Investigation into Impact of Ageing on Rubber Component in Used Engine Mount

By:

Lizhe Wang

A thesis submitted in partial fulfilment of the requirements for the degree of
Doctor of Philosophy

The University of Sheffield
Faculty of Engineering
Department of Mechanical Engineering

September 2019

Acknowledgements

Thanks to all the friends and colleagues I have met during these four years, and those who trusted my skills and capabilities.

Finally, many thanks to my parents Huanxian Wang, Huifang Liu, my girlfriend Kewei Chen and other family members for their supports and encouragement. It would be impossible for me to accomplish this without the support I have received.

Abstract

A 2014 KPMG customer survey report demonstrated the increasing demand of driving comfort and sustainable development. With the longer lifespan of modern vehicles, more attention has been placed on to products' lifetime performance. Ageing of rubber components in the engine mount was known to be one of the key elements related to the compromised driving experience in used vehicles. This thesis will investigate how the properties of the rubber component change, and why. Links among mechanical properties, microstructures and chemical composition of the aged carbon black filled vulcanised natural rubber used in a commercial engine mount are to be revealed.

By investigating used engine mounts, the changes of stiffness for rubber in the used engine mount was established, which were identified to be related to post-curing, thermal degradation, oxidative degradation, filler re-agglomeration and loss of additives. Among these ageing mechanisms, the most dominating factors were post-curing and loss of additives, which increased the stiffness of the rubber by 45% in a four-year-old car that has driven by 80 thousand kilometres.

The impact of the acting ageing mechanisms was identified through aerobic and anaerobic artificial ageing experiments. The artificial ageing experiments provided knowledge about how each ageing mechanism progresses in the material and how they interact with each other. It also demonstrated the limitations of artificial ageing on simulating certain ageing mechanisms.

This is the first time such a comprehensive investigation has been made to identify the causes of different ageing mechanisms on specimens from real vehicles and discuss how the ageing mechanisms impact on the material individually. Hopefully this work could provide useful information for the industry and other academics in the area when designing rubber relevant products or investigating ageing behaviour of similar materials.

Table of Contents

List of Abbreviations

6PPD	N'-phenyl-p-phenylenediamine
ABS	Anti-lock Braking System
BIIR	Bromobutyl Rubber
BR	Polybutadiene
CIIR	Chlorobutyl Rubber
CR	Chloroprene Rubber
CV	conventional vulcanization
DCM	Dichloromethane
DMA	Dynamic Mechanical Analysis
DMTA	Dynamic Mechanical Thermal Analysis
DPPD	N,N′-Diphenyl-p-phenylenediamine
EV	effective Vulcanization
FTIR	Fourier Transformation Infrared Spectroscopy
GC	Gas Chromatography
GPC	Gel permeation chromatography
HDPE	High-Density Polyethylene
IIR	Isobutylene-Isoprene Rubber
IR	Polyisoprene
LC	Liquid Chromatography
LDPE	Low-Density Polyethylene
MS	Mass Spectrometry
NBR	Nitrile Rubber
NIST	National Institute of Standards and Technology
NMR	Nuclear Magnetic Resonance
NR	Natural Rubber
RDC	Residual Dipolar Coupling
SBC	Thermoplastic Styrenic block copolymers
SBR	Styrene-Butadiene Rubber
SEM	scanning electron microscope

SEV	semi-effective Vulcanization
TEM	Transmission electron microscopy
TGA	Thermogravimetric Analysis
TPE-A	Thermoplastic polyamide elastomers
TPU	Thermoplastic Urethane Elastomers
UV Light	Ultraviolent Light

List of Figures

XII

XIII

List of Tables

XVI

CHAPTER 1. INTRODUCTION – DEMANDING AREAS OF AUTOMOBILE INDUSTRY

In the 1890s, a personal horseless carriage was a symbol of one's position in society [1]. Nowadays, people see cars more as a tool for transportation rather than a symbol of power. Automotive industry has grown dramatically in the last century. In the UK, an average of one car per household was achieved in 2008 [2]; the automobile has become an essential product for everyday life. The number of road vehicles has continued to rise in recent years, Figure 1.1 shows the global car sales from 2007.
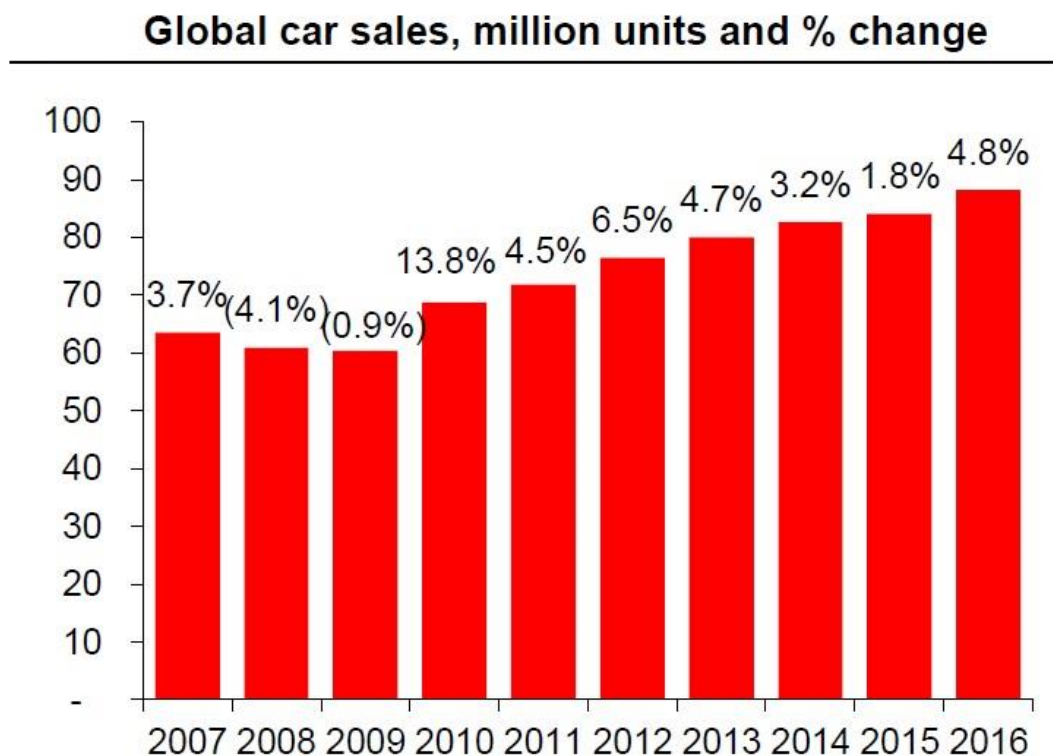
Figure 1.1 Global car sales [3]

When it still holds its symbolic meaning, the most demanding factor of a car is as a status symbol. However, when people start to see them as an everyday tool, they start to show interest in other factors. A 2014 survey by KPMG produced a list of the factors that most influence customers in purchasing a car; the results are shown in Figure 1.2.

Factors Customers Feel are Critical When Purching a Car

Enhanced vehicle lifespan

Environmental friendliness

Vehicle styling

■ Percentage of customer feel important

Ergonomics and comfort

Safety innovation

Fuel effiency

0   20   40   60   80   100
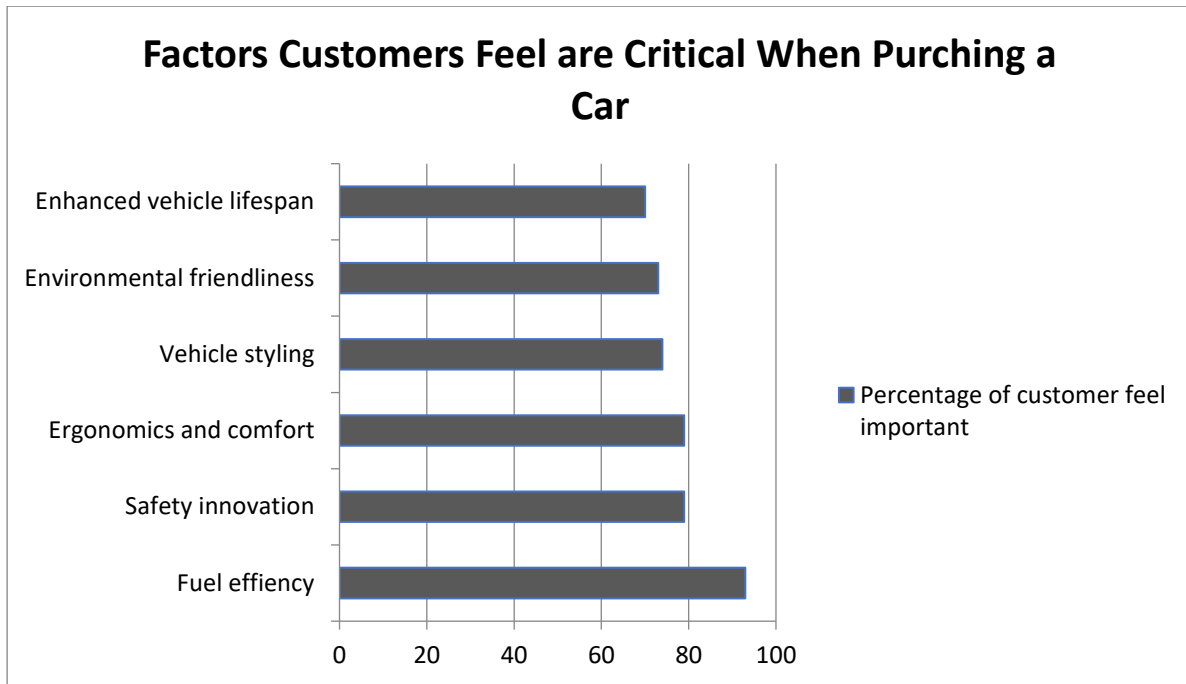
Figure 1.2 Factors customers feel are critical when purchasing a car. Only shows factors with an agreed rate above 70% [4]

As the survey results show, vehicle styling is demanded but fuel efficiency, which directly links with the cost and environmental factor of the car, has become the most influencing factor for one to purchase a car. Like all innovative products, people will pay for the idea and style at the beginning, and when the products start to become affordable to the public, cost becomes the most dominating factor. In recent years, the industry has made every effort to improve fuel efficiency in a number of ways, for example: energy recovery, fuel combustion, turbo/super charging, high efficiency transmission, lightweight chassis, etc.

As the cost of purchasing and maintaining a car becomes even cheaper, people have started to pay attention to the quality and durability of the product, which are represented by ergonomics, comfort and vehicle lifespan in the survey. Research in recent years also implies this changing focus. For the comfort of handling, researches on steering and braking systems can be found in a wide range of sources. For example, the development of the four-wheel steering system and anti-lock braking system (ABS) has certainly led to better handling capabilities [5] [6]. The presence of an ABS system reduces the vehicle's chances of crashing by 18%, according to statistical analysis [7], and the four-wheel steering system reduces the turning radius of a prototype car by 50% [6]. For the riding experience,

investigations were made into air conditioning and window glass in order to achieve better visual, acoustic, thermal and humid comfort [8] [9]. Researches on suspension systems, seat control, engine mount and material properties were conducted to reduce the discomfort caused by vibrations [10] [11] [12]. The development of an active or semi-active controlled suspension system and engine mount provides adjustable damping strength under different situations. Studies on materials also extended the vehicle's lifespan. Figure 1.3 shows the increasing average age of operating cars and light trucks in the US.
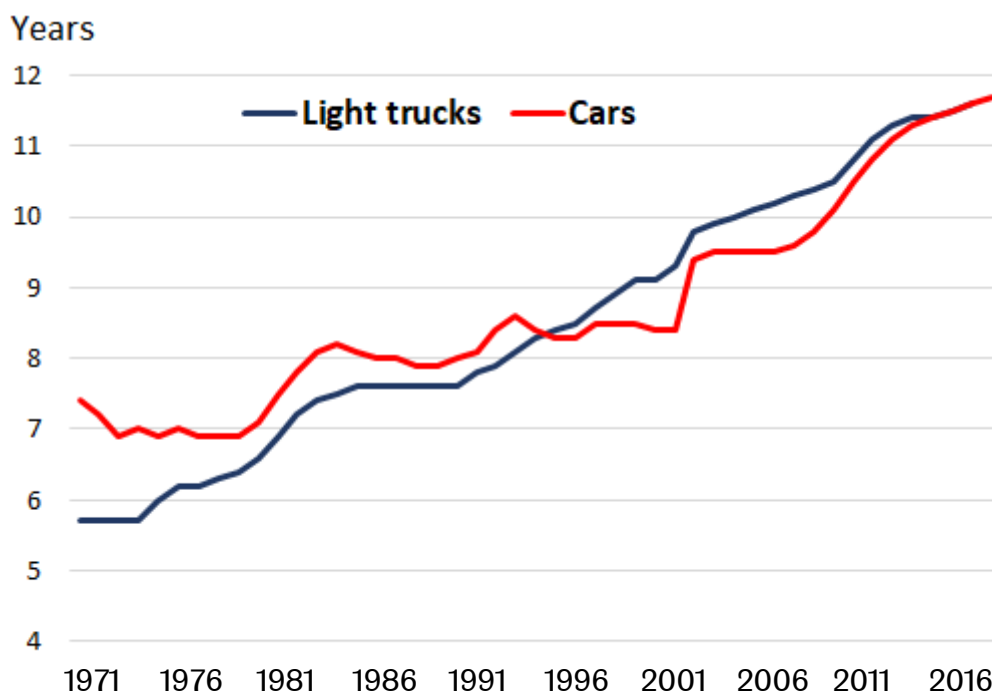
Figure 1.3 Average age of cars and light trucks [13]

This longer lifespan of vehicle and the demand on driving comfort generates a new challenge. The quality of a vehicle varies with time because of material ageing. Producing vehicles that maintain consistent performance over a long lifespan or considering this change of performance in the design cycle becomes important.

1.1 Engine Mounts in Vehicles

One of the components that could influence the performance and comfort of the car is the engine mount. Unlike rubber tires which wear out quickly and can be easily replaced, the engine mount functions as the joint between the engine and

the surrounding components. It is normally designed to reduce the vibration transmitted from the engine to the rest of the car. The dynamic response of the engine mount directly affects the reduction of vibration [14]. A worn engine mount could lead to undesirable noises and excessive vibration transmitted from the engine to the car [15]. From submarine to airplane, motorcycle to tank, an engine mount is installed in most applications that need an engine to produce power. There are various types of engine mount on the market for different purposes. The following examples represent the common engine mounts for land use vehicles.

1.1.1 Rigid mounts

A rigid mount is usually applied when accurate alignment between components is critical. The high stiffness means that rigid mounts have better rigidity to the chassis and lead to better shifting performance in a race. The rigid mount is often found in 1970s' sport vehicles. TRE Motorsport, an engine installation and re-conditioning specialist suggest, due to the high stiffness of the mount, more vibration and noise are transmitted into the car with this type of mount [16].

1.1.2 Resilient mounts

This type of mount uses rubber to avoid metal-metal contact between the engine and the car. The rubber provides resilience and damping to the mount and limits the production of noise and vibration. Figure 1.4 shows a Vulkan T Series resilient mount; the slash region represents the metal part and the dotted region represents the rubber. Rubber mounts with higher elastic modulus could provide better power transmission. This reduces the vibration absorption performance of the rubber part and leads to a harsh driving experience [14]. A mount that is too soft could lead to a bad component alignment for the components around the engine mount and allow it to vibrate around and reduce the lifespan of the engine [17] [18].
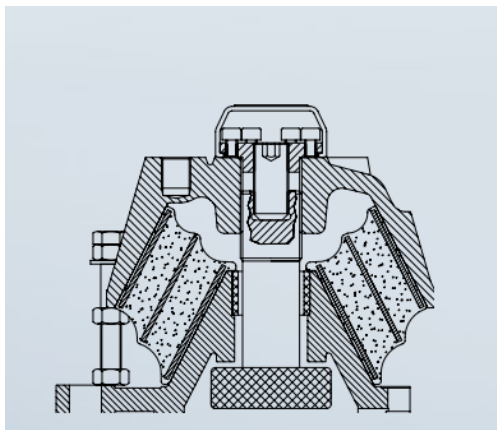
Figure 1.4 – Vulkan T Series resilient mount [19]

1.1.3 Hydraulic mounts

A typical design of a hydro-mount is illustrated in Figure 1.5. It consists of a body made of rubber, containing metallic frames to reinforce the mount's rigidity and metallic blocks act as junctions between the rubber part and the shaft. The fluid chamber brings extra viscous damping to the system at designed frequencies; usually it is set to counter the road shake [20] [21]. It therefore absorbs more vibrations and keeps relatively good component alignment. The hydro-mount was originally developed in the 1980s, and it has been heavily applied in the modern automotive industry due to its outstanding noise/vibration reduction performance [22]. The viscous performance of the mount relies heavily on the fluid chamber. The function of rubber in a hydraulic mount is mainly to provide resilience [23].
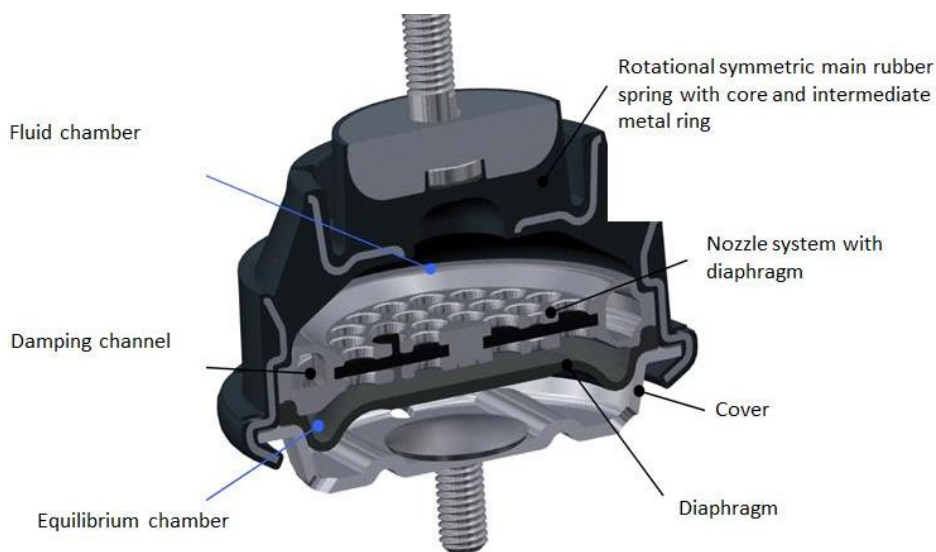
Figure 1.5 – A typical design of hydro-mount [24]

1.1.4   Active control mount

There is a trend to use active control techniques to further improve the driving experience. For example, in a Toyota Camry V6 a vacuum actuated engine mount is installed. This type of mount can adjust its stiffness according to the engine speed by changing the pressure in a hollowed vacuum chamber inside the rubber. In the Porsche 911 GT3, the combination of electromagnet and magnetorheological fluid allows the mount to adjust its damping coefficient according to its rate of deformation. The viscosity of the magnetorheological fluid depends on the surrounding magnetic field [25]. In Figure 1.6, the yellow chamber is filled with the magnetorheological fluid and the orange blocks are electromagnets that produce a magnetic field relating to the input voltage.
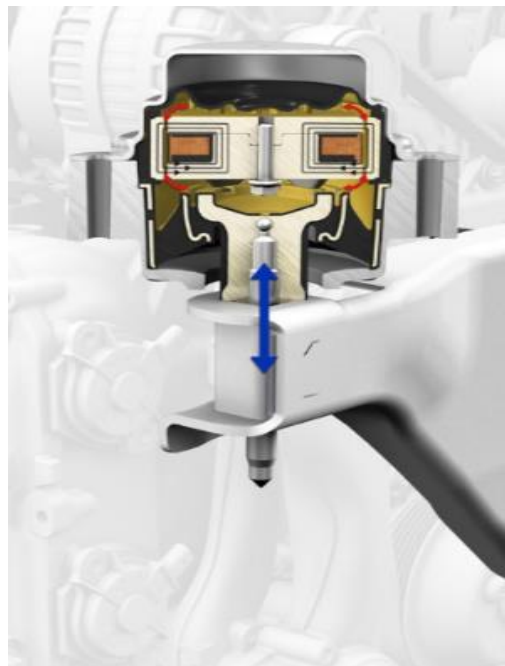
Figure 1.6 – Active engine mount in Porsche 911 GT3 [25]

The engine mount that will be investigated in this research is a hydraulic mount. Its structure is similar to the one shown in Figure 1.5, consisting of a rubber body and aluminium frames, with propylene glycol as the chamber fluid. The rubber used here is a carbon black filled vulcanised natural rubber with a filler content of 30%. It is covered under a steel outer case which protects the mount from physical contact and light.

1.2 Performance of the Engine Mount

There are many factors that can impact the dynamic response of the engine mount, including different loading conditions, operating conditions affected by weather or location differences, geometry change of the mount caused by creep [26] and property changes of rubber material caused by various ageing mechanisms [27] [28].

All these factors are related to the driving comfort. When the mount is severely worn, the engine may experience stronger vibration from the movement of the car body, which damages the engine system and reduces the lifespan of the vehicle [15]. Thus, it is crucial to understand how the mount behaves under various conditions when designing it. Although this could be achieved experimentally, the time and effort required for the experiments are unacceptable for commercial products.

This brings the demand of building a virtual model that is capable of making quick predictions on the performance of the engine mount during the design cycle.

1.2.1 Modelling its performance

Various types of analytical and numerical virtual models have been developed to simulate the performance of engine mounts with rubber or fluid chambers. For analytical solutions, like the one developed by Whear and Williams, assumed the mount is a complex spring-damper system. In order to match the performance of the actual mount, the model requires correlated stiffness and damping coefficient as the input. This method provides a perfect prediction of the specific loading conditions the model is designed for, which ranges from 0 to 50 Hz in this example [29]. However, property changes caused by ageing cannot be directly fed into the model. New correlated coefficients need to be evaluated again experimentally.

By understanding more of its operating physics, an analytical model that is developed from differential equations can be built, as Colgate et. al. did [30]. Although the prediction might be slightly off from the reality, this method can make predictions for more loading conditions, the aforementioned model covers 5 to

200 Hz excitation with different amplitudes. This type of model uses the physical properties of each individual component, hence these properties need to be measured again if the material properties change.

In the last 20 years, with more advanced computing techniques, the mount performance can be estimated using finite element analysis models. The required input becomes material properties of each individual material in the mount and the appropriate methods used to simulate them. Its accuracy is enough to make a good prediction on the performance of the mount in many loading conditions. Masahiro Fukazawa made a CAE model for predicting hydraulic mount behaviour under 200 to 1000 Hz [31].

As the changing material properties caused by ageing can be embedded into the model, this means the CAE model has the potential to make lifetime performance predictions for the engine mount. This makes the study of property changes of rubber in the engine mount during ageing desirable.

1.2.2 *Existing progress on studies relevant to rubber property changes*

Over the years, the automobile industry has made many attempts to predict the ageing behaviours of the rubber material. Experimental data exists from accelerated ageing tests that give insights about the performance changes of the material over time, theoretical models also exist that aim to predict this behaviour. However, the accelerated ageing data were captured in laboratories and the actual operating conditions for an engine mount are much more complex, which led the experimental results to be different from the reality. For the same reason, due to the complexity of the rubber matrix itself and the ageing conditions, theoretical models can only provide a non-accurate guidance about the material behaviour to designers. Thus, an understanding of how the ageing mechanisms affect rubber's properties is needed. With the knowledge of how each ageing mechanism affects the rubber and how multiple ageing mechanisms act together, the ageing behaviour of rubber could be predicted based on actual mechanisms instead of a black box.

The published investigation of ageing mechanisms of rubber is not comprehensive enough for this purpose. Those investigations are either focusing on property changes that are led by a single ageing mechanism or establishing property changes and discussing possible ageing mechanisms without investigating their acting rates individually.

This research will be focusing on establishing a comprehensive study identifying and analysing the ageing behaviour of rubber material used in a real-world engine mount, by investigating the connections between the changes on the specimen's mechanical properties and the changes on its microstructures and chemical composition. Lab-controlled ageing methods will be used to simulate and deduce impact of individual ageing mechanisms and compare with real-life samples taken from used engine mounts. As mentioned, the material used in these engine mount that would be investigated in this research is a carbon black filled vulcanised natural rubber.

This investigation could also be helpful for other applications involving long lifespan rubber components like in submarines [32] and bridges [33]. The flow chart shown in Figure 1.7 illustrates the progression of the study and this thesis.

Aim: Establish relationships between the mechanical properties changes and microstructure changes of rubber material during ageing.

Investigation of retrieved mount samples

Establish effect of ageing on elastic modulus

Investigate causes of elastic modulus changes

Crosslink Density Changes

Oxidative Degradation

Loss of Additives

Carbon Migration

Cracks

Accelerated ageing of mount and sheet samples

Establish how elastic modulus changes

Verify the feasibility of using sheet material to replicate mount material

Investigate behaviour of acting mechanisms

Anaerobic Accelerated Ageing for sheet samples

Establish elastic modulus changes of sheet material under oxygen-free environment

Investigate the relationship between acting ageing mechanisms and the existence of oxygen

Figure 1.7 Flow chart of this study

CHAPTER 2. ELASTOMERS AND THEIR PROPERTIES

Rubber is categorised as a type of elastomer, which implies that it is a type of polymer. Polymers were not invented by humans; millions of years ago, nature had already discovered them. Nowadays, they are everywhere on Earth. Protein, a kind of polymer, is the basis of most creatures on this planet. Collagen, keratin, silk and enzymes are all proteins. For green plants, one of the major components in their cell walls is a polymer – cellulose. Plants store energy by producing another kind of polymer – starch. The first rubber was also produced by plants and it is the first polymer humans ever used. Mesoamerican rubber balls were invented around 1600 BC and were used in the Mesoamerican ballgame.

After the Mayans, Charles Goodyear noticed that the rubber gum does not melt when heated in boiling sulphur, but charred. After many experiments to improve the whole process, the recipe for vulcanisation was found in 1839, which makes rubber more durable. The first synthetic plastic 'Bakelite' was produced in 1907 and was used for electrical insulators. From the 1920s, polymers started to be produced in large scale and became the most used material in 1976 [34]. The consumption of rubber material has kept increasing since the beginning of the 20th century, as shown in Figure 2.1.
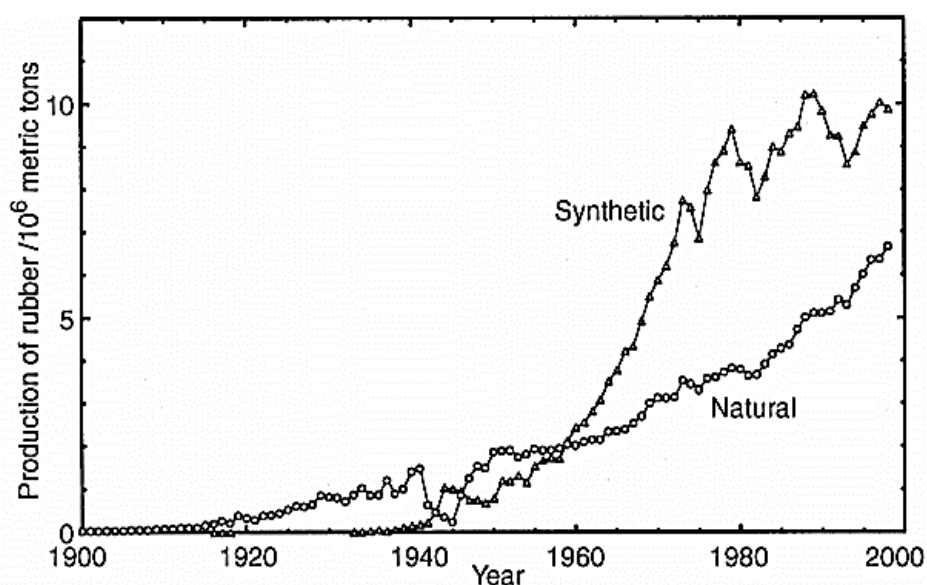
Figure 2.1 - Rubber production from 1900 [35]

The aim of this research is to provide a deeper understanding on the ageing behaviour of rubber material in the engine mount. This chapter begins by exploring polymer materials in general, before investigating the existing literature regarding rubber, its ageing mechanisms and common characterisation methods, in more depth.

2.1 Polymer Material

As discussed in the introduction, the ageing of rubber material in the engine mount is expected to impact the driving comfort of the vehicle. Rubber is a type of polymer, and, in order to understand its ageing behaviour, the basics of polymer materials are critical. In this chapter, the fundamentals of polymers and their applications are briefly introduced.

2.1.1 Formation of a polymer

A polymer represents a network of large molecules formed by repeating subunits. These subunits are called monomers; Figure 2.2 illustrates this relationship [36]. In this figure, the polymer chain represents a linear homopolymer – the polymer consists of only one type of monomer that forms long straight chains [37].
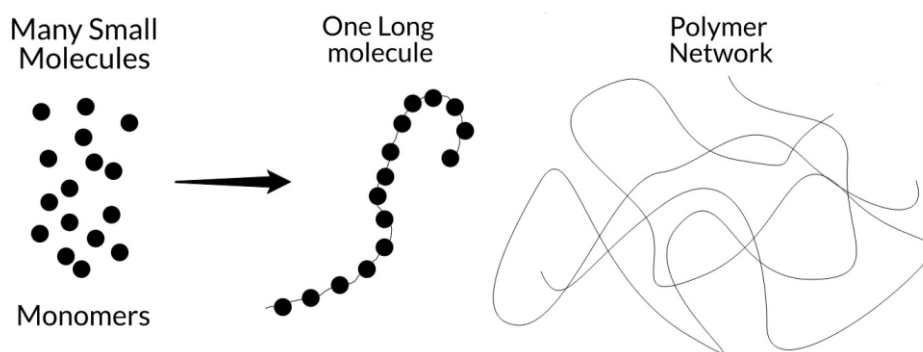
Figure 2.2 – Structure of linear homopolymer (left); A polymer network (right)

The process of transferring monomers into a polymer is called polymerisation. There are two main polymerisation processes: chain growth polymerisation and step growth polymerisation [37]. For chain growth polymerisation, there are three steps: initiation, propagation and termination. The process is illustrated in Equation

2-1, where R· represents free radicals with unpaired valence electron and M represents monomers. Initiators are needed to produce free radicals. The radicals will react with the monomers and become the new radicals that will react with other monomers. The polymer chain grows rapidly once the propagation is initiated, until it terminates with another growing chain.

Initiation:

$$Initiator => R \cdot$$

$$R \cdot + M => RM \cdot$$

Propagation:

$$RM_n \cdot + M => RM_{n+1}$$

Termination:

$$RM_n \cdot + \cdot M_m R => RM_n M_m R$$

Or
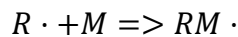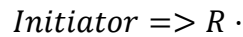
$$RM_n \cdot + \cdot M_m R => RM_n + M_m R$$

Equation 2-1 - Chain growth polymerisation process

For step growth polymerisation, no initiator is needed. Monomers react with each other and form dimers, which then react with the remaining monomers or other dimers to form trimers or tetramers. Those oligomers keep reacting with monomers or other oligomers to form a longer polymer chain. This process is shown in Figure 2.3. All reactions in this process have a considerably higher energy barrier and normally occur under a high temperature environment.
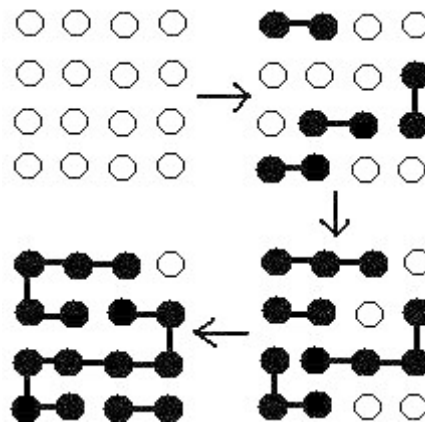
Figure 2.3 – Step growth polymerisation process [38]

The chain length depends on the reaction time and this polymerisation process is significantly slower than the chain growth process.

2.1.2 Structures of polymer

The formed polymer chains can be non-linear, which means branches can form on polymer chains. Those polymers are called branched polymers, the most linear chains in a branched polymer that represent the properties of the molecule the best are defined as the backbone chains. According to how the polymer chain branches, those polymers can be further categorised into comb polymer, brush polymer, star-shaped polymers, dendrimers and crosslinked polymers; Figure 2.4 illustrates their structures.
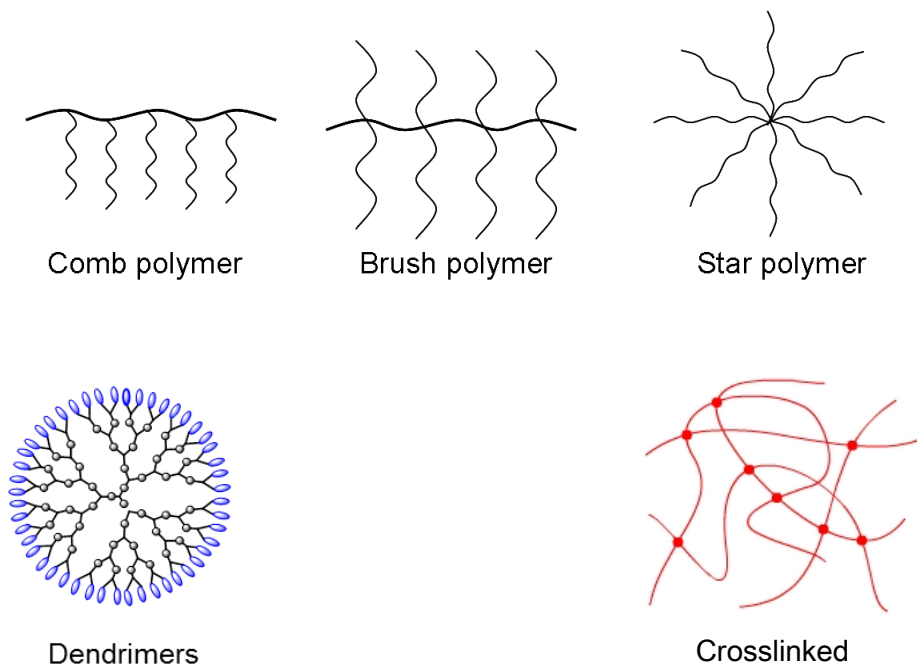
Figure 2.4 – Typical structures of polymer [37] [39]

Properties' dependence on structure for polymers

To explain the property changes caused by branching, a good example is HDPE (high-density polyethylene) and LDPE (low-density polyethylene). Figure 2.5 illustrates their chemical structure. HDPE consists of long linear chains with a low degree of branching, and LDPE has a much higher degree of branching [40]. This makes the chains in LDPE become impossible to be packed as densely as those in HDPE.
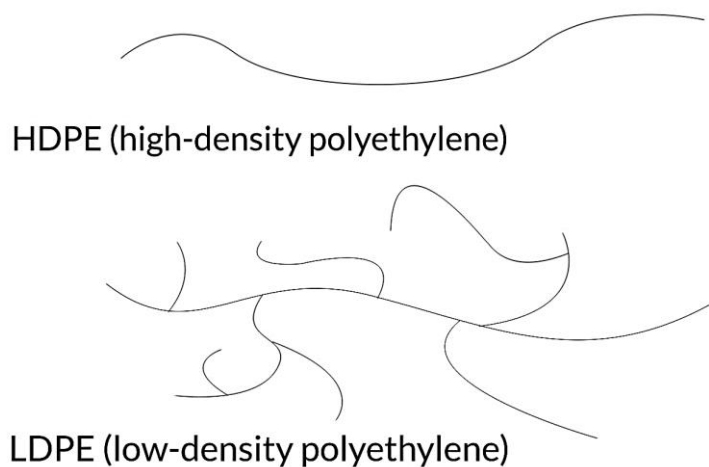
Figure 2.5 – Chain structure of HDPE and LDPE

This leads LDPE to have smaller density and weaker intermolecular force. Table 2-1 makes a comparison between these two materials on their thermal, mechanical and optical properties. Examples of application of each material are also given.

Material	HDPE	LDPE
Melting point	134.85°C	109.85°C
Tensile strength	43 MPa	24 MPa
Density	0.96 g/cm^3	0.92 g/cm^3
Transparency	Semi-transparent	Transparent
Applications	Toys, pipes, utensils, etc.	Plastic wraps, packaging foam, plastic bags, etc.

Table 2-1 – Properties and Applications of HDPE and LDPE

The branched polymer also has the chance to form a crosslinked network, in other words, instead of having free ends, the ends of branches are attached to other polymer chains as the one shown in Figure 2.4. This makes the polymer become stronger and maintain most of its mechanical properties under high temperatures. These connections are normally irreversible chemical connections. However, the good temperature tolerance comes with the fact that these crosslinked polymers are normally not recyclable. This type of polymer is called thermoset, which will be introduced further in later chapters. Due to the crosslinked structure, thermosets are not soluble which makes them unable to be tested by characterisation methods, which require specimens to be dissolved before testing. Methods exist that form crosslinks without turning the material into thermosets, which will also be introduced later.

Properties of polymers with special structures

For the star-shaped polymers shown in Figure 2.4, their unique molecular structure makes them highly compact and leads to a low radii of gyration and hydrodynamic radii, hence lowering the viscosity. Weaker intermolecular force results from its multi-arm structure, which leads to lower a melting point and

degree of crystallisation. They are often used as lubricants or an additive to motor oil as a viscosity control agent. It also contributes to hydrogels, ultrathin coatings, etc [41].

Dendrimers shown in Figure 2.4 are extremely difficult to be manufactured and can be much more expensive than gold. Their properties normally depend on the chemical group covering their surface, for example, loading hydrophilic group on a dendrimer's surface can make it water soluble. A well-known application for a dendrimer is medicine delivery, by loading a chemical group that can target the infected cells on its surface and carry the medicine in its interior. This can effectively lower the side effects of the medicine on healthy cells [42].

Copolymer

Copolymer means the type of polymer formed by different types of monomers. Copolymer with two types of monomer can be called a bipolymer, terpolymer for three types, quarterpolymer for four, etc.

The arrangement of different types of monomers in a copolymer can vary its properties; according to how those monomers are arranged, the copolymer can be further categorised. Table 2-2 shows the name of those different arrangements.

Name	Structure (X, Y represent different monomer)
Alternating copolymer	X—Y—X—Y—X—Y—X—Y—X—Y
Random copolymer	X—Y—Y—X—Y—X—Y—Y—X—X
Block copolymer	X—X—X—X—X—Y—Y—Y—Y—Y

Table 2-2 Types of copolymer

The properties of copolymers can vary a lot, even with a tiny change in its arrangement, therefore, it is difficult to summarise the specific benefits of copolymers compared to homopolymers. In general, this nano-scale blend of different monomers brought the possibilities of getting new and better properties, like the discovery of alloy in the early ages [43]. Many thermoplastic elastomers are copolymers, with part of the polymer providing resilience properties, and part of

the polymer forming reversible connections between polymer chains. Moreover, although homopolymers can be branched, the copolymerisation process makes the final structure of the polymer, and, therefore, its properties, more controllable.

Thermosets and thermoplastics

As mentioned in previous sections, thermosets are polymers that have developed an irreversible chemical bond — crosslinks between individual chains that cannot be un-linked and make the polymer unable to melt under high temperatures. Thermoplastics represent polymers that can be reshaped and remoulded under high temperatures. Thermoplastics can still develop 'crosslinks' to enhance their properties, but the crosslinks needed to be reversible. This is normally achieved by two approaches: ionomers and block copolymers. Ionomers are copolymers consisting of non-polar chains and some polar side groups, the polar ionic groups attract each other and form connections equivalent to crosslinks under low temperatures. The block copolymer method requires the copolymer that consists of chains that are difficult to be packed up, and chains that are easy to be packed up;, the part that can be easily be packed up can form crystalised regions which work as crosslinks in this case.

Crystallinity

The polymer network is usually described as a plate of spaghetti, each spaghetto (a single strand of spaghetti) represents a polymer chain. Unlike other materials, polymers have a significantly higher molecular weight, the long polymer chains are all entangled together and the intermolecular force holds them in place. The chains are able to move or rotate when there is enough activation energy. The polymer can be partially 'crystallised' and forms regions with order as shown in Figure 2.6, caused by different chain structures, or by certain methods like cooling, solvent evaporation or stretching. The remaining region is referred to as amorphous region.
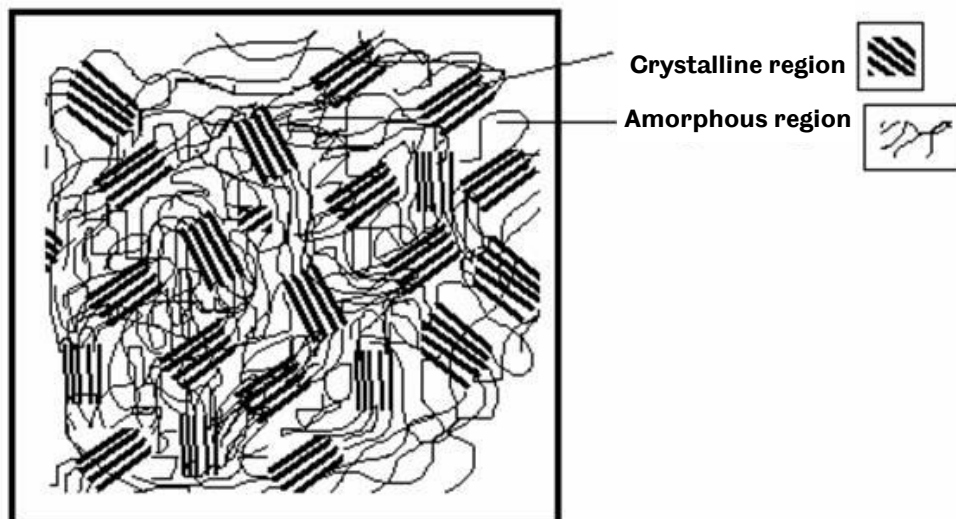
Figure 2.6 - Partially crystallised polymer [44]

These crystallised regions are called lamellae. Polymer chains in lamellae are closely packed and, therefore, dramatically increase the intermolecular forces inside these lamellae. Polymer chains that connect multiple lamellae are called tie molecules. This structure can, therefore, be considered as a reversible crosslinked network.

The ratio of crystallinity is closely related to the structure of the material. Considering the LDPE and HDPE case mentioned earlier, lamellae are easier to form in HDPE due to its less branched structure. Polymers with syndiotactic branches also tend to be easier to pack up than polymers with atactic branches.

Intermolecular forces

As mentioned in previous chapters, intermolecular force is related to the properties for polymers. Except from the crystallinity of the material, the forces between elements and chemical bonds can also affect it.

There are several types of intermolecular forces and the two that most closely relate to polymers are dipole-dipole force and London dispersion force [45]. Dipole-dipole force is produced when elements from different molecules with opposite charges attract each other. Figure 2.7 illustrates this relationship. In its special case of 'hydrogen bonding' this attraction force is much stronger. As the

chemical bond formed between a hydrogen atom and oxygen, nitrogen or fluorine atom provide large differences in their electronegativity.

$$\begin{array}{cc} \delta^- & \delta^+ \\ Cl\!\!-\!\!I & \\ \vdots & \vdots \\ I\!\!-\!\!Cl & \\ \delta^+ & \delta^- \end{array} \qquad \begin{array}{cccc} \delta^+ & \delta^- & \\ Cl\!\!-\!\!I \cdots Cl\!\!-\!\!I \end{array}$$
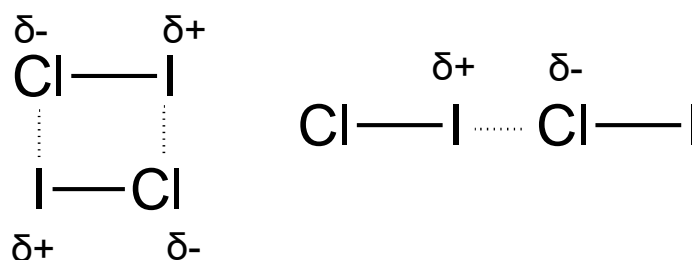
Figure 2.7 Dipole-dipole force

The London dispersion force exists when molecules temporarily develop a dipole due to the movement of electrons that attract each other. Figure 2.8 illustrates this behaviour, where the large red dots represent the nuclei and black dots represent electrons [45].
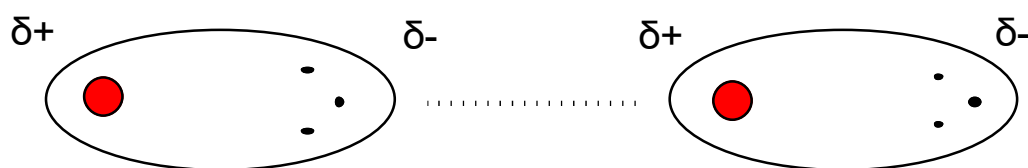
Figure 2.8 London dispersion force

Both the dipole-dipole force and the London dispersion force decay fast with the distance between the molecules. This makes intermolecular forces strong in the lamellae, as polymer chains are closely packed. By the difference on the overall strength of polymers' intermolecular force, they can be categorised into fibre, plastic and elastomer [45].

Fibres have strong intermolecular forces and a high degree of crystallinity, resulting in high stiffness and low flexibility.

Plastics have moderate intermolecular forces and demonstrate both good mechanical toughness and a certain level of flexibility [46]. When the stretching force is strong enough, it will break enough interconnections and make the deformation irreversible.

Elastomers have relatively low intermolecular force between chains, the reason for them to be flexible is because these chains, with weak intermolecular force, can be

easily twisted into different states under force. For a crosslinked elastomer, with chemical crosslinks or physical crosslinks, the chains can still return to their original configuration after large deformation. Figure 2.9 illustrates the elongation process of a network of chains, without and with crosslinks. In an un-crosslinked network, as chains are entangled together, they can still return to their original state if the deformation is under a certain limit.
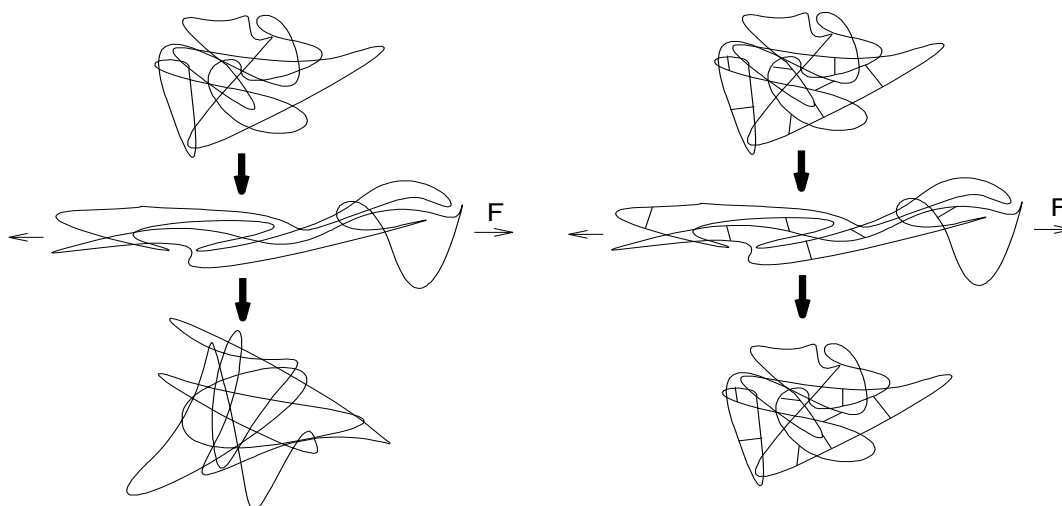
Figure 2.9 Elastomer network under stretch   (left) un-crosslinked   (right) crosslinked

By heating up polymer materials, they can become softer and for thermoplastics they will eventually melt into liquid. A high temperature environment will provide kinetics for the chains to transfer their states, because this kinetic acts against the intermolecular attraction force. On the contrary, under a low temperature environment, chains become very inactive and the polymer loses its flexibility.

2.2 Elastomer

As discussed in the previous chapter, the polymer material is a network of chains and those with weak intermolecular force between polymer chains are elastomers. It represents the type of material that has low stiffness and moderate yield strength, exhibits both elastic and viscous properties. Due to the unique behaviour of elastomers, they are often used in protective clothes, sports accessories, vibration absorbing devices, etc. The automobile industry has a high demand for elastomer materials, functionalities of car tires, and engine mounts heavily rely on their rubber components.

2.2.1 Dynamic response of elastomer

A major functionality of elastomer material in a product is to reduce the transmitted vibration. Changes on the dynamic response of the elastomer material directly affect the product's performance.

Elastomers normally have extraordinary flexibility. They can be stretched to several times their original length. For an elastic material, strain represents the existence of stress that has a magnitude directly linked with the material's modulus. Due to the chain network structure rubber has, it exhibits both elastic and viscous properties. Figure 2.10 illustrates some commonly used models for viscoelastic materials, they consist of damper and spring components and are applied in different scenarios.
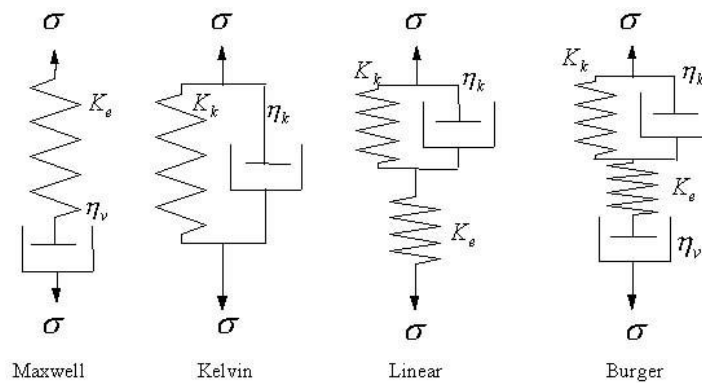
Figure 2.10 – Dynamic models for simulating viscoelastic materials [47]

Due to the existence of a damping effect, when an elastomer is subjected to periodical load, there is a delay between the strain applied and the force detected. The damping effect causes the input energy to partially dissipate to heat energy. An illustration of this delay is shown in the left hand side of Figure 2.11. Under dynamic loading, the elastic modulus of a rubber is related to both its elastic and viscous properties, which are represented by the so-called storage modulus and loss modulus, respectively. The storage modulus represents the energy stored in the deformed material and will be recovered when the force is removed. The loss modulus represents the dissipated energy in the system, those energy are transferred into heat during movement of molecules and fillers [48]. The combination of these two is called dynamic modulus which represents the force

response of rubber under a given test condition, as shown on the right hand side of Figure 2.11.
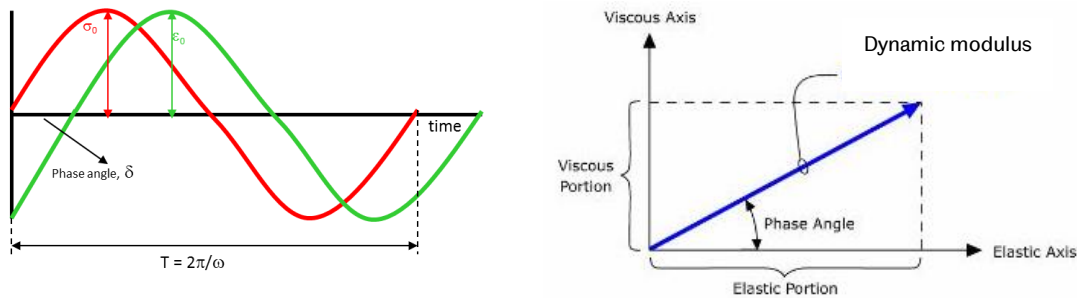
Figure 2.11 – Delay between stress and displacement (left) [49] / Viscous and elastic portion of dynamic modulus (right) [50]

The properties of elastomer materials make them special, but those properties come from their complex internal structures and make investigation of this material rather challenging. Its properties are affected by many factors: its chemical composition determines the structure of the formed network; its manufacturing method affects how polymer chains are connected to each other; its loading conditions change rubber's internal structure; its additives, most rubber materials used nowadays are composite materials, mixing rubber with other substances to achieve desired properties [27]; and its service time, the rubber's properties change over time as various mechanisms would occur when rubber is exposed to different environments for a long time.

Various researches have been carried out to establish a better understanding of the material and produce elastomers with more desirable properties. These studies include looking at possible additives or fillers to alter elastomers' properties; investigation into the formation of crosslinks during the material's forming process; conducting new characterisation techniques to reveal more insights about their physical and chemical properties; study of their degradation processes and property changes while ageing. All these researches aim to develop elastomers with better functionalities and establish better control of their properties.

2.2.2 Types of elastomer

As mentioned in previous chapters, polymers can be split into two categories; thermoplastics and thermosets. Elastomers can be categorised in the same way, a few examples of elastomers in both categories are introduced in this chapter.

Thermoplastics

Styrenic block copolymers (SBC)

SBCs consist of copolymer chains with polystyrene end blocks and a polydiene block in the middle. The polystyrene end blocks from different copolymer chains can be easily packed up and crystallised, which serves as crosslinks between the polydiene chains. The structure of SBCs can be seen in Figure 2.12.
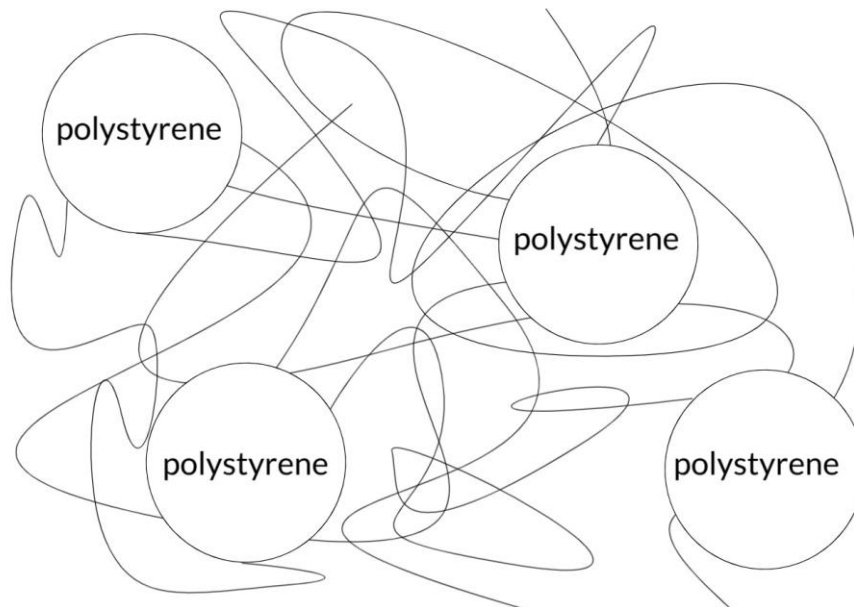
Figure 2.12 Structures for SBC

A typical SBC polydiene block can be butadiene, isoprene, ethylene-butylene or ethylene-propylene, which forms SBS, SIS, SEBS and SEPS with polystyrene, respectively [51]. SBCs generally have good electrical and mechanical properties and they also tend to have good abrasion resistance. This makes them a good choice for cables, wires and shoe soles.

Thermoplastic urethane elastomers (TPU)

TPU consists of copolymer chains with low polarity soft long chains and short high polarity urethane segments. The hydrogen bonding between the urethane

segments makes the connection very strong, forming crystalline or pseudo crystalline regions. The long chains in the middle provide resilience to the material, which is normally linear polyester or polyether. Its structure is illustrated in Figure 2.13. The properties of the TPU depend on the ratio between the soft and hard segments, and the component used for the soft long chain [51]. TPU can have good mechanical properties, as well as oxygen, ozone and abrasion resistance [52]. They can be used to make conveyor belts, footwear, hoses, etc.
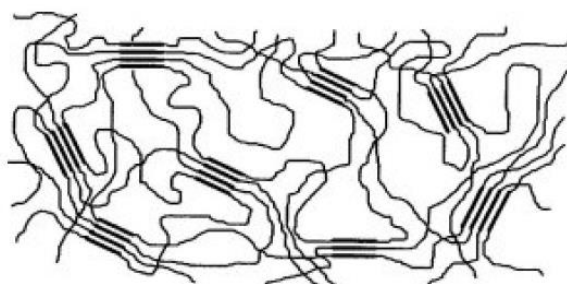
Figure 2.13 Structure of TPU [51]

Thermoplastic polyamide elastomers (TPE-A)

TPE-A also consists of soft segments and hard polyamide segments, where the soft segments can be polyester or polyether. The polyamide can be polyesteramide, polyetheresteramide, polyether-block-amide, etc [51]. The structure representing TPE-A is illustrated in Figure 2.14. The polyamide segments form crystalline regions with hydrogen bonding, TPE-A is considered to be one of the best thermoplastic elastomers due to its good performance and processability. They normally have good heat, chemical and abrasion resistance. They can be found in medical devices, sports equipment, motor systems, etc [53].
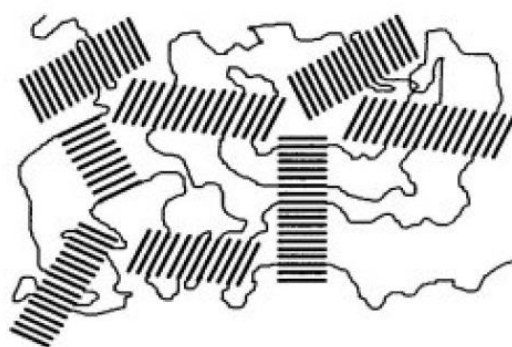
Figure 2.14 Structure of TPE-A [51]

25

Thermosets

Thermoset elastomers normally require the addition of curing agents during their manufacturing process for the crosslinks to be formed. Details of the curing process will be introduced in the next chapter.

Chloroprene rubber, polychloroprene (CR)

Polychloroprene was invented in the 1930 as one of the first synthetic rubbers [54]. It can be produced by free radical polymerisation, a type of chain growth polymerisation method. Figure 2.15 illustrates its structure. CR normally has good oil, ozone and abrasion resistance. It is also inflammable and would become stiffer under a high temperature environment. Its main applications include conveyer belts, gaskets, wetsuits, coated fabrics, etc [55].
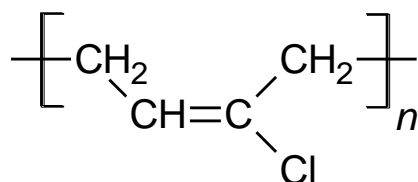
Figure 2.15 Structure of Polychloroprene

Silicone Rubbers

Silicon rubbers are inorganic as their backbone chains do not contain carbon. Figure 2.16 illustrates their structure; the backbone chain is formed by alternating silicone and oxygen atoms [51].
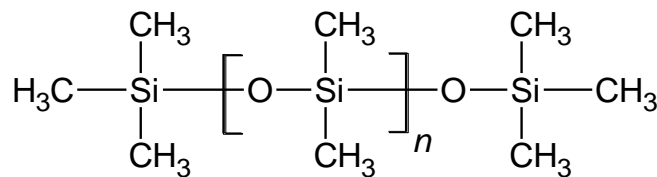
Figure 2.16 Structure of silicone rubber

Silicone rubbers are normally more stable than organic rubbers; they tend to have superior temperature and ageing resistance, good elasticity and electrical insulation. They can be found in various applications under extreme environments, such as cooking tools, sportswear, high temperature electronics, aeronautics industry, etc [56].

Butyl rubbers

Isobutylene-isoprene rubber (IIR), chlorobutyl rubber (CIIR) and bromobutyl rubber (BIIR) all belong to butyl rubbers [51]. The chemical expression of the copolymer IIR is shown in Figure 2.17. Some of its properties depend on the number of carbon-carbon double bonds, a low double bond density means a good oxygen and ozone resistance. Halogens can be added to enhance the properties of IIR. Adding chlorine or bromine can turn IIR into CIIR or BIIR which exhibit better chain flexibility and cure compatibility when blended with some other rubbers.
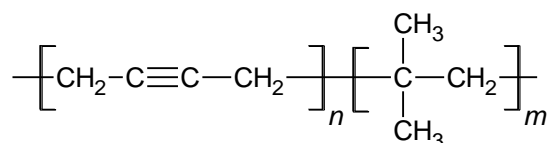
Figure 2.17 – Chemical expression of IIR

Butyl rubber shows a good long-term property stability and thermal stability, excellent ozone and weather resistance and low gas permeability. Its wear resistance is bad, and it also shows a relatively poor resilience. Typical applications are steam hoses, waterproof film, footballs and inner tyres [54].

Nitrile Rubber (NBR)

NBR is a copolymer consisting of butadiene and acrylonitrile, its chemical expression is illustrated in Figure 2.18.
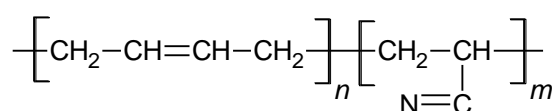
Figure 2.18 – Chemical expression of NBR

NBR has very good weather and heat resistance, and excellent oil and abrasion resistance, however, its ozone resistance is poor. NBR is a random copolymer and the percentage of acrylonitrile dominates the properties of the product [51]. A high acrylonitrile percentage leads to a high abrasion resistance, hardness, heat resistance and oil resistance with the risk of having poor cold resistance. NBR can be blended with IIR to achieve better weather resistance and thermal stability. Typical applications are non-latex gloves, protective clothes, seals and applications requiring good oil resistance.

Natural rubber

Natural rubber is one of the most demanded elastomers for commercial use [57]. It is harvested from the latex produced by the rubber tree – Hevea Brasiliensis. More than 200 species of plants produce natural rubber, but the rubber tree is the major source due to its commercial advantage on production rate. The chemical expression of natural rubber is shown in Figure 2.19 which represents cis-1,4-polyisoprene [40]. It has excellent mechanical properties such as tensile strength, elongation at break, tear resistance and wear resistance. However, it has relatively low weather and ozone resistance and is not suitable to be used under a high temperature environment. Typical applications are tyres, conveyor belts, footwear, latex products, etc [40].

$$\left[\begin{array}{c} CH_2 \\ \backslash\!\!= \\ H \end{array} \begin{array}{c} CH_2 \\ / \\ CH_3 \end{array}\right]_n$$
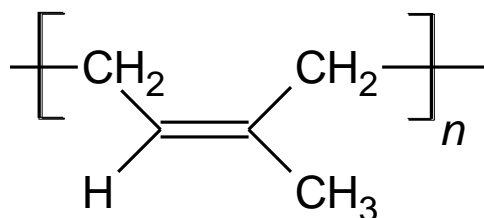
Figure 2.19 Chemical expression of natural rubber

Competing synthetic rubber

There are many synthetic rubbers that were developed as alternatives to natural rubber. Styrene-butadiene rubber (SBR), polyisoprene (IR) and polybutadiene (BR) can all fall into this category [51].

SBR is the most demanding synthetic rubber and it is a co-polymer consisting of the chemical units shown in Figure 2.20. Its properties are fairly similar to natural rubber as it was developed as an alternative for natural rubber during World War II. Its abrasion and ozone resistance are slightly better than natural rubber but it has a shorter elongation at break and lower modulus.

$$\left[CH_2-CH=CH-CH_2\right]_n \left[CH_2-CH\right]_m$$
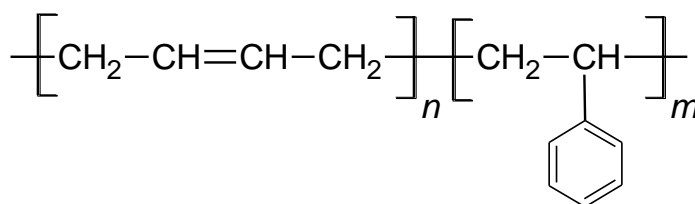
Figure 2.20 – Chemical expression and components of SBR

IR is the synthetic version of natural rubber as they share the same chemical formula. It is purer than natural rubber harvested from the rubber tree as natural rubber has other organics in it like proteins, fatty acids, resins, etc. For this reason, IR has a better property consistency compared to NR, and does not have the allergenic problems caused by tree organics [58]. Moreover, the industrial manufacturing process of IR means it has significantly better processability than NR. However, due to the isomerism problem, the IR can consist of other isomeric structures of polyisoprene, as shown in Figure 2.21 [51]. Although, by controlling the polymerisation conditions, the composition can be controlled fairly well, the percentage of cis-1,4-units still cannot reach 100% as NR have. The result is that the material has a lower degree of crystallisation and leads to a slightly lower modulus.

cis-1,4 polymer   trans-1,4 polymer

1,2 polymer   3,4 polymer
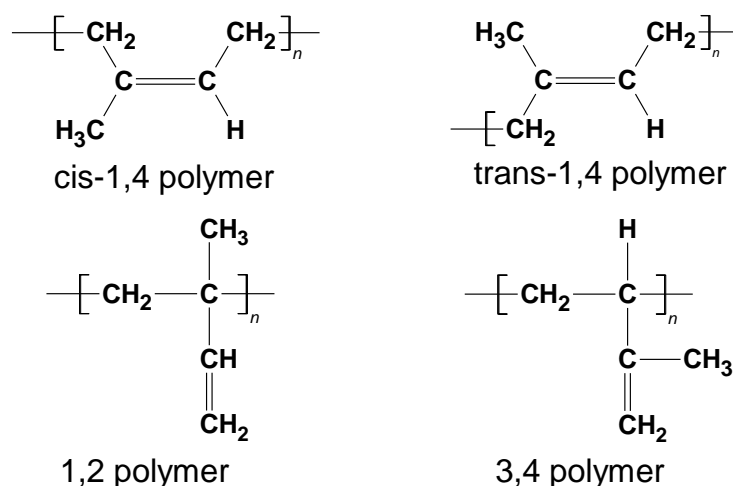
Figure 2.21 – Chemical expression and variations of IR

BR was developed due to its excellent cold resistance, it also has very high resilience. It is difficult to process unless blended with other elastomers. In most applications SBR, IR and BR will be blended with natural rubber to achieve desired properties [51]. The percentage of each component varies depending on the demanded performance of the product. The applications of these materials are all similar to natural rubber.

2.3 Factors Affecting Properties of Rubber

As mentioned in the previous section, rubber's properties are affected by many factors. This chapter reviews the most general ones and those that are closely

related to this research, as well as factors that affect their properties, including their manufacturing processes, composition, microstructures and operating conditions.

2.3.1 Manufacturing method

There are various manufacturing methods available for elastomer materials, including extrusion, compression moulding, injection moulding, transfer moulding, etc [59].

Dong (2013) showed NEXPRENE samples prepared with compression moulding and injection moulding can get about ±20% difference on storage modulus, even with the same mould temperature. The chamber pressure in compression moulding affects the material differently under different temperatures [60]. For example, at 177 °C, storage modulus of NEXPRENE samples manufactured under 103 bars of pressure were 30% lower than samples manufactured under 138 bars. But, under 221 °C, the storage modulus of a sample made under 103 bars were 25% higher than samples made under 138 bars [60].

Skrobak et al. (2016) showed an increase of about 10% on tensile strength for injection moulded NR BR blend when compared with compression moulded samples, even under the same mould temperature and chamber pressure [61], and suggested the difference could be caused by different chain arrangements in the samples. Skrobak et al. (2018) showed similar modulus difference on EPDM rubber manufactured with both methods under the same temperature and pressure, where injection moulded samples have a 10% higher tensile modulus [62].

2.3.2 Radiation

When rubber is exposed to a radioactive environment, chain-scission and crosslinking would be triggered, the dominating mechanism depends on the type of rubber. Kopal et al. (2018) illustrated the tensile modulus of nitrile rubber blend increased by 40% to 200% with an increasing radiation dose [63]. Shubhra et al. (2010) showed that the tensile modulus of polypropylene/natural rubber

composite increased by 10% to 200% for different radiation doses and composite compositions [64].

2.3.3 Oxidation

Oxidation could trigger chain scission or crosslinking in rubber material. Colin et al. (2007) showed that the tensile modulus of polyisoprene could decrease by more than 50% when aged in air under various temperatures [65]. Gu et al. (2006) showed that the tensile modulus of high damping rubber used in bridge bearing increased by more than 100% when aged in air under 70 °C [66].

There are two important factors that this process depends upon, apart from contacting oxygen: temperature and UV-light intensity [67]. The temperature provides kinetics to the Oxidation process, and UV-light can significantly accelerate the process of producing radicals. Gu et al. (2006) showed that the tensile modulus of tested rubber increased by 50% under UV radiation [66]. The detailed process will be introduced in Chapter 2.4.1.

Ozonation

Ozonation is triggered when the elastomer reacts with ozone in the atmosphere. The ozonation process leads to a well-known phenomenon called ozone cracking, an example on a vehicle tire is shown in Figure 2.22.
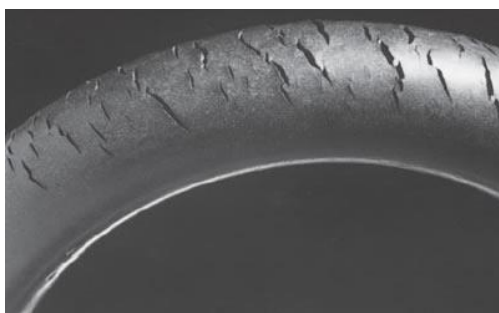
Figure 2.22 – Ozone attack caused cracks on a tyre [68]

2.3.4 Hydrolysis

Some polymers or elastomers could react with water molecules, which normally leads to chain scission to the polymer network, and, therefore, reduces the elastic

modulus. Furukawa et al. (1999) showed more than 15% of elastic modulus reduction on polyesterurethane elastomers with various side groups caused by hydrolysis [69]. Wanamaker et al. (2008) showed a decrease of elastic modulus up to 50% on a thermoplastic elastomer (polylactide-polymenthide-polylactide triblock copolymer) caused by chain scission introduced by hydrolysis [70].

2.3.5 Fillers and additives

Fillers

Fillers are added to modify elastomers' stiffness, abrasion resistance, friction coefficient, chemical resistance, etc. Carbon black is the most recognised filler in the industry due to its great balance between cost and reinforcement performance. There are some other kinds of filler which are used to meet special requirements. Silica fillers provide higher stiffness but lower tensile strength, calcium carbonate is suitable for cheaper and lighter colour applications [71] [72]. Kamal et al. (2009) showed that the storage modulus of natural rubber could be increased by 150% after adding 73% weight calcium carbonated fillers, 200% with 49% weight carbon black filler and 1400% with 54% weight silica fillers [71]. The fillers interact with rubber chains next to them and constrains their movement. More detailed explanations are given in the next chapter.

Vulcanisation additives

For most raw thermoset elastomers described in previous chapters, their mechanical properties are not strong enough to be used. The chains would flow with the deformation and can easily be permanently deformed. Their mechanical properties rely heavily on the surrounding temperature; a hot environment makes them soft and a cold environment makes them brittle. Most applications mentioned previously require the rubber used to be vulcanised beforehand. In the vulcanisation process, curatives are added to the rubber and the rubber is then put into a high temperature and high pressure environment. Those added curatives will act as bridges between polymer chains.

As mentioned previously, the polymer chains are entangled together, and are free to rotate under stress, when they are linked to each other, the movement of polymer chains will be constrained and lead to a higher overall stiffness. This link between polymer chains is referred to as crosslinks, shown in Figure 2.23 where grey atoms are carbon, write atoms are hydrogen and yellow atoms are sulphur. Due to the strong connecting force from covalent bonds, even under an extreme temperature environment, the movement of elastomer chains are well constrained and lead to a good thermal stability [37].
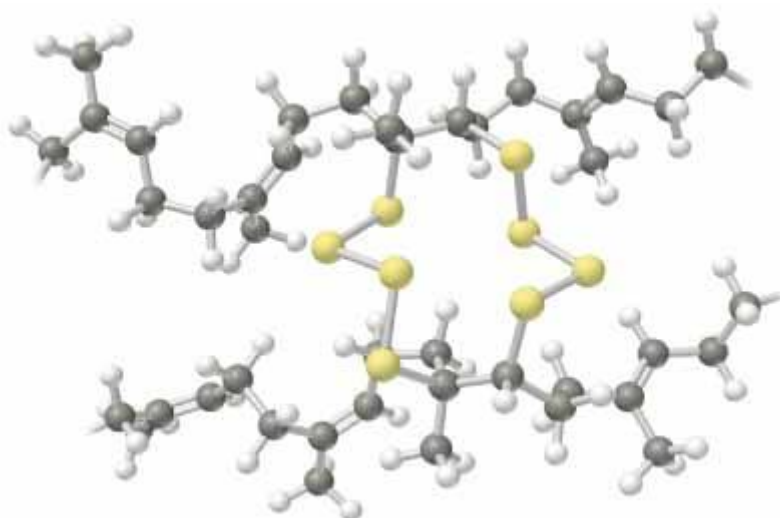
Figure 2.23 Crosslink between polymer chains [73]

The commonly used curatives are polymeric sulphur and peroxides. The selection of curative is based on their solubility in different elastomers. Sometimes accelerators and activators are needed to achieve a designated crosslinking rate and quantity for obtaining the desired property enhancement [74]. Thiazoles, Thiurams and Sulfenamides are all common choices for accelerators in the vulcanisation process, and zinc fatty acid ester, which is formed by fatty acid and zinc oxide inside the material, is a common activator [74]. Figure 2.24 illustrates the chemical structures of the mentioned curatives and accelerators.
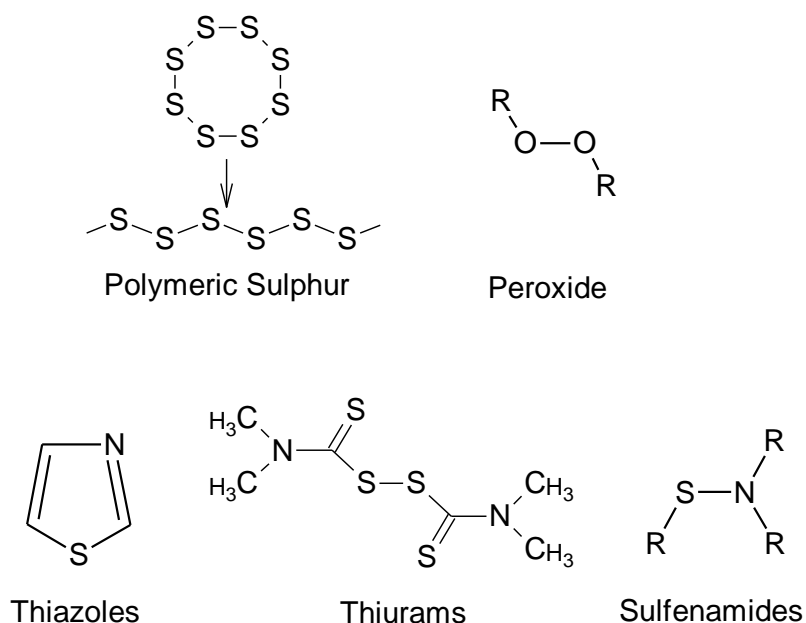
Figure 2.24 Chemical structures for common vulcanisation additives

Kruželák et al. (2016) reviews the difference between sulphur-cured rubbers and peroxide-cured rubbers. Sulphur cured normally has better mechanical properties, such as tear strength, abrasion resistance and fatigue resistance [75]. Their work in 2017 showed that the tensile strength of sulphur-cured natural rubber is 100% higher than peroxide natural rubber [76]. Peroxide cured rubber tends to have better heat-ageing stability and electrical properties. Stelescu et al. (2016) suggests that this difference is caused by the higher bond strength between carbon-carbon crosslinks formed in the peroxide system, making them harder to be separated but more rigid [77].

The amount of vulcanisation agent and additives added in the vulcanisation process affects the formed crosslinks. According to the composition, the curing system can be categorised into conventional vulcanisation (CV), effective vulcanisation (EV) and semi-effective vulcanisation (SEV) systems. Rohana Yahya et al. (2011) found that the tensile strength of CV-cured natural rubber could be 100% higher than EV cured rubber [78]. The composition and pros and cons of those systems are listed in Table 2-3, where phr stands for per hundred rubber.

Curing System	Sulphur	Accelerator	Properties
CV	2-3.5 phr	0.4-1.2phr	Network consists of more than 95% di- and polysulphidic links, which are unstable under heat. However, it provides excellent mechanical properties.
EV	0.4-0.8 phr	2-5 phr	Primarily formed by monosulphidic and disulphidic bonds. Although it provides lower modulus, it means EV cured rubbers have better heat and oxidation resistance. However, EV cured rubbers are usually not suitable for dynamic applications due to their poor fatigue resistance.
SEV	1-2 phr	1-2.5 phr	An intermediate curing method between CV and EV. Usually selected when the application needs both heat and fatigue ageing resistance.

Table 2-3 Differences between curing methods

Protective chemicals

Various chemicals can be added into the elastomer materials to enhance their capabilities of working under different harsh environments. Those chemicals are added to protect the elastomer from reacting with environmental hazards. For example, antioxidants are added to reduce the chemical reaction between the elastomer material and oxygen. Figure 2.25 illustrates the chemical structures of some common protective chemicals.

Hindered Phenols   Phosphites

Hindered Amine Light Stabiliser (HALS)   p-Phenylenediamine
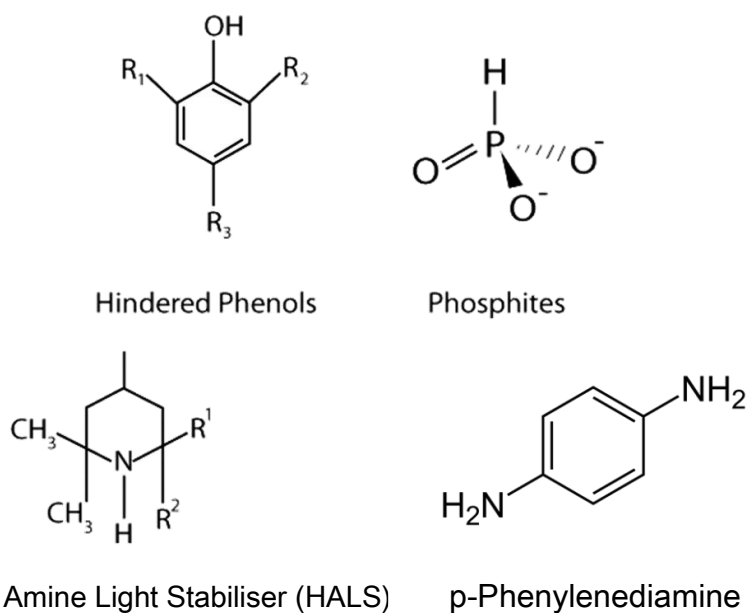
Figure 2.25 Protective chemicals in rubber materials

Although these antioxidants and antiozonants have no direct influence on the mechanical properties of the material, their existence delays the progress of oxidation.

Paraffin wax can be used as a protective additive, too. Instead of interacting with the chemical reactions, it forms a protective layer on the surface of the elastomer. Although paraffin wax's function is to protect the material from the surrounding environment, Abu-Abdeen (2000) showed the Young's modulus of a SBR/NR blend decreased by 150% by increasing the paraffin wax content, from 0% to 40% [79]. There are also other protective additives commercially available that increase the elastomer's heat resistance, radiation resistance, corrosion resistance, ultraviolet resistance, etc.

Functional chemicals

Functional chemicals are added into the elastomer material to adjust its physical properties. Plasticisers are added to increase the softness of an elastomer and enhance the dispersion of fillers. Commonly used plasticisers include mineral oil, ester plasticisers, phthalate-based plasticisers, adipate-based plasticisers, etc. Włoch et al. (2019) showed the tensile modulus of carbon black filled natural rubber decreased by 20% when increasing plasticiser amount from 2% to 8% [80]. The measured crosslink density also changed in some works, however, the

measurement did not consider the weight change caused by extraction of additives during the swelling process [81].

Tackifier resins are added to products that require good tackiness between the elastomer material and its contacting surface like tyres or V-belt. Tackifiers tend to be sticky materials that have a low molecular weight. They disperse in the elastomer product and, therefore, enhance the material's tackiness.

2.3.6 Volume swell

When a rubber component encounters certain liquid, it may swell and lead to an increase in volume which affects the performance of the product [82]. Zielińska et al. (2016) suggested that the swollen specimen could get lower elastic modulus due to breakdown of filler-filler bonds, as well as the presence of a void in the rubber network caused by swelling [83]. Qamar et al. (2010) showed a volume increase of more than 100% for an EPDM-type elastomer swelled in water and oil, the hardness of the specimen kept decreasing in the process from above 70 Shore A to below 40 Shore A [84].

2.3.7 Under dynamic loading

Due to the complexity of rubber's material structure, its elastic modulus also depends on the operating conditions. The most significant dominators are strain rate, temperature and elongation. As described previously, the rubber is a network formed by polymer chains and the chains are entangled all the time. If the deformation is slow, the chains will take their time to transfer smoothly to the next stage. However, if the deformation is relatively fast, the chains will start to show a greater resistance on the deformation. Thus, a fast deformation will lead to a high elastic modulus. The temperature acts in a similar way; under a low temperature the material would behave like glass, as low temperatures increase the energy required for the chains to move around. This temperature is known as the glass-transition temperature. Figure 2.26 shows the dynamic modulus of viscoelastic material under different temperatures and frequencies.
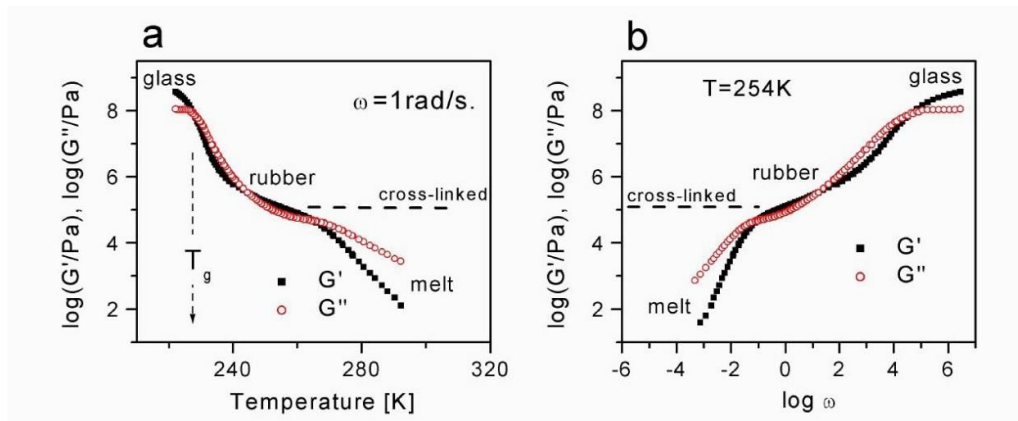
Figure 2.26 – Variation of elastic modulus under different temperatures/frequencies [85]

After the rubber is manufactured, the chains are likely to be at their lowest energy state, however, it is also possible that there exists an even lower energy state but it requires a certain activation energy for the chain to transform into it. Or, some chains could be permanently broken due to a large deformation. Thus, whenever rubber is stretched to a new maximum strain, a reduction on the elastic modulus before this maximum strain is expected. This is the Mullins effect, and it is shown in Figure 2.27. When the material is deformed to a certain strain for the first time, the stress required is represented by curve 1,4 and 7. The reduced stress is represented by curve 3, 6 and 9. In reality, multiple loading cycles are required for this reduction of modulus to become stable. In filled rubber, some permanent loss of connections between polymer chains and fillers would also lead to this effect.
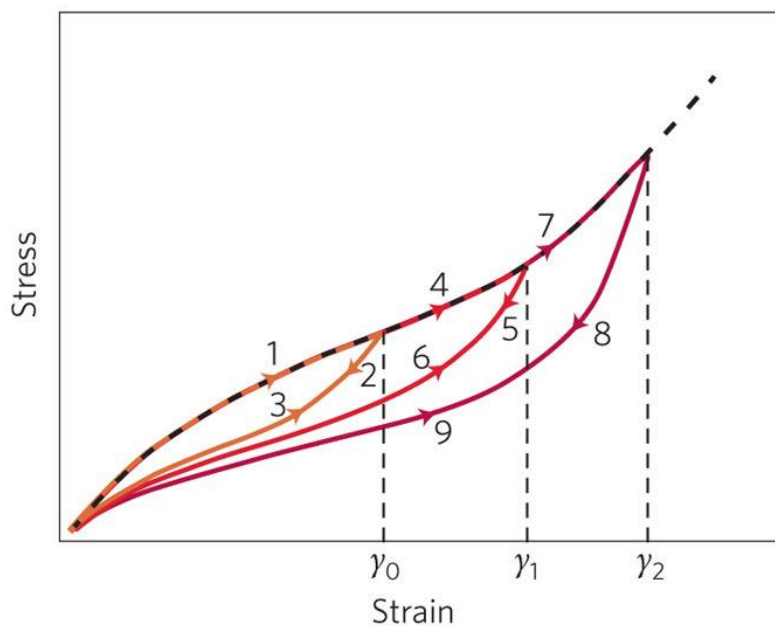
Figure 2.27 – Mullins effect on elastomers [86]

Another well-known strain related phenomenon for filled rubbers is the Payne effect. In a filled rubber, there exists chain-filler interfaces. This connection can be broken under a large strain and lead to a lower elastic modulus. This is the Payne effect and Figure 2.28 illustrates this behaviour. At around 20% strain, most of the chain-filler connections are temporarily broken, the elastic modulus of the material will be close to its original modulus before the reinforcement. However, when the force is removed, most of the broken chains will be reconnected and, hence, this loss of modulus is not permanent [87]. Elastic modulus is usually measured by using dynamic (thermal) mechanical analysis technique. However, depending on the condition of the sample, a hardness test and nano-indentation can be used to obtain properties that can represent elastic modulus of the material.
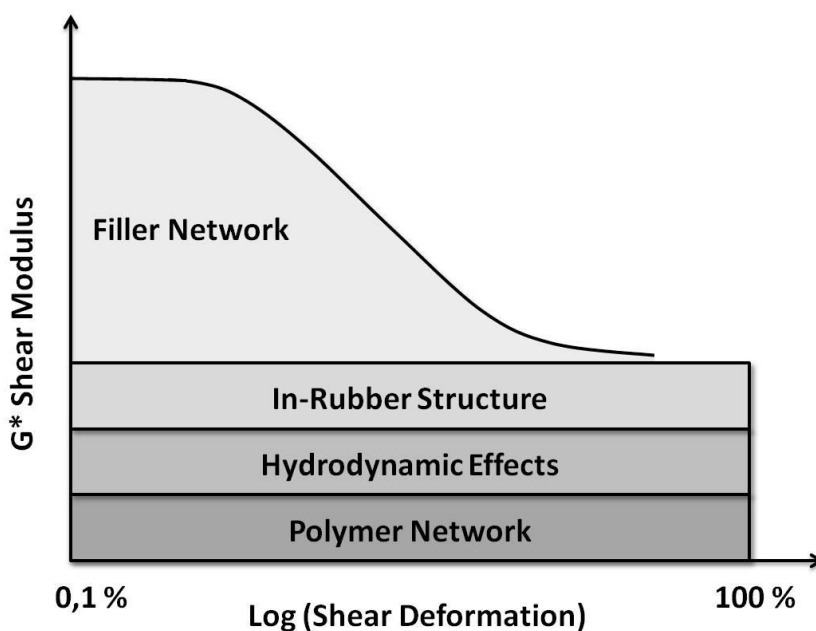
Figure 2.28 – Payne effect on filled elastomers [88]

2.4 Underlying Causes and how to Measure Them

As described in the Chapter 2.3, elastomers are affected by many factors. This chapter briefly explains how they alter the material structures and lead to impact on the elastic modulus of the material.

2.4.1 Crosslink density

Crosslink density represents the number of crosslinked points in a unit volume [89], which is known to be directly related to the modulus of the material. Sperling (1986) indicated that there is a direct connection between the Young's modulus (E) of the elastomer and its crosslink density [90]. This relationship is shown as Equation 2-2.

$$E = vRT$$

v	R	T
Crosslink Density	Gas Constant	Kelvin Temperature

Equation 2-2 Crosslink density and Young's modulus

Fei Zhao et al. (2011) showed this linear relationship for an unfilled natural rubber. Although Young's modulus is representing the elastic modulus of the rubber in quasistatic measurements, it could indicate that the dynamic modulus of the elastomer is directly related to its crosslink density [91].

Both crosslinking and chain scission changes the measured crosslink density [92] [93]. As mentioned in the previous chapter, the curing process for rubber products is the stage when the crosslinks develop. Oxidation, ozonation, radiation and hydrolysis can all effectively impact the measured crosslink density.

Vulcanisation process

The vulcanisation process is one of the most important discoveries in the rubber industry. Its development is closely related to many applications of elastomer materials. Figure 2.29 illustrates this process, although the chemical expression is simple and clear, the process is time consuming and inefficient. The original process takes about six hours under a temperature of 140 °C, on average, the crosslinks consist of more than 40 sulphur atoms.
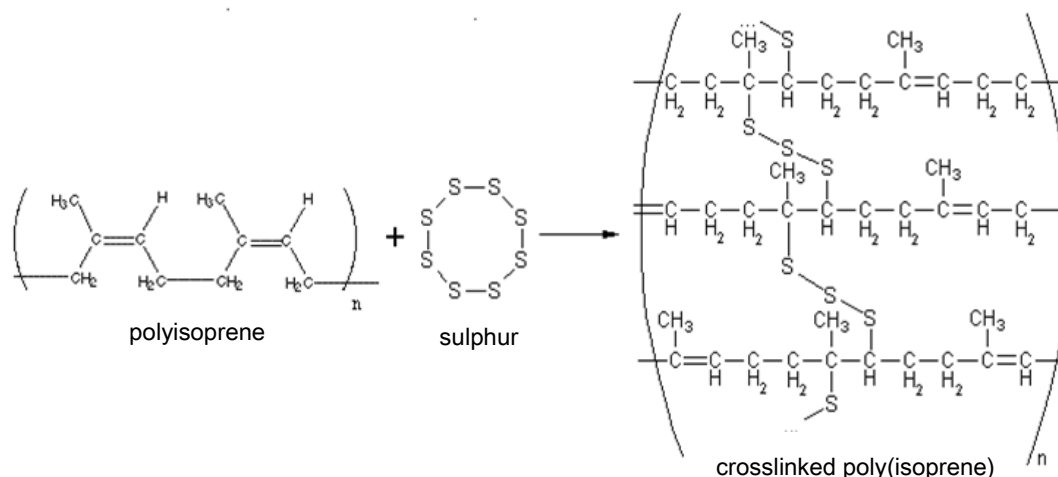
Figure 2.29 Sulphur vulcanisation [94]

After years of research, various additives were discovered to accelerate and increase the efficiency of the process. Vulcanisation agents other than sulphur were also discovered. The mechanisms involved in the vulcanisation process are complex and still not fully understood, except some widely accepted basic steps. Accelerators usually consist of nitrogen and hydrogen atoms, they speed up the vulcanisation process by helping to convert the sulphur molecule into crosslinks. N-oxydiethylene-2-benzothiazole sulphonamide (MBS) is a typical sulphenamide accelerator, its chemical expression is shown in Figure 2.30.
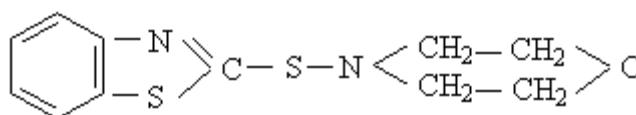
Figure 2.30 MBS chemical expression [94]

Figure 2.31 illustrates how MBS is transferred into active accelerator BtSSBt.
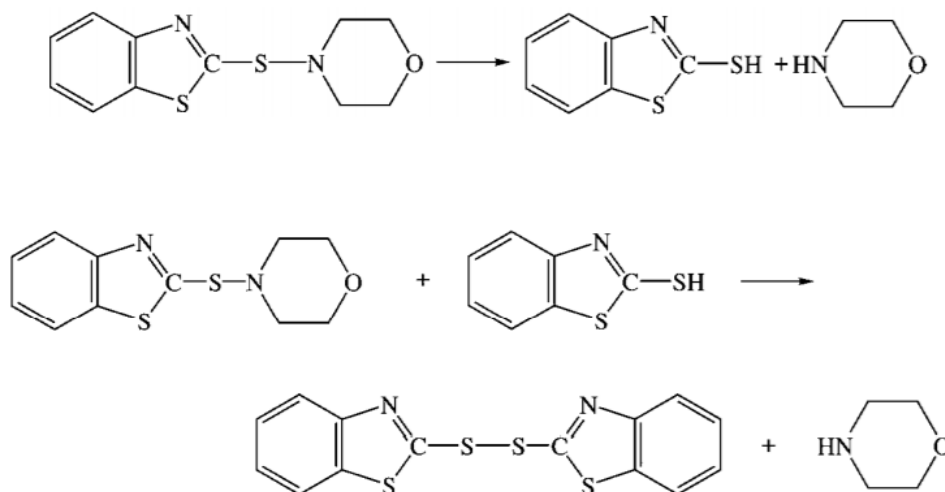
Figure 2.31 MBS transfer to active accelerator [94]

The active accelerator can then transfer into crosslink precursor, as shown in Figure 2.32.
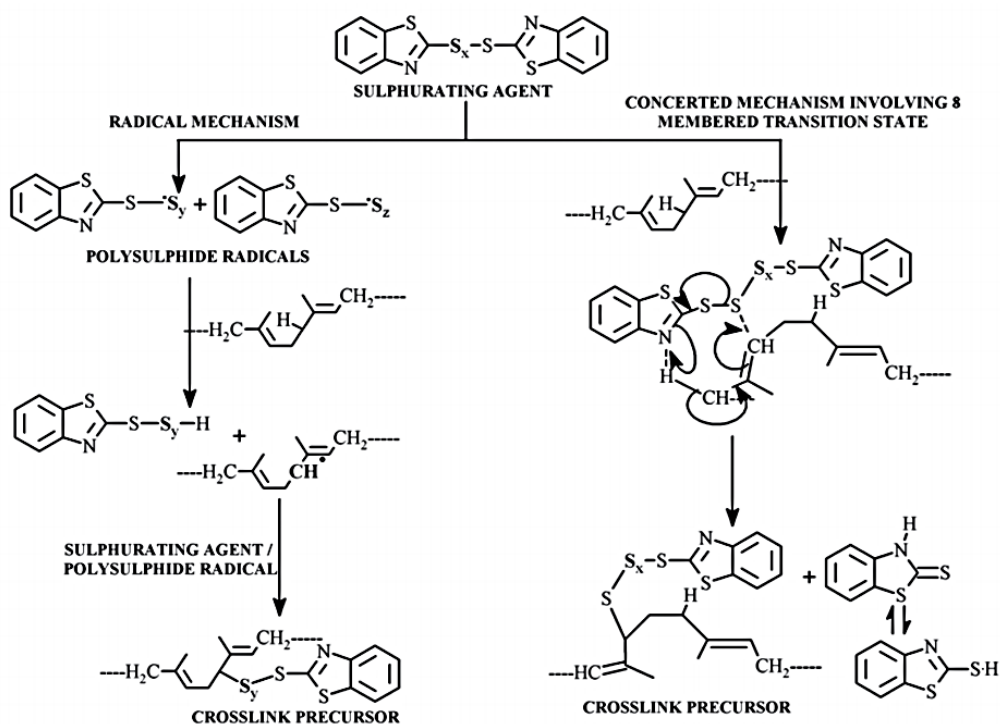
Figure 2.32 Transferring from active accelerator to crosslink precursor [94]

The addition of activator leads to the formation of another active accelerator – BtSZnSBt. It also increases the efficiency of the process by reducing the formation of monosulphidic radicals, a chemical that terminates without forming crosslinks. This behaviour is shown in Figure 2.33.
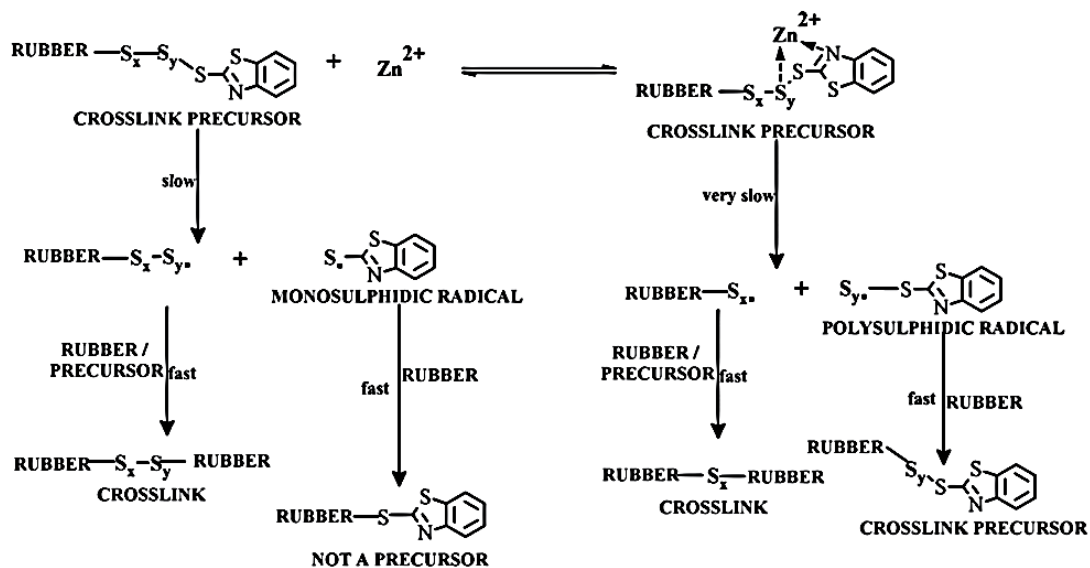
Figure 2.33 Comparison between crosslink precursor with and without the addition of Zn [94]

With the addition of accelerator and activator, the energy barrier in the vulcanisation process is brought down from 210KJ/Mole to less than 125KJ/Mole [95].

The formed crosslinks and side product during the process can be in the states illustrated in Figure 2.34.
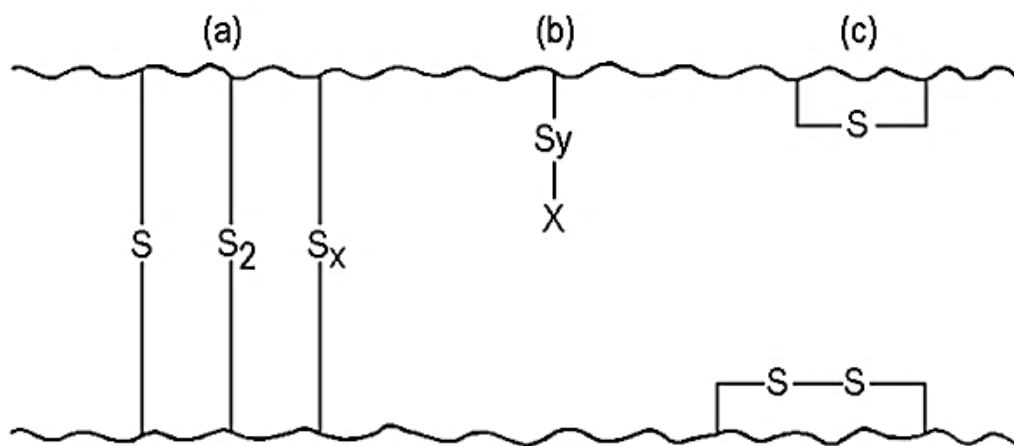
a) monosulphide, disulphide or polysulphide
b) pendent sulphides
c) cyclic monosulphides and disulphides

Figure 2.34 Different types of crosslinks [78]

When using peroxide curatives, the vulcanisation process between peroxide and natural rubber is illustrated in Figure 2.35.
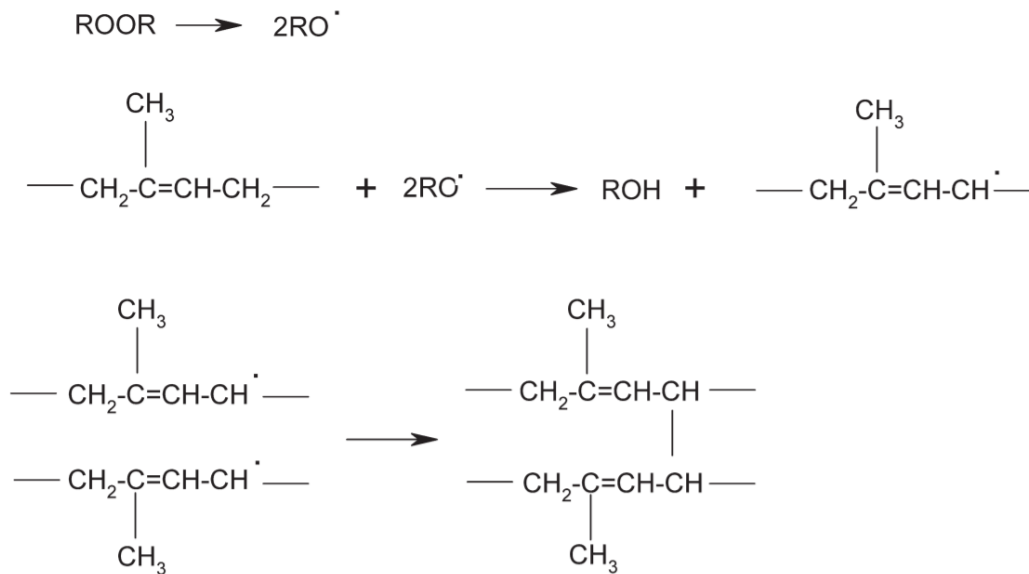
Figure 2.35 Peroxide curing process [75]

Ionising radiation

As mentioned in Chapter 2.3.2, radiation can trigger crosslinking or chain scission. When the natural rubber is exposed under radiation with enough energy (ionisation energy of hydrogen is 14eV [96]), the C-H bond starts to dissociate and produces free radicals, as illustrated in Equation 2-3 [97]. The $NR - H$ represents the C-H bond in the natural rubber and the symbol $(\cdot)$ stands for free radical.

$$NR - H => NR - H \cdot \quad (active\ with\ radiation)$$

$$NR - H \cdot => NR - H^+ + e^- \quad or \quad NR - H => NR \cdot + H \cdot$$

$$NR - H^+ + NR - H => NR \cdot + NR - H_2^+$$

$$NR \cdot + NR - H_2^+ + e^- => NR - NR \quad (crosslinking)$$

$$H \cdot + NR - H => NR \cdot + H_2$$
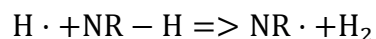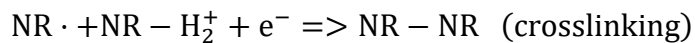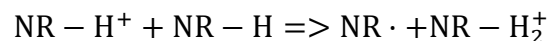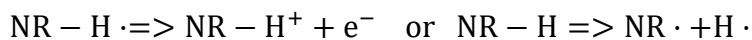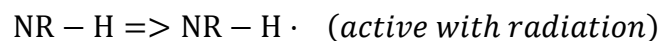
Equation 2-3 Progresses of ionising radiation

The dominating mechanism varies in different materials. The occurrence rate of crosslinking is about 20 times more than chain scission in natural rubber, which means that natural rubber is likely to be crosslinked and become stronger under radiation.

Oxidation

As mentioned in the previous chapter, oxidation can significantly influence the mechanical properties of the rubber material. oxidation is a problem for many materials as oxygen in the atmosphere is extremely reactive. By oxidising the material, its chemical composition will be changed due to the reaction between oxygen and rubber chains. It also triggers chain scission and crosslinking that changes the crosslink density. The general process of oxidation in rubber material is shown in Equation 2-4. Where R stands for rubber, H stands for hydrogen atom and O stands for oxygen [98].

Initiation:

$$RH => R \cdot + H \cdot$$

Propagation:

$$R \cdot + O_2 => ROO \cdot$$

$$ROO' + RH => ROOH + R \cdot$$

Branching:

$$ROOH => RO \cdot + \cdot OH$$

$$RH + \cdot OH => R \cdot + H_2O$$

$$RO \cdot + RH => ROH + R \cdot$$

$$RO' => RO + R \text{ (Chain scission)}$$

Termination:

$$ROO \cdot + ROO \cdot$$

$$ROO \cdot + R \cdot \qquad \text{All triggers crosslinking}$$

$$R \cdot + R \cdot$$
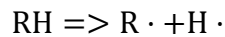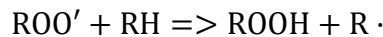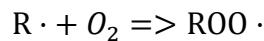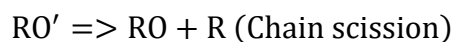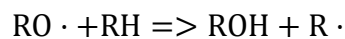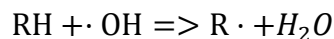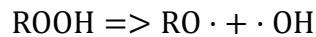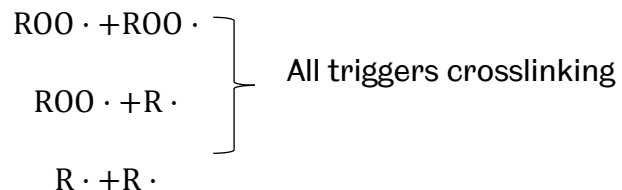
Equation 2-4 Steps of oxidative degradation

There are two important factors that this process depends on, apart from oxygen: temperature and UV-light intensity. A higher temperature increases the reaction

rate of the oxidation process, and UV-light can significantly accelerate the process of producing radicals. This relationship is illustrated in Figure 2.36.

$$\text{Polymer (RH)} \xrightarrow{\text{UV light or heat}} R^\bullet \xrightarrow{\quad O_2 \quad} ROO^\bullet$$

$$R^\bullet \xleftarrow[\;RH\;]{} \qquad \qquad \downarrow RH$$

$$RO^\bullet + OH^\bullet \xleftarrow{\qquad\qquad} \textcircled{R}^\bullet + ROOH$$
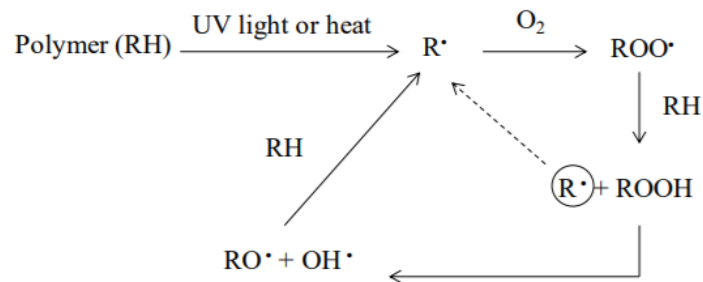
Figure 2.36 Oxidation cycle of polymer [67]

Once the oxidation occurs, both crosslinking and chain scission process are triggered. Crosslinking leads to a stronger connected polymer network, increase the material's modulus and reduce the elongation at break [75], as the entangled polymer chains are restricted from moving freely. Chain scission caused by oxidation can happen on both the existing crosslinks and the backbone chains. When the chain scission occurs at the backbone chains, it leads to a shorter average backbone chain length. The elongation at break of polymer material relies on stretching up the entangled polymer chains, shorter chain length reduces the elongation at break as well as the modulus of the material [99]. The occurring rate for both mechanisms depends on the material. The occurrence of chain scission is at a predominate position for natural rubber [100] and the material tends have lower modulus and elongation at break once oxidised [101].

Bonfils et al. (1999) have suggested the possibility of changing the dominating mechanism (from chain scission to crosslinking) inside natural rubber during ageing, due to the shortage on oxygen diffused into the interior of rubber samples. This is because the recombination of free radicals produced in the initiation and propagation stages in Equation 2-4 become more frequent [102], as the lack of oxygen reduces the formation of $ROO\,\cdot$ and therefore $RO\,\cdot$, which leads to chain scission. Especially, according to R. L. Clough and K. T. Gillen (1991), the rapid oxygen consumption near the surface region during the oxidation process together with antioxidants behave as a barrier, prevent oxygen from diffusing into the interior of the material [103].

Ozonation

Ozone reacts with the double bonds in elastomer materials and causes chain scission to occur, Figure 2.37 illustrates this process. The breakdown of backbone chains could make the material lose its extensibility. It would generate tiny cracks, especially under deformation, which grow with time, leading to the ozone cracking.
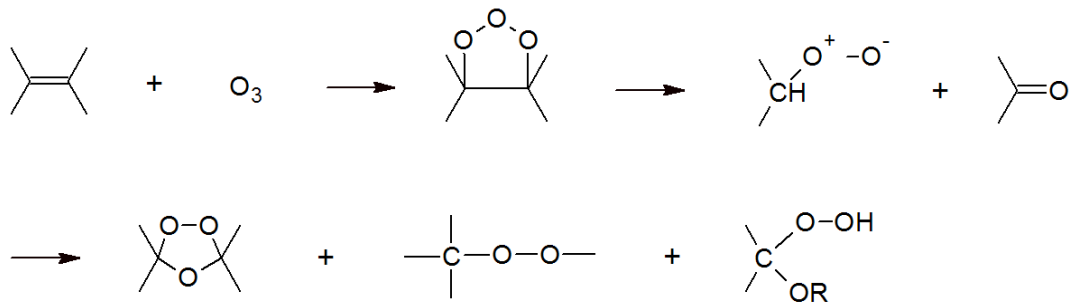
Figure 2.37 - Ozonation of elastomer [104]

Critical depth

These processes rely on oxygen and ozone to take place, and hence, it mainly occurs at the near surface region of the material. The depth of the effect is related to the ageing time and temperature, ranging from millimetres to decimetres depending on the material. Muramatsu et al. (1995) discovered the depth at which the material is relatively unaffected by oxidation is proportional to the exponential of the reciprocal of the ageing temperature [105]. This is called the 'critical depth' of oxidation, Equation 2-5 illustrates this relationship.

$$d = \alpha e^{\frac{\beta}{T}}$$

d	α & β	T
Critical depth	Constant to be determined	Temperature

Equation 2-5 Critical depth of oxidation

The calculation of the constants requires testing the same material aged under different temperatures. Y. Itoh et al. (2009) made a correlation for natural rubber used in bridge bearing, based on properties changes of the material aged under 60, 70 and 80 degrees Celsius at varies depth throughout the sample [33].

Hydrolysis

Another mechanism that can lead to chain scission that damages the elastomer's performance is hydrolysis. For example, when certain elastomers contact water or hydroxyl ion, the process shown in Figure 2.38 would occur.
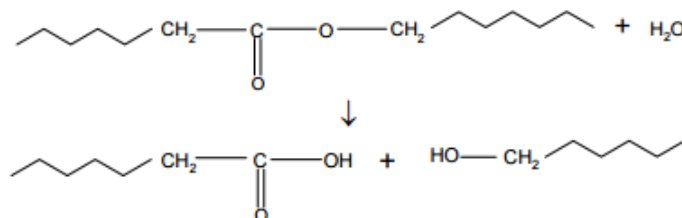
Figure 2.38 – Process for chemical degradation [106]

Measuring techniques for mechanisms that lead to crosslink density changes

The swelling technique is the most common method to measure the crosslink density of an elastomer [107]. Saleesung et al. (2015) and Young Kee Chae et al. (2010) used NMR (nuclear magnetic resonance) to produce comparable crosslink density measurements, which correlates results from the swelling technique well [108] [109].

2.4.2 Chemical composition

Oxidation, ozonation, and hydrolysis lead to chemical reactions and changes on the chemical composition of the material. Methods for measuring these phenomena can, therefore, be Fourier-transform infrared spectroscopy (FTIR) and Raman spectroscopy. With the FTIR technique, Rohana Yahya (2011) found that the intensity of C=O bond increased due to oxidation of natural rubber [110], Ik-Sik Kim et al. (2016) observed intensity increases on the O-H, C-O and C=O double bond [111]. Wu and Zhang (2019) used Raman spectrometry to find indicators of oxidation for silicone rubber [112].

2.4.3 Filler dispersion and distribution

The addition of fillers increases the stiffness of the material because it constrains the movement of polymer chains [72]. The gaps between polymer chains are occupied by those fillers and leave them less space to transform.

Filler particles normally range from 10 to 100 nm in diameter and fuse together to form aggregates in the rubber network. The aggerates then flocculate others via Van der Waals force to form agglomerates. The interaction between elastomer chains and fillers is crucial to the performance of the reinforcement. The interacting rubber chains are called bound rubber, and, according to the way the chains are incorporated with the fillers, they are categorised as rubber shell, occluded rubber and trapped rubber, as shown in Figure 2.39, the reinforcement strength reduces as chains get further away from the fillers. Fei et al. (2012) showed the addition of carbon black filler increased the measured crosslink density of natural rubber by 15% [113].
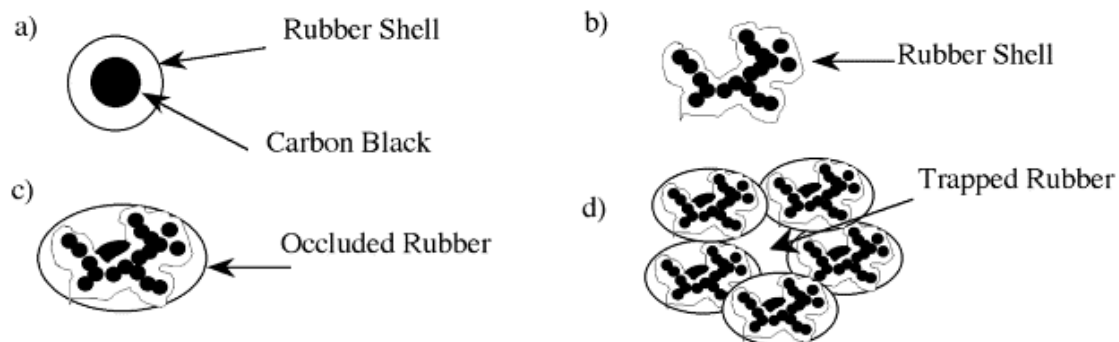
Figure 2.39 Types of bound rubber [114]

The size, composition, dispersion, distribution and morphology of the filler particles, therefore, affect the performance of the product. Filler dispersion represents sizes of formed aggregates and distribution represents space between clusters of fillers, as shown in Figure 2.40.
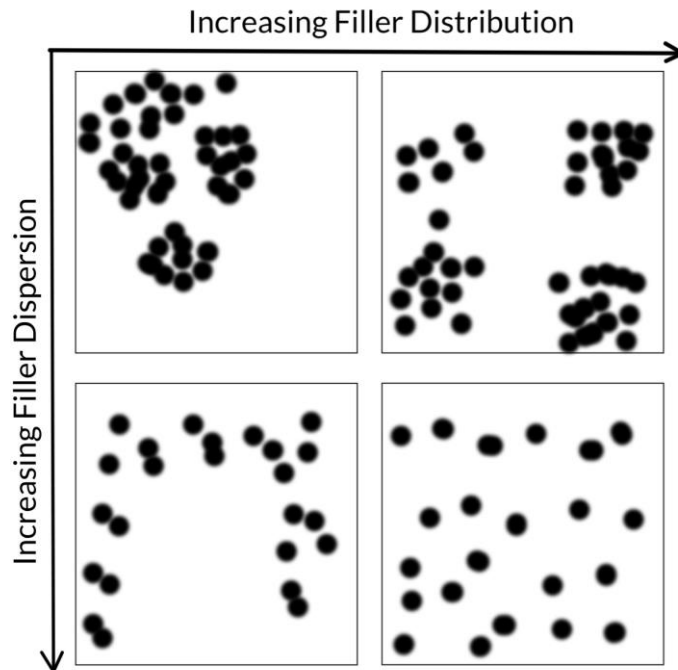
Figure 2.40 Filler dispersion and distribution

Wen Fu et al. (2019) showed that, from 0% to 60% carbon black filler content, the tensile modulus increased by about 20% to 500% and the measured crosslink density varied from about -50% to 130% [115]. Sihwan Kim et al. (2016) showed for the epoxy-carbon nano tube composites, the elastic modulus of a sample with good dispersion can be 5% to 20% higher than the sample with poor dispersion [116].

SEM (scanning electron microscope) has been used to detect the carbon black distribution [117] [118], TEM (transmission electron microscopy) can also be used [119]. Syed K.H. Gulrez et al. (2014) has suggested the electrical conductivity of filled polymer is also related to the filler distribution and dispersion. The poorly distributed but well dispersed filler network can provide the best conductivity as continuous conductive paths can be formed [120]. Gustavo et al. (2003) also suggested that the changes to conductivity can be caused by aggregates movement in the carbon black filled rubber [121].

2.4.4 Additive concentrations

Antioxidants protect the product in several different ways. Sterically hindered phenols react with free radical scavengers and terminate the oxidation process. Phosphites decompose the peroxides that would cause further oxidation [122]. Hindered amine is also a commonly used additive that is usually used to prevent the photo-oxidation process of polymer materials. Some of the diamine additives are often used to cope with ozone that reacts with C=C bond in elastomers. After antioxidants are consumed in the process, the material would become vulnerable to oxidation.

Plasticisers normally have a low molecular weight and fit in between elastomer chains. The increased space between elastomer chains makes the chains require less energy to move around. As mentioned in the previous chapter, the concentration of plasticisers and paraffin wax are related to the material's elastic modulus. The additives were added to modify the rubber's properties, concentration changes of additives often lead to changes of properties.

Both the activated carbon method and TGA (thermogravimetric analysis) can be used to measure the content of volatile additives [123] [124]. Liu et al. (2017) used GC-MS (gas chromatography-mass spectrometry) to identify the concentration changes of additives in nitrile rubber and suggest the possible identity of these additives [125]. Kump et al. (1996) used X-ray fluorescence to examine metal elements in rubber material to deduce relevant additives [126].

2.4.5 Cracks

Cracks can cause changes in mechanical performance, but ozonation causes the cracking. It can significantly reduce the tensile strength of an elastomer [127]. Cracks are damaging to the material's integrity and lead to a different stress distribution [128]. Interfaces created when the crack forms generate extra friction inside the material, stress concentration at the crack tips also changes the stress distribution in the material. The changing of the size and distribution of the cracks is difficult to be observed by the naked eye, but can be measured by SEM [129].

2.4.6 Swelling

When chemicals with a low molecular weight are added into a solvent, if the strength of the chemical's inter molecular interaction is weaker than the molecule-solvent interaction then the chemical will eventually dissolve in the solvent. For polymers, however, the chains are entangled together and, even though the attraction force from the solvent is strong, the polymer cannot be easily dissolved. Because solvent has strong interactions with polymer chains, the polymer will disperse eventually with a much longer time for dissolving. As for those solvents that have a relatively lower interaction force, the solvent is likely to be absorbed by the polymer without further dispersing process. The volume and compliance of the material will increase due to this absorption of solvent and a diagram illustrating this process is shown in Figure 2.41. The degree of swelling can be measured by comparing the weight or volume changes before and after soaking the elastomer in the interested liquid.

Figure 2.41 – Dissolving and swelling process for polymers [130]

2.5 Effect of Time and environment

Some of the factors mentioned in previous chapters are time dependent, and some are related to the operating conditions of the rubber product, which means these factors only impact when continuously exposing the material under certain environmental conditions. These factors, that change over time, are the ageing mechanisms of the material. This chapter summarises these ageing mechanisms and discusses the time of ageing.

2.5.1 The ageing mechanisms

The factors that require chemical reactions to occur are time related, as reactions take time. The factors that could be affected by diffusion of particles would also likely to be related to ageing, as the migration of a solid substance can be significant over a long period of time.

Post-curing and thermal degradation

These two mechanisms are considered together, as for vulcanised rubbers they occur simultaneously. The addition of curatives connects nearby polymer chains during the vulcanisation process to develop crosslinks. The rubber with the curatives will be sent into a heating chamber to accelerate the crosslinking process. However, as Choi (2000) pointed out, the post-curing effect can take place after the manufacturing process caused by the remaining curatives in the system, which leads to an increase of crosslink density and stiffening of the material. The reaction between pendent sulphides groups can also contribute to this stiffening effect [131]. This phenomenon usually occurs in conventional cured rubbers due to the higher usage of curatives in the system and, therefore, is less significant in rubbers made by the effective vulcanisation process [131]. The crosslink density of conventional cured natural rubber increased by 20% after five days under 60 °C and 40% under 100 °C. In the case of thermal degradation, Onyshchenko (2016) pointed out that, under elevated temperatures, the decomposition reaction can lead to loss of crosslinks [78]. Reid Shelton and Winn (1944) showed tensile modulus of Buna-S rubber increased by at least 20% under 80 °C for more than 2 days in nitrogen gas [132].

Ionising radiation

Ionising radiation are waves or particles travelling with energy. The carried energy ionises the molecules when it encounters the material. The total energy received is represented by the absorbed dose, which is related to the strength of the radiation and the exposure time [133]. Both work from Kopal et al. (2018) and Shubhra et al. (2010) showed the increasing impact caused by increasing absorbed dose [63] [64].

Oxidative degradation, ozonation and hydrolysis

All these mechanisms involve reaction with substances in the environment and belong to chemical degradation. The reaction involved requires time to act and the reactive substance also needs time to diffuse into the material.

Kim et al. (2016) showed that under UV-light, the intensity of O-H bonds in the natural rubber samples kept increasing with increasing exposure time. The relative abundance of O-H bonds, which is calculated from FTIR peak, representing the O-H bonds intensity, increased by 10 times after nine days of ageing [111]. Their work in 2019 showed the relative abundance of C=O relevant groups kept increasing for 33 days under an ozone environment.

Celina et. al (1997) showed that on the surface of 2mm thick nitrile rubber, the intensity of C=O bond increased by 12 times after eight days into ageing under 140 °C and seven times after 28 weeks into ageing under 100 °C. The C=O bond intensity in the centre of the sample aged under 140 °C is unchanged, the intensity of C=O bond increased by six times across the entire sample for the one aged under 100 °C [134]. This difference is caused by the critical depth mentioned in the previous chapter.

Furukawa et al. (1999) aged polyesterurethane elastomers under 100 °C water for five days and the elastic modulus of the sample kept decreasing during this process [69].

Filler re-agglomeration

For filled rubber, the filler particles inside can diffuse around during ageing. As mentioned in previous chapters, the size and shape of filler clusters can impact the properties of the elastomer. This process can be accelerated with energy input, Zhang et al. (2014) showed cyclic loading can lead to changes on the filler network, which may be responsible for about 2.5% changing on storage modulus for rubber that has experienced 100k cycles [119]. Garnier et al. (2013) indicated that, after the stress softening caused by the Mullins effect, releasing of occluded rubber can lead to a reduction of elastic modulus for rubber under cyclic loading [28] [119]. Zhang also suggested that the filler particles would gather up again in a more

uniform format, and the reformed aggregates would contain polymer chains that try to penetrate through. Both factors can lead to an increasing of elastic modulus.

Azura and Leow (2019) suggested that the electrical property changes on natural rubber composites after six days of ageing under 100 °C could be caused by the movement of carbon aggregates [135].

Loss of additives

Most additives are physically blended into the elastomer system. Paraffin wax, antioxidant and antiozonant tend to migrate to the near surface region and form protective layers [136]. They migrate in the rubber system and some of them can be consumed during usage. As they degrade over time, certain ageing mechanisms like oxidation could accelerate. Plasticisers also tend to diffuse out from the system and the diffusing rate depends on the molecular weight of the plasticiser [137]. The diffusion processes and reaction rate of the additives can accelerate in a high temperature environment. Liu et al. (2017) illustrated the process of losing additives in nitrile rubber over 40 days of ageing. The additive is lost faster under 150 °C than under 125 °C [125].

Swelling

Kader and Bhowmick (2003) showed the exponentially decaying swelling rate for 20 hours between acrylate rubber/fluororubber blend and various polar solvents under room temperature [138]. Graham et al. (2005) showed the volume increase of nitrile rubber contacting different types of aromatic blend under room temperature for 3 days [139].

2.5.2 Artificial ageing

A tremendous amount of work related to the artificial ageing test of rubber materials has been done. Including the literature mentioned in the previous section. The aims of these tests are to provide a controlled environment for the ageing mechanisms to develop, and to simulate the long ageing process in a relevantly short time. Except monitoring the properties changes of the material

during the ageing period, this method can also be used to predict the lifespan of a product.

Accelerated ageing

The reduction of ageing time is achieved by increasing the speed of ageing, the factors related to the ageing of the material are applied with an increased quantity. Temperature is one of these factors that is known to be directly related to the rate of diffusion and reaction. Some literature introduced in the last section also showed that the ageing mechanisms would be accelerated under higher temperatures [125] [131] [134] [138]. Other common factors include, humidity, radiation, cyclic loading, etc., the term 'load level' will be used to describe the quantity of the ageing factor the material is exposed to. Numbers of investigations has been made to correlate the load level and the ageing speed. Several numerical models have been developed for different factors, Table 2-4 summarizes the common form of some models. The term 'acceleration factor' represents the ratio between the ageing speed of material under real-life and accelerated conditions, the term 'ageing speed' can be representing rate of reaction, rate of degradation, rate of moisture absorption, rate of creep, etc.

R_a	R_r	L_a	L_r	k_1 - k_5
Accelerated ageing speed	Real-life ageing speed	Load level in accelerated condition	Load level in real-life condition	Constants in corresponding models.
Name		Acceleration factor		Practical Cases
Arrhenius Relationship		$$\frac{R_a}{R_r} = e^{\left(\frac{k_1}{L_a} - \frac{k_1}{L_r}\right)}$$		Relationship between reaction rate and temperature for chemical reaction [106].
Eyring Relationship		$$\frac{R_a}{R_r} = \frac{L_r}{L_a} e^{\left(\frac{k_2}{L_a} - \frac{k_2}{L_r}\right)}$$		Relationship between reaction rate and temperature for chemical reaction [140]. Relationship between ageing speed and humidity [141].

Inverse Power Law Relationship	$\dfrac{R_a}{R_r} = (\dfrac{L_r}{L_a})^{k_3}$	Relationship between ageing speed and voltage/pressure applied on a product [142].
Williams–Landel–Ferry Relationship	$\dfrac{R_a}{R_r} = e^{\left(\frac{-k_4(L_a-L_r)}{k_5+(L_a-L_r)}\right)}$	Relationship between creep rate and temperature for viscoelastic material [143] [144].

Table 2-4 Accelerated ageing models

Most ageing mechanisms considered in this project are related to chemical reactions, both the Arrhenius relationship and the Eyring relationship showed capabilities on correlating chemical reaction rate with temperature changes. Investigations have shown these two models are interchangeable under a temperature of 1000 Kelvin [145] [146].

Arrhenius relationship is selected for this research, which was developed by Svante Arrhenius in 1889. Equation 2-6 shows this relationship, illustrating the temperature dependence of the reaction rate.

$$R = Ae^{\frac{-E_A}{RT}}$$

R	A	E_A	R	T
Rate constant	Pre-exponential factor	Activation energy of the reaction	Universal gas constant	Temperature

Equation 2-6 The Arrhenius equation

The Arrhenius equation can be used to estimate the length of accelerated ageing. The relationship between accelerated ageing time and real-world time is shown in Equation 2-7, Q_{10} is set to 2 according to ASTM f1980 [147].

$$AAT = \frac{RT}{Q_{10}^{[(T_{AA}-T_R)/10]}}$$

AAT	RT	Q_{10}	T_{AA}	T_R
Accelerated ageing time	Real time	Reaction rate increase for every 10 Kelvin increase	Accelerated ageing temperature	Real temperature

Equation 2-7 Estimation of accelerated ageing time [147]

Many existing works have utilised high temperature ageing to shorten the test period for investigating the impact of ageing. Besides those that have already been listed, many other studies indicated that the ageing mechanisms evolve faster under a high temperature environment [148] [149]. Davies and Evrard (2007) used the Arrhenius theory to investigate the polyurethane used in marine environments, simulating its ageing behaviour beyond 20 years into service by accelerated aging the specimen in 50 °C water [150]. Gu and Itoh (2016) simulated 96 years of ageing for the surface region of natural rubber bridge bearing serving in Tokyo in lab conditions, keeping the specimen at 70 °C environment for 64 days [151].

Environmental ageing

Lab controlled environmental ageing exposes the specimen to a desired environment under controlled temperature. Davies and Evrard (2007) put the polyurethane specimens in artificial sea water to simulate the marine environment [150].

Shelton and Winn (1944) and Amerongen (1955) investigated the impact of oxidation by comparing anaerobic and aerobic environmental ageing results. In most cases, oxidation on the surface of the material is not avoidable in temperature accelerated ageing tests [132] [152]. For natural rubber, as described previously, the chain scission process is at the predominating position, which makes its impact entangled with post-curing and thermal degradation. Thus, to investigate the sole impact of oxidation, they performed anaerobic temperature ageing on natural rubber and compared with results obtained from aerobic temperature ageing [152].

In order to simulate the static and dynamic deformation experienced by many rubber products, numbers of mechanical ageing tests have been done in previous researches. The nucleation and propagation of crack and carbon network evolution are directly linked with mechanical cyclic loading and creep is linked with static loading [153] [154]. Both the previously mentioned works by Zhang et al. (2014) and Garnier et al. (2013) applied cyclic loading to the specimen to investigate its impact [28] [119].

Garnier et al. (2013), in particular, made a comparison between cyclic loaded ageing tests under high temperature and low temperature environment [28]. The dominating factor is indicated to be the over vulcanisation (post-curing) process according to the test results. The complex behaviour shown in the low temperature test is, therefore, insignificant. However, another work by Garnier et at. (2013) indicated that the cyclic loading is still making significant contributions on the microstructure changes in the material during the ageing process [155].

Drawbacks and limitations

First, exposure to high temperature would never be experienced by the specimen in a real-life situation and could alter its ageing behaviour. Davies and Evrard (2007) have highlighted this concern during accelerated ageing polyurethane in a marine environment. New ageing mechanisms could be triggered at higher temperatures [150].

Second, as shown in Equation 2-6, the Arrhenius equation, the reaction rate is related to the activation energy required by the reaction to occur. This value determines the Q10 in Equation 2-7 which represents the reaction rate increase for every 10 Kelvin increase. A recommended value is 2, which suggests the reaction would occur twice as fast for every 10 Kelvin increase in temperature [127] [147] [156] [157]. However, this rate actually varies for every ageing mechanism listed, meaning that under higher temperatures some mechanisms could be accelerated more than the others. This suggests that the ageing behaviour of accelerated aged samples could be different from the real-life sample, as different ageing mechanisms progress at different rates.

Third, Neuhaus et al. (2017) showed the impact of discontinuous ageing on fatigue life of natural rubber [158], suggesting that the constant accelerated ageing temperature is ignoring the impact of intermittent heating in real life.

It is important to discuss these factors when designing the experiment or analysing the results.

2.6 Material Characterisation Methods

2.6.1 Measuring elastic modulus

<u>Dynamic mechanical analysis/ dynamic mechanical thermal analysis</u>

The aim of DMA is to measure the material's elastic modulus. For a DMA machine, two tests are commonly used for elastomer materials: tension compression test and shear test. By measuring the resisting force while applying strain to the specimen, based on the stressed surface area of the sample, the elastic modulus of the specimen can be calculated. As described in previous chapters, the elastic modulus of elastomers changes under different frequencies and temperatures. DMA provides the capability of measuring the elastic modulus of the sample while performing cyclic loading under different frequencies and strains, DMTA adds the temperature control into the experiment.

For the shear test, according to BS ISO 4664-1:2011 [159], experimental configuration shown in Figure 2.42 is required, and, in order to eliminate the effect of bending moment, samples should be similar in size and placed symmetrically. The test result is the shear modulus of the specimen.
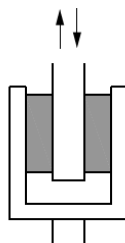
Figure 2.42 – Experimental configuration for shear DMA test, the white block in the middle represents the vibrating wall and the grey blocks represent samples [159]

For the tension compression test, a single sample is placed between two flat plates. One plate for supporting the sample and the other one applies strain as shown in Figure 2.43. The sample is glued onto the holders to ensure its steadiness during the test, the output is the elastic modulus of the sample.
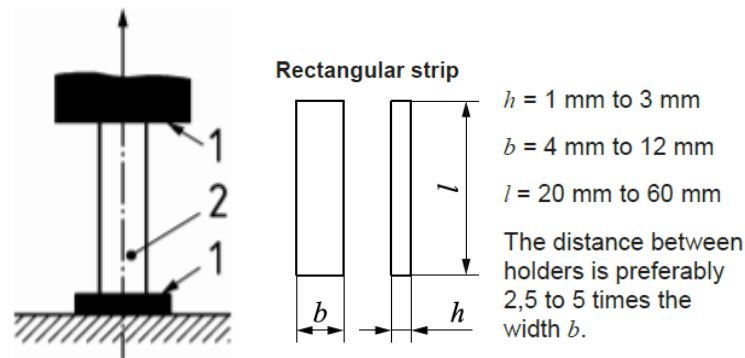
Figure 2.43 – Experimental configuration for tension compression DMA test. 1 are the holders and 2 is the sample [159]

The samples are glued on the holders, therefore the two ends of the sample are constrained on lateral movement, which makes it unable to expand. This would impact the measured elastic modulus, especially under large strain. The significance of this impact is related to the shape factor of the sample, which is calculated by $Shape\ Factor = \frac{bh}{2l(b+h)}$.

According to experiments performed by Acrotech Inc. on urethane elastomer shown in Figure 2.44, the shape factor starts to make a huge impact on the measured modulus when it exceeds 0.25.
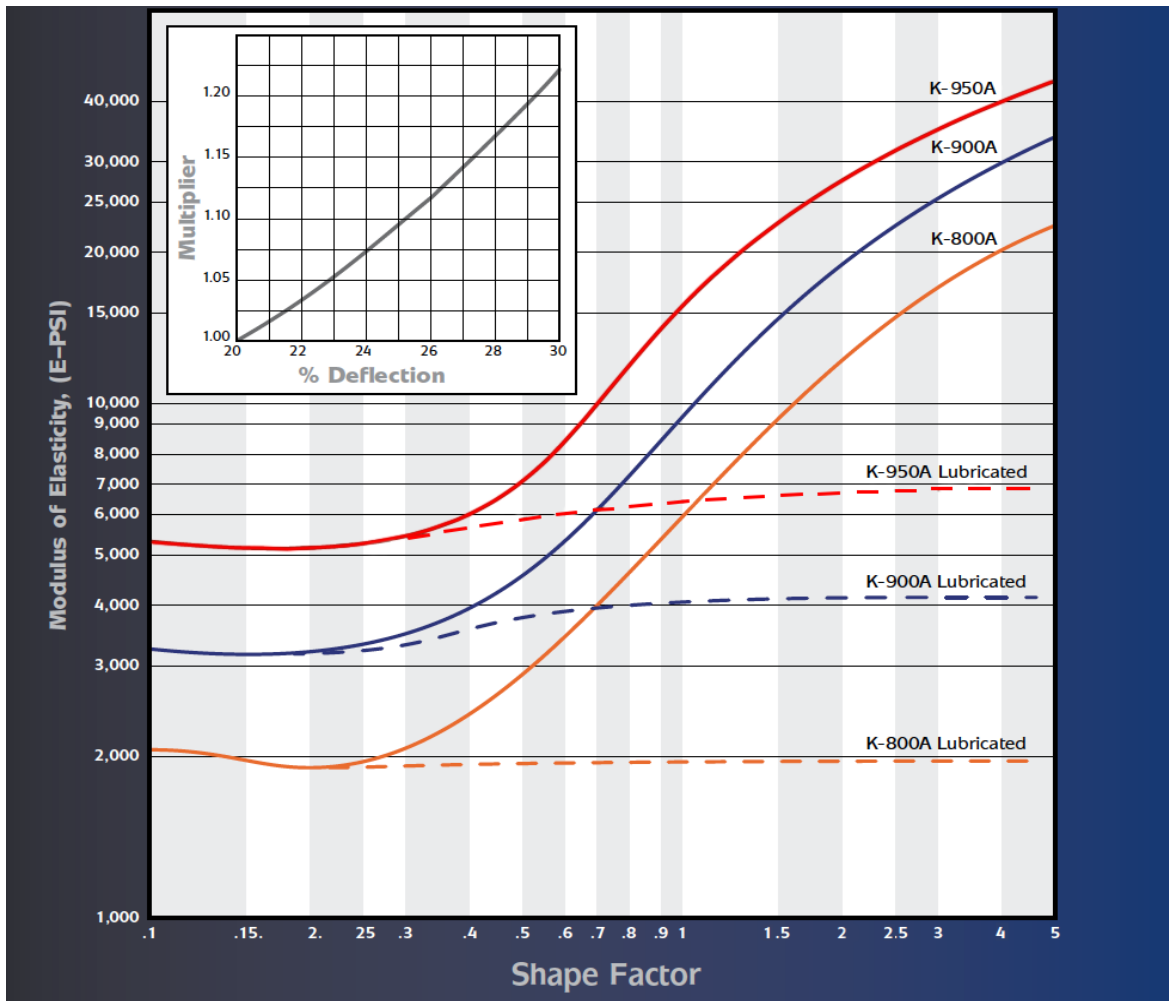
Figure 2.44 – Variation of modulus with shape factor [160]

Hardness test

Hardness is a property that can be correlated to the elastic modulus of rubber. To measure the hardness of a material, a force meter connected to a tip with known geometry (called a durometer) is needed. By recording the force applied and depth of the tip pushed into the specimen surface, the hardness of the specimen can be calculated. The reading needs to be taken after the tip of the durometer is pressed into the material and allowed to rest for 15 seconds. Shore A hardness is known to be directly related to the elastic modulus, Equation 2-8 illustrates this relationship.

$$E = \frac{0.0981 \times (56 + 7.62336 \times S)}{0.137505 \times (254 - 2.54 \times S)}$$

Equation 2-8 Shore A hardness to elastic modulus [161]

Where E represents the elastic modulus of the material and S represents the measured shore A hardness. This correlation stops matching with the experimental result when S is smaller than 40. Another correlated formula recorded in the British standard that gives a better fit is shown in Equation 2-9 where erf represents the error function.

$$S = 100 \times \text{erf}\left(3.186 \times 10^{-4} \times E^{\frac{1}{2}}\right)$$

Equation 2-9 Correlation between shore A hardness and elastic modulus for softer material [162]

Although this technique cannot control frequency and strain, the correlation can provide a rough estimation for elastic modulus that can be compared between samples.

Nano-indentation and DMA

Using this technique, a material's properties can be measured on smaller samples. The principle of nano-indentation is similar to other hardness tests and is applied to very small subjects. This technique records the full hysteresis data, and, therefore, mechanical properties like stiffness can be extract from the results. The process is fully automated, as shown in Figure 2.45 and can be very consistent.
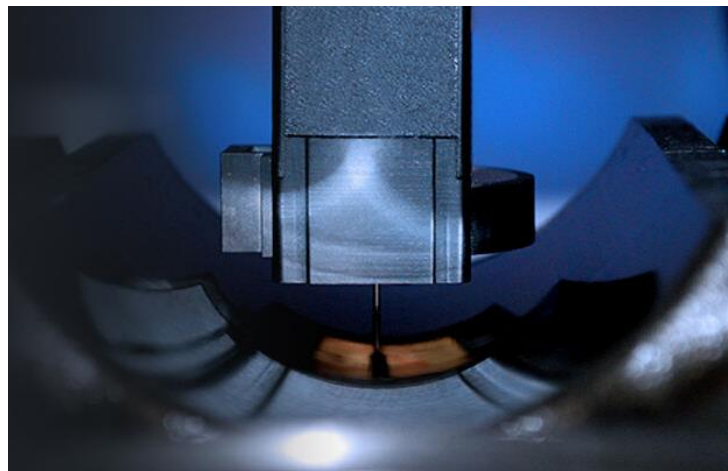
Figure 2.45 – Nano-indenter by Hysitron [163]

Nano-DMTA is Nano-indentation with a controllable operational temperature and frequency range. Li and Herrmann (2014) have presented works for using the nano-DMA technique to test filled natural rubber samples taken from different depths of a tire [164]. The drawback of this technique is that the strain of the test cannot be controlled.

Summary

DMA can be used to measure rubber's elastic modulus for any given strain, temperature and frequency, directly. Nano-DMA can also measure the elastic modulus directly, but the corresponding strain is not defined due to the nonuniform strain distribution around the tip of the indenter. Nano-DMA requires samples with flat and smooth testing surfaces, and the surface roughness of the sample can affect the test results [165]. When considering that samples were taken from used engine mounts with irregular geometry, such samples can be difficult to obtain. Non-uniformity of properties can also be problematic. For hardness test, Shore A hardness can be converted into elastic modulus by Equation 2-8. However, the corresponding strain, frequency, and temperature are all undefined. As this research involves comparing samples with different ageing conditions, and the risk of unknown strain distribution could introduce extra uncertainties, DMA was the most appropriate choice of technique.

2.6.2 Measuring crosslink density

Swelling technique

When a crosslinked polymer is placed in a suitable solvent, instead of being dissolved completely, it will absorb the solvent due to the existence of a crosslink. The absorption stops when the mixing force and connecting force from crosslinks reaches an equilibrium. By measuring the volume change before and after the material is swollen, using Equation 2-10 the crosslink density can be determined.

$$V_x = -\frac{\ln(1 - v_2) + v_2 + \chi_1 v_2^2}{\varphi\left(v_2^{1/3} - v_2/2\right)}$$

V_x	v_2	χ_1	φ
crosslink density	volume fraction of polymer in a fully swelled sample	Flory interaction parameter relates to the interaction between solvent and solute	molar volume of the solvent

Equation 2-10 Relationship between swell and crosslink density

A detailed derivation can be found in [166]. The volume fraction of the polymer in the swelled sample is calculated from its weight before and after the sample is swelled. The sample needs to be dried and weighed again to counter any loss of additives or polymer chains in the swelling process.

Nuclear magnetic resonance

NMR can be used to identify chemical content and structure of the material by studying the spin of nuclei. The spinning nuclei can be imagined as a spinning top, as the nuclei is charged, this spinning produces a magnetic moment. For any nuclei under magnetic field it has two spin states, one has a magnetic moment aligned with the external magnetic field and one against. The nuclei prefer to spin with the external magnetic field which is a lower energy state and the gap between the two spin states depends on the strength of the external magnetic field and the chemical environment it experiences. A picture illustrating this gap is shown in Figure 2.46.
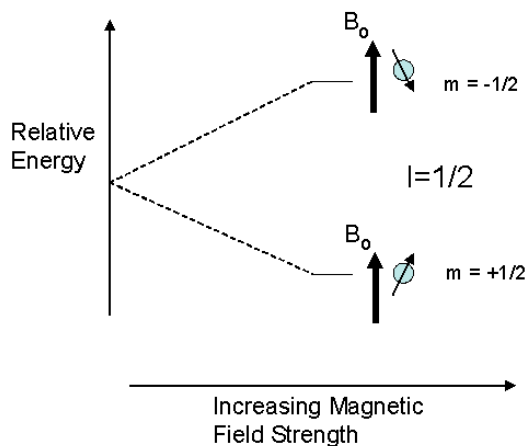
Figure 2.46 – Spin mode for atoms and their energy level [167]

In an NMR machine, the sample is under an external magnetic field and hit by a radio pulse covering different frequencies. For nuclei at the lower energy state, they will flip between the higher and lower spin state after experiencing magnetic waves with their resonant frequencies. As the nuclei flip, they will jump back from a higher to lower energy state, and, during this process, energy is emitted in the form of magnetic waves with frequencies depending on the energy gap between the two spin states of nuclei. Figure 2.47 illustrates this process, and the signal received during the jumping back process can be used to distinguish the amount of

interested nuclei under different chemical environments, which can help to deduce the chemical composition of the sample.
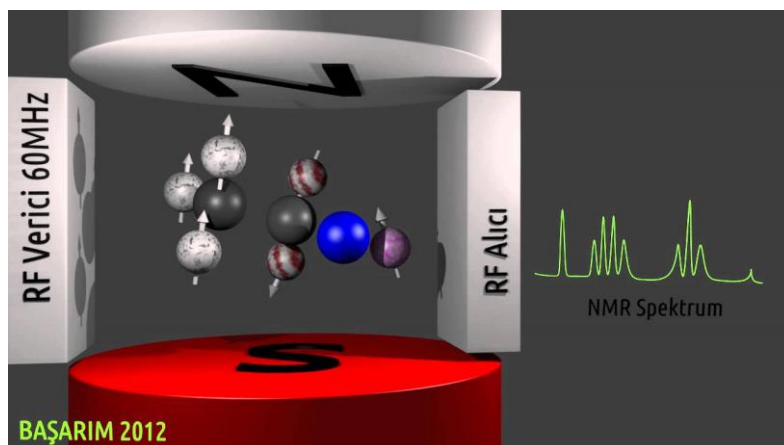
Figure 2.47 – Signal network in the NMR machine [168]

Chae et al. (2010) suggests using 1H NMR to indirectly measure the crosslink density of elastomers [108]. As mentioned previously, the energy difference between spin states depends on the chemical environment around the nuclei. Hence, the frequency of the released magnetic wave implies the nature of this environment. According to Chae, when toluene is absorbed by natural rubber, pi electrons in rubber and toluene will interact when their molecules are very close to each other. The chemical environment experienced by hydrogen inside the interacted toluene is changed and the energy difference between its two spin states is reduced. In Figure 2.48, the darker area near the rubber chain illustrates the area where toluene can interact with rubber.
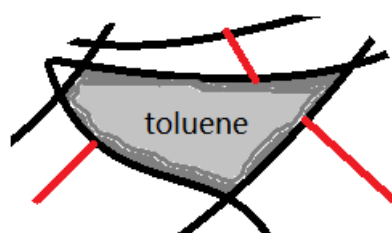
Figure 2.48 Interacting toluene (dark grey) and unaffected toluene (light grey) inside rubber network

Toluene inside the darker area and brighter area exchanges rapidly. The NMR machine can only detect a combined broad signal over a range of frequencies as shown in Figure 2.49. The location of the combined peak is related to the ratio between the amount of toluene inside the two areas. In a network with low

crosslink density, the interacted toluene is outnumbered by the unaffected toluene due to the large space the rubber network can provide. The peak of the resulting wave will be at the high-energy side as shown in Figure 2.49, and vice versa. Therefore, the location of the peak can provide information about the level of crosslink in the material.
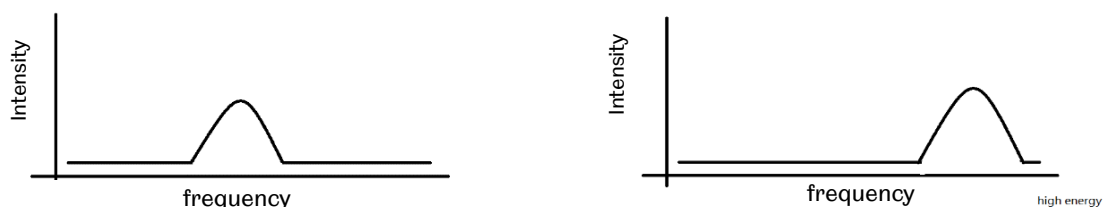
Figure 2.49 (left) Detected signal in NMR, (right) When unaffected toluene is more the sample releases wave with higher energy

There is another method using NMR to measure the crosslink density of vulcanised rubber. Before a normal NMR test, the atoms inside the solution are aligned by the external magnetic field, all giving spin in the same direction. If the atoms are only partially aligned, atoms with different spin directions will interfere with the chemical environment of nearby atoms. The degree of unalignment is measured as the residual dipolar coupling (RDC) [109]. As mentioned previously, energy emitted from atoms with different chemical environments are different. Many atoms with the same chemical environment give a sharp peak, but many atoms with a similar but different chemical environment will bring a broad peak. With a higher crosslink density, mobility of atoms in the rubber network is poorer, and, hence, lead to a higher RDC and broader peak [169]. Therefore, both the width of the peak or the measured RDC can correlate to crosslink density. This method is designed for ^{13}C solid state NMR. However, both methods can only compare samples that have the same composition and are unable to provide quantitative results.

Summary

Although both NMR methods can provide comparable results, the effect of additives to the chemical environment is not clear. Therefore, swelling test was selected, toluene would be used as the solvent as it is commonly used in swelling tests for natural rubber.

2.6.3 Measuring chemical composition

Fourier transformation infrared spectroscopy:

Known as FTIR, a commonly used technique for measuring chemical composition on the surface of the specimen. Chemical bonds in a substance normally stay at their lowest energy state and a fraction of them will be in their excited state according to the temperature. The energy required to reach a higher energy state depends on the elements forming the bond. Those chemical bonds have many vibration modes, examples of vibration mode of chemical bonds are shown in Figure 2.50.

symmetric stretching   asymmetric stretching

scissoring   rocking
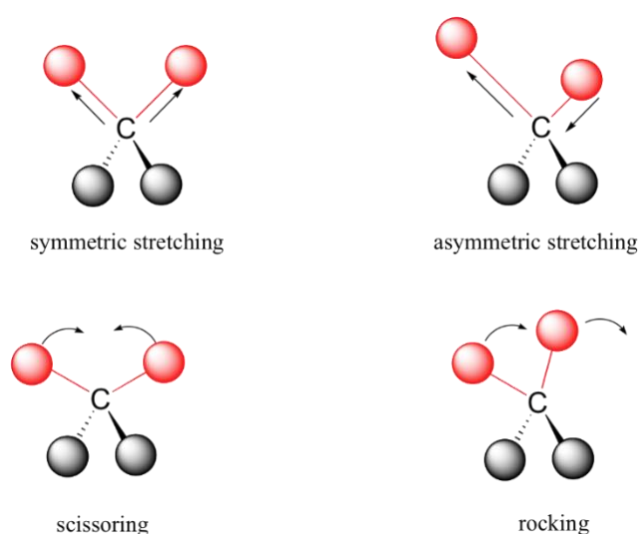
Figure 2.50 Modes of bond vibration [170]

By emitting infrared light toward the sample, the part of the infrared light that is at the resonant frequency of those vibration modes would be absorbed. That is saying that the photon carries energy identical to the energy difference between the ground state and the excited state of the molecule which is absorbed by the molecule. As $E = hv$, where E is the energy of the photon, h is the plank's constant and v is the frequency. By monitoring the absorbed frequencies, existence of certain chemical bonds or elements can be defined [171]. However, not all bond vibrations absorb infrared light. Only vibration modes that change the dipole moment of the molecule would be excited by infrared light, which are the vibrations that change the distance between charged particles in the molecule. Figure 2.51 shows vibration modes of a carbon dioxide molecule, the symmetric stretching mode (v1) does not change the molecule's dipole moment as the change

in distance between charged particles in each bond are equal and in the opposite direction. Therefore, this mode cannot absorb energy from infrared.
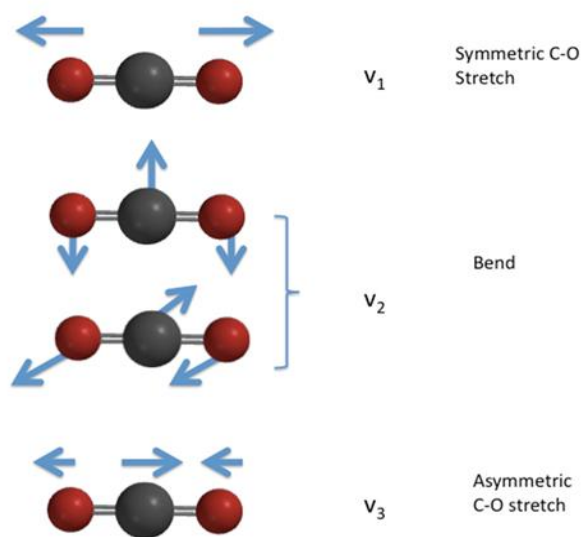
Figure 2.51 Vibrational modes and dipole moment [172]

The attenuated total reflectance (ATR) technique is often used to take measurements. An infrared beam is emitted to a crystal at a certain angle that triggers the total reflection inside the crystal. The sample is then pressed against this crystal, the infrared beam creates evanescent waves at the reflecting points which penetrate the sample for a certain depth [173]. The corresponding frequencies in the evanescent wave would be absorbed by the sample before it returns to the crystal. Figure 2.24 illustrates this idea, the penetration depth is normally a few micrometres, and it depends on the reflective index of the crystal, incident angle of the beam and the wavelength of the beam. ATR-FTIR requires minimal sample preparation to obtain consistent results, the only requirement is that the sample must make intimate contact with the crystal. The shallow sampling depth makes it capable of measuring materials with strong infrared absorbance like carbon filled rubber.
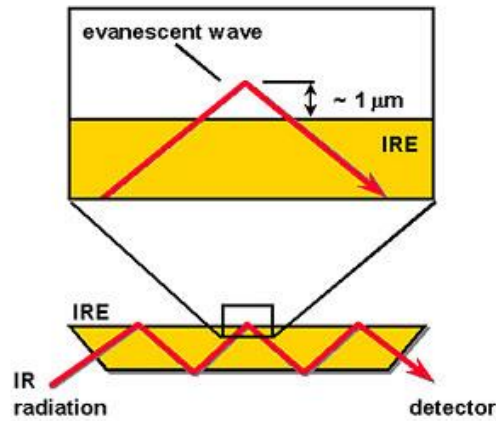
Figure 2.52 Attenuated total reflectance [174]

Raman spectroscopy

Raman spectroscopy is based on detecting Raman scattering from the Raman effect. When photons with frequencies different from the resonant frequencies of the molecule hit it, it can still be absorbed by the molecule due to the uncertainty principle. The absorbed photon pushes the molecule into a higher virtual energy state for an instant and then the molecule will return to its ground energy state. It emits the energy in the form of a photon with energy the same as the one it absorbed with a random direction, as shown in Figure 2.53. This phenomenon is called Rayleigh scattering.
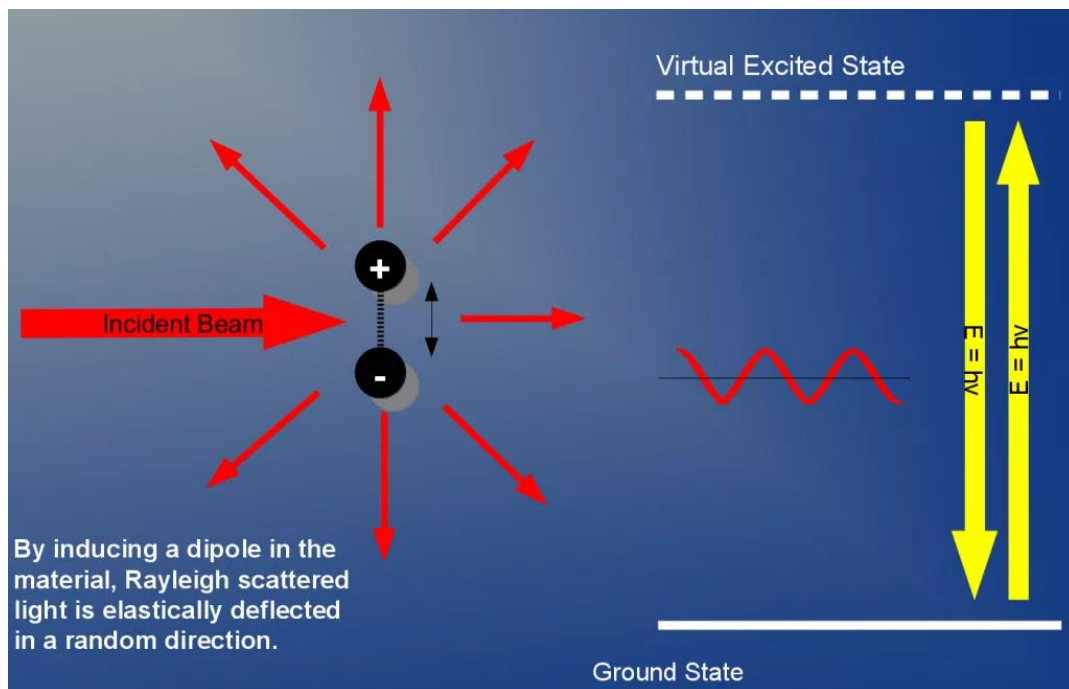
Figure 2.53 Rayleigh scattering [175]

70

However, there is a chance that the molecule will not return to its ground state and return to a vibrational energy state, which means that the emitted photon carries less energy than the absorbed photon. The energy difference between the incident photon and the scattered photon reflects the frequency of the specific vibrational mode the molecule returns to. This incomplete scattering is the Raman effect. However, this only happens when there is a change in the polarisability of the molecule during the vibration [176]. Polarisability is reflected by the stability of electrons forming the bond and it is related to the distances between atoms in the molecule. The electrons form chemical bonds between atoms due to the attractions from nuclei, the distance between the electrons and the nuclei decides how stable the electrons are. Therefore, for Raman effect to take place, the distance between the electron in one atom and the nucleus from the other atom need to change at the vibration peaks. For the vibration modes of carbon dioxide, shown in Figure 2.51, the symmetric stretching mode is the only one that changes the polarisability of a molecule and triggers Raman effect. The Raman scattering can be detected and, due to the uniqueness of the bond vibration frequencies, elements and bonds in the molecule can be defined.

Summary

Chemical reactions generate new chemical bonds in the specimen. By FTIR or Raman spectrometer, intensity of these bonds and, therefore, the severity of the chemical reaction in the sample can be determined. FTIR is selected for this research due to its larger user base and accessibility, most of the literature mentioned previously used FTIR to be the examining method for oxidation in rubber.

2.6.4 Measuring changes in filler dispersion and distribution
Scanning electron microscope

SEM is a technique for obtaining micrometre scale photographs of the specimen by emitting electrons to the sample surface and monitoring the reflected electrons [177]. The sample can be very small, but a good surface condition is needed to

obtain images with good quality, especially when detecting the secondary electrons. Secondary electron is the electron from the specimen that interacts with the electron beam emitted by SEM and becomes a product of ionisation. When the electron beam is emitted to an edge on the sample surface, the depth of the escape route for the secondary electron becomes shorter and more secondary electrons can be collected by SEM. This is called the edge effect and is shown in Figure 2.54.
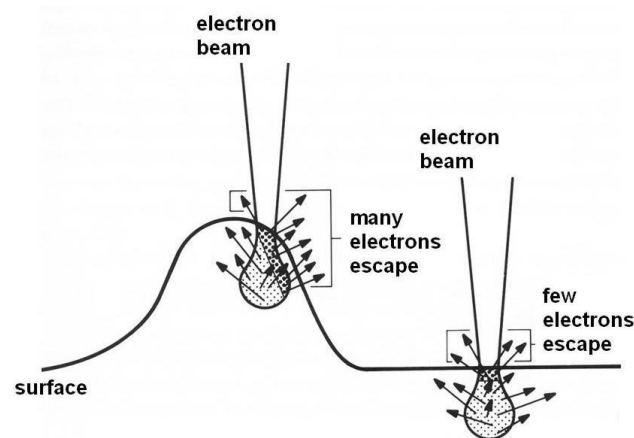
Figure 2.54 Edge effect of SEM [178]

To detect specimens that consist of materials with different atomic numbers, back scattered electrons can be collected exclusively using a specific detector. Back scattered electrons are one type of reflected electrons which bounce back to their emitting direction after colliding with the specimen atoms. Which means the dense part can reflect more electrons due to its higher atom density [179]. This technique can be used to distinguish the carbon black fillers in the rubber.

Transmission electron microscope

Instead of collecting scattered electrons, TEM collects the electrons transmitted through the specimen [180]. This makes the size, especially the thickness, of the specimen crucial to the test. The result is a 2D image that cumulates all the information through the thickness of the sample. Therefore, by capturing a TEM image of the same specimen at different angles, a 3D structure can be constructed.

Figure 2.55 shows the 3D structure of a piece of silica-filled natural rubber. The radius and amount of filler clusters can be obtained.
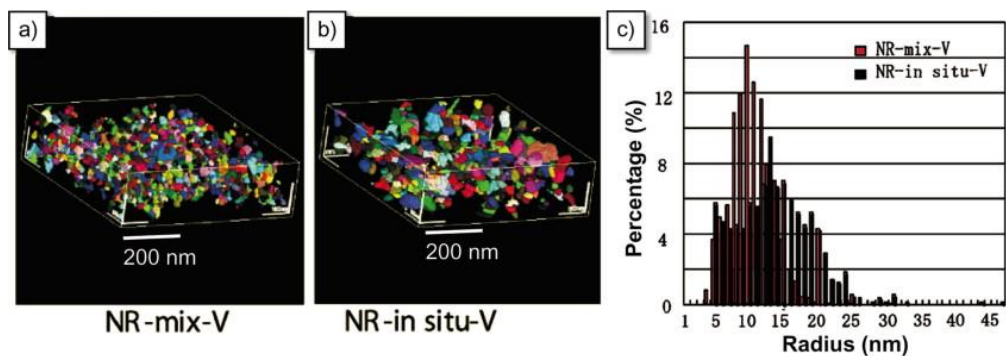
Figure 2.55 -- 3D TEM image of silica filler natural rubber [181]

Summary

Although TEM has the potential to give a 3D illustration of the carbon network, its measured size is small compared to SEM. When considering the possible non-uniform distribution of the carbon particle and more achievable sample requirements, SEM is the most appropriate for this test. It was also selected for measuring cracks, as suggested in Chapter 2.4.5.

2.6.5 Measuring additives in rubber

Activated carbon

Activated carbon technique is a standard method for measuring the volatility of plasticisers in a polymer. The specimen should be prepared in disk form and placed at the bottom of a metal container with lid [123]. The disk specimen should be covered with activated carbon and put into an oven at 70 °C for 24 hours. Plasticisers will partially migrate and react with the activated carbon according to their volatility, leading to a weight change to the specimen. This technique can be used to compare the amount of additive in a sample and their volatility.

Thermogravimetric analysis

Substances in a composite material have different vaporising points and flashing points. Thermogravimetric analysis offers continuous weight measurement while the temperature increases. By recording the weight changes of the specimen, weight fraction of major ingredients in the specimen can be defined. In the case of rubber, there are three major weight loses. They represent the loss of volatile

additives, pyrosis of the rubber network and combustion of the resulted/filled carbon black. Hence this technique can be used to measure the weight fraction of known constituents of the specimen.

Chromatography

Chromatography is a technique capable of separating different substance in a mixture. Chromatography pushes the mixture through a structure containing a substance that can interact with constituents in the mixture and cause them to travel at different speeds. The pushing is done by a liquid solvent or gas, which is the mobile phase. The substance affecting the constituents' travelling speed is called stationary phase. The difference on the mobile phase categorises chromatography into gas chromatography and liquid chromatography [182].

In gas chromatography, the specimen is normally heated up to volatilise its constituents. The vaporised substance is then pushed into the structure containing stationary phase material. This structure is normally a long coil tube with stationary phase material on the wall. When the mixture gas travels through, gas from different constituents meets the stationary material and would condense or dissolve for different time periods. The time for the substance to travel through the whole coil is called the retention time. Although rubber network and carbon black would not vaporise, this method can be used to separate additives in the system. The test requires the mixture to condense and vaporise multiple times in the process so that the chemicals can be well separated. This makes the selection of testing temperature important.

Liquid chromatography is a well-established technique for measuring the molecular weight distribution of a polymer. In order to use this technique, the polymer needs to be fully dissolved which means all individual chains in the solution have no interactions with others. The solution is injected to a column filled with porous particles with appropriate hole sizes for the subject polymer. Shorter chains with smaller molecular length would travel through much more holes than the longer chains as the longer chains are more difficult to fit into small holes. Thus, the time the chain takes to travel through the container is related to its

molecular weight. The left hand side of Figure 2.56 is an example of the pores and on the right, the picture illustrates the process.
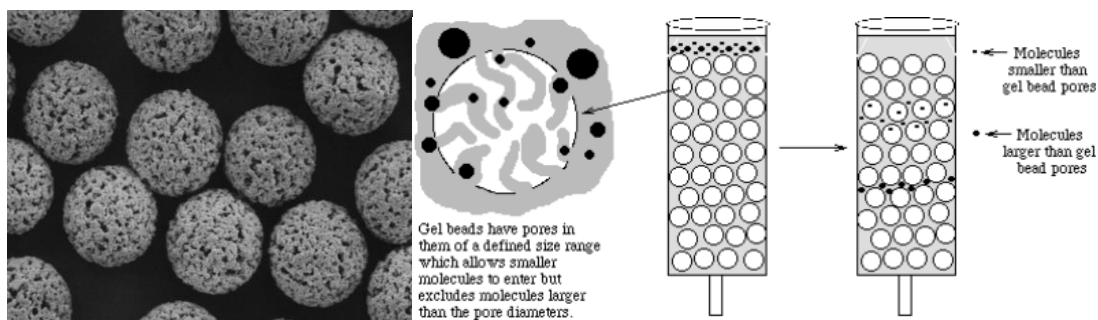
Figure 2.56 – Porous particles (left) [183] and GPC process (right) [184]

Chemicals need to be dissolved in a suitable solvent, which carries the chemicals through the stationary phase. The selected solvent must not affect the interested chemicals.

Mass-spectrometry

This is a technique that measures the mass-to-charge ratio of ions. Together with chromatography, it can give suggestions on the structure and amount of atoms in the additives in the sample. It breaks molecules into charged fragments with different masses by ionisation process. Fragments with different mass to charge ratio are separated by a magnetic field that tries to redirect the movement of the charged fragments, this process is shown in Figure 2.57.
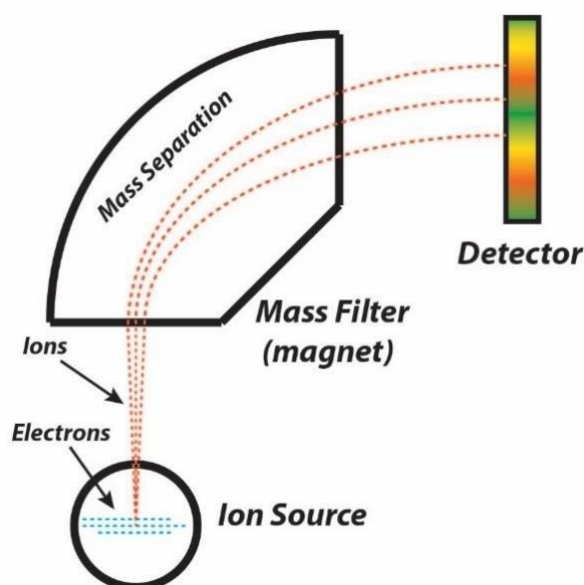
Figure 2.57 Mass spectrometry distinguishes fragments [185]

When the chromatography technique sends out chemicals separately, the mass-spectrometry machine will detect the mass-to-charge ratio of charged fragments of each detected chemical. The resulting mass spectrum of the detected chemical is then compared with the database which can suggest possible chemical structures for the detected chemicals.

X-ray fluorescence

X-ray fluorescence is a technique highly sensitive to a single element. It uses high energy particles to knock off electrons on the K-orbit of an element, causing electrons from higher energy orbit to fall on the K-orbit and releases energy in the X-ray region as shown in Figure 2.58. As the energy gap between orbits is unique for each element, the element can be defined by collecting the fluorescent energy. As the technique requires an electron filling process in the atom, most commercial products can only detect elements heavier than sodium. This makes this technique useful to detect additives containing metal elements in elastomers. However, it can only measure the intensity of metal elements in the specimen, further deduction and tests are required to conclude more detailed information about the additives [186].
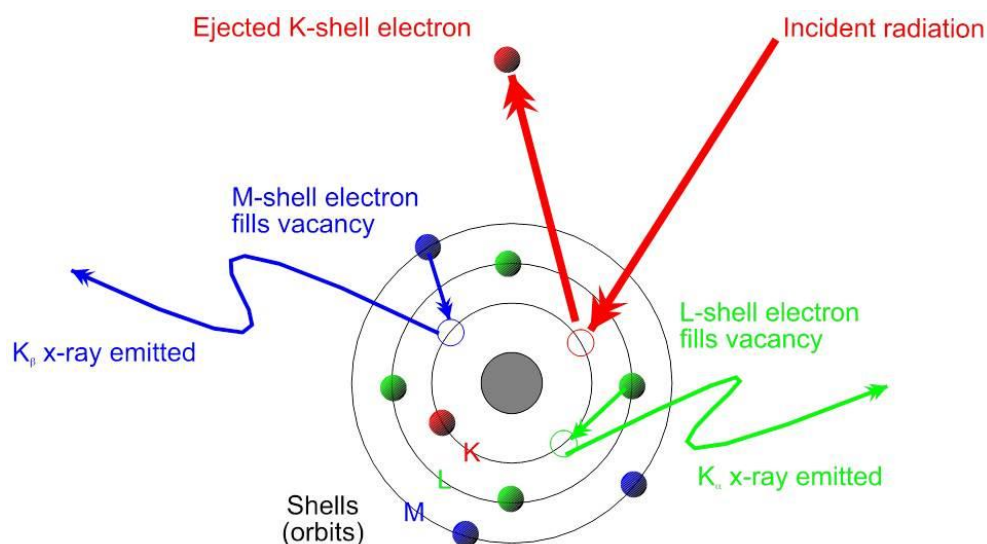
Figure 2.58 - Principle of XRF [187]

Summary

Both the TGA and activated carbon methods can be used to determine the volatility of the additive and are potentially useful to determine the total amount of

remaining additives. TGA is especially useful for determining the content of carbon black filler in the rubber. However, carbon black particles form large aggregates that are trapped in the network have no known degradation process like other polymeric additives, therefore, loss of carbon black is not considered. Although X-ray fluorescence can give the intensity of atoms with an atom number larger than 14, how they form into a molecule cannot be determined. The common additives listed in Chapter 2.3.5 also consist of atoms with a smaller atom number, which cannot be detected by this method. Gas chromatography coupled with mass spectrometry is, therefore, selected due to its ability to determine the chemical structure of the detected chemicals.

2.6.6 Summary of ageing mechanisms and test methods

Table 2-5 summarised the ageing mechanisms and their corresponding effects on microstructure. How each mechanism can be measured and their relativity to this research is also listed.

Factor causing property change	Underlying cause	Selected measuring techniques	Triggering ageing condition	Relativity to this research
Crosslink density changes by crosslinking or chain scission	Post-curing and thermal degradation	Swelling technique	Time and temperature	**Yes**, the material is vulcanised and operates under high temperature environment
	Ionising radiation		Radiation	**No**, no known radiative source
	Oxidative degradation	FTIR for chemical composition changes	Contact with oxygen	**Yes**, the material is exposed to air
	Hydrolysis		React with water	**No**, natural rubber does not react with water

Changes on Filler distribution	Carbon re-agglomeration	SEM	Temperature and cyclic loading	**Yes**, the material is filled with carbon black and experienced cyclic loading
Changes on additives' concentrations	Loss of additives	GC-MS	Time and temperature or oxygen	**Yes**, the material has additives
Crack	Crack propagation	SEM	Cyclic loading, ozonation	**Yes**, the material is exposed to ozone and experienced cyclic loading
Swelling	Swelling	Weight scale	Encounter weak resisted chemical	**No**, the interaction between natural rubber and propylene glycol (the chamber fluid) is neglectable [188] [189].

Table 2-5 Ageing mechanisms with their corresponding microstructure changes, required ageing conditions and measuring technique

CHAPTER 3.   RESEARCH PLAN

This research aims to identify and understand the ageing behaviour of carbon filled vulcanised natural rubber used in an engine mount. In order to achieve this, the following steps have been defined.

		Milestones
Existing engine mount	Step 1	Investigate elastic modulus changes of rubber from existing used engine mounts.
	Step 2	Investigate the cause of any change in stiffness, with respect to the potential ageing mechanisms identified in Chapter 2.
Controlled ageing	Step 3	Investigate causes identified in step 2 in a more controlled ageing environment by applying artificial ageing tests on new samples.
Overall comparison	Step 4	Combine the results from steps 1, 2 and 3 to provide an in-depth explanation of the ageing mechanisms involved and the ageing behaviour of the rubber used in the engine mount.

Table 3-1 Project milestones

The flow chart shown in the introduction also progressed to the one shown in Figure 3.1, indicating the planned experimental work and aim of each step.

Aim: Establish relationships between the mechanical properties' changes and microstructure changes of rubber material during ageing.

Investigation of retrieved mount samples

DMA on Retrieved Mount Samples

Crack Observation In SEM

GC-MS on retrieved mount samples

FTIR on retrieved mount samples

Crosslink Density test on retrieved samples

SEM on retrieved mount samples

Crosslink Density test at different locations

To obtain repeatable data with controllable ageing conditions. Learn the full ageing behaviour of the material.

Aerobic Artificial Ageing for mount and sheet

DMA on aerobic aged mount and sheet samples

Crosslink Density test on aerobic aged mount and sheet samples

GC-MS on aerobic aged sheet samples

SEM on aerobic aged sheet samples

To separate the impact of oxidation from other ageing mechanisms. Deduce impact of each ageing mechanism

Anaerobic Artificial Ageing for sheet samples

DMA on aerobic aged sheet samples

Crosslink Density test on aerobic aged sheet samples

GC-MS on aerobic aged sheet samples
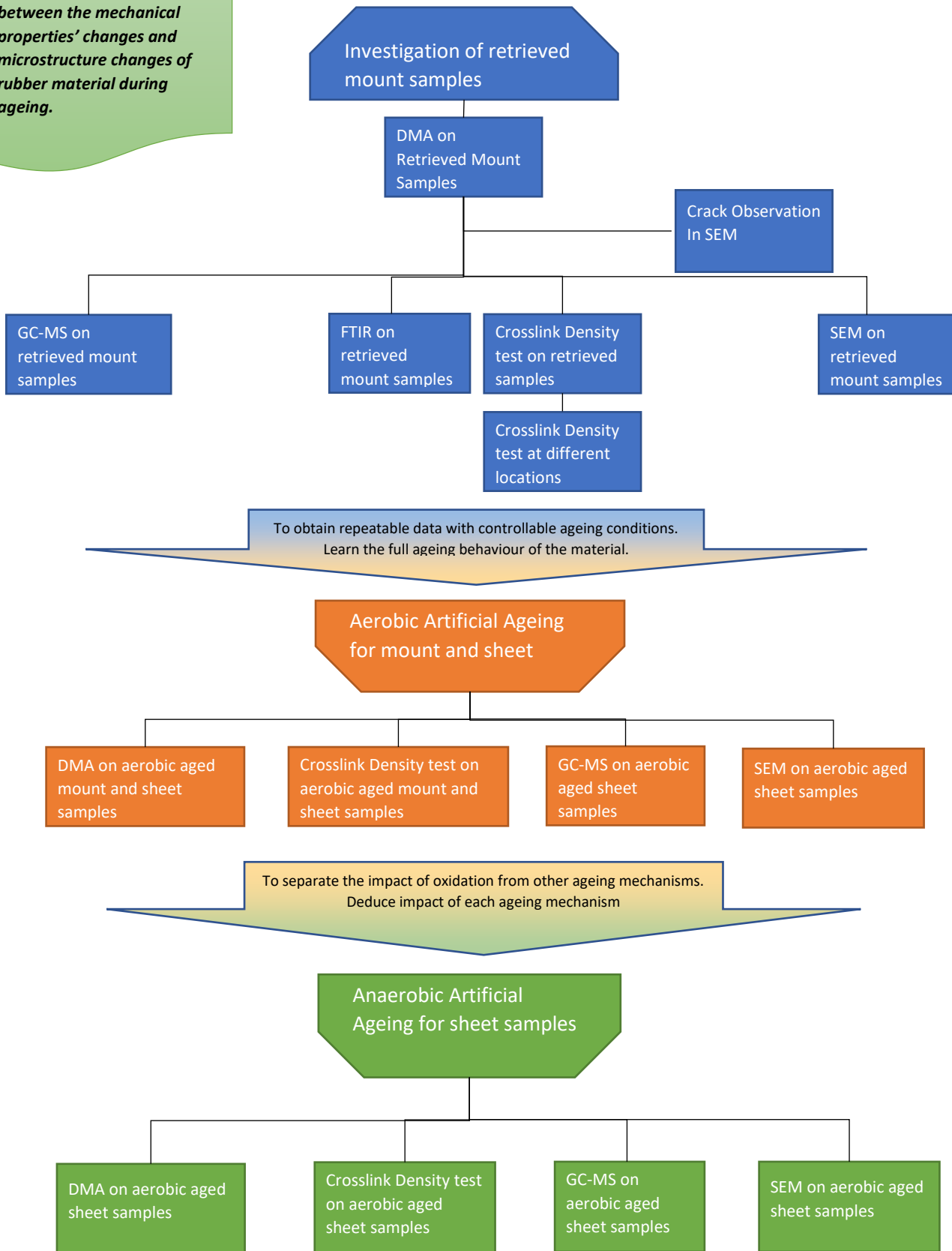
SEM on aerobic aged sheet samples

Figure 3.1 Experimental works flow chart

CHAPTER 4. BENCHMARKING OF REAL-WORLD ENGINE MOUNT

In order to gain knowledge about the rubber ageing behaviour in real-life conditions, rubber samples from engine mounts that were retrieved from used vehicles were tested.

The used engine mounts were provided by Jaguar Land Rover. They were sent from Dubai due to the high temperature operating environment they experienced, which ranged from 14 ℃ to above 95 ℃. As mentioned in Chapter 2.5.2, high temperatures can accelerate many ageing mechanisms, which suggested that these mounts would provide a 'worst case' scenario for testing.

4.1 Elastic Modulus

As mentioned in Chapter 1.1, the rubber part's main function in an engine mount is to provide resilience, and its elastic modulus is closely related to the mount's performance. Whilst anecdotal evidence suggests that the elastic modulus changes as the mount ages, this has not been tested scientifically. This section, therefore, focuses on investigating the change of elastic modulus across the range of aged mounts provided.

4.1.1 Sample selection

The ageing conditions of an engine mount are mainly represented by its mileage and time in service. Time in service is directly related to the ageing time of the mount and mileage reflects the dynamic loading the mount has experienced. Whilst each mount came with a known mileage and time in service, little else was known about driver style and other aspects which may vary. Moreover, frequency of the vehicle being driven can be reflected by the ratio between the mount's mileage and its time in service. Four mounts with similar average mileage per month and a new mount were selected for the initial investigation to identify whether ageing changes the properties of the rubber. Table 4-1 shows their mileage, time in service and average distance travelled per month.

Mount ID	Distance Travelled (km)	Time in Service (Month)	Average Ratio (km/Month)
1	0	0	N/A
2	82249	52	1581
3	92041	48	1917
4	96638	57	1695
5	145926	55	2653

Table 4-1 Ageing conditions for selected mounts

4.1.2 Methodology

As mentioned in Chapter 2.6.1, DMA, Nano-DMA and hardness can all provide a direct or indirect measurement of elastic modulus of the material. DMA can be used to measure rubber's elastic modulus for any given strain, temperature and frequency, directly. Nano-DMA can also measure the elastic modulus directly, but the corresponding strain is not defined due to the nonuniform strain distribution around the tip of the indenter. Nano-DMA requires samples with flat and smooth testing surfaces, and surface roughness of the sample can affect the test results [165]. When considering that samples were taken from used engine mounts with irregular geometry, such samples can be difficult to obtain. Non-uniformity of properties can also be problematic. For hardness test, Shore A hardness can be converted into elastic modulus by Equation 2-8. However, the corresponding strain, frequency, and temperature are all undefined. As this research involves comparing samples with different ageing conditions, and the risk of unknown strain distribution could introduce extra uncertainties, DMA was the most appropriate choice of technique.

4.1.3 Sample preparation

A cross section of the engine mount is shown in Figure 4.1, the metal part is made of aluminium and the hollow at the bottom is the fluid chamber. When force is transmitted from the connecting shaft, rubber next to the fluid chamber provides resilience properties to the mount. As mentioned in Chapter 2.4.1, oxidation at the near-surface region may cause changes to the rubber's properties and lead to properties' gradient. The effects of each ageing mechanism are not clearly understood; therefore, to maintain consistency, all samples were taken from the centre part of this region (the region inside the orange box).
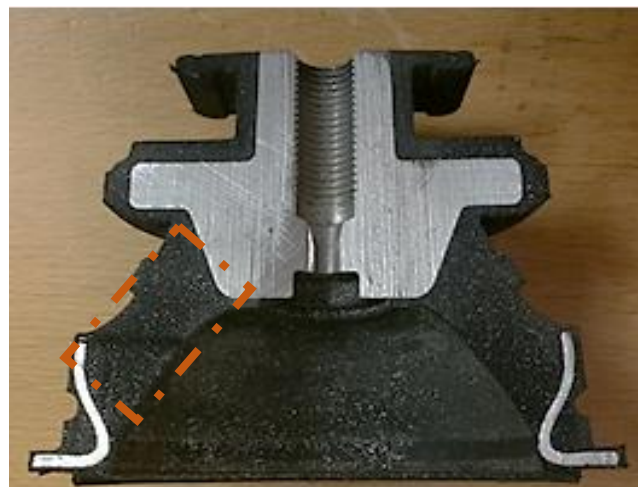
Figure 4.1 Cross section of the engine mount (shell removed)

Elastic modulus can be measured by a shear test or tension compression test. For this work, the tension compression test was selected as it directly generates the elastic modulus of the material. The samples were, therefore, cut into cuboid blocks, as suggested by ISO 4664. The required shape is illustrated in Figure 4.2 where 1 represents the clamps and 2 represents the sample.

Figure 4.2 Tensile DMA test

83

The mount was cut into layers with a band saw and then cut manually into small cuboid blocks. Due to the flexibility of rubber material, cutting thin samples often leads to uneven cut surfaces, especially for large cut surfaces. To avoid this problem, the samples were cut to have thicker 'h' than the standard. For the same reason, the height 'l' was also slightly lower than the standard, to reduce the size of the cut surface.
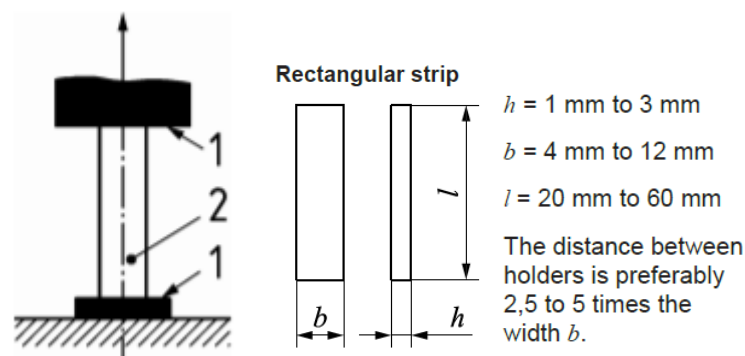
Although the lateral contraction of the specimen would make a larger impact on the result, as described in Chapter 2.6.1, the samples were cut with similar shape factors so that they are still comparable. Large shape factor can lead to inaccurate measurement. Thus, samples were cut with shape factor smaller than 0.25.

Three DMA samples were cut from each selected mount to account for any uncertainties caused by nonuniformity of the material properties. The locations of the cuts are shown in Figure 4.3. The picture on the left-hand side illustrates where the layers were cut, the sample layer on the right-hand side is the region between the white lines. The two rectangular spaces in the image on the right illustrate the DMA samples' cut location.

Figure 4.3 – Cut location for DMA samples

An uncertainty on dimension of $\pm 25\%$ on the thickness was generated in the band saw cutting process. Further uncertainty from manual cutting led to a $\pm 20\%$ difference to the width and $\pm 12\%$ difference on the height. The experiment requires a flat contact surface between the sample and the supporting plates, some samples needed to be trimmed down further. Table 4-2 shows the sample

dimensions with their corresponding shape factors. The nature of the cutting process led to some variation in the exact size of the specimens. However, as discussed in Chapter 2.6.1, modulus variation for samples with shape factors under 0.25 are relatively small. Furthermore, this variation of modulus caused by size differences will be factored out during the experiment, details will be included in the results section.

Mount ID	Sample	Height (mm)	Width (mm)	Thickness (mm)	Shape Factor
1	1	18	6	8	0.1
	2	20	5	5	0.06
	3	21	5	5	0.06
2	1	20	6	6	0.08
	2	21	5	5	0.06
	3	16	5	5	0.09
3	1	18	4	6	0.07
	2	16	4	5	0.07
	3	12	5	6	0.11
4	1	22	5	6	0.06
	2	18	6	6	0.08
	3	18	6	6	0.08
5	1	16	5	5	0.08
	2	18	5	5	0.07
	3	14	5	5	0.09

Table 4-2 Sample size for DMA test

4.1.4 Experimental configuration

The machine selected was the Metravib Viscoanalyser VA 2000. To calculate the elastic modulus of the sample, the machine applied sinusoidal stretching to the sample with defined strain, frequency and temperature, then captured the force signal and the displacement signal with built-in sensors.

In order to gain a better understanding of the Payne effect mentioned in Chapter 2.3.7 and its influence upon elastic modulus, dynamic strain sweep tests were conducted with different static strains. The maximum dynamic strain for tension compression test was set to be 10%, as this covers most operating strain for the actual engine mount. To avoid problems caused by buckling, the samples were loaded with tensile static strains. The test takes 49 measurements from each sample, calculating the elastic modulus of the sample from 0.3% (the minimum value selectable) to 10.3% static and dynamic strain. Figure 4.4 illustrates the measuring conditions of the DMA test.
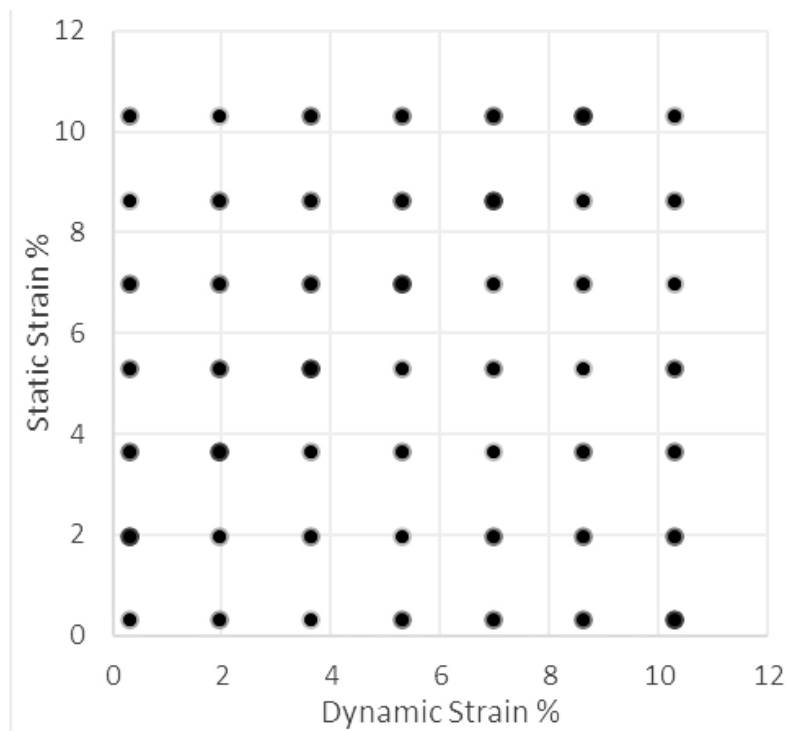

Figure 4.4 Measuring conditions for DMA tests

As mentioned in Chapter 2.3.7, temperature and operating frequency could affect the measured elastic modulus. Although small changes of both the frequency and temperature would not lead to a significant impact on the results as the modulus is proportional to the log of them, the frequency was set to 1Hz and the temperature was set to 30 °C in order to obtain a comparable result. Because the material would never experience strain above 20% during service, all samples were temporarily stretched with a 20% strain before the test to eliminate the Mullins effect mentioned in Chapter 2.3.7.

4.1.5 Results

The calculation shown in Equation 4-1 converts the measured force displacement information into a value of elastic modulus.

$$K = \frac{\Delta F_A}{S_A} \qquad\qquad E' = K\, Fc\, (height/S_e)\, cos\delta$$

$$F_C = 1/(1 + 2(S_e/SI)^2) \qquad E = E'(1 + i \tan \delta)$$

K	ΔF_A	S_A	δ	E
stiffness	amplitude of the force signal	amplitude of the displacement signal	phase shift	elastic modulus
E'	F_C	S_e	SI	i
storage modulus	geometry correction factor	excited surface area of the sample	free surface area	imaginary unit

Equation 4-1 Calculation of elastic modulus in VA2000 [190]

Figure 4.5 shows the measured material's elastic modulus for sample 1 of mount 1 at different strains. The results from other samples are similar and are attached in Appendix A i.
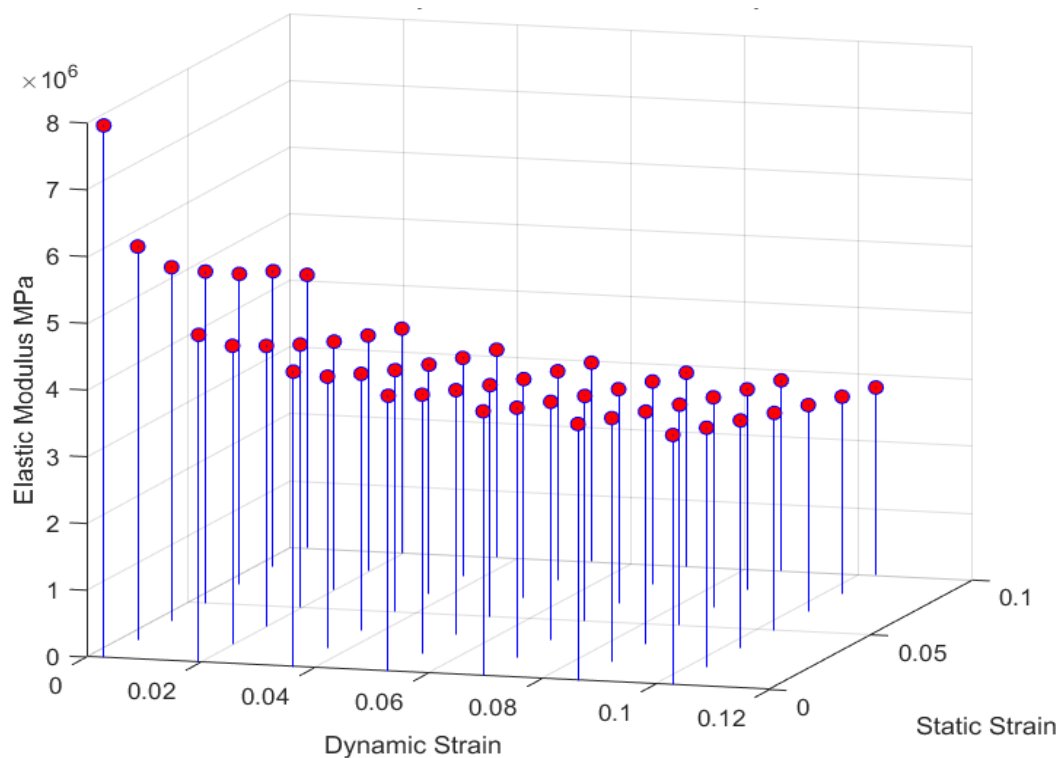

Figure 4.5 – Strain sweep test, strain vs. elastic modulus for mount ID 1, the new mount

As expected, due to the Payne effect, the elastic modulus of the sample decreases as the strain increases. Due to the strain dependence of elastic modulus, comparisons must, therefore, be made among same strain conditions. Figure 4.6 shows the elastic modulus of samples obtained from each selected mount at 10% static strain and 10% dynamic strain with different ageing conditions, as a higher strain could eliminate the effects of the Mullins effect and reduce uncertainties caused by friction inside the DMA machine.
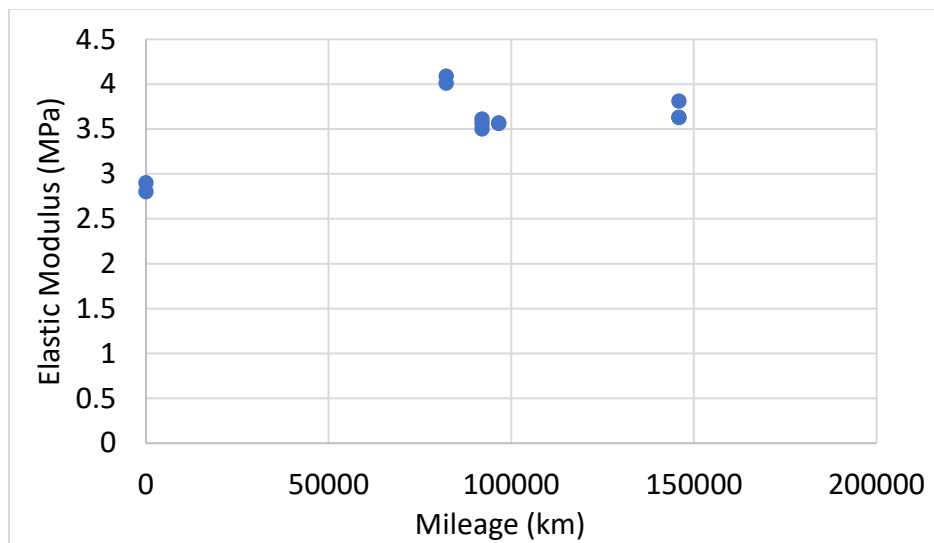

Figure 4.6 – Elastic modulus vs. mileage of the mount

It can be seen that there is a difference between the unused and used mounts, with all used mounts having a higher elastic modulus than the unused mount. Whilst it is not possible to draw conclusions related to the specific manner in which ageing affects elastic modulus, it is clear that it does lead to an increase of 17% to 35%. The next step for this research is to establish the mechanisms leading to this increase in stiffness.

4.2 Investigation of Ageing Mechanisms

As shown in Table 3-1, the next step is to define the active ageing mechanisms for the selected product. The rubber samples to be tested are taken from the same selected engine mounts. As the mount is not exposed to light and radiation, and its interaction with the chamber fluid (in this mount is propylene glycol) is negligible [188] [189], Table 2-5 in Chapter 2.6.6 is simplified into Table 4-3, which provides a

summary of which of these ageing mechanisms are relevant for this study. This chapter will go through the characterisation process of these mechanisms.

Mechanisms	Evidence of Necessity	Impact
Post-curing and thermal degradation	Vulcanised rubber exposed to high temperature environment	Crosslink density
Oxidative degradation	Exposed to air	Crosslink density Chemical composition
Filler re-agglomeration	Experienced cyclic loading and high temperature	Carbon filler distribution
Loss of additives	Exposed to air and high temperature environment.	Concentrations of additives
Cracks	Exposed to air and experienced cyclic loading	Forming and propagation of cracks

Table 4-3 Necessity of investigation for ageing mechanisms

4.2.1 *Post-curing and thermal degradation*

As crosslink density is closely related to the elastic modulus, changes to the elastic modulus indicate possible changes to the crosslink density of the material. In order to identify whether any post-curing and thermal degradation have changed the measured crosslink density of the material, this chapter examined the changes on crosslink densities of the rubber taken from different locations in used mounts. As different locations experienced different ageing conditions, by comparing the differences among the measured crosslink density, the impact of different ageing conditions can be revealed. The swelling technique was applied, as it can calculate

the crosslink density of the specimen by soaking it in toluene and weighing it before and after the soaking process.

Sample preparation

Due to the difficulty of manual cutting mentioned previously, differences of sizes of samples are unavoidable. Although they would be cut into similar sizes, the samples needed to be swelled thoroughly to eliminate the uncertainties caused by different swelling statuses between small and large samples. This makes smaller samples preferable. However, toluene is relatively volatile and if the samples are too small or too thin, significant amounts of toluene could escape before being weighed. Thus, the samples were cut into approximately 4mm cubes, weighing at least 70 milligrams.

These samples are smaller than the DMA samples, which enabled the possibility of taking samples from different locations on the mount. As mentioned in Chapter 2.4.1, oxidative degradation can lead to changes to crosslink density, which predominately happens at the near-surface region of the material. Other regions would also experience different forms of ageing, thus, samples were taken from four different locations on the engine mount.

The orange boxes shown in Figure 4.7 represent the sampling locations. Location A is at the surface of the mount, and away from the part of rubber that provides resilience properties to the mount. Samples taken from location A can be assumed to have experienced the oxidative degradation without experiencing cyclic loading during their service period. Samples from location B were also taken from the surface, in areas where they would have experienced cyclic loading during the service period. Samples taken from location C are 3mm away from the surface and will not have experienced any cyclic loading during service, and, the influence of oxidative degradation should be smaller or eliminated. Samples from location D are 10mm away from the mount surface so the effects of oxidative degradation should be even less or eliminated. These samples will have experienced cyclic loading during the service period and this is where the DMA samples were taken.
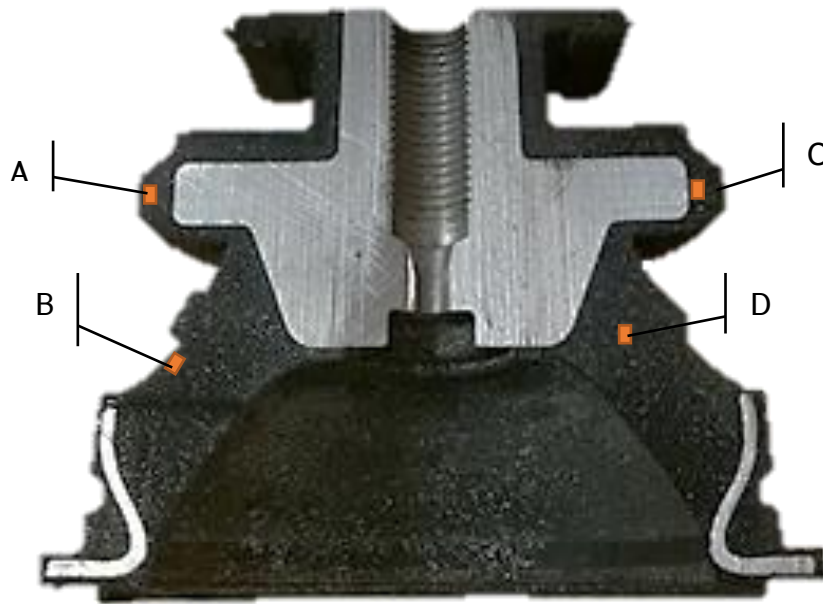
Figure 4.7 Sampling locations for swell test

At least 5 samples were cut from each location of each mount to account for any uncertainties introduced by geometry differences.

Experimental configuration

A set of samples has been put into toluene and their weight changes was recorded, the changes after two weeks became negligible. Thus, the experimental procedure for the swelling technique measurement is shown below:

1.   Swell the sample in toluene for two weeks to approach equilibrium.

2.   Take a sample and dip it in a bottle of acetone.

3.   Gently and quickly dry sample surfaces with tissue followed by a gentle blow to evaporate the remaining acetone.

4.   Measure the weight of the sample, obtain W_wet.

5.   Put samples in a vacuum oven under 60 °C for two days to ensure the removal of the remaining solvent.

6.   Measure the weight of the sample, obtain W_dry.

Result

Equation 4-2 was applied to obtain the crosslink density of each sample. Using the weight of dried samples is because the original sample weight included the weight of additives and unbonded chains that could dissolve in the solvent.

$$V_x = -\frac{\ln(1 - v_2) + v_2 + \chi_1 v_2^2}{\varphi\left(v_2^{1/3} - v_2/2\right)} \quad , \quad v_2 = \frac{\rho_s}{\rho_r\left(\frac{w_{wet}}{w_{dry}} - 1\right) + \rho_s}$$

V_x	v_2	χ_1	φ
crosslink density	volume fraction of polymer in a fully swelled sample	Flory interaction parameter relates to the interaction between solvent and solute	molar volume of the solvent
ρ_s	ρ_r	w_{wet}	w_{dry}
Density of the solvent	Density of natural rubber	Weight of the soaked sample	Weight of the dried sample

Equation 4-2 Calculating crosslink density

Figure 4.8 shows the results of samples taken from location D. The result shows that the crosslink density of rubber samples increased with increases in mileage, peaking and ending at a 39% increase. The behaviour is similar to that observed from the DMA test shown in Figure 4.6.
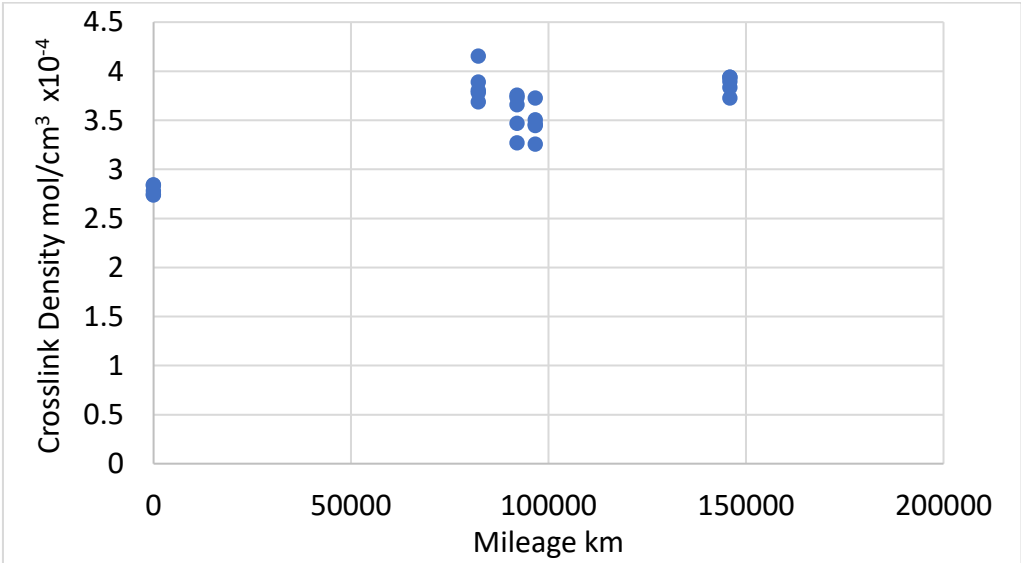

Figure 4.8 Crosslink density of samples taken from location D

Test results for samples taken from location A, B, and C are plotted in Figure 4.9, Figure 4.10 and Figure 4.11, respectively. All the samples taken from A, B and C show a decrease in crosslink density. In particular, the samples taken from the surface of the mount show lower crosslink density compared to the samples taken from locations away from the surface.
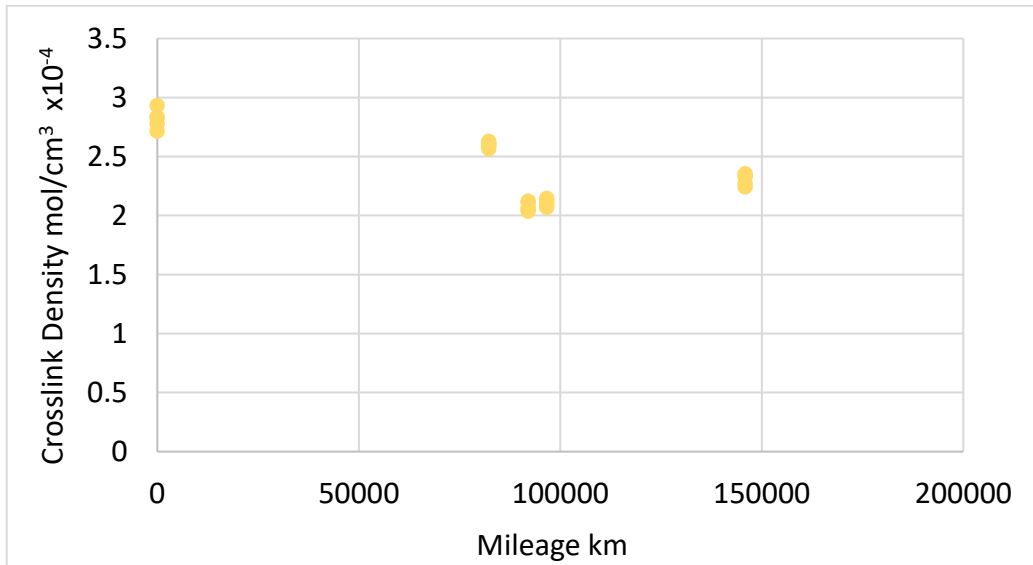

Figure 4.9 Crosslink density of samples taken from location A

Samples taken from location A showed an overall decrease in crosslink density of between 18% and 26%.
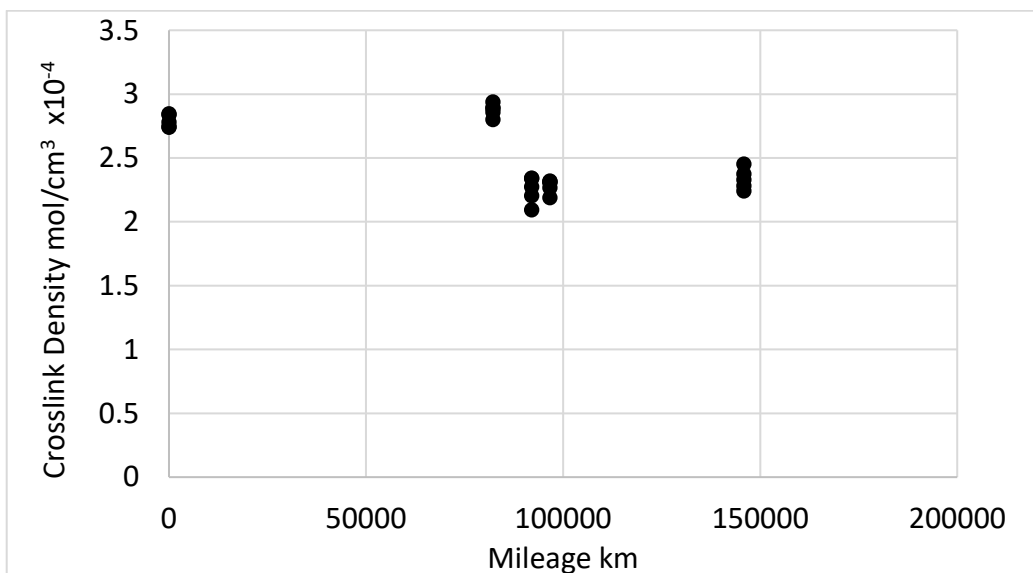
Figure 4.10 Crosslink density of samples taken from location B

The average crosslink density of samples from location B showed a decrease in crosslink density up to 19%.
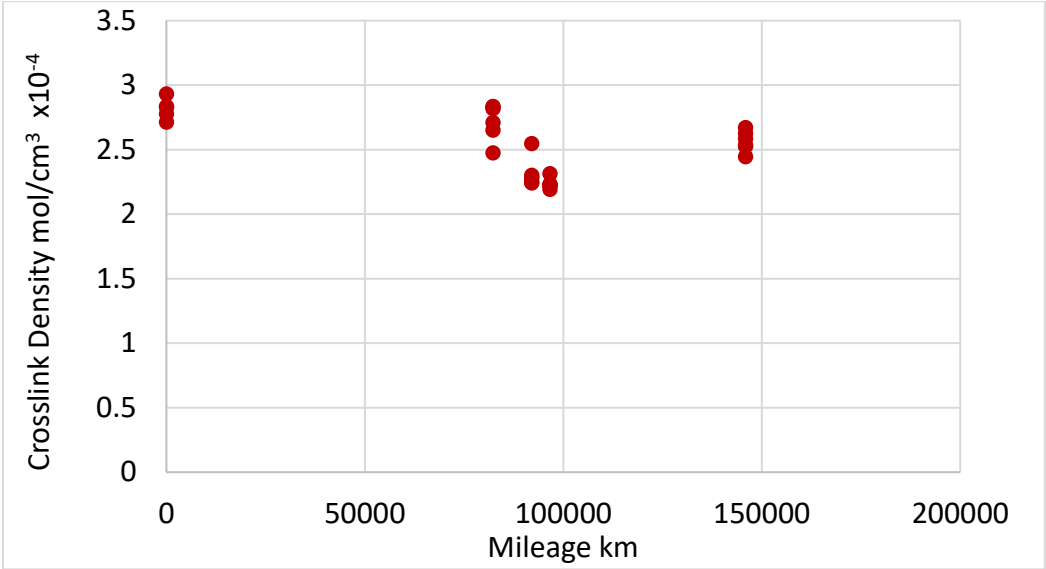
Figure 4.11 Crosslink density of samples taken from location C

Samples from location C showed a decrease in crosslink density of between 8% and 20%.

Discussion

Comparing with measured elastic modulus

Figure 4.12 shows the plot between the elastic modulus of rubber samples and the measured crosslink density from location D. As suggested by literatures, higher crosslink density corresponds to higher elastic modulus, except for samples taken from Mount ID 2 and 5 which show different elastic modulus with the same crosslink density, which are the newest and oldest used mounts. This is likely to be caused by other existing ageing mechanisms, i.e., carbon and additive migration.
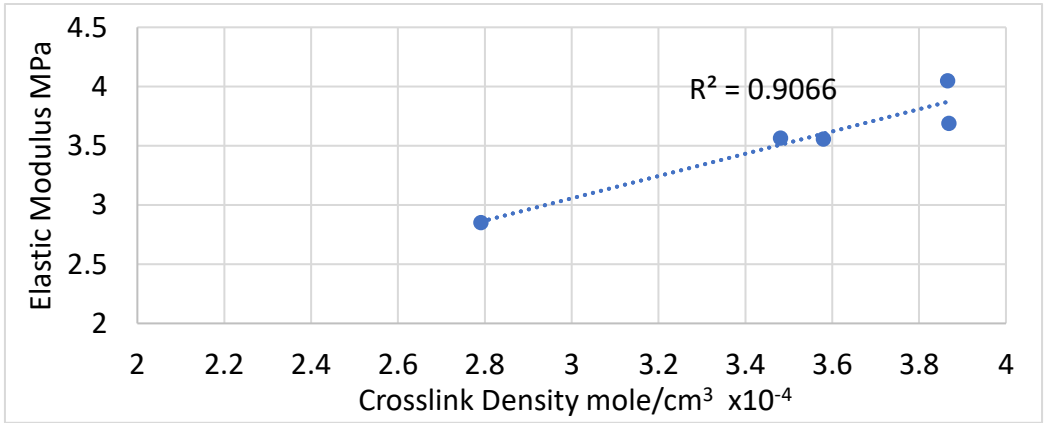
Figure 4.12 Relationship between crosslink density and elastic modulus

Comparing samples from different locations on the mount

With comparing the percentage changes of crosslink densities of samples taken from different locations, differences in the behaviour of crosslink density changes were observed. Figure 4.13 illustrates that there is a clear difference between samples taken from location D and samples taken from other locations.
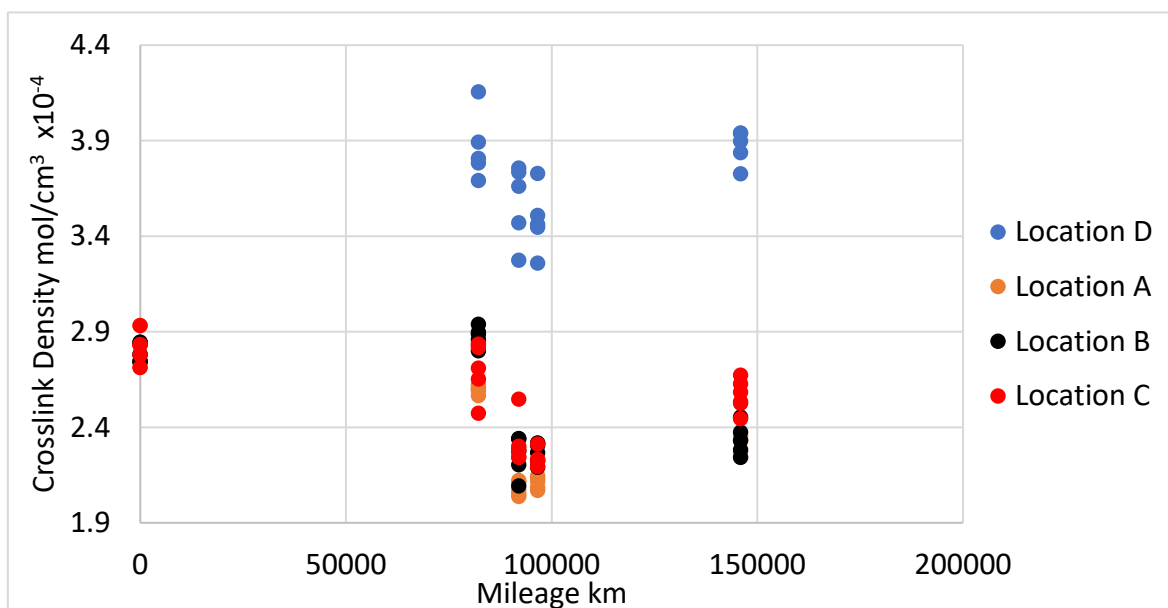

Figure 4.13 Crosslink density changes of samples taken from different locations from real-world mounts

Average standard deviations of measured crosslink densities at different locations are shown in Table 4-4. Although the variations of results at every sampling location were relatively small, a larger standard deviation can be observed for the measured crosslink density of samples taken from surface locations. This is likely to be caused by non-uniform ageing behaviour inside the mount, causing differences in the absolute distance between the sampling locations and outer surfaces, crucial for the results. The possible non-uniform ageing behaviour includes oxidation and additive migration.

	Near Surface		Away from surface	
Location	A	B	C	D
Standard Dev	3.08×10^{-6}	6.53×10^{-6}	8.62×10^{-6}	1.43×10^{-5}

Table 4-4 Standard deviation of measured crosslink densities

Based on the sampling locations, they would have been affected by ageing conditions shown in Table 4-5. Besides from those, all locations were affected by post-curing and thermal degradation.

Sampling location	Ageing condition
Sample from location A	Oxidative degradation
Sample from location B	Oxidative degradation + cyclic loading
Sample from location C (3mm from surface)	None/lesser oxidation and ozonation
Sample from location D (10mm from surface)	Cyclic loading

Table 4-5 Ageing conditions at each sampling location

Effect of Oxidative degradation

A and C were both taken from locations that never experienced cyclic loading, and B and D were both from locations which would. By subtracting the values measured at the bulk region from those at the surface, the effect of oxidative degradation can be identified. Figure 4.14 illustrates the differences in measured crosslink densities for both the set that experienced cyclic loading and the set that never experienced cyclic loading. Both sets showed that oxidative degradation reduced the measured crosslink density and the impact continues with increasing mileage. The error bar is calculated based on the standard deviation of each sampling location, shown in Table 4-4. For example, the pair without cyclic loading has the error bar representing $\pm$ (standard deviation of location A + location C).
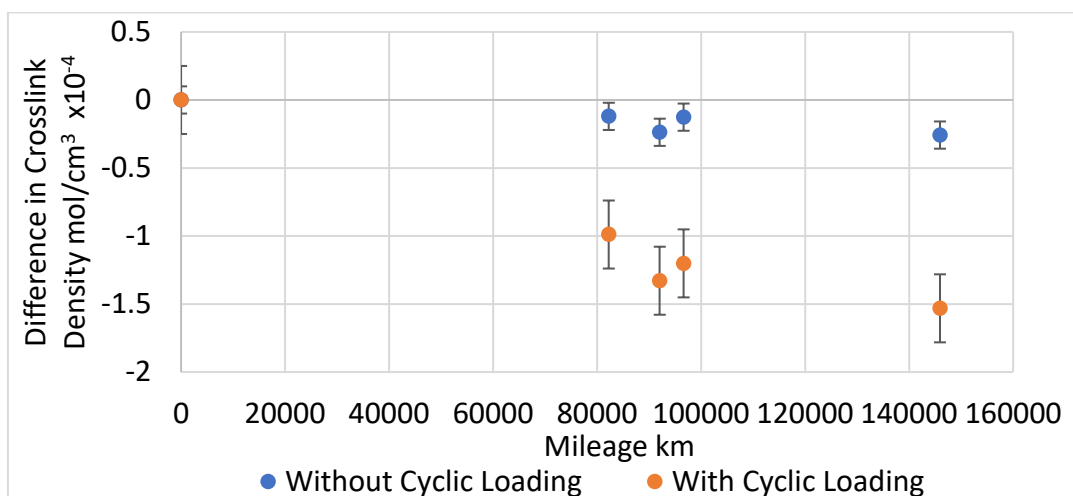

Figure 4.14 Effect of oxidative degradation

The influences of the oxidative degradation are clearly shown by the difference in the set that experienced cyclic loading (B and D), a decrease in crosslink density up to 50% of the new mount's crosslink density, which is expected to be the result of oxidation according to Veith (1957), who suggested that chain scission takes the predominate position in the oxidation process of natural rubber [191].

The effect is not as pronounced in the set without cyclic loading (A and C), which might be caused by the smaller distance difference between the sampling locations.

Effect of cyclic loading

A and B were both taken from the surface, and C and D were from regions away from the surface. By subtracting the value measured from the locations that never experienced cyclic loading from the locations that experienced cyclic loading, the impact of cyclic loading can be identified.

Figure 4.15 illustrates the differences between measured crosslink densities of both pairs. There is a pronounced increase of difference in crosslink density between the pair away from the surface. However, as suggested previously, this could be caused by the fact that location C is closer to the surface than location D and has been affected by oxidative degradation. The error bar was calculated with the same method used in Figure 4.14.

The difference between the pair taken from the surface showed that the impact of cyclic loading on measured crosslink density is insignificant.
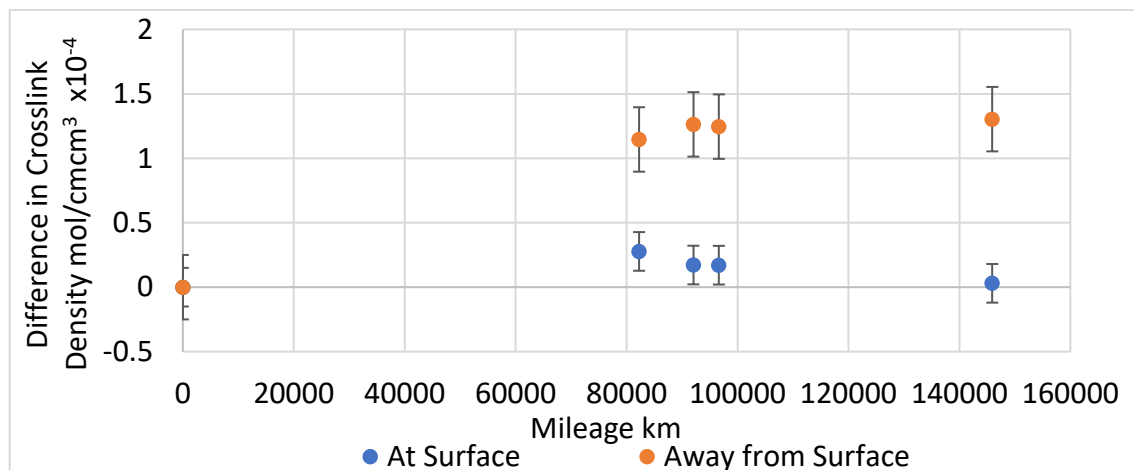

Figure 4.15 Effect of dynamic loading

4.2.2 Oxidative degradation

Oxidation in natural rubber is dominated by chain scission [191]. It also triggers the formation of new compounds in the material, which changes the material composition. The chain scission leads to a decrease of overall crosslink density, which is entangled with the impact of post- curing and thermal degradation processes. Knowledge about the progression of oxidation can help separate the effect of oxidative degradation from the others.

As mentioned in Chapter 2.4.2, the new compounds formed during oxidation contain O-H bond, C-O bond and C=O bonds, their intensities increase with the progression of oxidation. FTIR was used to examine the possible chemical composition change caused by oxidation by comparing the chemical composition of the outer surface of used and unused mount rubber. Except from comparing the intensities of the oxidation related bonds, other significant differences in the appearance of the spectrum were also noted, to identify if there are other changes upon the chemical composition caused by ageing.

Sample preparation

The testing apparatus was the PerkinElmer Frontier FTIR, which uses attenuated total reflectance technique for taking measurements. As described previously, oxidation mainly occurs when the material comes into contact with air, therefore, its effect is likely to be more significant on the surface of the material. Thus, all measurements were taken from the outer surface of the mount that are exposed to air. Specimens were taken from the surface of the mount, cut into 2mm thick and at least 3mm in width and length. Two samples were taken from the new mount (mount ID 1) and two from the oldest mount (mount ID 5) for the maximum age difference. Seven measurements in total were taken from samples from each mount.

Experimental configuration

The testing crystal was cleaned with acetone and lab paper towels after each test followed by a two minute drying period. The 'background' process, which records and eliminates changes from the atmosphere was done after every three tests to

counter any possible environmental changes. The scan covers wave numbers from 800cm^{-1} to 4000cm^{-1}, which covers all bonds formed by oxidation of natural rubber mentioned in Chapter 2.6.3.

Result

Figure 4.16 shows an example of the measurement taken from the surface of the rubber component in a new engine mount. Lower transmittance represents a higher intensity of a certain bond as the bond absorbs the energy resonance with its vibration modes. If intensities of bonds produced by the oxidation process increased, the progression of oxidation can be identified.
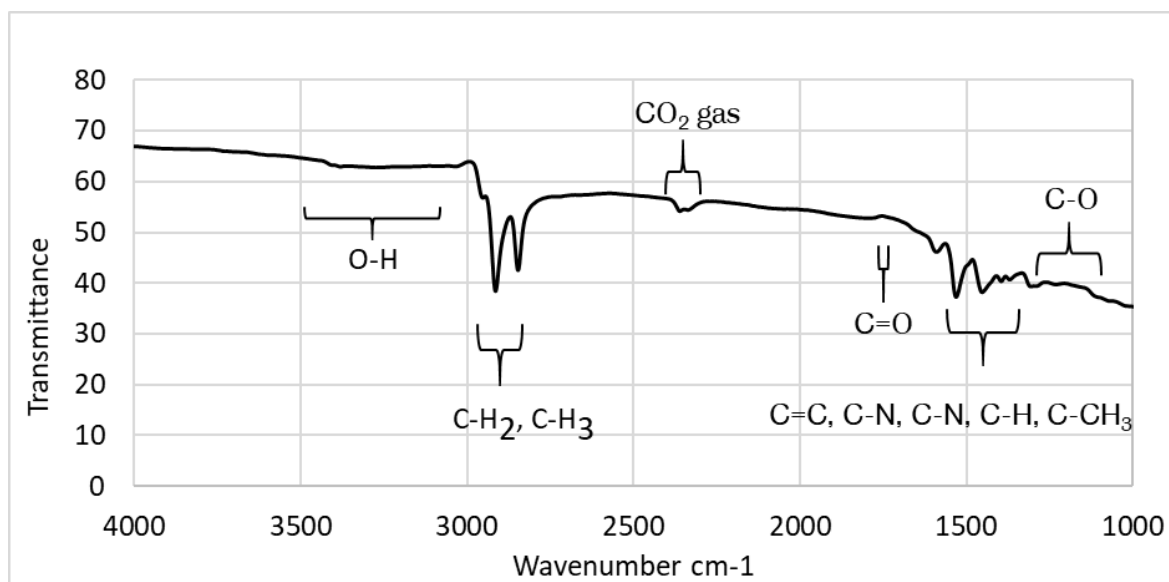
Figure 4.16 Example of measurement taken from the rubber surface of new engine mount

Table 4-6 shows the chemical bonds corresponding to the observed peaks. Possible sources of these peaks were also suggested [192] [193]. A variation on transmittance around 3200 cm^{-1} shows the existence of O-H bond in the new sample, the sharp peaks around 2900 cm^{-1} represent the methylene groups and methyl group. Peaks at 2330 cm^{-1} were reported to be caused by CO_2 in the atmosphere. Peaks around 1520 cm^{-1} and 1440 cm^{-1} were clustered together and unable to be separated.

Wave number cm^{-1}	3200 (broad)	Peaks near 2900	Peaks at 2330	1730	Peaks around 1520	Peaks around 1400
Corresponding chemical bond	O-H	C-H in CH$_2$ and CH$_3$	CO$_2$ gas	C=O	C-O, C=C, C-N	C-N, C-H, C-CH$_3$
Source	Oxidation, additives	Rubber chains, additives	CO$_2$ in environment	Oxidation, additives	Oxidation, additives	Curing agent, additives

Table 4-6 Chemical bonds corresponding with observed peaks

Figure 4.17 shows all measurements made on the surface of the new engine mount, and Figure 4.18 shows all the measurements made on the surface of the oldest mount.
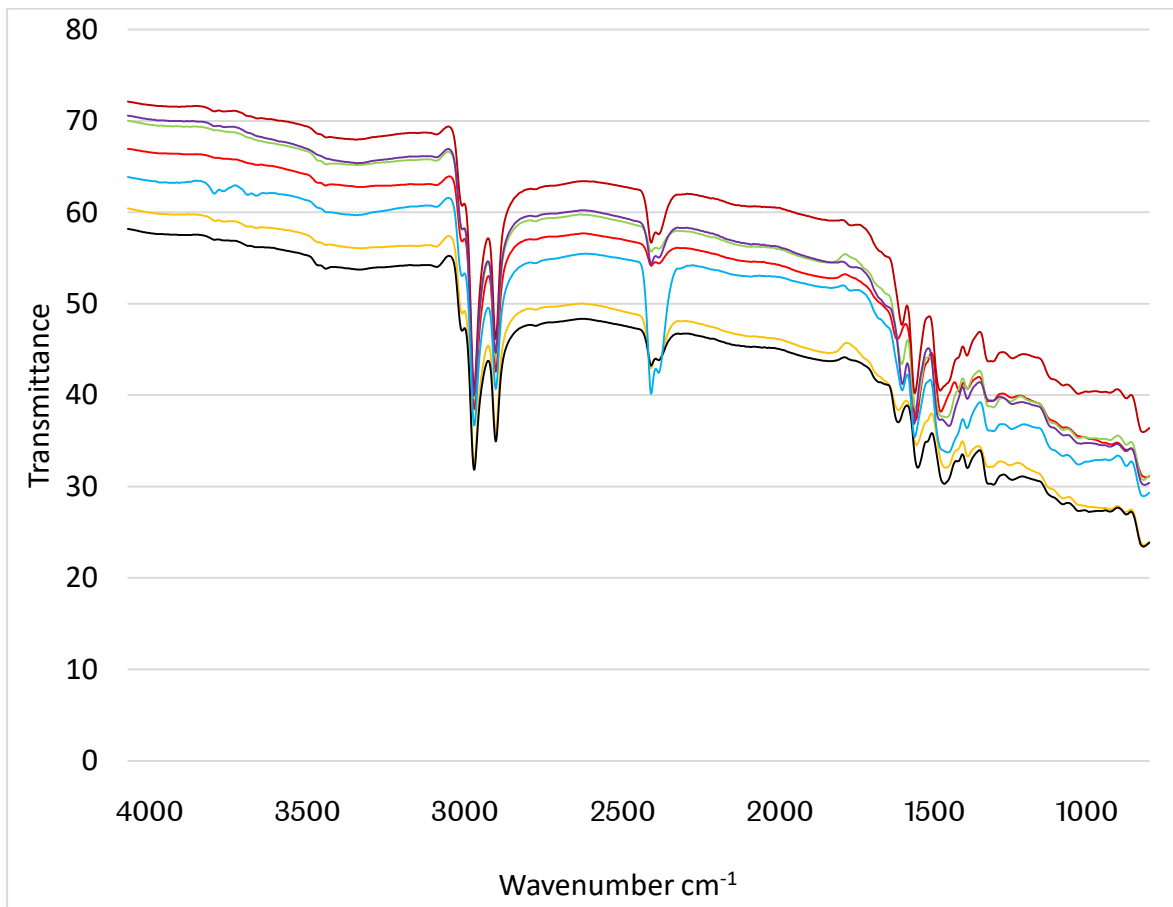
Figure 4.17 FTIR spectrum of samples from surface of new mount
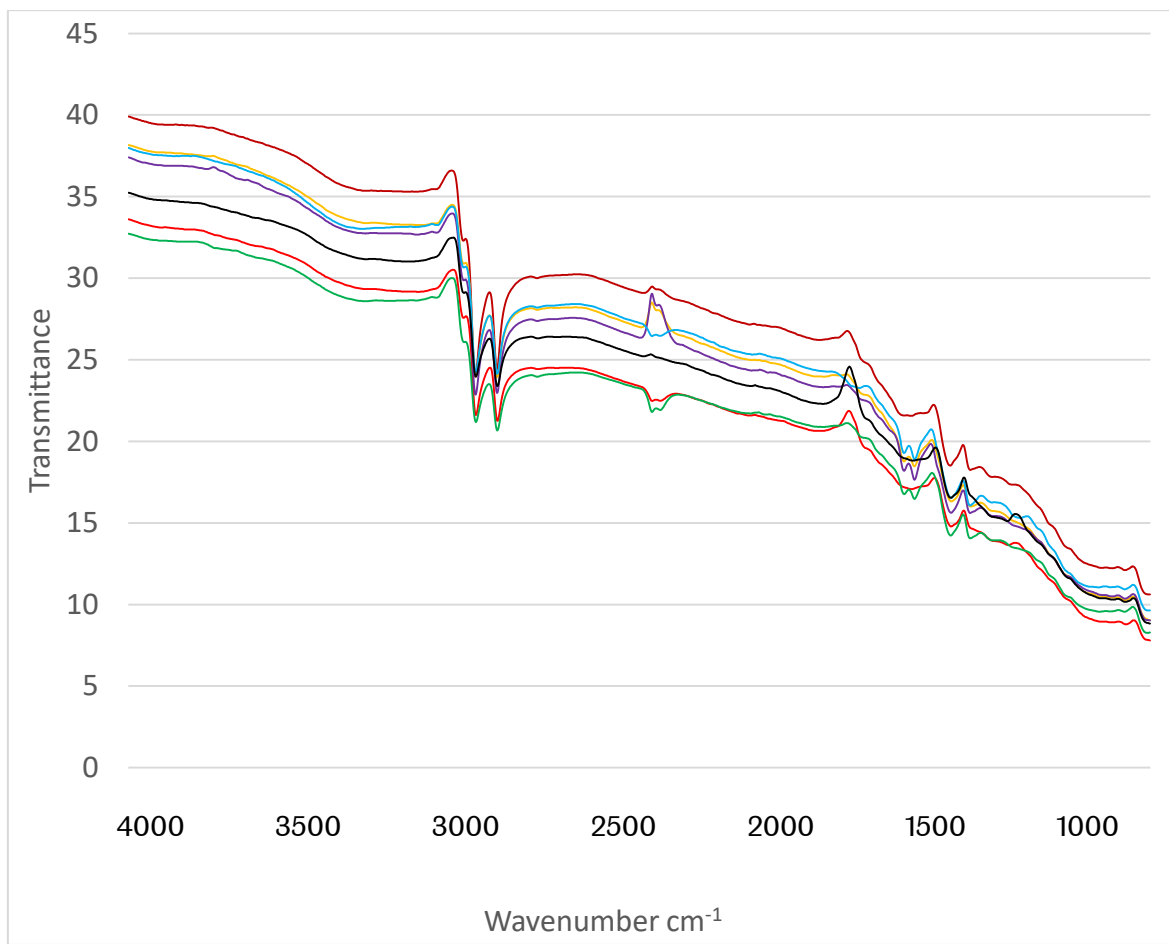
Figure 4.18 FTIR spectrum of samples from surface of the oldest mount

The transmittance line does not overlay for the samples taken from the same mount and a continuous decrease of transmittance was observed in every measurement. Carbon black is a strong absorber of infrared, which is known to be responsible for the all frequency range absorbance and the incline of the baseline [194]. As mentioned in Chapter 2.6.2, the penetration depth of the evanescent wave is a few micrometres and the carbon filler particles can have a diameter within 100nm. This means that the content of interfering carbon black of each test can be different among tests due to the non-uniformity of carbon black distribution at small scale [195]. However, except from the peak at around 2330 cm^{-1}, the peaks' location and behaviour are similar for samples taken from the same mount.

Discussion

The baseline transmittance is different between the new mount samples and the oldest mount samples. Lower transmittance of the oldest mount samples suggests the carbon particles in the surface region of the mount were not as intense as in the oldest mount.

Figure 4.19 shows the zoomed comparison between samples taken from the new and the oldest mount, stacked up with 35 transmittance in between. At regions representing O-H (at around 3300 cm^{-1}) bond intensity and C=O (at around 1750 cm^{-1}), C-O (at around 1200 cm^{-1}) bonds intensity. No significant changes have been observed in the regions corresponding to O-H and C=O bonds. Intensity reduction can be observed at the four peaks around 2900 cm^{-1} (representing C-H), and peaks around 1440 cm^{-1} and 1520 cm^{-1} (representing C-O, C=C and C-N).
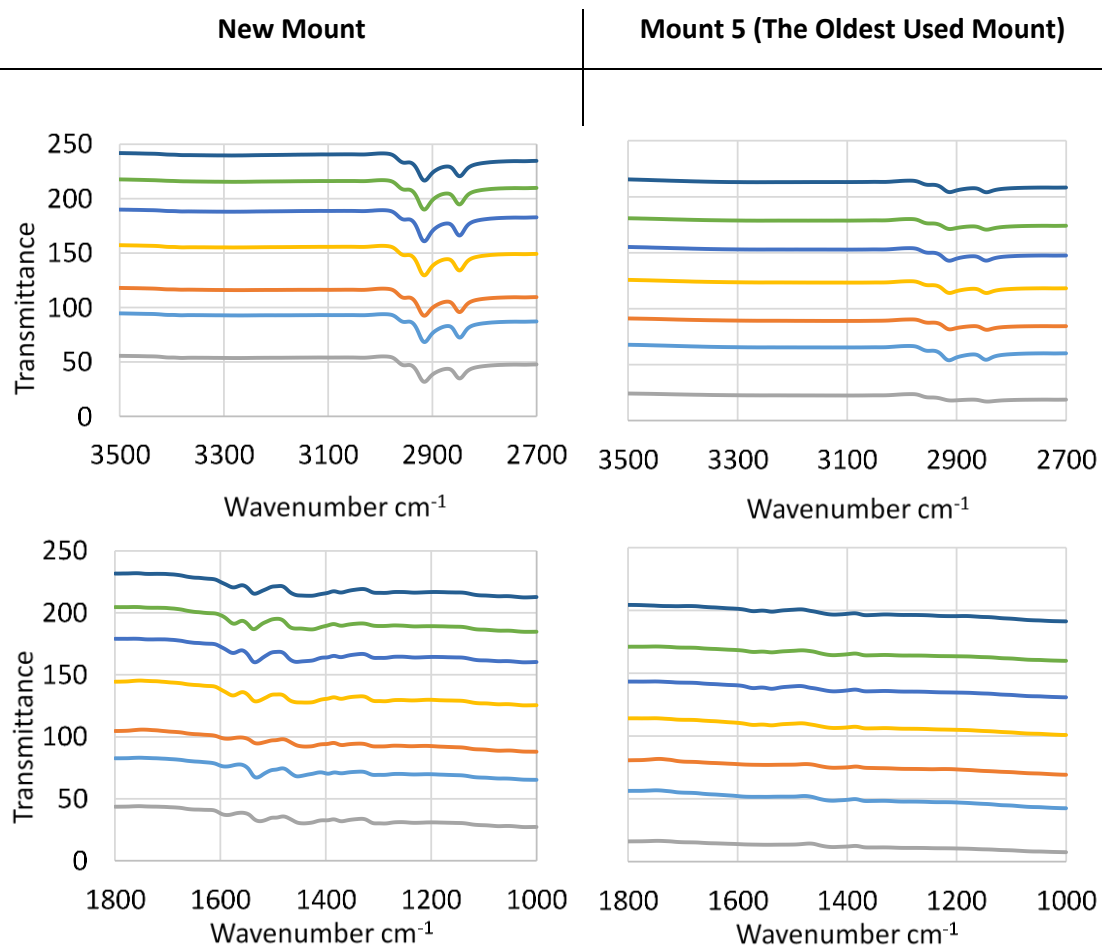
Figure 4.19 Comparing samples taken from new and used mount's surface, zoomed at regions corresponding to oxidative related bonds -- O-H bond (top)/ C=O & C-O bond (bottom)

The intensity reduction observed at 2900 cm^{-1}, 1730 cm^{-1} and 1550 cm^{-1} could be the result of additive migration. Listed in Table 4-6, these peaks could be representing bonds in the additives. The 2900 cm^{-1} peaks reflect the amount of C-H bonds, which are the main constituent of mineral oil, a common plasticiser. C=O bond exists in various additives, from plasticiser to curing agent. The peaks around 1550 cm^{-1} can represent many bonds, the variation can be related to the C-H bond for reasons listed above and the C-N bond, a common constituent in many antioxidants. A similar behaviour was discovered by Liu et al. (2017), who also suggested that this could be led by overlaps between oxidation and loss of additives [125].

4.2.3 Filler re-agglomeration

As mentioned in Chapter 2.4.3, ageing could lead to re-configuration of carbon filler network inside the rubber material. Scanning electron microscopy was used in order to attempt to observe whether this has occurred in used mounts.

Sample preparation

To investigate the existence of carbon filler re-agglomeration in a used engine mount, and its relationship with temperature, time and cyclic loading, samples were taken from location C and D (Both locations are away from the surface of the mount, where C has never experienced cyclic loading and D has.) of the new engine mount and three used mounts have different mileage and time in service (Mount ID 3,4,5 in the DMA test).

Three samples were prepared for each interested location. The cryo-fracture method was used to prepare the samples. The rubber samples were soaked in liquid nitrogen for three minutes until bubbles were no longer produced from the sample surface. The sample was quickly transferred to a workbench and cut at the middle with a sharp razor blade. To ensure the image was not distorted by surface defects, only samples with a comparably clean and flat surface were used.

Experimental configuration

Helios NanoLab SEM was selected due to its outstanding performance under low voltage conditions. After loading the samples into the chamber, the Everhart-Thornley Detector (ETD) and through the lens detector were used to achieve 10,000 times magnification. The voltage was set to below 5 KV to reduce any problems caused by overcharging. A Backscatter detector was then used to capture an image reflecting atom number density difference between constituents of rubber. Atom number density is calculated by $N = \frac{\rho \times N_A}{M}$, where ρ represents the material's density, N_A represents the Avogadro's number and M represents the molar mass of the material. Carbon black has 9×10^{-22} atoms per unit volume and natural rubber network has 8×10^{-21} atoms per unit volume. This means carbon black should be able to reflect more back scattered electrons than the rubber network and, therefore, is expected to be brighter in the images. The captured images were analysed by Fiji – an image processing software, to analyse the particle size and their distribution.

To avoid the problem caused by the possible non-uniform distribution of carbon fillers and to ensure the sample amount, seven images were captured from random locations across three samples of each mount.

Result

In the raw image, although the artefacts caused by cryo-fracture were avoided when capturing the images, there are still parts that are over-exposed and out of focus areas. This is likely to be caused by the high roughness brought by large carbon black particles. Thus, out of focus areas in the images were not included when counting the particles. Figure 4.20 to Figure 4.24 illustrate the processing procedures for pictures taken from location D of mount 5 as an example. The image was first smoothened to eliminate fake small particles caused by noise. It was then cropped to ensure the quality of the area to be analysed. Then, it was transferred into a black and white image with a brightness threshold based on the known volume fraction of carbon black in the sample (15%). The number and sizes of particles in the cropped area were then measured with the built-in particle

counting function. All raw images and processed images can be found in Appendix B i to xvii.
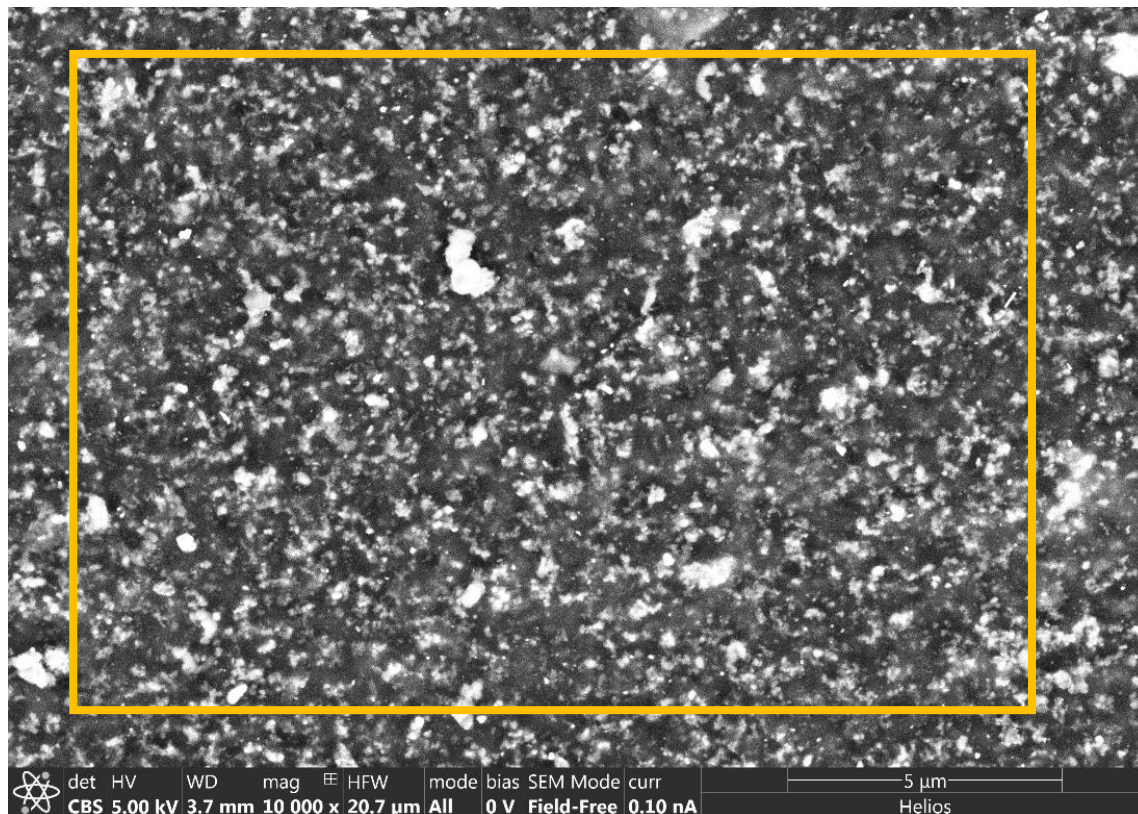
Figure 4.20 An example SEM image taken from mount 5 sample
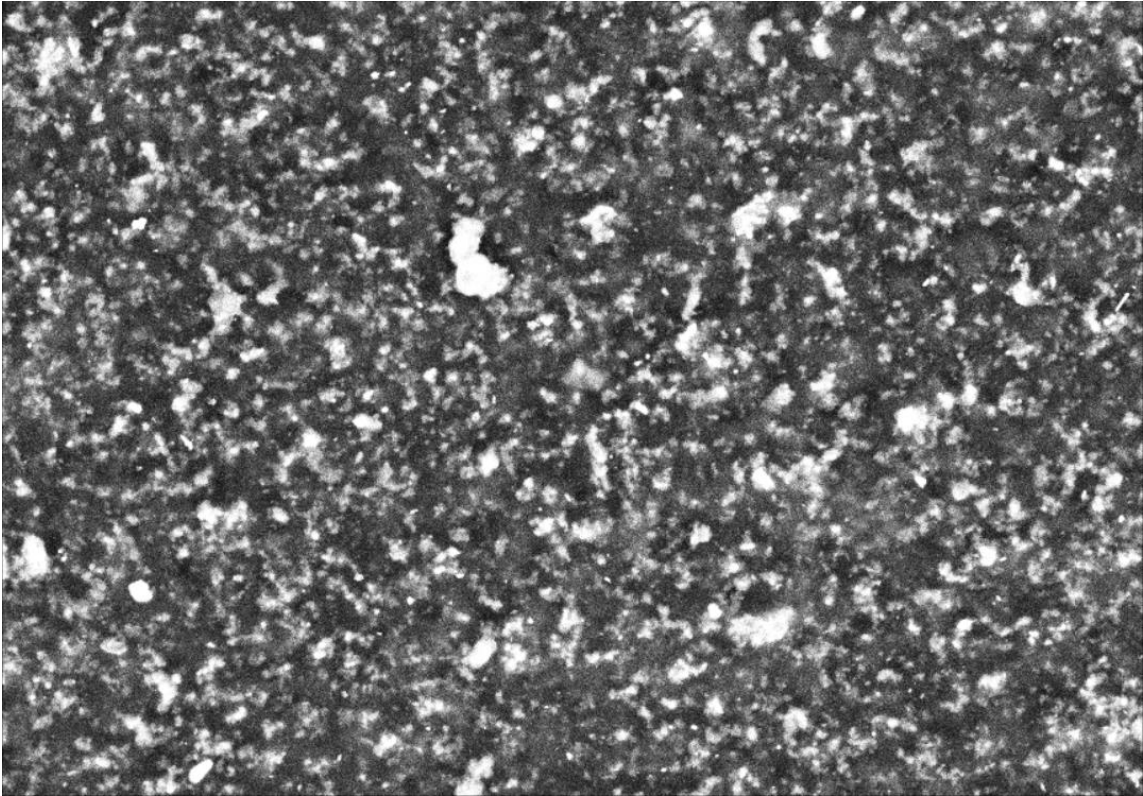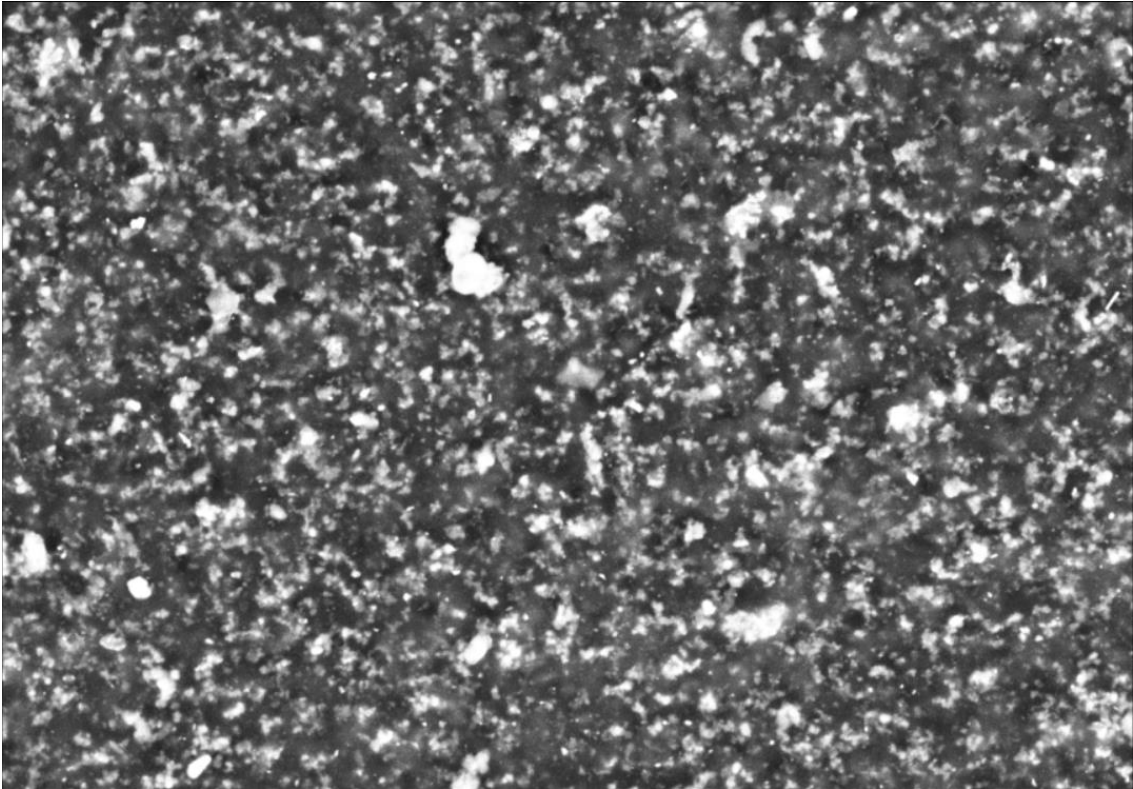
Figure 4.21 Area selected to be examined
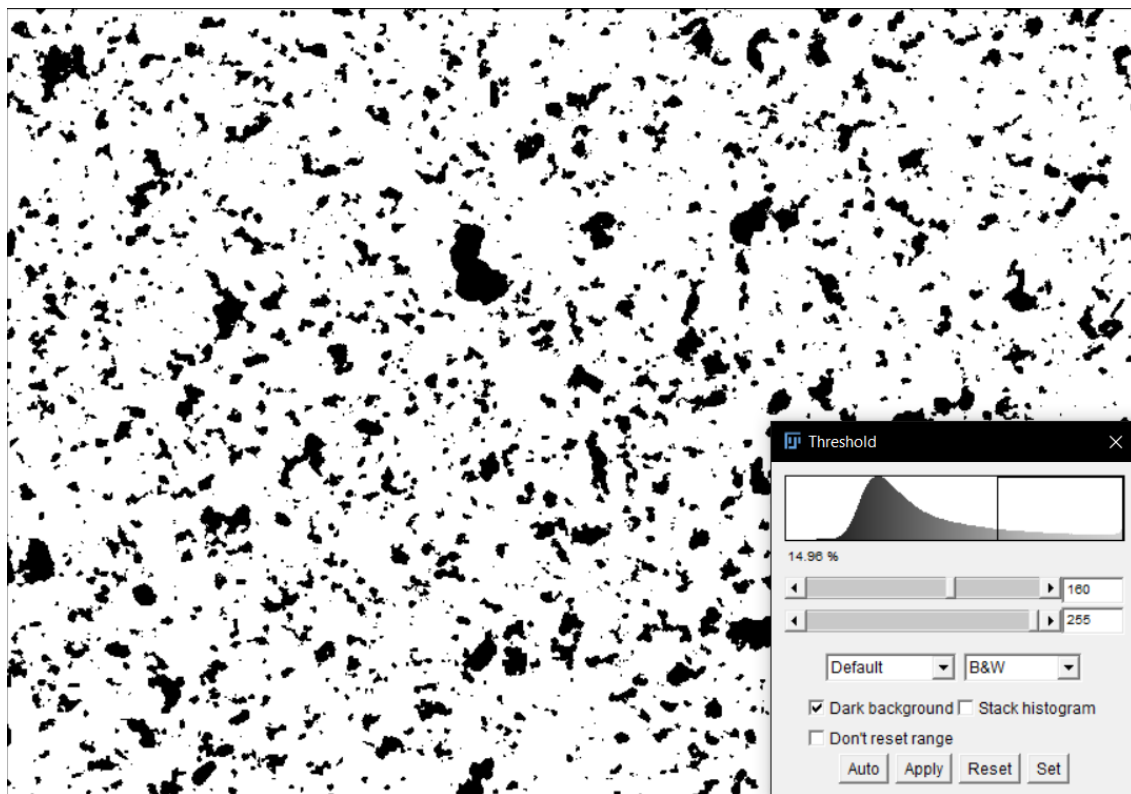

Figure 4.22 Smoothened and cropped image

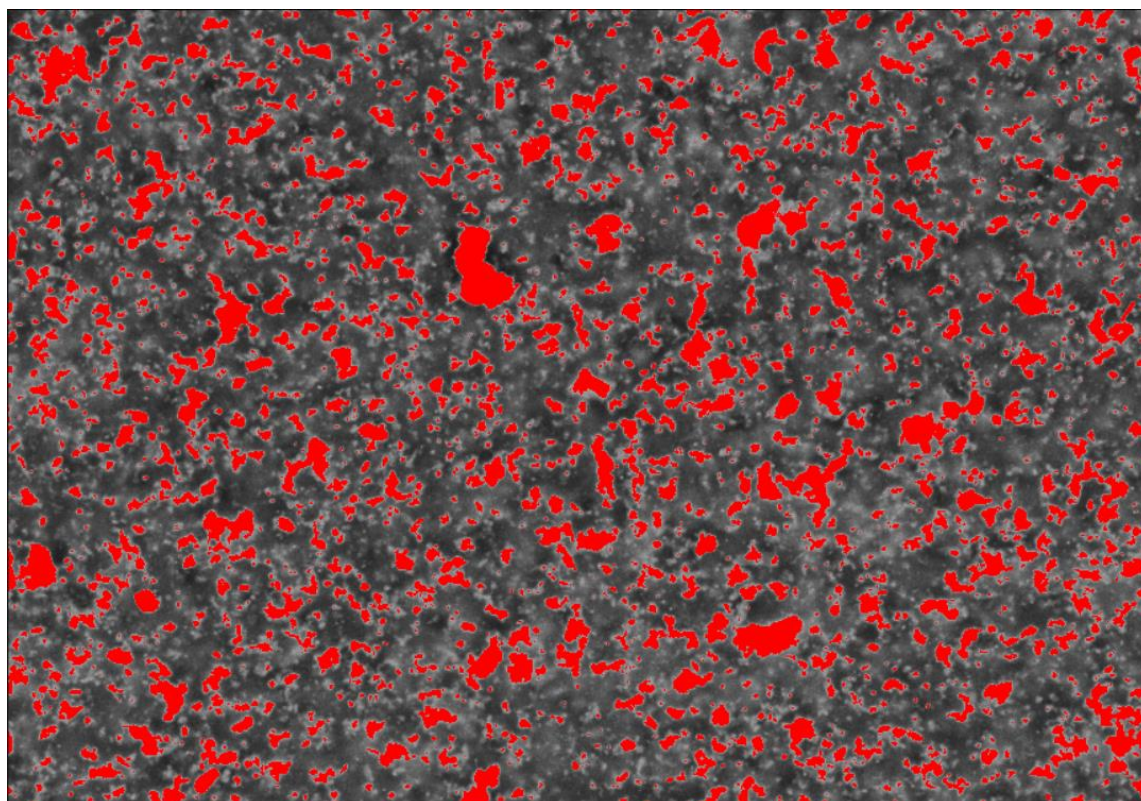**Figure 4.23 Black and white image after setting the threshold**

Figure 4.24 Overlaying the black and white image with the cropped area

Discussion

The analysis was separated into three parts, the first part compared images taken from the new engine mount and the oldest mount to identify if this phenomenon had occurred. Location D was selected, as Zhang et al. (2014) suggested cyclic loading has direct effects on the carbon re-agglomeration [119]. The surface was avoided, as a new mount would not have experienced the same level of oxidation; the influence of oxidation on the imaging and carbon re-agglomeration is unknown.

The second part compared images taken from location D from a different mount to investigate the relationship between carbon re-agglomeration and mileage of the mount. Part three compared samples taken from location C and D from mounts with Mount ID 3,4 and 5.

Existence of carbon re-agglomeration

The carbon particles in those images were categorised into different size groups, and the number fraction of each size group among all particles was calculated. This was achieved using the number of particles of each size group divided by the total amount of particles in each image.

The number of particles at different size ranges was added up across all seven pictures for the same mount to create a larger data pool. The fractions of the amount of carbon particles at different sizes were then calculated, to give an estimation of the percentage of particles at different sizes – the particle size distribution of each mount.

The particle size distribution of the sample taken from location D of the new mount and the sample taken from the oldest mount (Mount ID 5) are shown in Figure 4.25.
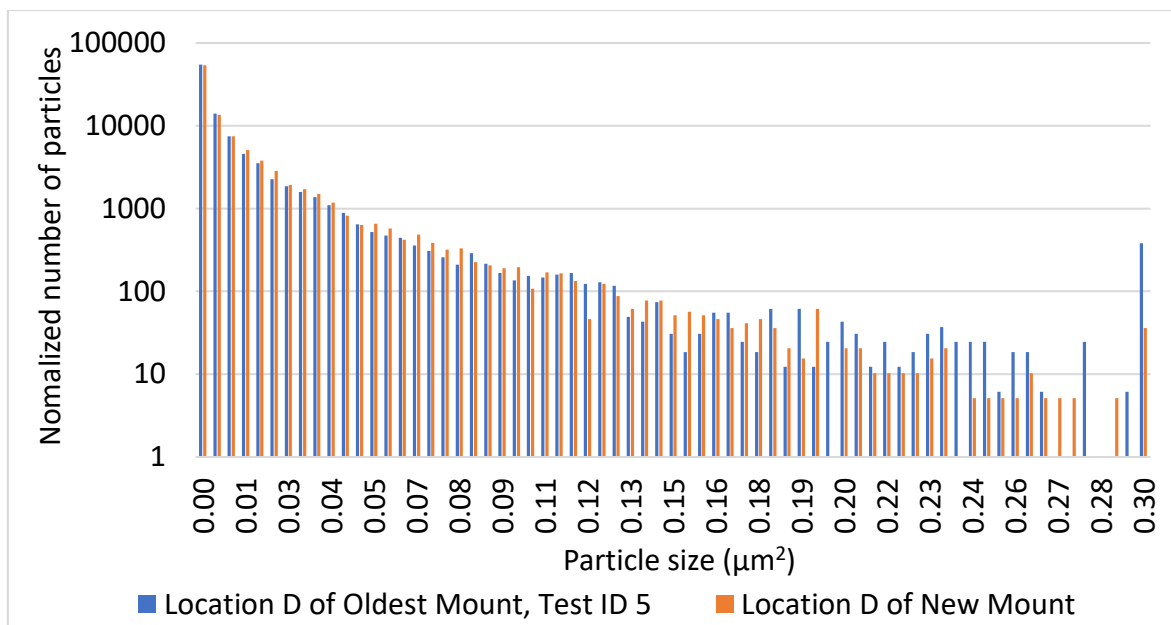
Figure 4.25 Particle size distribution of mount 5 and new mount

To compare the amount of particles at each size group, Figure 4.26 shows the ratio of number of particles at different sizes between the new mount and the oldest mount.
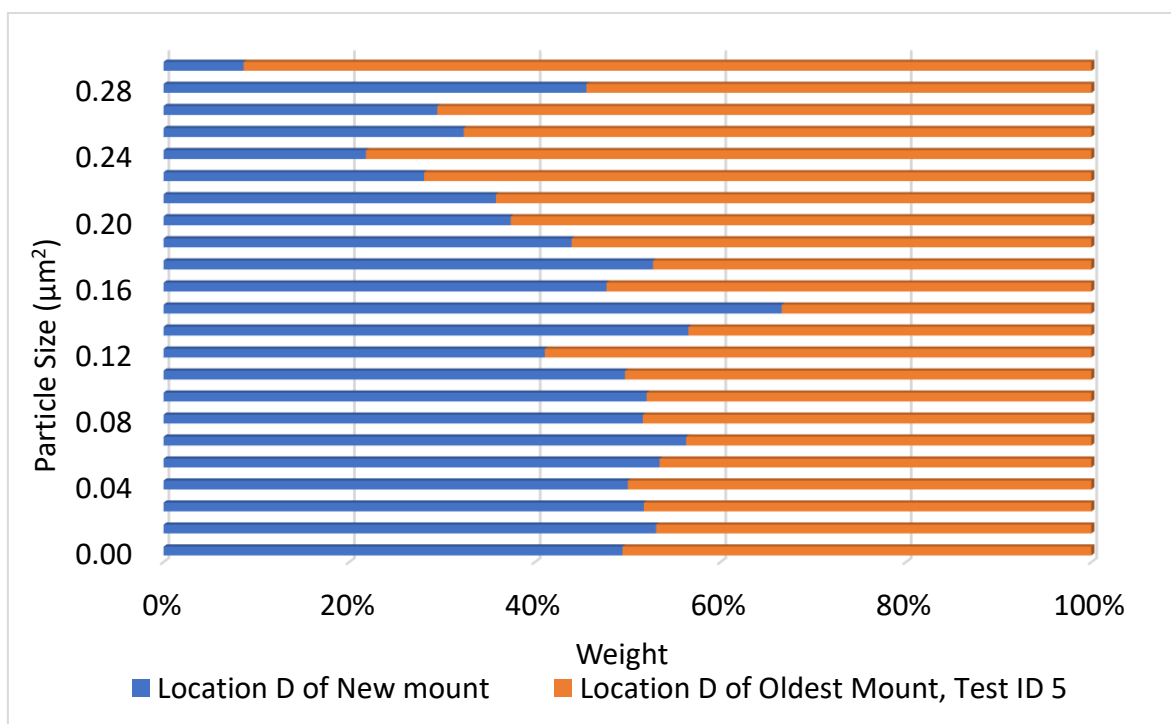
Figure 4.26 Ratio of number of particles at different sizes between new and oldest mount

Clearly, carbon fillers in mount 5 (the oldest mount) have more large aggregates. Although there may be some noise in the results, mount ID 5 showed a higher

occupation rate for particles larger than 0.16 μm^2, which indicates that carbon particles were likely to group up in the used mounts.

Relationship between mileage and carbon re-agglomeration

Figure 4.27 shows the percentage change of particle size distribution of each size group for each used mount. The mileage increases with increasing Mount ID.
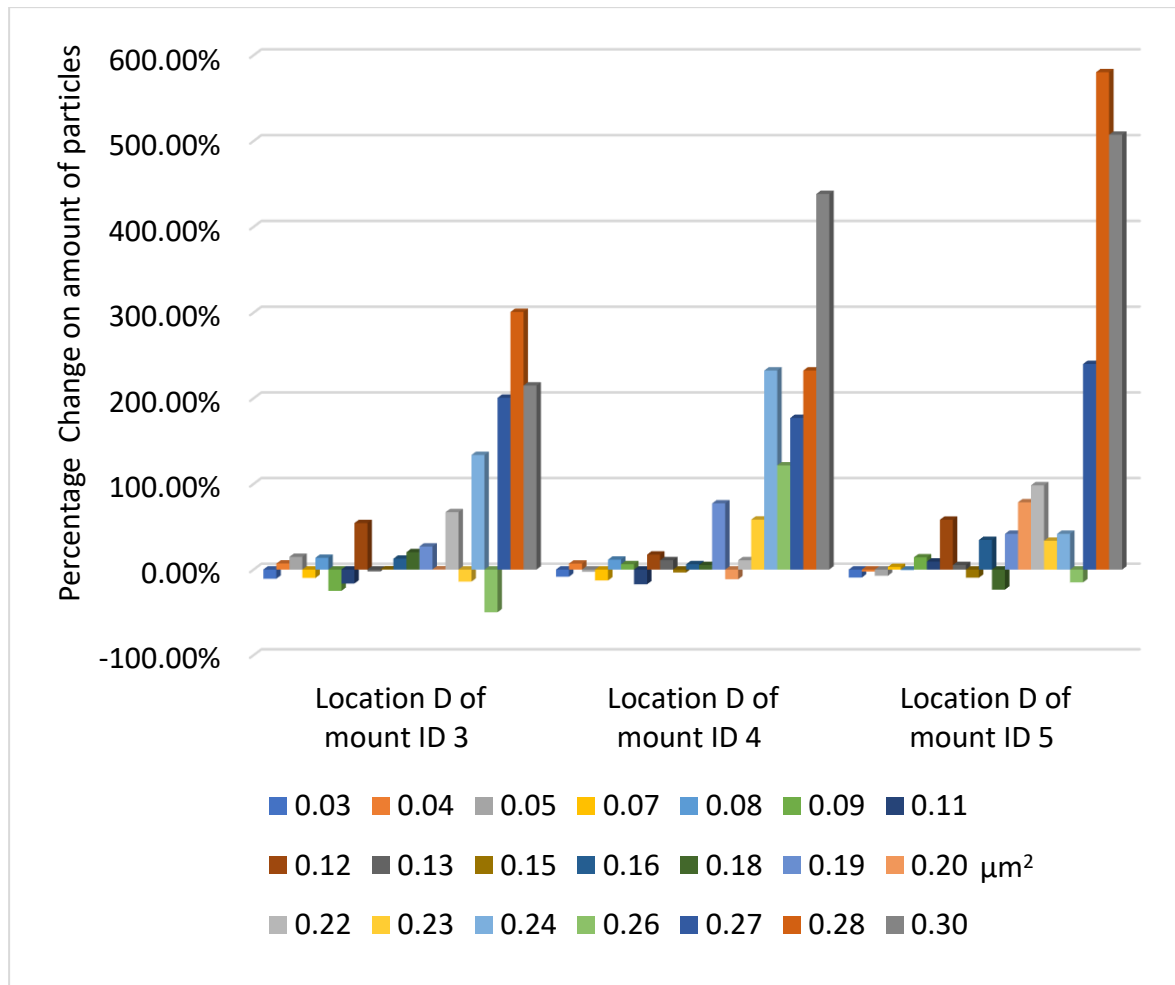
Figure 4.27 Percentage change of particle size distribution for mount 3, 4 and 5

The amount of large particles in mount ID 4 and mount ID 5 is more than large particles in mount ID 3. Although mount ID 5 has 50% more mileage than mount ID 4, the difference between them is not more significant than the difference between mount ID 3 and 4. This suggested that time in service might also be an important factor for this mechanism, as mount ID 4 and 5 only have 2 months difference in time in service. Table 4-7 reviews the ageing conditions of the tested mounts.

Mount ID	Mileage (km)	Time in Service (Months)
3	92041	48
4	96638	57
5	145926	55

Table 4-7 Ageing conditions of the tested mounts

Influence of cyclic loading

For samples taken from locations on each tested mount that never experienced cyclic loading, a bad conductivity was noticed upon testing. As reviewed in Chapter 2.4.3, differences of conductivity could imply differences on the filler arrangement, However, this change of conductivity affected the quality of the SEM image, made the comparisons with samples taken from location D unreliable.

4.2.4 Loss of additives

As mentioned in Chapter 2.4.4, another possible ageing mechanism can be through loss of additives. Gas chromatography coupled with mass spectrometry was selected to investigate this phenomenon due to its ability to determine the concentration and chemical structure of the detected chemicals.

Sample preparation

Gas chromatography works by heating up and vaporising the interested chemicals in a solvent, then separating these chemicals according to their physical properties, as introduced in Chapter 2.6.5. The identity of chemicals can then be analysed with mass spectrometry. In order to investigate loss of additives at regions near the surface and away from the surface, one portion of a 300 milligrams sample was cut from each of location B (surface) and location D (bulk) from both the new mount and the oldest mount. The samples were cut into powder like segments and soaked in dichloromethane (DCM) for 24 hours as DCM can effectively extract additives from the rubber sample. Some insolubles were also extracted, as shown in Figure 4.28, they are likely to be carbon black fillers, escaped due to an increase of space between polymer chains. Therefore, the solvent was filtered before the GC/MS test, as insolubles can damage the machine.

111

Figure 4.28 Insolubles in the solvent

Experimental configuration

After the samples were soaked in DCM for 24 hours, they were loaded into the GC-MS machine. The machine used was the 7250 Accurate-Mass Q-TOF. The samples were heated up from 60 °C to 300 °C with 10 °C per minute increment and 60 minutes constant heating afterwards to clear any remaining chemicals in the column. The time and temperature used have clearly separated the peaks representing each chemical in the solvent. The result would show the retention time of each detected chemical. In the mass spectrometry, the intensities of charged fragments of each separated compound were obtained and compared within the NIST (National Institute of Standards and Technology) database in order to identify the best matching chemical.

Chapter 4 -- Benchmarking of real-world engine mount

Result

Raw results obtained from all samples are shown from Figure 4.29 to Figure 4.32, the graphs plot the time taken for vaporised chemicals to go through the entire GC column. Each peak represents a separated chemical, and the area beneath the peak indicates the concentration of this specific chemical. Significant column bleeding can be observed after 20 minutes, which may indicate that a certain additive in the sample reacts with the column material.
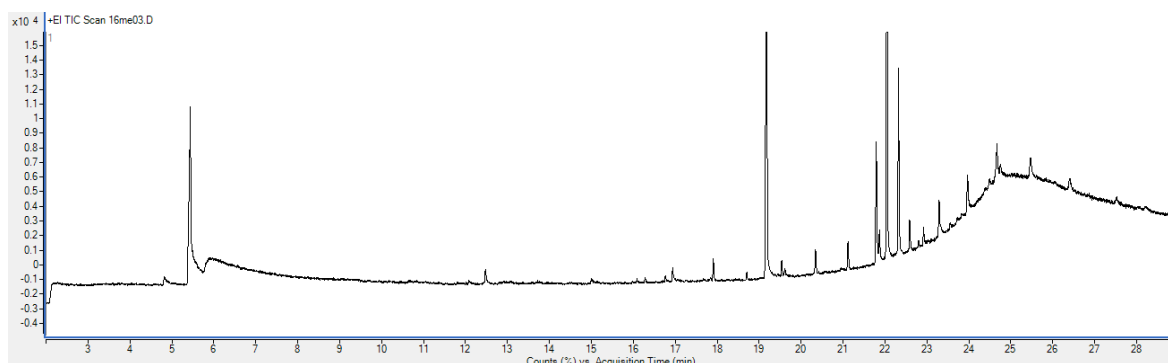
Figure 4.29 GC result of sample taken from location D (bulk) of the new mount
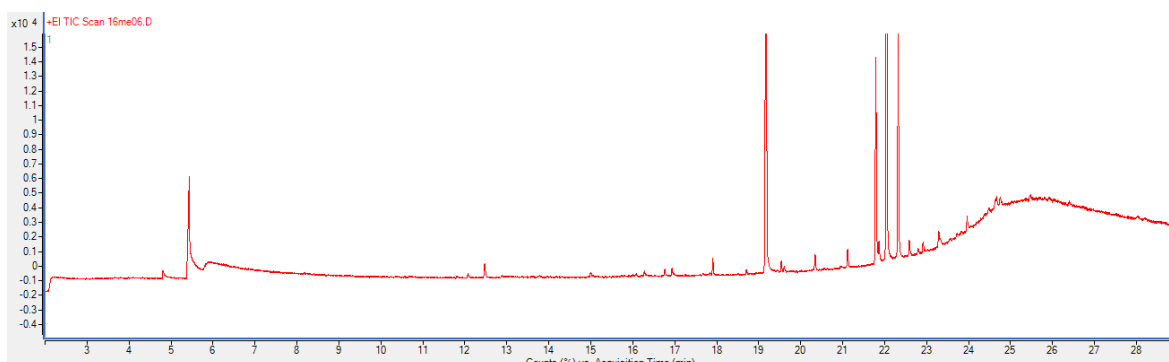
Figure 4.30 GC result of sample taken from location B (surface) of the new mount
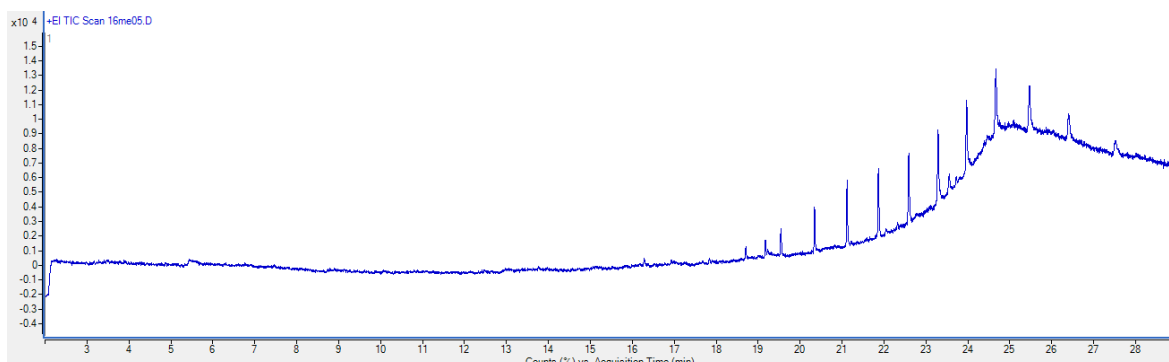
Figure 4.31 GC result of sample taken from location D (bulk) of the oldest mount
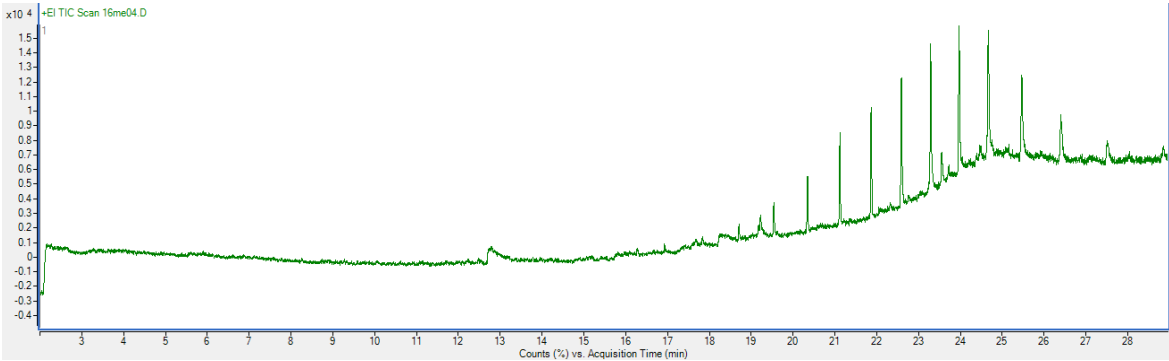
Figure 4.32 GC result of sample taken from location B (surface) of the oldest mount

The peaks would be selected individually, and the mass spectrometry result for the selected regions would be extracted. Figure 4.33 and Figure 4.34 show the mass spectrometry result extraction process for the peak with a retention time of 19.9 minutes, as an example.
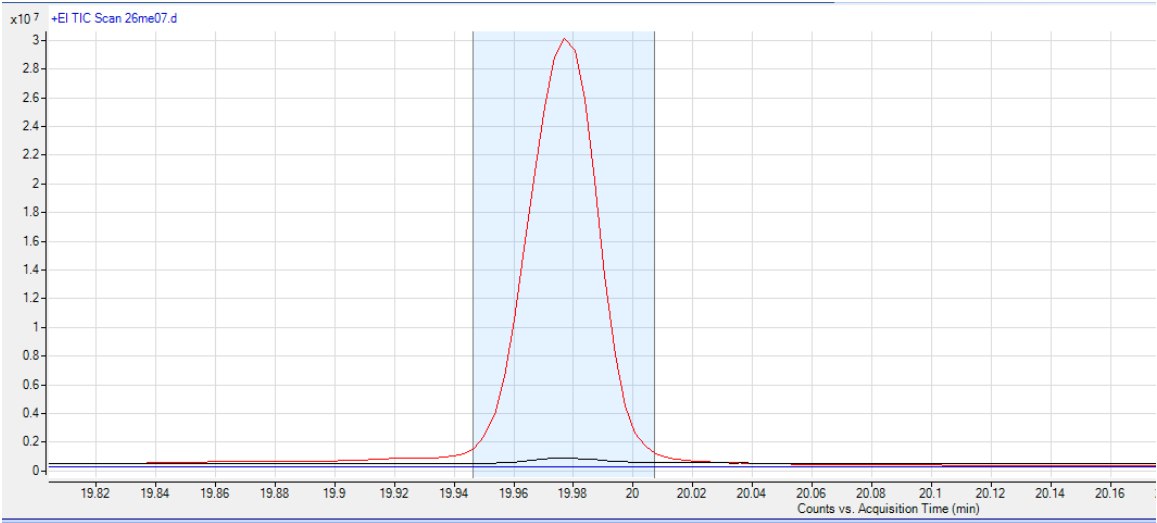
Figure 4.33 Peak with retention time of 19.9 minutes
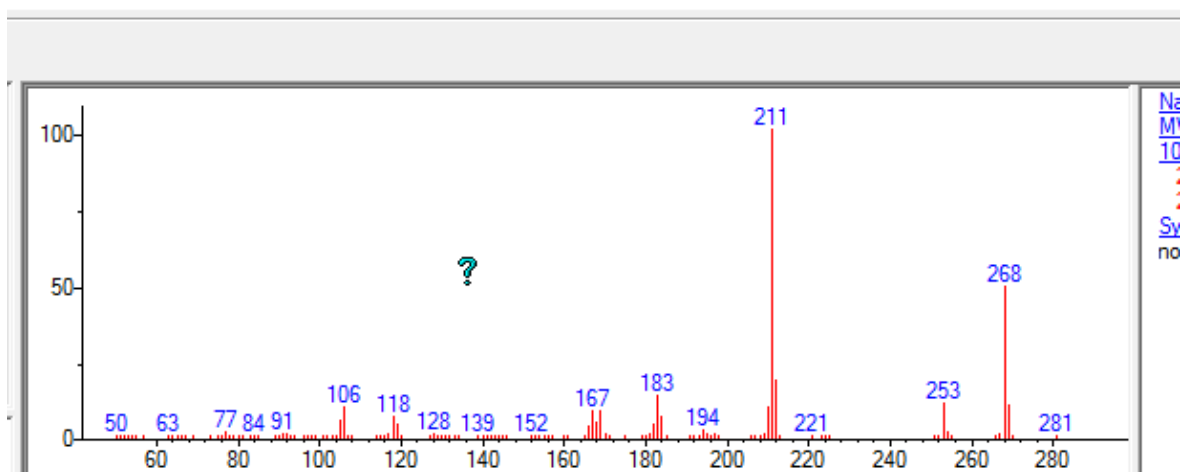
Figure 4.34 Mass spectrometry of peak at 19.97 minutes

The extracted spectra were compared with spectra of known chemicals from the NIST database. The chemicals with similar spectra were listed with a suggested possibility based on how similar the spectra are. The structure of the suggested chemicals and their spectra in the database was also shown. Figure 4.35 and Figure 4.36 illustrates this process for the peak observed at 19.9 minutes.

#	Lib.	Match	R.Match	Prob. (%)	Name
⊞1	M	913	922	98.0	1,4-Benzenediamine, N-(1,3-dimethylbutyl)-N'-phenyl-
⊞2	R	799	837	98.0	1,4-Benzenediamine, N-(1,3-dimethylbutyl)-N'-phenyl-
3	M	661	680	0.98	Benzoimidazol-2-one, 1-adamantan-1-yl-1,3-dihydro-
⊞4	M	627	655	0.25	3,4-Dimethoxyphenol, tert-butyldimethylsilyl ether
⊞5	R	610	727	0.13	1,4-Benzenediamine, N-(1-methylethyl)-N'-phenyl-
⊞6	M	591	632	0.06	Cyclohexene, 3-butyl-3,5,5-trimethyl-1-(trimethylsilyloxy)
⊞7	R	583	714	0.13	1,4-Benzenediamine, N-(1-methylethyl)-N'-phenyl-
⊞8	M	583	682	0.13	1,4-Benzenediamine, N-(1-methylethyl)-N'-phenyl-
9	M	578	718	0.04	Pyrimidine, 2-(4-pentylphenyl)-5-propyl-
10	M	576	838	0.03	Propanoic acid, 3-(1,2,3,5,6,11b-hexahydro-11H-pyrr
11	M	576	707	0.03	6-Methyl-2-pyridinecarbaldehyde phenylhydrazone
12	M	570	605	0.03	Benzaldehyde, 2-butoxy-5-(4-methylphenyl)-
13	M	568	702	0.02	6H-Pyrido[2,3-b][1,4]benzodiazepin-6-one, 5,11-dihyd
14	M	559	561	0.02	Uleine, dihydro-
15	M	555	741	0.01	2,6-Diethyl-4-phenylpyridine
16	M	554	700	0.01	1-Methyl-1,2,6,7,8,9-hexahydropyrro[1,2,3-j,k]carbazo
17	M	553	665	0.01	Indole, 1-acetyl-3-(3,5-dimethylpyrazol-1-yl)-
⊞18	M	551	552	0.01	Dasycarpidan-1-one
19	M	549	564	0.01	3,4-Quinolinedicarbonitrile, 5,6,7,8-tetrahydro-2-(4-mor
20	M	548	698	0.01	2-(4-Fluorophenyl) indole
21	M	545	671	0.01	β-Carboline, 1-methyl-3-hydroxymethyl-
22	M	542	805	0.01	4-Amino-1-phenylpyrazolo(3,4-e)pyrimidine
⊞23	M	542	669	0.01	Phenol, 2-[[(4-methylphenyl)imino]methyl]-
24	M	538	712	0.00	Acridine-9-thiole
25	M	538	663	0.00	3-Dimethylaminodiphenylmethane
26	M	535	706	0.00	6-Ethyl-2,3-dimethyl-4-phenylpyridine
⊞27	R	535	557	0.00	Equilin
28	M	534	686	0.00	4-Amino-4'-hydroxystilbene

Figure 4.35 Suggested chemical matches with spectrum peak at 19.9 minutes
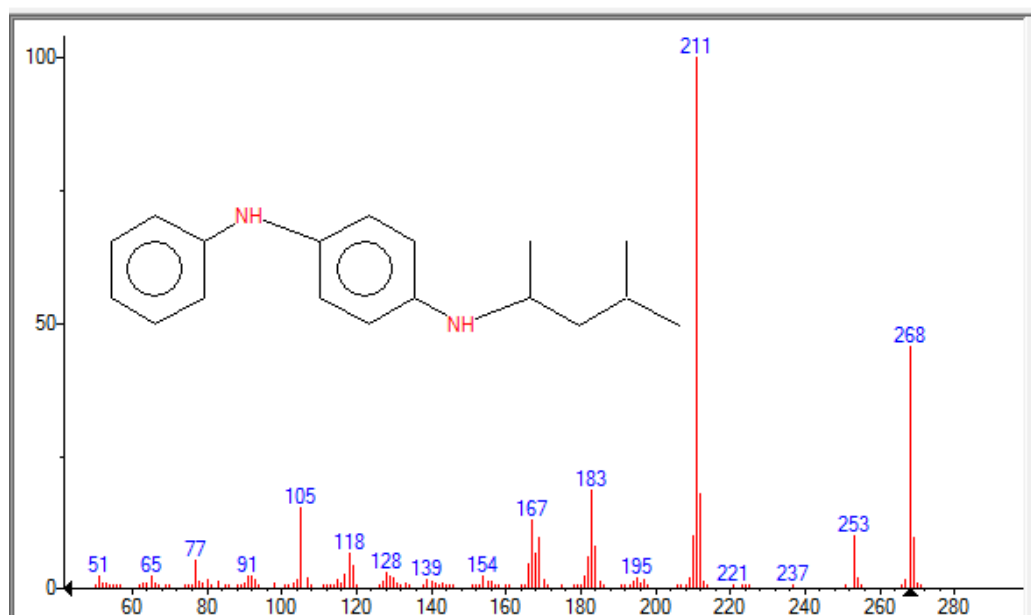
Figure 4.36 Chemical structure with the highest matching rate for the peak at 19.9 minutes

Figure 4.37 shows the peaks representing the identified chemicals in the new mount bulk region sample. Table 4-8 shows the peak retention times and corresponding chemical compounds.

The sample was sent by the material supplier of the engine mount and many additives may relate to the company's intellectual property and were not published. The names of those additives were unable to be defined by the software. Thus, some of the peaks had significant changes were unable to be identified. Only the peaks with known chemical structure and functionalities are investigated.
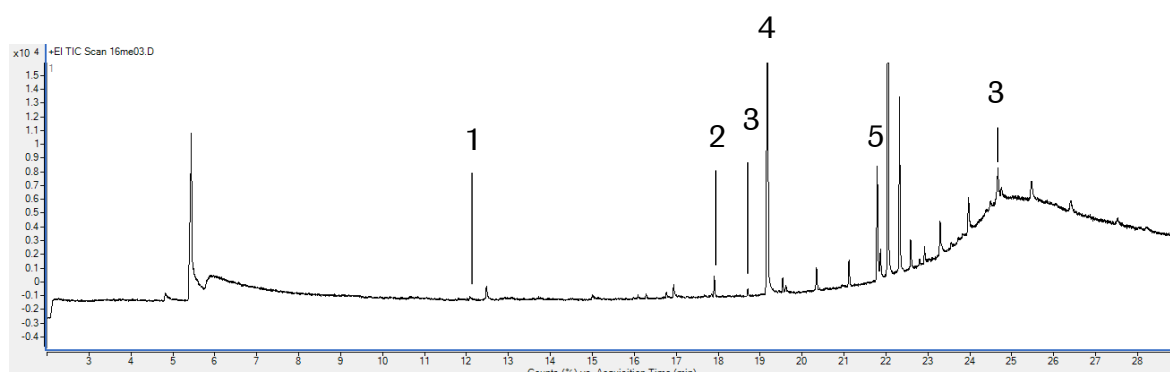
Figure 4.37 Identified peaks in the GC result of sample from the bulk region of the new sample
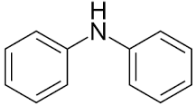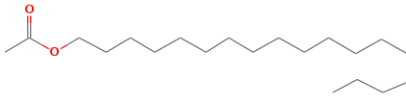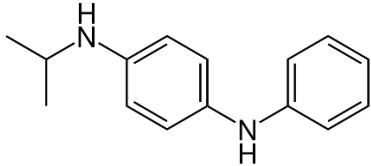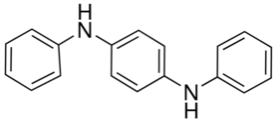
Peak number	Retention time	Chemical structure	Name Functionality
1	12		**Diphenylamine** Antioxidant
2	17.9		**Octadecyl acetate** Plasticiser
3	17; 17.8; 18.6 19.5; 20.3; 21.1; 21.9; 22.7; etc	Higher alkanes from C23 – C35	**Paraffin wax** Antiozonant, preventing cracks
4	19.9		**6PPD** Antioxidant
5	21.8		**DPPD** Antiozonant

Table 4-8 Possible corresponding chemical for detected peaks

Discussion

Figure 4.38 plots the results from new and oldest samples from location B (at the surface region). Baselines differences were caused by the different maximum chemical concentration in the solvents, it is better to make the comparison based on the differences between areas beneath the peak instead of height. Solvent volatilisation was noticed after the samples were prepared and before the test. Since the time taken for each test was long and DCM is a relatively volatile solvent, samples tested later (sample from the oldest mount) tend to have a higher concentration.
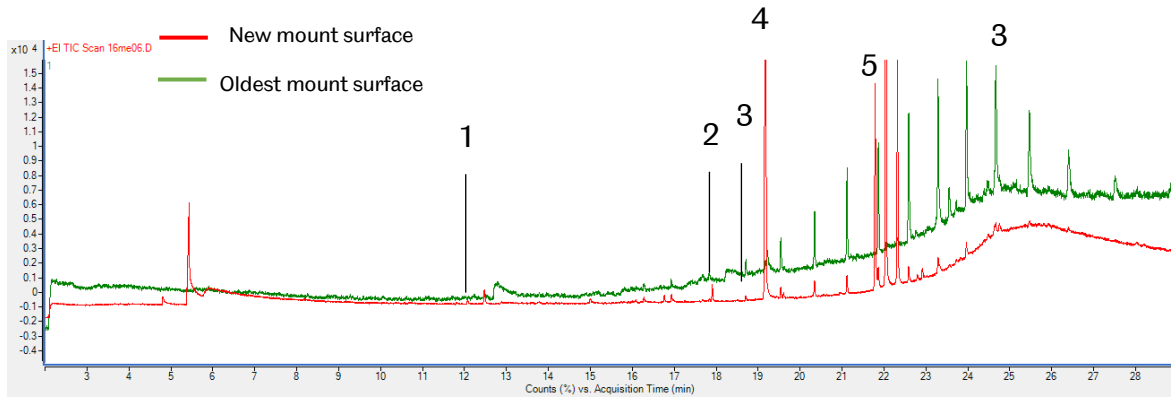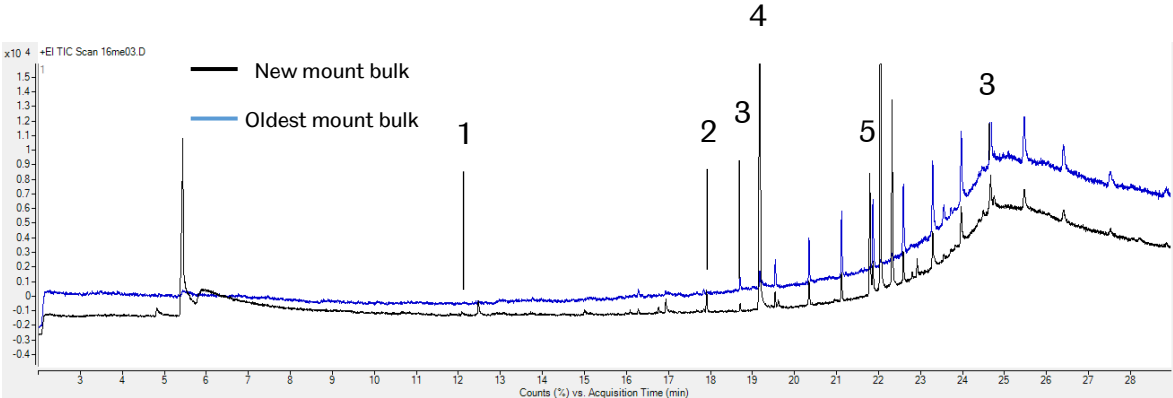
Figure 4.38 GC-Result from location B of aged (green) and unaged (red) mount

Figure 4.39 to Figure 4.42 illustrates the changes on the peaks representing the identified chemicals in the surface region of the material. The reduction of intensities on these peaks represent the existence of loss of additives.
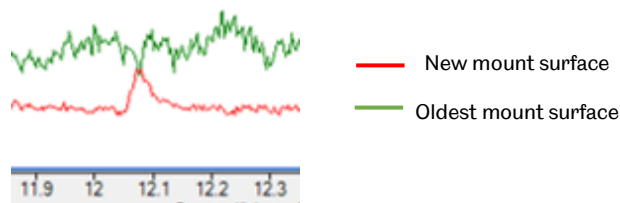
Figure 4.39 Peak 1 - diphenylamine in the surface region

The peak representing diphenylamine has vanished, where diphenylamine is a widely used antioxidant in the industry.
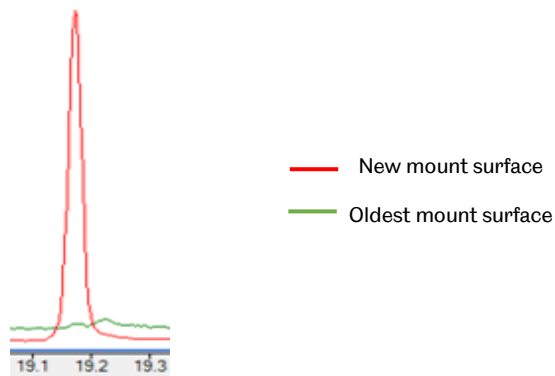
Figure 4.40 Peak 4 - 6PPD in the surface region

The peak representing 6PPD has also almost vanished, it's the highest peak in the GC result of the new mount sample which shows it has a high concentration in the material. 6PPD is also a wildly used antioxidant. The depletion of diphenylamine

and 6PPD at the surface region means the material became vulnerable to oxidative degradation during ageing.
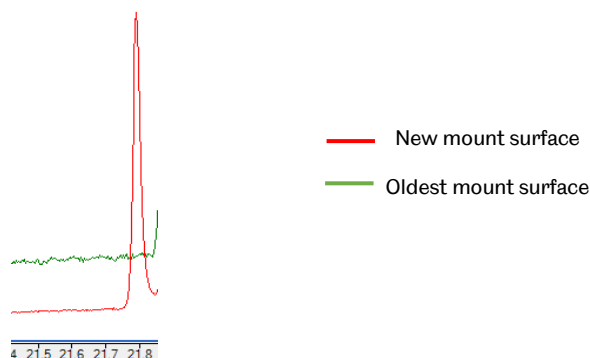
Figure 4.41 Peak 5 – DPPD in the surface region

The peak representing DPPD, a common antiozonant disappeared in the result representing the oldest mount. This suggests that the material became vulnerable to ozonation during ageing.
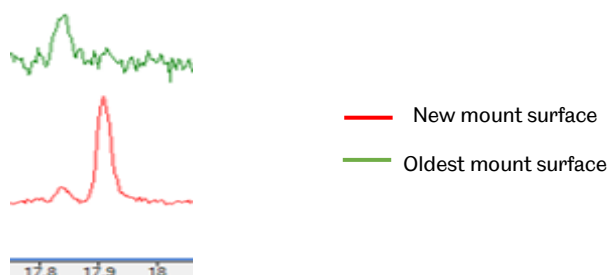
Figure 4.42 Peak 2 - octadecyl acetate in the surface region

The peak representing octadecyl acetate was not shown in the oldest mount. Octadecyl acetate is a commonly used plasticiser and the depletion of it could lead to an increase of elastic modulus as mentioned in Chapter 2.3.

Figure 4.43 plots the results from new and oldest samples from location D.

Figure 4.43 GC result from location D of aged (blue) and unaged (black) mount

Figure 4.44 to Figure 4.47 illustrates the changes on the peaks of identified chemicals at the bulk region of the material.
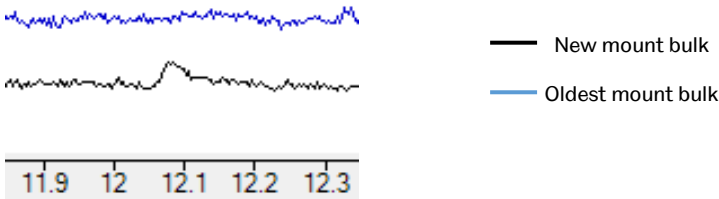
Figure 4.44 Peak 1 – diphenylamine in the bulk region
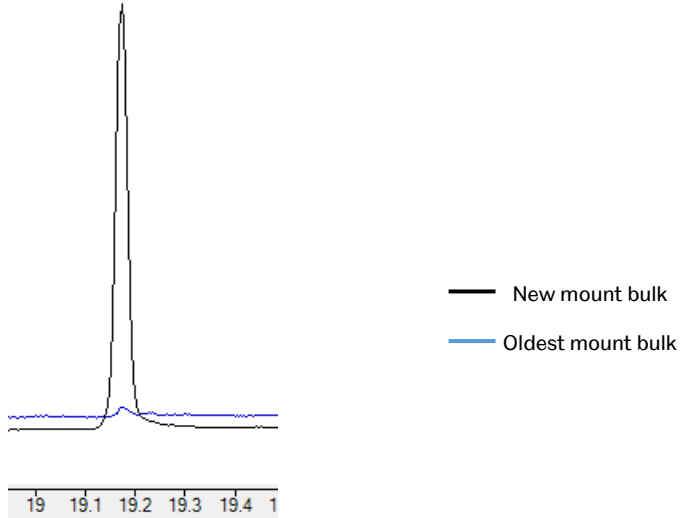
Figure 4.45 Peak 4 - 6PPD in the bulk region

120
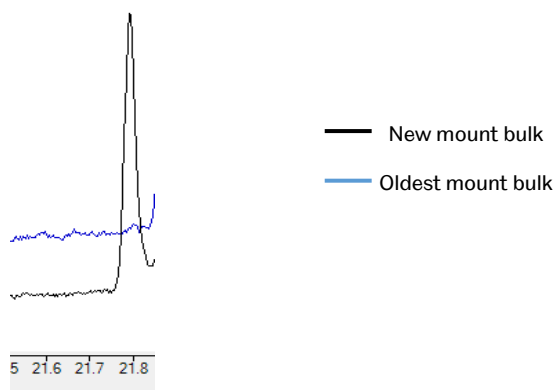
Figure 4.46 Peak 4 DPPD in the bulk region

The peaks representing diphenylamine 6PPD and DPPD have vanished or dramatically reduced. The concentration reduction of these additives in the bulk region represents the consumption of antioxidants and antiozonants in the surface region, which triggered the migration of additives.

Figure 4.47 Peak 3 - octadecyl acetate in the surface region

The concentration of octadecyl acetate decreased in the bulk region of the material, together with the loss of antioxidants and antiozonants, showed the additives that migrated in the entire rubber component. No significant difference was noticed between the behaviour of additives in the surface region and in the bulk region. The antioxidants that migrated from the bulk to the surface postponed the effect of oxidative degradation. The loss of plasticiser in both regions means the stiffening of the material during ageing caused by loss of additives was throughout the rubber component in the mount.

4.2.5 Cracks

Cracks can also affect the mechanical properties of the specimen. When deforming the mount surface, no discontinuation was noticed, which means no visible cracks were found on the mount surface. SEM is the most commonly used method to observe smaller cracks, due to the edge sensitivity of secondary electrons described in Chapter 2.6.4. As described in Chapter 2.4.5, potential cracks in the mount are likely to affect the sample's mechanical performance, as it changes the stress distribution and adds friction inside the material.

Sample preparation

Three samples containing 4mm of the mount surface with thickness and width of 1.5 mm were prepared with the cryo-fracture technique. Due to the bad flatness of the actual surface, the observation was made at multiple locations on the cross-section of the mount. When considering the geometry and functionality of the rubber part on the engine mount, cracks are likely to propagate in the radial and azimuthal directions due to the compression and bending the rubber part suffers. As described in Chapter 2.4.1, cracks are especially likely to be generated on the surface due to ozonation. Thus, the near-surface regions of the cross-section shown in Figure 4.48 were selected to be examined. Samples were cut from a new mount and Mount ID 5, the oldest mount, is the one that has the highest possibility to have cracks.

Figure 4.48 Sampling location for finding cracks on used mount

Experimental configuration

Multiple samples were loaded, the operator navigated through edges corresponding to the mount surface of each sample and took pictures when the crack was observed.

Result

Only one large crack was found on all examined surfaces, which is shown in Figure 4.49. It was captured on the surface of the oldest mount.
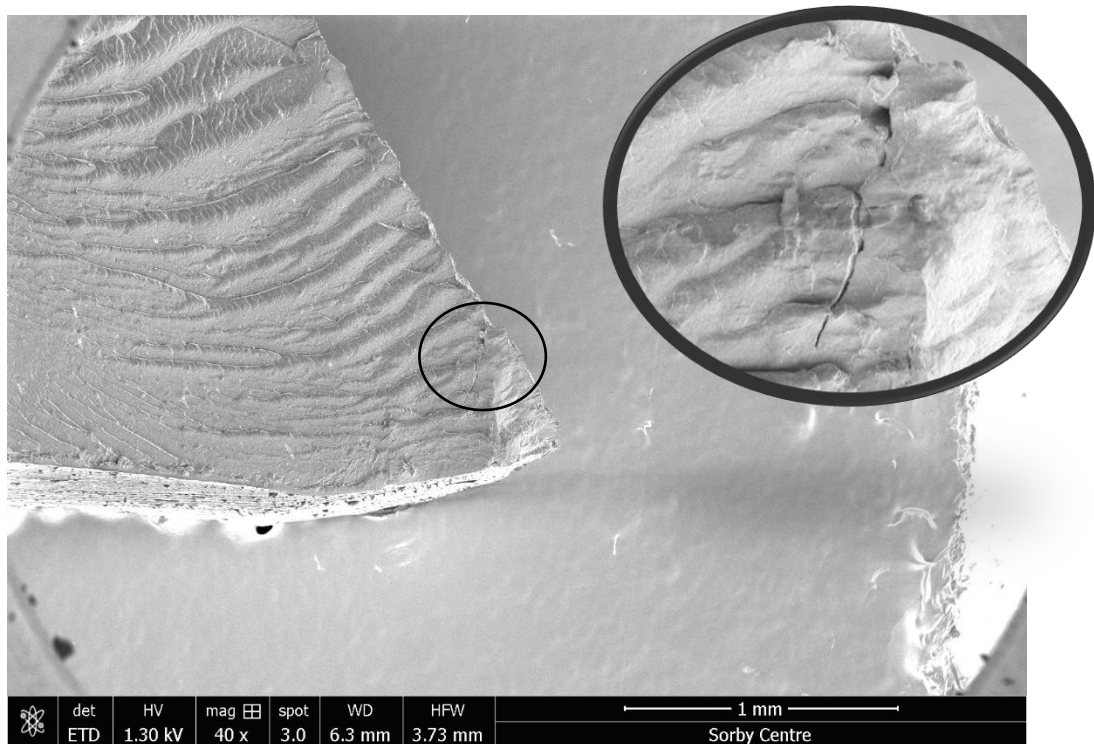

Figure 4.49 Crack on the surface of Mount ID 5, the oldest mount

Discussion

Only a single crack was found from a 1 cm long surface. There is no evidence of mass formation of cracks in the used engine mount, thus, further investigation on cracks was stopped.

4.3 Summary

This chapter has shown that the elastic modulus of rubber taken from used mounts increased during ageing. Material characterisations have shown that, among the possible ageing mechanisms, evidence has been found for post-curing and thermal degradation, oxidative degradation, carbon re-agglomeration and loss of additives. In order to build up a more rigorous understanding of these ageing mechanisms, they needed to be investigated under environments with controllable ageing conditions.

Due to the limitation on the sample amount, the number of repeating samples were cut to minimum. This does not affect the conclusions have been drawn from the previous tests, as the tests have been repeated for a few times showed that the error is significantly smaller than the changes observed.

CHAPTER 5.   ARTIFICIAL AGEING (IN AIR)

The previous chapter showed how the elastic modulus, crosslink density, carbon filler distribution and quantity of additives intensities of the rubber in the engine mount were affected by ageing. As the samples taken from used engine mounts were unable to provide repeatable data due to different driving preferences of drivers, samples with more controllable ageing conditions are required. As described in Chapter 2.5.2, artificial ageing is a common method for investigating ageing behaviour of rubber materials. This was, therefore, identified as a suitable method for investigating samples aged in an oven, with the presence of air.

5.1   Ageing parameters

5.1.1   Material

Due to the limitation on the amount of the actual mount material, a few 6mm thick rubber sheets with the same composition as the mount rubber were acquired from the material supplier. The sheets were produced by compression moulding instead of injection moulding, which may affect the material's properties while maintaining a similar ageing behaviour. A set of samples taken from a new engine mount was also aged in this section to allow a comparison to be made. Most tests were not repeated, as the expected properties changes are larger than errors generated in the experiment. This is for ensuring the remaining material is sufficient for further tests.

5.1.2   Atmosphere

This test was performed in air, as the engine mount was exposed to air during service. Anaerobic accelerated ageing, which is used to investigate the bulk material's properties that are expected not to be affected by air, will be discussed in the next chapter.

5.1.3 Temperature

The temperature was set to 95 °C, the highest temperature the mount could have experienced in Dubai according to the product supplier, in order to ensure the oven aged samples did not experience higher temperatures than likely in real life. All samples were put in the oven above a thick layer of sand to maintain their surrounding temperature when opening the oven.

5.1.4 Length of time

The purpose of the artificial ageing is to investigate how properties of the rubber samples change in the presence of air. The length of the artificial ageing needed to be long enough to cover what the rubber could have experienced in real life. Thus, the entire artificial ageing process could be considered a combination of accelerated ageing and environmental ageing, with the accelerated ageing part representing the time the vehicle is not being used and the environmental ageing part representing when the vehicle is in operation.

For the accelerated ageing part, according to the Arrhenius Equation mentioned in Chapter 2.5.2, the ageing under room temperature (in a garage) for the duration of 52 months can be achieved in 10 days under 95 °C. The calculation is shown in Equation 5-1.

$$\frac{RT}{Q_{10}^{[(T_{AA}-T_R)/10]}} = AAT$$

RT	Q_{10}	T_{AA}	T_R	AAT
Real time	Reaction rate increase for every 10 Kelvin increase	Accelerated ageing temperature	Real temperature	Accelerated ageing time
52 months	2 (as recommended for unknown reactions)	95 °C	23 °C (recommended room temperature)	10 days

Equation 5-1 Calculation for accelerated ageing time

126

For the environmental ageing part, among the examined retrieved mounts, the highest average mileage per month is 2806 km/month. This suggests that the average mileage per day is 66 km. Assuming an average driving speed of 50 km/h, the time that the engine experienced 95 °C is no more than 130 days. Thus, together with the 10 days from the accelerated ageing part, the total length of the test was set to 140 days.

5.2 Investigation of properties with ageing

Changes to elastic modulus, crosslink density, carbon filler distribution and additives intensities have been confirmed to be related to ageing in the previous chapter. These properties were, therefore, chosen to be measured for the accelerated aged samples. To avoid any uncertainties caused by differences on testing environments such as room temperature and humidity, all tests for the same interested property were performed at the same time, after all the samples had been taken out and acclimatised.

5.2.1 Elastic modulus:

DMA tests were applied to measure how the elastic modulus of the material changes under a controlled ageing environment. It also verified whether the sheet samples could be used to represent the rubber material in the engine mount.

Test method

DMA tests were performed on the Metravib VA2000 again under 1 Hz and 30 °C. Measurements of elastic modulus were made under 10% dynamic and static strains.

Sample preparation

Samples taken from both the new engine mount and the rubber sheet were prepared for the elastic modulus measurement. The samples were prepared manually as described in Chapter 4.1.3. The samples were cut to 5mm x 6mm x 16mm ±1.5mm blocks.

Sampling frequency

The sampling frequency for the samples is shown in Table 5-1.

Sample type	Sampling amount	Sampling frequency
DMA test (mount)	1	Every 7 days
DMA test (sheet)	1	Every 7 days

Table 5-1 Sampling elastic modulus samples

Result

Figure 5.1. shows the result of this testing on the mount samples. The 88 day old sample broke during the test and therefore is not recorded.
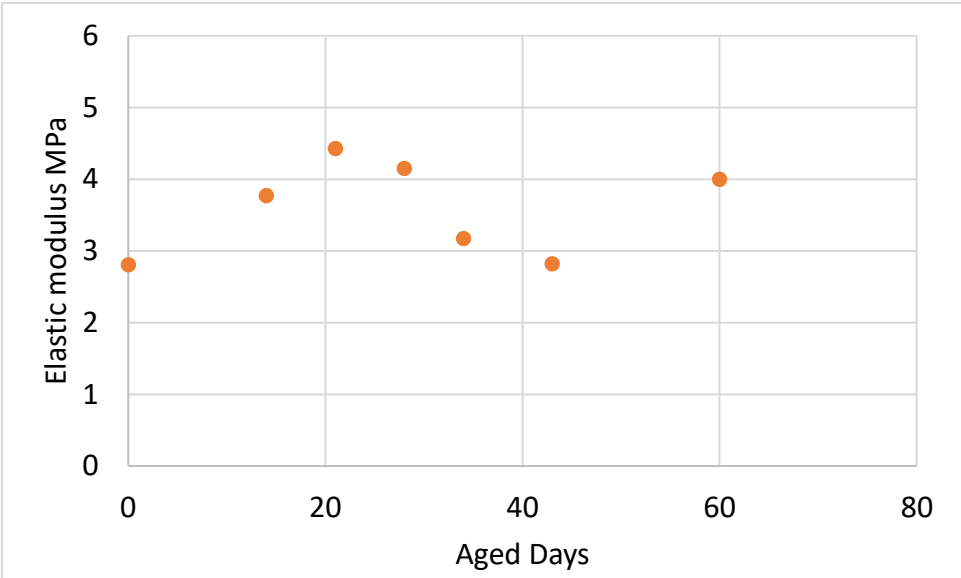
Figure 5.1 Elastic modulus of aged mount samples

It can be seen that there is an increase to a peak at around 21 days, followed by a subsequent decrease until around 43 days. A final increase is observed after this, which is likely to be related to a final loss of resilience of the material, as the samples aged 88 days were broken during the test.

Figure 5.2 shows the elastic modulus of the sheet samples. A similar trend was observed; the sheet material did not break at 88 days into ageing, which could be caused by the expected property difference from different manufacturing methods.
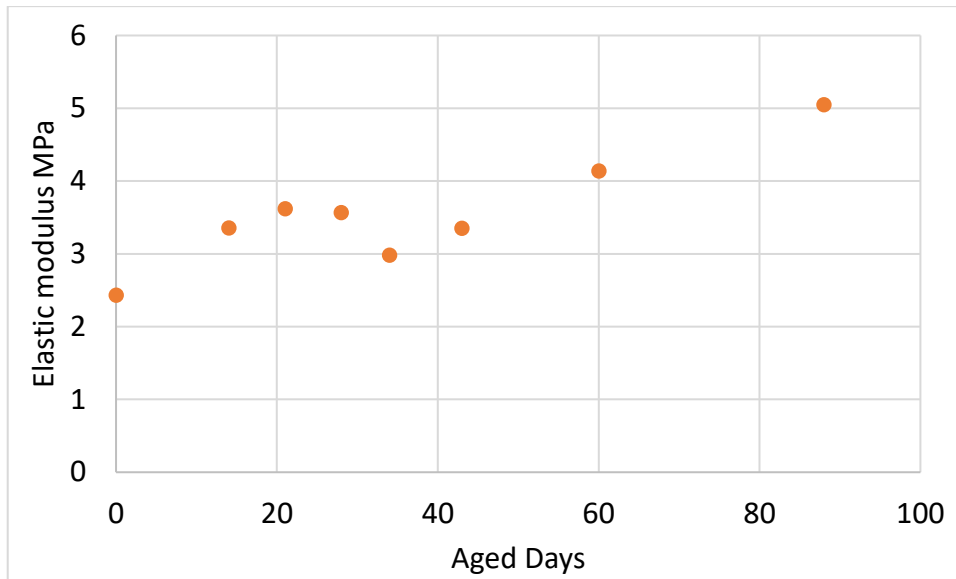
Figure 5.2 Elastic modulus of aged sheet samples

Discussion

All results indicated the same ageing behaviour, for both the sheet samples and the mount samples under both strain conditions. Figure 5.3 shows the percentage changes of elastic modulus for both materials under 10% dynamic and static strain conditions.
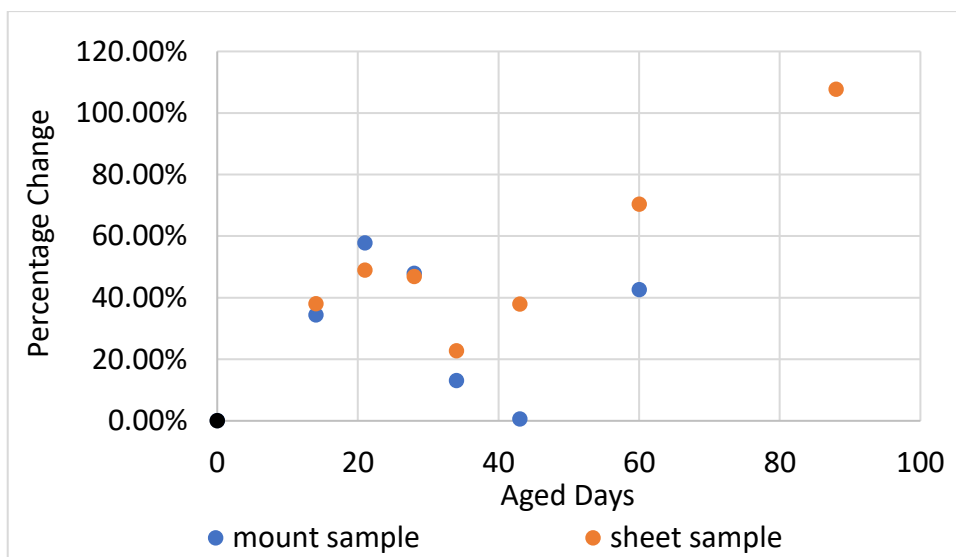
Figure 5.3 Change of elastic modulus of aged mount and sheet samples under 10% dynamic strain

These results suggested that, although the exact properties may differ between the mount and the sheet material, the sheet material should provide a good indication of trends caused by ageing and are likely to share similar microstructure changes.

5.2.2 Crosslink density

Crosslink density of samples taken from different locations in the used engine mount had different ageing behaviours. As a property closely related to the elastic modulus of the material, the swelling technique was, therefore, conducted on the artificially aged samples.

Test method

Crosslink density was investigated with the swelling technique described in Chapter 4.2.1.

Sample preparation

The samples were cut manually to 4mm x 4xmm x 4mm ±1mm cubes using the method described in Chapter 4.2.1. The critical depth for oxidation for similar materials under 95 °C ranges from 4mm to 6mm based on the theory mentioned in Chapter 2.4.1, which means oxidation mainly takes place at the first 1-2mm, as the effects exponentially decay with depth. The difference between the whole sample and the surface removed sample can be used to identify the impact of oxidative degradation observed in previous tests. Two sets of sheet samples were, therefore, prepared, in order to investigate the effect of oxidative degradation - the first set was tested as normal, the second set were tested with 1mm removed from each surface.

Sampling frequencies

The samples were sampled in rates shown in Table 5-2.

Sample type	Sampling amount	Sampling frequency
Mount sample	1	Every 7 days
Sheet sample (surface included)	1	Every 7 days
Sheet sample (surface removed)	1	Every 7 days

Table 5-2 Sampling frequencies for crosslink density tests

Result

Figure 5.4 shows the crosslink densities of the tested samples. The crosslink density of the mount samples raised to a peak at 21 days into ageing followed by a subsequent decrease until 43 days. The measured crosslink density of mount samples continued to increase afterwards.

The surface included sheet samples that showed a decrease of crosslink density and reached a trough at around 28 days, followed by a subsequent increase till the end of the ageing period.

The crosslink density of the surface removed sheet samples increase for the sample 5 days into ageing, followed by a decrease until 34 days into ageing, then continued to increase afterwards.
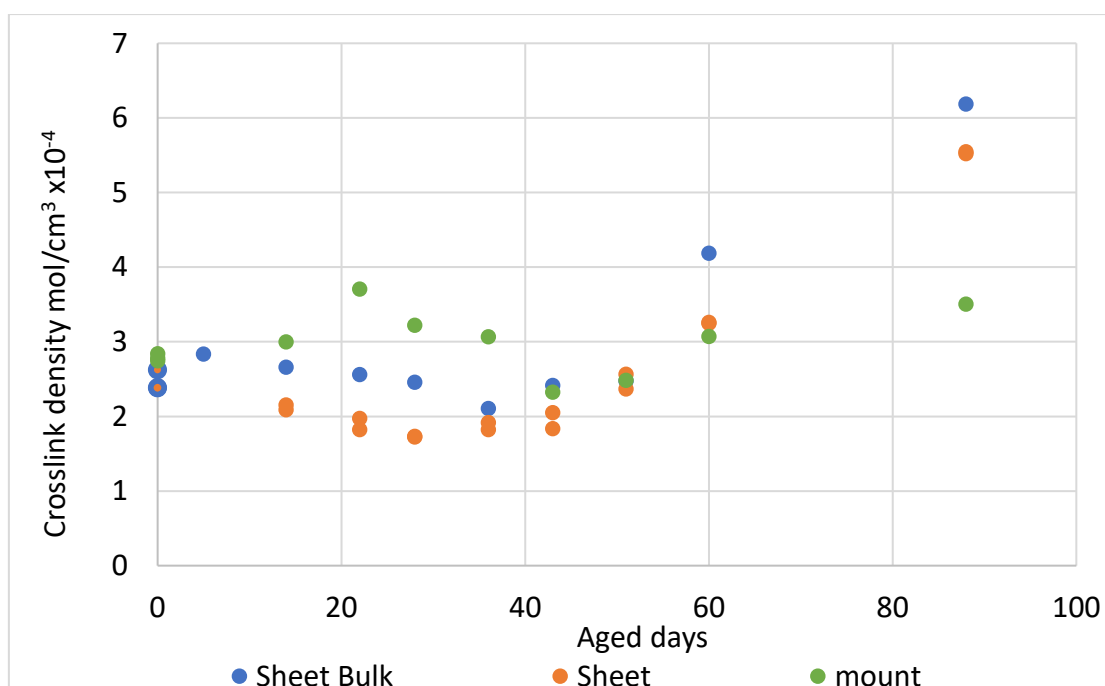
Figure 5.4 Crosslink density changes of aerobic aged samples

Discussion on crosslink density

The different crosslink density changes between the sheet and mount samples could be caused by the different chain arrangements as suggested by Skrobak (2016), mentioned in Chapter 2.3.1 [61]. Although the composition of the materials were the same, different manufacturing methods could have affected how

crosslinks formed internally and led to a difference on the post-curing and thermal degradation behaviour.

At any particular days into ageing, the crosslink density of the sheet sample is higher than the surface removed sheet sample. Thus, the decrease of crosslink density was caused by oxidative degradation. This decrease kept throughout the 90 days ageing period in the near surface region of sheet samples.

5.2.3 Filler re-agglomeration

Increase of the aggregates' sizes were observed on the rubbers taken from used engine mounts. Its impact on artificially aged samples needs to be investigated.

Test method

SEM images were taken by the Helios NanoLab SEM machine described in Chapter 4.2.3 to look at the carbon filler distribution of the material. SEM images were taken from the new sheet sample and the aged sheet sample. The images were processed and analysed with the methods used in previous tests.

Sample preparation

The SEM samples were prepared using the cryo-fracture technique described in Chapter 4.2.3. The samples were prepared to be thinner than 1mm to reduce the problems caused by charging.

Sampling frequency

The sheet sample aged the most was tested, which was 137 days into ageing. Seven SEM images were taken from the new sheet sample and another seven from the 137 days aged sheet sample.

Result

Figure 5.5 and Figure 5.6 show example images taken from the new sheet sample and the 137 days aged sheet sample, respectively. The rest can be seen in Appendix B xii to xv. The analysing method was the same as in Chapter 4.2.3.
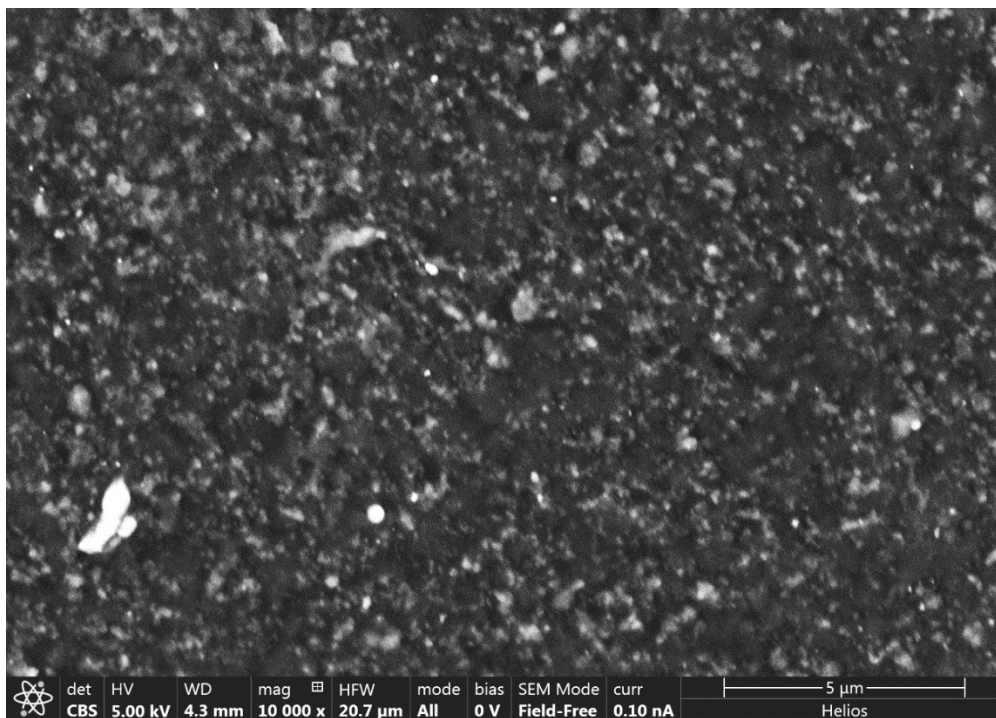
Figure 5.5 New sheet sample
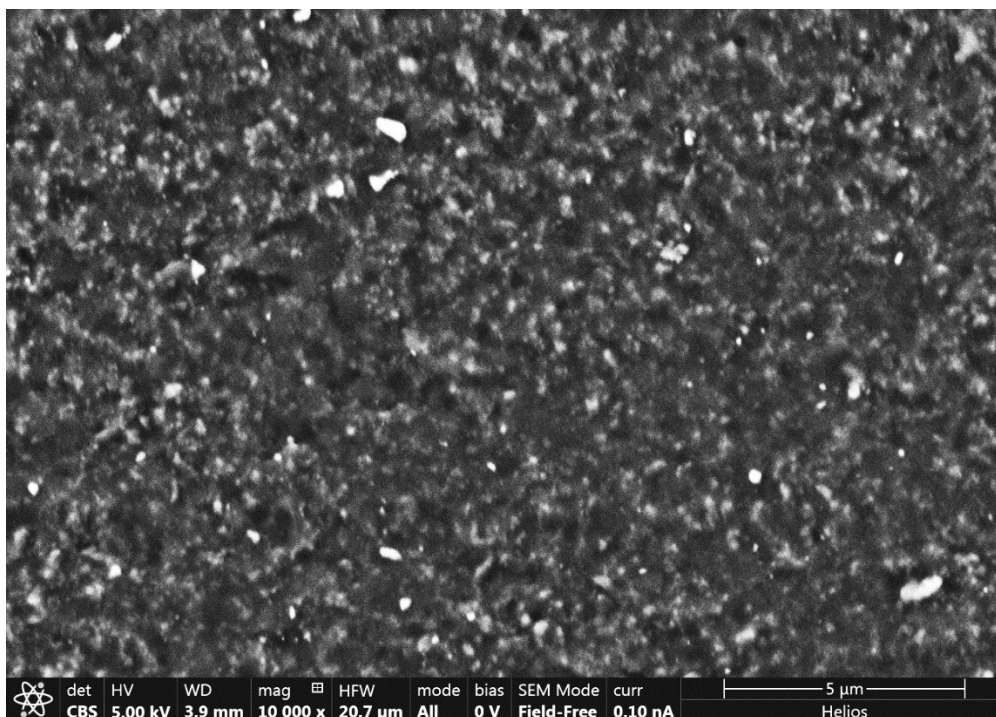
Figure 5.6 Sheet sample aged 137 days

Discussion on carbon re-agglomeration

Figure 5.7 shows the ratios of the amount of carbon particles between the two samples under different size ranges.
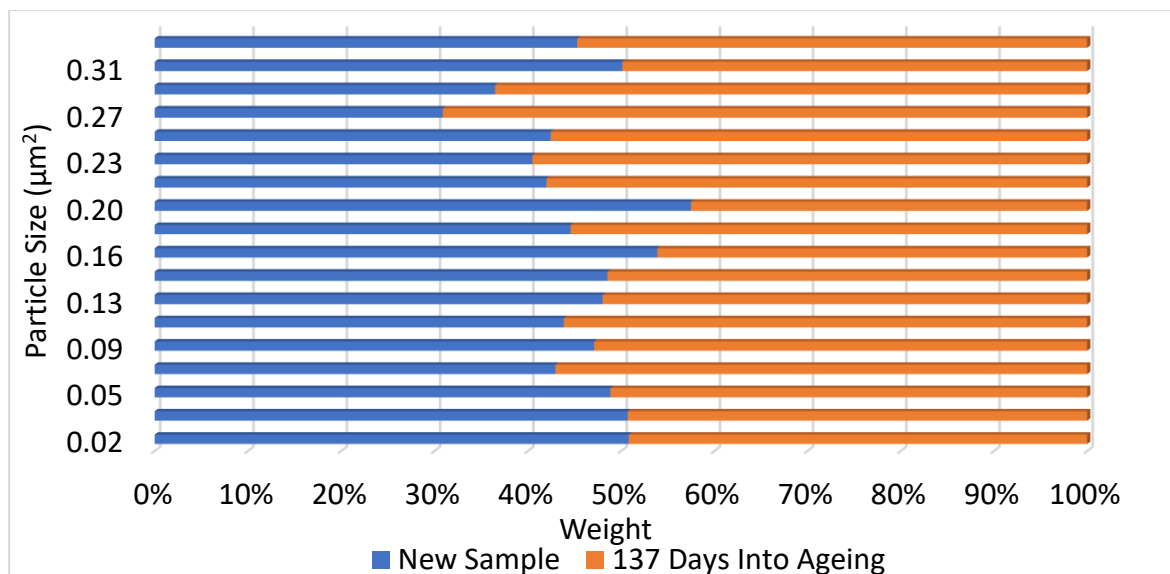
Figure 5.7 Comparison of size distribution between new and aerobic aged sample

It can be seen that although the difference between the two samples were not as significant, the 137 days aged sample showed a higher proportion of large aggregates, as was seen in aged mounts in Chapter 4.2.3. This will be discussed further in Chapter 7.

5.2.4 Loss of additives

Many additives that relate to the properties of the rubber material have depleted inside the used engine mount. To investigate how variations on the concentration of these additives are related to the elastic modulus changes, additive intensities were measured for sheet samples at different days into ageing.

Test method

Additives of differently aged sheet samples were extracted from the sample by DCM, as mentioned in Chapter 4.2.4. The solutions were then tested by the same GC-MS machine.

Sample preparation

Samples were prepared to powder like fragments as mentioned in Chapter 4.2.4. In the previous test, it was noticed that the long experimental time made the DCM solvent used to extract the sample evaporate while queuing. To normalise the

concentration between samples, the same amount of dodecane was added into each extracted solvent. Intensities of each interested additive could be normalised by the concentration of dodecane before comparison. The filtering process was also removed, the solvent was carefully drawn with a pipette with smaller inlet nozzle to prevent extracting the insoluble material. To obtain more accurate results, the drawing amount of the GC machine also increased from 0.1ml to 0.3ml to enhance the signal and reduce the effect of noise.

Sampling frequency

Sheet samples were sampled in dated listed in Table 5-3. The sampling was more frequent at the beginning of the test as the additives were expected to deplete faster in the beginning. One extra sample was taken on day 0 and day 56, to investigate the error in the test. One extra sample was introduced for day 0 and day 56, to provide knowledge about uncertainties introduced in the sample preparation process.

Sampling days	0	4	7	16	24	36	45	56	72	92
Increment (days)	0	4	3	8	8	12	11	11	16	20

Table 5-3 GC-MS sampling days

Result

Figure 5.8 to Figure 5.10 shows the results from a new sheet sample, a 16 days aged sample and a 72 days aged sample. The peaks were analysed using the method described in Chapter 4.2.4. Table 5-4 shows the peaks match well with chemicals that have known functionalities; more peaks were defined due to the improvement of the test method. As described in Chapter 4.2.4, many peaks were unable to be clearly identified and are, therefore, not discussed here.
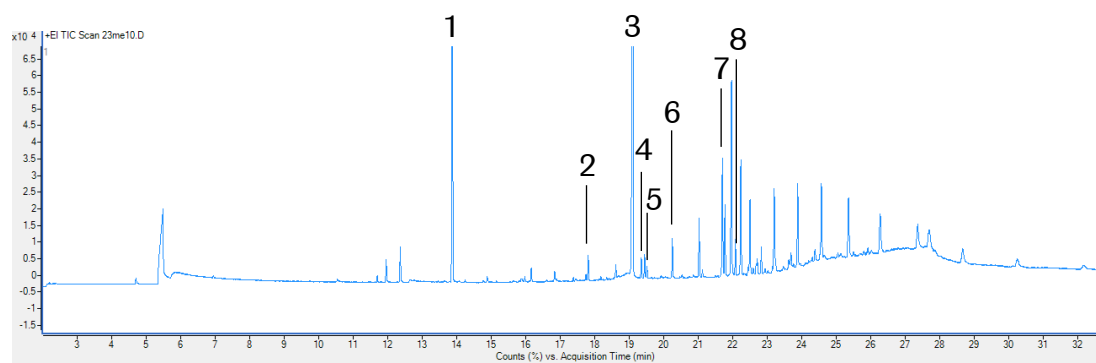
Figure 5.8 GC result for a new sheet sample
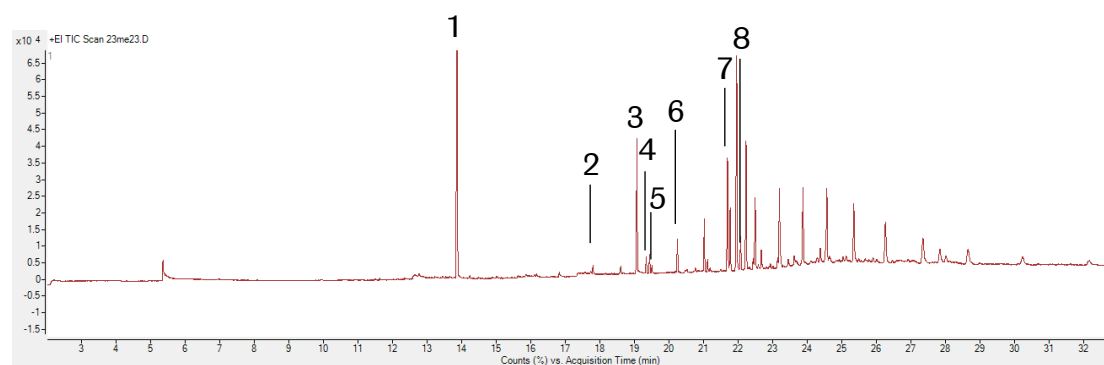
Figure 5.9 GC result for sheet sample aged 16 days
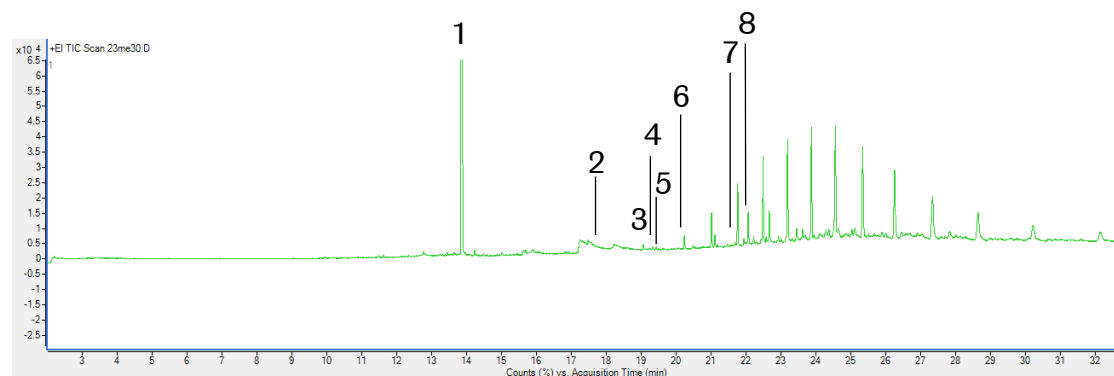
Figure 5.10 GC result for sheet sample aged 72 days
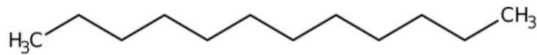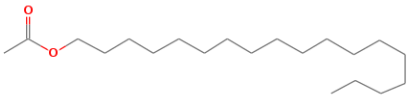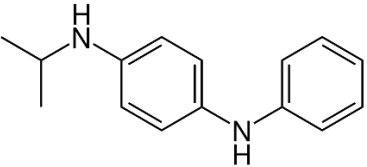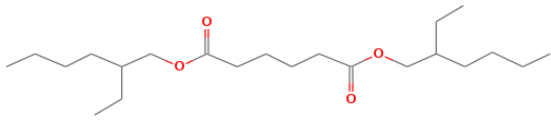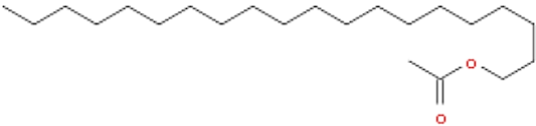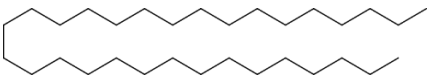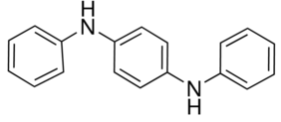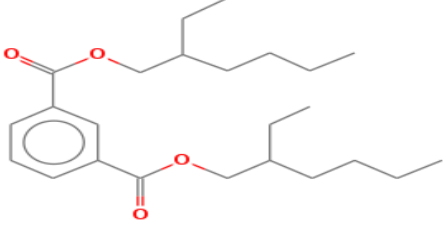
Peak number	Retention time	Chemical structure	Name and functionality
1	13.85		**Dodecane**, reference chemical
2	17.9		**Octadecyl**, Plasticiser 1
3	19		**6PPD**, Antioxidant
4	19.3		**Adipol 2EH**, Plasticiser 2
5	19.5		**Eicosyl acetate**, Plasticiser 3
6	17; 17.8; 18.6 19.5; 20.3; 21.1; 21.9; 22.7; 23.2; etc	Higher Alkanes from C23 – C35	**Paraffin wax**, protection layer, plasticiser
7	21.8		**DPPD**, Antiozonant
8	22.05		**Dioctyl isophthalate**, Plasticiser 4

Table 5-4 Possible names and functionalities of identified chemicals

Figure 5.11 shows the built in integral function for identifying the concentration of a certain chemical. Due to the potential vaporisation of solvent before the test, all results were normalised by the concentration of dodecane before further comparisons. A table of measured concentration of these chemicals are included in Appendix C i.
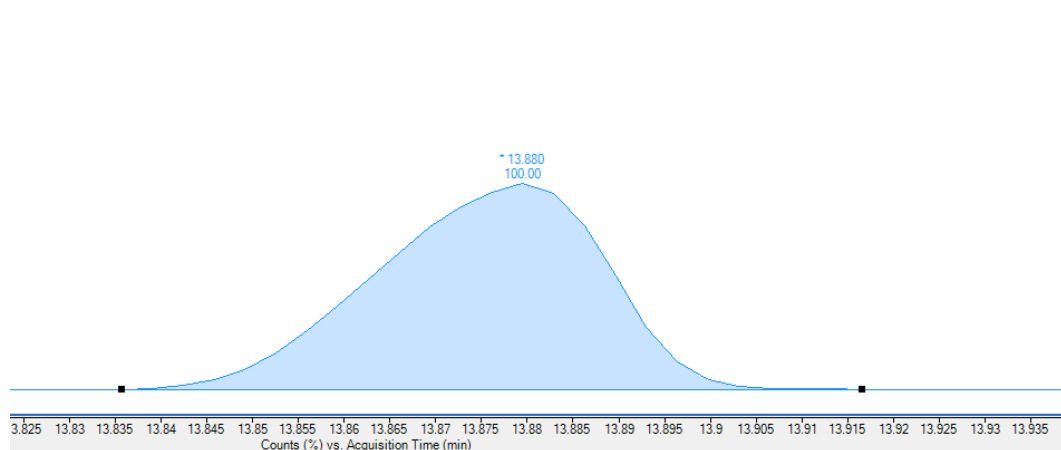
Figure 5.11 Built in integral function

Discussion

Figure 5.12 shows the concentration changes of dodecane in the new sample, 16 days aged sample and 72 days aged sample. The concentration of dodecane increases with time, which confirms the possible phenomenon of solvent evaporation mentioned in Chapter 4.2.4.
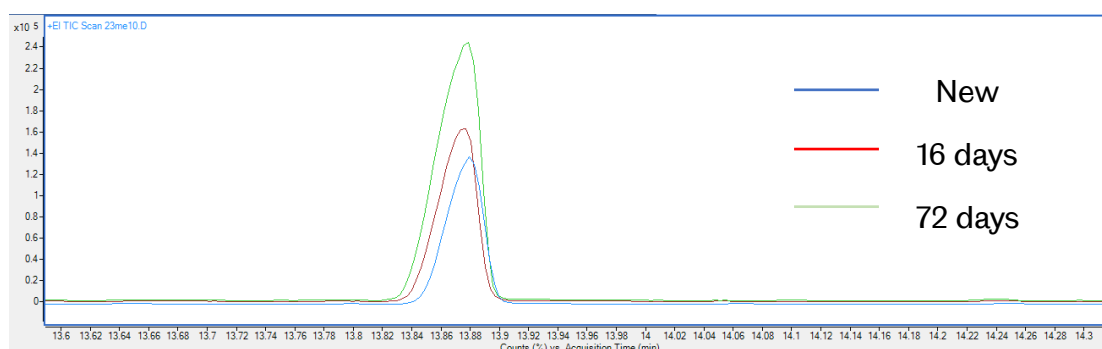
Figure 5.12 Intensity of dodecane in samples with different days into ageing

Figure 5.13 to Figure 5.19 illustrates the normalised concentration changes of these chemicals in samples with different aged days.
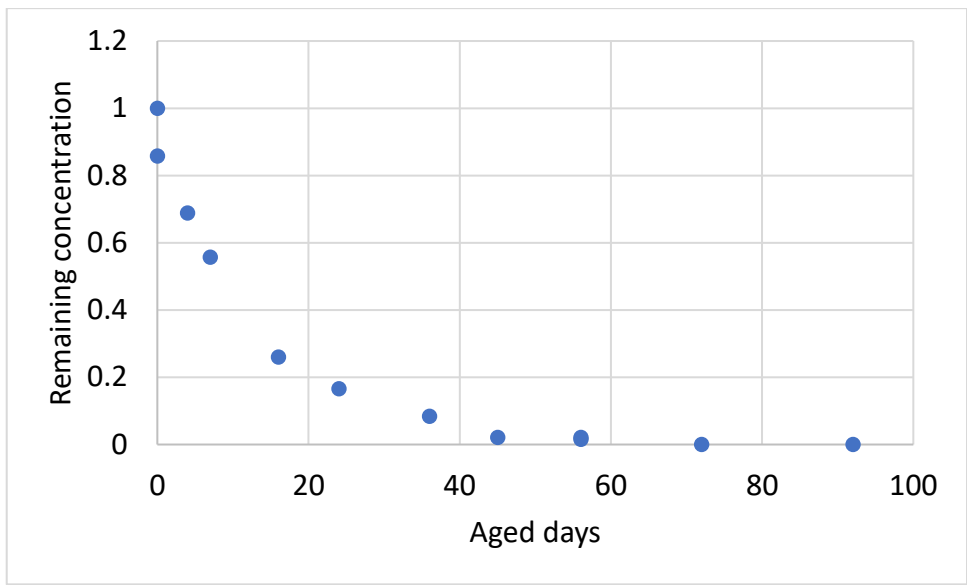
Figure 5.13 Concentration changes of plasticiser 1 - octadecyl
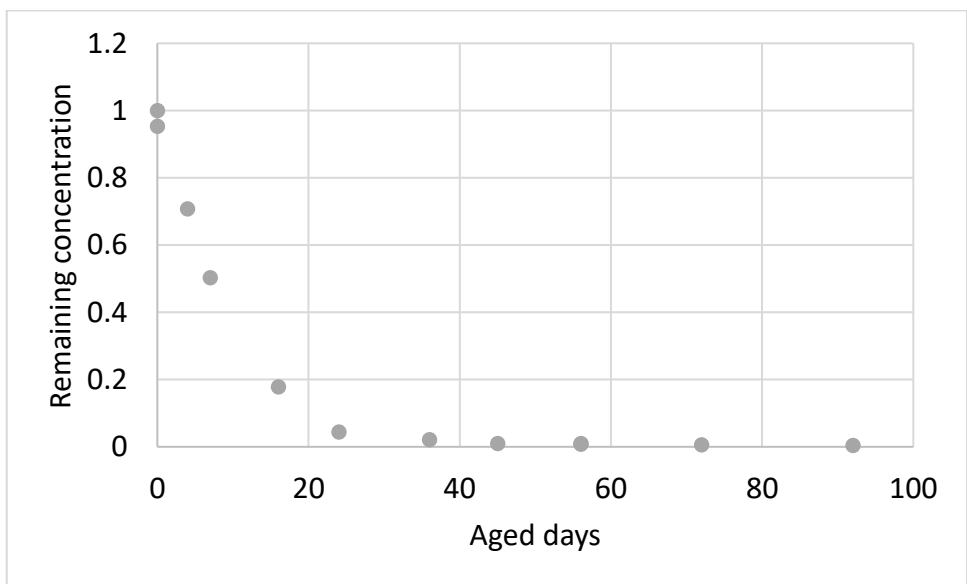
Figure 5.14 Concentration changes of antioxidant - 6PPD
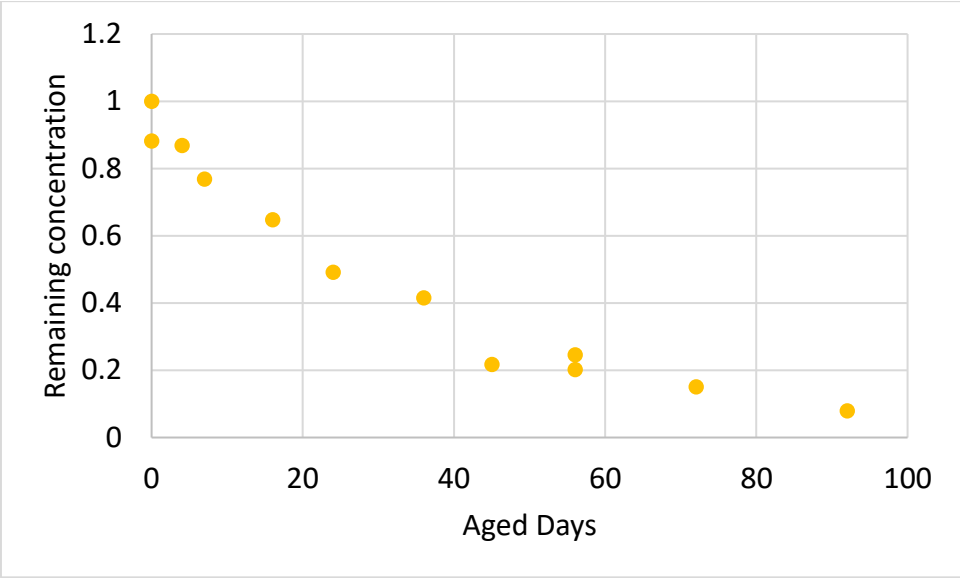
Figure 5.15 Concentration changes of plasticiser 2 - adipol 2EH
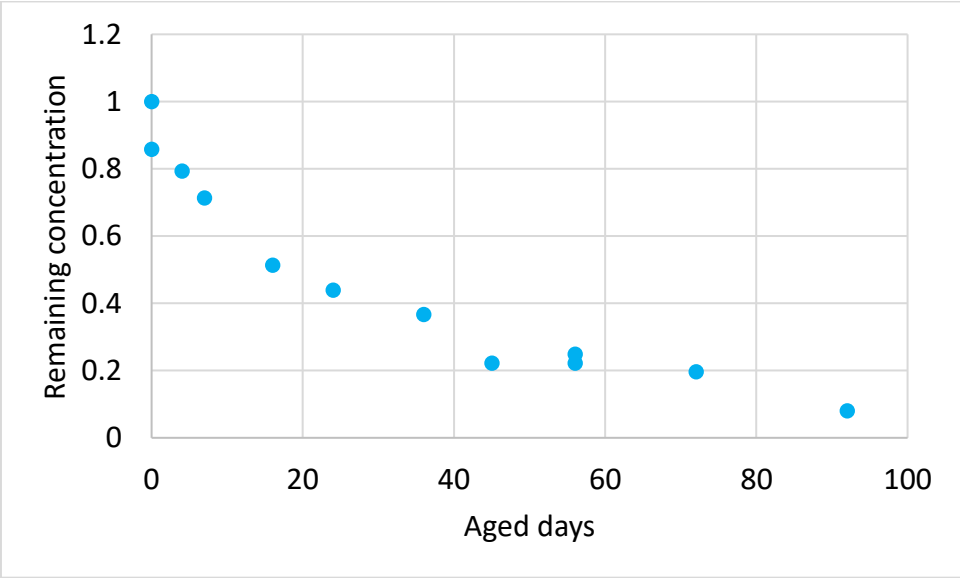
Figure 5.16 Concentration changes of plasticiser 3 - eicosyl acetate
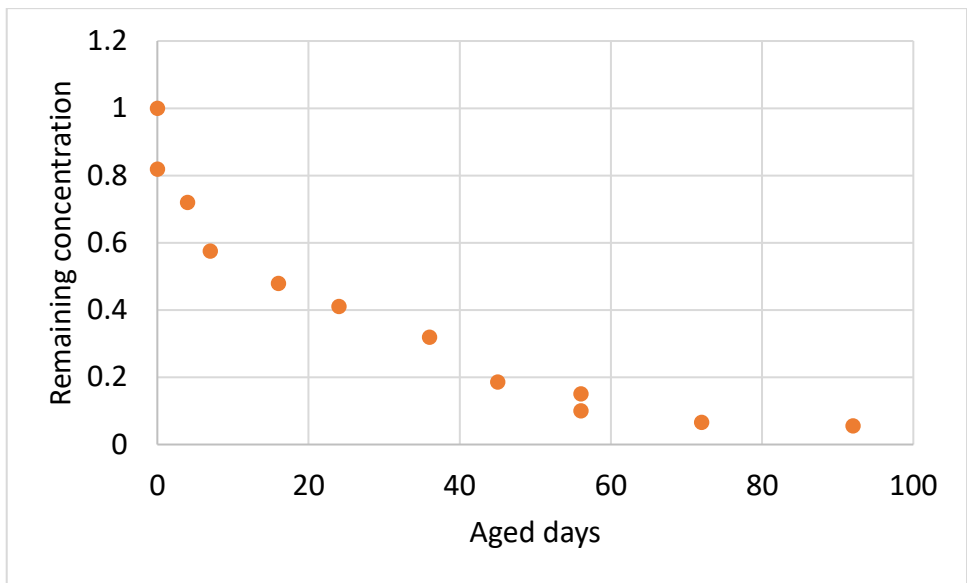
Figure 5.17 Concentration changes of paraffin oil/wax
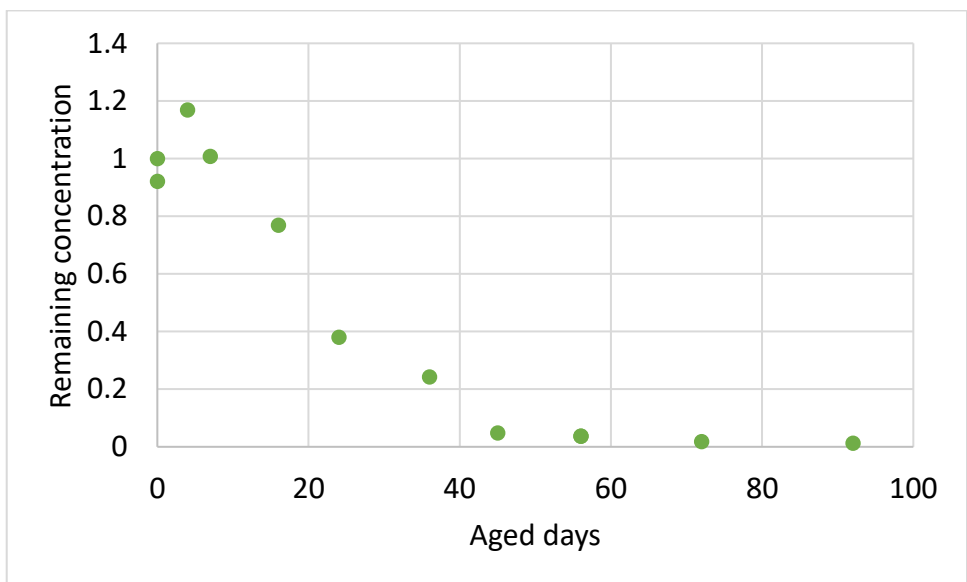
Figure 5.18 Concentration changes of antiozonant - DPPD
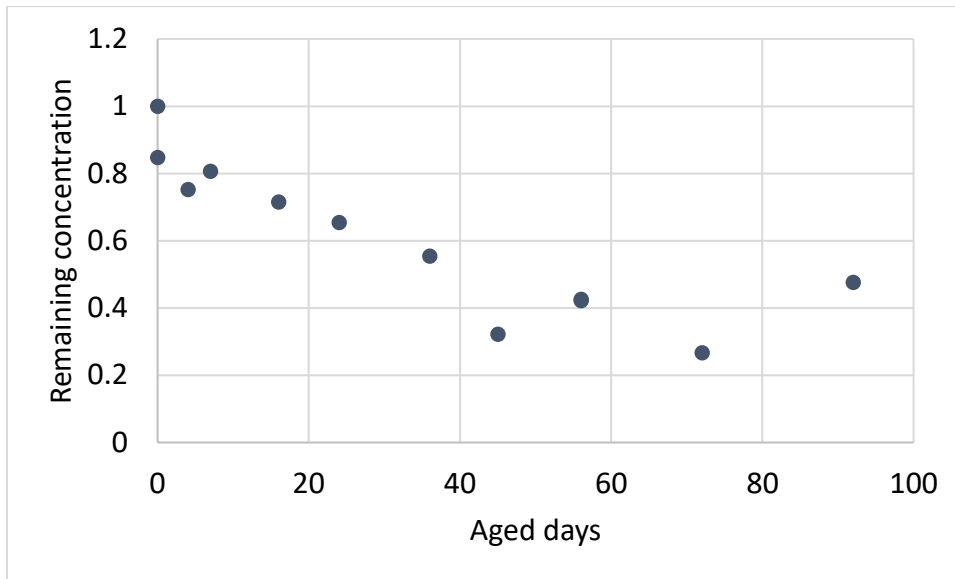
Figure 5.19 Concentration changes of plasticiser 4 - dioctyl isophthalate

It can be seen that the concentration of all the additives decreased over time, with key points at around 24 days and 43 days. The reduction of concentration of all additives became slower at these key points. The reduction of plasticisers could lead to an increase in the sample's elastic modulus. The depletion of antioxidants and antiozonants makes the material became more vulnerable to oxidative degradation during ageing.

The samples prepared from the same day showed (day 0 and day 56) the uncertainties caused by sample preparation could be up to around 20% of the additive's concentration.

The concentration of plasticiser 4 shows an increase at 56 days and 92 days into ageing. Other additives also showed a slight fluctuation at these periods. The increase of concentration observed on plasticiser 4 and wobbles from other additives were likely to be caused by uncertainty introduced in sample preparation process. The wobbles observed from all additives were observed from the same sample, this means that these changes were highly likely to be caused by the uncertainties introduced during sample preparation. As shown in Chapter 5.2.4, plasticiser 4 is less volatile than other additives, which makes this introduced uncertainty more significant as it is related to the concentration of the additive.

5.2.5 Hardness

In addition to the factors identified in Chapter 2, Shore A hardness is often linked to stiffness of the material. Therefore, a hardness test was added as an extra investigation in this experiment.

Test method

Shore A durometer was used to measure the Shore A hardness of the sample manually. The reading was taken after the tip of the durometer was pressed into the sample and allowed to rest for 15 seconds, for reasons described in Chapter 2.6.1. The test would be performed after resting the samples on a metal plate for 30 minutes to acclimatise to the environment. The samples would then be put back into the oven until the next test.

Sample preparation

The samples were prepared into 12mm x 12mm x 6mm blocks. Two mount samples and four sheet samples were prepared.

Sampling frequency

The temperature variation is not avoidable when opening the oven, to investigate if this variation would affect the elastic modulus of the samples, hardness samples were categorised into three sets with different sampling frequencies to identify the impact of discontinuous ageing described in Chapter 2.5.2.

Sample type	Sampling amount	Sampling frequency
Hardness sample (mount)	2	Every day at the beginning and less frequent later
Hardness sample (sheet)	2	Every day at the beginning and less frequent later
Hardness sample (sheet)	1	Every 7 days
Hardness sample (sheet)	1	137 days

Table 5-5 Sampling frequencies for hardness tests

Result

The hardness for all tested samples is plotted in Figure 5.20. The hardness of the samples increased to a peak at around 27 days, followed by a subsequent decrease to around 60 days. A final increase was observed after this. The samples tested every 7 days follow the samples tested every day until 90 days into ageing. The sample tested only at the end gave a similar result to the sample tested every 7 days. After 90 days into ageing, the locations that had been tested previously gave a significantly smaller reading than locations that had never been tested.
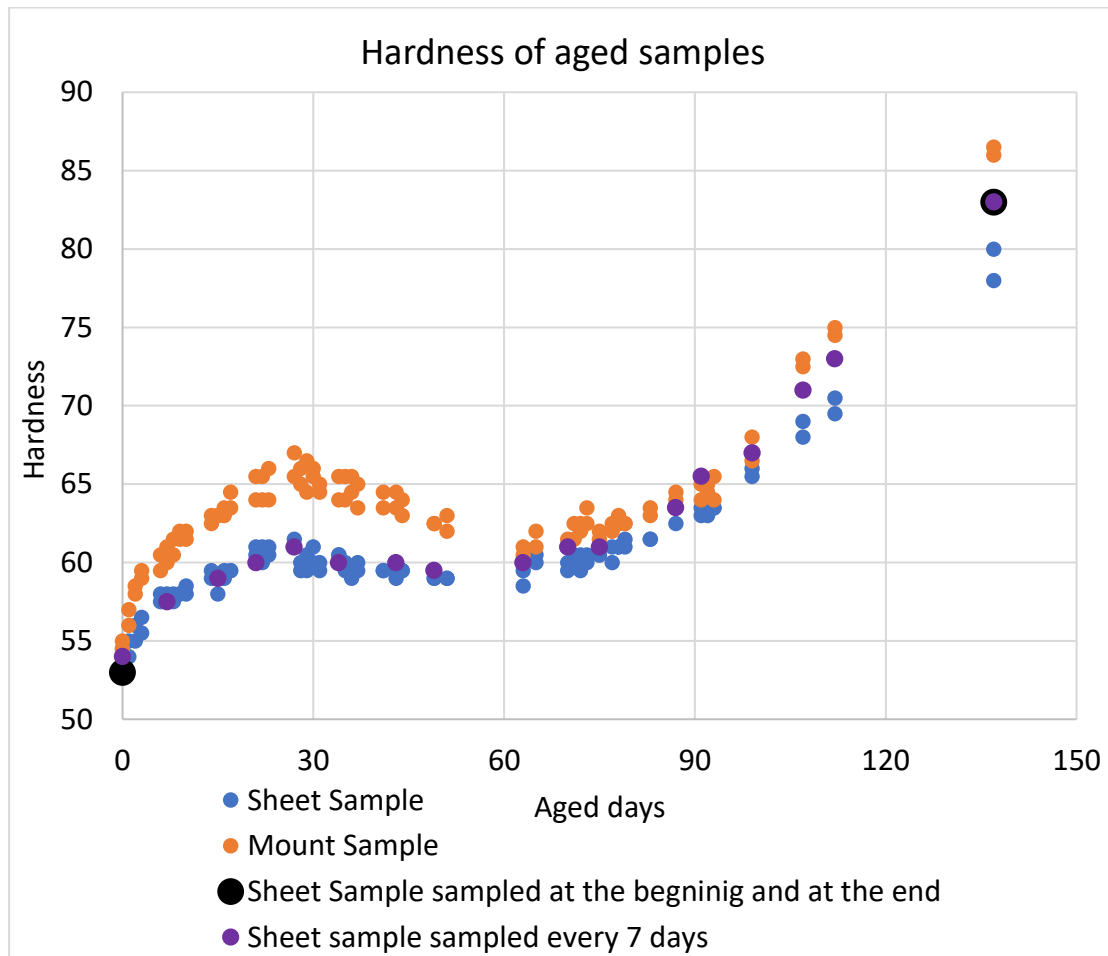
Figure 5.20 Hardness of accelerated aged mount and sheet samples

Discussion on hardness test

The changes were significant and relatively slow, which validated the designed sampling frequencies for other tests. The different intermittent heating setup did not show significant impact to samples aged less than 90 days. The reason for samples that were sampled every day being softer after 90 days into ageing is likely

to be caused by the damage received by the sample. As mentioned in Chapter 4.1, the material lost its resilience during ageing and the elongation at break is near 20% for the 90 days aged mount sample. The sheet sample is expected to experience the same problem and, therefore, when the tip of the durometer was pressed into the sample, it could have damaged the integrity of the polymer network.

5.3 Discussion

5.3.1 *Comparing DMA result with result from the hardness test*

The measured Shore A hardness was transferred into elastic modulus using Equation 5-2 mentioned in Chapter 2.6.1, where E represents elastic modulus and S represents Shore A hardness.

$$E = \frac{0.0981 \times (56 + 7.62336 \times S)}{0.137505 \times (254 - 2.54 \times S)}$$

Equation 5-2 Shore A hardness to elastic modulus according to Gent (1958) [161]

In Figure 5.21, the transferred hardness results are compared with elastic modulus measured with DMA.
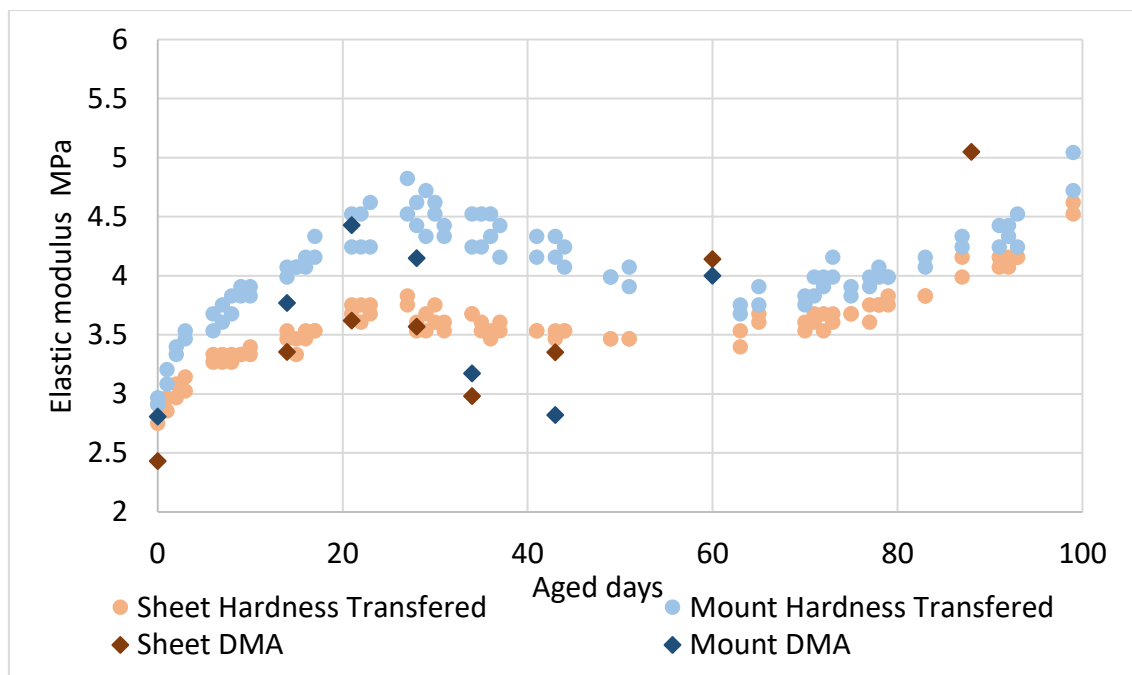
Figure 5.21 Comparing hardness transferred elastic modulus to DMA measured result

It shows the results obtained by both methods had a similar behaviour. The magnitude of changes for results from the hardness test is smaller than the DMA results, which could be caused by human error.

5.3.2 Comparing change of elastic modulus and crosslink density

Figure 5.22 shows the crosslink density vs. elastic modulus of accelerated aged samples. The correlation is not very good, which could suggest a changing of elastic modulus caused by ageing mechanisms irrelevant to crosslink density.
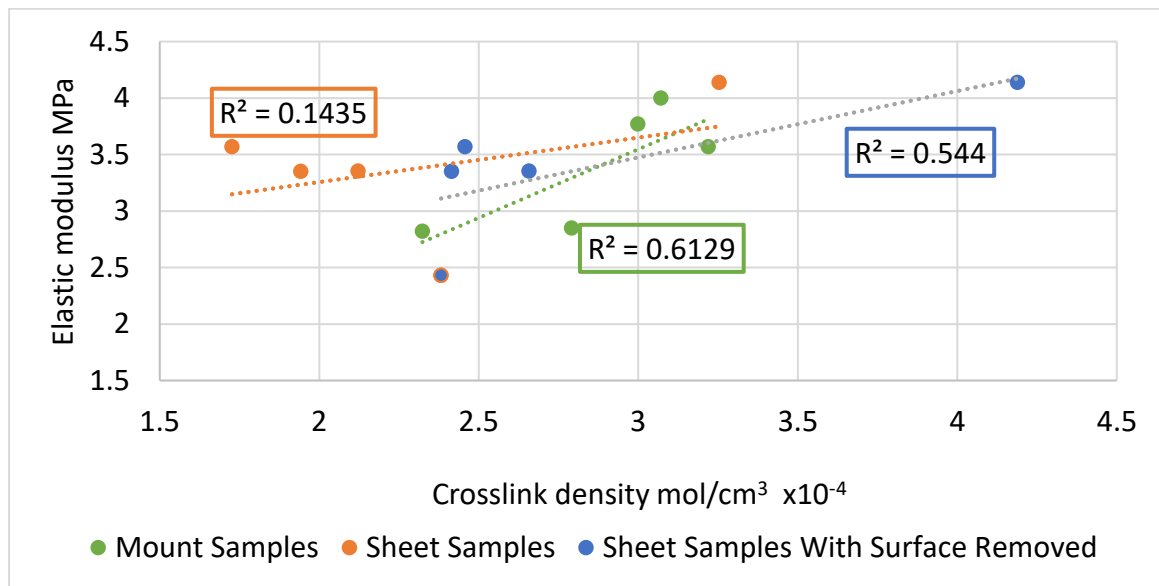
Figure 5.22 Crosslink density vs. elastic modulus for aerobic aged samples

5.3.3 Loss of additives and changes to elastic modulus

Plasticisers were added to the material to reduce its stiffness. The decreases of plasticisers' intensities are likely to be related to the stiffening of the material before 28 days into ageing. As shown in Figure 5.23, the elastic modulus of the material reached a peak between 21 to 28 days. Most plasticisers lost more than 50% of their initial intensities after 24 days into ageing.
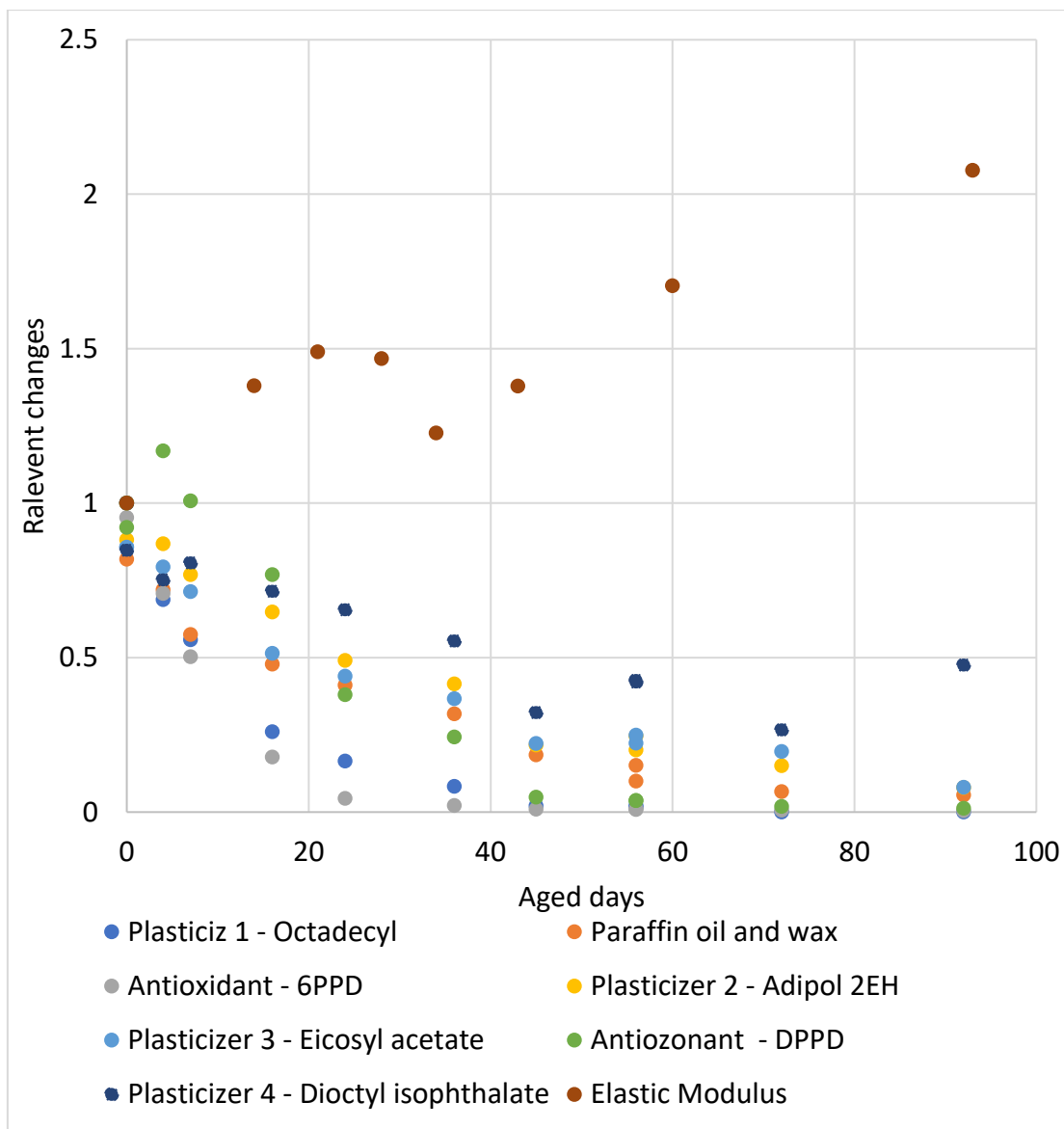
Figure 5.23 Loss of additives and changes on elastic modulus

Paraffin wax was added as a protective chemical, however, its existence reduces the elastic modulus of the material as described in Chapter 2.3.5. The remaining paraffin wax in the material also reached below 50% which could contribute to the stiffening of the material.

The antioxidant and antiozonant also depleted during this period, which may allow the oxidative degradation related reactions to take place more rapidly.

5.3.4 Potential impact of oxidation

The failure of the 90 days aged mount sample during the DMA test suggests that the material has lost its resilience at this stage which could be caused by the breakdown of polymer backbone chains during the chain scission process caused by oxidation, which makes the material lose its flexibility.

In the sheet sample, more than 50% of antioxidants and paraffin wax were lost before 24 days into ageing and depleted at around 60 days into ageing, which suggests oxidative degradation related reactions became more rapid after day 24. As mentioned in Chapter 2.4.1, it is possible that the dominating mechanism of oxidation for regions away from the surface transferred from chain scission to crosslinking, which could be causing the increase of crosslink density after 50 days into ageing. This can be seen in Figure 5.24, where black and grey markers represent the measured crosslink density of original and surface removed samples, respectively.
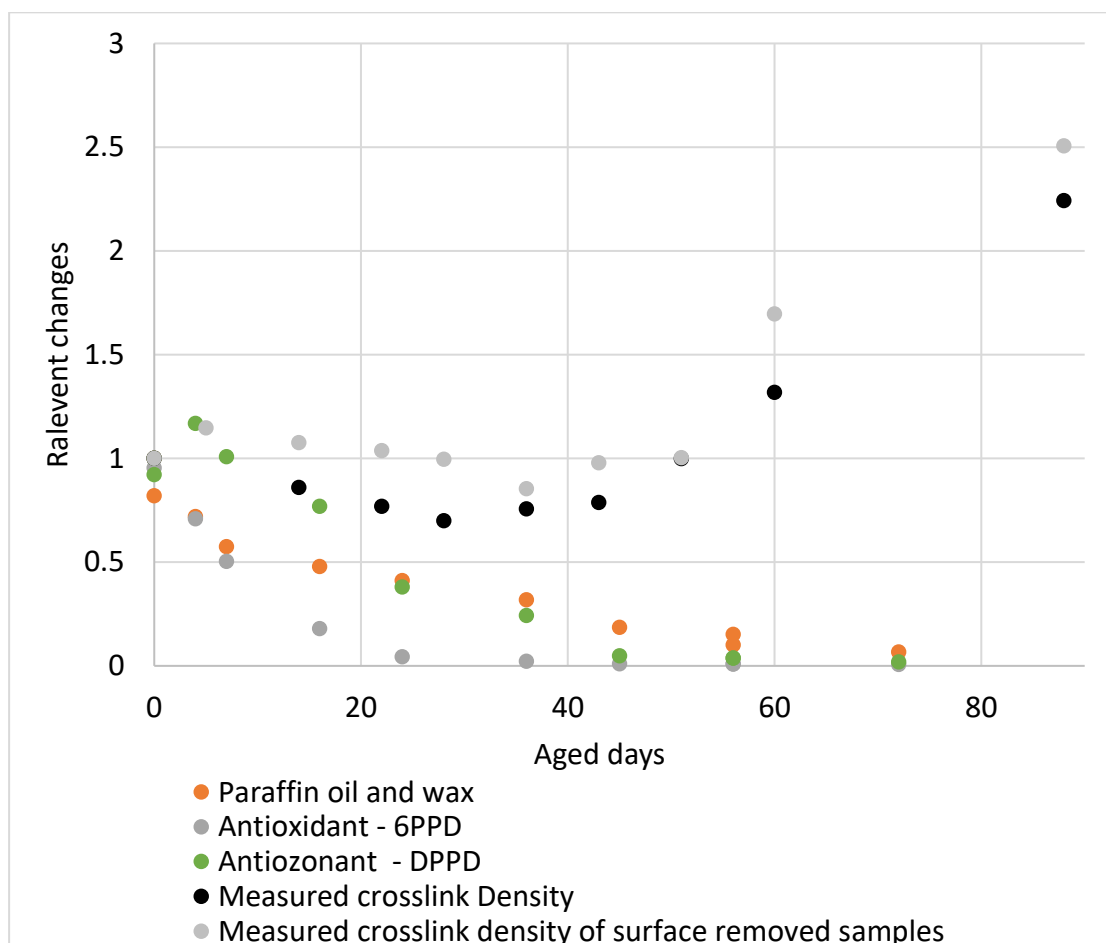
Figure 5.24 Measured crosslink density and concentration changes on relevant additives

5.4 Summary

Although the possible causes of some changes of elastic modulus of material have been identified, the impact of these ageing mechanisms are still entangled. In particular, the effect of oxidation is likely to conceal the effects of other ageing mechanisms causing changes to crosslink density.

The following chapter will, therefore, focus on investigating the same factors without the presence of oxygen.

CHAPTER 6.   ARTIFICIAL AGEING (IN NITROGEN)

Both the accelerated ageing test and results obtained from used engine mounts indicate that the oxidative degradation is causing chain scission to the material. Due to the existence of certain additives, the FTIR test was unable to provide the degree of oxidation. Its impact on crosslink density was also linked to post-curing and thermal degradation. This made the deduction of the sole impact of oxidation inapplicable without further investigation. Thus, samples taken from the rubber sheet were artificially aged under an anaerobic environment. When comparing results obtained from the aerobic accelerated ageing test, the impact of the presence of oxygen and other ageing mechanisms can be deduced.

6.1   Ageing parameters

6.1.1   Material

All samples were prepared from the rubber sheet; its similarity with the mount rubber on ageing behaviour has been confirmed in previous tests.

6.1.2   Atmosphere

To create an anaerobic environment for multiple samples with different designated ageing times, it is crucial that the samples are separated from each other, i.e., the anaerobic environment of each sample would not be disturbed when removing samples as they reach their designated ageing time.

The samples cut for different characterisation methods were, therefore, put into 20ml vials filled with nitrogen gas. The number of samples, their purpose and the number of the prepared vials are listed in Table 6-1.

Vial type	Vial configuration	Number of vials
Vial type 1	1 x DMA sample	27
	2 x crosslink density samples	
Vial type 2	1 x GC sample	9
	1 x SEM sample	

Table 6-1 Anaerobic test vial configuration and sampling frequencies

Samples with the same purpose were put into different vials to reduce the impact of the unlikely event of nitrogen gas leaking. Headspace vials were used, with caps that have PTFE/silicone septum acting as seals to ensure good airtightness while ageing. Figure 6.1 illustrates the cap of the vial; the white disc is the PTFE/silicone septum, which has good thermal capabilities [196] [197].

Figure 6.1 Caps with PTFE/silicone septum

Figure 6.2 illustrates the gas filling procedure. The nitrogen gas was fed into the bottle at 100 ml/min through the needle. Samples were put away from each other and leant towards the wall of the bottle; this is to reduce the possibility of trapping air between contacting surfaces. The gas filling step was set to 10 mins to ensure that the majority of the air inside the bottle was replaced by nitrogen gas. The bottle was gently brought down and the cap was crimped on the bottle as soon as the needle left the bottle. The needle directing nitrogen gas was bent with a desired curve and length, ensuring the tip of the needle is close to the bottom of

the bottle and can leave the bottle easily. The sealed vial is then transferred into the oven.
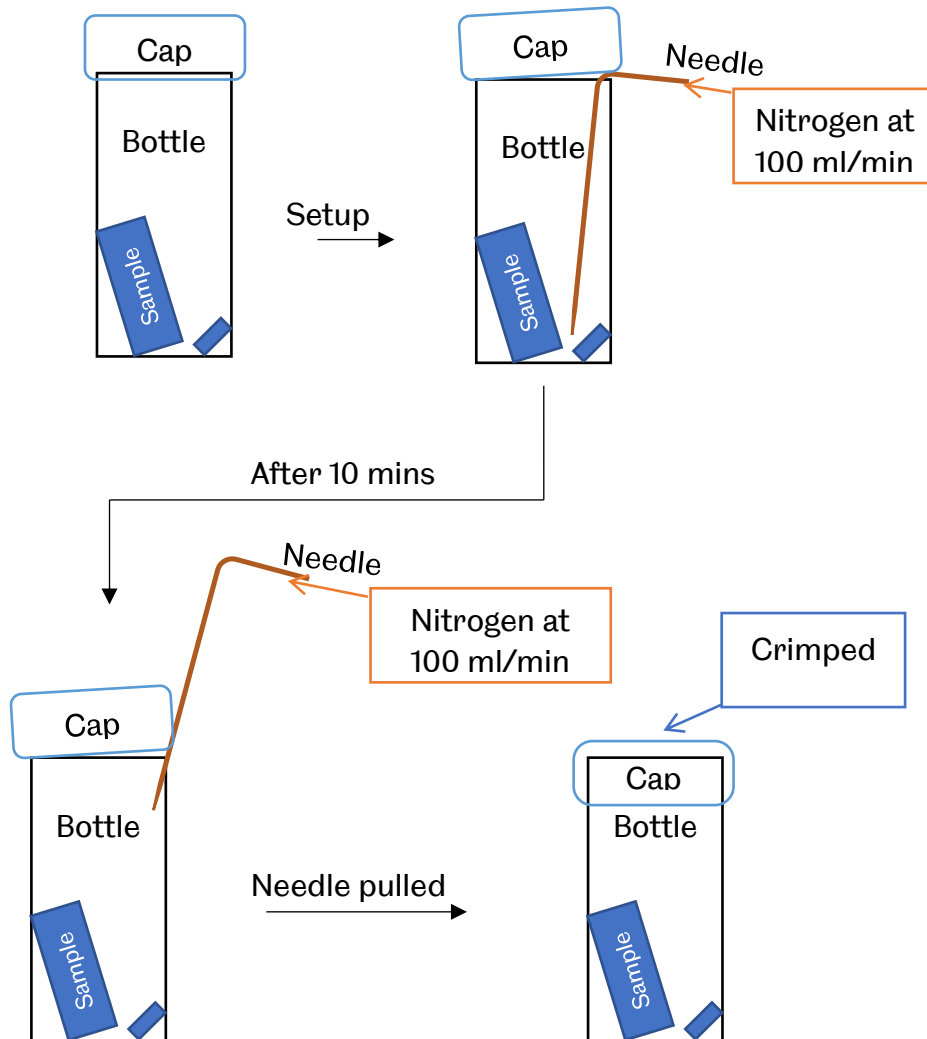
Figure 6.2 Anaerobic vials preparation

6.1.3 Temperature

The temperature was set to 95 °C, the same as in Chapter 5. The bottles were buried in a sand bath to maintain a more stable surrounding temperature when the oven door needed to be opened.

6.1.4 Length of time

The total ageing time was set to 90 days, as samples artificially aged in air lost their resilience and became a different material after 90 days into ageing. Comparison

between samples aged under anaerobic and aerobic environments after this date is meaningless.

It was noticed that most property changes in the previous test were more complex before 43 days into ageing, which indicates a faster property-changing rate in this period. Thus, the sampling days were set to be more frequent at the beginning of the test. Thus, 3 vials containing DMA/crosslink density test samples and 1 vial containing GC-MS/SEM samples were taken at days shown in Table 6-2. Vials were taken in a random order to balance out the uncertainties caused by the possible variation of ageing conditions at different locations in the oven.

Sampling days	0	6	12	19	28	38	49	60	74	88
Increment (days)	0	6	6	7	9	10	11	11	14	14

Table 6-2 Anaerobic test sampling days

6.2 Investigation of properties with anaerobic ageing

The properties measured in the aerobic accelerated ageing test were measured again, including elastic modulus, crosslink density, carbon re-agglomeration and additives intensities. All tests for the same interested property were performed at the same time, regardless of the time the samples were taken out of the oven.

6.2.1 Elastic modulus

Test method

As described in Chapter 5.2.1, the samples were tested with 10% dynamic and static strain.

Sample preparation

The samples were prepared with the manual cutting method described in the previous test. The samples were cut to 5mm x 6mm x 16mm ±1.5mm blocks.

Sampling frequency

3 Samples were acquired on days listed in Table 6-3.

Sampling days	0	6	12	19	28	38	49	60	74	88
Increment (days)	0	6	6	7	9	10	11	11	14	14

Table 6-3 Sampling frequencies for elastic modulus samples

Result

Figure 6.3 shows the results of the 10% static and dynamic stain test. The changes to the elastic modulus of anaerobic aged sheet samples were insignificant before 20 days into ageing. It then decreased to trough at around 50 days into ageing and increased afterwards.
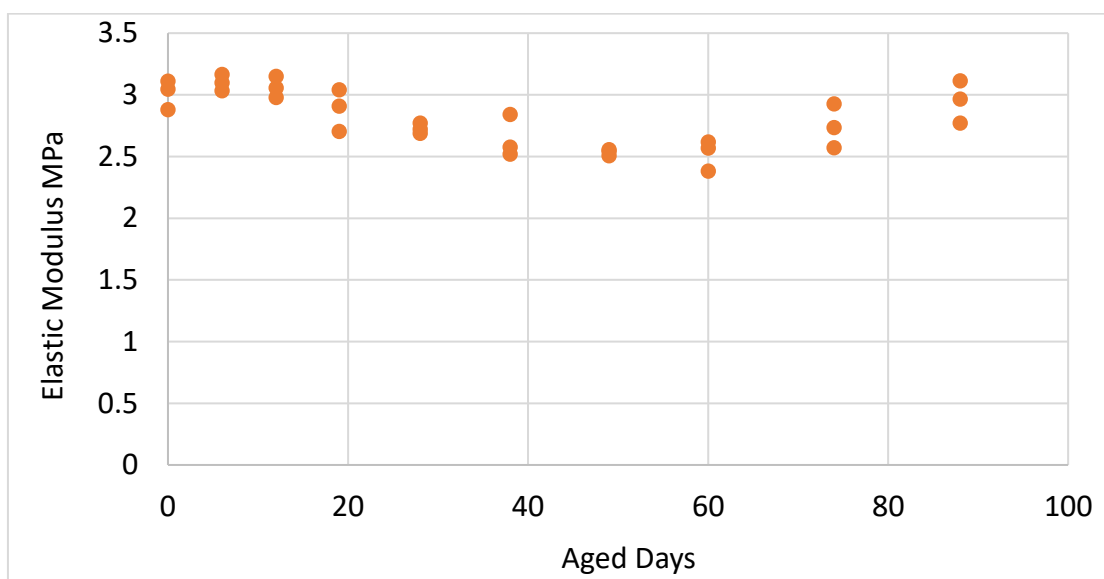
Figure 6.3 Elastic modulus changes of anaerobic aged samples under 10% static and dynamic strain

6.2.2 Crosslink density

Test method

The exact measuring process described in Chapter 4.2.1 was applied.

Sample preparation

The samples were cut manually into 4mm x 4xmm x 4mm ±1mm cubes as described in the previous test.

Sampling frequency

Six samples were acquired on days listed in Table 6-4. Samples were kept in vials that also contained DMA samples.

Sampling days	0	6	12	19	28	38	49	60	74	88
Increment (days)	0	6	6	7	9	10	11	11	14	14

Table 6-4 Sampling frequencies for crosslink density samples

Result

As shown in Figure 6.4, the crosslink density of the samples decreased after 10 days into ageing and reached a trough at around 50 days into ageing.
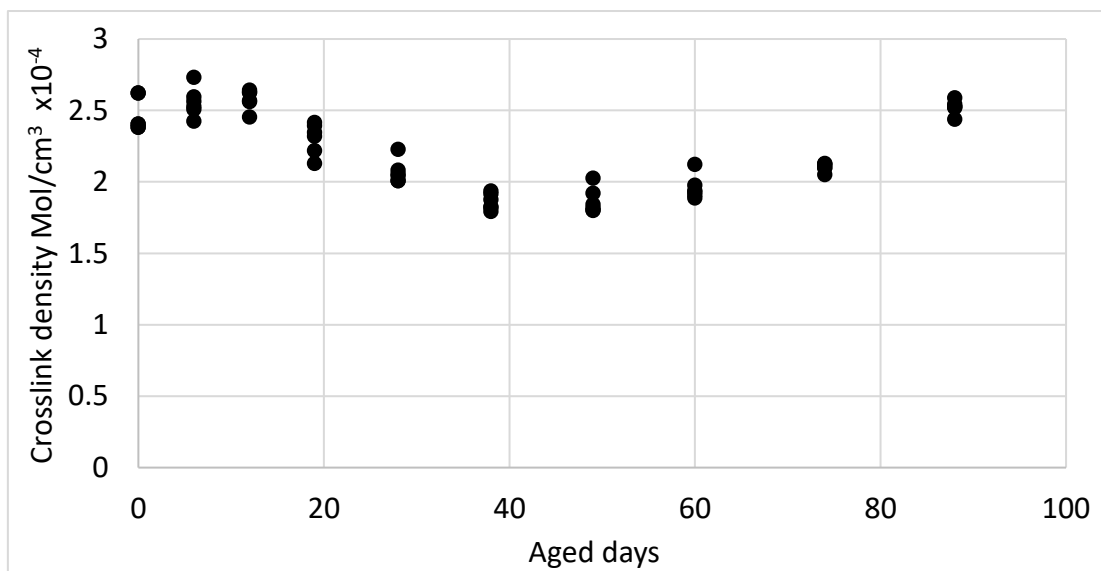
Figure 6.4 Crosslink density changes of anaerobic aged samples

6.2.3 Carbon re-agglomeration

Test method

SEM images were taken by the Helios NanoLab SEM machine used previously. The analysis method described in Chapter 4.2.3 was applied again.

Sample preparation

The SEM samples were prepared with the cryo-fracture technique and then manually cut to 1mm thick, as mentioned in Chapter 5.2.3.

Sampling frequency

Seven images were captured from the new sheet samples and the 90 days anaerobic aged samples.

Result

The images can be seen in Appendix B xvi to xvii. The analysation method was the same as in Chapter 4.2.3. Figure 6.5 shows the ratios of the amount of carbon particles between the two samples under different size ranges.
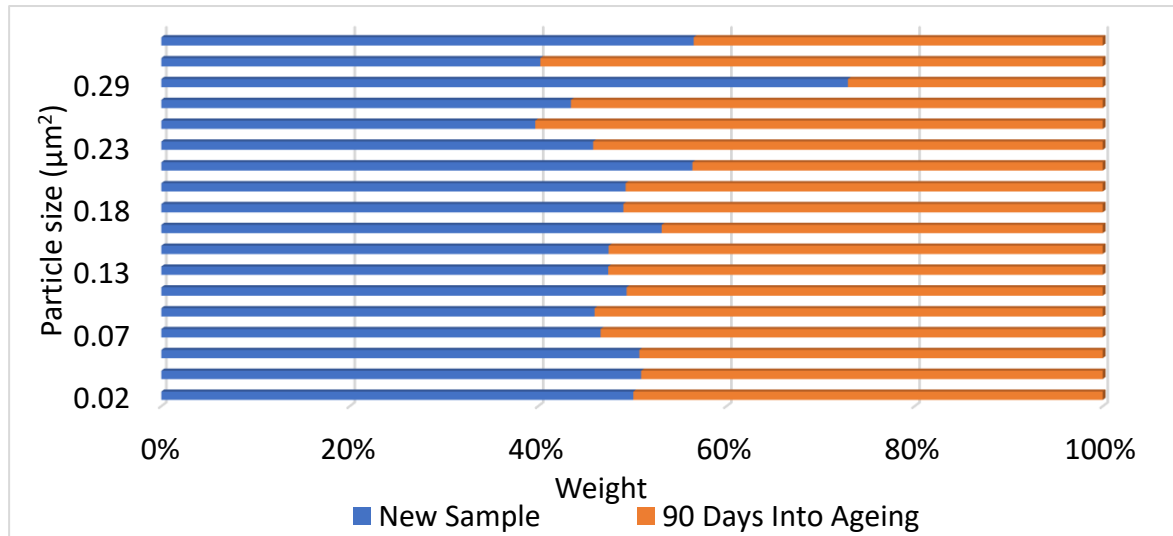
Figure 6.5 Particle size ratios between 90 days anaerobic aged sample and new sample

Differences can be observed at individual size categories with no clear trend. Although the sample is only 90 days into ageing, no precursor of carbon re-agglomeration has been observed.

6.2.4 Loss of additives

Test method

Intensities of additives were measured using the method described in Chapter 5.2.4.

Sample preparation

The sample preparation process was identical to the process described in Chapter 5.2.4.

Sampling frequency

Samples were taken in days listed in Table 6-5.

Sampling days	0	6	12	19	28	38	49	60	74	88
Increment (days)	0	6	6	7	9	10	11	11	14	14

Table 6-5 Sampling days for GC-MS samples

Result

The measured intensities of each interested chemical are listed in Appendix C ii. Figure 6.6 shows the normalised results of these chemicals.
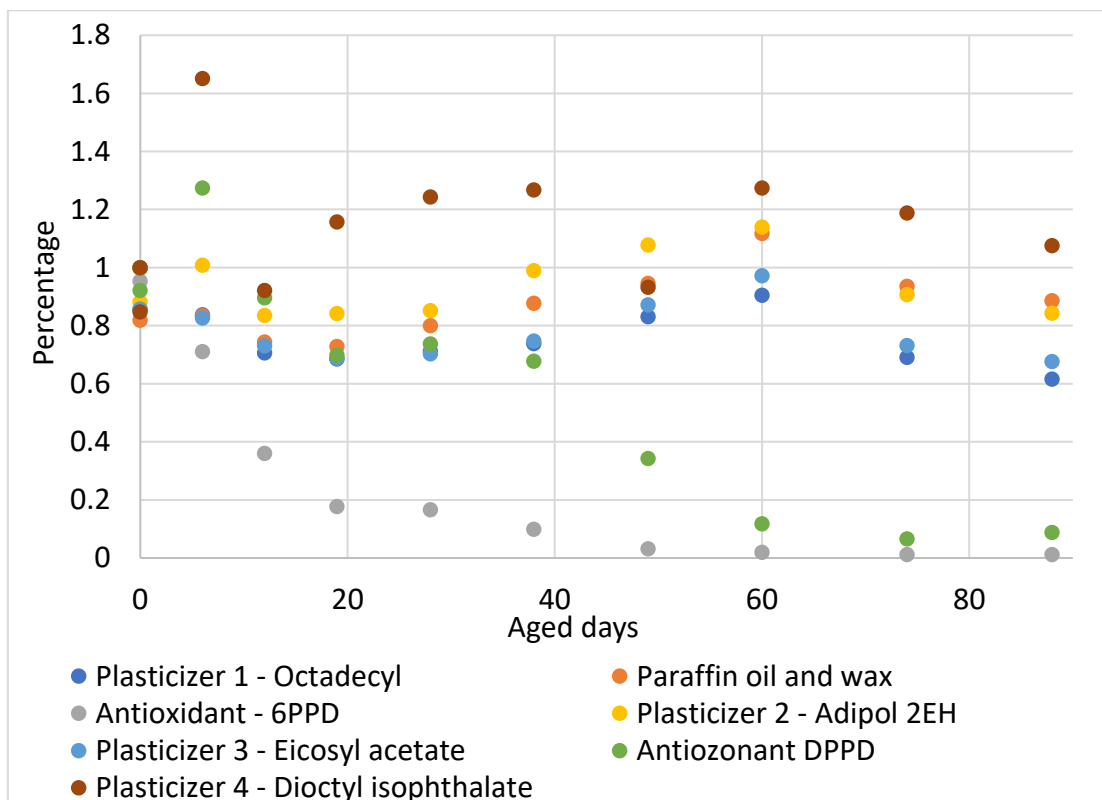
Figure 6.6 Concentration changes of interested additives in anaerobic aged samples

Concentration of 6PPD, the antioxidant, and DPPD, the antiozonant, reduced in the first 60 days into ageing. The reduction could be caused by the migration of the chemical, as both 6PPD and DPPD are volatile chemicals.

It clearly showed that, under an anaerobic environment, the plasticisers and paraffin oil/wax in the material remained stable throughout the ageing period, making them irrelevant to the changes to the elastic modulus.

concentrations of plasticisers and paraffin oil/wax wobbles at various days but showed no significant trends. The concentrations that increased to above 100%

were likely to be caused by uncertainties, as no known mechanism could increase the concentration of these additives.

6.3 Discussion

As can be seen in Figure 6.7, the measured crosslink density correlates very well with elastic modulus. This suggests crosslink density changes are responsible for elastic modulus changes in the anaerobic aging test.
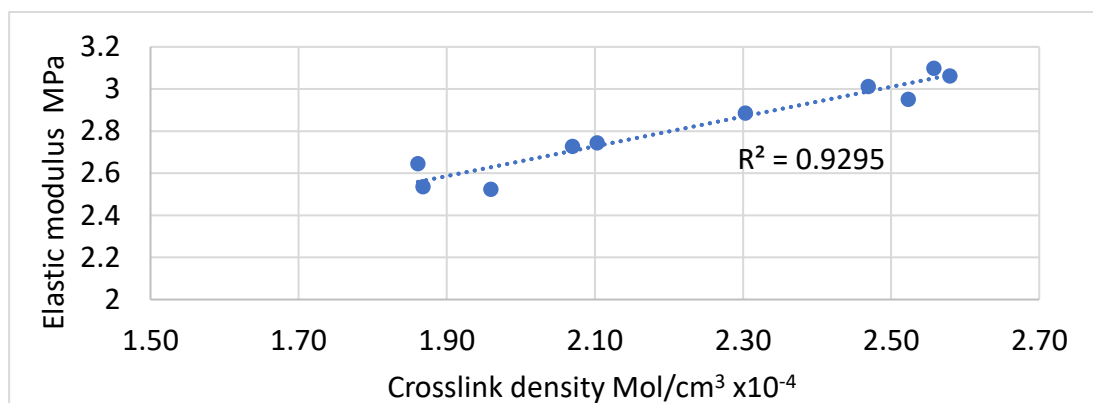
Figure 6.7 Crosslink density vs. elastic modulus of anaerobic aged samples

All measured properties behave differently under anaerobic ageing conditions, which suggests that they were related to air contact. The changes observed on carbon black distribution and concentrations of plasticisers are not significant under anaerobic environment. Although the loss of antioxidants and antiozonants still occurs, slow depletion rate suggests that this reduction of concentration could be caused by the migration process and volatilisation.

The changes of crosslink density under the anaerobic environment are likely to be caused by post-curing and thermal degradation. As the other ageing mechanisms related to crosslink density – oxidation and carbon re-agglomeration were not observed.

CHAPTER 7.   DISCUSSION

7.1   Introduction

The ageing behaviour of samples aged under three different ageing conditions were examined, including samples taken from real-life used engine mounts, samples that experienced oven ageing in air, and samples that experienced anaerobic artificial ageing. This chapter compares the results across samples aged in these three environments, attempting to conclude the differences between the lab aged samples and real-life aged samples, and to deduce the ageing behaviour of rubber material in the engine mount.

7.2   Ageing Behaviour of the Mount in Real-Life Scenario

As described in Chapter 2, an increase of elastic modulus was observed on rubber in the used engine mounts. The acting ageing mechanisms were defined to be post-curing and thermal degradation, oxidative degradation, carbon re-agglomeration and loss of additives. All these mechanisms could be the reason behind the stiffening of the material. Table 7-1 summarises the potential influence of these mechanisms.

Ageing mechanisms	Potential impact based on literature
Post-curing and thermal degradation	Stiffening or softening, or a mix of both, during ageing by changing the crosslink density of the material, the actual impact depends on how crosslinks were formed inside the material during manufacturing.
Oxidative degradation	Based on the difference in crosslink density measured at locations near and far from the surface of the mount, it was confirmed that oxidative degradation causes chain scission to the material. However, the dominating mechanism changing from chain scission

	to crosslinking suggested by Bonfils (1999) could be happening inside the material [102].
Filler re-agglomeration	The carbon black filler grouped up during ageing to form larger aggregates which could potentially decrease the elastic modulus, as larger aggregates size reduces the reinforcement performance and can be considered as poor dispersion. For locations that never experienced deformation, the newly formed larger aggregates are likely to trap rubber chains and lead to an increase in crosslink density. This is not likely to affect the material's elastic modulus, as the chains would break free when the material is deformed.
Loss of additives	The loss of various plasticisers and paraffin wax could potentially lead to an increase of elastic modulus. Loss of antioxidants and antiozonants made the material became vulnerable to oxidative degradation during ageing.

Table 7-1 Effects of acting ageing mechanisms

The good correlation between elastic modulus and crosslink density changes of samples taken from the bulk region of the mount proved that the dominating mechanisms are the ones causing changes to crosslink density.

The impact of cyclic loading on crosslink density was concluded as insignificant in Chapter 4.2.1, but, during the SEM imaging process, it was noticed that regions that experienced cyclic loading had better conductivity than regions that never experienced cyclic loading in used mounts. Mentioned in Chapter 2.4.3, the conductivity could be affected by re-agglomeration of carbon fillers, suggesting the cyclic loading process may have influences on other properties of the material.

Although the acting mechanisms were identified, how they impacted through the ageing process was not clear as, in a real-life scenario, the driver's driving preferences could make these ageing mechanisms progress differently in each

aged mount. The discussion about how these ageing mechanisms evolved will be made later after more understanding of them is gained.

7.3 Use of Artificial Ageing to Simulate Real-Life Behaviour

In order to obtain samples with controllable ageing parameters, artificial ageing experiments were conducted. The mount samples have been artificially aged in air and changes to their elastic modulus and crosslink density were clearly presented. Figure 7.1 compares the elastic modulus changes of samples taken from used engine mounts and samples aged artificially. Although the aged days and mileage were unable to be correlated due to the uncertainties caused by the driver's driving preferences, it shows that the magnitude of the changes were similar between the two sets of samples.
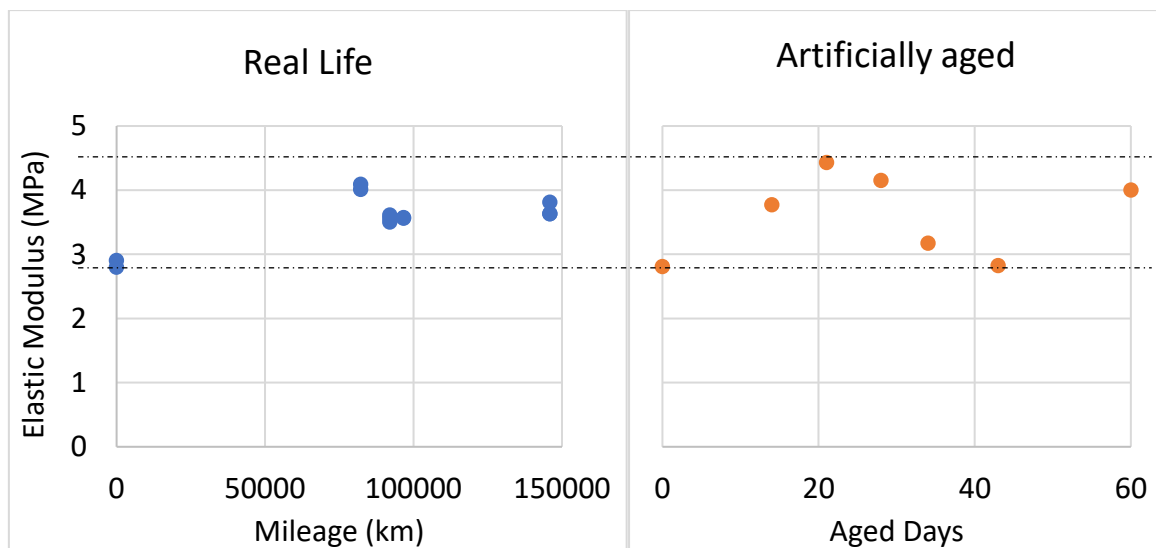
Figure 7.1 Elastic modulus changes under 10% dynamic strain and 10% static strain in samples taken from real-life and artificially aged

Unlike samples taken from the real engine mounts, a bad correlation between elastic modulus and crosslink density were noticed. Figure 7.2 shows this difference.
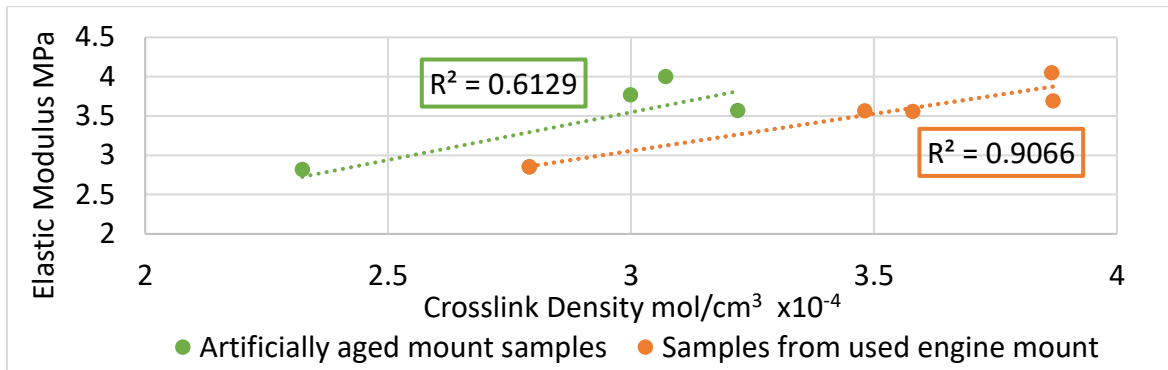
Figure 7.2 Crosslink density vs. elastic modulus for samples aged in lab and real-life

This could be caused by the impact of factors not influencing crosslink density, or the non-uniform crosslink density changes through the sample caused by oxidative degradation. Figure 7.3 illustrates the percentage changes of elastic modulus and crosslink density of aged mount samples.
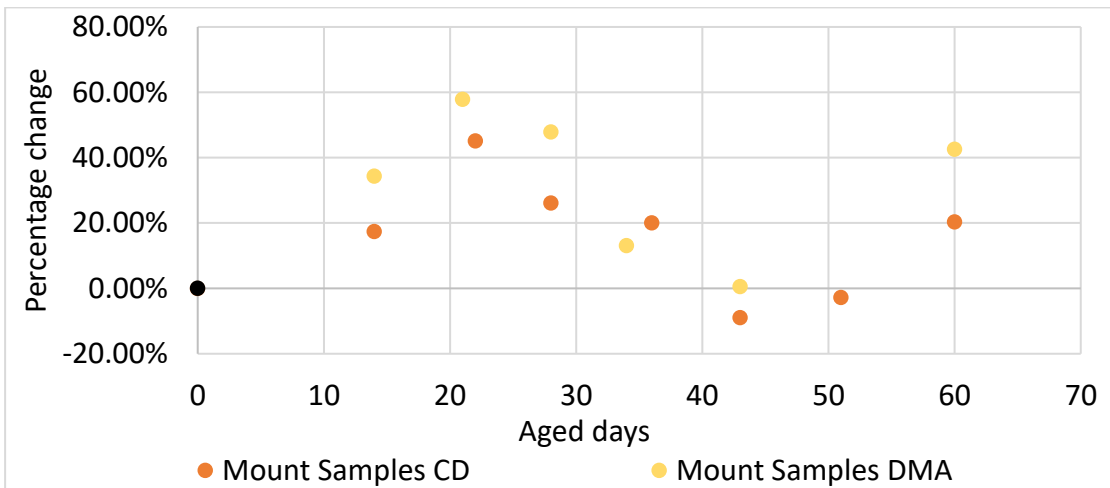
Figure 7.3 Percentage changes of elastic modulus and crosslink density for aged mount samples

Although loss of additives could contribute to the increase of elastic modulus before 21 days, it does not affect crosslink density. The increase of crosslink density could be caused by the post-curing and thermal degradation processes.

The magnitude of the decrease of elastic modulus after 24 days is not likely to be caused by oxidation and ozonation only, as they mainly acted at the surface region. Therefore, it is possible that post-curing and thermal degradation also contributed to this decrease of crosslink density after 24 days into ageing for the mount rubber, and together with oxidation lead to this strong decrease of elastic modulus. Although carbon re-agglomeration is also able to reduce the crosslink

density and elastic modulus of the material, it is not likely that it contributed to this decrease, for reasons that will be explained later.

Post-curing, thermal degradation and oxidative degradation could be responsible for the final increase of the modulus, and made the material lose its resilience. Further discussion on their behaviour is discussed later.

7.3.1 Differences between rubber from the used engine mount and aerobic aged samples

As mentioned in Chapter 2.3, the critical depth of oxidation is related to the temperature of ageing. This depth could range from 5 mm to 30 mm for temperatures from 100 to 25 °C, based on calculations from literature [33]. Except for the more significant oxidation caused by a high temperature environment, which mainly happens in the surface region, oxidation under lower temperatures during the service time could slowly penetrate through the entire rubber component. This means that material in the rubber component in the engine mount is influenced differently by oxidative degradation when compared with the smaller samples used in the artificial ageing test.

Another potential difference between them could be the content of additives. As described in Chapter 4.2.4, the additives in the bulk region of the rubber component in an engine mount could migrate to the surface region during ageing. This could have delayed the breakdown of the polymer network caused by oxidation and ozonation. The tested sample taken from the mount aged the most still maintains its resilience. This allows the material to survive longer and provide time for other mechanisms to develop further. These mechanisms include carbon re-agglomeration and crosslinking caused by oxidation due to lack of oxygen in the interior of the material. As the protection layer formed by antioxidants and oxidised rubber in the surface region prevents oxygen from diffusing into the bulk region of the mount, the changing dominating mechanism phenomenon mentioned in Chapter 2.4.1 can occur. However, due to the limited amount of new mount material, it was not possible to test the concentration changes of additives in the

artificially aged samples. Rubber sheets provided by the material supplier were used as a substitute for further investigations.

7.4 Use of Sheet Sample to Simulate Mount Rubber's Ageing Behaviour

Due to the limitation on the amount of new mount samples, sheet samples were used for further investigation, attempting to represent the ageing behaviour of the rubber in the engine mount.

7.4.1 Similarities and differences between mount and sheet samples

As the mount and sheet samples share the same composition, the same ageing mechanisms are expected to be acting. The way they affect the material is also expected to be similar, except for post-curing. As mentioned in Chapter 2.3, the post-curing process is related to the manufacturing and curing processes. Figure 7.4 has been shown in Chapter 4.1.5, it illustrates the similar ageing behaviour of the mount and sheet samples.
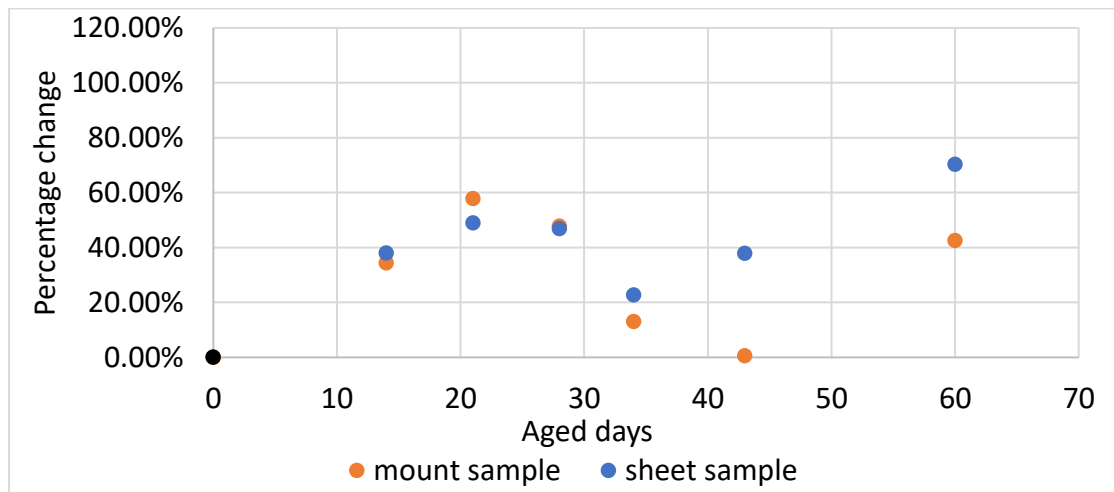
Figure 7.4 Elastic modulus change of mount and sheet samples under 10% dynamic strain

The elastic modulus of mount samples shows a higher initial increase. The decrease between 20 to 40 days into ageing was stronger for the mount samples, and its final increase came later than the sheet samples. Figure 7.5 shows the difference in crosslink density changes between air aged mount samples and sheet samples.

164
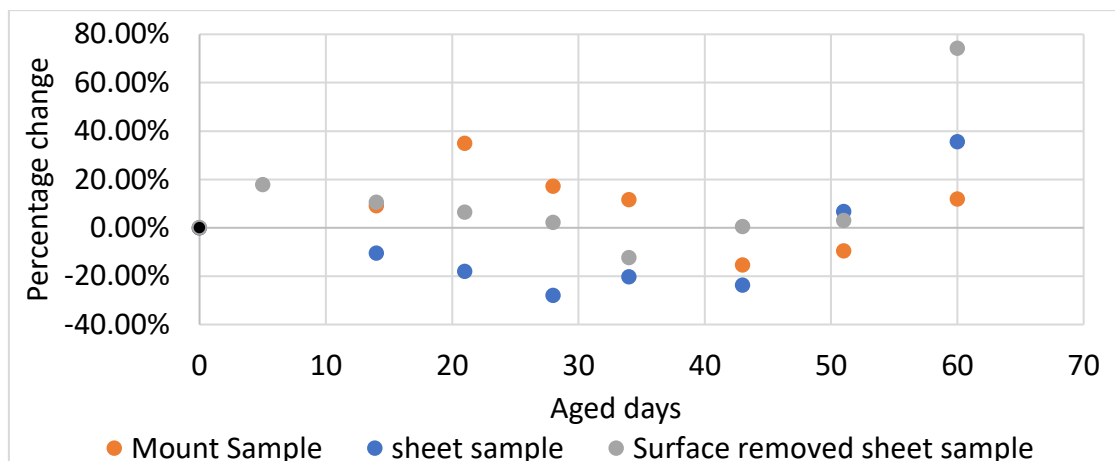
Figure 7.5 Percentage crosslink density changes of mount and sheet samples

The main difference that can be seen is the stronger increase at the beginning for mount samples which is suspected to be caused by the different post-curing and thermal degradation behaviour. The decrease on the mount sample was also more significant after 24 days into ageing. All samples started to increase with different magnitudes between 34 to 43 days into ageing.

7.4.2 Behaviour of carbon re-agglomeration and loss of additives in sheet sample

In Chapter 4, the results clearly showed that the carbon re-agglomeration on the sheet sample was less significant than what have been observed in the used mount. Although the material was different, the dependence of ageing time of carbon re-agglomeration was noticed in Chapter 4.2.3 when comparing distribution of carbon aggregates between used engine mounts. Artificial ageing under a high temperature environment was unable to simulate the whole effect of this mechanism.

The rubber in the engine mount was under cyclic loading during service, two articles suggested the effect of cyclic loading on rubber experienced 10^5 to 10^6 cycles, respectively, none of them are close to the conditions of a real engine mount [28] [119]. However, both of them suggested an increase of elastic modulus could be caused by cyclic loading, Zhang et al. (2014) suggested that this is because the reformation of fillers during cyclic loading improved the filler distribution [119].

This implies carbon re-agglomeration in the short artificial ageing experiment may increase the elastic modulus of the material, rather than decrease it.

The concentrations of additives with known functionalities decreased by more than 50% in the first 30 days and most of them depleted before 60 days into ageing, which indicated that it could be responsible for the increase of elastic modulus before 21 days into ageing. However, the significance of this mechanism in this stiffening of the material remains unknown. Although the measured crosslink density did not show an increase in this period for the sheet samples, it could be that the chain scission caused by oxidative degradation in the surface region concealed the actual crosslink density changes in the entire sample. The need to identify the impact of post-curing and thermal degradation led to the anaerobic artificial ageing experiment, which could then reveal or confirm the impact of other ageing mechanisms.

7.5 Aerobic Verses Anaerobic Artificial Ageing for Sheet Samples

7.5.1 Difference on elastic modulus changes

When comparing elastic modulus changes on samples from both lab-ageing tests in Figure 7.6, the increase at the beginning is not shown for the anaerobic aged samples and the increase at the end of it was weaker. The difference observed upon the initial elastic modulus could be caused by the ageing of the material in real life between the aerobic test and the anaerobic test, which is 1.5 years. The increase of the elastic modulus at the beginning and at the end are caused by air contact, as they were not observed in the anaerobic aged samples.
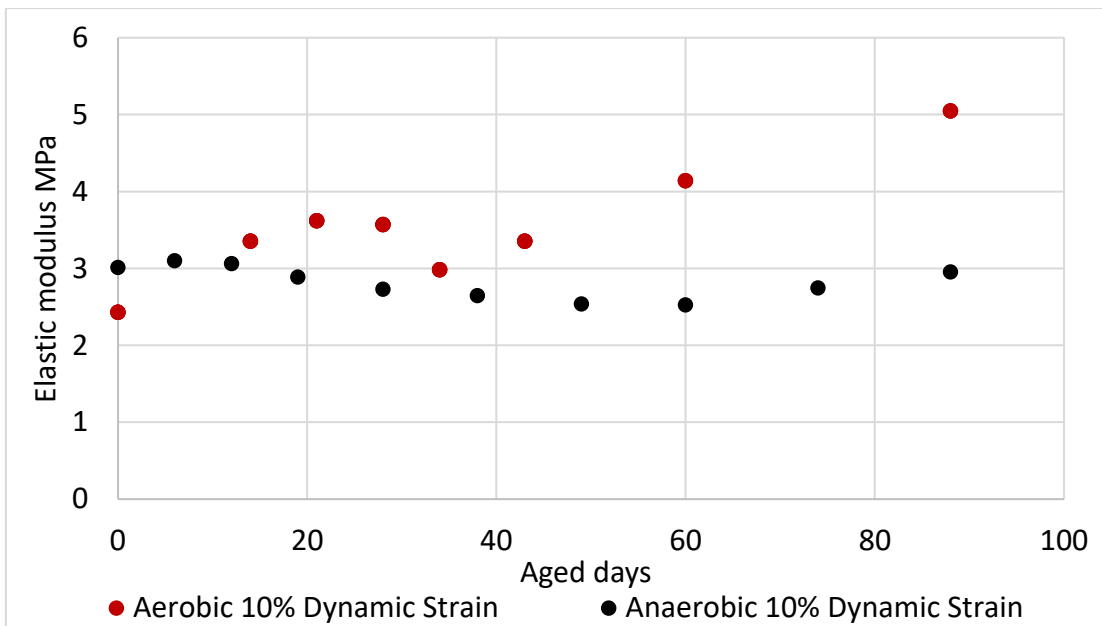
Figure 7.6 Comparing elastic modulus changes of aerobic aged samples and anaerobic aged samples

7.5.2 Difference on crosslink density changes

Figure 7.7 compares the crosslink density changes of the aerobic aged samples and the anaerobic aged samples. The crosslink density of samples aged in air started decreasing earlier than the samples aged in nitrogen. The increase after 40 days into ageing was stronger for samples aged in air.
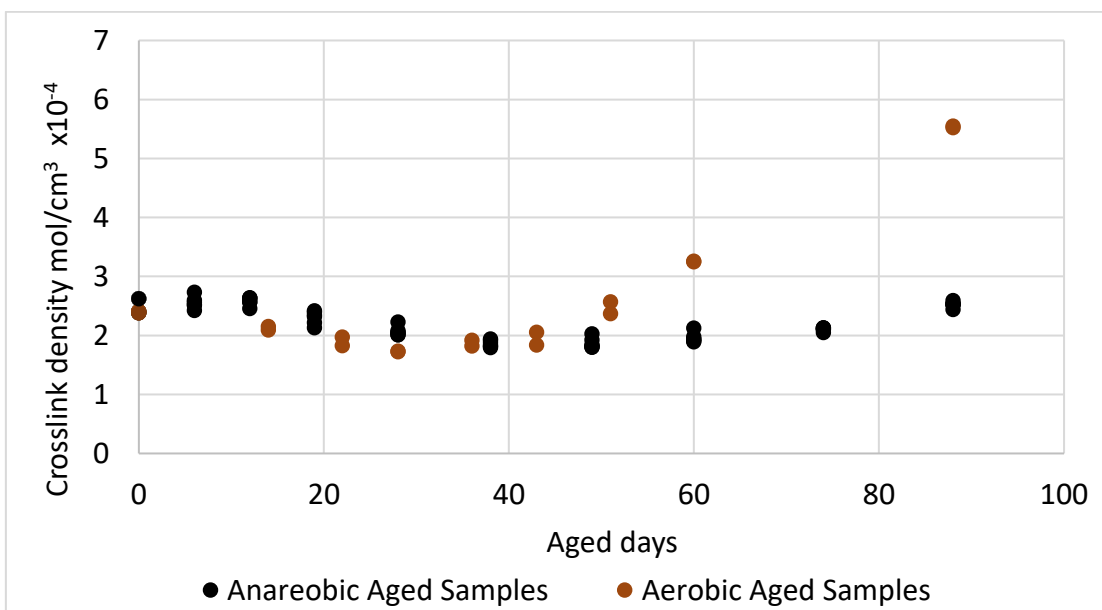
Figure 7.7 Crosslink density changes of aerobic and anaerobic accelerated ageing test

Figure 7.8 compares the crosslink density changes of the aerobic aged surface removed sheet samples and the anaerobic aged sheet samples. Their trends are similar before 30 days into ageing. This close match is expected, as the effects from oxidation and ozonation are expected to be insignificant in the bulk of the material at the beginning stage of the ageing process.
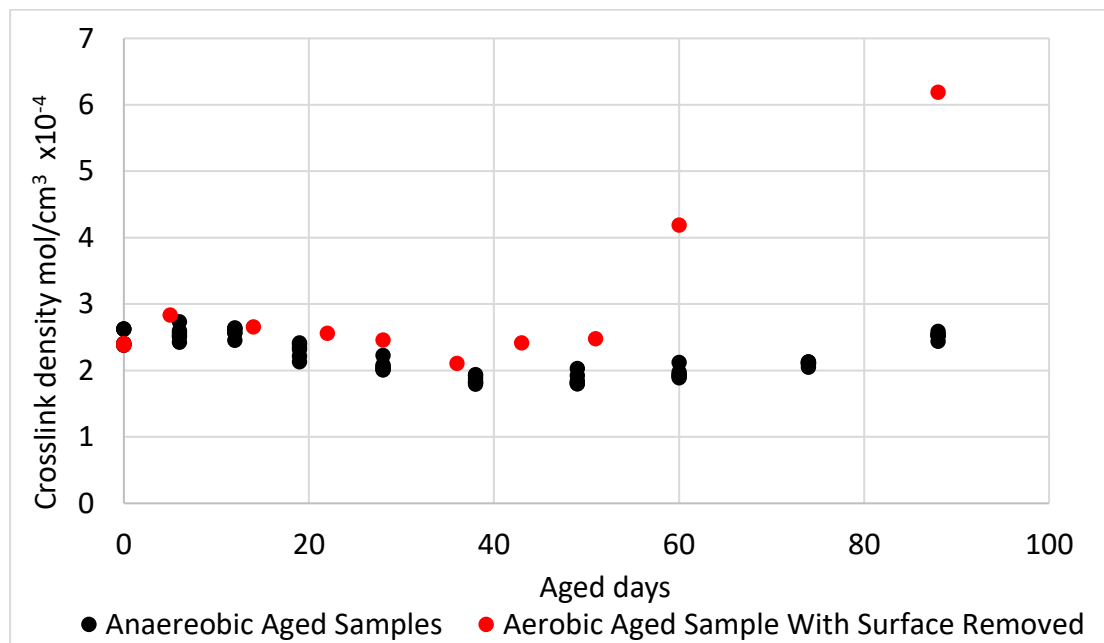
Figure 7.8 Crosslink density changes of aerobic aged and anaerobic aged samples

7.5.3 Differences on carbon filler distribution and additives' concentrations changes

The carbon re-agglomeration and loss of plasticisers/paraffin wax observed in the aerobic ageing test was not observed from samples in the anaerobic ageing test. The loss of antioxidants occurs in both tests, but the depletion rate was much higher under aerobic condition.

The difference on loss of additives between aerobic and anaerobic aged samples suggests that the plasticisers at the surface of the material may also be oxidised and depleted. The depletion of additives at the surface of the material then triggers the migration of additives inside the material. It is also possible that the fast depletion and migration of antioxidants and paraffin-wax might have lowered the activation energy for other additives to migrate, as the environment became more dynamic.

7.5.4 The relationship between overall ageing behaviour of elastic modulus and ageing mechanisms

Table 7-2 summarises the changes of each measured property during the aerobic and anaerobic accelerated ageing test. At the first turning point of elastic modulus changes of samples aged in air at around 20 days into ageing, the changing mechanisms included crosslink density (in nitrogen) and concentrations of additives.

Property	Aged days / Environment	0-20 days	20-40 days	40-60 days	60-90 days	137 days
Elastic modulus	Air	Increase	decrease	increase	increase	Increase
	Nitrogen	Stable	Slowly decrease	Stable	Slowly increase	N/A
Crosslink density	Air	Slowly decrease	Slowly decrease	Increase	Increase	Increase
	Nitrogen	Stable	Slowly decrease	Stable	Slowly increase	N/A
Carbon filler size	Air	N/A	N/A	N/A	N/A	Minor increase
	Nitrogen	N/A	N/A	N/A	Stable	N/A
Concentration of plasticisers	Air	Decrease	Slowly Decrease	Slowly Decrease	Slowly Decrease	N/A
	Nitrogen	Stable	Stable	Stable	Stable	N/A
Concentration of Antioxidants	Air	Decrease	Slowly decrease	Depleted	Depleted	
	Nitrogen	Slowly decrease	Slowly decrease	Slowly decrease	Stable	N/A

Table 7-2 Property changes of sheet samples during ageing

Figure 7.9 shows the percentage changes of both the elastic modulus and the crosslink density changes of aerobic aged samples. This increase of elastic modulus before 20 days into ageing was not caused by the crosslink density

changes. Under both the aerobic and anaerobic environments, crosslink density did not increase during this period. As discussed in the previous chapter, the peak elastic modulus was also at the same period when most of the identified plasticisers depleted. It can be deduced that the loss of plasticisers and paraffin wax increased the elastic modulus of the sample in the first 20 days into ageing.
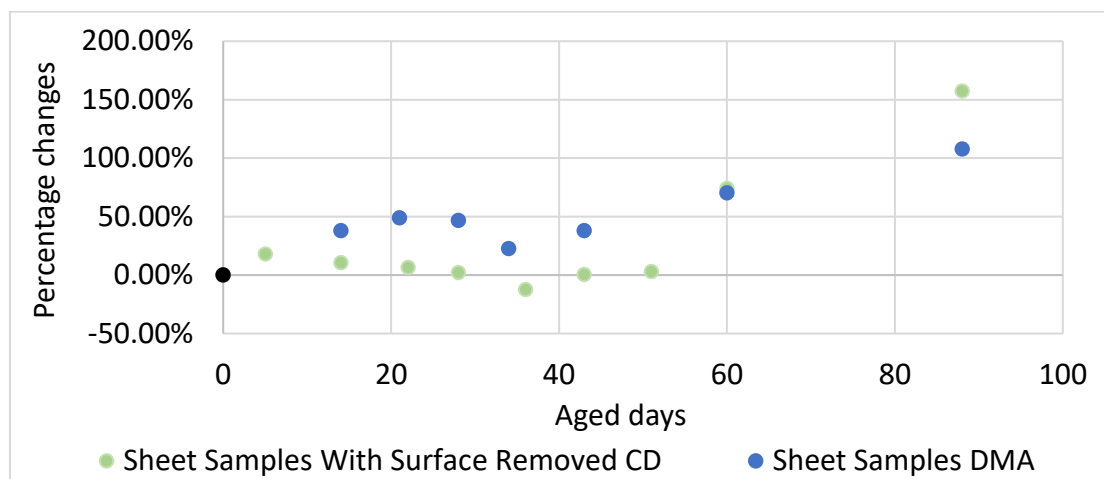
Figure 7.9 Percentage changes of crosslink density and elastic modulus of aerobic aged samples

The impact of air contact is represented by the difference between the aerobic and anaerobic accelerated ageing tests results. The impact of oxidation and ozonation can, therefore, be deduced. Although the behaviour of loss of additives and carbon re-agglomeration were different for samples aged in different environments, the impact of loss of additives has no proven connection with the crosslink density as mentioned in Chapter 2.3.5. The carbon re-agglomeration was weak on the sample aged 137 days in the aerobic test and was insignificant on the sample aged 90 days in the anaerobic test. When considering the possible impact of carbon dispersion mentioned in Chapter 2.3.5 and 2.4.3, its impact on elastic modulus and crosslink in the anaerobic artificial ageing test can be negligible.

Although oxidation and ozonation reduced the measured crosslink density, its impact on the overall elastic modulus is less significant as the chain-scission mainly occurs at the surface region of the sample. It may still contribute to the decrease of the elastic modulus, as the accelerated aged samples were relatively small and are covered by the predicted critical depth. Hence, the decrease of the elastic modulus could be caused by both the oxidation/ozonation and the post-curing

phenomenon. This explains why the decrease of elastic modulus between 20-40 days is more significant for the samples aged in air.

The increase of elastic modulus and crosslink density after 40 days is likely to be initiated by the post-curing effect. The changing dominating mechanism for oxidation due to the lack of oxygen mentioned in Chapter 2.4.1 could also contribute to this.

The changes on the measured crosslink density and elastic modulus was on the same amplitude until 50 days into ageing. As mentioned in Chapter 2.3, the changes on elastic modulus of a rubber should be similar to its crosslink density changes. The severely damaged rubber network could be the reason causing this different increasing rate between crosslink density and elastic modulus after day 50, as the material is losing its identity as an elastomer. It is possible that carbon re-agglomeration also contributed to the increase of crosslink density. As mentioned in Chapter 2.3, trapped rubber is generated during the manufacturing process when the aggregates form. In this accelerated ageing test, the filler that migrates under a high temperature environment means that the newly formed large aggregates can potentially trap polymer chains during their formation. This increase was not shown in the measured elastic modulus, as this constraint can be easily broken down when the 10% static strain is applied.

7.5.5 Ageing behaviour of all the ageing mechanisms and the elastic modulus sheet rubber

Effect of post-curing and thermal degradation

The impact of post-curing and thermal degradation was confirmed, which is the measured ageing behaviour of the anaerobic accelerated aged samples. A possible increase smaller than 5% on both properties was observed before 12 days into ageing. It then decreased the material's crosslink density by 25% and elastic modulus by 15%. Between about 20 to 50 days into ageing, it increased by 25% for crosslink density and 15% for elastic modulus until 90 days into ageing.

Post-curing and thermal degradation were considered as a whole thing. Because both are triggered by temperature and time, making it impossible to separate their impact. Although based on the acting mechanisms, post-curing is responsible for crosslinking and thermal degradation is responsible for chain-scission.

Effect of oxidation

Oxidation primarily occurs at the surface region of the material, its effects decay with depth. Based on the differences between the aerobic and anaerobic accelerated ageing test, its impact was deduced. It reduces the crosslink density and hence elastic modulus of the material before 50 days into the aerobic artificial ageing test. It then caused a dramatic increase of both properties due to the severely damaged polymer network. Or, as suggested by Bonfils et al. (1999) the insufficient oxygen atom diffused in the interior of the material makes crosslinking the dominanting effect [102].

Effect of carbon re-agglomeration

Carbon re-agglomeration is likely to be related to the time of ageing and, therefore, it was not significant in the artificial ageing tests. However, it was possible that carbon re-agglomeration caused an increase in the elastic modulus of the material aged over a short period. Both Zhang et al. and Garnier et al. suggested the re-formation of fillers, in the short-term, could improve the filler distribution [28] [119].

Effect of loss of additives

More than 50% of most plasticisers including paraffin wax in sheet rubber samples have been lost before 25 days into aerobic accelerated ageing, with one major plasticiser reaching 20% of its original concentration. The antioxidant 6PPD has reached 5% of its original concentration in this period and DPPD, the antiozonant, reaches 5% at around 45 days into ageing. The concentrations of additives keep decreasing with a slower decreasing rate.

The loss of plasticisers and paraffin wax would increase the elastic modulus of the material, thus, this phenomenon keeps hardening the material with a decreasing

hardening rate. The depletion of antioxidant makes the material more vulnerable to oxidation.

Ageing behaviour of aerobic aged sheet rubber explained

At this stage, the ageing behaviour of the accelerated aged sheet samples can be thoroughly explained. The impact of each individual ageing mechanism acting on the sheet samples were identified or deduced. Table 7-3 summarises the dominating mechanisms at each stage of elastic modulus changes.

	0-20 days	20-40 days	40-137 days
Elastic modulus	**Increase**	**Decrease**	**Increase**
Crosslink density	**Slowly decrease**	**Slowly decrease**	**Increase**
Dominating ageing Mechanism	Loss of paraffin wax and plasticisers increased the elastic modulus; oxidation on the outer surface led to the decrease on crosslink density.	Oxidation and thermal degradation caused chain scission, reduced both the elastic modulus and crosslink density.	Scission of backbone chains caused by oxidation made the rubber lost its resilience. The formation of trapped rubber during carbon re-agglomeration might contribute to the increase of crosslink density.

Table 7-3 Ageing behaviour of sheet rubber and responsible ageing mechanisms

7.6 Ageing Behaviour of Artificially Aged Mount Samples and Rubber in the Ageing Mount

7.6.1 *Artificially aged mount samples*

The ageing behaviour of mount samples was expected to be similar to the sheet samples. Based on the discussion made on their differences on the post-curing and

thermal degradation behaviour, their impact on mount samples were deduced. They were likely to significantly increase the material's crosslink density and elastic modulus before 20 days into ageing, then decrease both properties after 20 days into ageing. It was not possible to deduce its behaviour after 50 days into ageing. Table 7-4 summarises the explanation of the ageing behaviour of mount samples.

	0-20 days	20-40 days	40-137 days
Elastic modulus	**Increase**	**Decrease**	**increase**
Crosslink density	**Increase**	**Decrease**	**Increase**
Dominating ageing Mechanism	Increase of the elastic modulus was caused by the loss of additives and post curing, post curing also increased the crosslink density.	Oxidation and thermal degradation caused chain scission, reduced both the elastic modulus and crosslink density.	Scission of backbone chains caused by oxidation made the rubber lost its resilience. The formation of trapped rubber during carbon re-agglomeration might contribute to the increase of crosslink density.

Table 7-4 Ageing behaviour of mount sample

7.6.2 *Rubber in used engine mount*

The rubber component contains regions contacting air and away from air. Based on established effects of individual ageing mechanisms acting on artificially aged samples, this section attempts to explain the ageing behaviour of rubber in the used engine mount.

Unlike anaerobic aged sheet samples, loss of additives and carbon re-agglomeration has been observed on samples taken from the bulk region of used rubber mounts. The depletion of surface region additives could trigger the migration of additives in the bulk region, as the additives tend to flow to regions with lower additive concentration [136].

The behaviour of ageing mechanisms acting on the mount is summarised in Table 7-5, there is no clear connection between the rate of occurrence across the mechanisms. The rate of each mechanism is closely related to the ageing condition of the engine mount, which depends on the driving habits of each driver.

Mechanism Age		Beginning	Middle	End
Post-curing	Impact on material	Crosslinking	Chain scission (deduced)	Unknown
	Impact on elastic modulus	Increase	Decrease	Unknown
Oxidation (mainly at surface region)	Impact on material	Chain scission	Chain scission	·Chain scission ·Crosslinking (Literature)
	Impact on elastic modulus	Decrease	Decrease	·Decrease (outside) ·Increase (inside)
Loss of additives	Impact on material	Loss of additives	Loss of additives	Depletion
	Impact on elastic modulus	Increase	Increase	None
Carbon re-agglomeration	Impact on material	Reformation of aggregates (literature)	Forming larger aggregates (predicted)	Forming larger aggregates (predicted)
	Impact on Elastic Modulus	Increase	Decrease	Decrease

Table 7-5 Effects of each ageing mechanism, measured, deduced, or predicted

Figure 7.10 shows the percentage changes of the elastic modulus and crosslink density of the samples taken from the bulk region of the rubber component in used engine mounts.
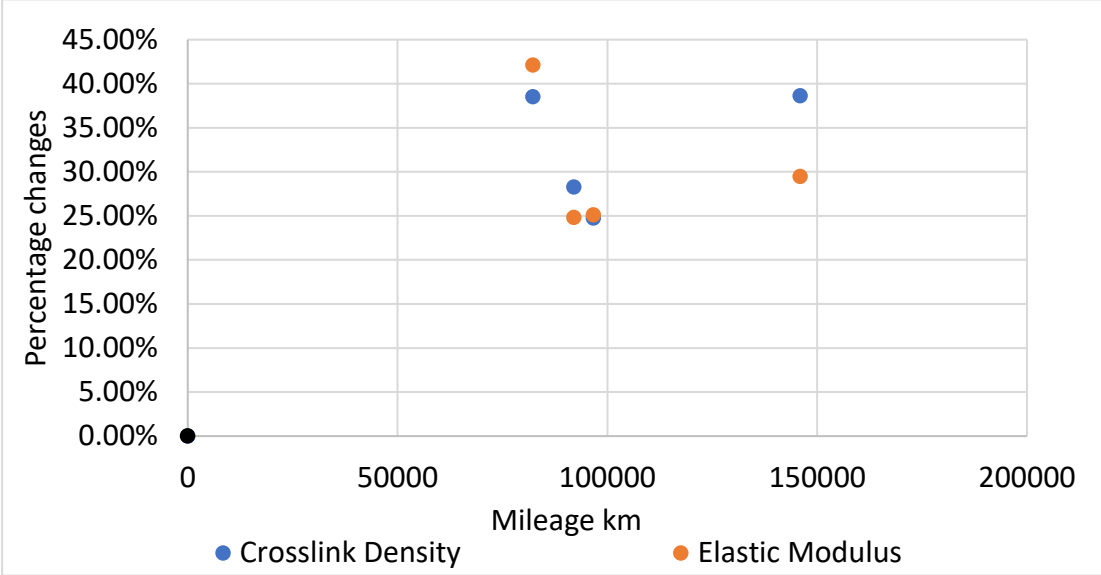
Figure 7.10 Percentage changes of elastic modulus and crosslink density of used mount samples

The overall increase was likely to be caused by both the post-curing effect and loss of additives. The observed decrease of elastic modulus and crosslink density after the newest used mount is also possible. The increase of elastic modulus for the newest used mount is about 40%, lower than the maximum (60%) observed in the aerobic artificial ageing test. Although the maximum can be different due to the different ageing conditions, it is possible that the newest used mount has passed the peak of elastic modulus and is on the downhill. Clearly, both the carbon re-agglomeration and the post-curing effect could lead to this reduction. For the mount aged the most, the higher crosslink density could be caused by oxidation, as its high temperature operating time was 40% more than other used mounts and the sampling location was in the bulk where oxygen atoms could be insufficient.

Figure 7.11 shows the crosslink density changes of samples taken from other locations on the engine mount. As they were all close to the surface of the mount, the behaviours are dominated by chain scission caused by oxidation. Except from the decrease of crosslink density caused by oxidation, the behaviour of crosslink density changes at these three locations after the first used mount are similar to the behaviour of the bulk region.
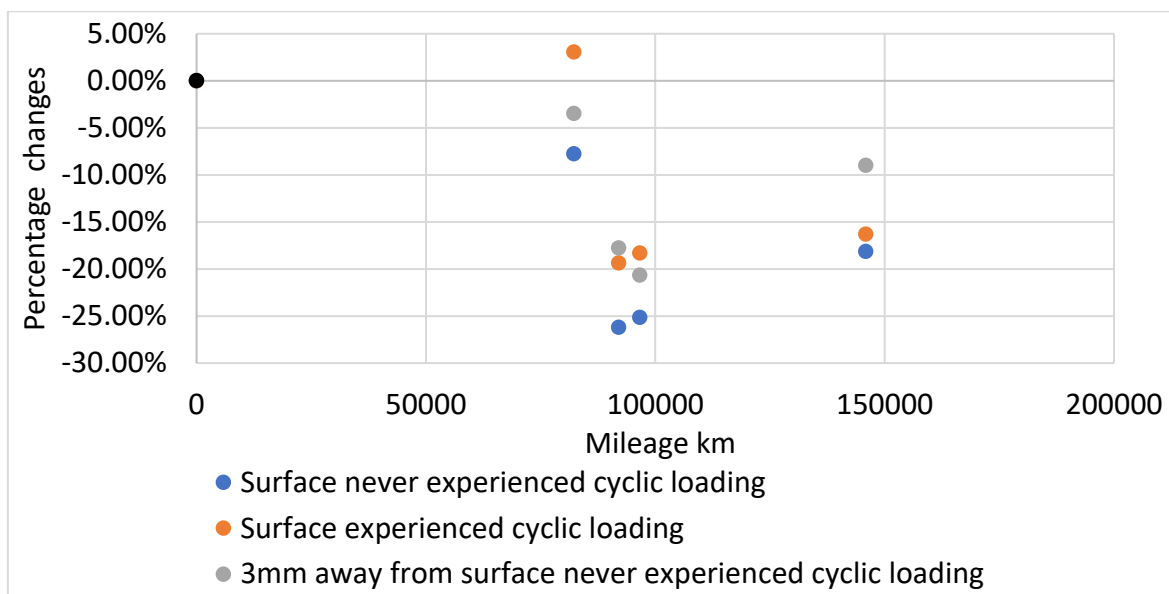
Figure 7.11 Crosslink density changes at other locations on the mount

It can be seen that the crosslink density changes of samples taken from the location that experienced cyclic loading is slightly different from the two that never experienced cyclic loading. This difference was observed in Chapter 4.2.1, but the knowledge of different ageing mechanisms was insufficient to make any deduction.

At the beginning, the crosslink density increased for samples taken from the location that experienced cyclic loading. This could be caused by the reforming of aggregate suggested by literature [28]. The increase before the mount aged the most was less significant for samples taken from this location when compared to samples from locations that never experienced cyclic loading. This could be caused by the increase of trapped rubber under a pure high temperature environment as discussed in section 7.5.4. The rubber chains would be harder to trap when the rubber is frequently deformed.

CHAPTER 8.   CONCLUSION AND FUTURE WORK

8.1 Conclusion

This work has demonstrated an explanation for the ageing behaviour of rubber used in an engine mount, based on separating and investigating the impact of individual acting ageing mechanisms. This is the first time similar work has been done in such a comprehensive way for such a long period of ageing time.

Through investigating rubber samples taken from real-life used engine mounts, aerobic accelerated aged rubber samples and anaerobic accelerated aged rubber samples, the impact and time each acting ageing mechanism occurred have been identified or deduced, as well as the overall impact on the material during ageing. Key conclusions are as follows:

8.1.1   Ageing behaviour of rubber in used mounts

The elastic modulus of rubber increased by at least 25% for all used mounts. Samples from the least aged increased by 45% and the most aged mount increased by 30%. Crosslink density changes were similar with the elastic modulus changes in the bulk area of used mount. Lower crosslink densities were observed at near surface regions.

Loss of additives and post-curing of mount material could have led to the increase of elastic modulus. Thermal degradation, carbon re-agglomeration and oxidation were likely to be responsible for the decrease of elastic modulus.

There is an ageing gradient for the oxidative degradation, its effect is stronger at the surface region and reduces through depth; deep inside, crosslinking may become the dominating mechanism. This led to the difference between crosslink density changes at different locations.

8.1.2 Relationship between elastic modulus changes and acting ageing mechanisms

Initially, elastic modulus of artificially aged rubber samples increased by 50% for the sheet sample and 60 % for the mount sample in the first 20 days into oven accelerated ageing in air. In this period, loss of plasticiser occurred on both sheet samples and mount samples. For the mount sample, its crosslink density has increased due to the possible post-curing mechanism during this period.

After 20 days into ageing, the elastic modulus decreased by 30% for the sheet sample and 60% for the mount sample. Thermal degradation has caused a reduction of crosslink density for the sheet samples in this period. The same mechanism was also found to be happening on the mount samples. The oxidative degradation is likely to be accelerated after a few days into ageing due to the fast depletion of antioxidant. Ozonation and oxidation caused chain scission, which decreased the crosslink density of the material.

A final increase of elastic modulus was observed after around 45 days into ageing before the samples no longer behave like a rubber and lost their resilience. The stiffening was 100% for the sheet samples and 40% for the mount samples. Chain scission caused by oxidation is expected accelerate after the antioxidant depletes, which breaks down the polymer network at the end. Insufficient oxygen atoms for the fast oxidative degradation inside the material could trigger crosslinking inside the material.

8.1.3 Viability of using sheet samples

While showing some differences on the overall properties, the sheet samples provided guidelines on the impact of each ageing mechanism, under the circumstance of insufficient mount material.

8.1.4 Aerobic and anaerobic artificial ageing

The impact of post-curing and thermal degradation varies between materials and could be complex. However, its impact on crosslink density is often entangled with

oxidative degradation when taking the measurements. The comparison between results from aerobic ageing and anaerobic artificial ageing experiments was critical for identifying the actual impact of each ageing mechanism.

8.1.5 *Impact of cyclic loading*

The impact of cyclic loading on crosslink density was insignificant, however, it had influenced the electrical properties of the material, which is related to the carbon filler distribution in the material.

8.1.6 *Suggestions on mount design*

Antioxidants and antiozonants were found to be more volatile than other additives. They would migrate and evaporate without the presence of air. Since oxidative degradation was the main reason for damage to the polymer network, antioxidants that can last longer are suggested to increase the life span of the engine mount.

The elastic modulus increase caused by loss of additives is unavoidable and took place at the beginning of the ageing process. In order to keep the overall performance of the mount unchanged, another mechanism that can counter its impact is needed. Therefore, it is suggested to design a curing recipe that can make the material reduce its crosslink density at the beginning of the ageing process.

8.2 Recommended Future Work

8.2.1 *Effect of carbon filler's structure*

Differences on conductivity were noticed between locations that have experienced cyclic loading and those that have never experienced cyclic loading. As mentioned in Chapter 2.4.3, changes to conductivity were likely to be related to the re-configuration of the carbon network [121]. Although the size distribution showed no significant differences, the filler structure could be different, which leads to the

possible investigation on how structures of filler aggregates changed during ageing and how cyclic loading impacts.

8.2.2 Effect of TMF – Thermo Mechanical Fatigue

The effect of cyclic loading on mechanical properties was not thoroughly investigated. Although the impact was proposed to be not as significant as the temperature effect based on the initial investigation, its impact upon elastic modulus of the material requires further investigation to be confirmed.

8.2.3 Link the changes with resistance to creep which leads to geometry changes

Although creep does not have known effects on elastic modulus, creep and the consequent geometry change is known to be related to the overall mechanical properties of the product. Thus, the changes on creep resistance of the material while ageing could be important for predicting the product performance.

8.2.4 Understanding the chain mechanisms in post-curing and thermal degradation for rubber manufactured with different techniques

The post-curing and thermal degradation mechanisms are affected by both manufacturing method and the curing method. An understanding of the chain mechanisms during the post-curing and thermal degradation process for rubbers that have been prepared differently is critical, as this can help to predict the impact of post-curing and thermal degradation, which can only be measured in experiments, currently.

8.2.5 Investigating thicker material and the property gradient

The existence of properties' gradient caused by ageing gradient of certain mechanisms was confirmed. Although the current method can provide explanation

on properties in a coarse scale, detailed gradient of changes of each related mechanism is essential for predicting properties of thicker materials.

8.2.6 Progression of acting ageing mechanisms under different ageing conditions

This work showed the progression of each ageing mechanism under 95 °C on small block specimens, and how different ageing mechanisms dominate at different times in the whole ageing process. The operating environment keeps changing for the real-life engine mounts; therefore, how different temperatures and cyclic loading conditions influence the progression speed of each acting ageing mechanisms can be investigated. Which could then predict the level of progression of ageing mechanisms in real-world rubber materials, according to the mileage, time in service, average driving speed and the sampling location.

8.2.7 Investigate the relationship between the level of each mechanism and percentage change on elastic modulus.

This work showed how elastic modulus of the material changes with specific levels of progression of each ageing mechanism. The influence of them may not be a simple addition. A model between the elastic modulus of the material and the level of progression of each ageing mechanism is desired. Together with the previously mentioned recommended works, the full ageing behaviour of an engine mount with known ageing conditions could be predicted.

CHAPTER 9. REFERENCES

[1]   E. Eckermann, World History Of The Automobile, Sae International, 2001.

[2]   D. Leibling, "Car Ownership In Great Britain," 10 2008. [Online]. Available: Http://Www.Racfoundation.Org/Assets/Rac_Foundation/Content/Downloadables/Car%20ownership%20in%20great%20britain%20-%20leibling%20-%20171008%20-%20report.Pdf. [Accessed 26 09 2016].

[3]   D. Scutt, "2016 Was A Record-Breaking Year For Global Car Sales, And It Was Almost Entirely Driven By China," Business Insider, 19 01 2017. [Online]. Available: Https://Www.Businessinsider.Com.Au/2016-Was-A-Record-Breaking-Year-For-Global-Car-Sales-And-It-Was-Almost-Entirely-Driven-By-China-2017-1. [Accessed 12 08 2019].

[4]   K. International, "Kpmg's Global Automotive Executive Survey 2014," 2014. [Online]. Available: Https://Www.Kpmg.Com/De/De/Documents/Global-Automotive-Executive-Survey-2014-Kpmg.Pdf. [Accessed 26 09 2016].

[5]   M. Elizabeth N, R. G. W, S. B. H. G And S. Andrew, "Examination Of Abs-Related Driver Behavioral Adaptation – On-Road Microdas Study," 12 2002. [Online]. Available: Http://Www.Nhtsa.Gov/Dot/Nhtsa/Nrd/Multimedia/Pdfs/Vrtc/Ca/Capubs/Nhtsaabs7-2finalreport.Pdf. [Accessed 26 09 2016].

[6]   M. D. Akhtar, "Wheel Steering System," *International Journal Of Engineering Research And Technology.,* Vol. 6, No. 3, Pp. 393-398, 2013.

[7]   Racv, "Effectiveness Of Abs And Vehicle Stability Control System," Royal Automobile Club Of Victoria Ltd, 2004.

[8]   Glassforeurop, "Characteristics Of Automotive And Transport Glass," [Online]. Available: Http://Www.Glassforeurope.Com/En/Products/Automotive-Transport-Glass-Charateristics.Php. [Accessed 26 09 2016].

[9]   Shu Jun Wang And Jun Jie Gu, "International Refrigeration And Air Conditioning Conference," Purdue, 2004.

[10]   M. P. Reed, "Survey Of Auto Seat Design Recommendations," University Of Michigan, Michigan, 2000.

[11]   Z. Zhang, H. R. Karimi, H. Huang And K. G. Robbersmyr, "Vibration Control Of A Semiactive Vehicle Suspension System Based On Extended State Observer Techniques," *Journal Of Applied Mathematics,* Vol. 2014, 2014.

[12]   M. Ishihama, S. Satoh, K. Seto And A. Nagamatsu, "Vehicle Vibration Reduction By Transfer Function Phase Control On Hydraulic Engine Mounts," *Jsme International Journal. Ser. C, Dynamics, Control, Robotics, Design And Manufacturing,* Vol. 37, No. 3, Pp. 536-541, 1994.

[13]   W. Richter, "Average Age Of Cars & Trucks By Household Income And Vehicle Type Over Time," Wolf Street Corp, 21 8 2018. [Online]. Available: Https://Wolfstreet.Com/2018/08/21/Average-Age-Of-Cars-Trucks-Vehicles-By-Household-Income-Vehicle-Type/. [Accessed 11 8 2019].

[14]   C. Threewitt, "Will New Motor Mounts Increase Engine Response?," Howstuffworks, [Online]. Available: Https://Auto.Howstuffworks.Com/New-Motor-Mounts-Increase-Engine-Response.Htm. [Accessed 12 08 2019].

[15]   T. Charlet, "How Long Do Engine Motor Mounts Last?," Yourmechanic , 02 12 2015. [Online]. Available: Https://Www.Yourmechanic.Com/Article/How-Long-Do-Engine-Motor-Mounts-Last. [Accessed 11 08 2019].

[16]   T. M. Sport, "Rsr Engine/Trans Mount," [Online]. Available: Http://Tremotorsports.Com/Engine/Rsr-Enginetrans-Mount. [Accessed 28 09 2016].

[17]   T. B. Blog, "Marine Engine Mounts And System Alignment," Marine.Com, 14 02 2012. [Online]. Available: Https://Go2marine.Wordpress.Com/2012/02/14/Marine-Engine-Mounts-And-System-Alignment/. [Accessed 2019 08 13].

[18]   A. P. Inc, "Marine And Industrial Engine Mounts," Av Products Inc, [Online]. Available: Https://Www.Avproductsinc.Com/Mobile-Marine/Fail-Safe-Mounts.Html. [Accessed 13 08 2019].

[19]   Vulkan_Couplings, "Resilient Mounts Technical Data," Vulkan Couplings, Herne, 2014.

[20]   N. Rana, "Conventional Vs Hydro Mount Use For Automotive Powertrain," Cae/Nvh At Zhongding Group, 09 10 2017. [Online]. Available: Https://Www.Linkedin.Com/Pulse/Conventional-Vs-Hydro-Mount-Use-Automotive-Powertrain-Nitin-Rana/. [Accessed 13 08 2019].

[21]   Amalji, "Default Hydraulic Engine Mounts Vs Rubber Engine Mounts," Team-Bhp, [Online]. Available: Https://Www.Team-Bhp.Com/Forum/Technical-Stuff/136184-Hydraulic-Engine-Mounts-Vs-Rubber-Engine-Mounts.Html. [Accessed 13 08 2019].

[22]   L. Carley, "Tech Feature: Active Motor And Trans Mounts," Babcox Media, 27 06 2011. [Online]. Available: Https://Www.Brakeandfrontend.Com/Tech-Feature-Active-Motor-And-Trans-Mounts/. [Accessed 13 08 2019].

[23]   M. Lu, "Study Of Automotive Hydromount Mechanism," Western Michigan University, Michigan , 2001.

[24]   Partinfo, "Engine Mounts - The Inside Story," [Online]. Available: Http://Www.Partinfo.Co.Uk/Articles/169. [Accessed 20 10 2016].

[25]   B.-H. Lee And C.-W. Lee, "Model Based Feed-Forward Control Of Electromagnetic Type Active Control Engine-Mount System," *Journal Of Sound And Vibration,* Vol. 323, No. 3-5, Pp. 574-593, 2009.

[26]   N. Tang, P. Soltani, C. Pinna, D. Wagg And R. Whear, "Ageing Of A Polymeric Engine Mount Investigated Using Digital Image Correlation," *Polymer Testing,* Vol. 71, No. 1, Pp. 137-144, 2018.

[27]   J.-H. Choi, H. J. Kang, H.-Y. Jeong, J.-H. Choi, H. J. Kang And H.-Y. Jeong, "Heat Aging Effects On The Material Property And The Fatigue Life Of Vulcanized Natural Rubber, And Fatigue Life Prediction Equations," *Journal Of Mechanical Science And Technology,* Vol. 19, No. 6, P. 1229–1242, 2005.

[28]   P. Garnier, J.-B. L. Cam And M. Grédiac, "The Influence Of Cyclic Loading Conditions On The Viscoelastic Properties Of Filled Rubber," *Mechanics Of Materials,* Vol. 56, Pp. 84-94, 2013.

[29] R. Whear And H. And Williams, "Advanced Hydraulically Damped Elastomeric Component Models," *Sae Technical Paper 2005-01-1065,* P. 5, 2005.

[30] J. Colgate, C.-T. Chang, Y.-C. Chiou, W. Liu And L. Keer, "Modelling Of A Hydraulic Engine Mount Focusing On Response To Sinusoidal And Composite Excitations," *Journal Of Sound And Vibration,* Vol. 184, No. 3, Pp. 503-528, 1995.

[31] M. Fukazawa, T. Murao And S. And Unigame, "The Method To Predict The Vibration Transfer Function Of Hydraulic Engine Mount On A Vehicle," *Sae Technical Paper 2016-01-1321,* P. 8, 2016.

[32] P. H. Mott And C. M. Roland, "Aging Of Natural Rubber In Air And Seawater," *Rubber Chemistry And Technology,* Vol. 74, No. 1, Pp. 79-88, 2001.

[33] Y. Itoh And H. S. Gu, "Prediction Of Aging Characteristics In Natural Rubber Bearings Used In Bridges," *Journal Of Bridge Engineering,* Vol. 14, No. 2, Pp. 122-128, 2009.

[34] M. D. Bowles, Chains Of Opportunity: The University Of Akron And The Emergence Of The Polymer Age, University Of Akron Press, 2008.

[35] K. Cornish, "Biochemistry Of Natural Rubber, A Vital Raw Material, Emphasizing Biosynthetic Rate, Molecular Weight And Compartmentalization, In Evolutionarily Divergent Plant Species," *Natural Rubber Product,* Vol. 18, No. 2, Pp. 182-189, 2001.

[36] D. W. Ball, Introductory Chemistry, Cleveland: Saylor Foundation, 2011.

[37] R. O. Ebewele, Polymer Science And Technology, New York: Crc Press Llc, 2000.

[38] A. Ravve, Principles Of Polymer Chemistry, New York: Springer-Verlag New York, 2012.

[39] H. Feng, X. Lu, W. Wang, N.-G. Kang And J. W. Mays, "Block Copolymers: Synthesis, Self-Assembly, And Applications," *Polymers,* Vol. 9, No. 10, P. 494, 2017.

[40] S. T. Sam, M. A. Nuradibah, H. Ismail, N. Z. Noriman And S. Ragunathan, "Recent Advances In Polyolefins/Natural Polymer Blends Used For Packaging Application," *Polymer-Plastics Technology And Engineering,* Vol. 53, No. 6, Pp. 631-644 , 2014.

[41] N. Aloorkar, A. Kulkarni, R. Patil And D. Ingale, "Star Polymer: An Overview," *Internatinal Journal Of Pharmaceutical Sciences And Nanotechnology,* Vol. 5, No. 2, Pp. 1675-1684, 2012.

[42] K. Madaan, S. Kumar, N. Poonia, V. Lather And D. Pandita, "Dendrimers In Drug Delivery And Targeting: Drug-Dendrimer Interactions And Toxicity Issues.," *Journal Of Pharmacy And Bioallied Sciences,* Vol. 6, No. 3, Pp. 139-150, 2014.

[43] A.-V. Ruzette And L. Leibler, "Block Copolymers In Tomorrow's Plastics," *Nature Materials ,* Vol. 4, No. 1, Pp. 19 - 31 , 2005.

[44] R. F. Boyer, "Glassy Transitions In Semicrystalline Polymers," *Journal Of Polymer Science: Polymer Symposia,* Vol. 50, No. 1, Pp. 189-242, 1975.

[45] J. H. Williams, "Order From Force," In *Jeffrey H Williams*, Morgan & Claypool Publishers , 2015 , Pp. 9-1 -- 9-18.

[46] R. M. J. A. Sabu Thomas, Rheology And Processing Of Polymer Nanocomposites, Wiley, 2016.

[47] Q. Wu, O. N. Lee, Z. Cai And D. Zhou, "Creep Behavior Of Borate-Treated Strandboard: Effect Of Zinc Borate Retention, Wood Species, And Load Level," *Maderas. Ciencia Y Tecnología,* Vol. 11, No. 1, Pp. 19-32, 2009.

[48] S. M.Nagaraja, Anasmujtaba And Mariobeiner, "Quantification Of Different Contributions To Dissipation In Elastomer Nanoparticle Composites," *Polymer,* Vol. 111, Pp. 48-52, 2017.

[49] B. B. G.S.Aglietti, "Innovative Viscoelastic Material Selection Strategy Based On Dma And Mini-Shaker Tests For Spacecraft Applications," *Acta Astronautica,* Vol. 131, Pp. 18-27, 2017.

[50] A. H. Abedali, "Predicting Complex Shear Modulus Using Artificial Neural Networks," *Journal Of Civil Engineering And Construction Technology,* Vol. 6, No. 3, Pp. 15-26, 2015.

[51] K. Hanhi, M. Poikelispää And H.-M. Tirilä, "Elastomeric Materials," Tampere University Of Technology, The Laboratory Of Plastics And Elastomer Technology, Tampere, 2007.

[52] Basf, "Thermoplastic Polyurethane Elastomers: Elastollan® – Material Properties," Basf, 2017.

[53] G. Holden, "Rubber Technology," In *Thermoplastic Elastomers*, Springer, 1973, Pp. 465-481.

[54] C. Chandrasekaran, "Anticorrosive Rubber Lining," In *11 - Raw Materials For Rubber Lining Compounds*, William Andrew, 2017, Pp. 77-86.

[55] F. Pacheco-Torgal, S. Jalali And A. Fucic, Toxicity Of Building Materials, Woodhead Publishing, 2012.

[56] A.Y.Coran, The Science And Technology Of Rubber, Academic Press, 2013.

[57] Malaysian Rubber Board , "Natural Rubber Statistic," Malaysian Rubber Board, Malaysian , 2018.

[58] K. Turjanmaa, T. Palosuo, H. Alenius, F. Leynadier, J.-E. Autegarden, C. André, H. Sicard, M. Hrabina And T. X. Tran, "Latex Allergy Diagnosis: In Vivo And In Vitro Standardization Of A Natural Rubber Latex Extract," *Allergy,* Vol. 52, No. 1, P. 41–50, 1997.

[59] J. G. Drobny, Handbook Of Thermoplastic Elastomers, William Andrew, 2007.

[60] Y. Dong, "Effects Of Processing Techniques On Mechanical Properties Of Selected Polymers," University Of North Texas, Texas, 2013.

[61] A. Skrobak, V. J. M. Stanek, D. Manas, M. Ovsik, V. Senkerik And M. Reznicek, "Mechanical Properties Of Injection Molded And Compression Molded Samples From Nature-Butadiene Rubber," In *20th International Conference On Circuits, Systems, Communications And Computers (Cscc 2016)*, Corfu Island, 2016.

[62] A. Škrobák, M. Řezníček, M. Ovsík And V. Janoštík, "The Influence Of Injection Molding On Tensile And Tear Properties Of Epdm Rubber," *Wseas Transactions On Applied And Theoretical Mechanics.,* Vol. 13, Pp. 150-156, 2018.

[63] I. Kopal, J. Vršková, I. Laba, J. D. Ondrušová, P. Hybler, M. Harničárová, J. Valíček And A. M. Kušnerová, "The Effect Of High-Energy Ionizing Radiation On The Mechanical Properties Of A Melamine Resin, Phenol-Formaldehyde Resin, And Nitrile Rubber Blend," *Materials (Basel),* Vol. 11, No. 12, P. 2405, 2018.

[64]   Q. T.H.Shubhra And A.K.M.M.Alam, "Effect Of Gamma Radiation On The Mechanical Properties Of Natural Silk Fiber And Synthetic E-Glass Fiber Reinforced Polypropylene Composites: A Comparative Study," *Radiation Physics And Chemistry,* Vol. 80, No. 11, Pp. 1228-1232, 2001.

[65]   X. Colin, L. Audouin And J. Verdu, "Kinetic Modelling Of The Thermal Oxidation Of Polyisoprene Elastomers. Part 3: Oxidation Induced Changes Of Elastic Properties," *Polymer Degradation And Stability,* Vol. 92, No. 5, Pp. 906-914, 2007.

[66]   H. Gu, "Ageing Effects On High Damping Bridge Rubber Bearing," In *6th Asia-Pacific Structural Engineering And Construction Conference*, Kuala Lumpur, 2007.

[67]   P. Toh-Ae, B. Junhasavasdikul, N. Lopattananona And K. Sahakaro, "Mechanical Properties And Stability Towards Heat And Uv Irradiation Of Natural Rubber/Nanotitanium Dioxide Composites," In *Recent Advances In Materials, Minerals And Environment (Ramm) & 2nd International Postgraduate Conference On Materials, Mineral And Polymer (Mamip)*, Penang, 2015.

[68]   K. G, Paterson And J. R. Mihelcic, "Air Resource Engineering," In *Environmental Engineering: Fundamentals, Sustainability And Design*, Michigan, John Wiley & Sons, 2008.

[69]   M. Furukawa, T. Shiiba And S. Urata, "Mechanical Properties And Hydrolytic Stability Of Polyesterurethane Elastomers With Alkyl Side Groups," *Polymer,* Vol. 40, No. 7, Pp. 1791-1798, 1999.

[70]   C. L. Wanamaker, W. B. Tolman And M. A. Hillmyer, "Hydrolytic Degradation Behavior Of A Renewable Thermoplastic Elastomer," *Biomacromolecules ,* Vol. 10, No. 2, P. 443–448, 2009.

[71]   M. M. Kamal, J. Clarke And M. A. Ahmad, "Comparison Of Properties Of Natural Rubber Compounds With Various Fillers," *Journal Of Rubber Research,* Vol. 12, No. 1, Pp. 27-44, 2009.

[72]   A. Mujkanović, L. Vasiljević And G. Ostojić, "Non-Black Fillers For Elastomers," In *13th International Research/Expert Conference*, Hammamet,, 2009.

[73]   P. H. Education, "Polymers," [Online]. Available: Http://Wps.Prenhall.Com/Wps/Media/Objects/3312/3391650/Blb1202.Html. [Accessed 20 10 2016].

[74]   N. P. Cheremisinoff, Condensed Encyclopedia Of Polymer Engineering Terms, Butterworth-Heinemann, 2001.

[75]   J. Kruželák, R. Sýkora And I. Hudec, "Sulphur And Peroxide Vulcanisation Of Rubber Compounds - Overview," *Chemical Papers,* Vol. 70, No. 12, Pp. 1533-1555, 2016.

[76]   J. Kruželák, R. Sýkora, I. Hudec, Bratislava And Slovakia, "Sulfur And Peroxide Curing Of Rubber Compounds Based On Nr And Nbr. Part I: Cross-Linking And Physical-Mechanical Properties," Kgk-Rubberpoint, Heidelberg, 2017.

[77]   M. D. Stelescu, E. Mănăilă, G. Crăciun, M. Sönmez, M. Georgescu And M. (. Nițuică, "Influence Of Crosslinking Method On The Properties Of Natural Rubber Mixtures," In *H International Conference On Advanced Materials And Systems*, Bucharest, 2016.

[78]   E. Onyshchenko, "Characterisation Of Network Structure In Recycled Rubber," London Metropolitan University, London, 2016.

[79] M. Abu-Abdeen, "Degradation Of The Mechanical Properties Of Composite Vulcanizates Loaded With Paraffin Wax," *Applied Polymer,* Vol. 81, No. 9, Pp. 2265-2270, 2001.

[80] M. Włoch, U. Ostaszewska And J. Datta, "The Effect Of Polyurethane Glycolysate On The Structure And Properties Of Natural Rubber/Carbon Black Composites," *Journal Of Polymers And The Environment ,* Vol. 27, No. 6, P. 1367–1378, 2019.

[81] H. Nabil, H. Ismail And A. Azura, "Optimization Of Accelerators On Curing Characteristics, Tensile, And Dynamic Mechanical Properties Of (Natural Rubber)/(Recycled Ethylene-Propylene-Diene-Monomer) Blends," *Journal Of Vinyl And Additive Technology,* Vol. 21, No. 2, Pp. 79-88, 2015.

[82] W. A. Woishnis And S. Ebnesajjad, Chemical Resistance Of Thermoplastics, William Andrew, 2012.

[83] M. Zielińska, R. Seyger, W. K. Dierkes, D. Bielinski And J. W. Noordermeer, "Swelling Of Epdm Rubbers For Oil-Well Applications As Influenced By Medium Composition And Temperature I: Literature And Theoretical Background," *Elastomery,* Vol. 20, No. 2, Pp. 6-17, 2016.

[84] S. Z. Q. T. Pervez, M. Akhtar And M. S. Al-Kharusi, "Material Behavior Of Water-Swelling And Oil-Swelling Elastomers," In *Conference: International Conference On Applied Mechanics, Materials And Manufacturing ,* Muscat, 2010.

[85] M. P. Group, "Brush Macromolecules," The Matyjaszewski Polymer Group, [Online]. Available: Http://Www.Cmu.Edu/Maty/Materials/Properties-Of-Well-Defined/Brush-Macromolecules.Html. [Accessed 07 10 2016].

[86] K. M. Schmoller And A. R. Bausch, "Similar Nonlinear Mechanical Responses In Hard And Soft Materials," *Nature Materials,* Vol. 12, P. 278–281, 201.

[87] B. Jiang, "Effect Of The Microstructure Of A Filled Rubber On Its Overall Mechanical Properties," *Acta Mechanica,* Vol. 225, No. 4, Pp. 1121-1140, 2014.

[88] M. Galimberti, "Rubber Clay Nanocomposites," In *Advanced Elastomers - Technology, Properties And Applications*, Intech, 2012.

[89] K. Mok And A. Eng, "Characterisation Of Crosslinks In Vulcanised Rubbers: From Simple To Advanced Techniques," Malaysian Rubber Board, Malaysian, 2017.

[90] S. Lh, Introduction To Physical Polymer Science, New York: Wiley, 1986.

[91] F. Zhao, W. Bi And S. Zhao, "Influence Of Crosslink Density On Mechanical Properties Of Natural Rubber Vulcanizates," *Journal Of Macromolecular Science, Part B ,* Vol. 50, No. 7, Pp. 1460-1469, 2011.

[92] P. Gilormini, E. Richaud And J. Verdu, "A Statistical Theory Of Polymer Network Degradation," *Polymer,* Vol. 55, No. 16, Pp. 3811-3817, 2014.

[93] C. B. Reinitz Sd, L. Ra And V. C. Dw, "Crosslink Density, Oxidation And Chain Scission In Retrieved, Highly Cross-Linked Uhmwpe Tibial Bearings.," *Biomaterials,* Vol. 35, No. 15, Pp. 4436-4440, 2014.

[94] P. Ghosh, S. Katare, P. Patkar, J. M. Caruthers, V. Venkatasubramanian And K. A. Walker, "Sulfur Vulcanization Of Natural Rubber For Benzothiazole Accelerated Formulations: From Reaction

Mechanisms To A Rational Kinetic Model," *Rubber Chemistry And Technology,* Vol. 76, No. 3, Pp. 592-693, 2003.

[95] V. M. L. Almeida, "Characterization Of The Factors Involved In The Tire Production Process," The University Of Minho, Braga, Portugal, 2012.

[96] A. Hösl And C. M. Franck, "Swarm Parameter Measurement In Hydrogen, Considering Secondary Photonic Electron Emission," Arxiv, 2018.

[97] E. Manaila, M. D. Stelescu And G. Craciun, "Aspects Regarding Radiation Crosslinking Of Elastomers," In *Advanced Elastomers - Technology, Properties And Applications*, Intech, 2012.

[98] E. M. Kornacka, "Applications Of Ionizing Radiation In Materials Processing," In *Radiation-Induced Oxidation Of Polymers*, Warszawa, Institute Of Nuclear Chemistry And Technology, 2017, Pp. 183-191.

[99] E. J. Clark, Molecular And Microstructural Factors Affecting Mechanical Properties Of Polymeric Cover Plate Materials, Gaithersburg: U.S. Department Of Commerce, 1985.

[100] K. R.W, "Oxidation And Ozonation Of Rubber," *Rubber Chem. Techn,* Vol. 58, Pp. 637-652, 1985.

[101] E. F. Ngolemasango, M. Bennett And J. Clarke1, "Kinetics Of The Effect Of Ageing On Tensile Properties Of A Natural Rubber Compound," *Journal Of Applied Polymer Science,* Vol. 102, No. 4, Pp. 3732-3740, 2006.

[102] F. Bonfils, J. Laigneau, H. De Livonniere, S. Beuve And J. Sainte Beuve, "Study Of Natural Rubber Degradation In A Pri Oven," *Kautschuk Gummi Kunststoffe,* Vol. 52, No. 1, Pp. 32-36, 1999.

[103] R. L. Clough And K. T. Gillen, "Oxygen Diffusion Effects In Thermally Aged Elastomers," *Polymer Degradation And Stability ,* Vol. 38, Pp. 47-56, 1992.

[104] P. P. Database, "Ozonation Reactions And Ozone Cracking In Elastomers," Polymer Properties Database, [Online]. Available: Https://Polymerdatabase.Com/Polymer%20chemistry/Ozone.Html. [Accessed 2019 07 14].

[105] Muramatsu Y.; Nishikawa I, "A Study For The Prediction Of The Long-Term Durability," *Showa Electric Wire Review,* Vol. 45, No. 1, Pp. Pp44-49, 1995.

[106] A. S. Maxwell, W. R. Broughton, G. Dean And G. Sims, "Review Of Accelerated Ageing Methods And Lifetime Prediction Techniques For Polymeric Materials," National Physical Laboratory , Teddington, 2005.

[107] I. Chambridge Polymer Group, "Swelling Measurements Of Crosslinked Polymers," Chambridge Polymer Group, Inc, Chambridge.

[108] Y. K. Chae, W. Y. Kang, J.-H. Jang And S.-S. Choi, "A Simple Nmr Method To Measure Crosslink Density Of Natural Rubber Composite," *Polymer Testing,* Vol. 29, No. 8, P. 953–957, 2010.

[109] T. Saleesung, D. Reicher, K. Saalwachter And C. Sirisinha, "Correlation Of Crosslink Densities Using Solid State Nmr And Conventional Techniques In Peroxide-Crosslinked Epdm Rubber," *Polymer,* Vol. 56, No. 1, Pp. 309-317, 2015.

Chapter 9 -- References

[110] Y. S. R. Yahya, A. R. Azura And Z. Ahmad, "Effect Of Curing Systems On Thermal Degradation Behaviour Of Natural Rubber (Smr Cv 60)," *Journal Of Physical Science,* Vol. 22, No. 2, Pp. 1-14, 2011.

[111] I.-S. Kim, B.-W. Lee, K.-S. Sohn, J. Yoon And J.-H. Lee, "Characterization Of The Uv Oxidation Of Raw Natural Rubber Thin Film Using Image And Ft-Ir Analysis," *Elastomers And Composites,* Vol. 51, No. 1, P. 1~9, 2016).

[112] L. Wu And Y. Zhang, "Enhanced Thermal Oxidative Stability Of Silicone Rubber By Using Cerium-Ferric Complex Oxide As Thermal Oxidative Stabilizer," *E-Polymers,* Vol. 19, No. 1, P. 257–267, 2019.

[113] Z. Fei, C. Long, P. Qingyan And Z. Shugao, "Influence Of Carbon Black On Crosslink Density Of Natural Rubber," *Journal Of Macromolecular Science, Part B,* Vol. 51, No. 6, Pp. 1208-1217, 2012.

[114] D.J.Kohls And G.Beaucage, "Rational Design Of Reinforced Rubber," *Current Opinion In Solid State And Materials Science,* Vol. 6, No. 3, Pp. 183-194, 2002.

[115] W. Fu, Liwang, J. Huang, C. Liu, W. P. Peng, H. Xiao And S. Li, "Mechanical Properties And Mullins Effect In Natural Rubber Reinforced By Grafted Carbon Black," *Advances In Polymer Technology,* Vol. 2019, P. 11, 2019.

[116] S. Kim, W. I. Lee And C. H. Park, "Assessment Of Carbon Nanotube Dispersion And Mechanical Property Of Epoxy Nanocomposites By Curing Reaction Heat Measurement," *Journal Of Reinforced Plastics And Composites,* Vol. 35, No. 1, Pp. 71 - 80, 2016.

[117] L. Karásek And M. Sumita, "Review Characterization Of Dispersion State Of Filler And Characterization Of Dispersion State Of Filler And Composites," *Journal Of Materials Science,* Vol. 31, No. 2, Pp. 281-289, 1996.

[118] T. Xu, Z. Jia, J. Li, Y. Luo, D. Jia And Z. Peng, "Study On The Dispersion Of Carbon Black/Silica In Sbr/Br Composites And Its Properties By Adding Epoxidized Natural Rubber As A Compatilizer," *Polymer Composite,* Vol. 39, No. 2, Pp. 377-385, 2019.

[119] F. Zhang, Y. Chen, C. Sun, S. Wenbd And L. Liu, "Network Evolutions In Both Pure And Silica-Filled Natural Rubbers During Cyclic Shear Loading," *Rsc Advances,* Vol. 4, No. 51, Pp. 26706-26713, 2014.

[120] S. K. Gulrez, M. A. Mohsin, H. Shaikh, A. Anis, A. M. Pulose, M. K. Yadav, E. H. P. Qua And S. Al-Zahrani, "A Review On Electrically Conductive Polypropylene And Polyethylene," *Polymer Composites,* Vol. 35, No. 5, Pp. 900-914, 2014.

[121] G. A.Schwartz, S. Cerveny, Á. J.Marzocca, M. Gerspacher And L. Nikiel, "Thermal Aging Of Carbon Black Filled Rubber Compounds. I. Experimental Evidence For Bridging Flocculation," *Polymer,* Vol. 44, No. 23, Pp. 7229-7240, 2003.

[122] A. Shrivastava, Introduction To Plastics Engineering, William Andrew, 2018.

[123] I. O. F. Standardization, "Iso 176: Plastics -- Determination Of Loss Of Plasticizers -- Activated Carbon Method," International Organization For Standardization, Geneva, Switzerland, 2005.

[124] M. Harada, "Analytical Methods For Vulcanized Rubbers," *International Polymer Science And Technology,* Vol. 43, No. 2, Pp. 192-197, 2015.

[125] X. Liu, J. Zhao, R. Yang, R. Iervolino And S. Barbera, "Thermal Aging Of Hydrogenated Nitrile Rubber – Loss Of Additives And Its Influence On Elasticity Maintenance," *Polymer,* Vol. 2017, No. 7-8, Pp. 588-597, 2017.

[126] E. Kump, M. Ne~Emer, B. Smodis And R. Jacimovic, "Multielement Analysis Of Rubber Samples By X-Ray Fluorescence," *Applied Spectroscopy,* Vol. 50, No. 11, Pp. 1373-1377, 1996.

[127] P.Trapperk And Y.Volokh, "Cracks In Rubber," *International Journal Of Solids And Structures,* Vol. 45, No. 24, Pp. 6034-6044, 2008.

[128] K. Legorju-Jago And C. Bathias, "Fatigue Initiation And Propagation In Natural And Synthetic Rubbers," *International Journal Of Fatigue,* Vol. 24, No. 2-4, Pp. 85-92, 2002.

[129] Y. Liu, L. Li, Q. Wang And X. Zhang, "Fracture Properties Of Natural Rubber Filled With Hybrid Carbon Black/Nanoclay," *Journal Of Polymer Research,* Vol. 18, No. 5, P. 859–867, 2010.

[130] B. A. Miller-Chou And J. L.Koenig, "A Review Of Polymer Dissolution," *Progress In Polymer Science,* Vol. 28, No. 8, Pp. 1223-1270, 2003.

[131] C. Sung-Seen, "Influence Of Thermal Ageing On Change Of Crocesslink Density And Deformation Of Natural Rubber Vulcanizates," *Journal Of The Korean Chemical Society ,* Vol. 21, No. 6, 2000.

[132] J. R. Shelton And H. Winn, "Aging Of Gr-S Vulcanizates In Air, Oxygen, And Nitrogen," *Industrial And Engineering Chemistry,* Vol. 36, No. 8, Pp. 728-730, 1944.

[133] M. F.L'annunziata, Handbook Of Radioactivity Analysis, Academic Press, 2012.

[134] M. Celina, J. Wise, D. K. O. K. T. Gillen And R. L. Clough, "Oxidation Profiles Of Thermally Aged Nitrile Rubber," *Polymer Degradation And Stability,* Vol. 60, No. 2-3, Pp. 493-504, 1998.

[135] A.R.Azura And S.L.Leow, "Effect Of Carbon Black Loading On Mechanical, Conductivity And Ageing Properties Of Natural Rubber Composites," In *6th International Conference On Recent Advances In Materials, Minerals & Environment (Ramm) 2018, Ramm 2018*, Penang, 2018.

[136] F. Anthoine, Ignatz-Hoover And B. H. To, "Migration Of Additives In Rubber," *International Polymer Science And Technology,* Vol. 32, No. 11, Pp. 653-662, 2005.

[137] T. D. Stark, H. Choi And P. W. Diebel, " Influence Of Plasticizer Molecular Weight On Plasticizer Retention In Pvc Geomembranes," *Geosynthetics International,* Vol. 12, No. 2, Pp. 99-110, 2005.

[138] M.Abdulkader And A. K.Bhowmick, "Thermal Ageing, Degradation And Swelling Of Acrylate Rubber, Fluororubber And Their Blends Containing Polyfunctional Acrylates," *Polymer Degradation And Stability,* Vol. 79, No. 2, Pp. 283-295, 2003.

[139] J. L. Graham, R. C. Striebich, K. J. Myers, D. K. Minus And W. E. Harrison, "Swelling Of Nitrile Rubber By Selected Aromatics Blended In A Synthetic Jet Fuel," *Energy Fuels,* Vol. 20, No. 2, Pp. 759-765, 2006 .

[140] R. Chang, Physical Chemistry For The Biosciences, Usa: University Science Books, 2005.

[141] Raliasoft, Accelerated Life Testing Data Analysis Reference, Tucson, Arizona: Raliasoft, 2015.

[142] L. A. Escobar And W. Q. Meeker, "A Review Of Accelerated Test Models," *Statistical Science,* Vol. 21, No. 4, P. 552–577, 2006.

Chapter 9 -- References

[143] T. S. Gates, "On The Use Of Accelerated Test Methods For Characterization Of Advanced Composite Materials," Nasa, Hampton, 2003.

[144] H. Peng, J. Jiang, J. Lu And J. Cao, "Application Of Time–Temperature Superposition Principle To Chinese Fir Orthotropic Creep," *Journal Of Wood Science Volume,* Vol. 63, Pp. 455-463, 2017.

[145] M. D. Normand And M. Peleg, "Arrhenius Versus Eyring-Polanyi Model," Wolfram Demonstrations Project, Champaign, 2013.

[146] M. D. N. M. Peleg And M. G. Corradini, "The Arrhenius Equation Revisited," *Critical Reviews In Foods Science And Nutrition,* Vol. 52, No. 9, P. 830–851, 2012 .

[147] Astm Subcommittee F02.50 On Package Development, "Astm F1980 - 16 -- Standard Guide For Accelerated Aging Of Sterile Barrier Systems For Medical Devices," Astm, West Conshohocken, 2016.

[148] X. Hu, Y. Li, X. Liu And W. Luo, "Experimental Studies Of Thermal Aging Effects On The Tensile And Tearing Fracture Behavior Of Carbon Black Filled Rubbers," In *13th International Conference On Fracture* , Beijing, 2013.

[149] V. Pimolsiriphol, P. Saeoui And C. Sirisinha, "Relationship Among Thermal Ageing Degradation, Dynamic Properties, Cure Systems, And Antioxidants In Natural Rubber Vulcanisates," *Polymer-Plastics Technology And Engineering,* Vol. 46, No. 2, P. 113–121, 2007.

[150] P. Davies And G. Evrard, "Accelerated Ageing Of Polyurethanes For Marine Applications," *Polymer Degradation And Stability,* Vol. 82, No. 8, Pp. 1455-1464, 2007.

[151] H. Gu And Y. Itoh, "Ageing Behaviour Of Natural Rubber And High Damping Rubber Materials Used In Bridge Rubber Bearings," *Advances In Structural Engineering,* Vol. 13, No. 6, Pp. 1105-1113, 2016.

[152] G. J. V. Amerongen, "Oxidative And Nonoxidative Thermal Degradation Of Rubber," *Journal Of Industrial And Engineering Chemistry,* Vol. 47, No. 12, P. 2565–2574, 1955.

[153] N. Saintiera, G. Cailletaudb And R. Piques, "Crack Initiation And Propagation Under Multiaxial Fatigue In A Natural Rubber," *International Journal Of Fatigue,* Vol. 28, No. 1, Pp. 61-72, 2006.

[154] C. Chai And A. Thomas, "Creep And Recovery Of Unvulcanized Natural Rubber," *Polymer,* Vol. 22, No. 3, Pp. 399-404, 1981.

[155] P. Garnier, J.-B. L. C. M. Grédiaca, S. Ababou-Girardd And M. Dubois, "On The Evolution Of The Viscoelastic Properties And Its Microstructural/Chemical Origin In Filled Nbr Subjected To Coupled Thermal And Mechanical Loads," *Polymer Degradation And Stability,* Vol. 98, No. 10, Pp. 2102-2110, 2013.

[156] Eastman, "Https://Www.Eastman.Com/Literature_Center/S/Spmbs2023.Pdf," [Online]. Available: Https://Www.Eastman.Com/Literature_Center/S/Spmbs2023.Pdf. [Accessed 08 09 2019].

[157] A. Shema, "Shelf Life Studies Basics – Concepts – Principles," Mocon's Advanced Packaging Solutions, [Online]. Available: Http://Vertassets.Blob.Core.Windows.Net/Download/9210cb42/9210cb42-6d9d-4fd4-Bd3e-216849d3b35d/Shelflifestudies.Pdf. [Accessed 08 09 2019].

[158] Christoph Neuhaus; Paul Heuler; Alexander Lion; Michael Johlitz; Matthias Barkhoff; Frank Duisen, "Influence Of Discontinuous Thermo-Oxidative Ageing On The Fatigue Life Of A Nr-Compound Used For Engine-Mount Application," In *10th European Conference On Constitutive Models For Rubbers Eccmr*, Munich, 2017.

[159] International Organization For Standardization, "Rubber, Vulcanized Or Thermoplastic -- Determination Of Dynamic Properties," Nternational Organization For Standardization, 2011.

[160] Acrotech, "Shape Factor & Modulus Of Elasticity," Acrotech, [Online]. Available: Http://Www.Acrotechinc.Com/Shape-Factor-Modulus-Of-Elasticity/. [Accessed 10 10 2016].

[161] A. N. Gent, "On The Relation Between Indentation Hardness And Young's Modulus," *Rubber Chemistry And Technology,* Vol. 31, No. 4, Pp. 986-906, 1958.

[162] B. Standard, "British Standard 903 Methods Of Testing Vulcanised Rubber Part A7," British Standard, 1957.

[163] U. I. A. M. W. Poznaniu, "Mikroskopia Sił Atomowych," Uniwersytet Im. Adama Mickiewicza W Poznaniu, . [Online]. Available: Http://Www.Cnbm.Amu.Edu.Pl/Pl/Laboratoria/Mikroskopia-Sil-Atomowych. [Accessed 20 10 2016].

[164] A. H. Duanjie Li, "Viscoelastic Analysis Of Rubber With Nanoindentation Dma," Nanovea, Irvine, 2014.

[165] Wu-Guijianga, Jian-Junsu And Xi-Qiaofeng, "Effect Of Surface Roughness On Nanoindentation Test Of Thin Films," *Engineering Fracture Mechanics,* Vol. 75, No. 17, Pp. 4965-4972, 2008.

[166] R. Gamba, "Swell Ratio Tester Report," Indian Head Division , Naval Surface Warfare Center , Boston, 2003.

[167] J. C. Edwards, "Principles Of Nmr," Process Nmr Associates Llc, Danbury, 2009.

[168] M. Karakaplan, "008-Nmr.Mpg," 12 05 2012. [Online]. Available: Https://Www.Youtube.Com/Watch?V=Yzpizjtsce8. [Accessed 20 10 2016].

[169] A. B. A. B. Amu, "Estimation Of Crosslink Density By Solid-State Nmr Spectroscopy," In *Blends Of Natural Rubber*, Springer Science & Business Media, 1998, Pp. 40-52.

[170] E. O. A. L. Chemistry, "Infrared Spectroscopy," Ellesmere Ocr A Level Chemistry, [Online]. Available: Https://Sites.Google.Com/Site/Ellesmerealevelchemistry/Module-4-Core-Organic-Chemistry/4-2-Alcohols-Haloalkanes-And-Analysis/4-2-4-Analytical-Techniques/-A-B-C-D-E-Infrared-Spectroscopy. [Accessed 20 10 2016].

[171] T. Soderberg, "Infrared Spectroscopy," In *Organic Chemistry With A Biological Emphasis Volume I*, Morris, University Of Minnesota, 2010.

[172] P. Shapley, "Heat Absorbing Gases," University Of Illinois, 2011. [Online]. Available: Http://Butane.Chem.Uiuc.Edu/Pshapley/Genchem1/L15/2.Html. [Accessed 23 01 2019].

[173] P. Spencer And A. Misra, Material-Tissue Interfacial Phenomena, Woodhead Publishing, 2017.

[174] A. Voilleya, A.-M. S. R. Gougeona, T. Karbowiak, D. Chassagne And F. Debeaufort, "Transfer Of Water And Active Molecules At The Interfaces In Complex Food Systems: Theoretical And Practical Aspects," *Procedia Food Science,* Vol. 1, P. 879 – 885, 2011.

[175] J. A.-D. M. Rūmī, "Scattering Part Two: A Quantum Of Scattering," The Physics Mill, 30 03 2014. [Online]. Available: Http://Www.Thephysicsmill.Com/2014/03/30/A-Quantum-Of-Scattering/. [Accessed 16 07 2019].

[176] J. C. Lindon, G. E. Tranter And D. W. Koppenaal, Encyclopedia Of Spectroscopy And Spectrometry, Academic Press, 2017.

[177] R. Kohli And K. Mittal, Developments In Surface Contamination And Cleaning, William Andrew, 2016.

[178] F. Krumeich, "Sem: Imaging With Secondary Electrons," Eth Zürich, 05 01 2018. [Online]. Available: Https://Www.Microscopy.Ethz.Ch/Se.Htm. [Accessed 19 02 2020].

[179] V. Koncar, Smart Textiles For In Situ Monitoring Of Composites, Woodhead Publishing, 2019.

[180] S. Yaragalla, R. Mishra And H. J. Maria, Carbon-Based Nanofillers And Their Rubber Nanocomposites, Elsevier, 2019.

[181] Matthewweyland And P. A.Midgley, "Electron Tomography," *Materialstoday,* Vol. 7, No. 12, Pp. 32-40, 2004.

[182] N. Rifai, A. R. Horvath And C. T. Wittwer, Principles And Applications Of Clinical Mass Spectrometry, Elsevier, 2018.

[183] B. Den, "Gel Filtration," Biotechniques Den, [Online]. Available: Http://Biotechniquesden.Blogspot.Co.Uk/2012/12/Gel-Filtration.Html. [Accessed 07 10 2016].

[184] B. Den, "Gel Filtration," Biotechniques Den, [Online]. Available: Http://Biotechniques2.Rssing.Com/Chan-8470871/All_P1.Html. [Accessed 20 10 2016].

[185] E. Radauscher, "Design, Fabrication, And Characterization Of Carbon Nanotube Field Emission Devices For Advanced Applications," Department Of Electrical And Computer Engineering Duke University, Duke , 2015.

[186] N. P. Cheremisinoff, Polymer Characterization, William Andrew, 1996.

[187] Bruker, "Handheld Xrf: How It Works," Bruker, [Online]. Available: Https://Www.Bruker.Com/Products/X-Ray-Diffraction-And-Elemental-Analysis/Handheld-Xrf/How-Xrf-Works.Html. [Accessed 08 09 2019].

[188] S. S. Dasa, J. C. Coburna, C. Tackb, Matthew R. Schwerina And D. C. Richardsona, "Exposure Of Natural Rubber To Personal Lubricants – Swelling And Stress Relaxation As Potential Indicators Of Reduced Seal Integrity Of Non-Lubricated Male Condoms," *Contraception,* Vol. 90, No. 1, Pp. 86-93, 2014.

[189] M. R. A. E. Corp, "Chemical Resistance Chart," Moss Rubber, South San Francisco.

[190] M. R.D.S, *Va815, Va2000, Va4000 Viscoanalyzer User Manual,* Limonest : R.D.S, Metravib.

Chapter 9 -- References

[191] A. G. Veith, "Chain Scission Efficiency In The Oxidation Of Natural Rubber Vulcanizates," *Rubber Chemistry And Technology,* Vol. 30, No. 4, Pp. 1146-1161, 1957.

[192] J. Hubball, J. Groeger, M. Bolgar And S. Meronek, Handbook For The Chemical Analysis Of Plastic And Polymer Additives, Crc Press , 2015 .

[193] S. Mehri And A. Andersson*, "Drift Study Of The Oxidation And The Ammoxidation Of Toluene," *Journal Of Molecular Catalysis, ,* Vol. 81, Pp. 51-62 , 25 10 2013.

[194] Shimadzu, "Can You Tell Me Why The Spectrum Baseline Is Curved?," Shimadzu, [Online]. Available: Https://Www.Shimadzu.Com/An/Ftir/Support/Faq/5.Html. [Accessed 22 08 2019].

[195] Shimadzu, "Points To Note In Rubber Analysis : Black Rubber," Shimadzu, [Online]. Available: Https://Www.Shimadzu.Com/An/Ftir/Support/Tips/Letter11/Rubber.Html. [Accessed 22 08 2019].

[196] Restek, "Septum Selection Guide," Restek, [Online]. Available: Https://Www.Restek.Com/Techtips/Septum-Selection-Guide2. [Accessed 06 07 2019].

[197] F. Scientific, " Septum Selection Guide Rev 2," [Online]. Available: Https://Fscimage.Fishersci.Com/Cmsassets/Downloads/Segment/Scientific/Pdf/Septum_Selection_Guide.Pdf. [Accessed 07 06 2019].

Appendix A.   Elastic modulus changes

i.   Used Mount Samples
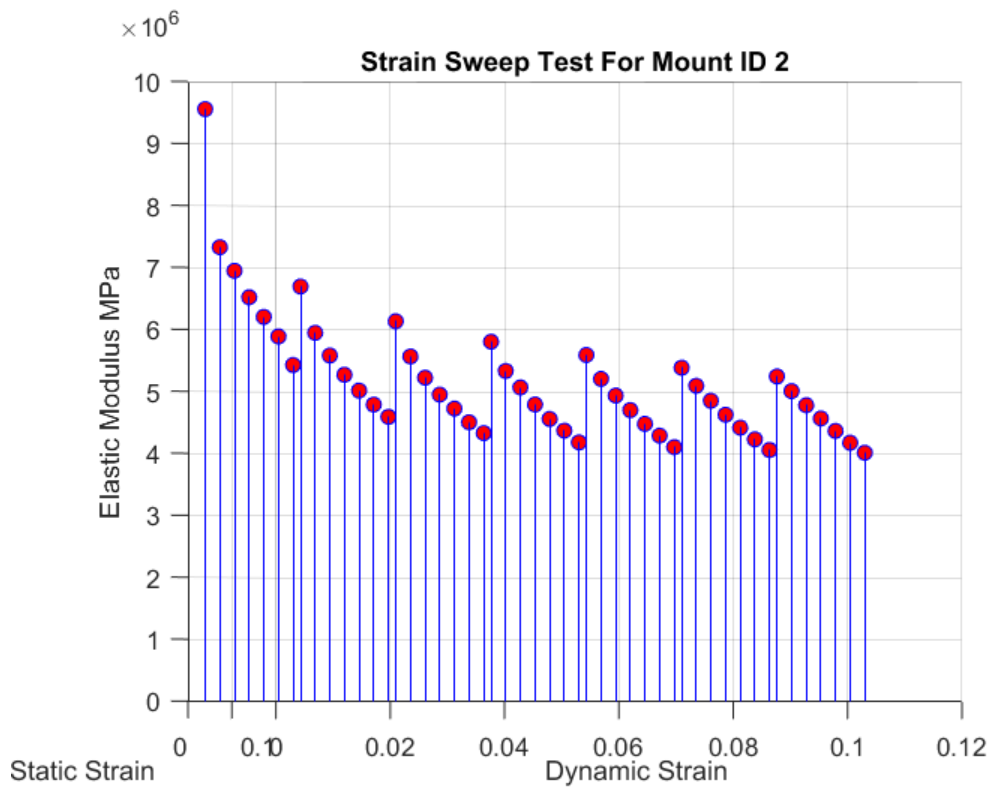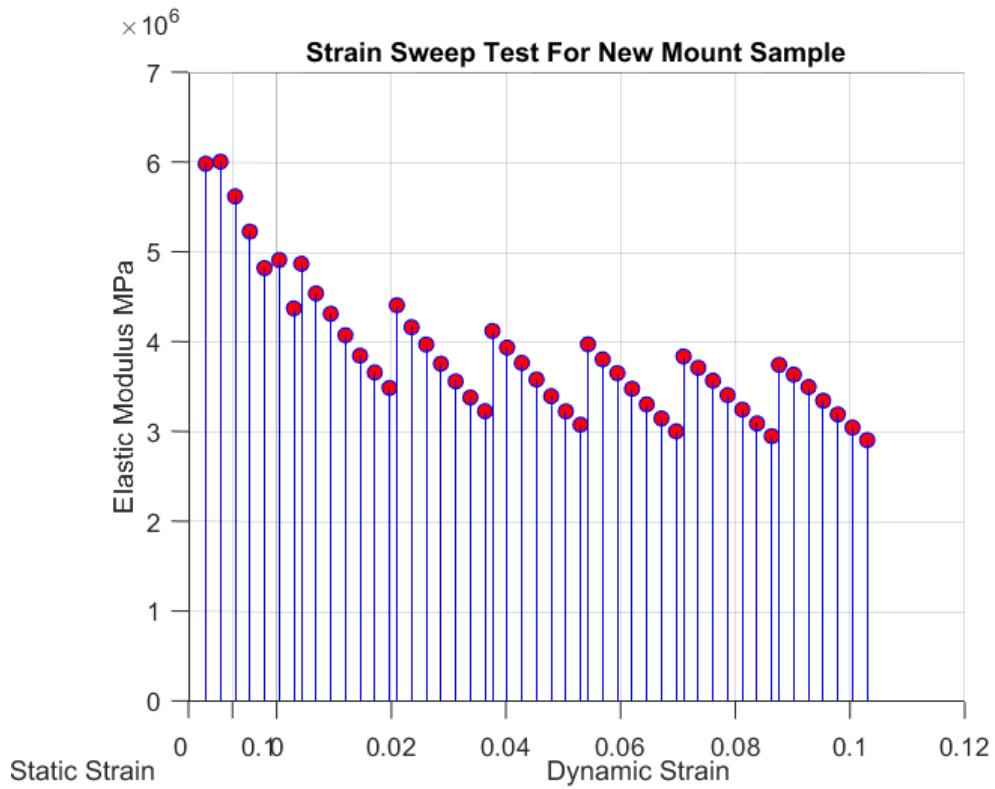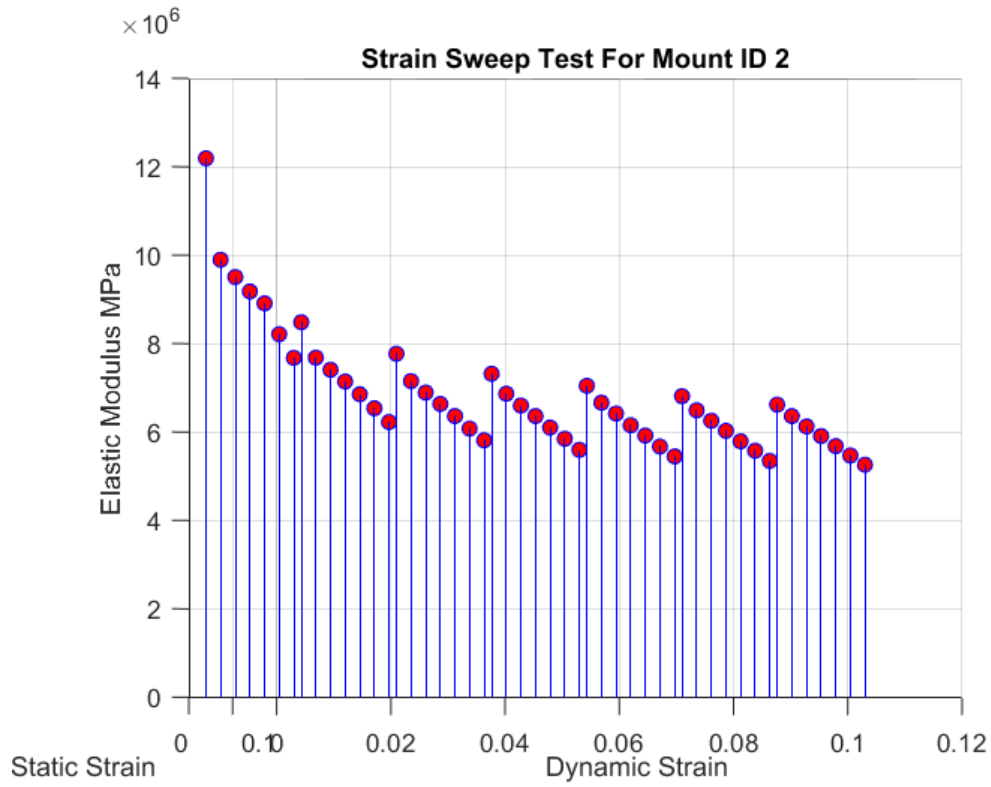
Odd when comparing with other ones and therefore removed from result

Strain Sweep Test For Mount ID 3

Strain Sweep Test For Mount ID 3

iii

Strain Sweep Test For Mount ID 4

Strain Sweep Test For Mount ID 4

iv

Strain Sweep Test For Mount ID 5

Strain Sweep Test For Mount ID 5

v

Strain Sweep Test For Mount ID 5
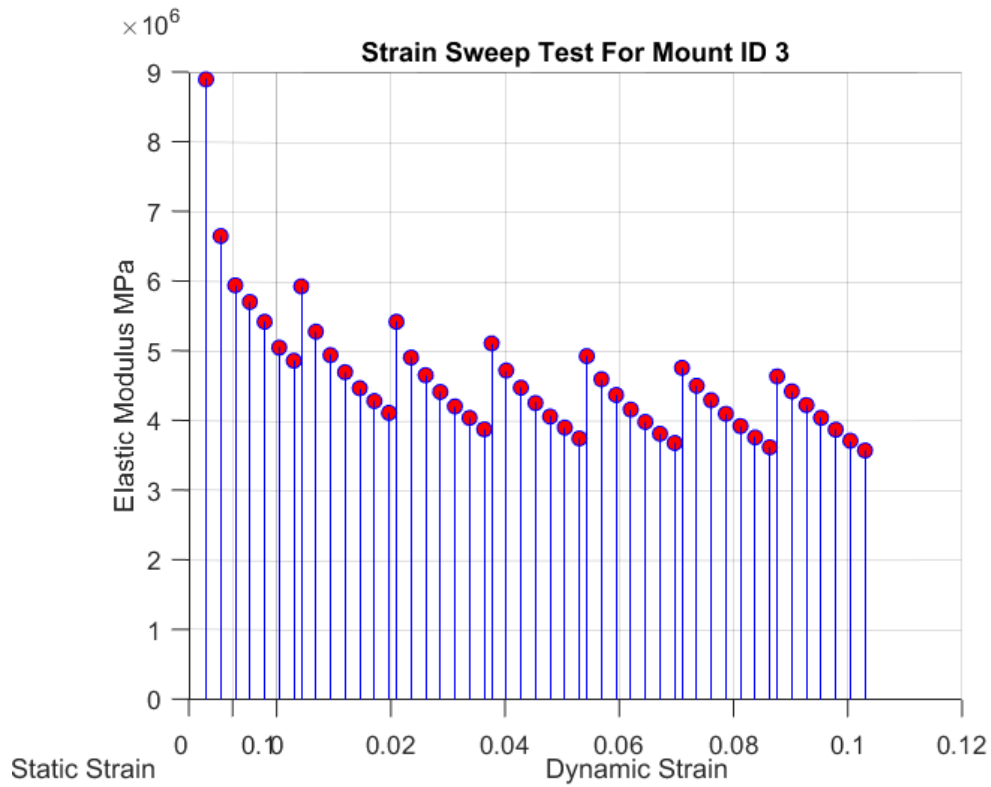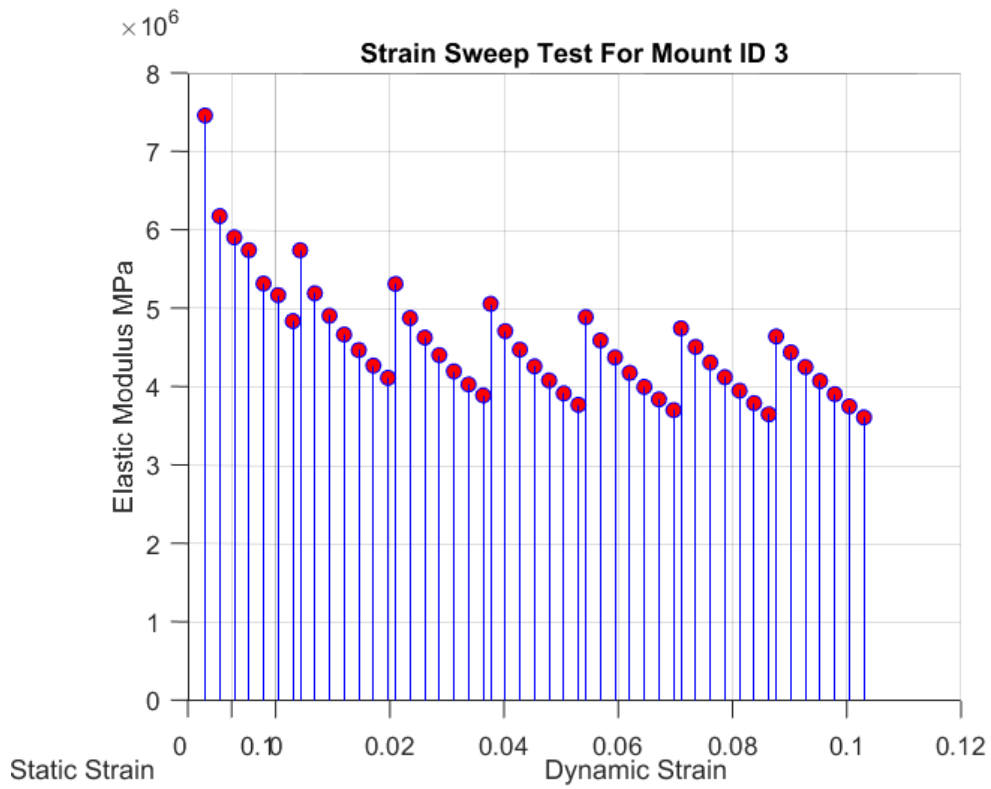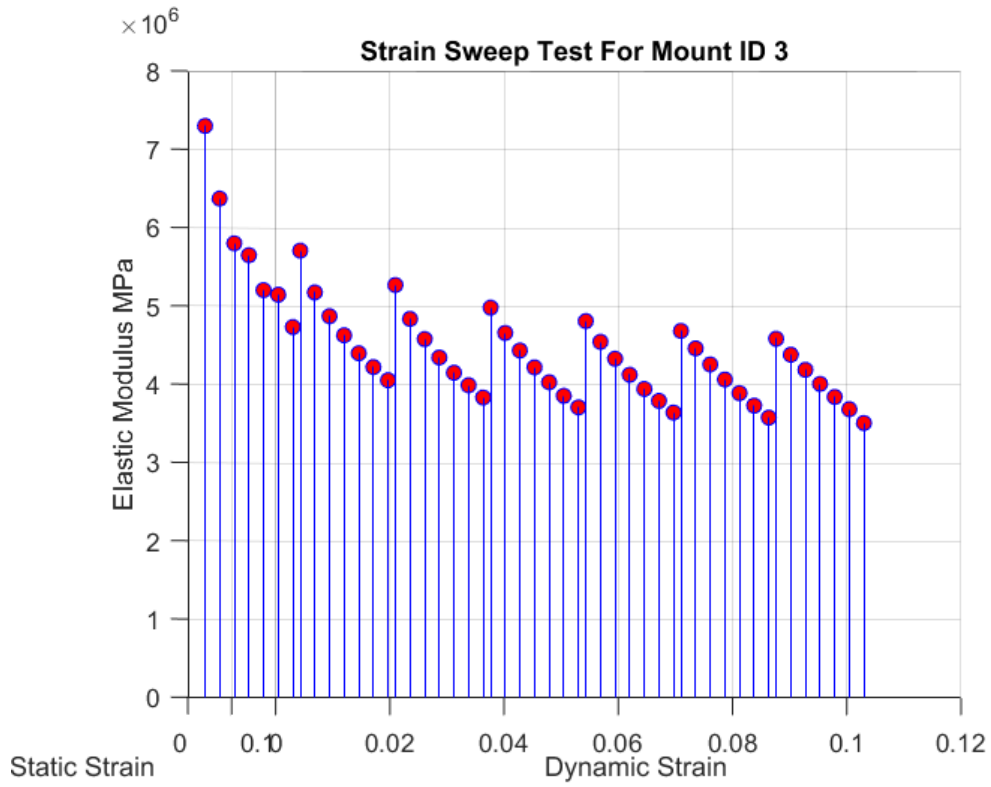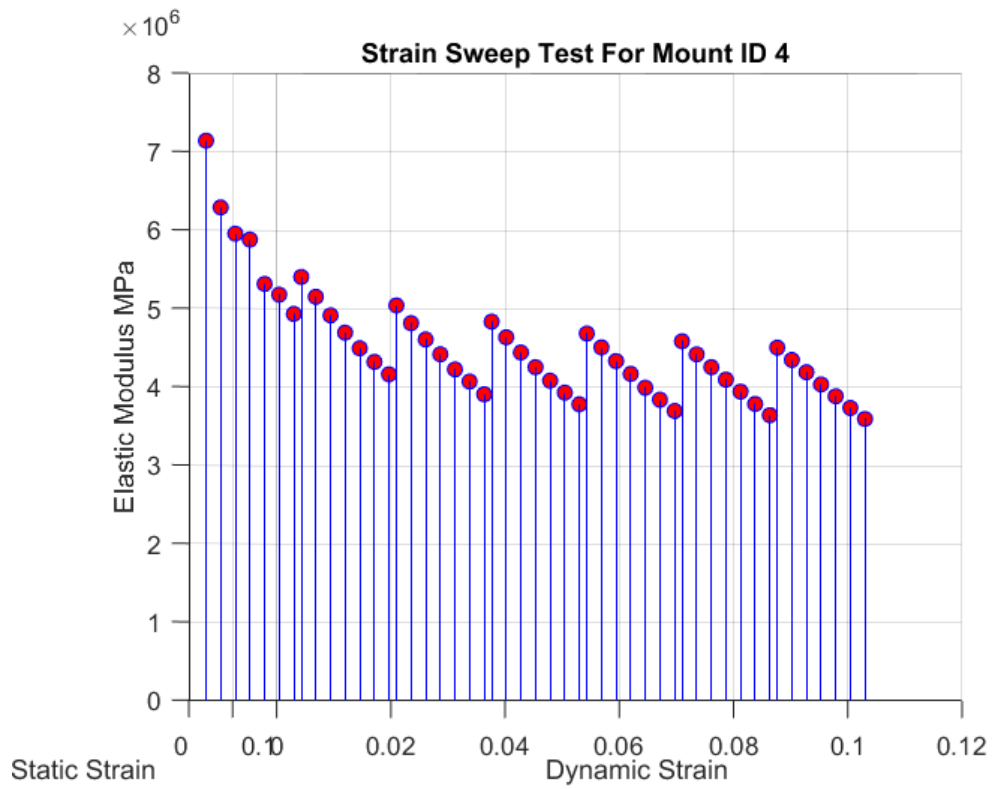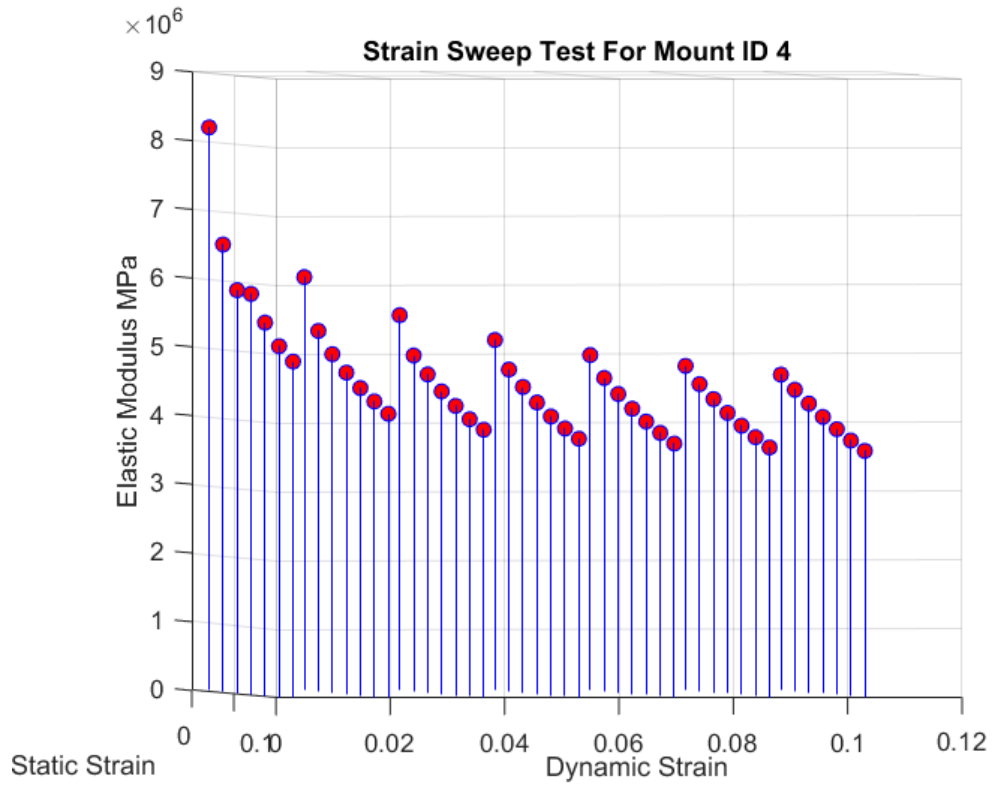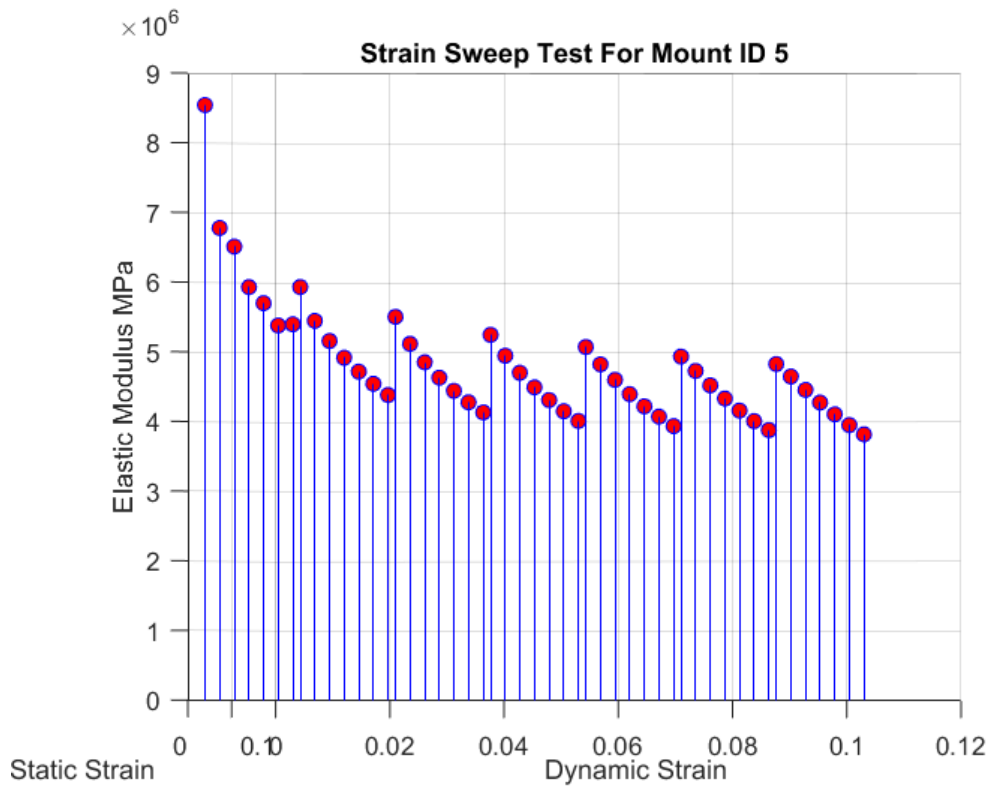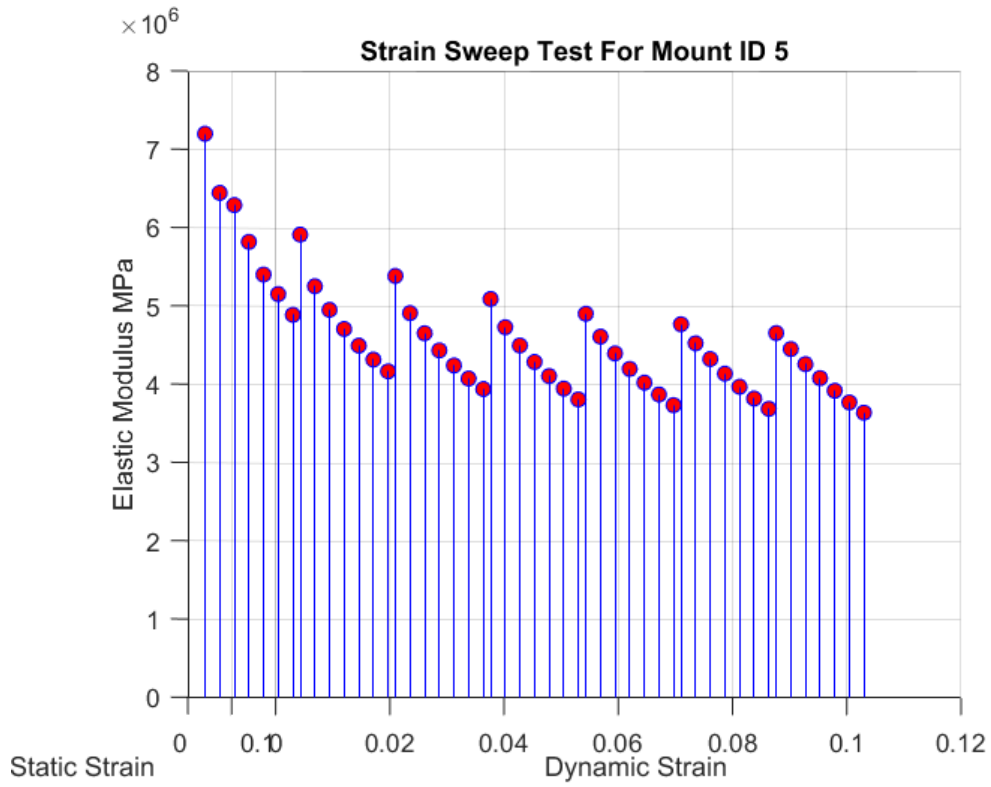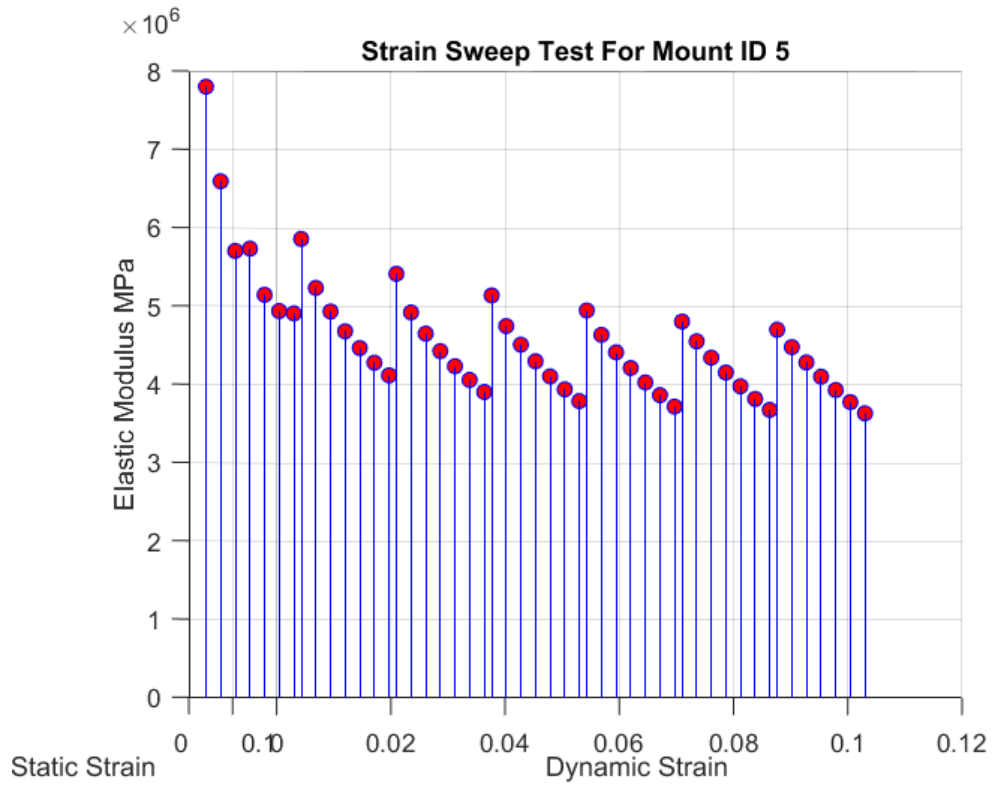
Appendix B.   SEM and processed Images

i.   New mount sample, Raw images

ix

det	HV	WD	mag	⊞	HFW	mode	bias	SEM Mode	curr	5 µm
CBS	5.00 kV	3.3 mm	10 000 x		20.7 µm	All	0 V	Field-Free	0.10 nA	Helios

x
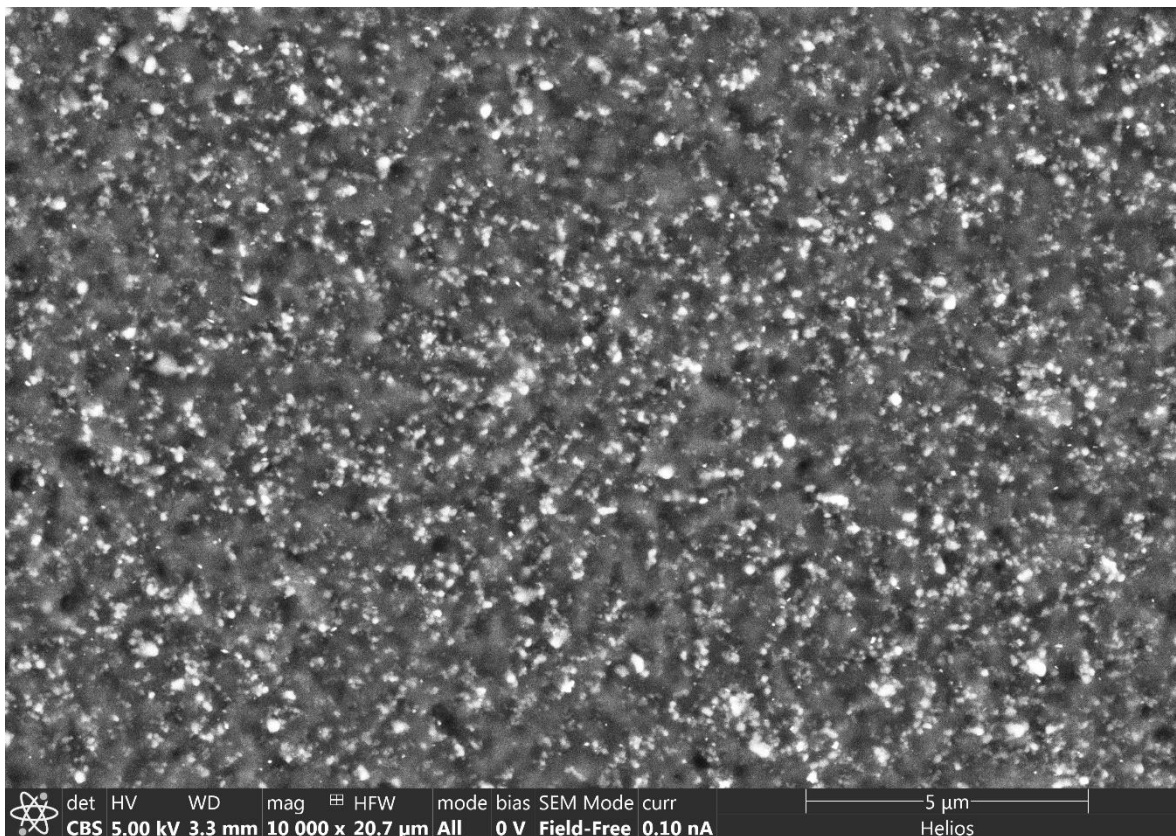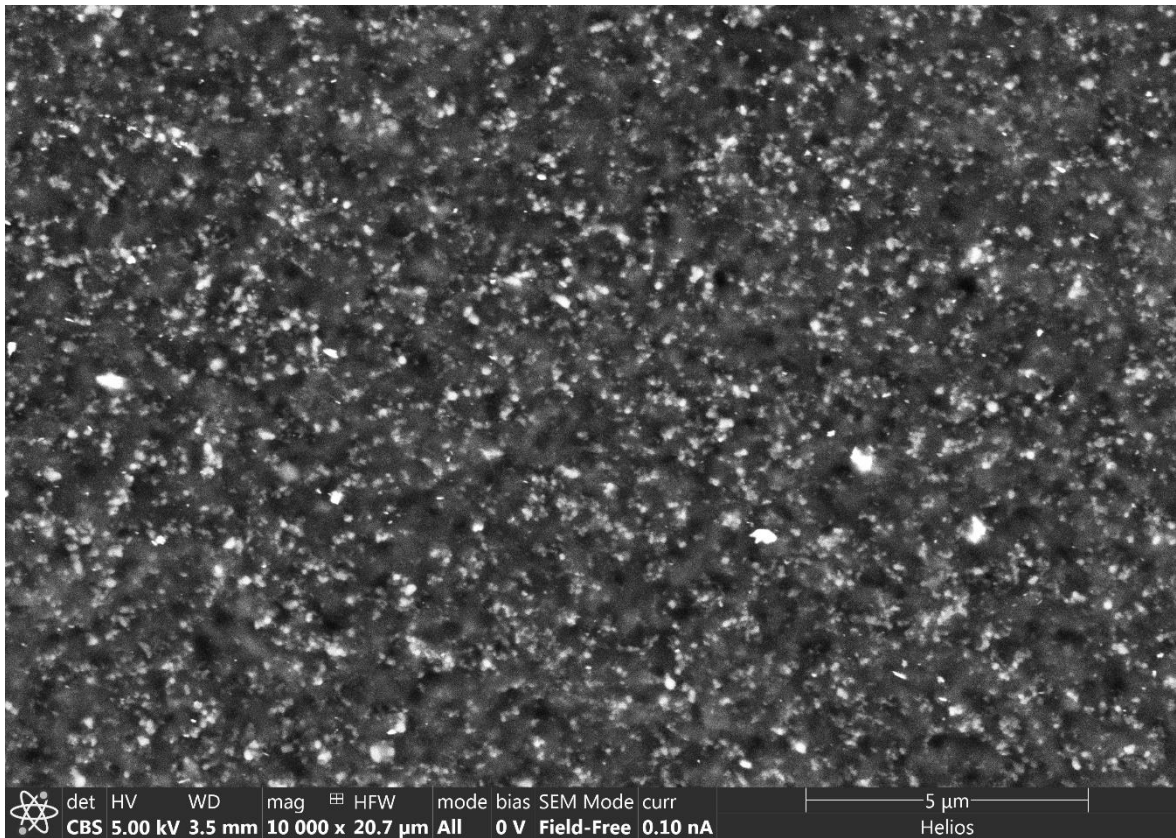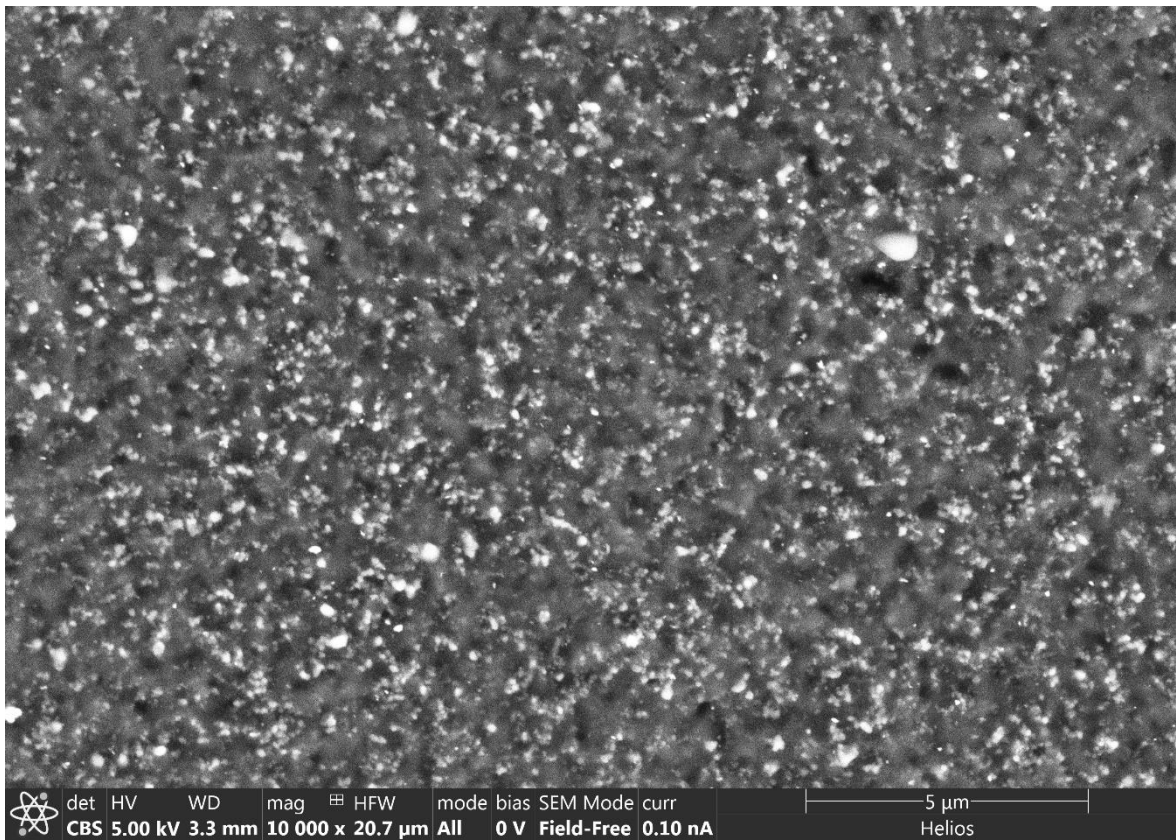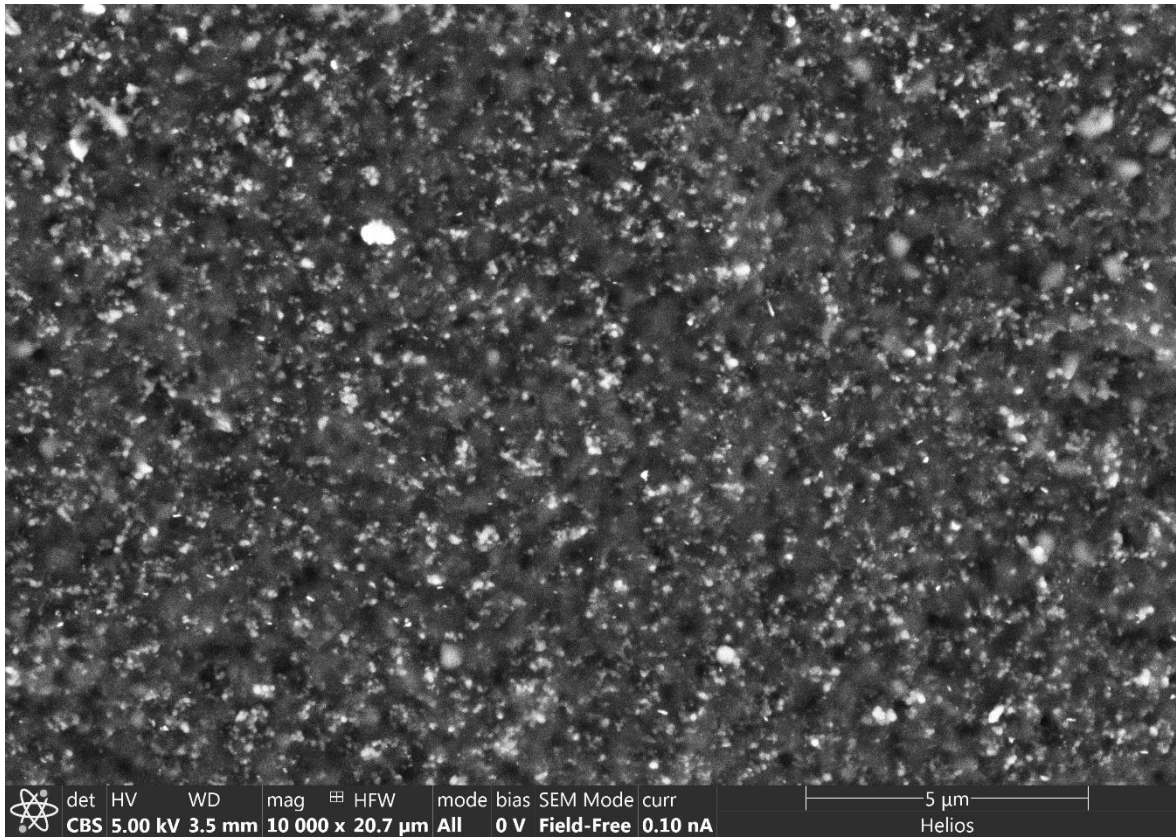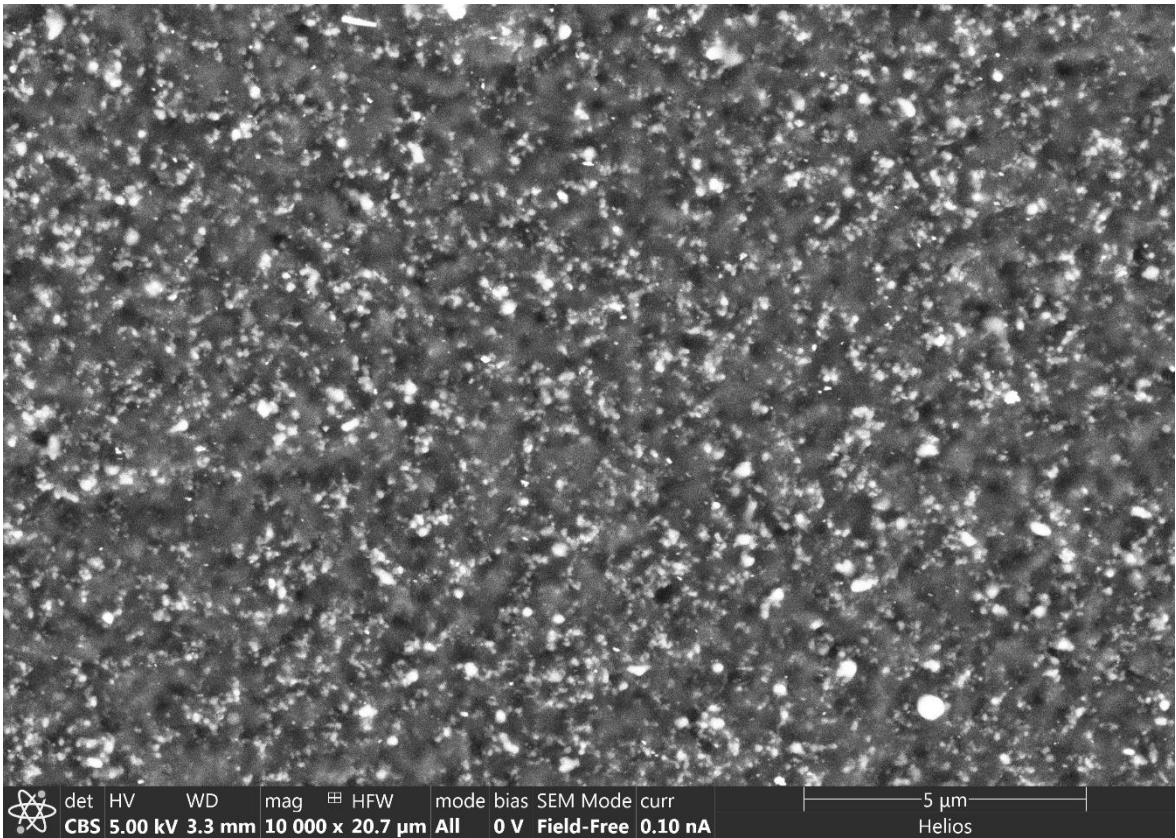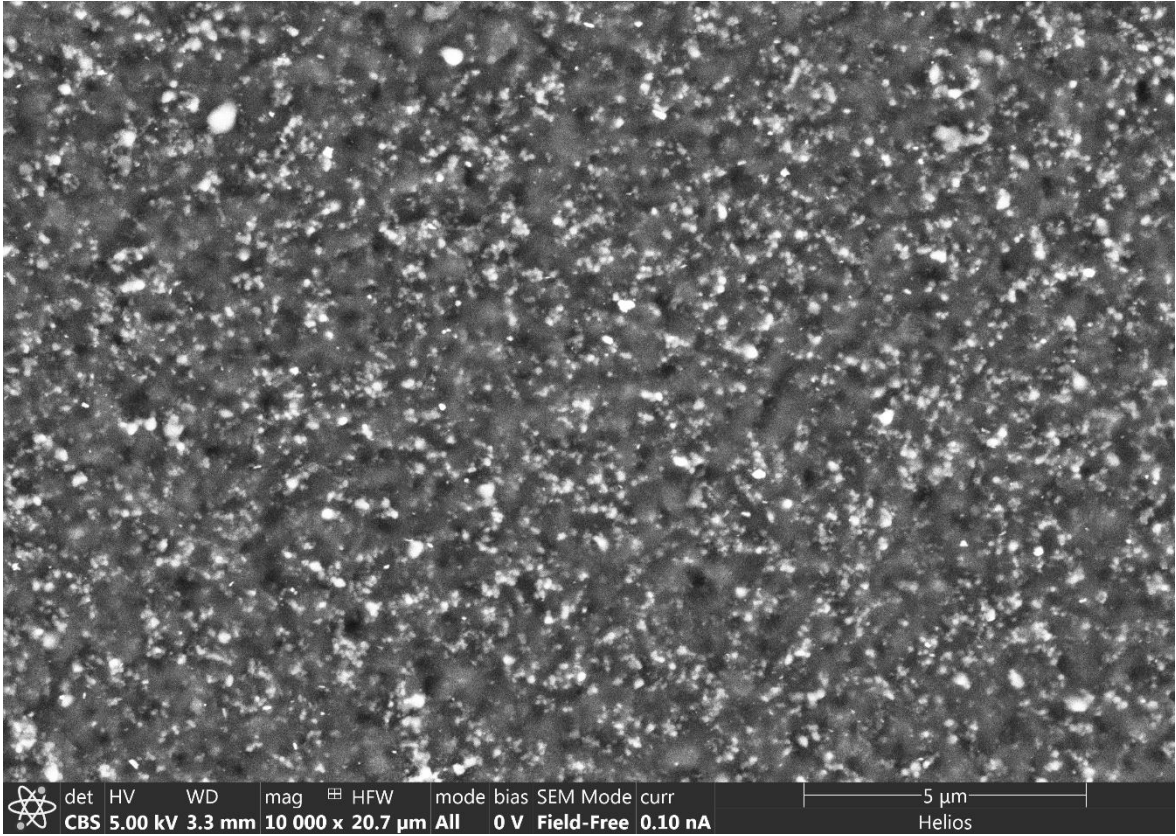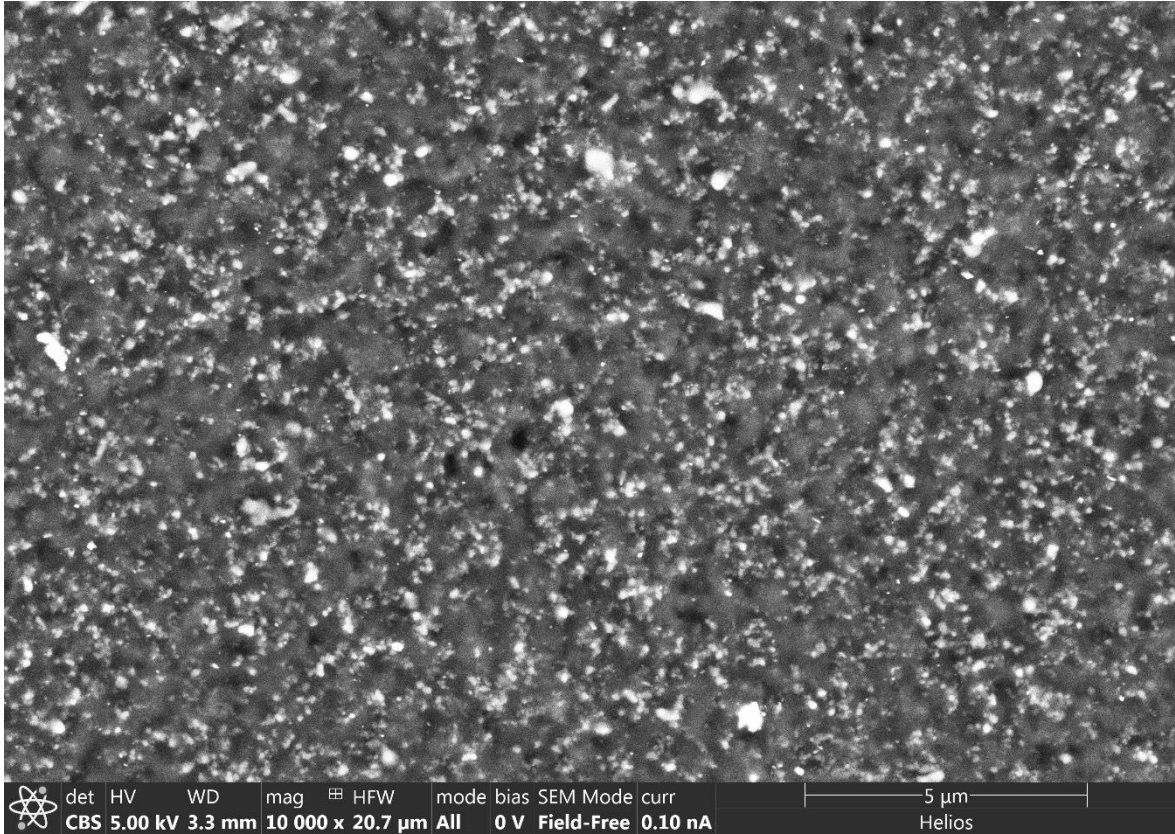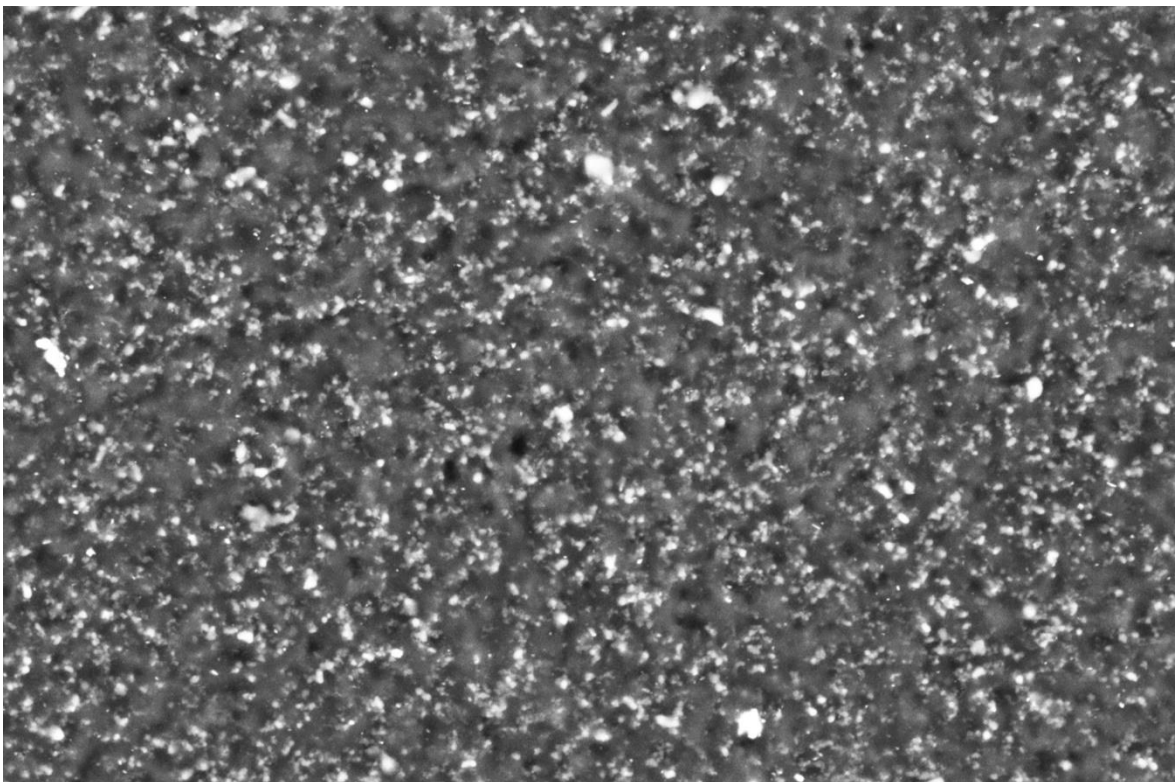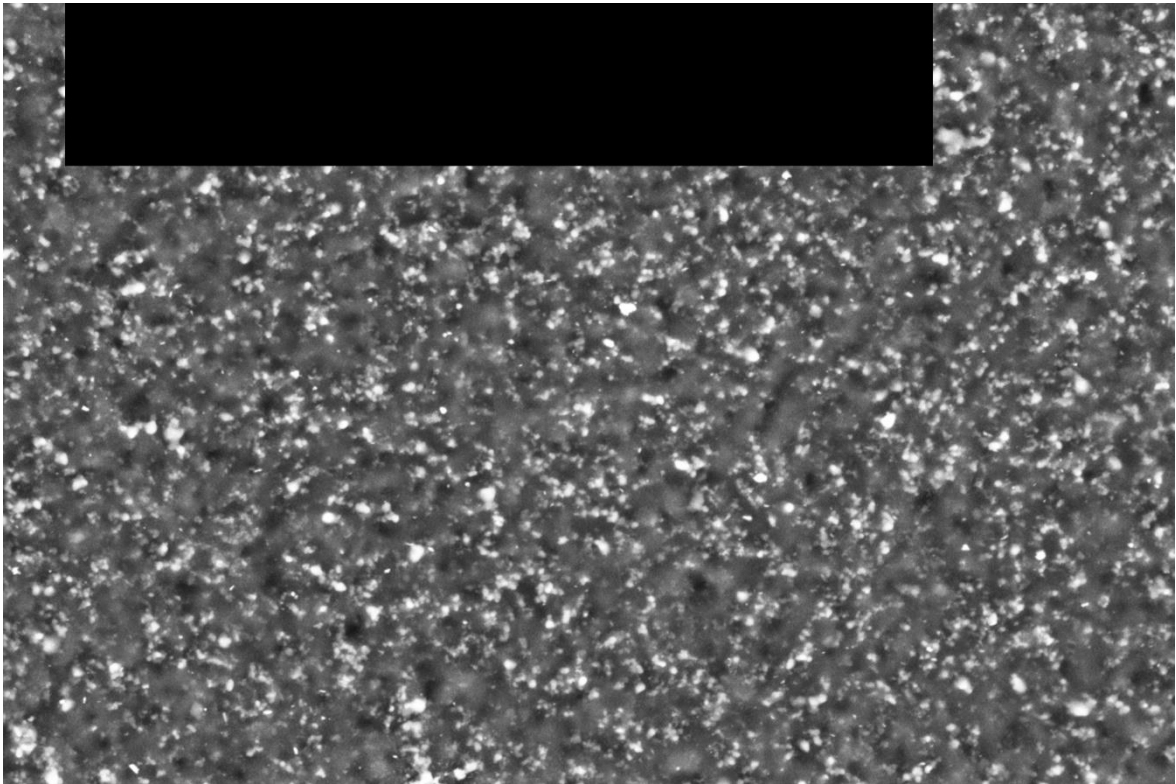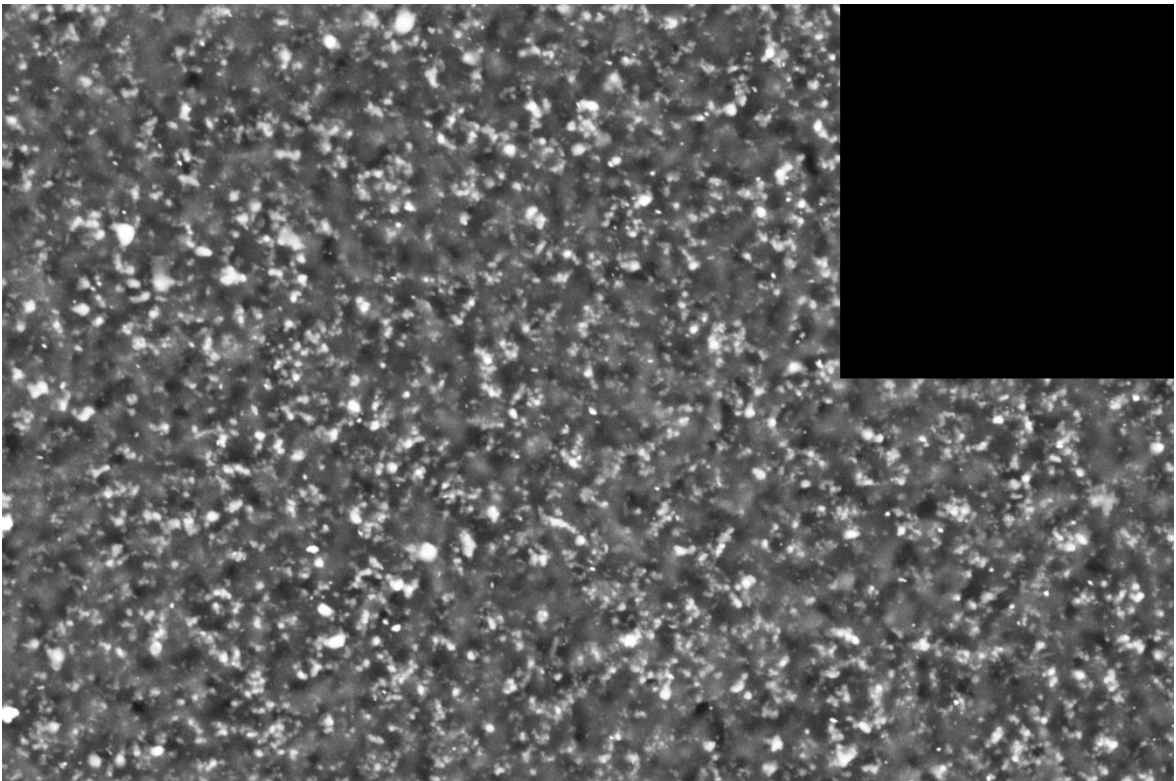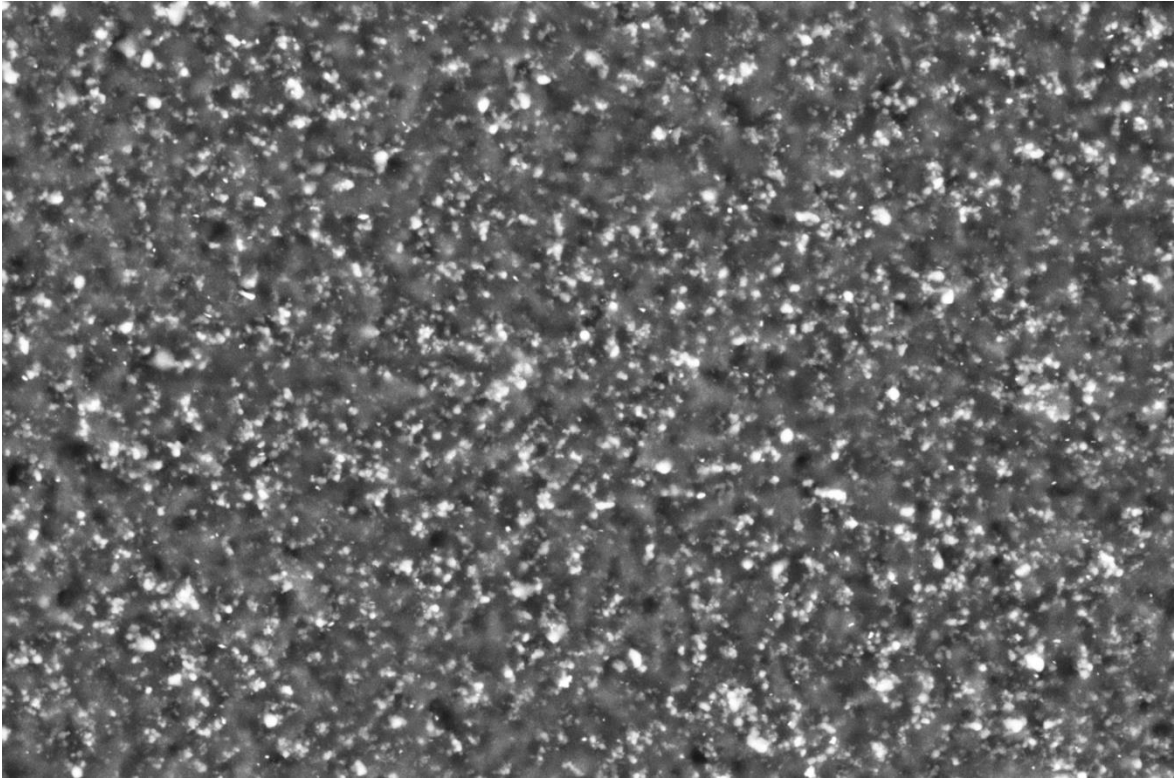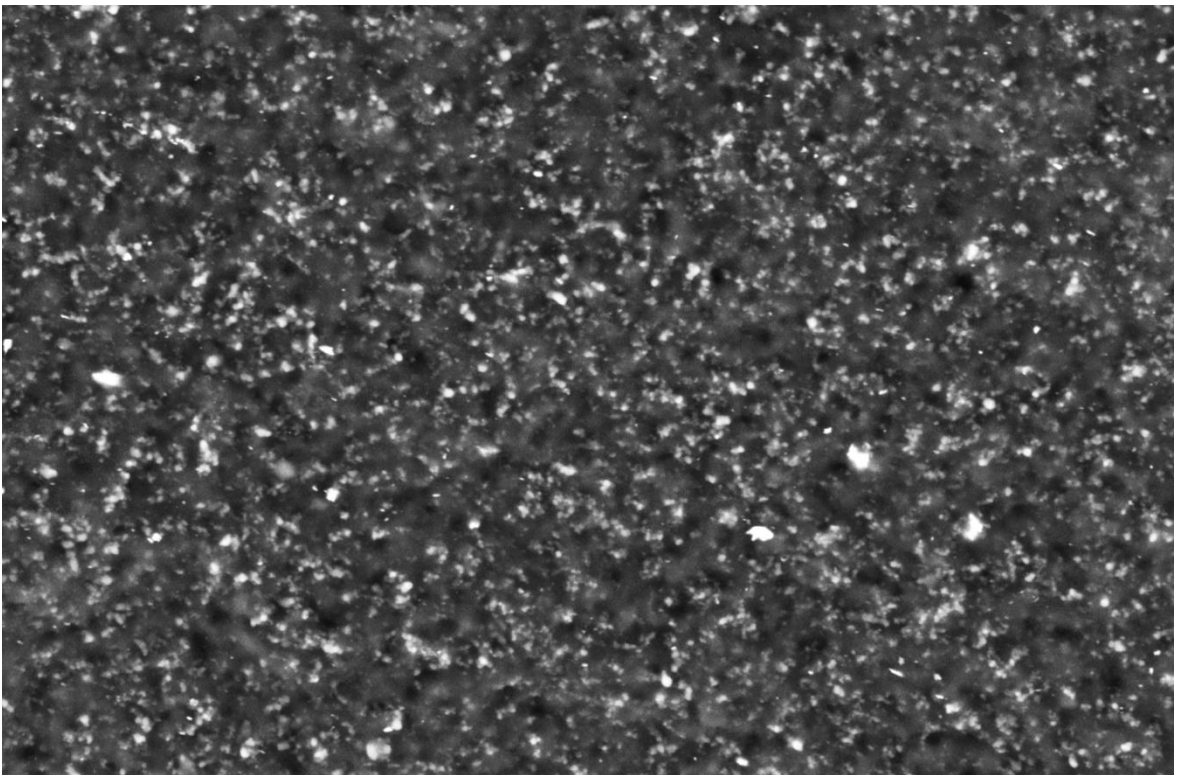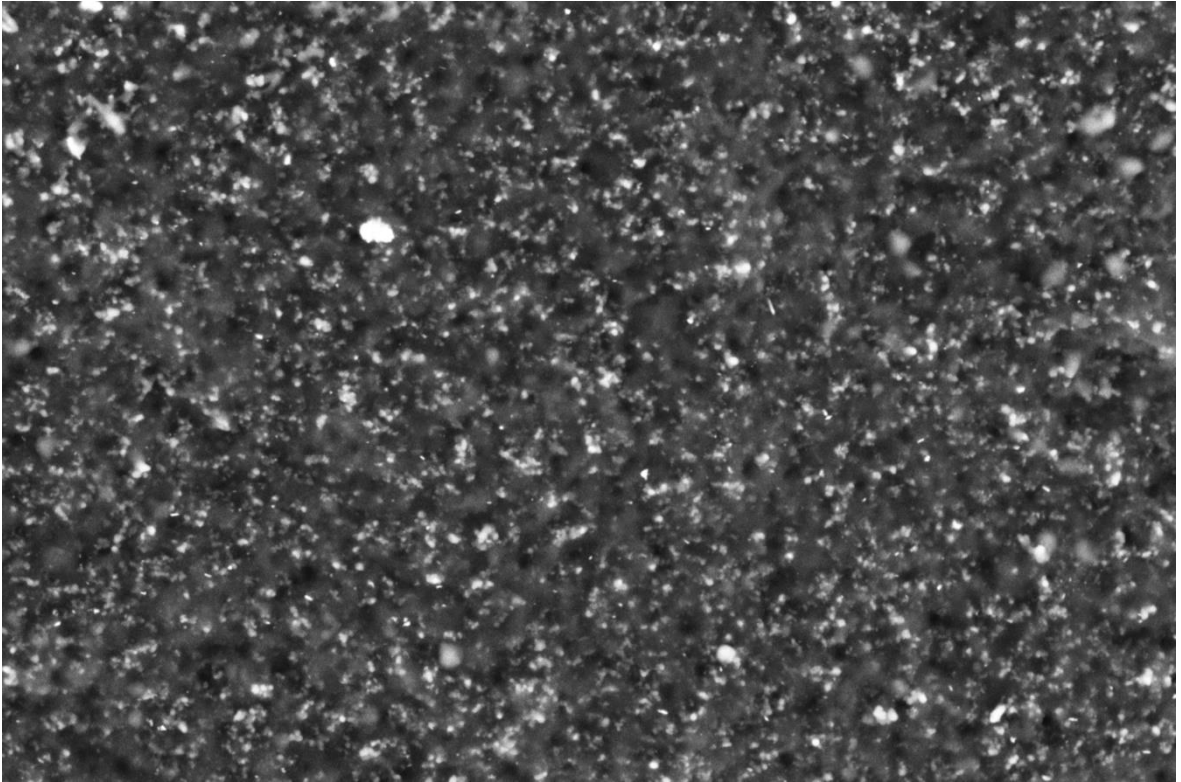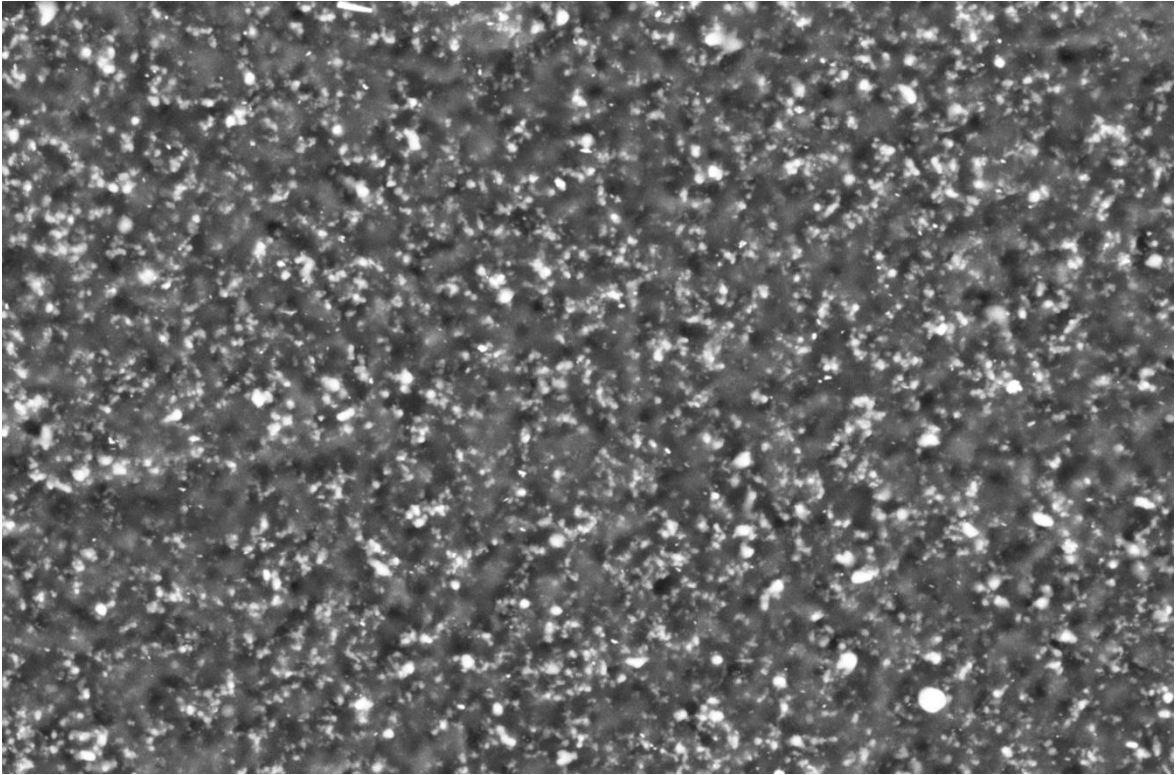
iii.   Mount ID 5 Location D, Raw Images
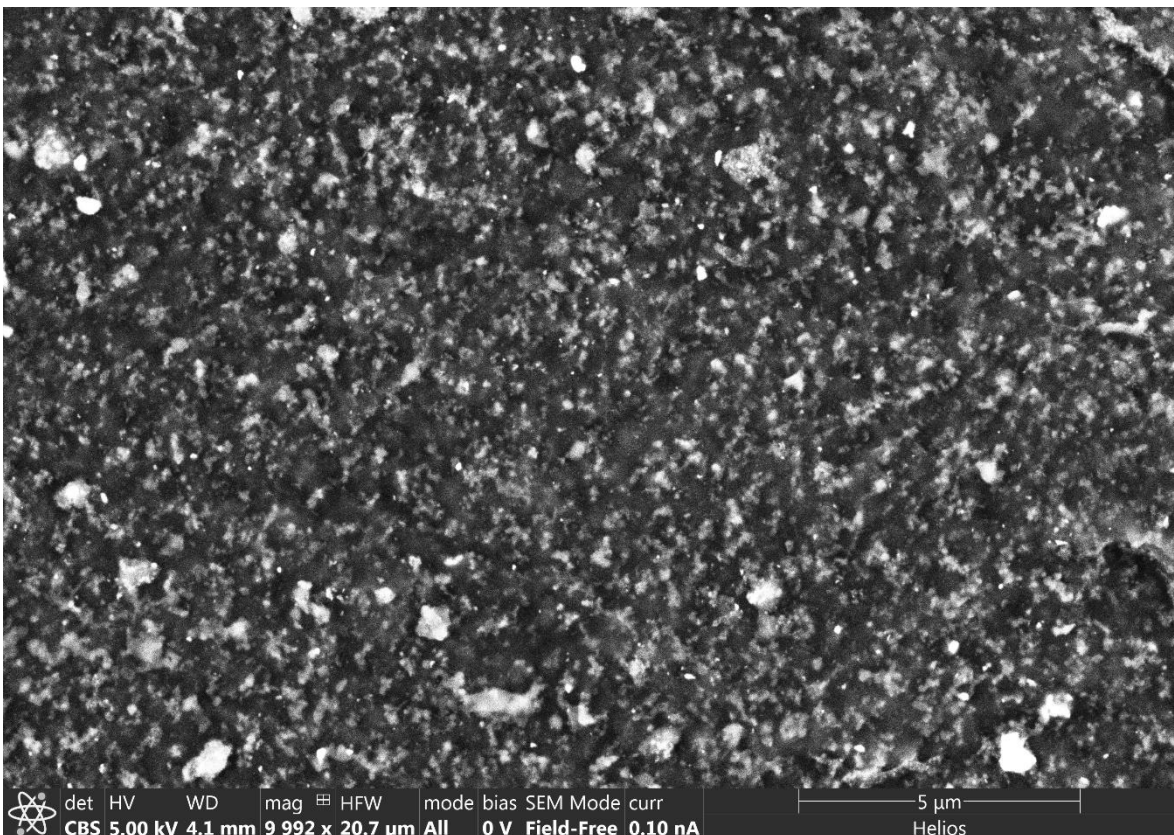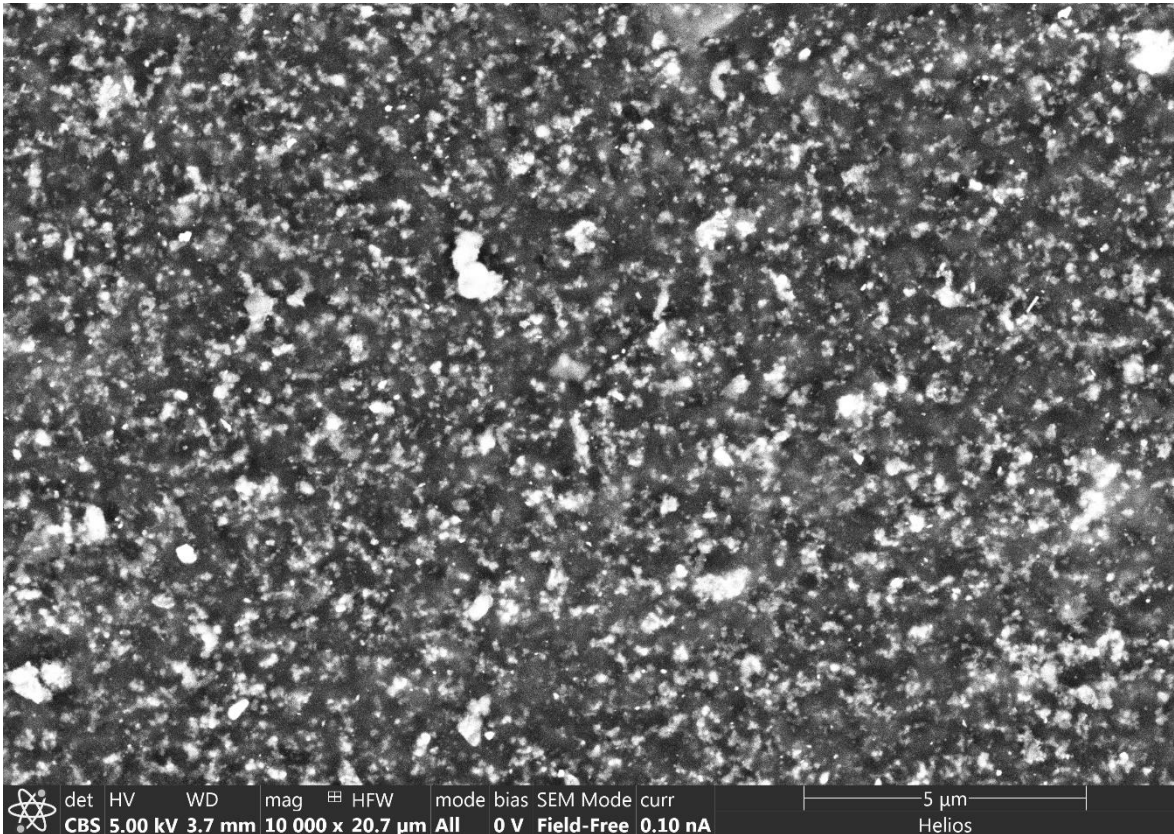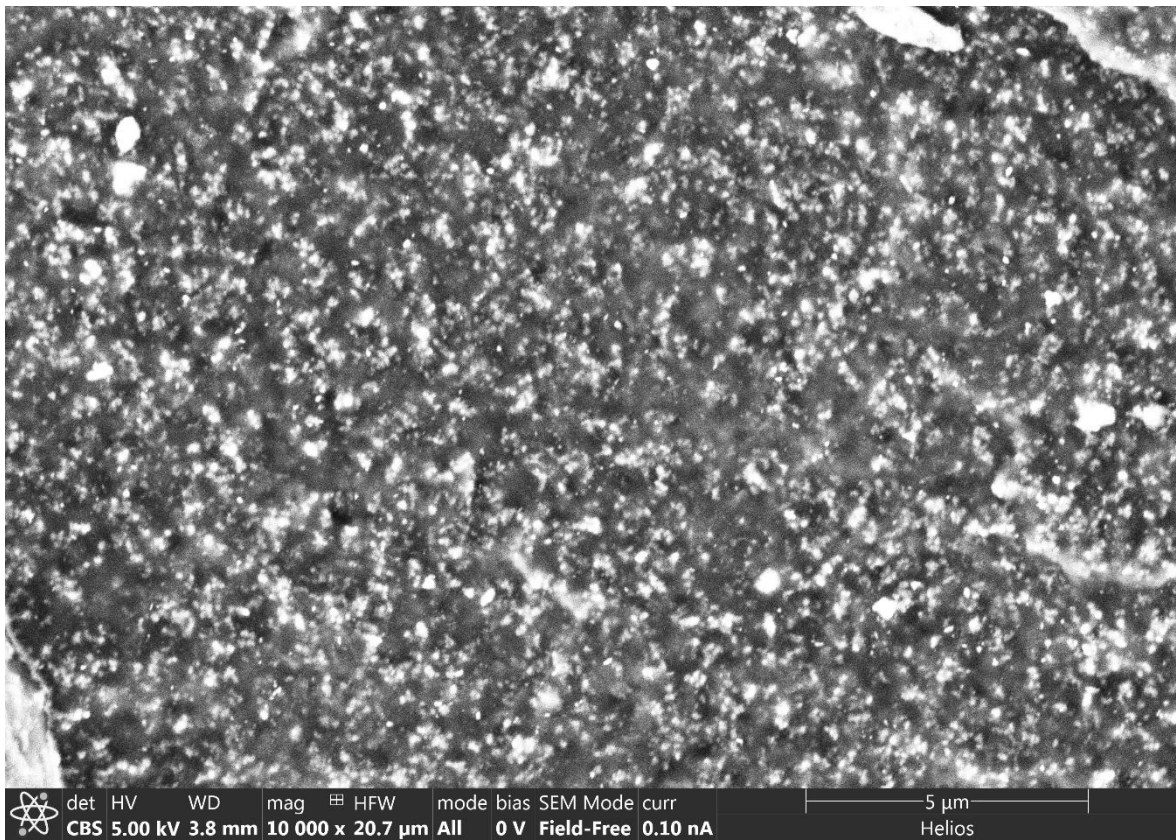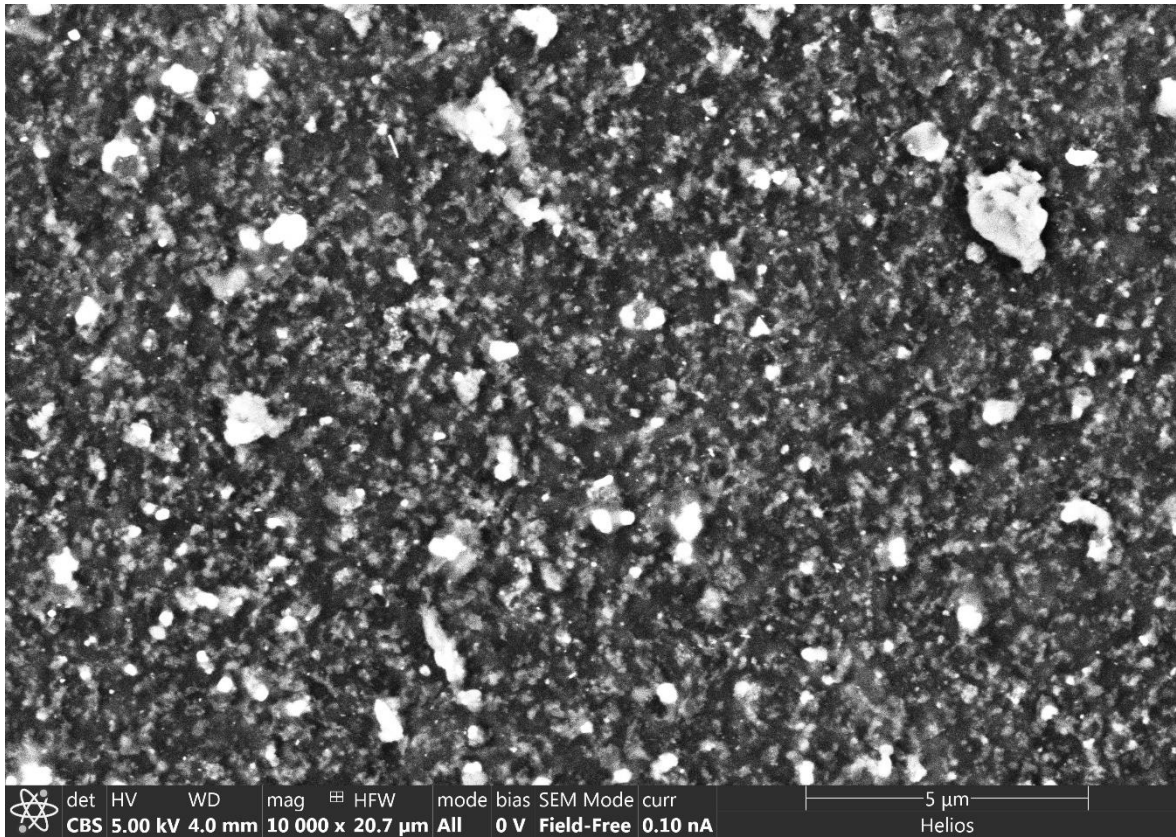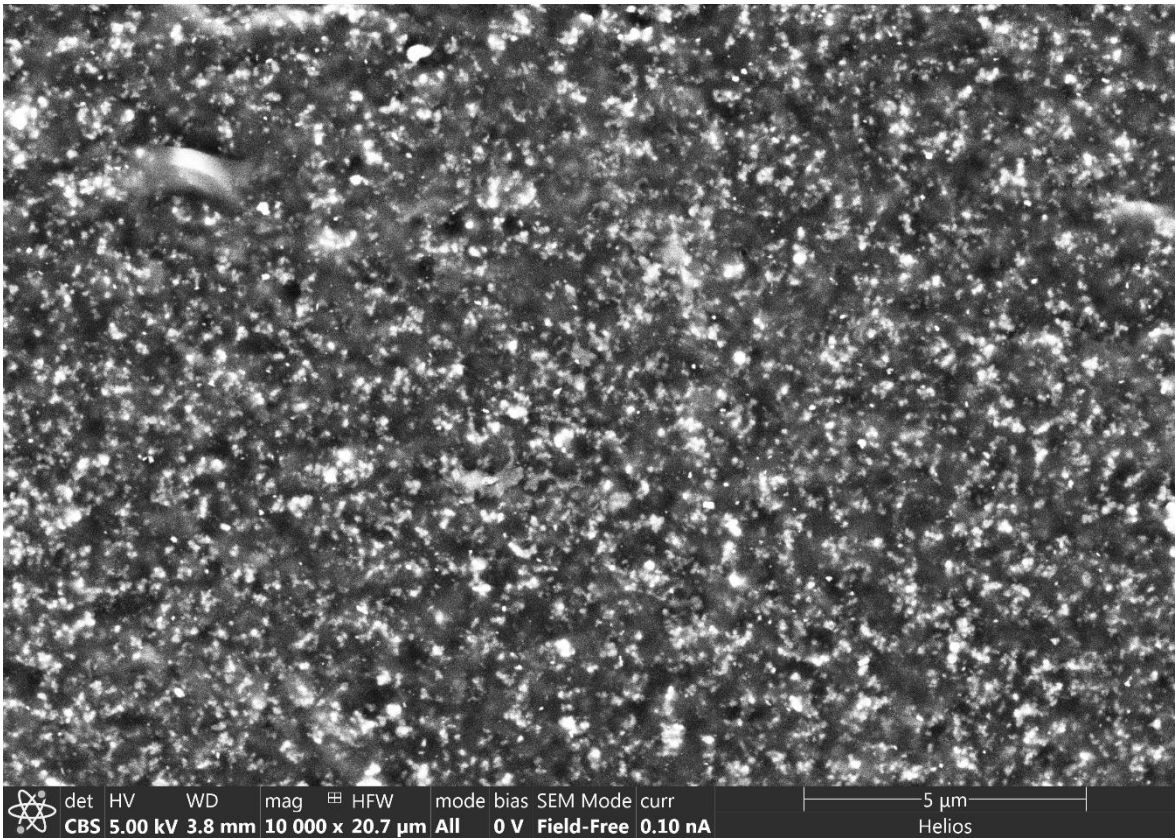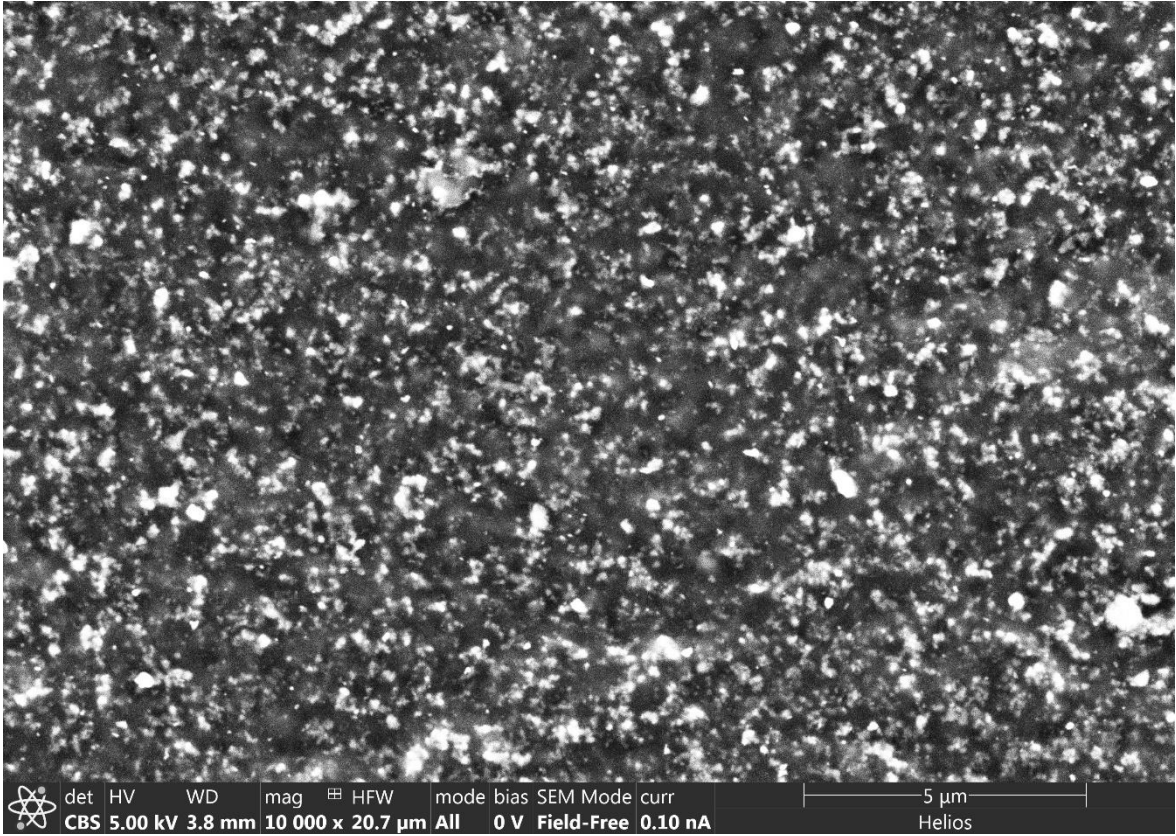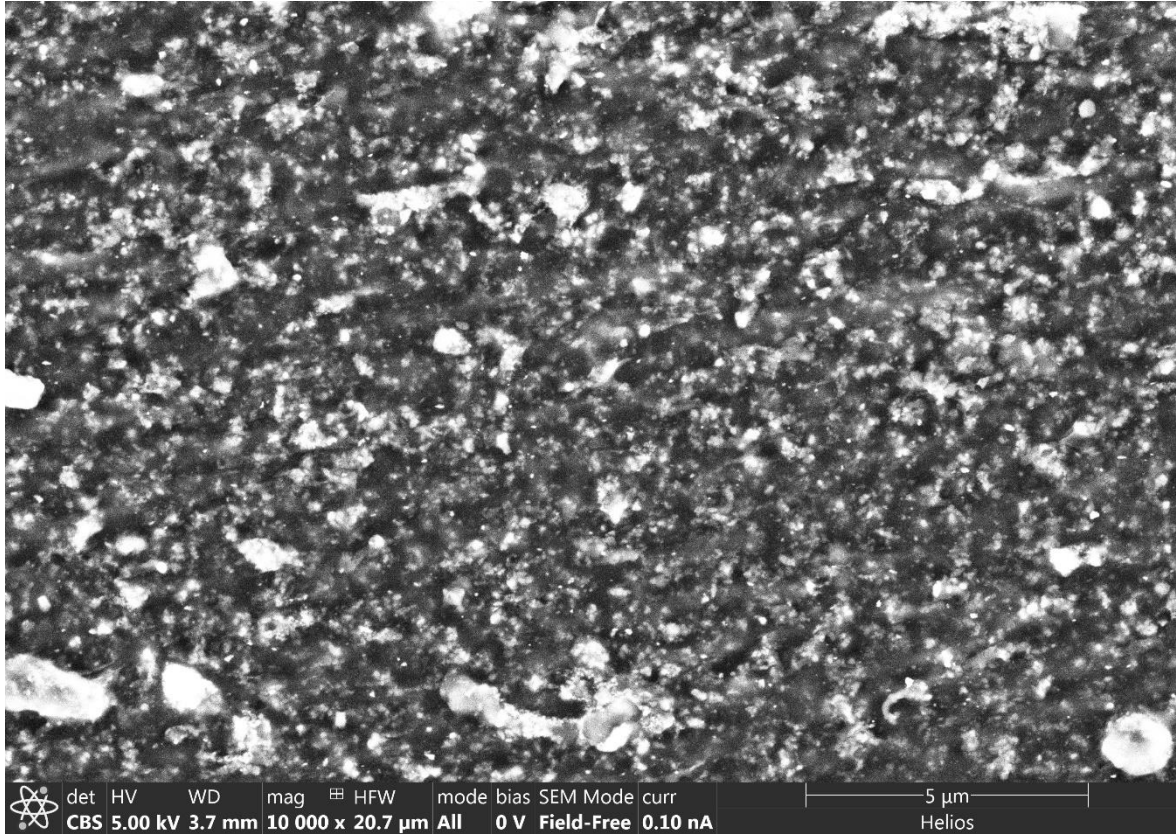
iv.　Processed Images, mount ID 5
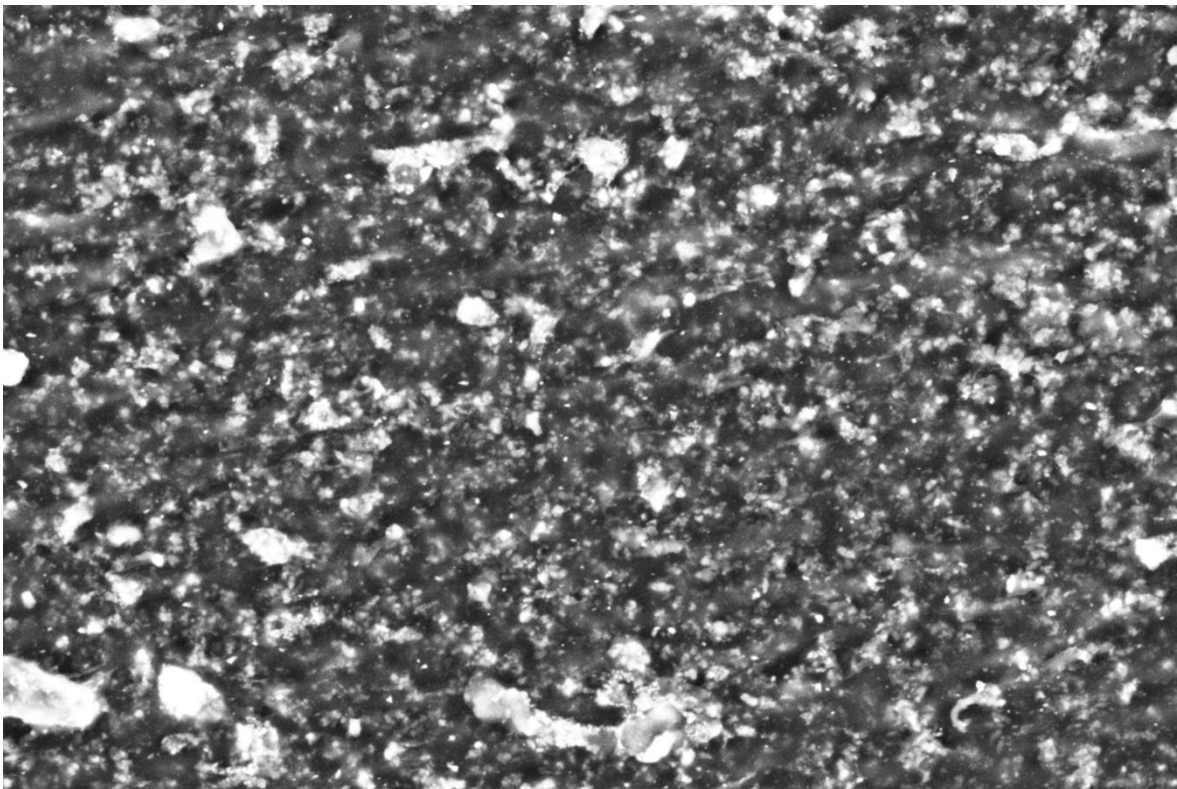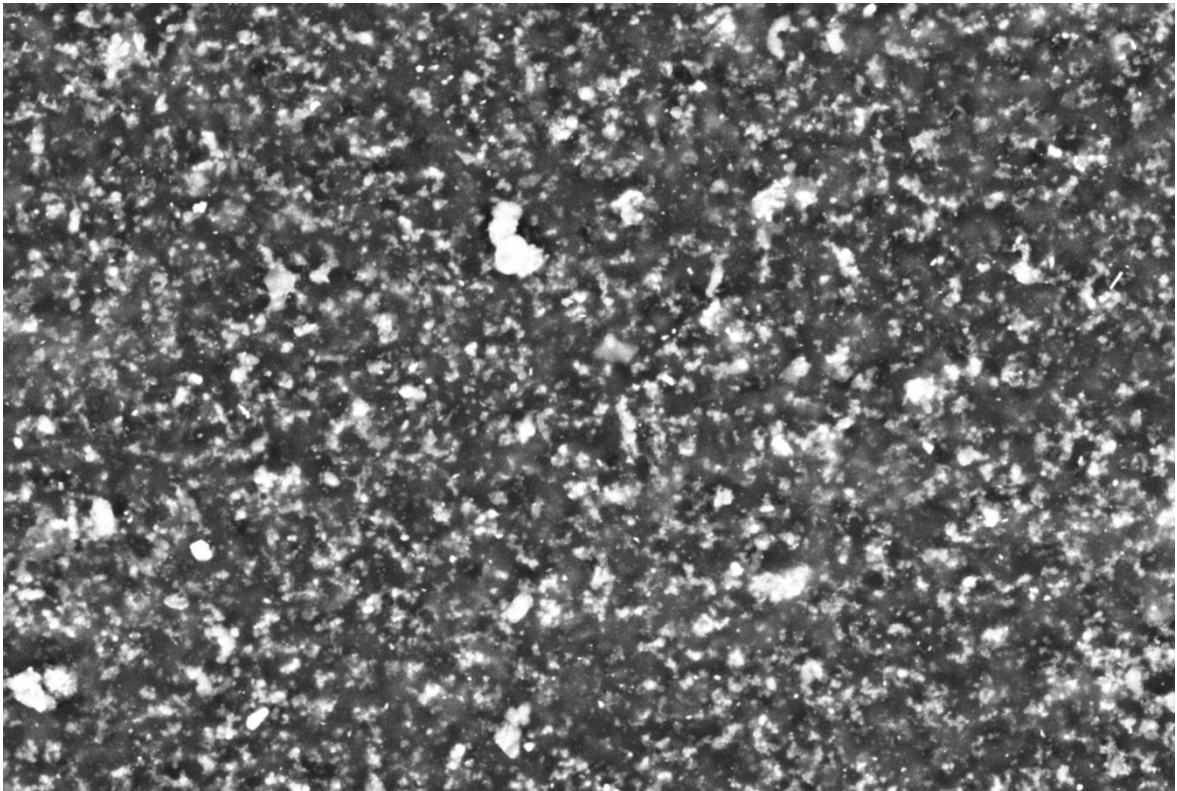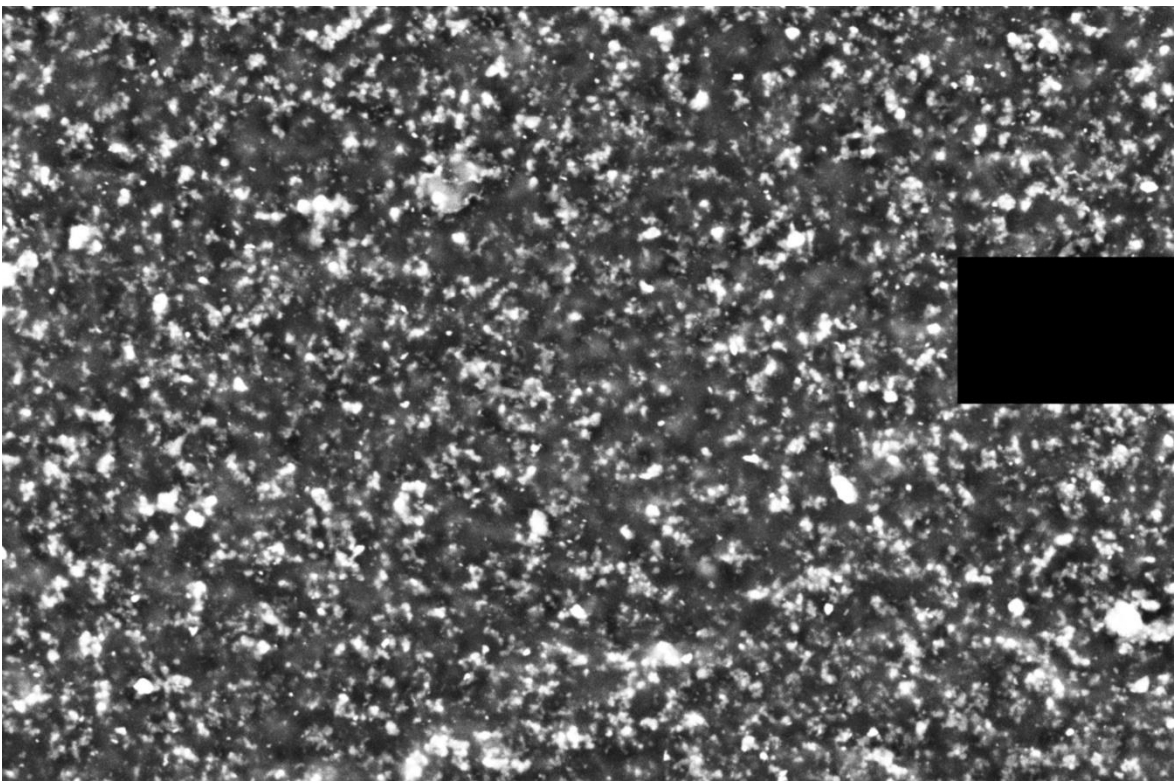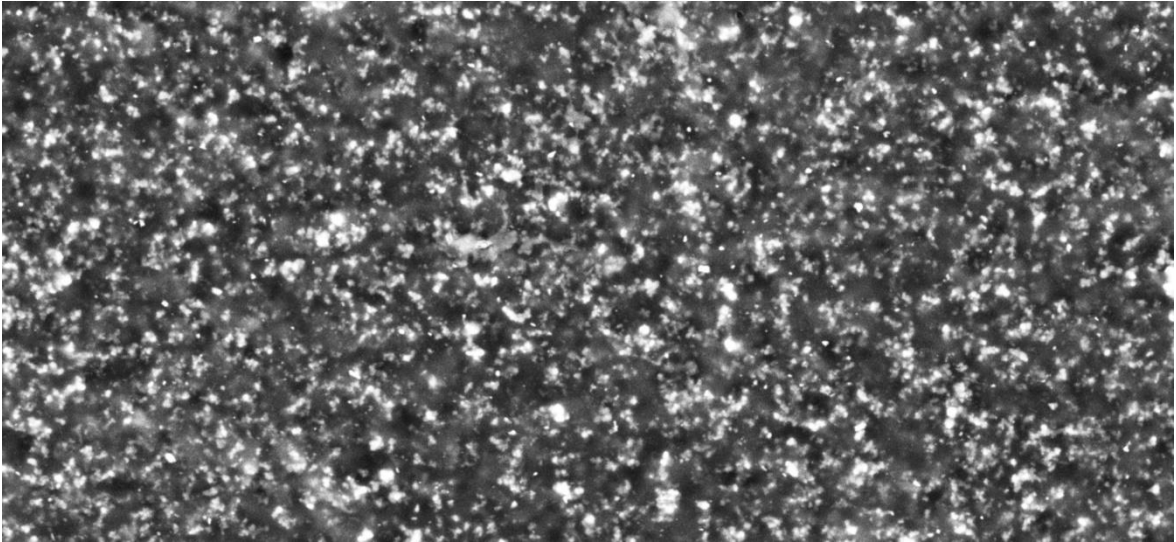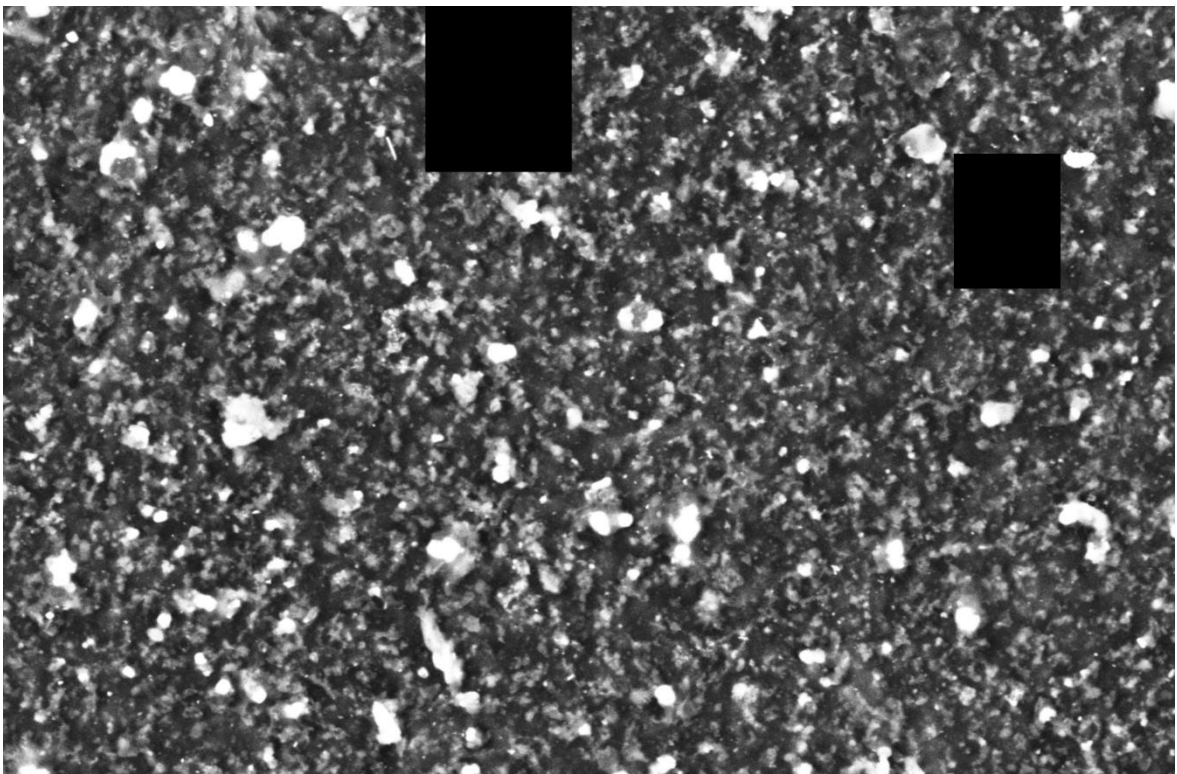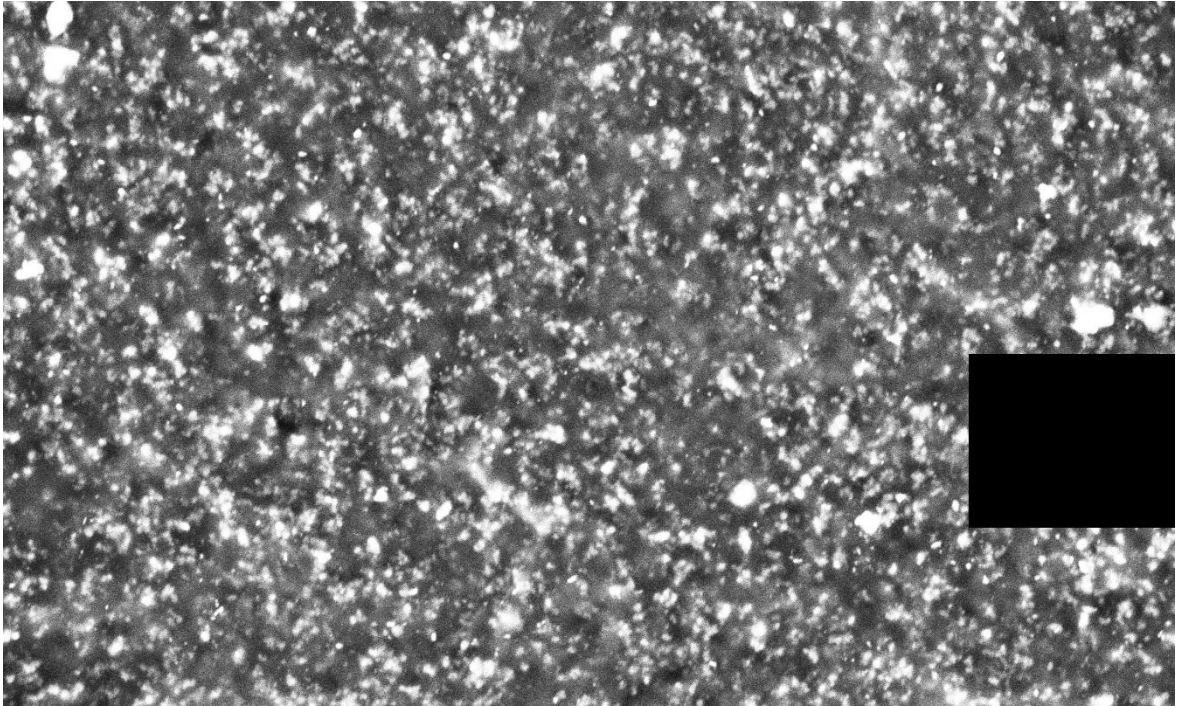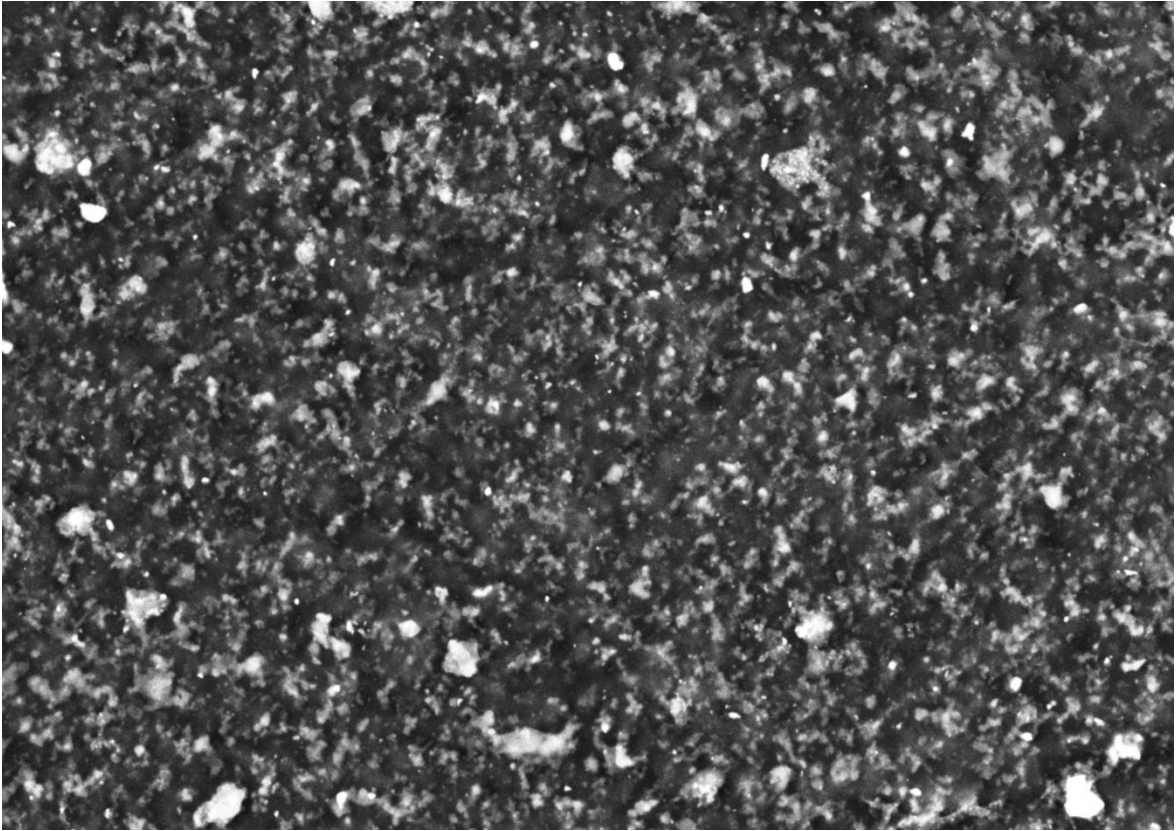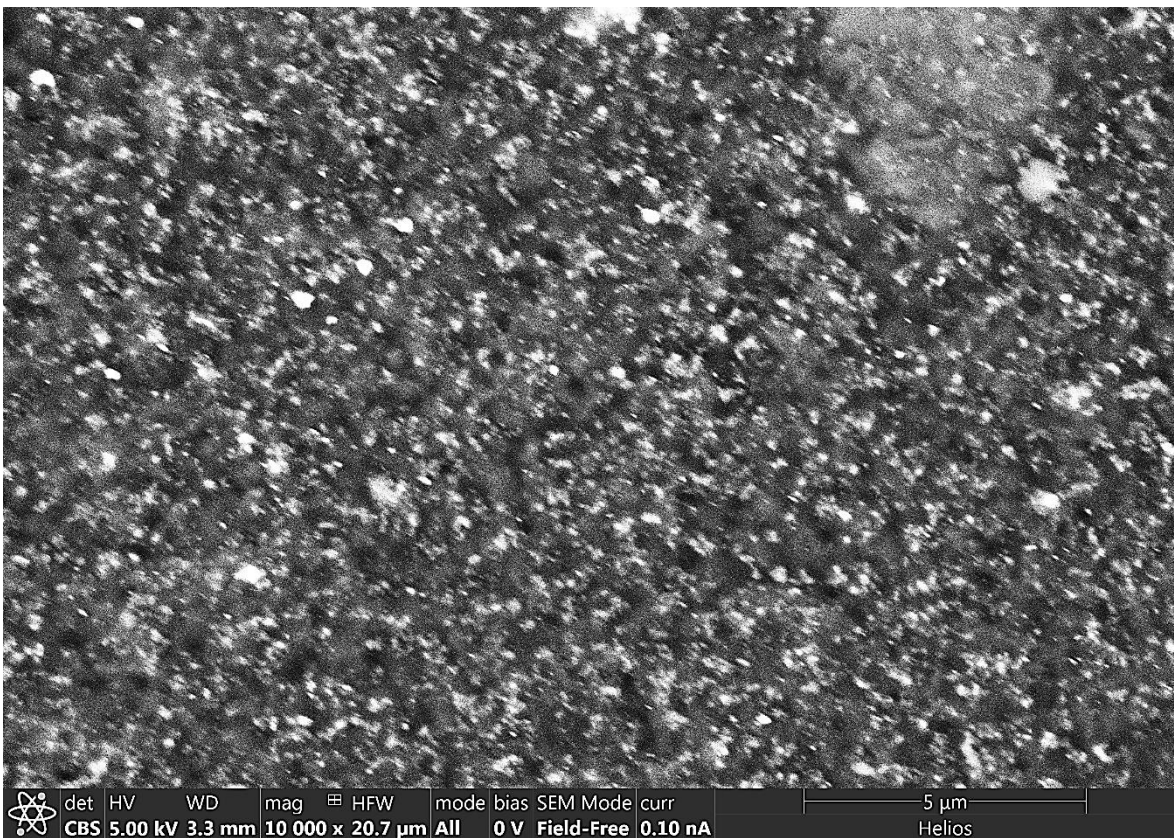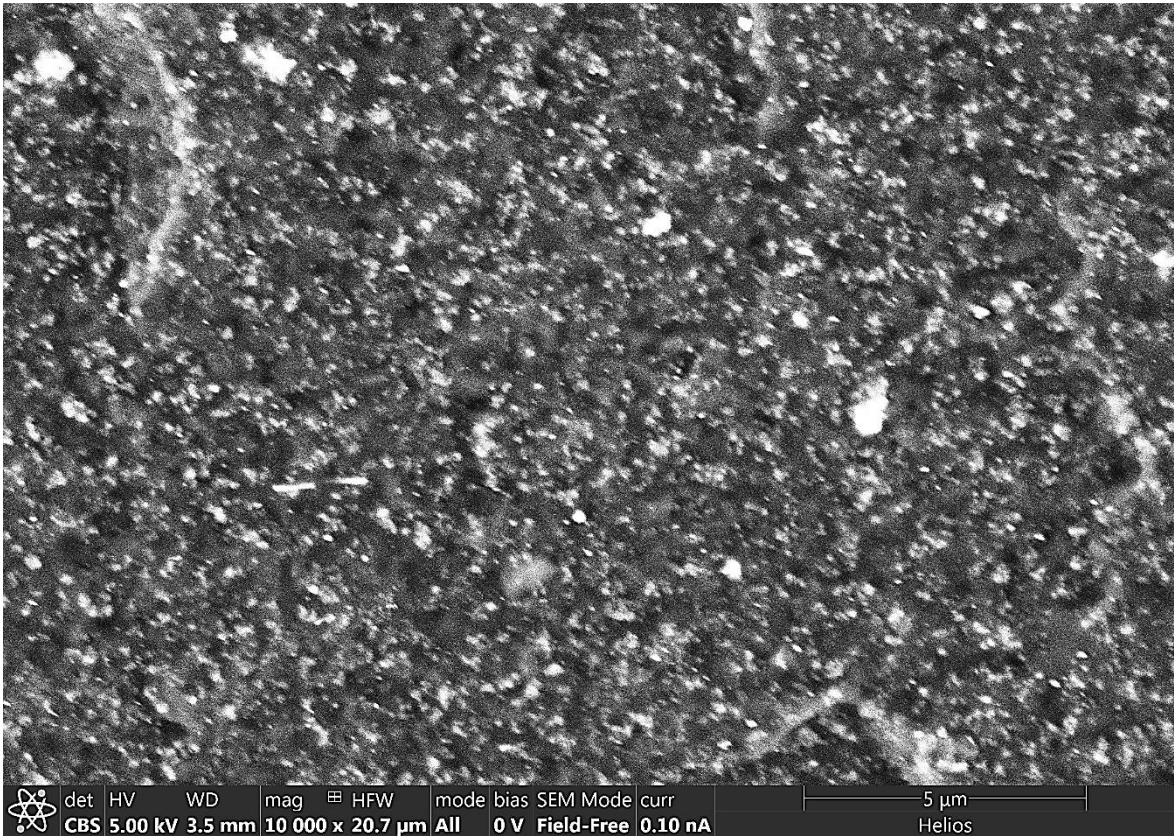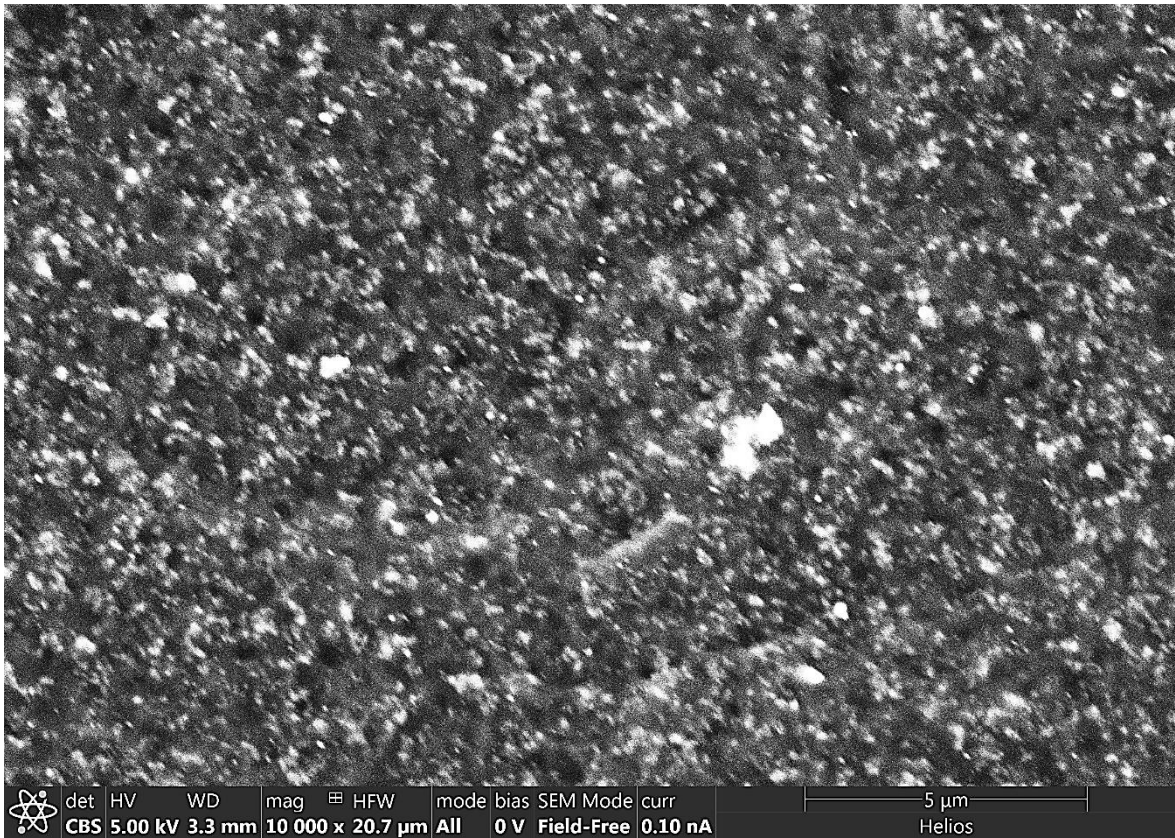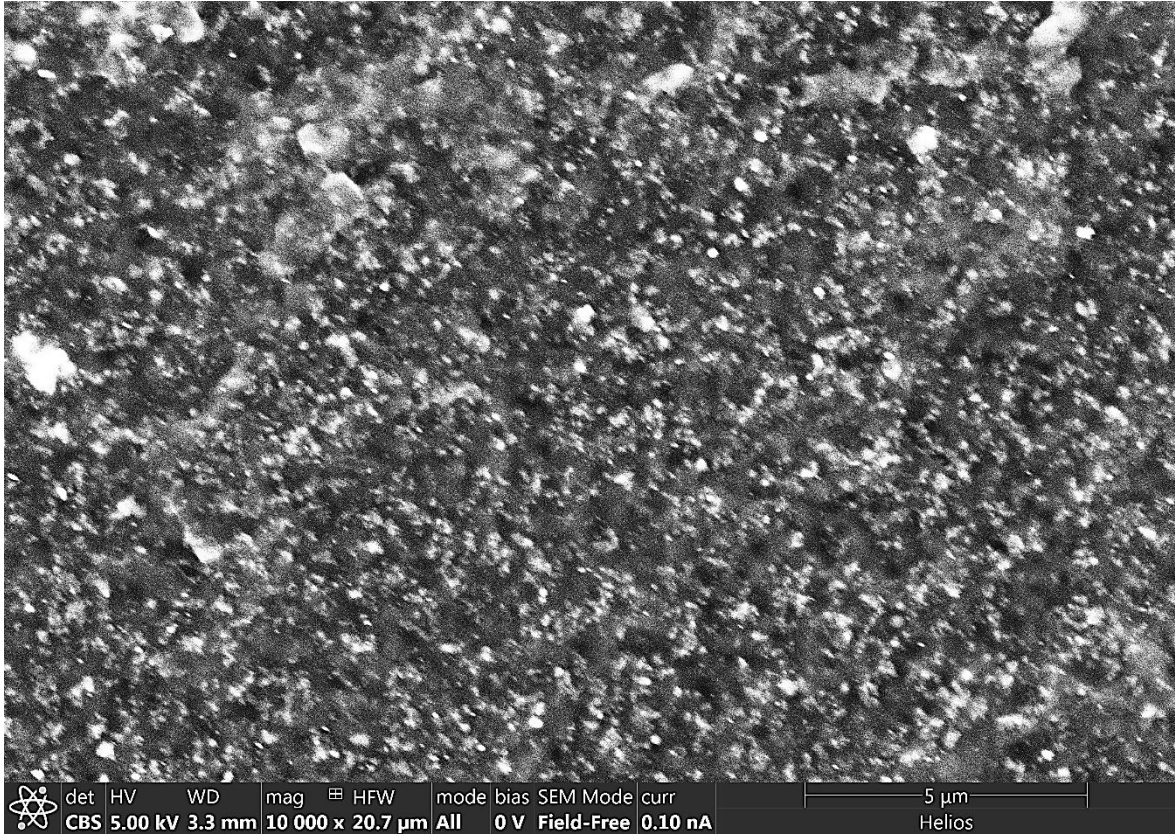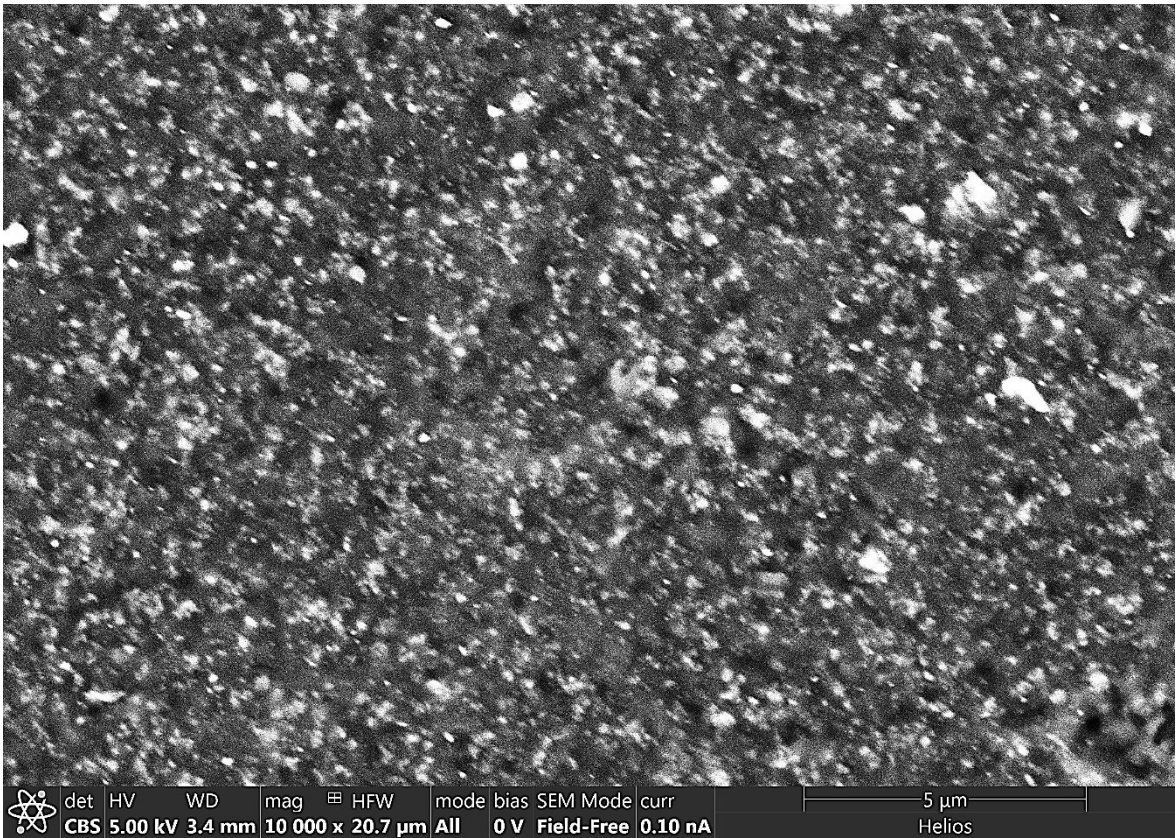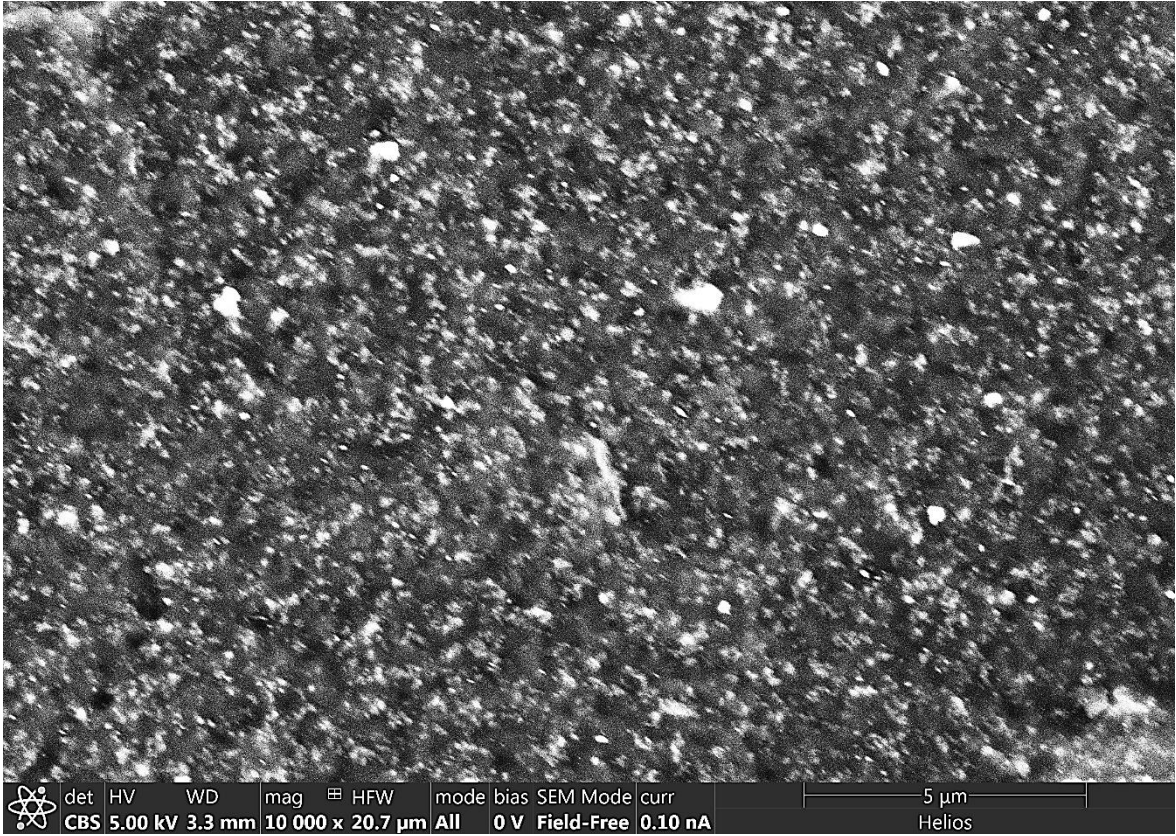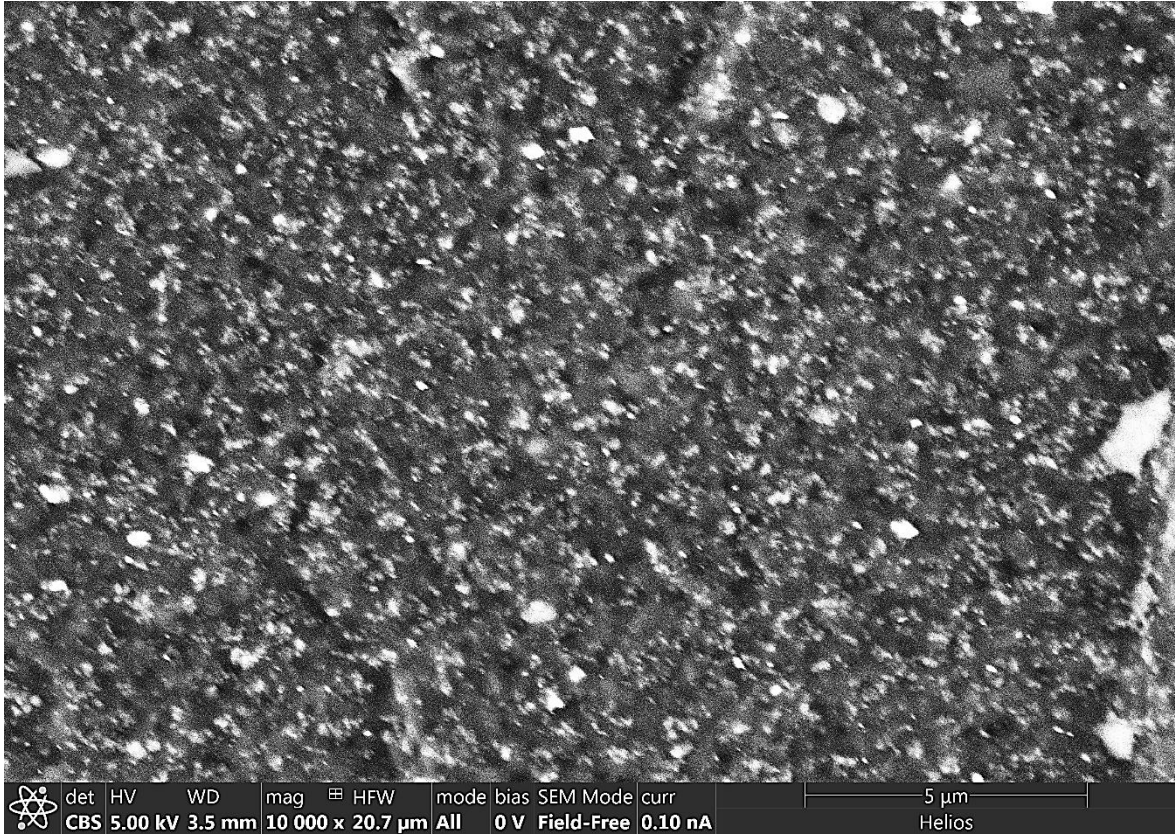
| det | HV | WD | mag | ⊞ | HFW | mode | bias | SEM Mode | curr | 5 µm |
| CBS | 5.00 kV | 3.5 mm | 10 000 x | | 20.7 µm | All | 0 V | Field-Free | 0.10 nA | Helios |

| det | HV | WD | mag | ⊞ | HFW | mode | bias | SEM Mode | curr | 5 µm |
| CBS | 5.00 kV | 3.3 mm | 10 000 x | | 20.7 µm | All | 0 V | Field-Free | 0.10 nA | Helios |

xxx
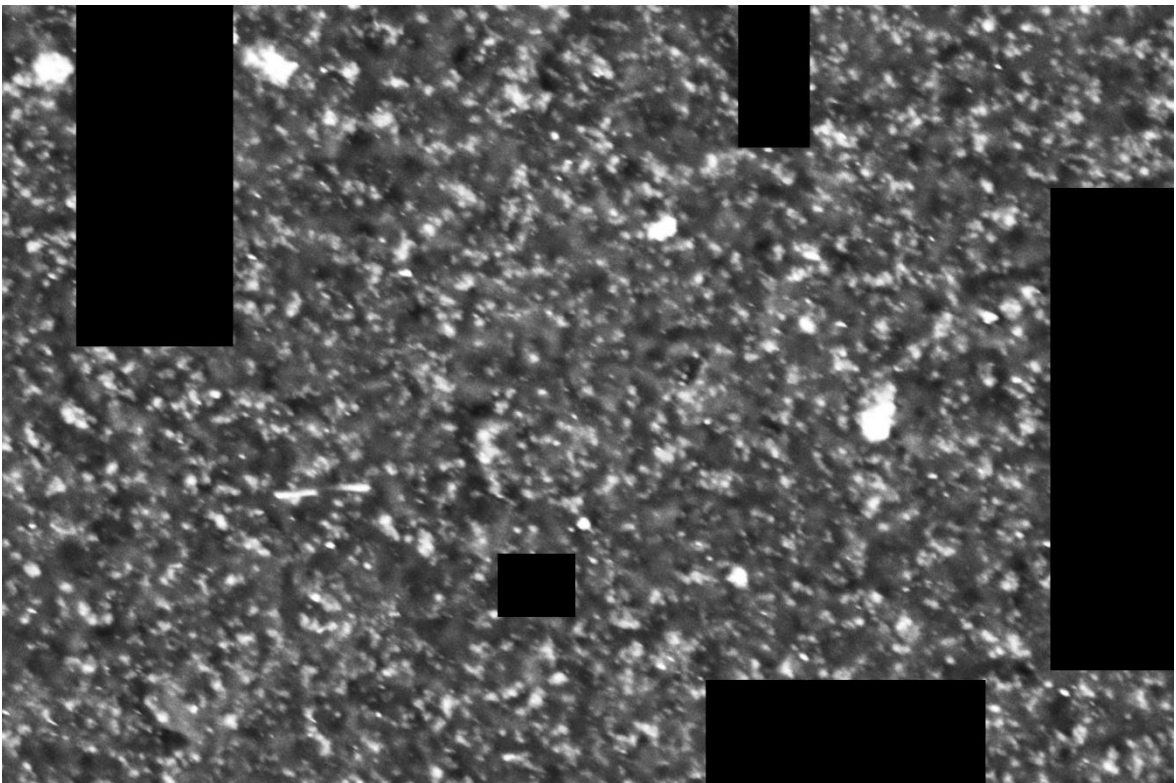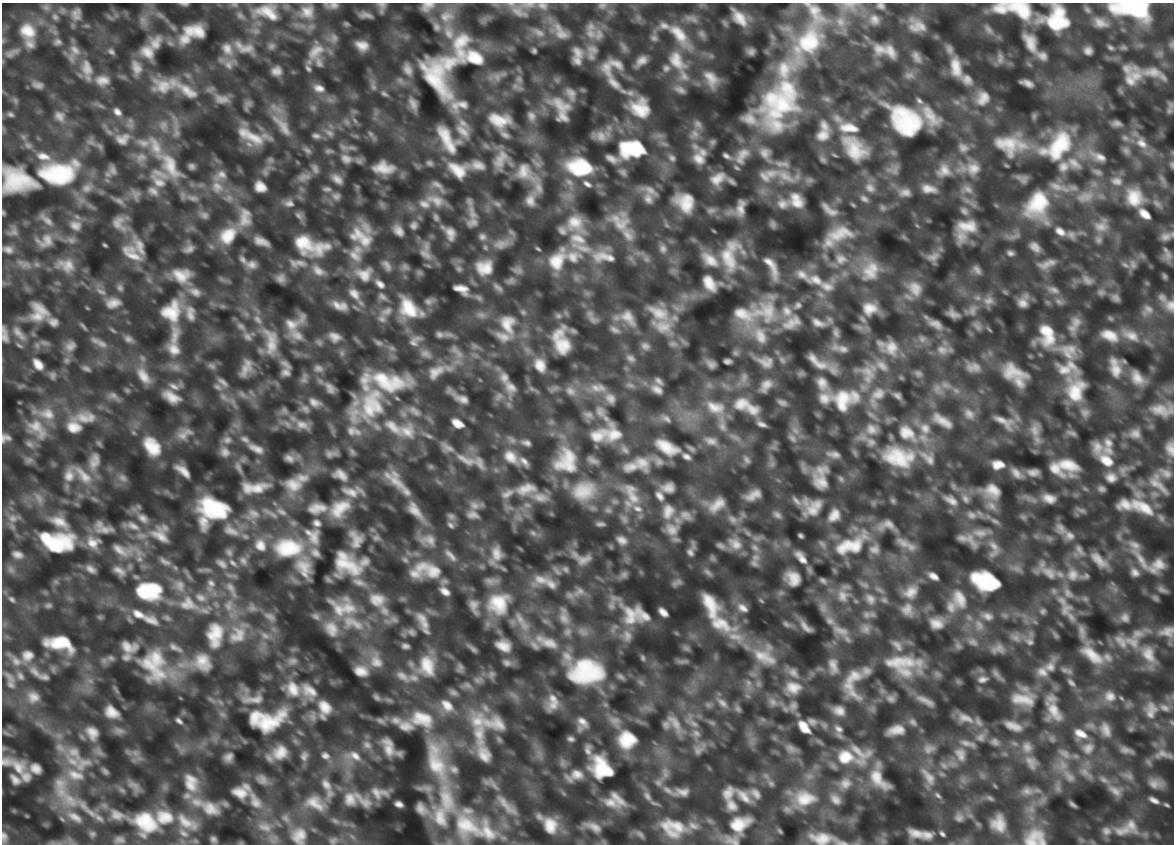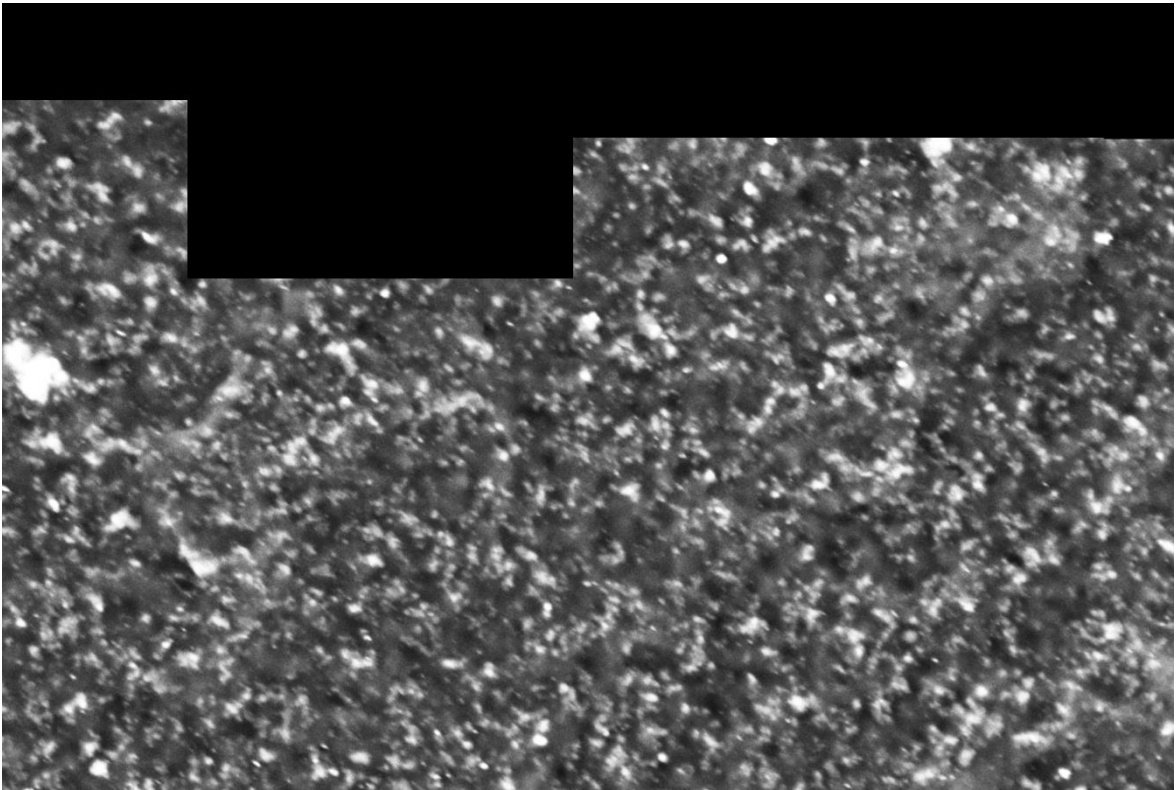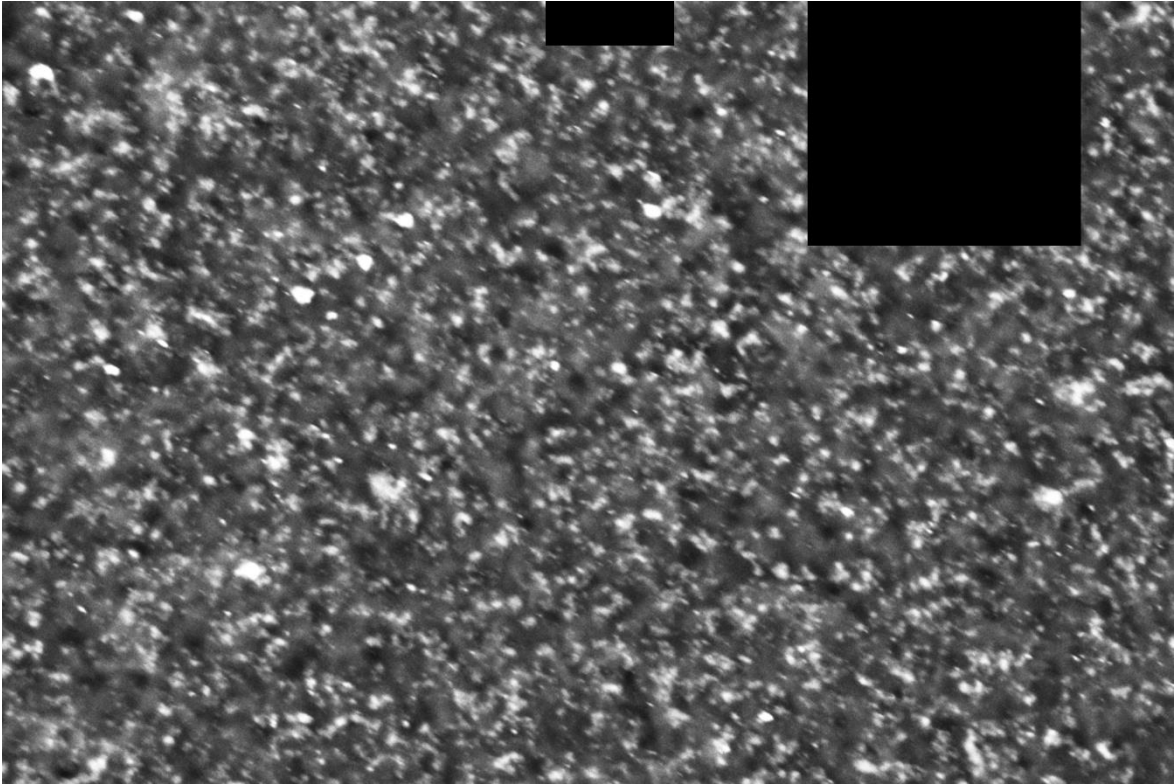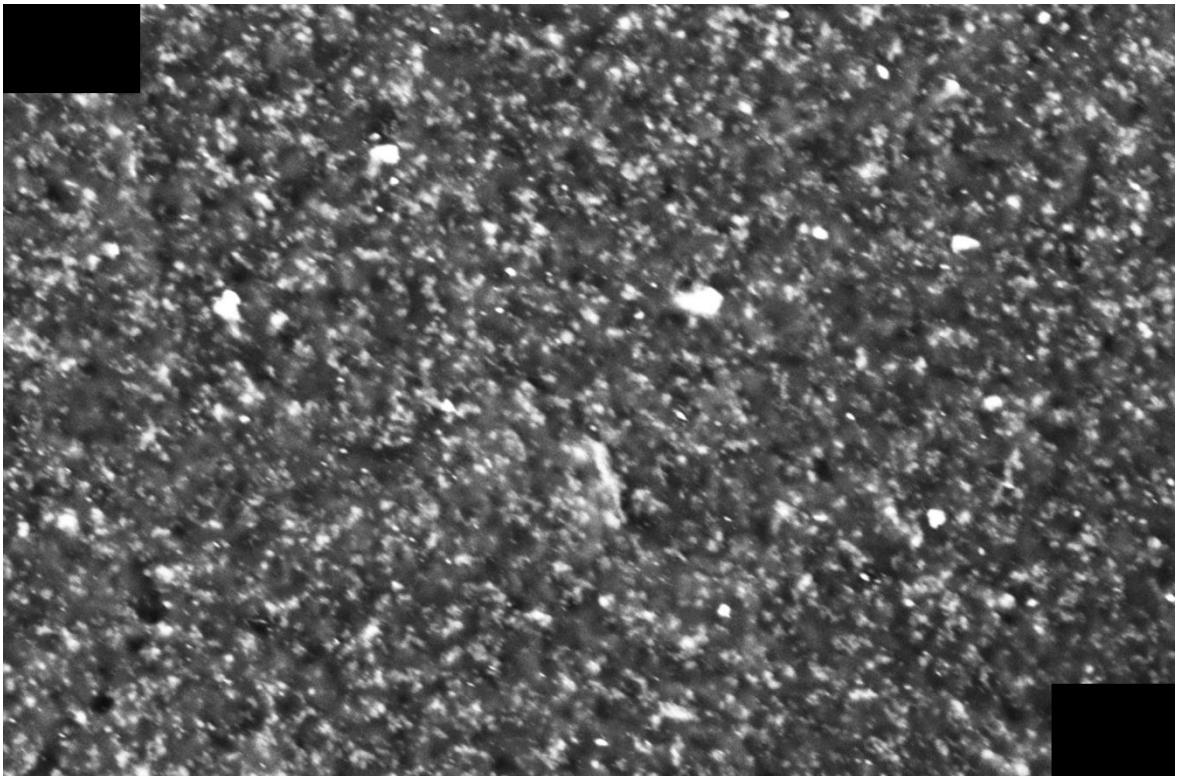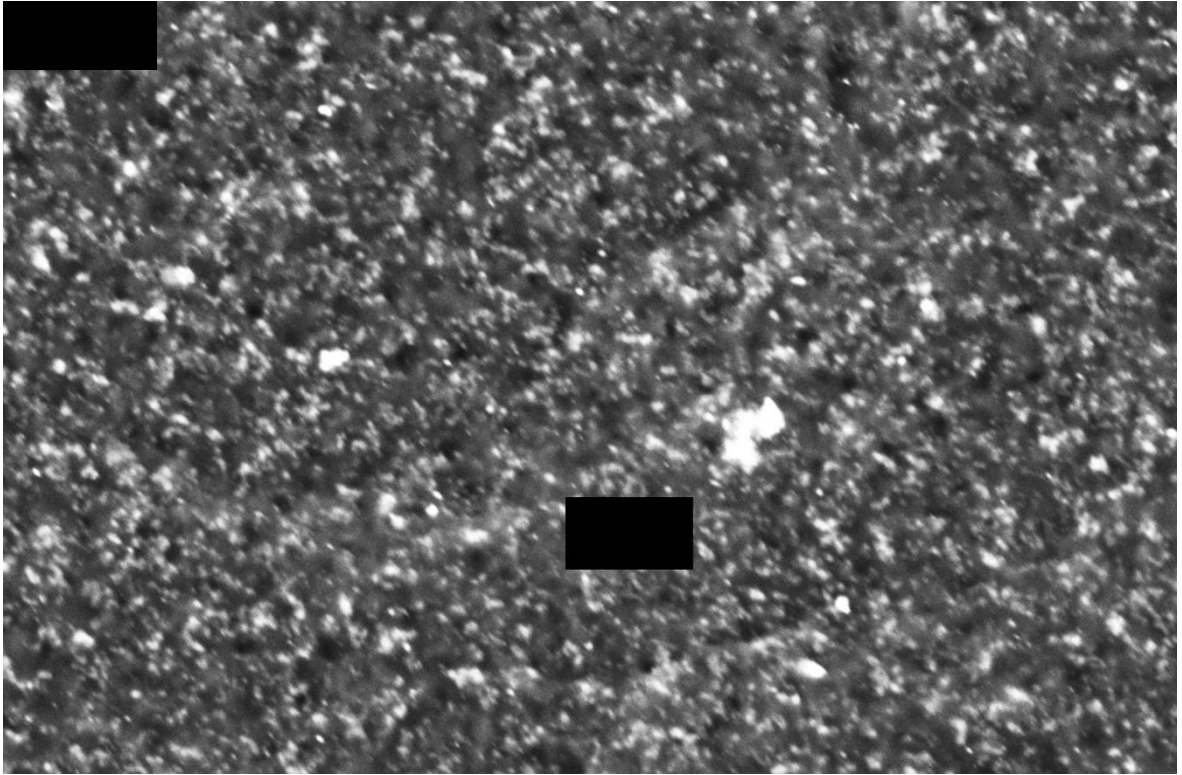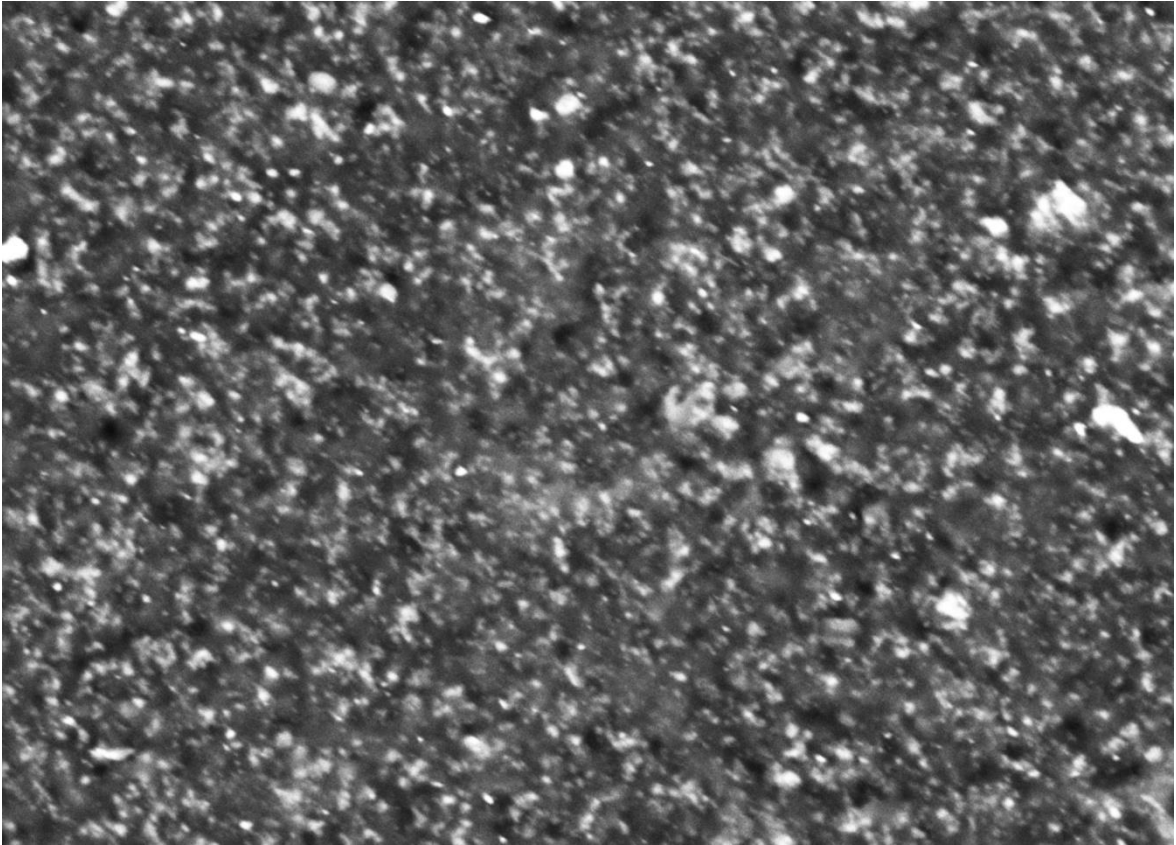
Mount ID 4 Location D, Raw Image
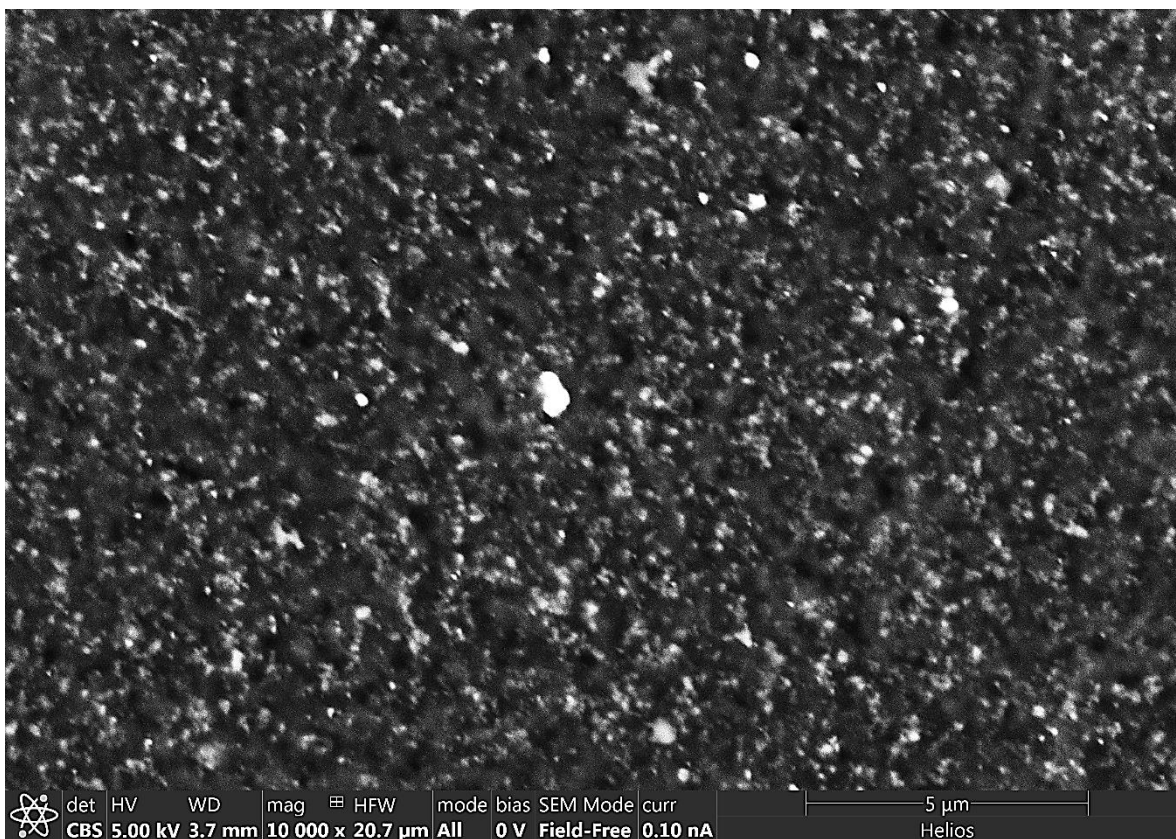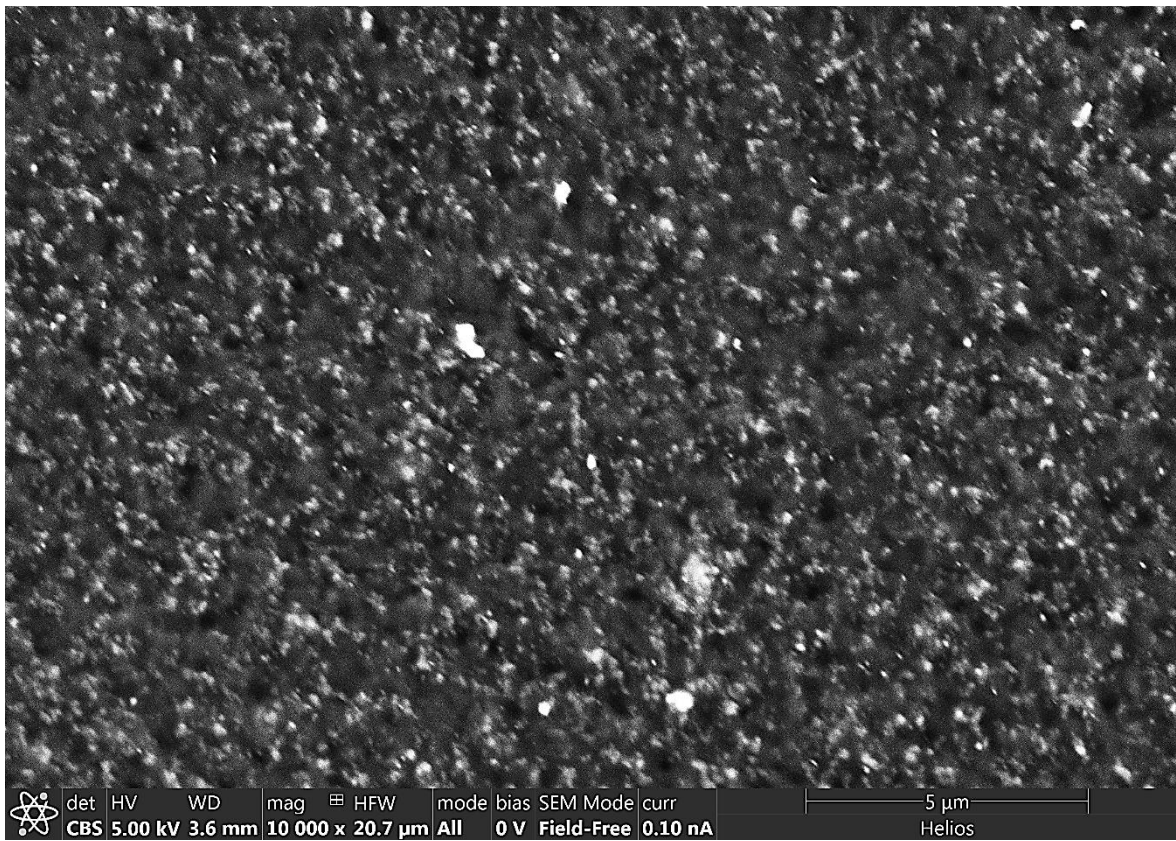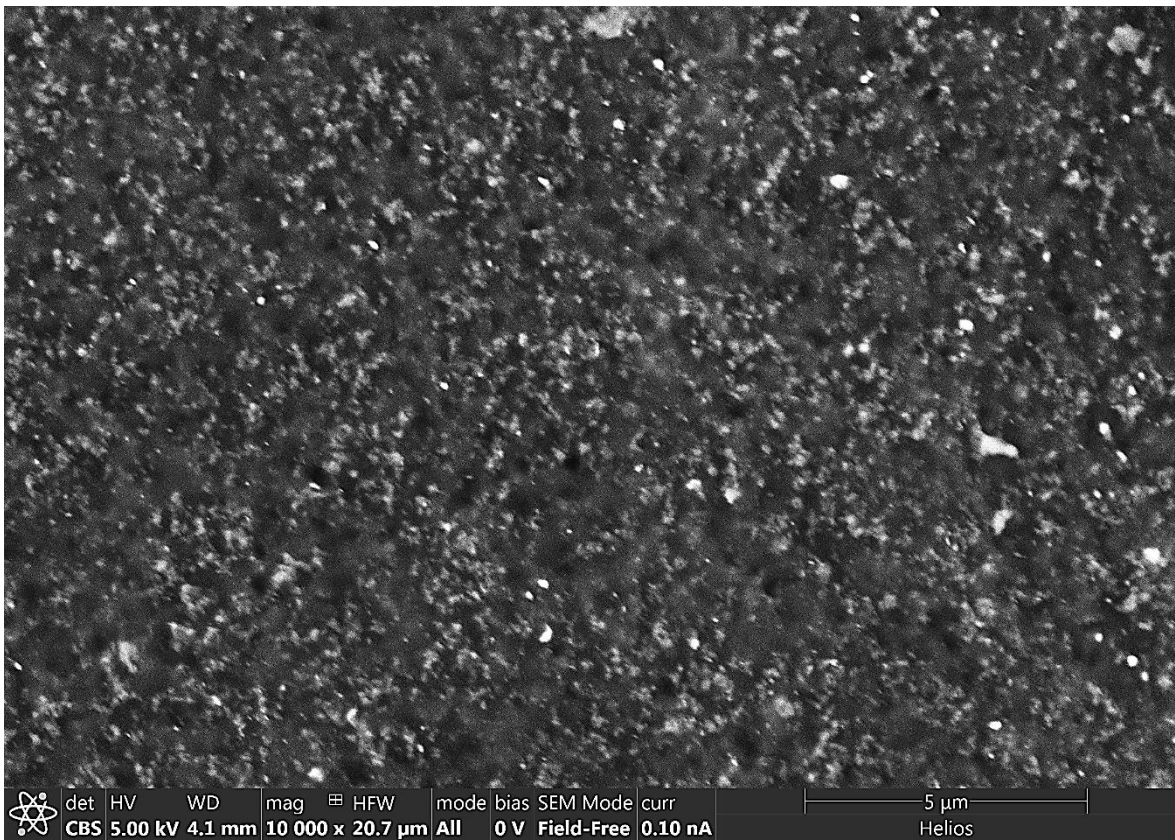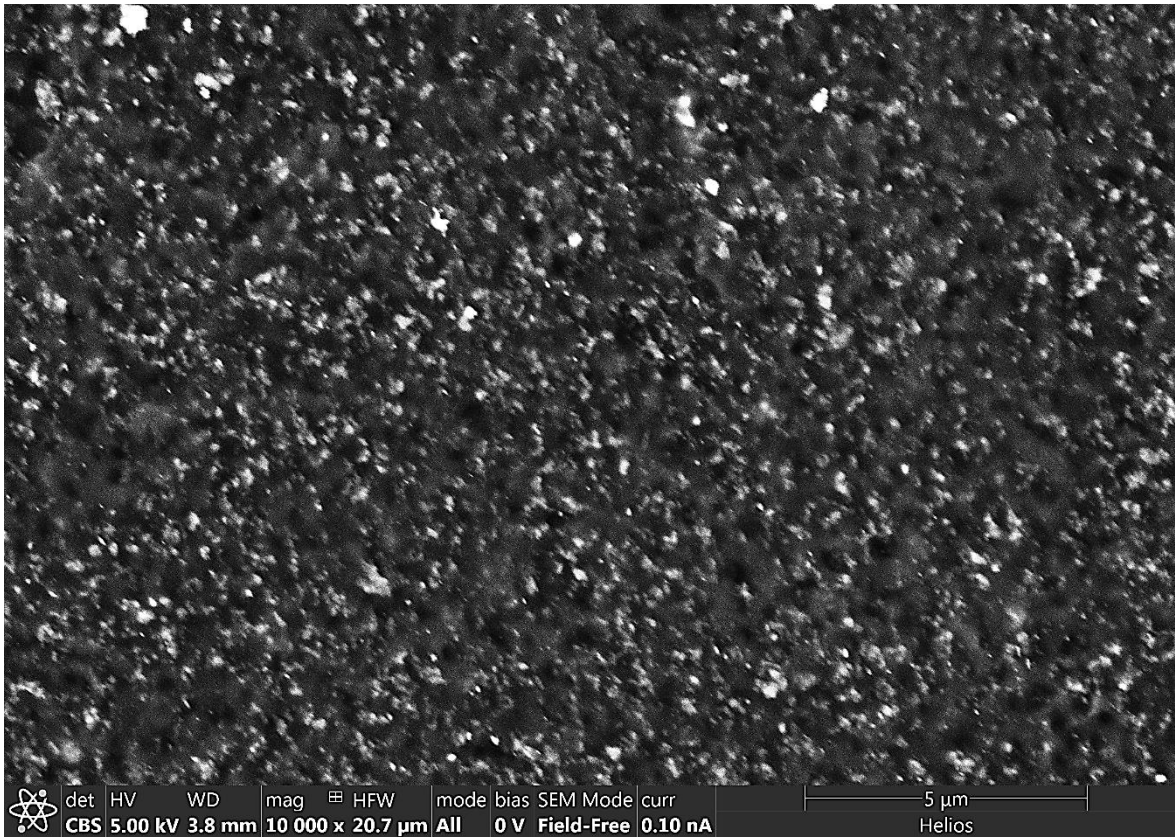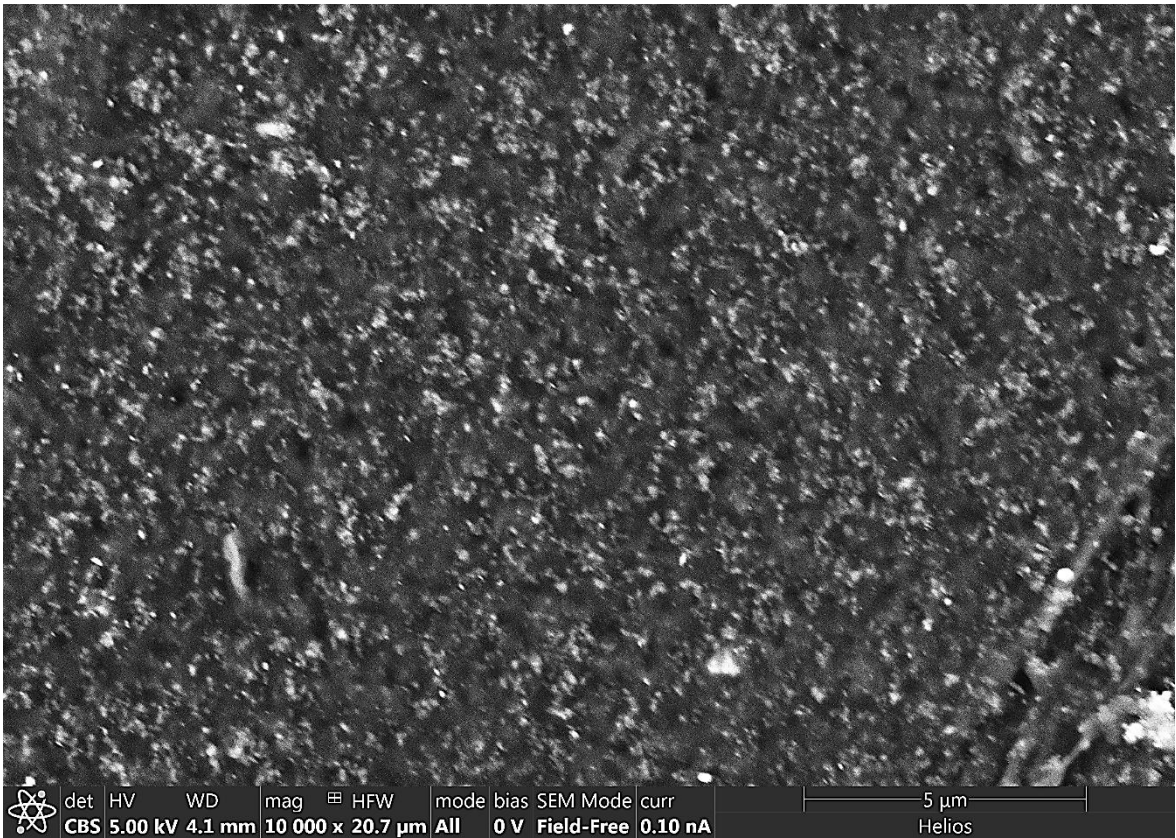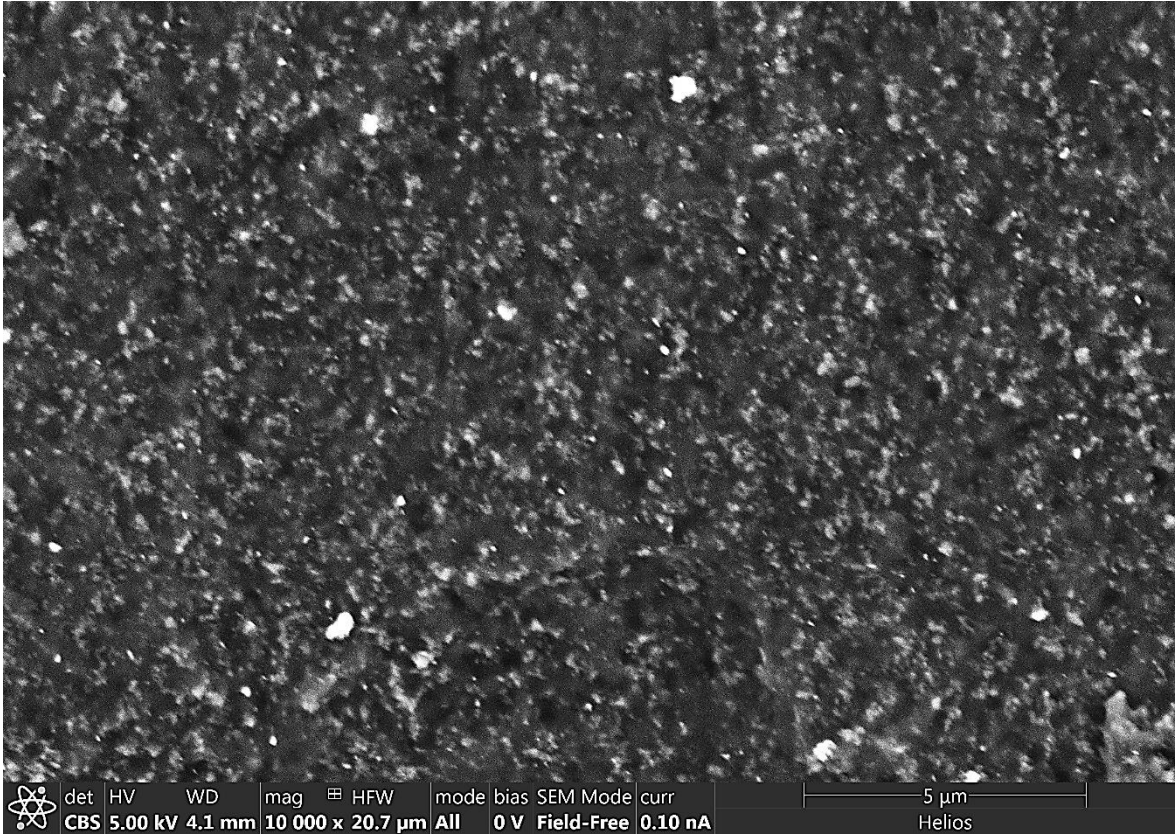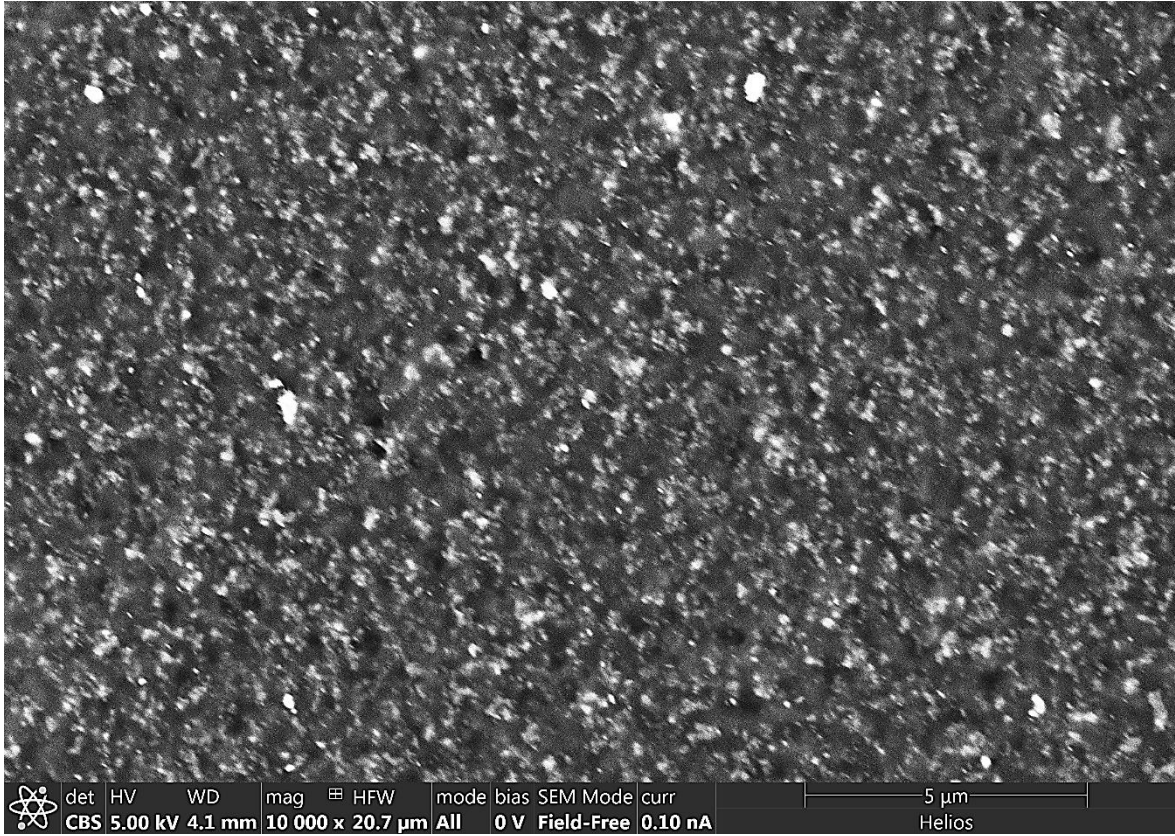
det	HV	WD	mag	HFW	mode	bias	SEM Mode	curr	5 µm
CBS	5.00 kV	3.8 mm	10 000 x	20.7 µm	All	0 V	Field-Free	0.10 nA	Helios

det	HV	WD	mag	HFW	mode	bias	SEM Mode	curr	5 µm
CBS	5.00 kV	4.1 mm	10 000 x	20.7 µm	All	0 V	Field-Free	0.10 nA	Helios

det	HV	WD	mag	HFW	mode	bias	SEM Mode	curr	5 µm
CBS	5.00 kV	4.1 mm	10 000 x	20.7 µm	All	0 V	Field-Free	0.10 nA	Helios
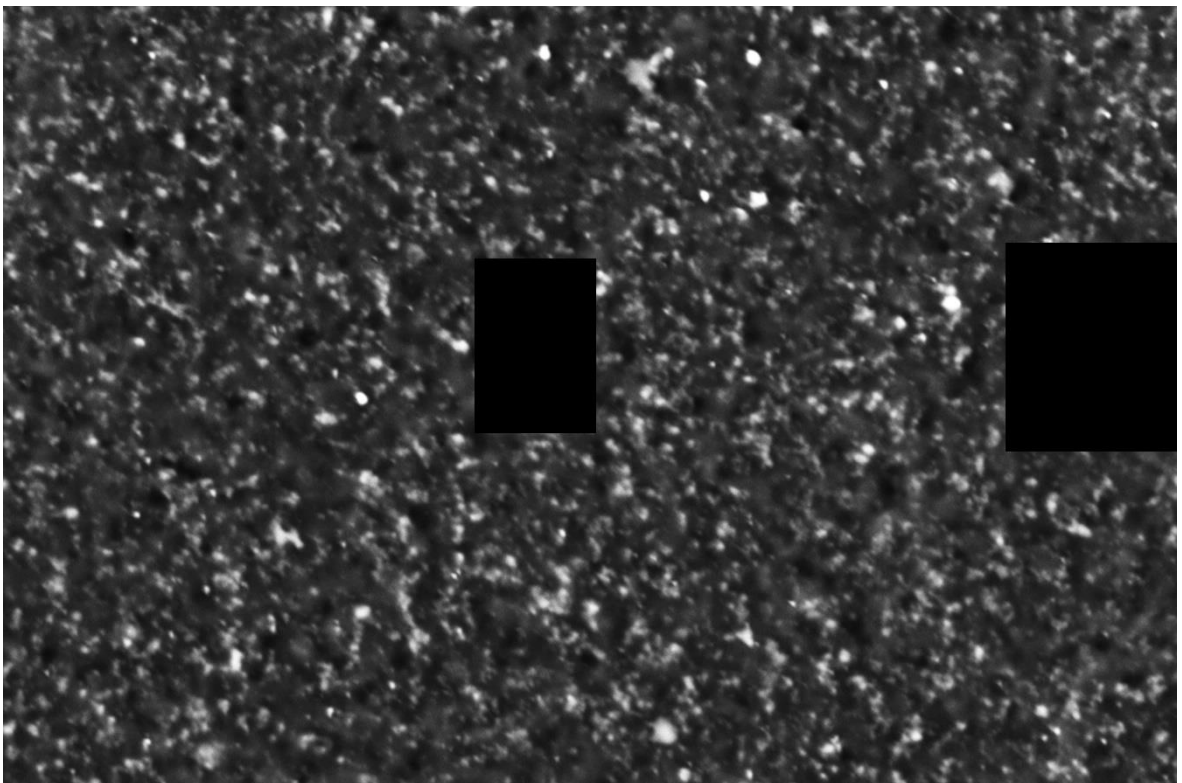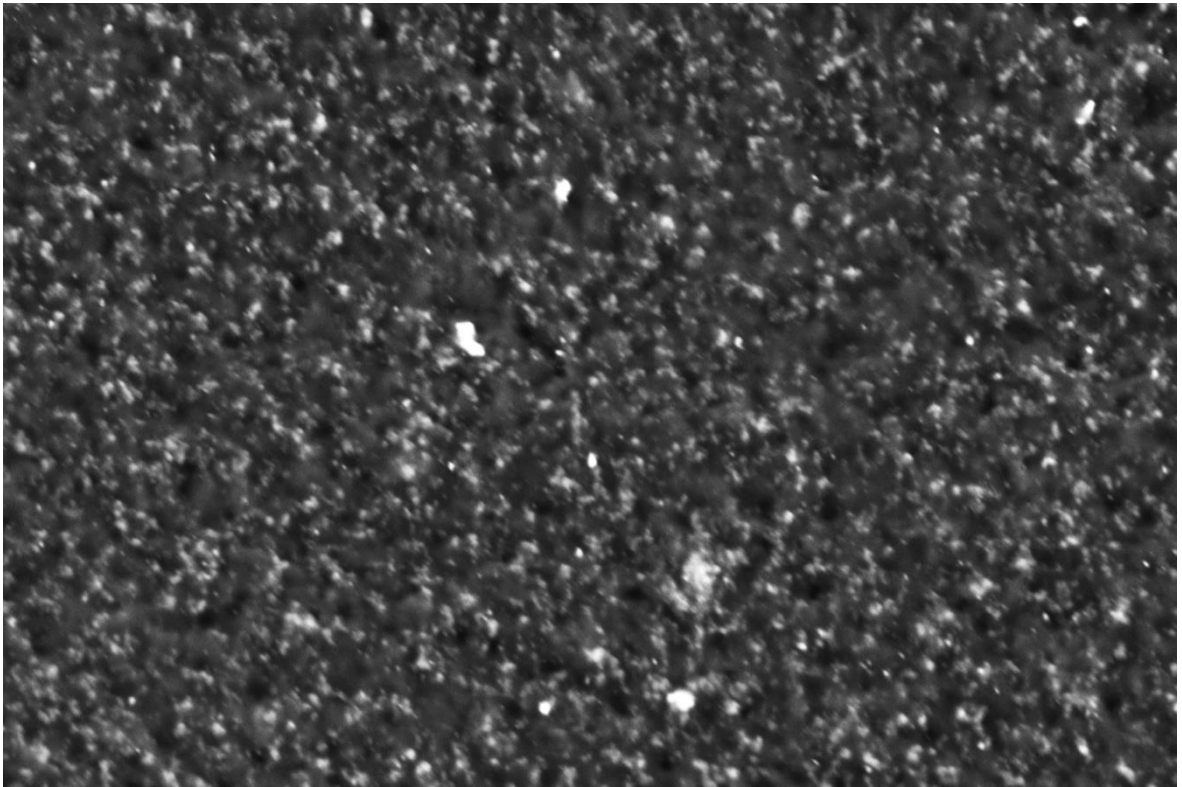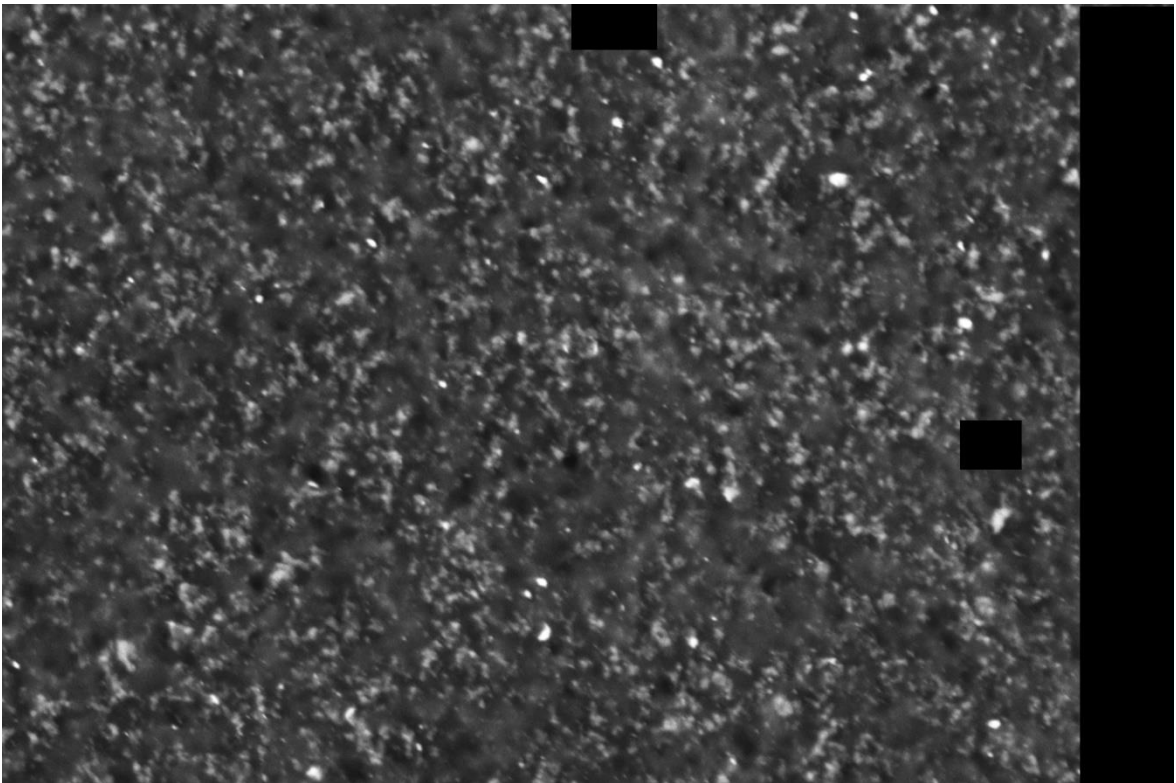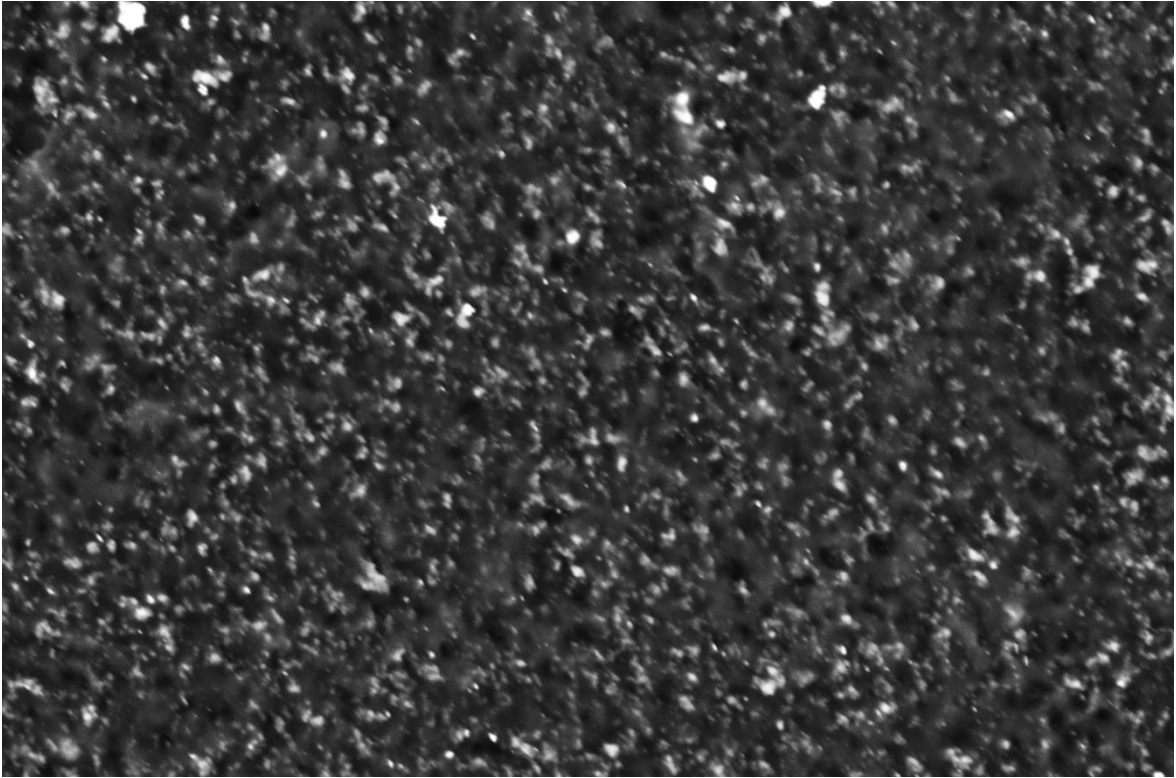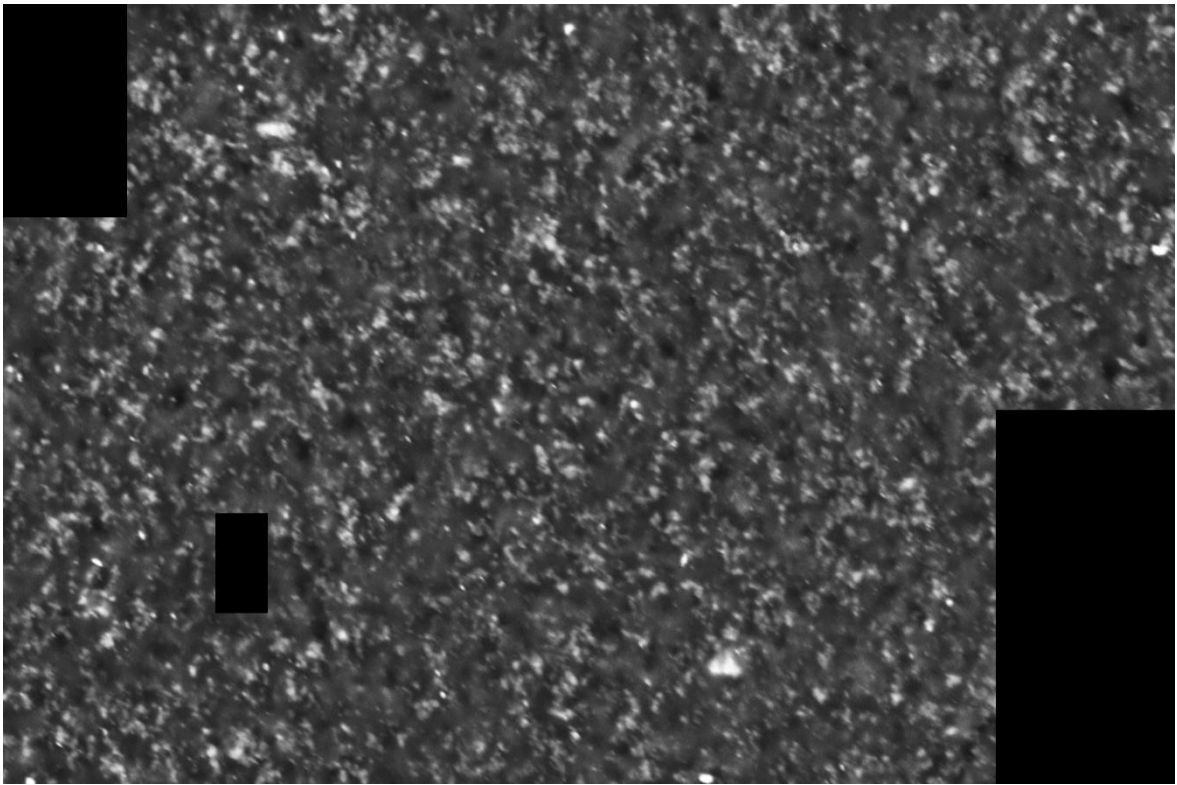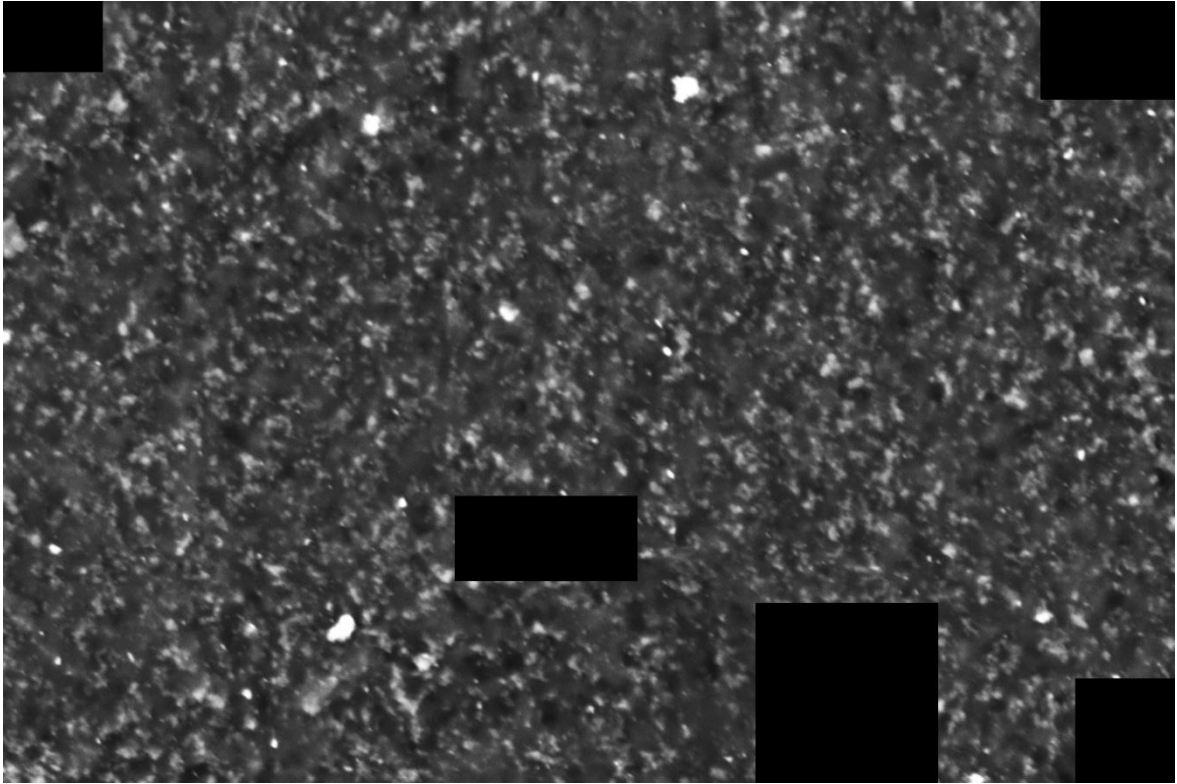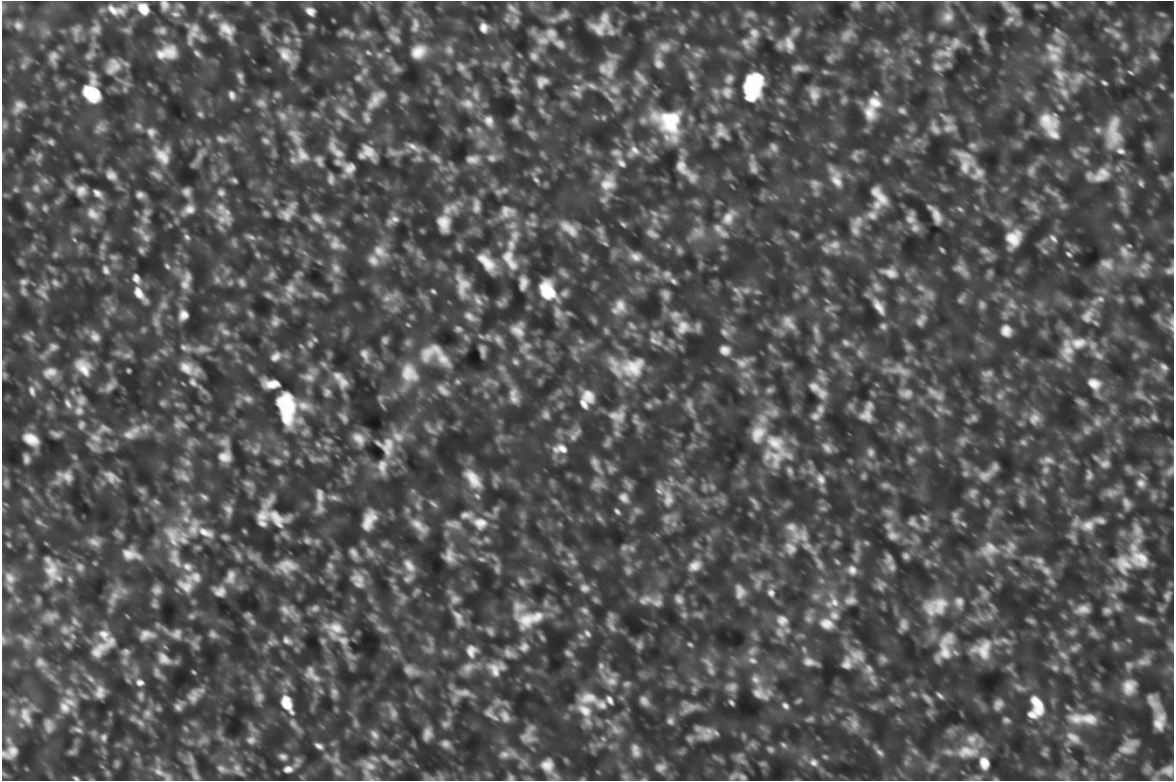
ix.   Mount ID 3 Location C, Raw Image

xl

det	HV	WD	mag ⊞	HFW	mode	bias	SEM Mode	curr	5 µm
CBS	5.00 kV	3.9 mm	10 000 x	20.7 µm	All	0 V	Field-Free	0.10 nA	Helios
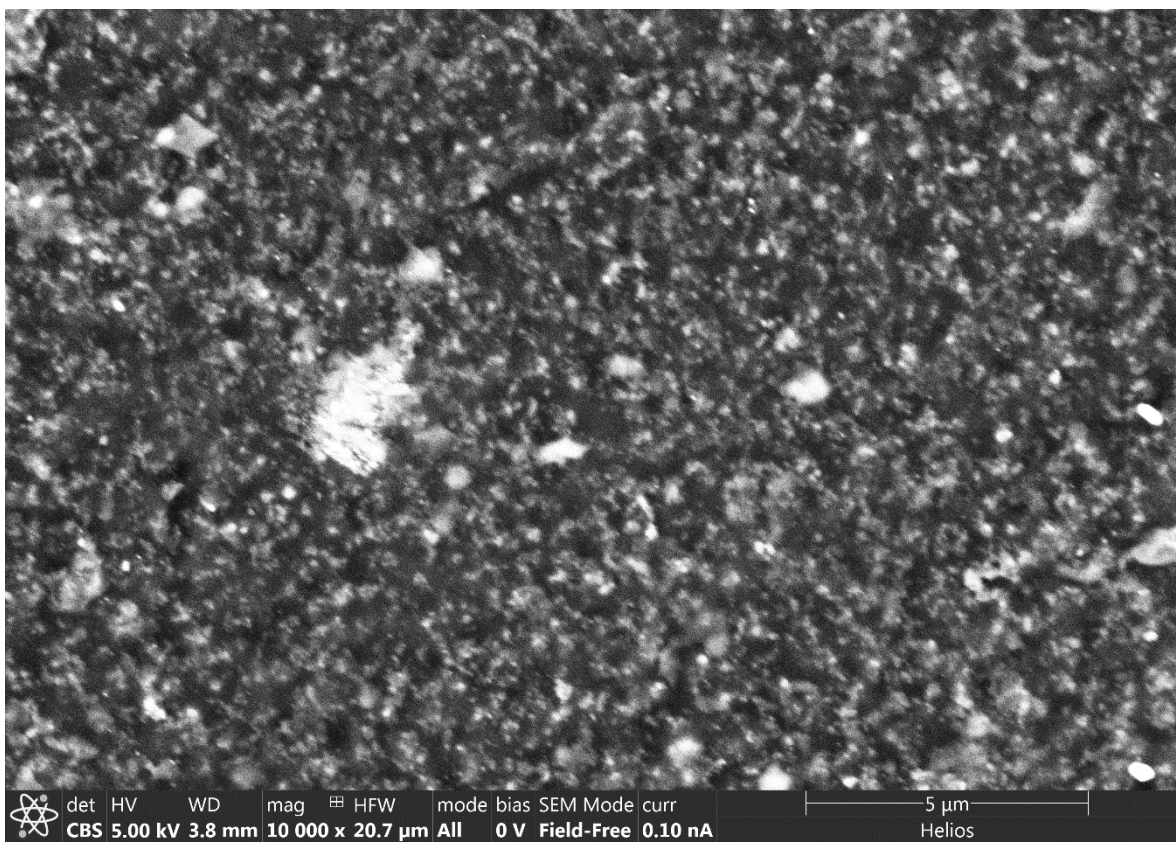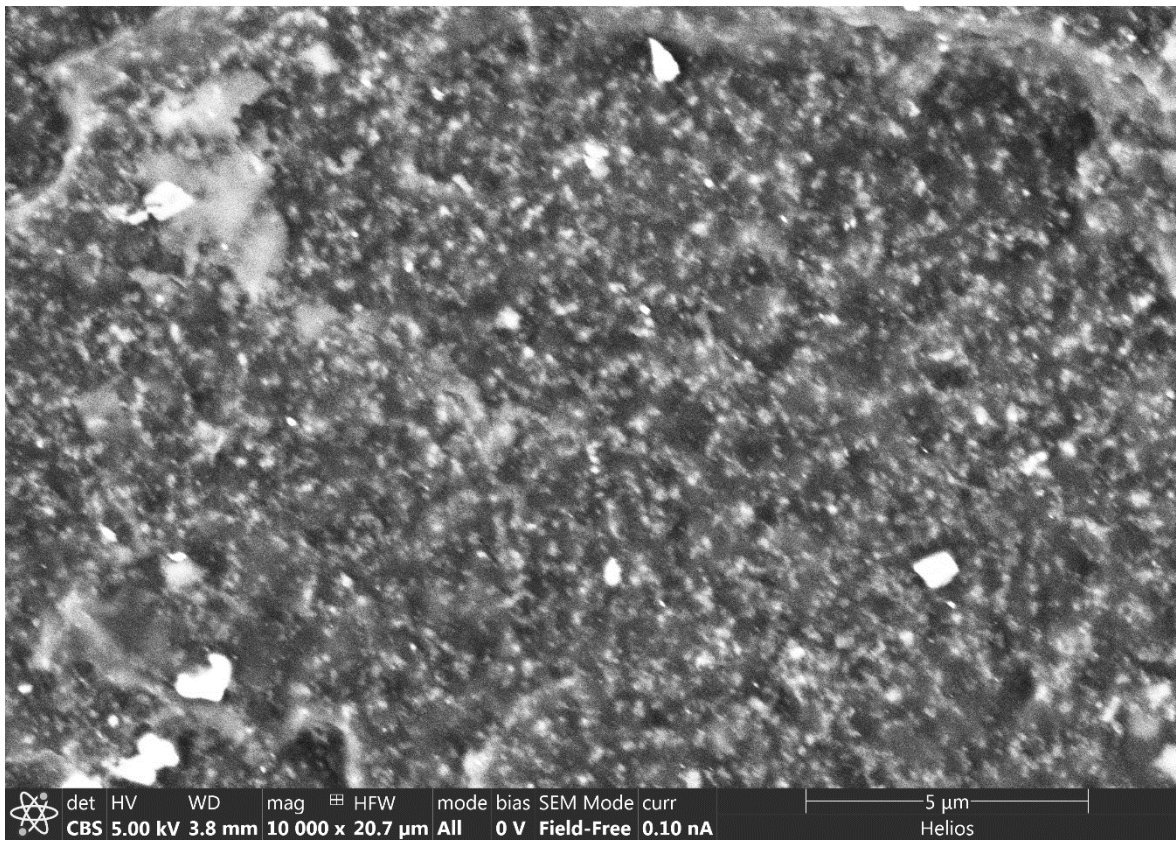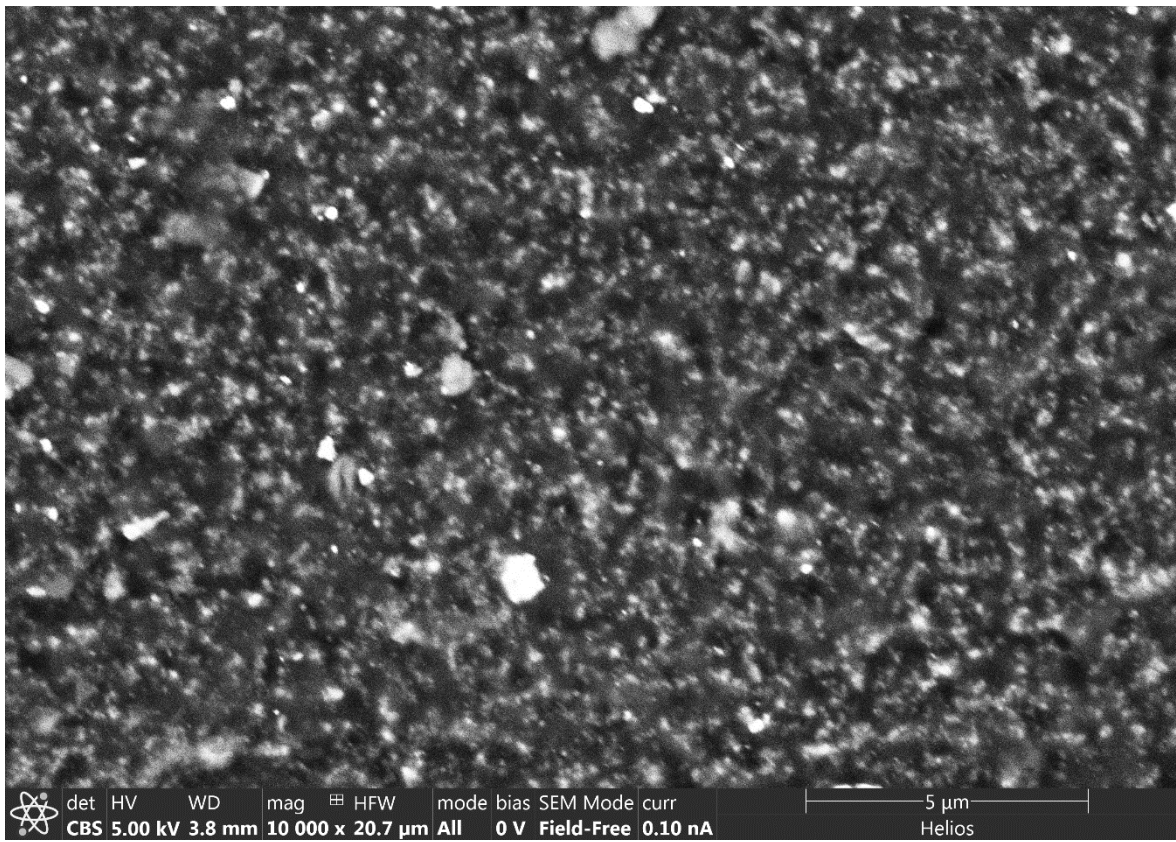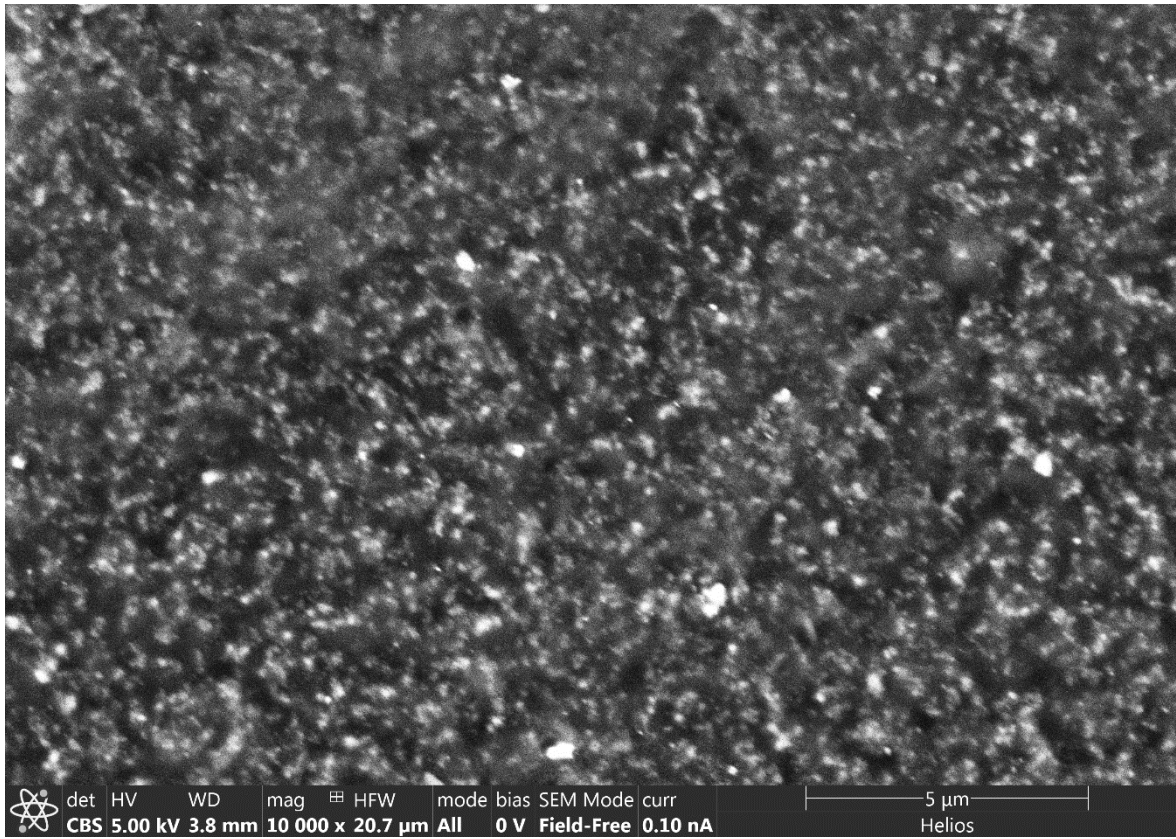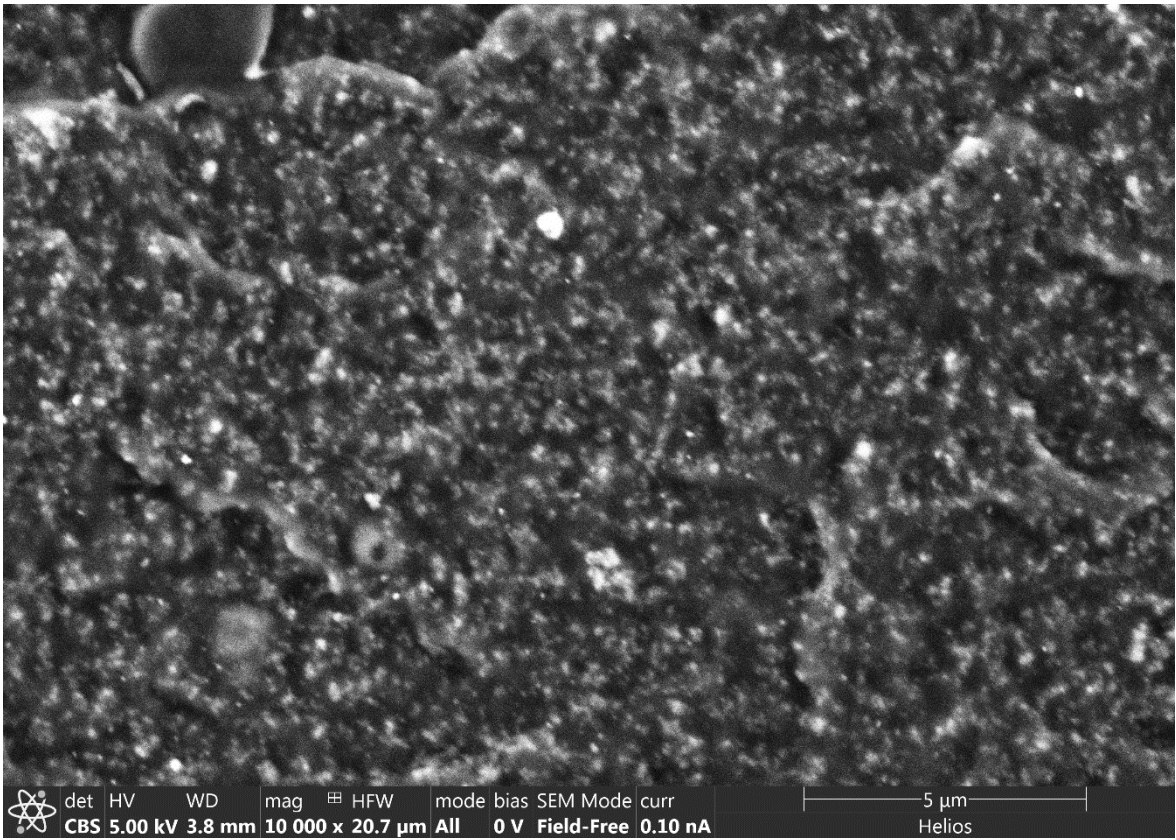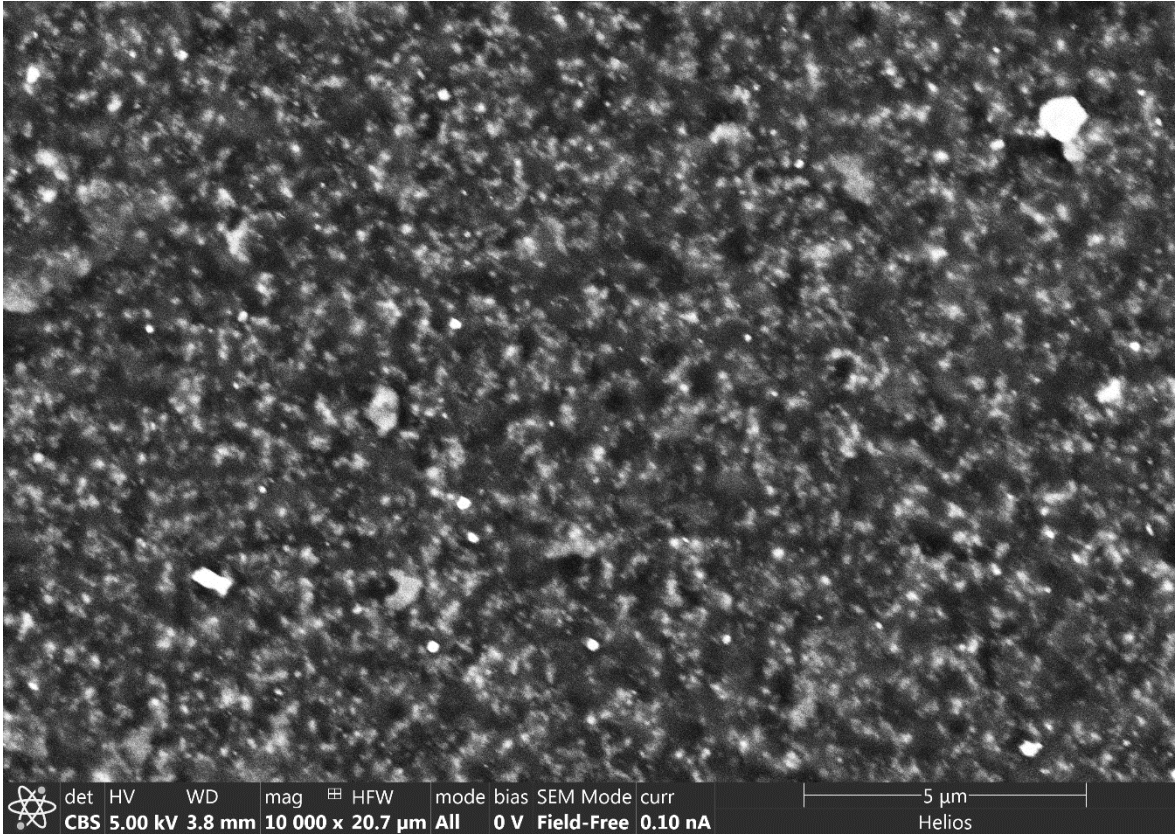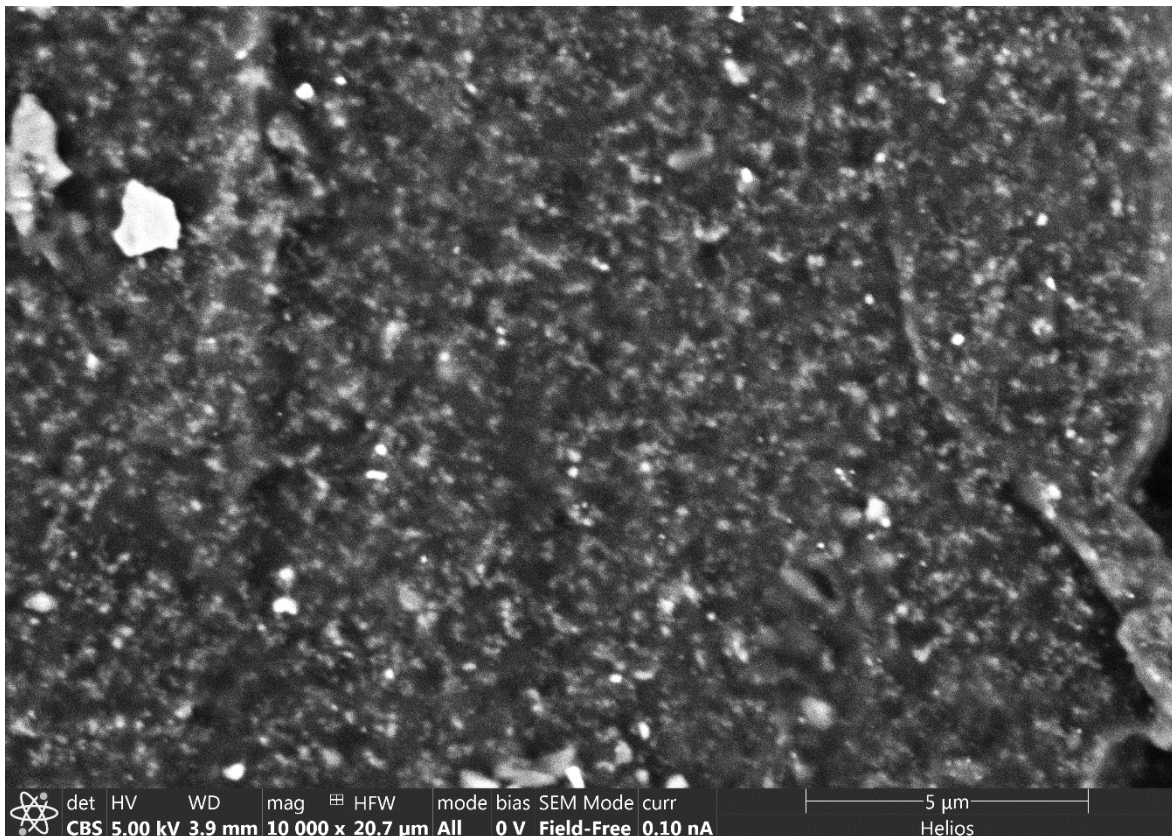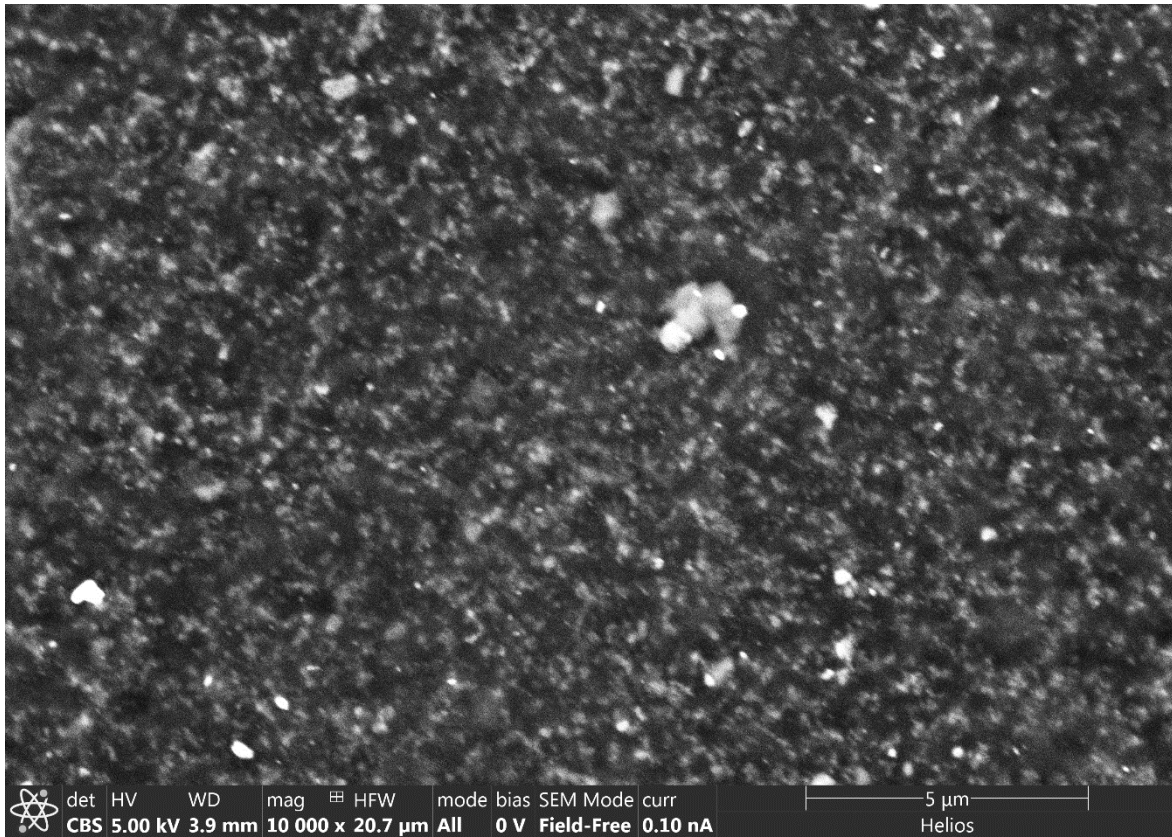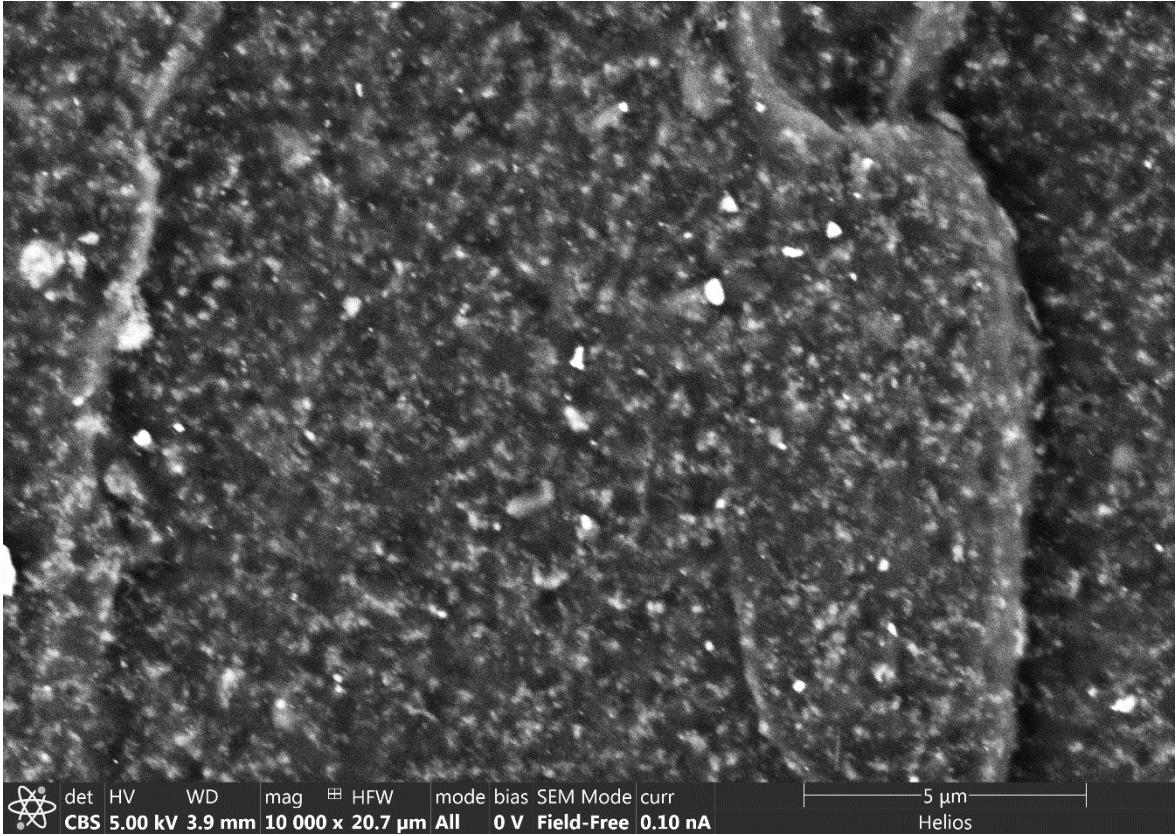
x.   Mount ID 4 Location C, Raw Image

det	HV	WD	mag ⊞	HFW	mode	bias	SEM Mode	curr	5 µm
CBS	5.00 kV	4.1 mm	10 000 x	20.7 µm	All	0 V	Field-Free	0.10 nA	Helios
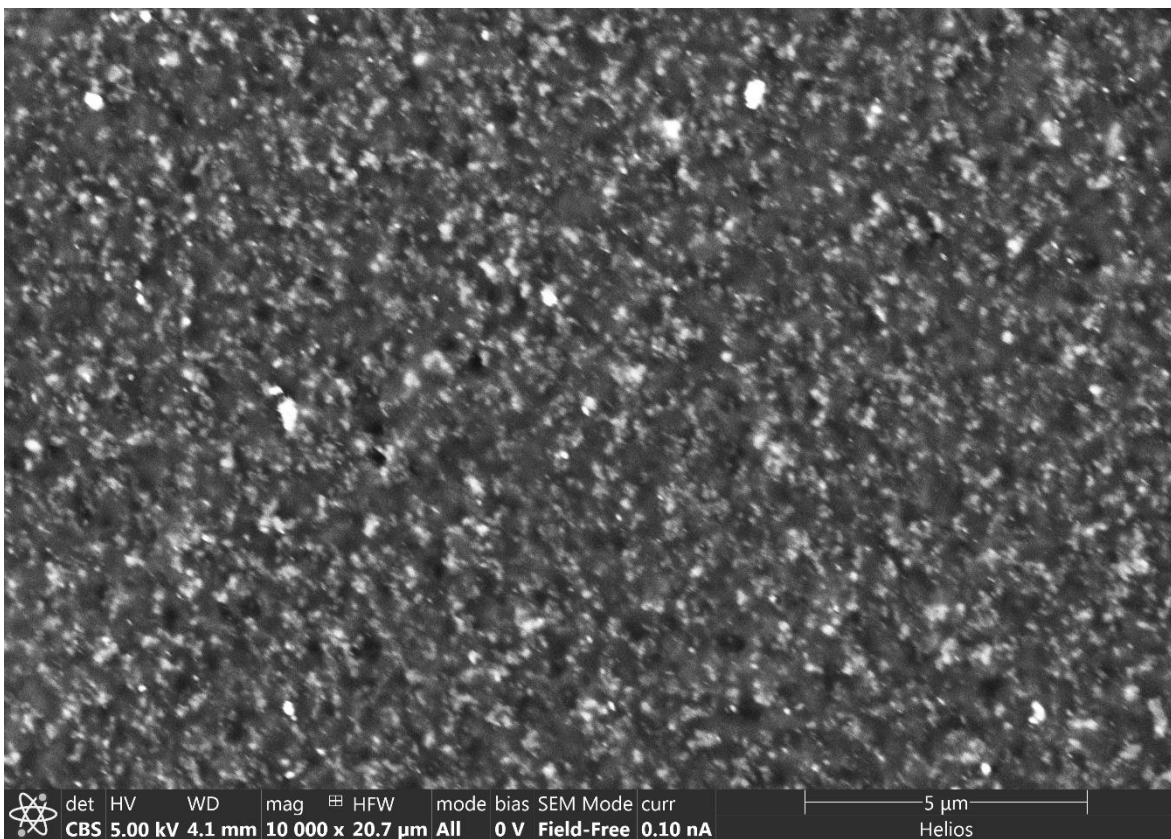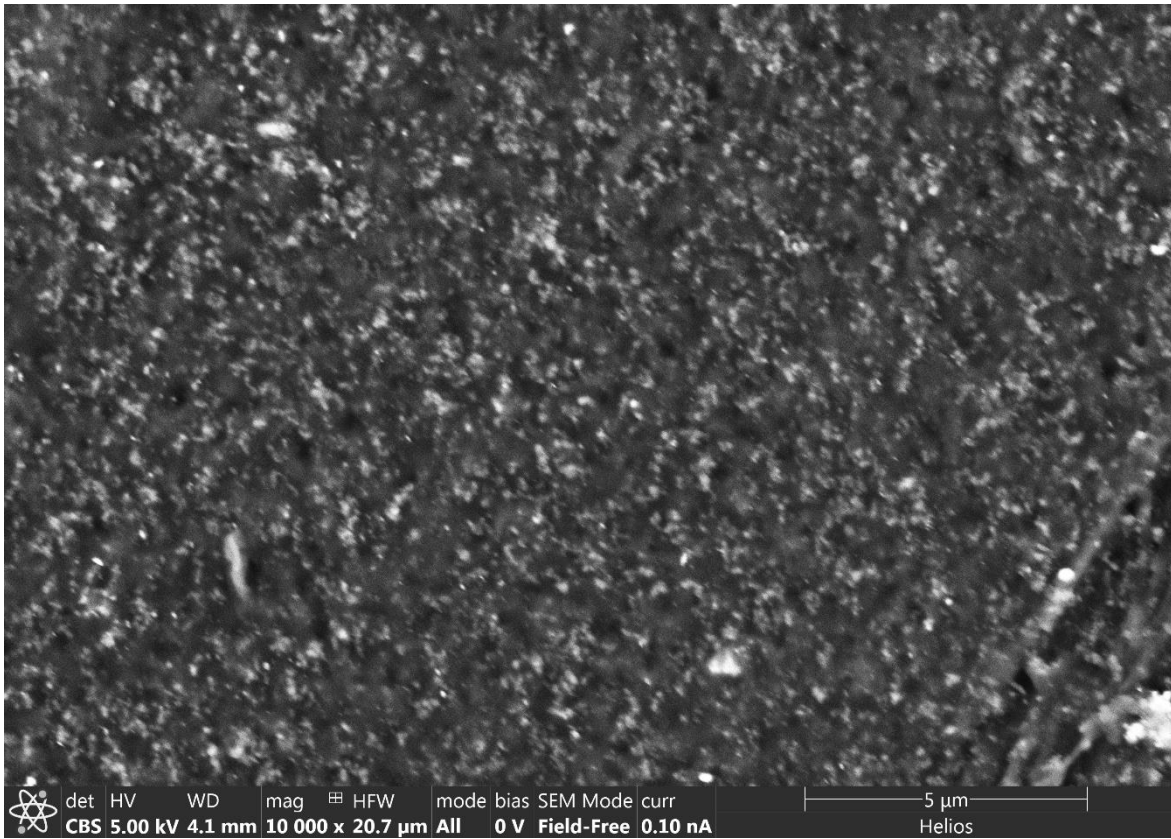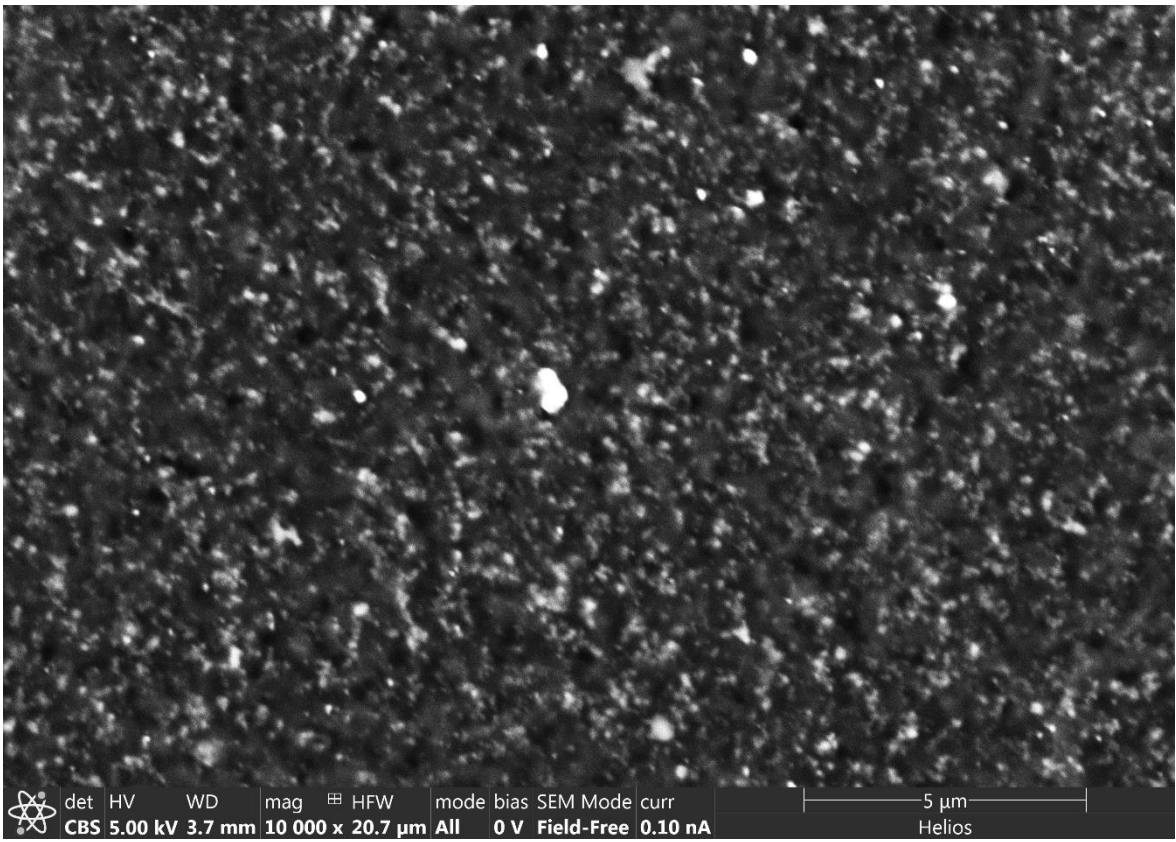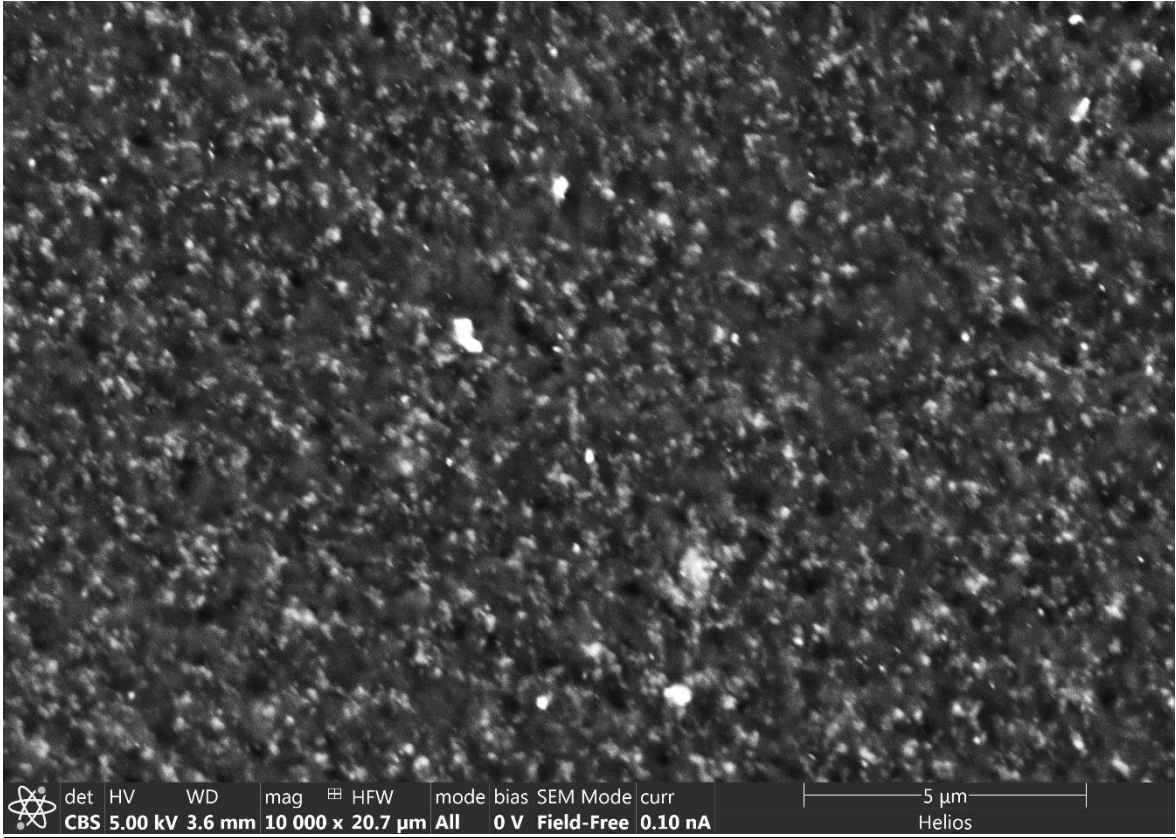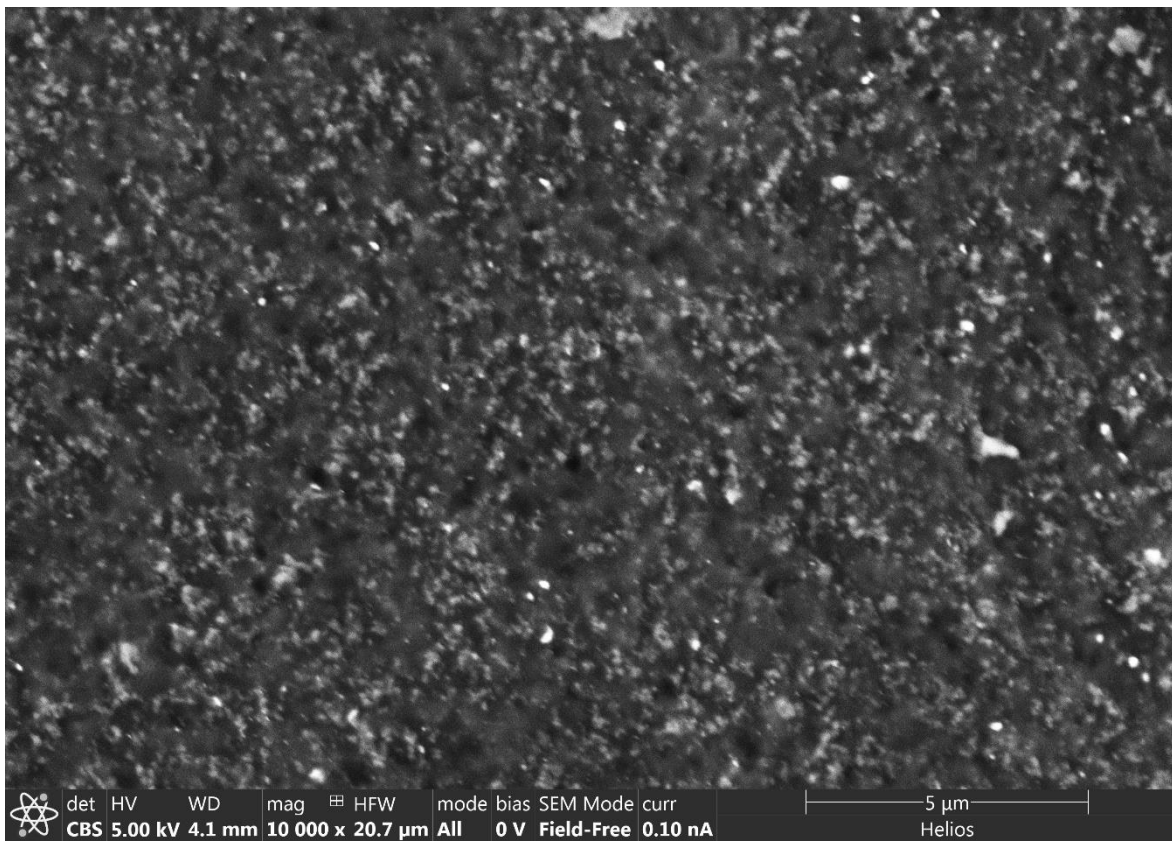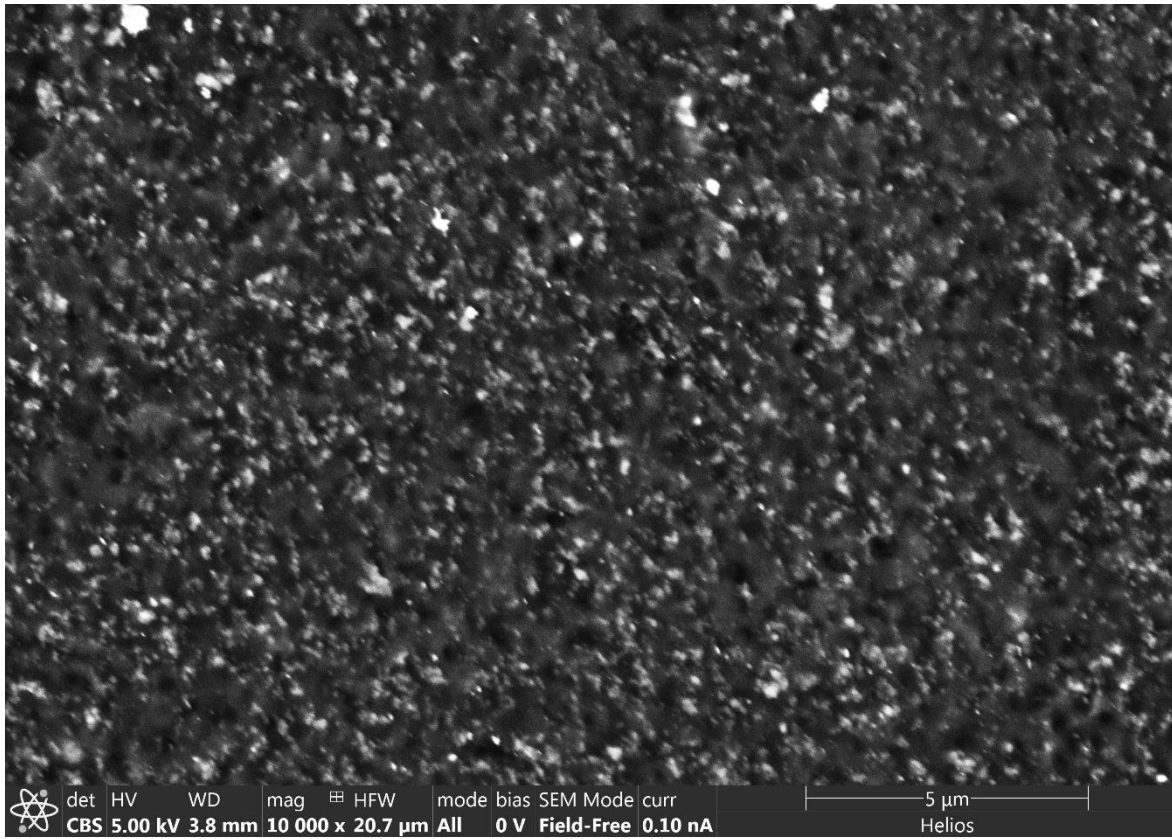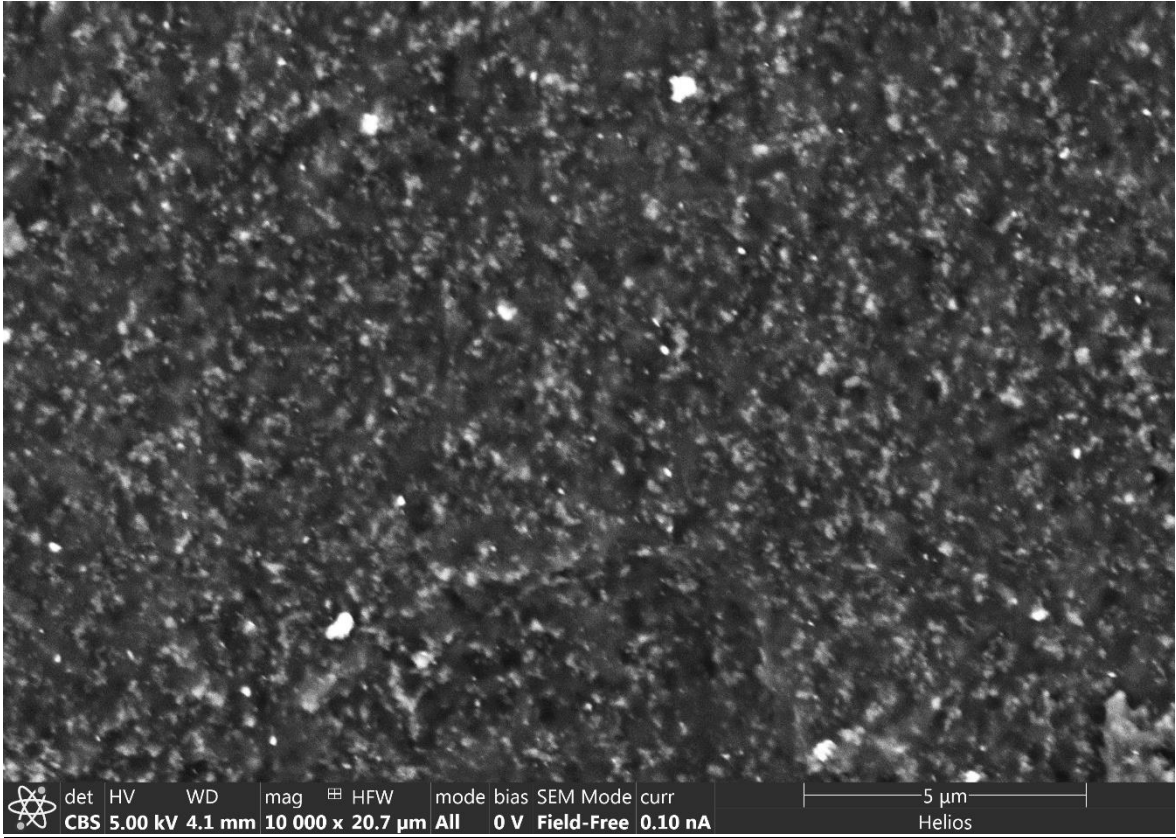
xi. Mount ID 5 Location C, Raw Image

li

det	HV	WD	mag ⊞	HFW	mode	bias	SEM Mode	curr	5 μm
CBS	5.00 kV	4.3 mm	10 000 x	20.7 μm	All	0 V	Field-Free	0.10 nA	Helios

det	HV	WD	mag □	HFW	mode	bias	SEM Mode	curr	5 µm
CBS	5.00 kV	4.3 mm	10 000 x	20.7 µm	All	0 V	Field-Free	0.10 nA	Helios

det	HV	WD	mag □	HFW	mode	bias	SEM Mode	curr	5 µm
CBS	5.00 kV	4.3 mm	10 000 x	20.7 µm	All	0 V	Field-Free	0.10 nA	Helios

det	HV	WD	mag ⊞	HFW	mode	bias	SEM Mode	curr	5 µm
CBS	5.00 kV	4.1 mm	10 000 x	20.7 µm	All	0 V	Field-Free	0.10 nA	Helios
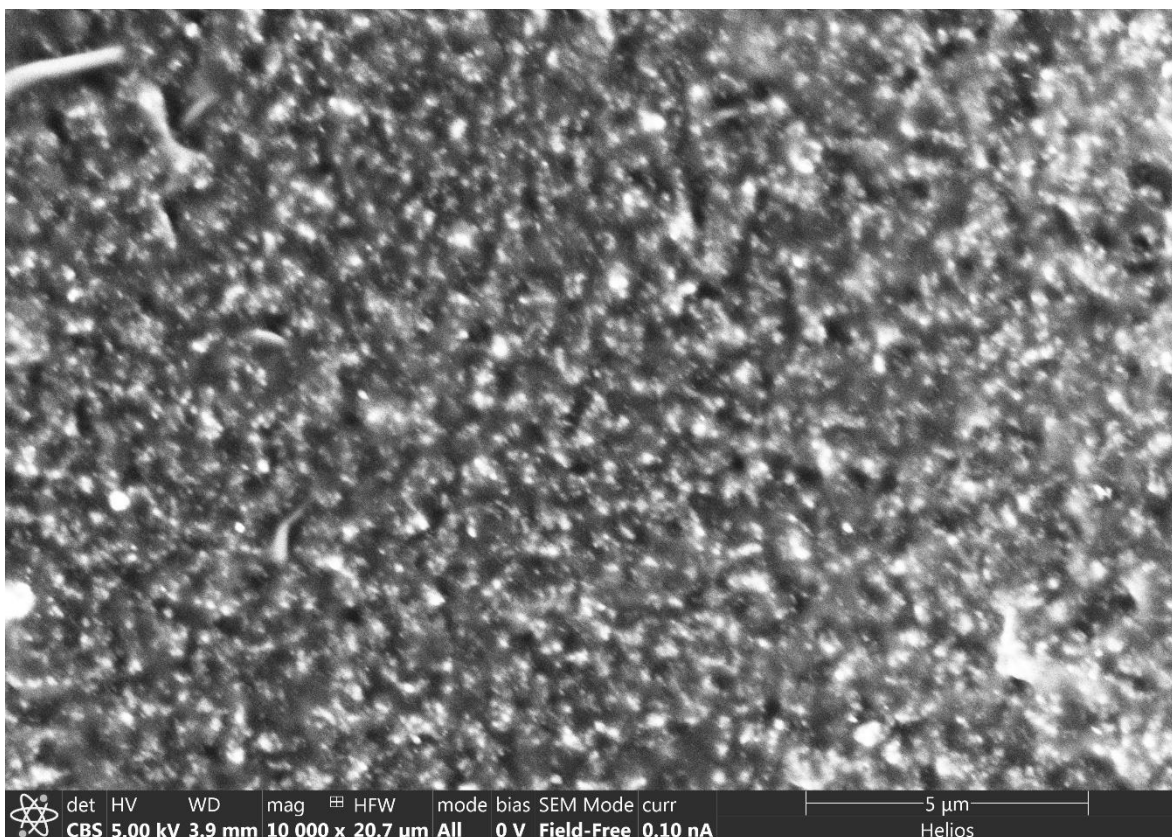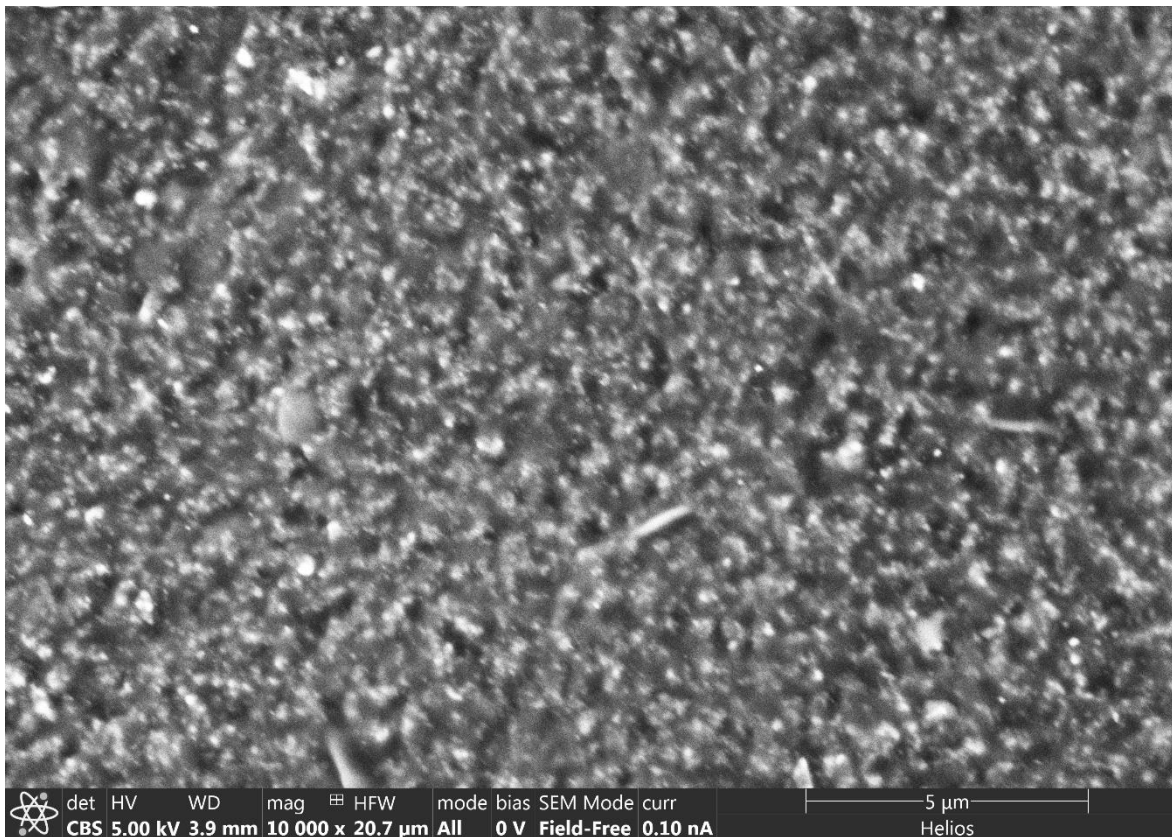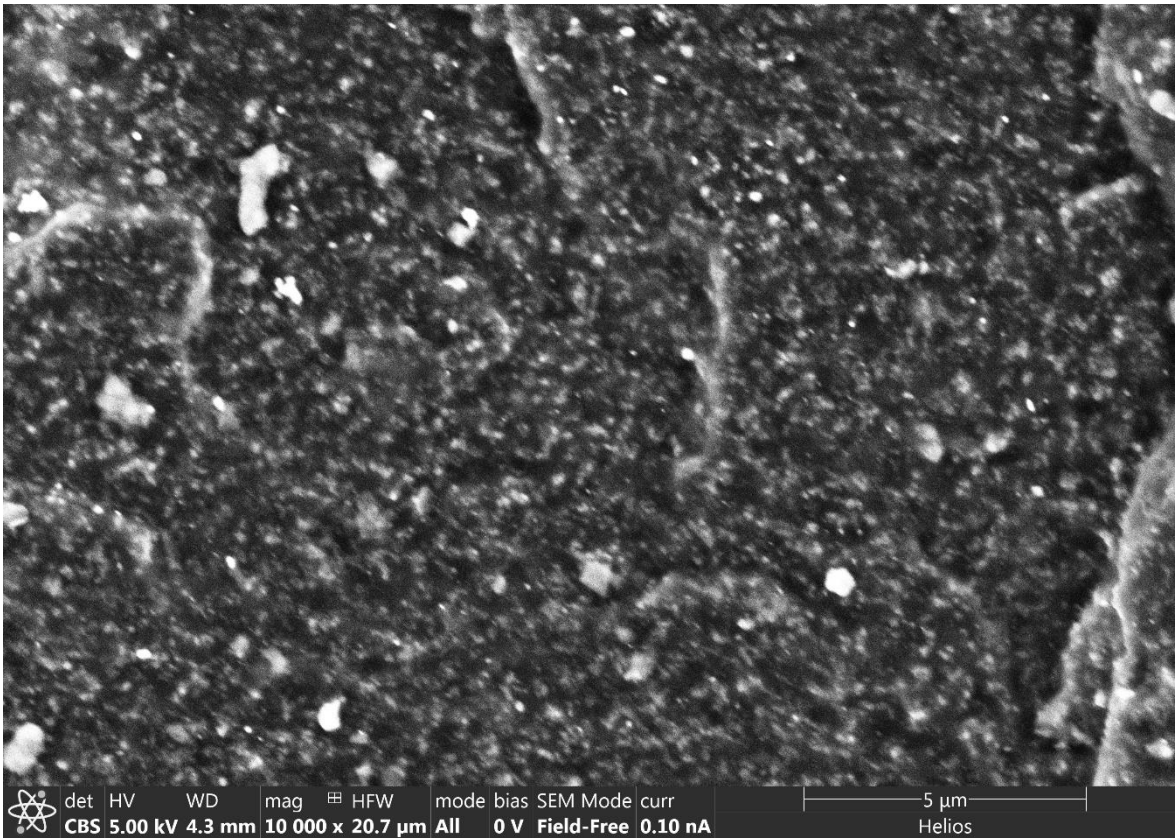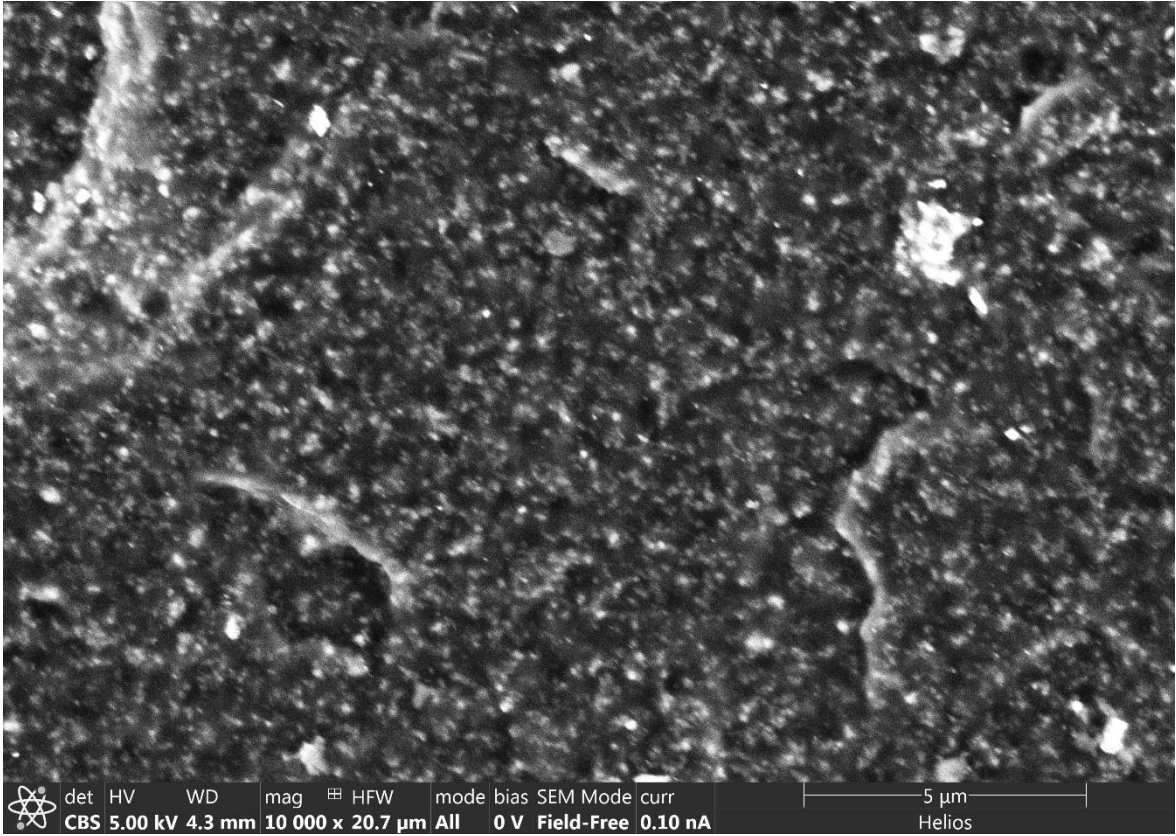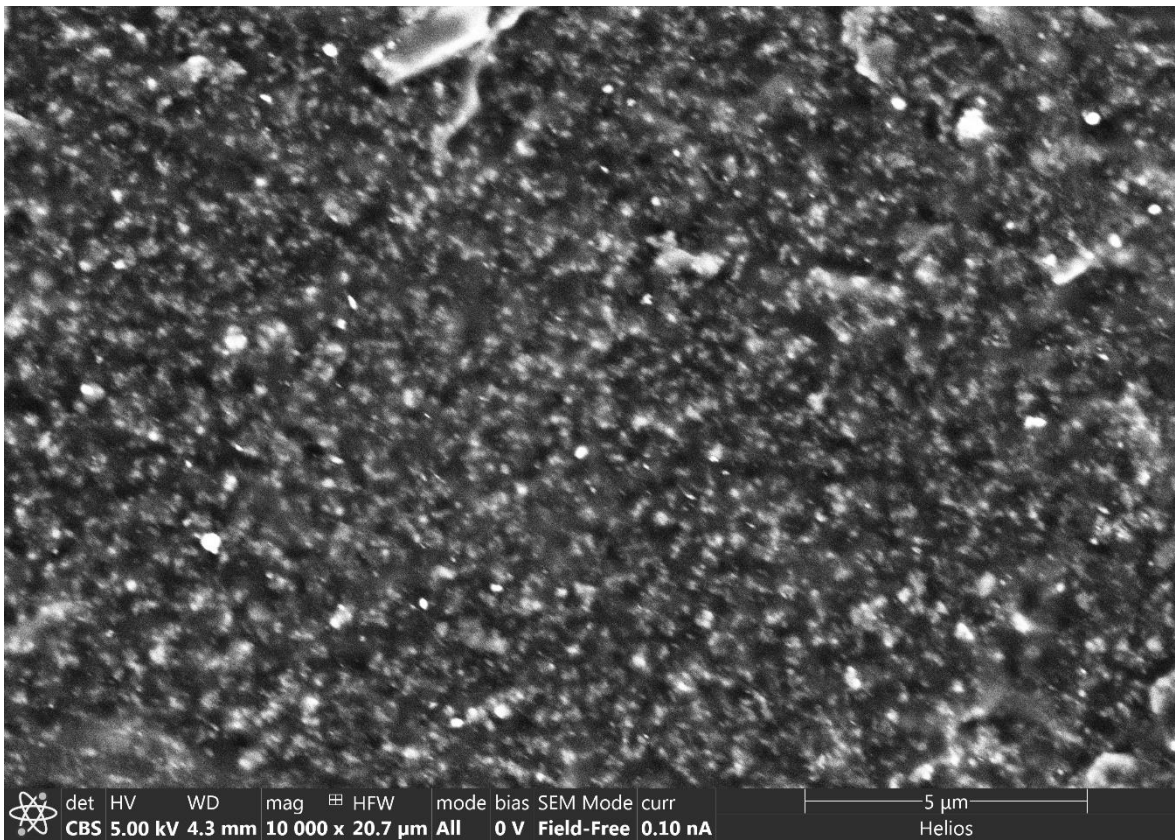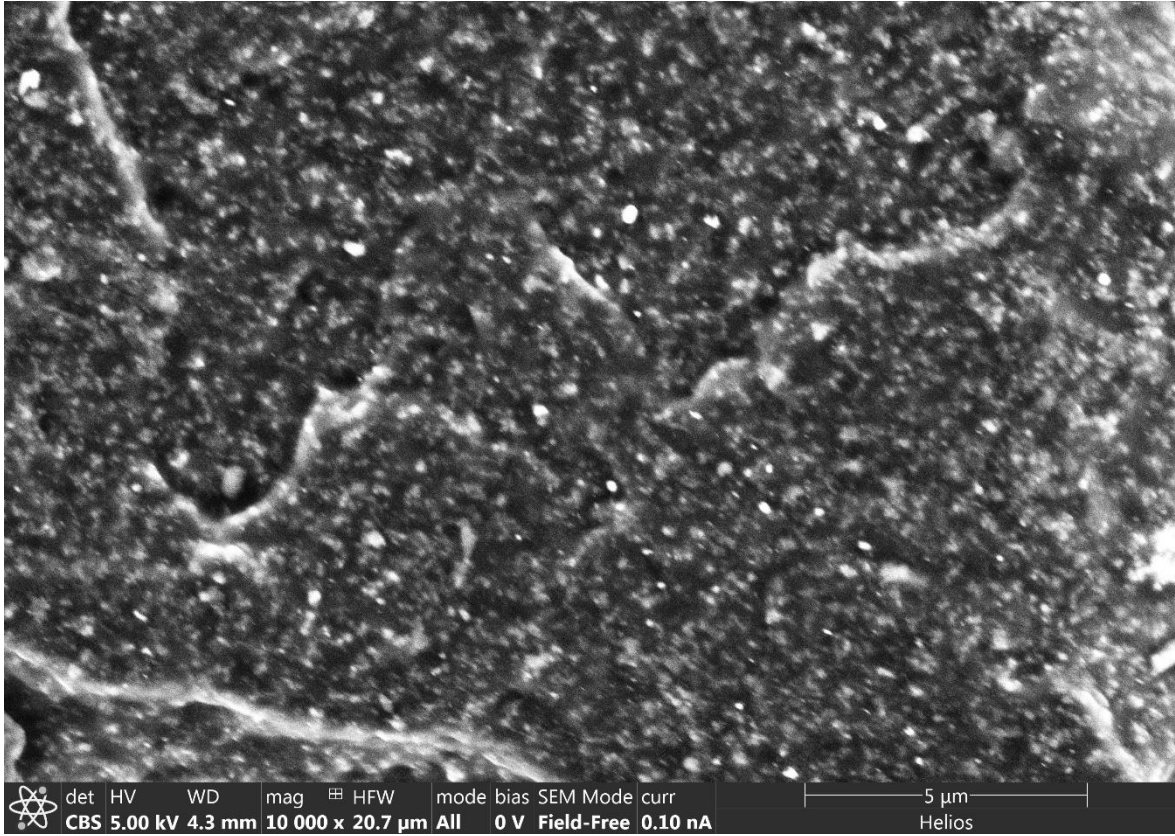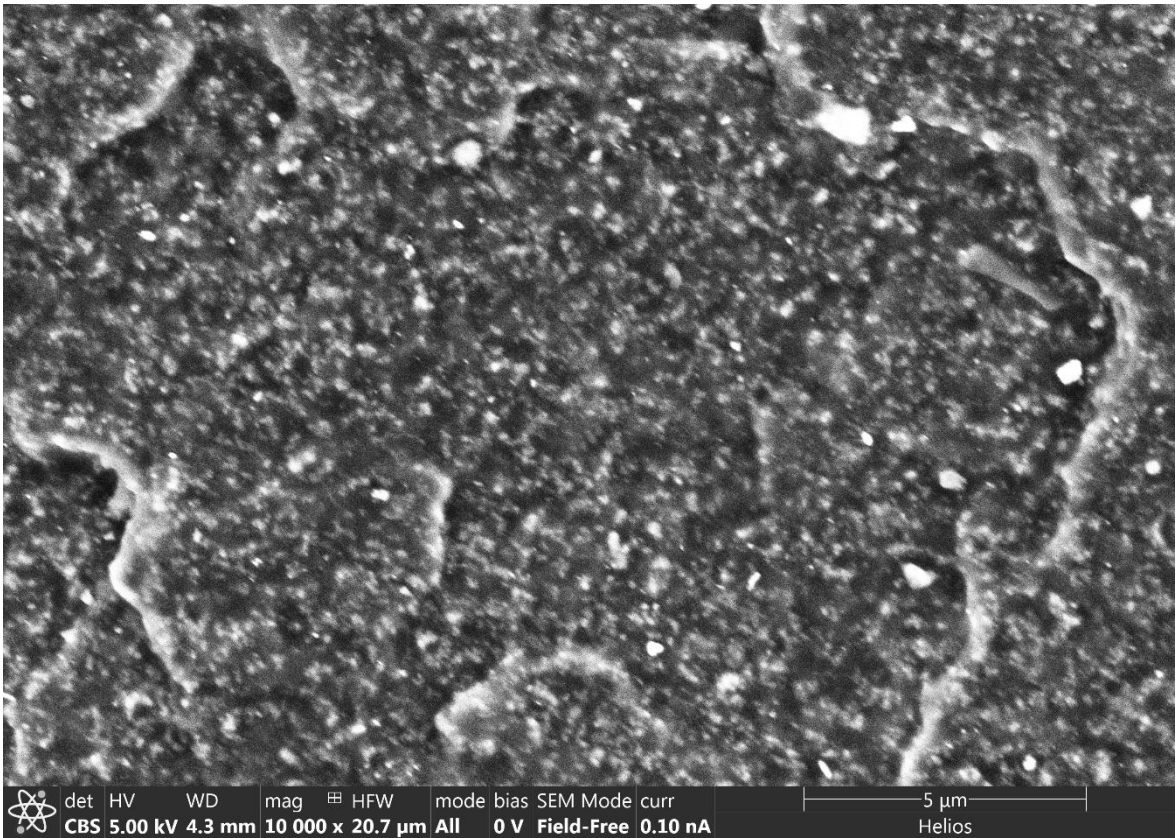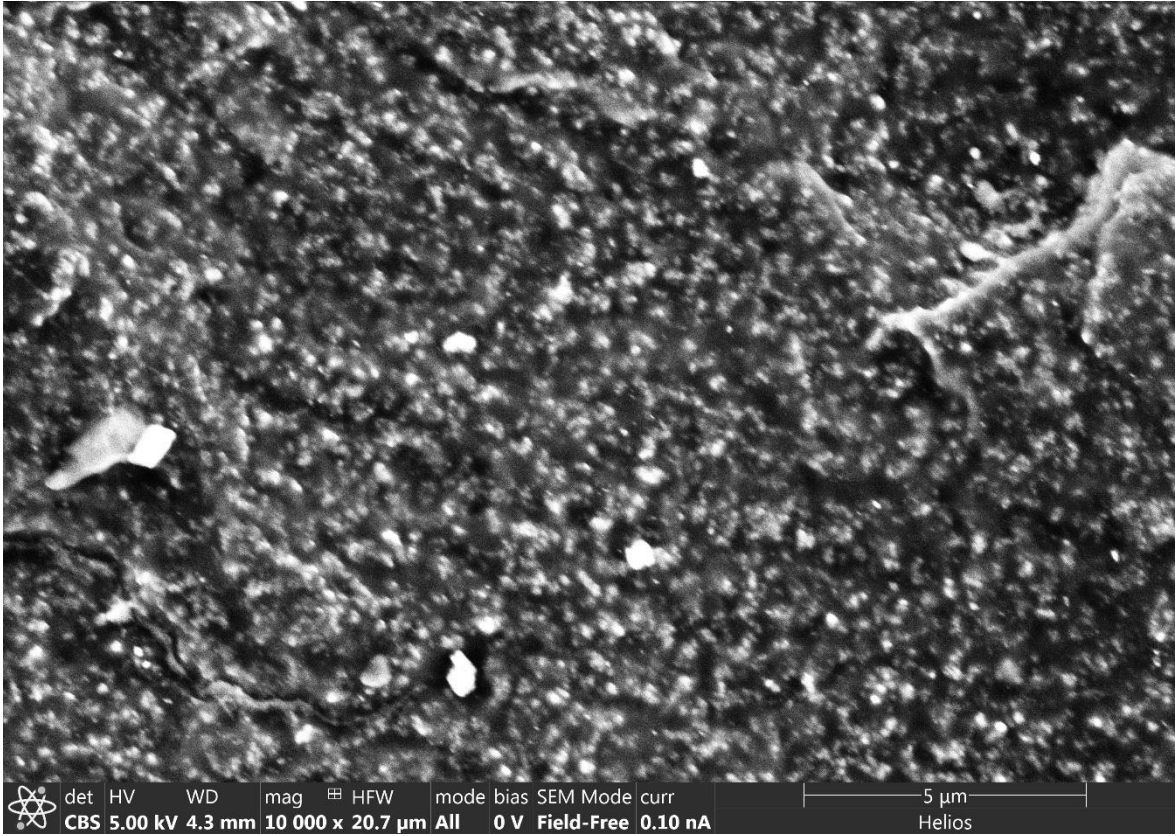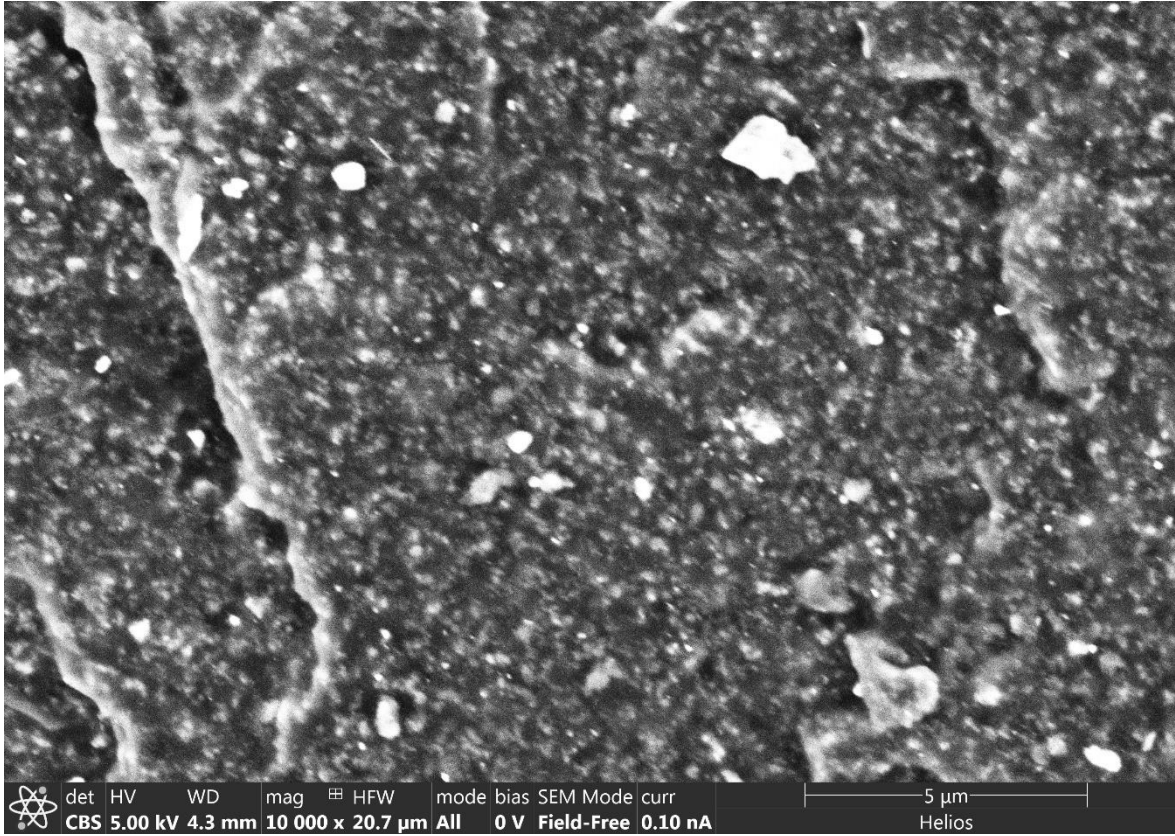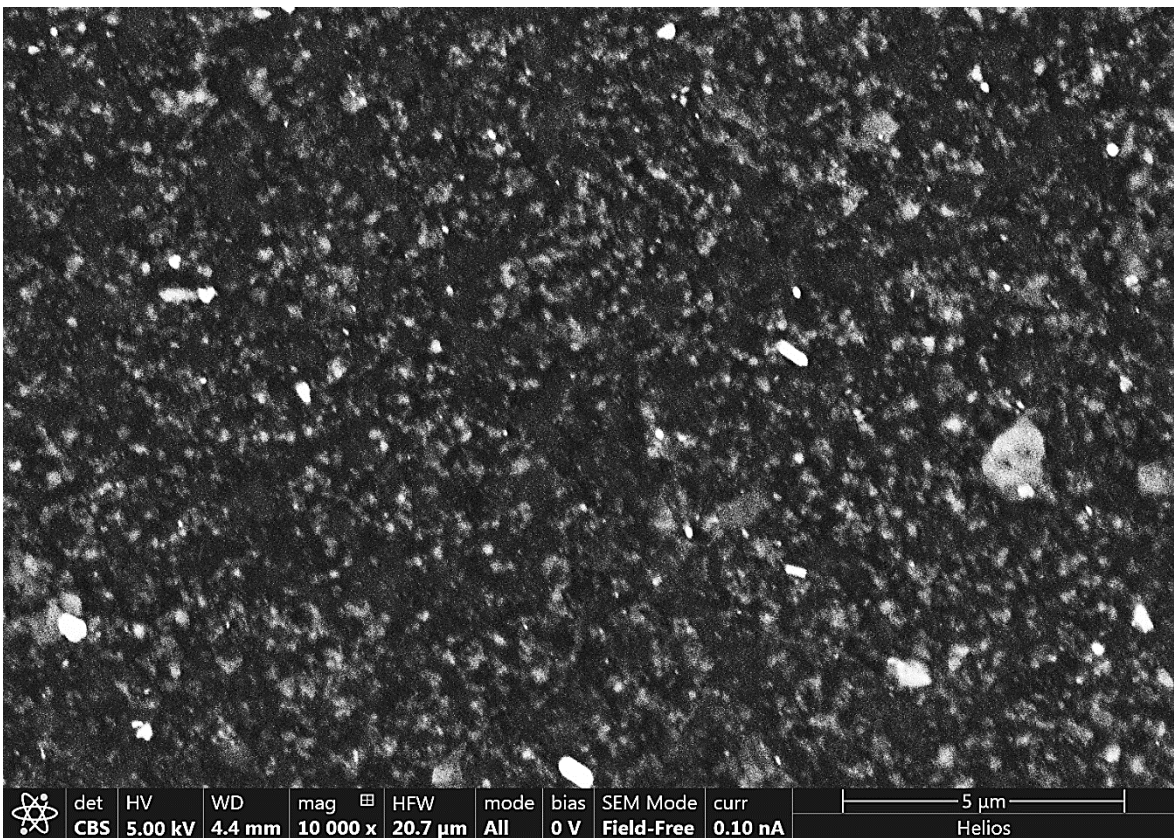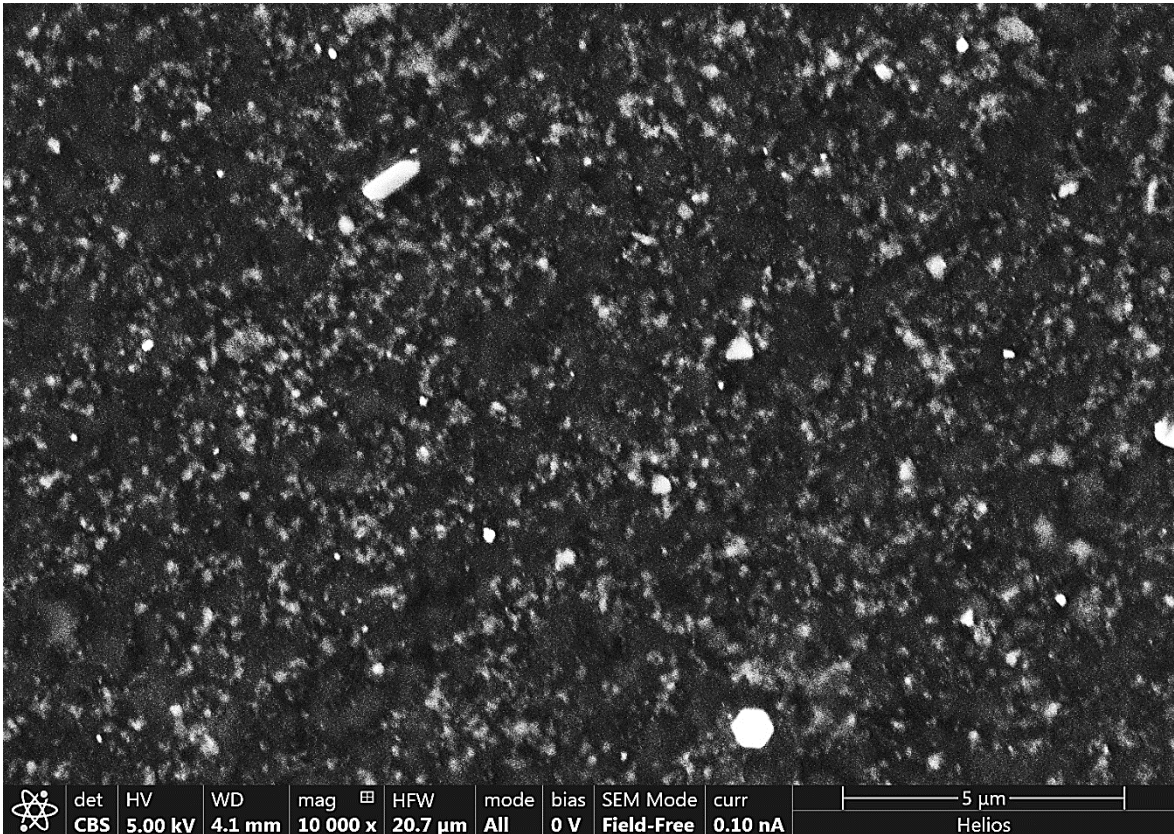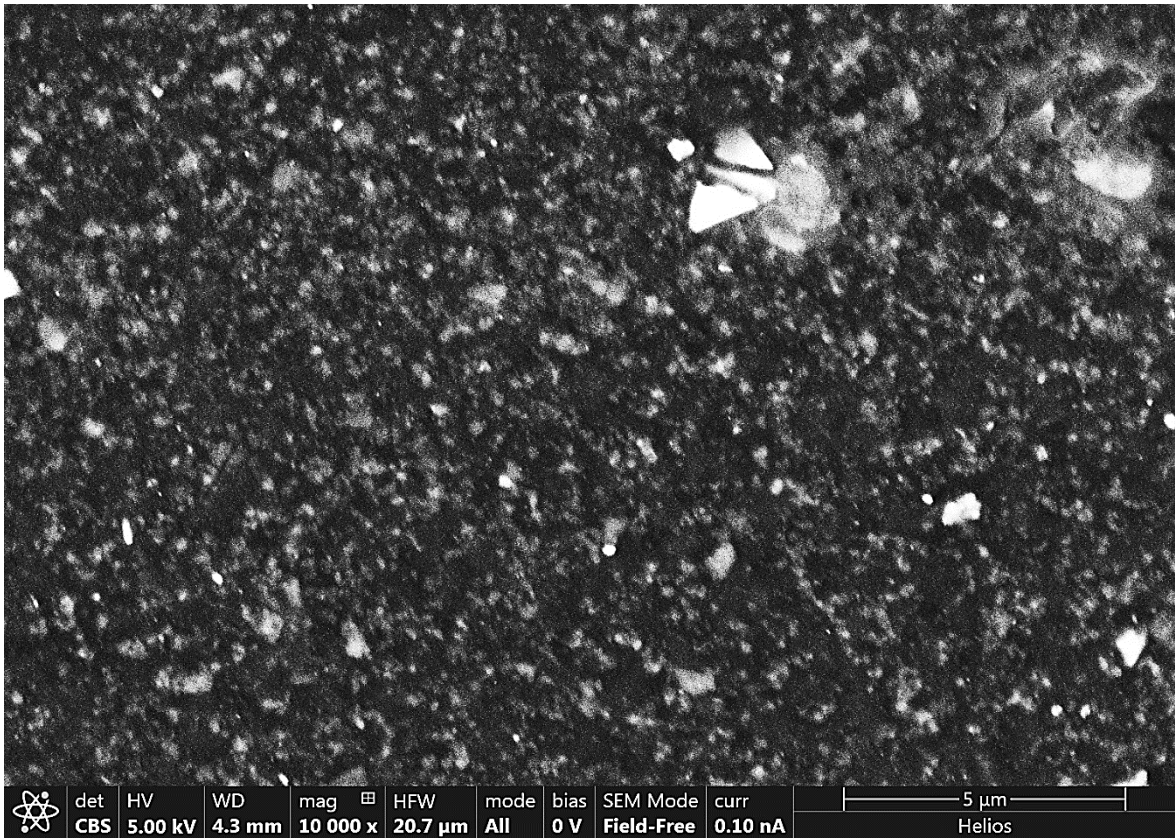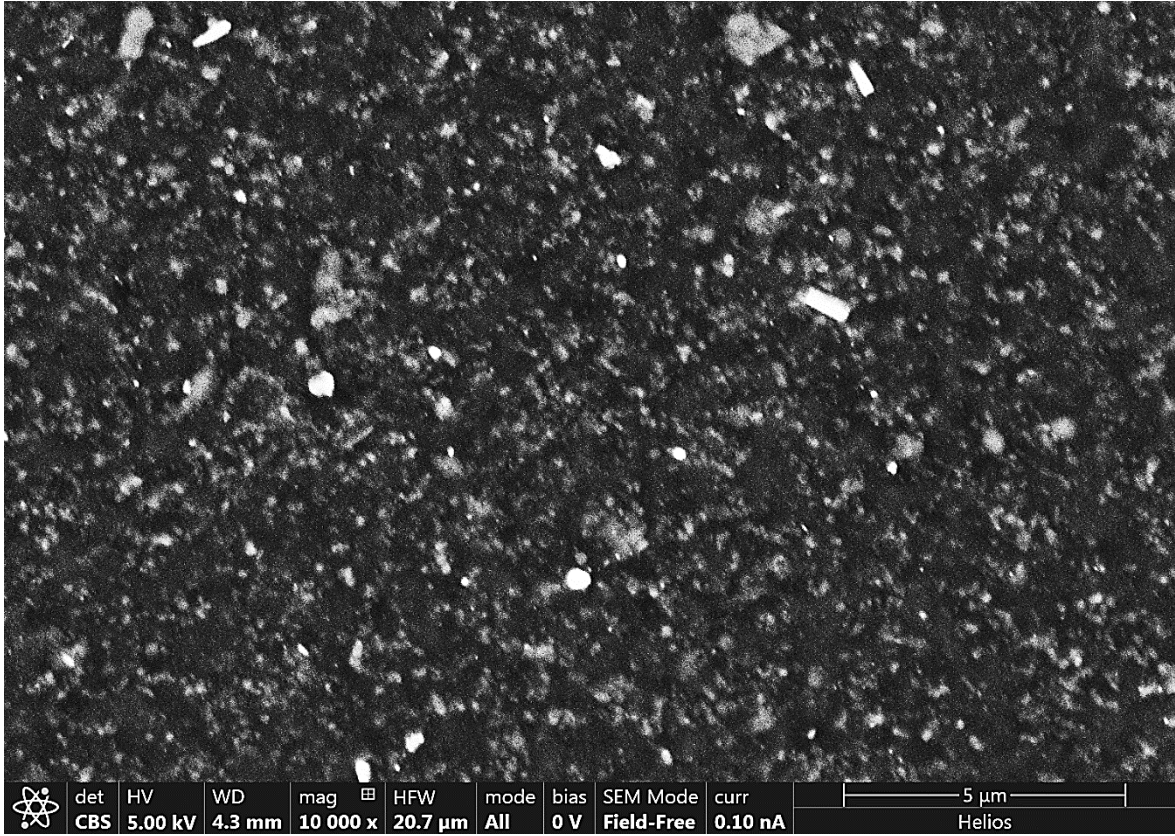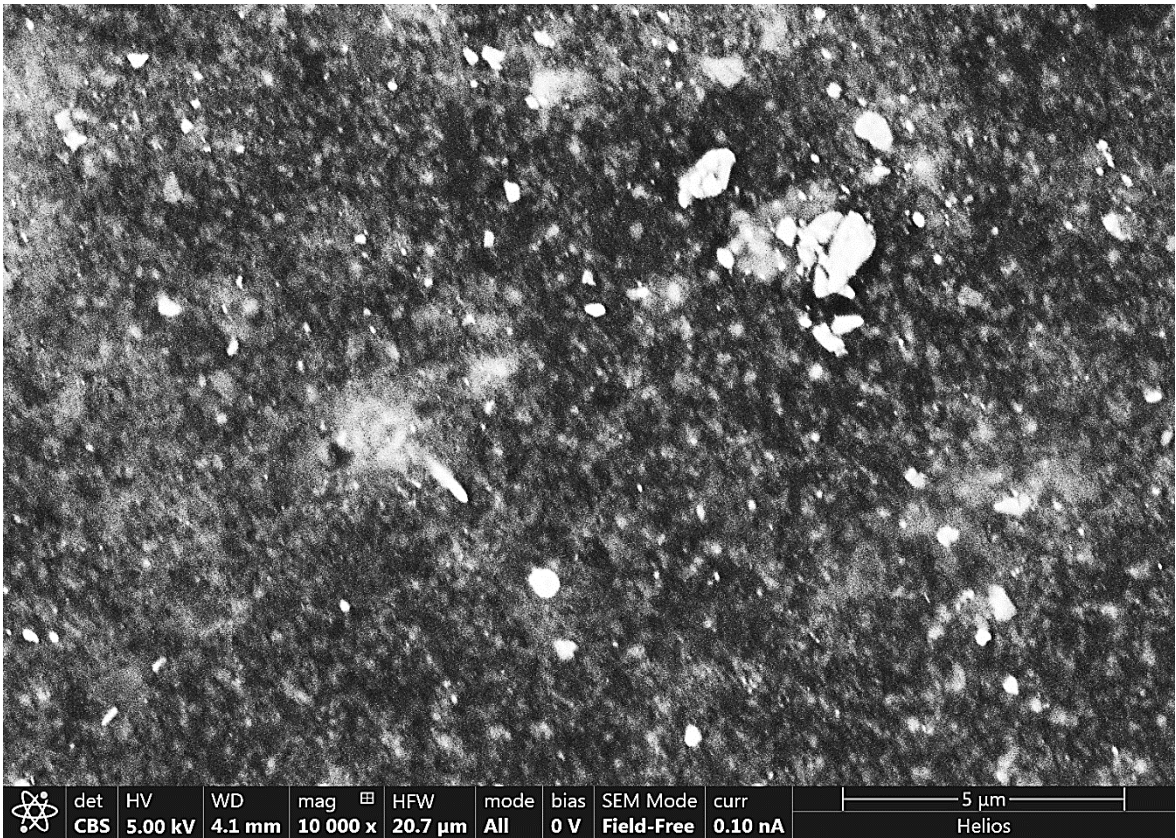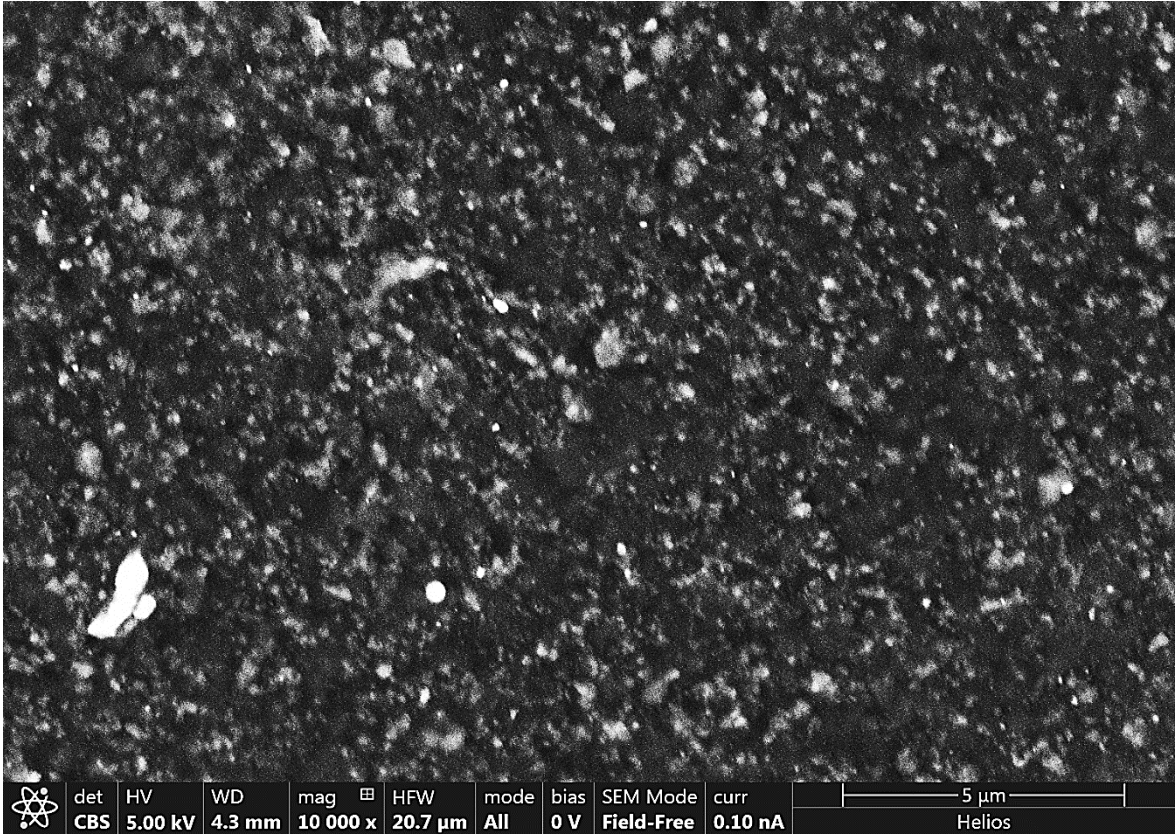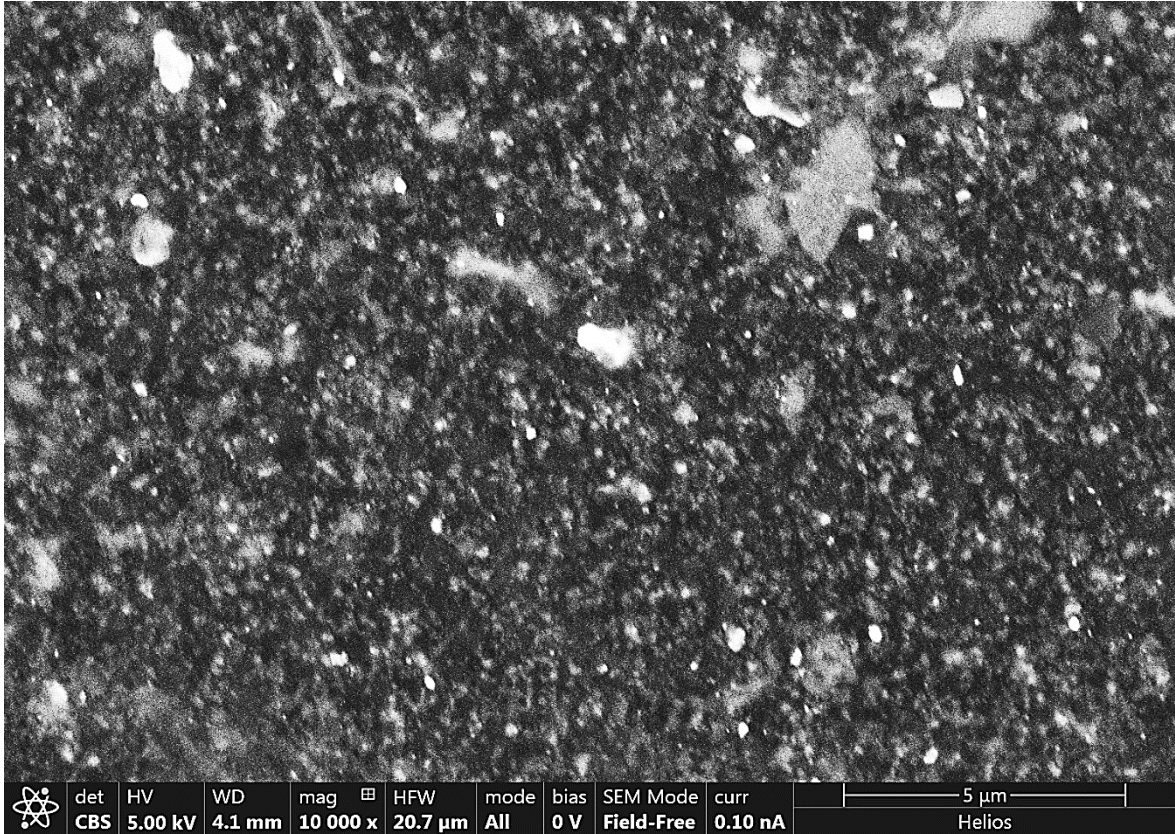
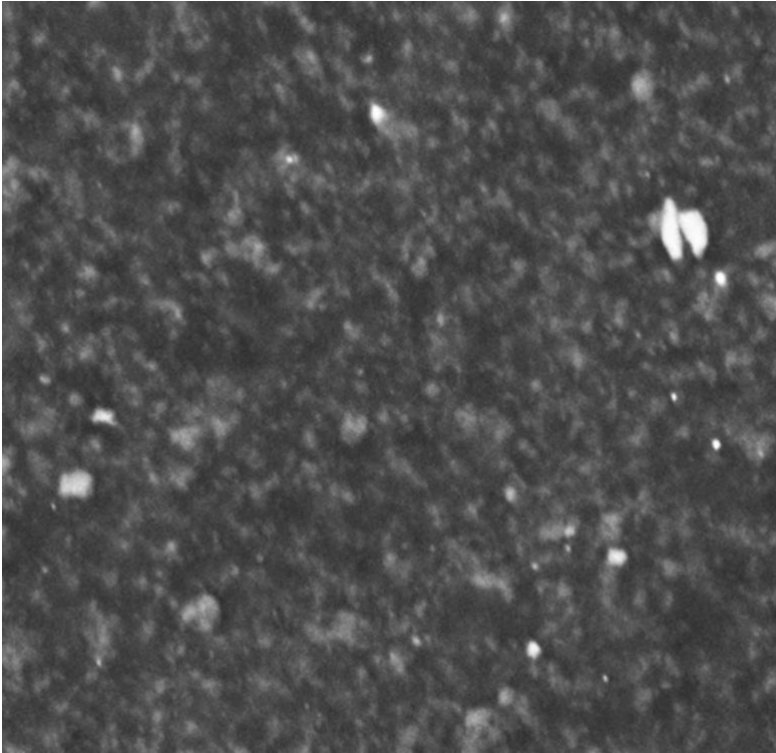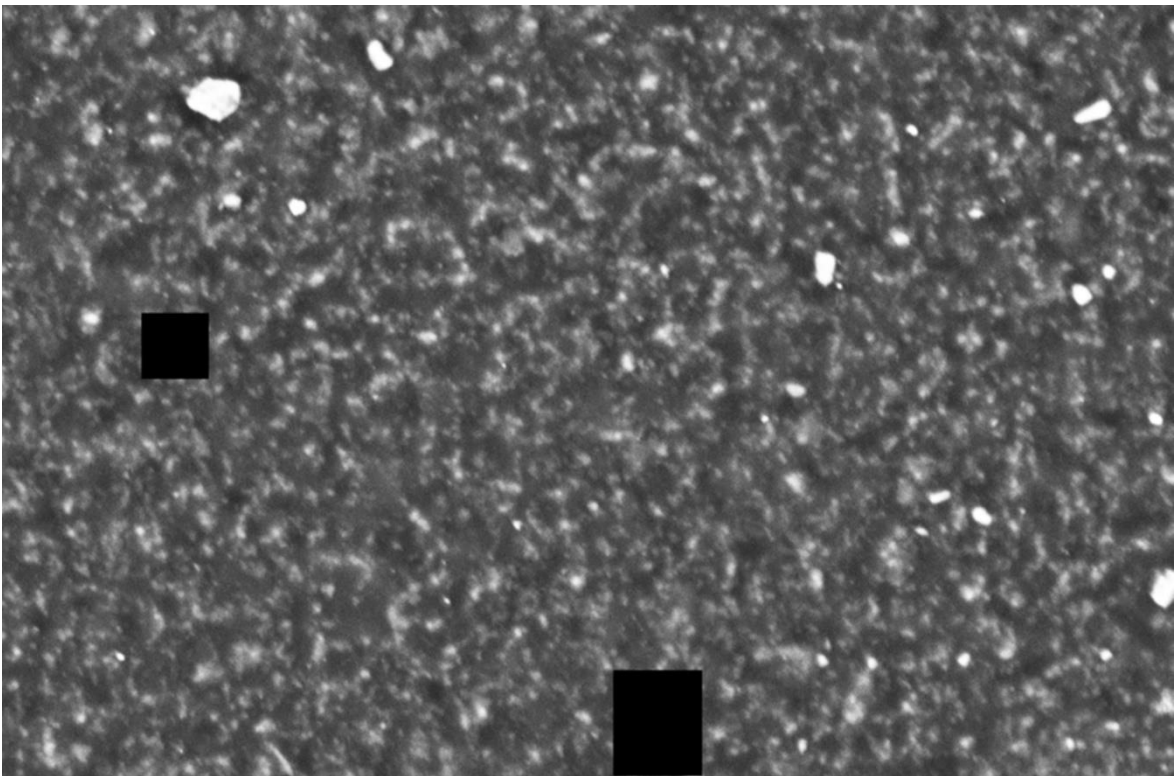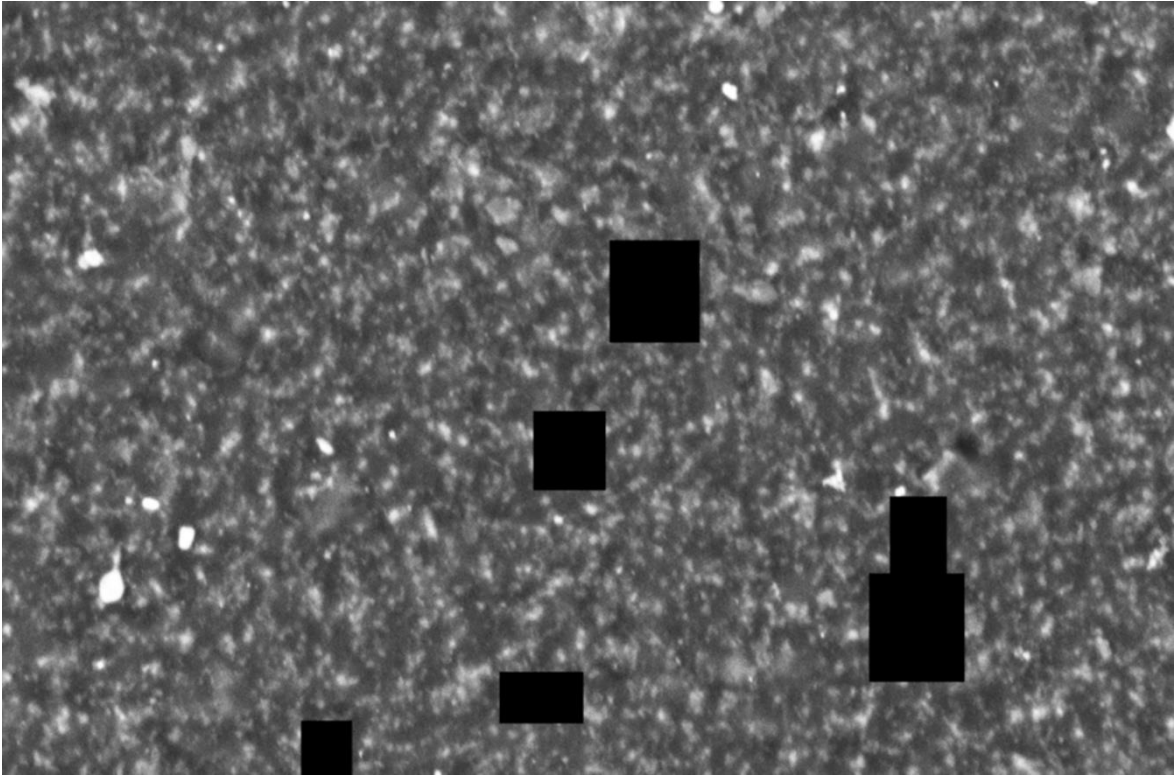xiii.   <u>Processed Image, New Sheet Sample</u>
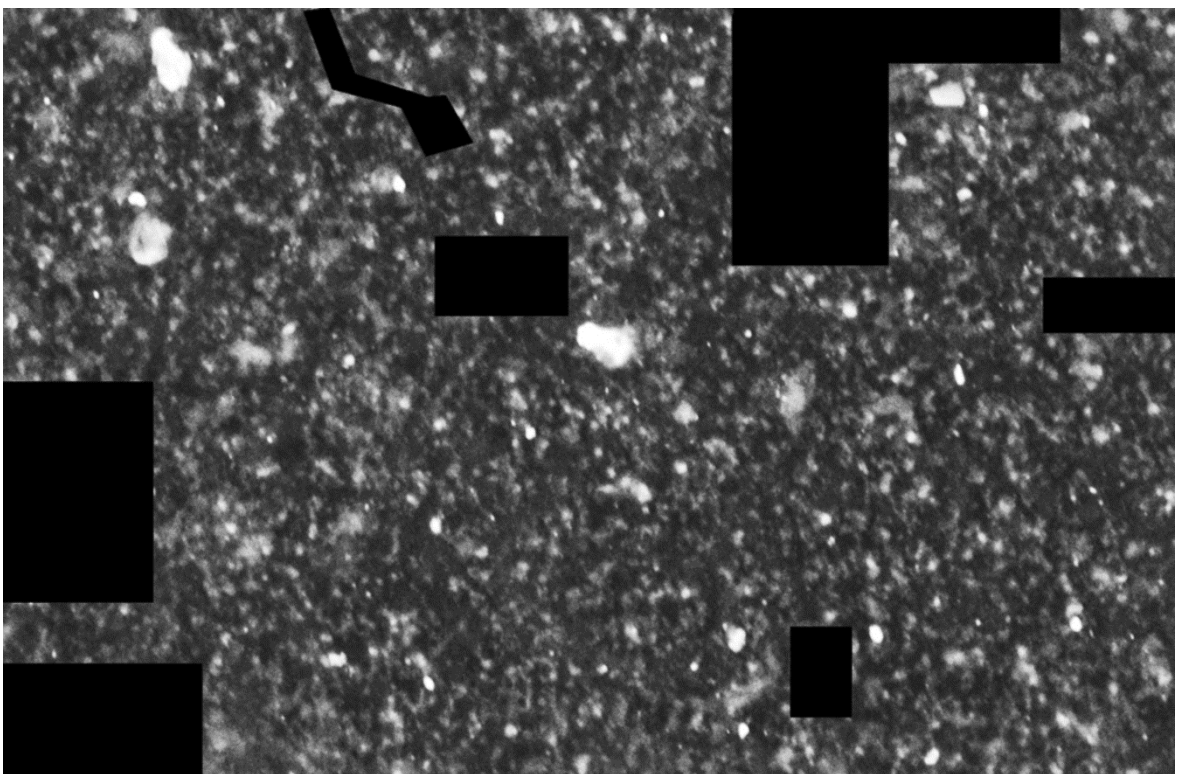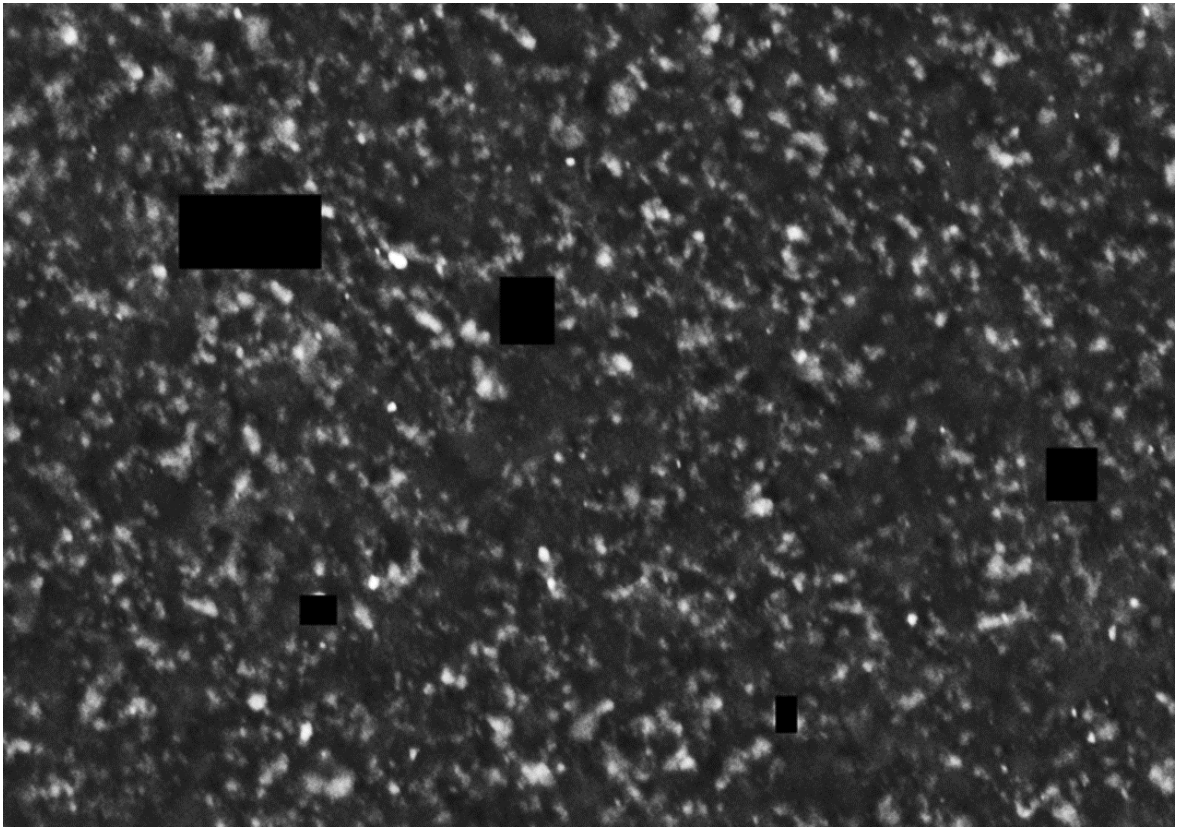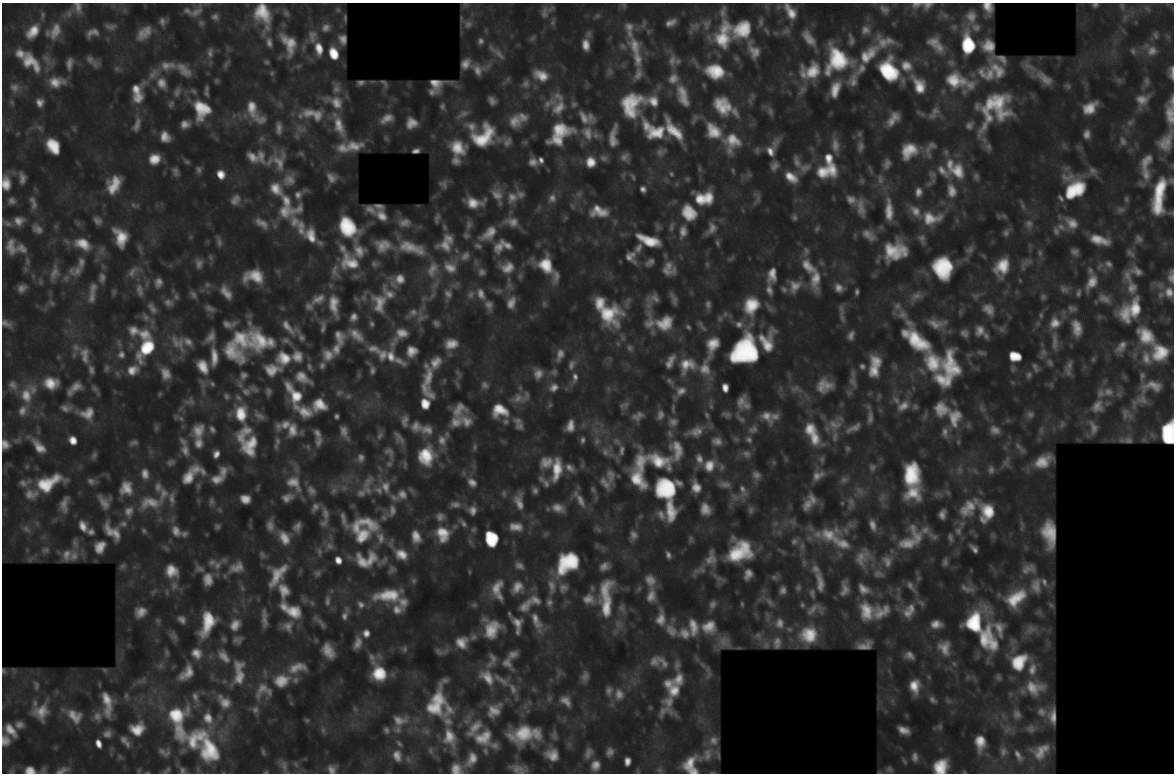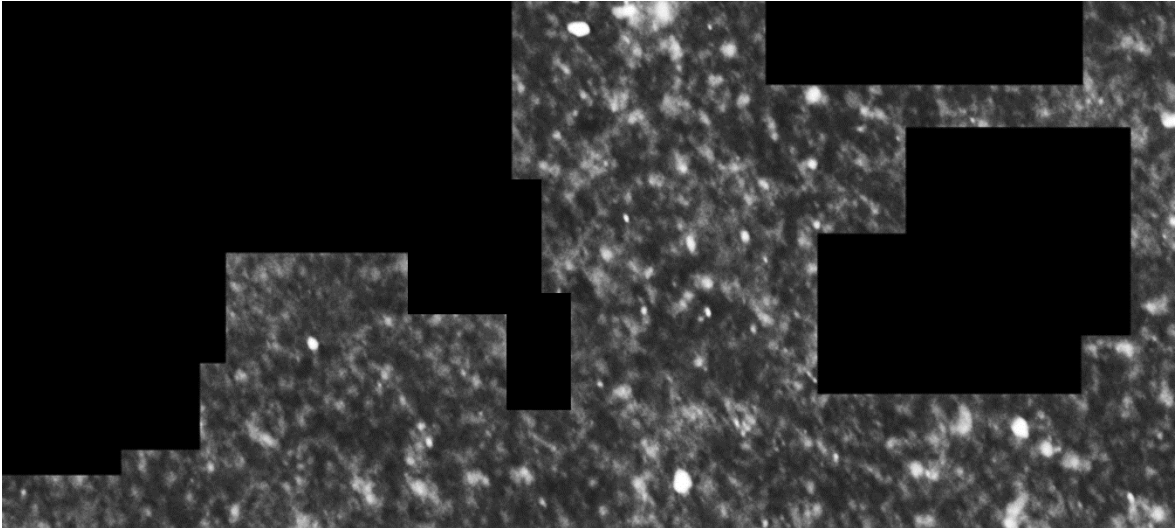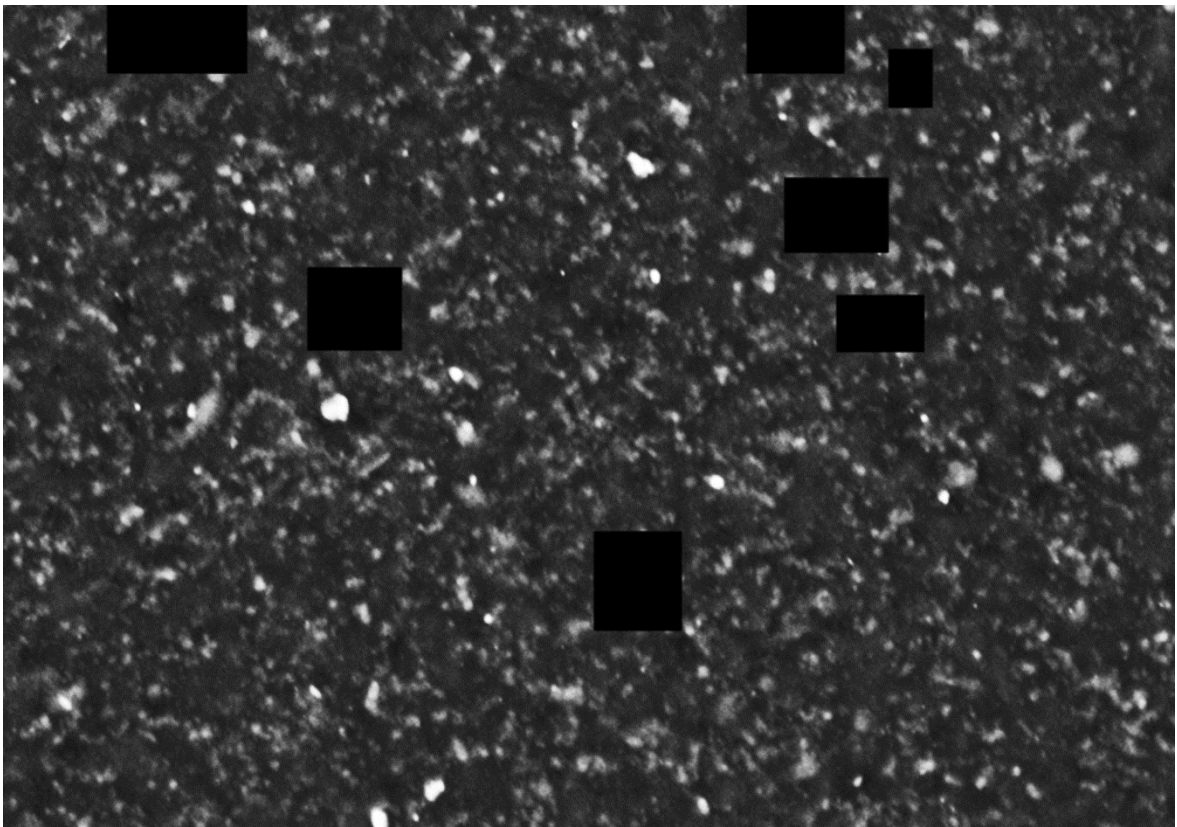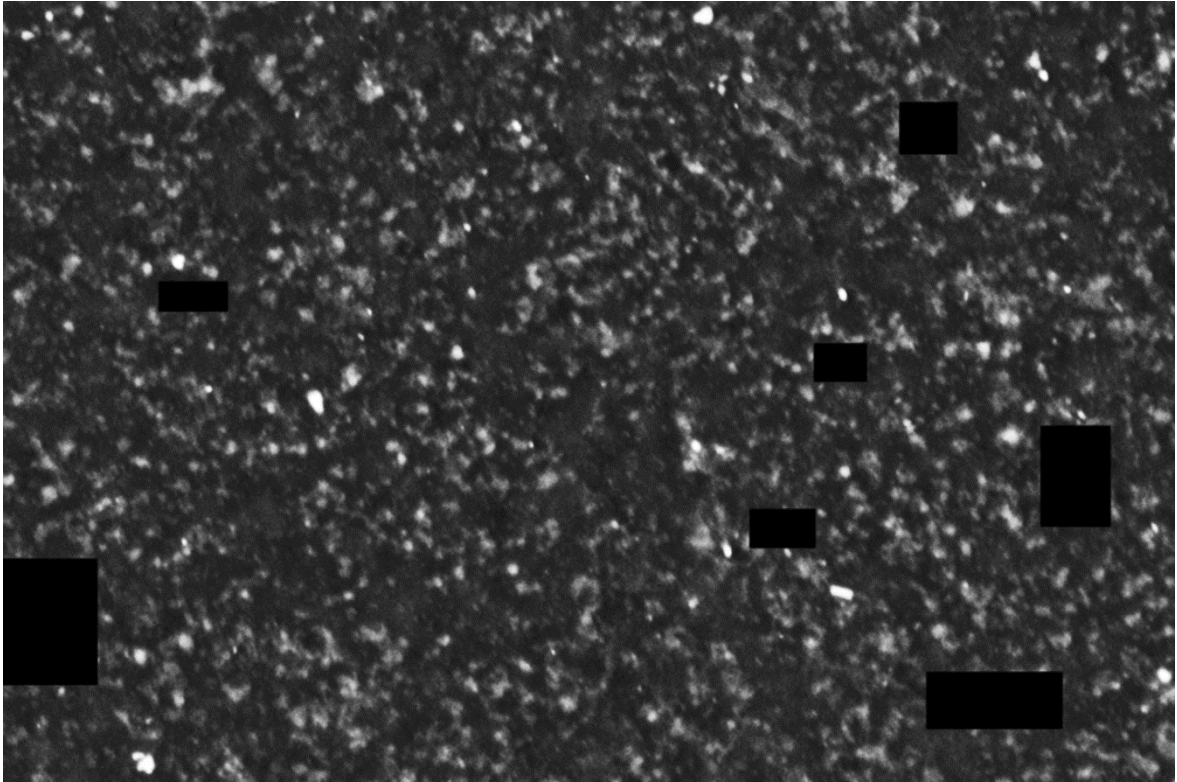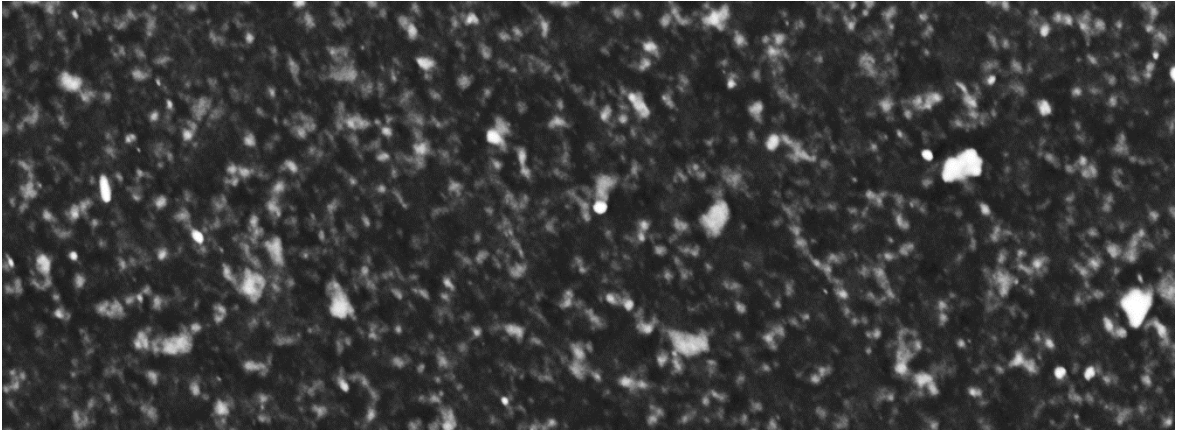
xiv.   137 Days Aerobic Aged Sample, Raw Image

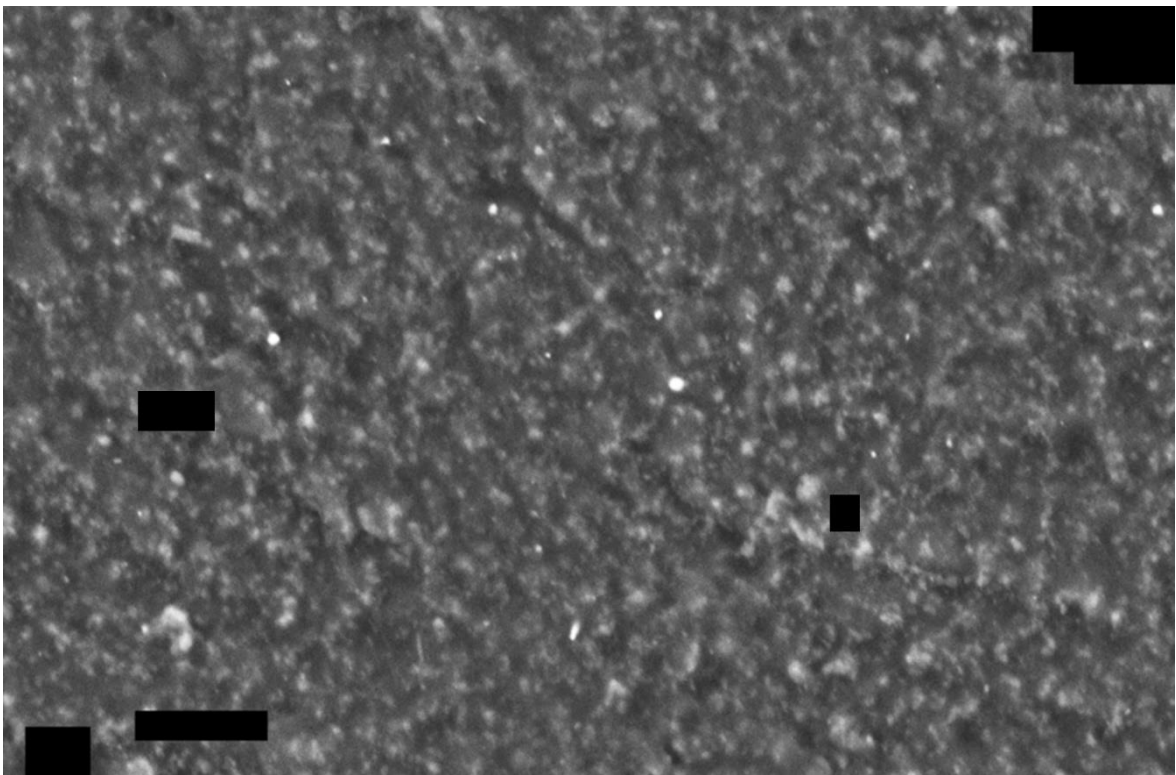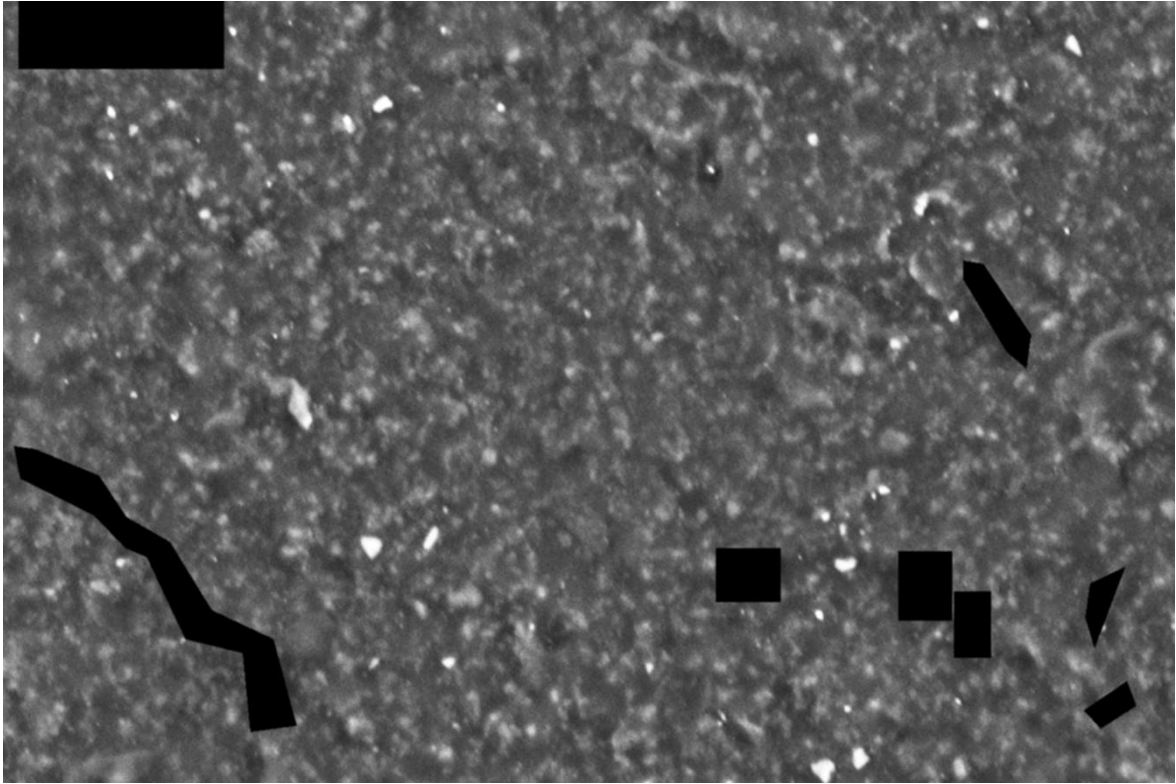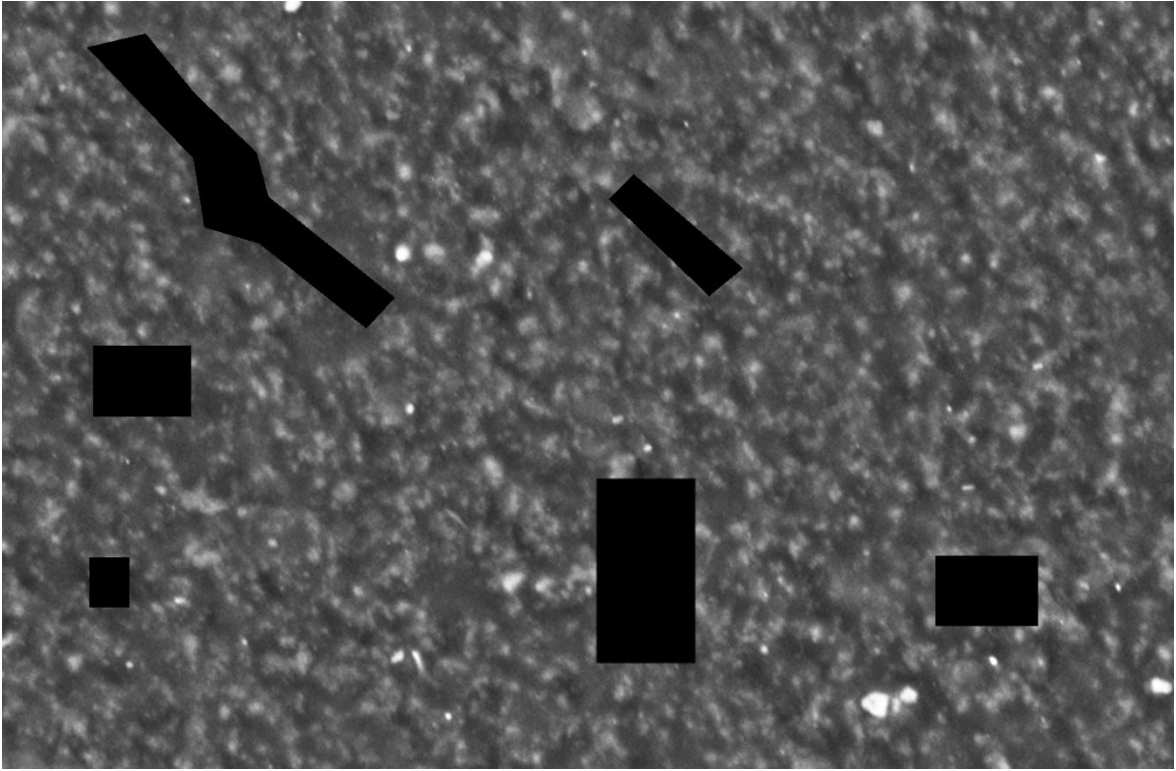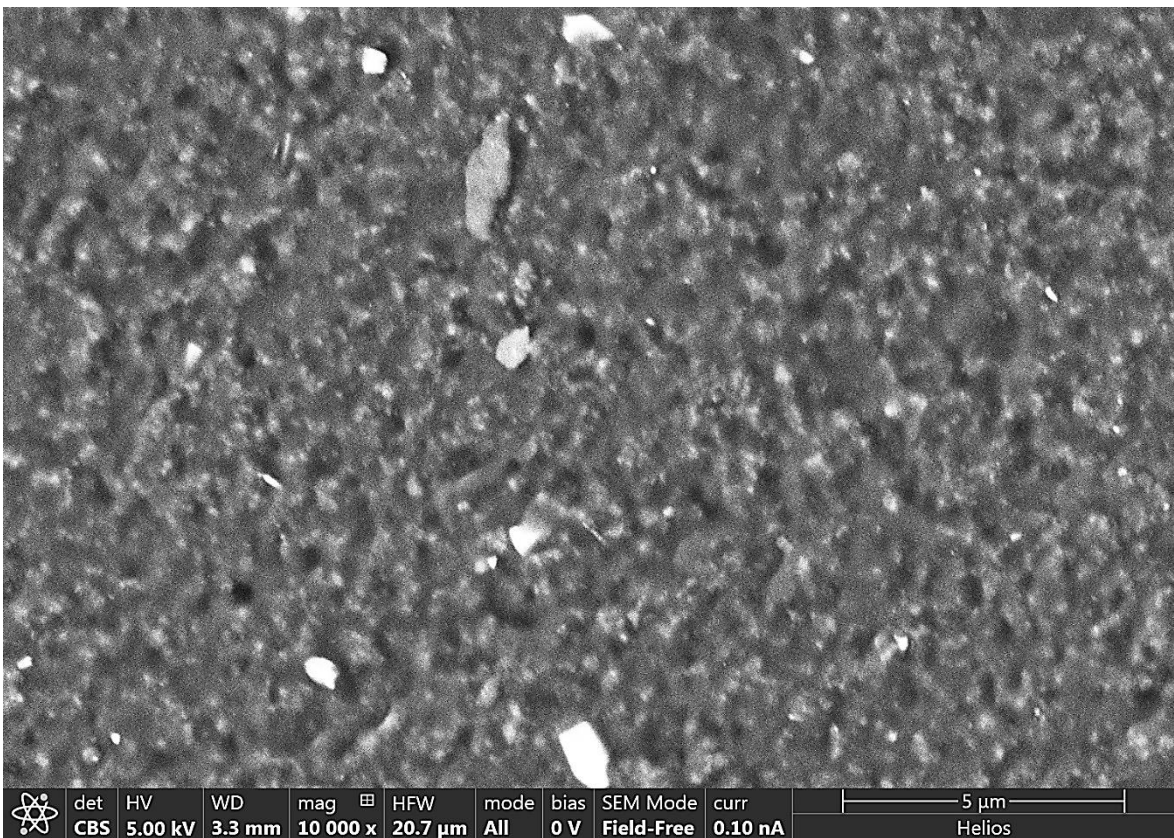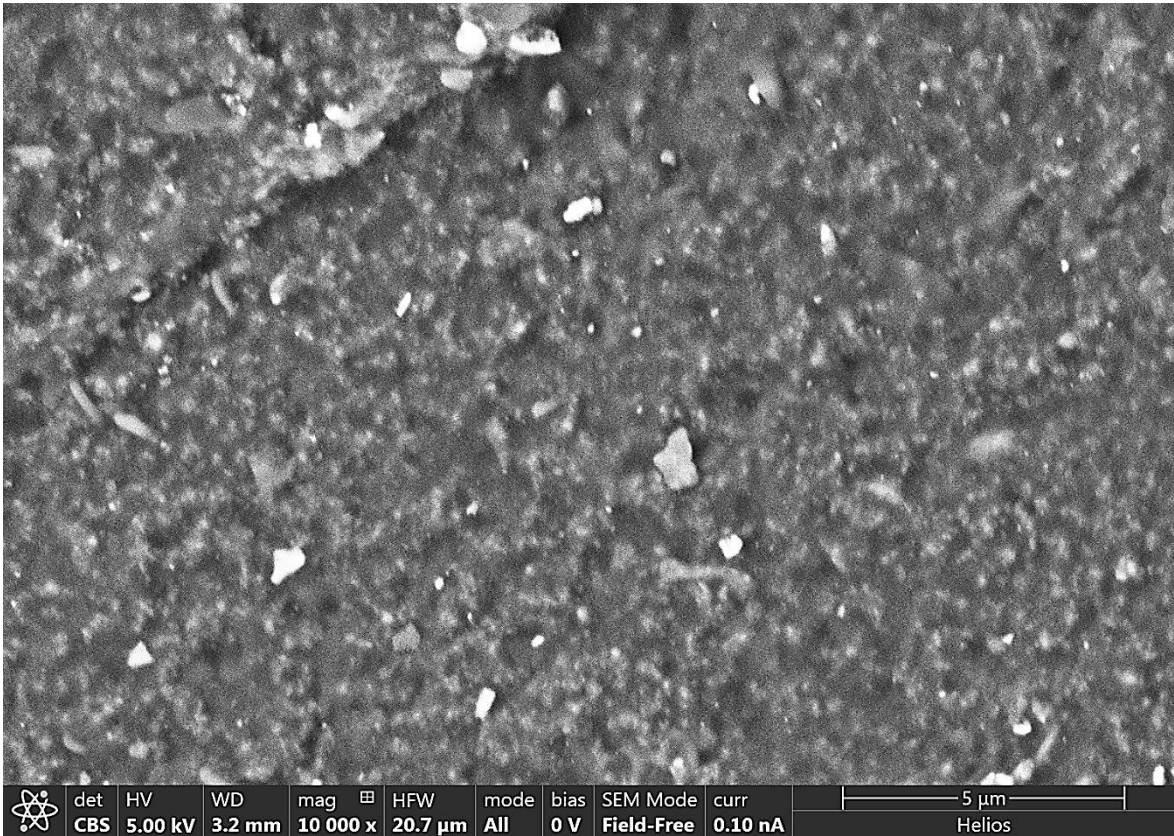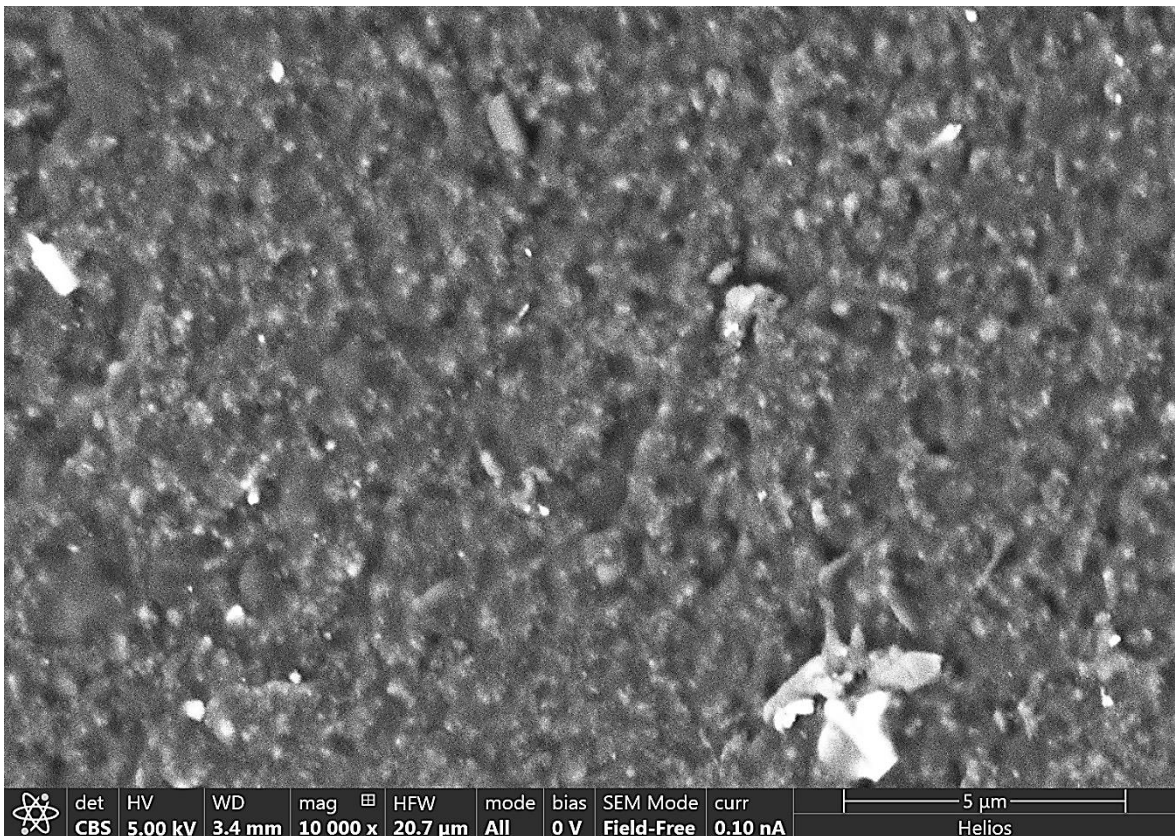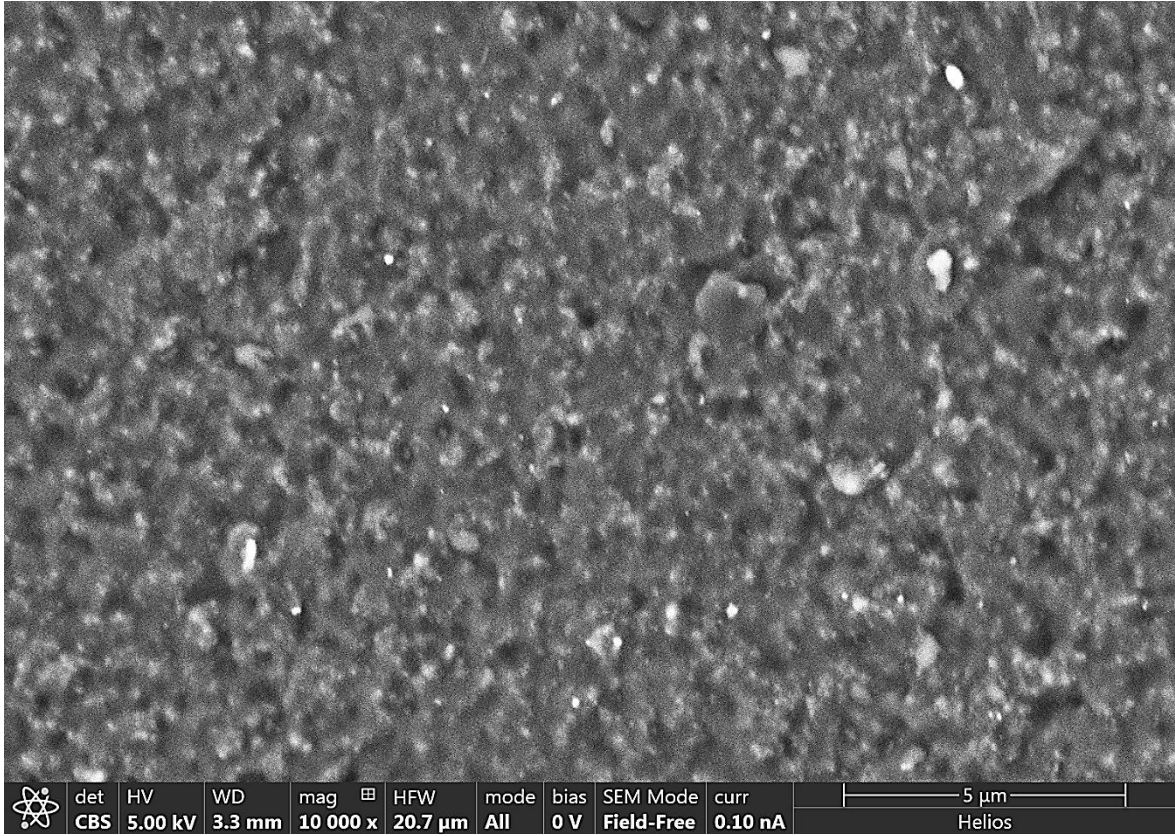| det	HV	WD	mag ⊞	HFW	mode	bias	SEM Mode	curr	5 μm
CBS	5.00 kV	3.1 mm	10 000 x	20.7 μm	All	0 V	Field-Free	0.10 nA	Helios
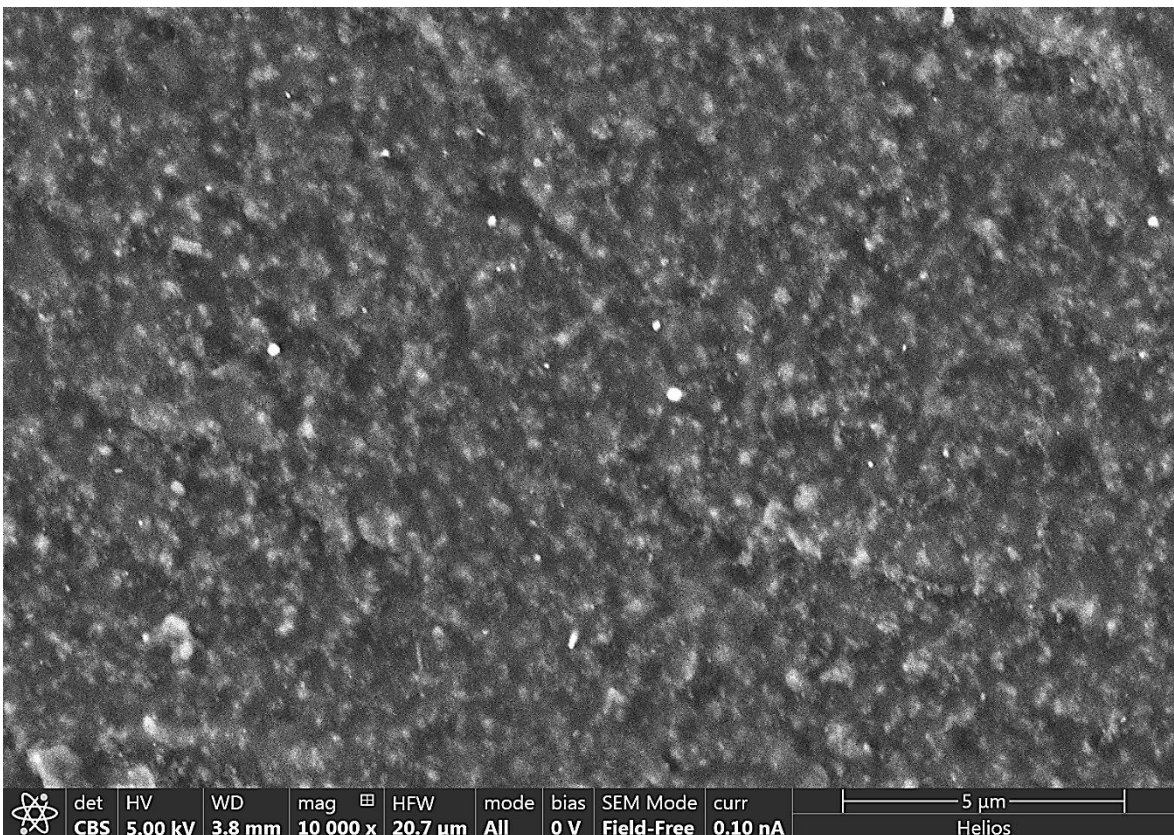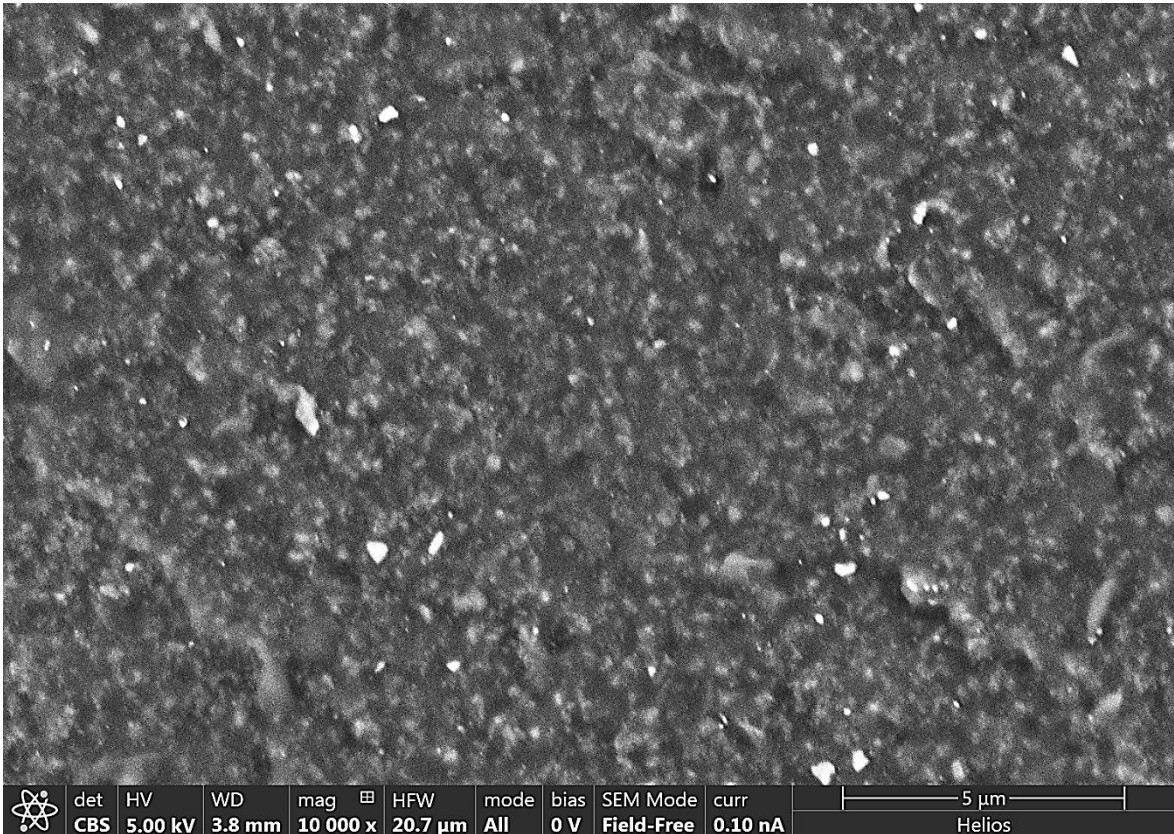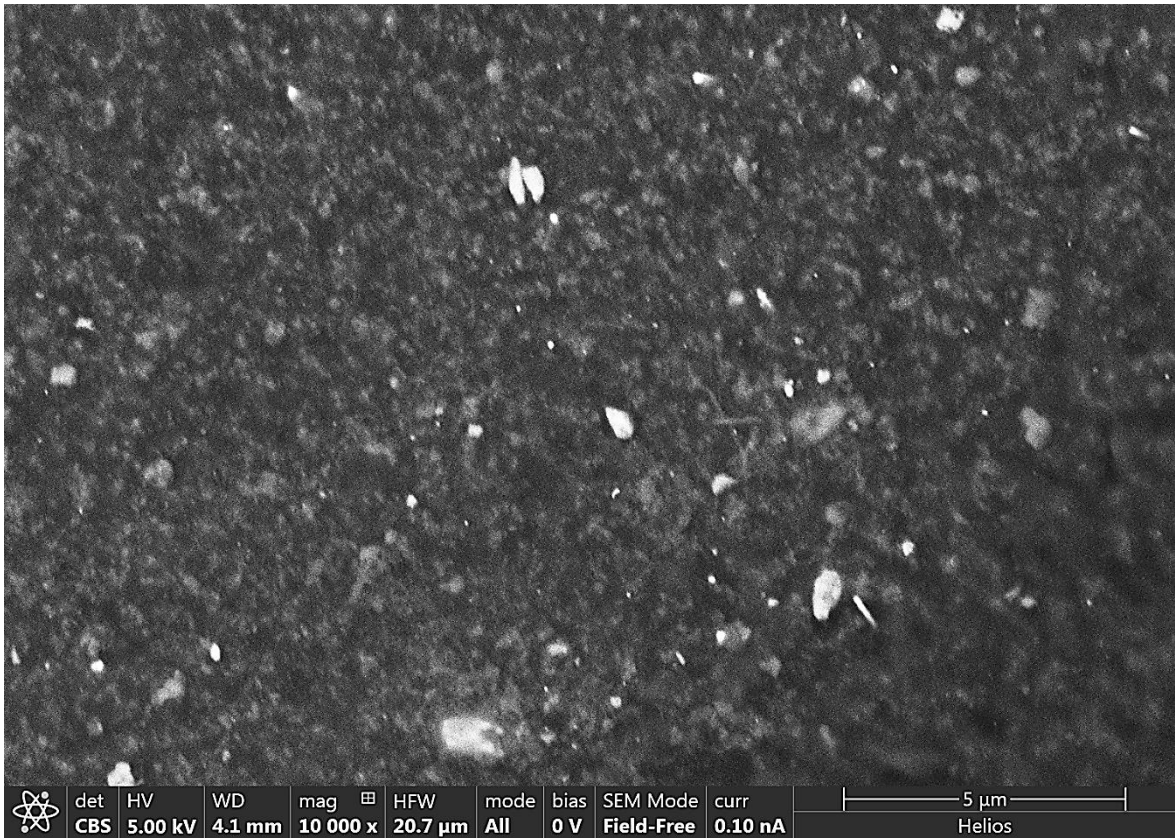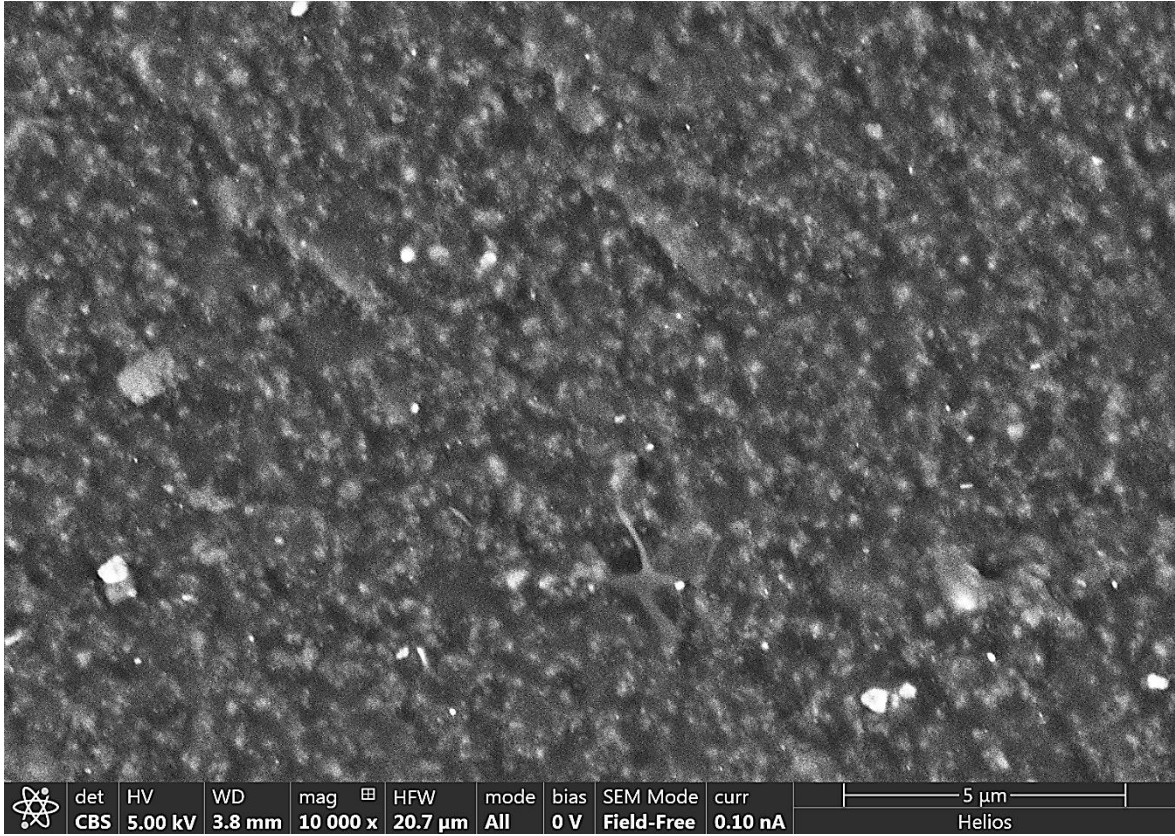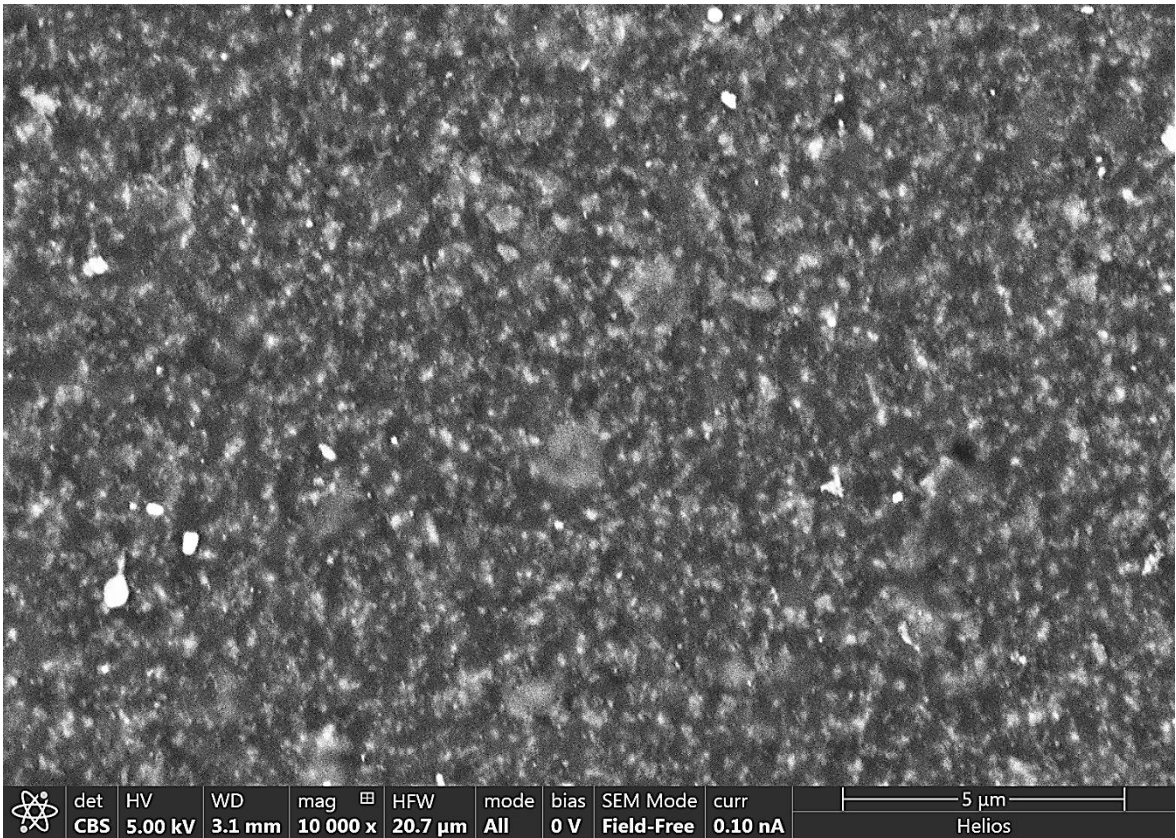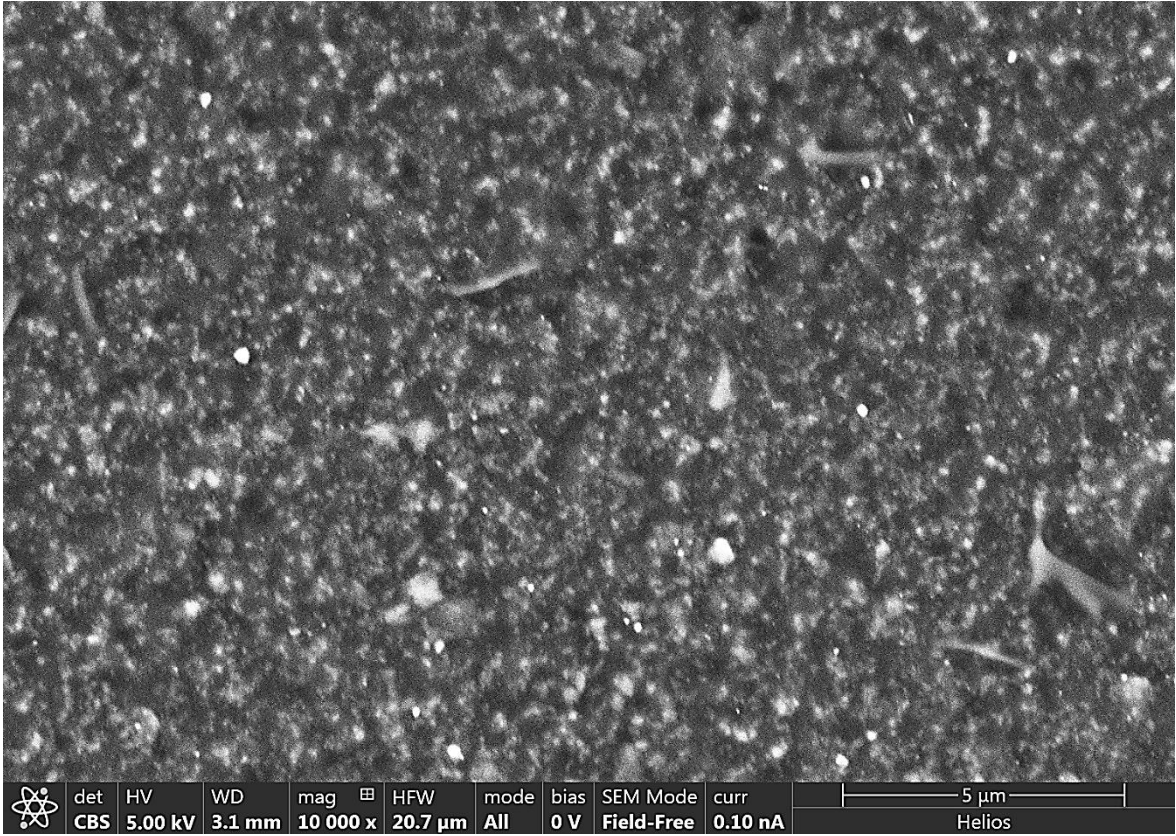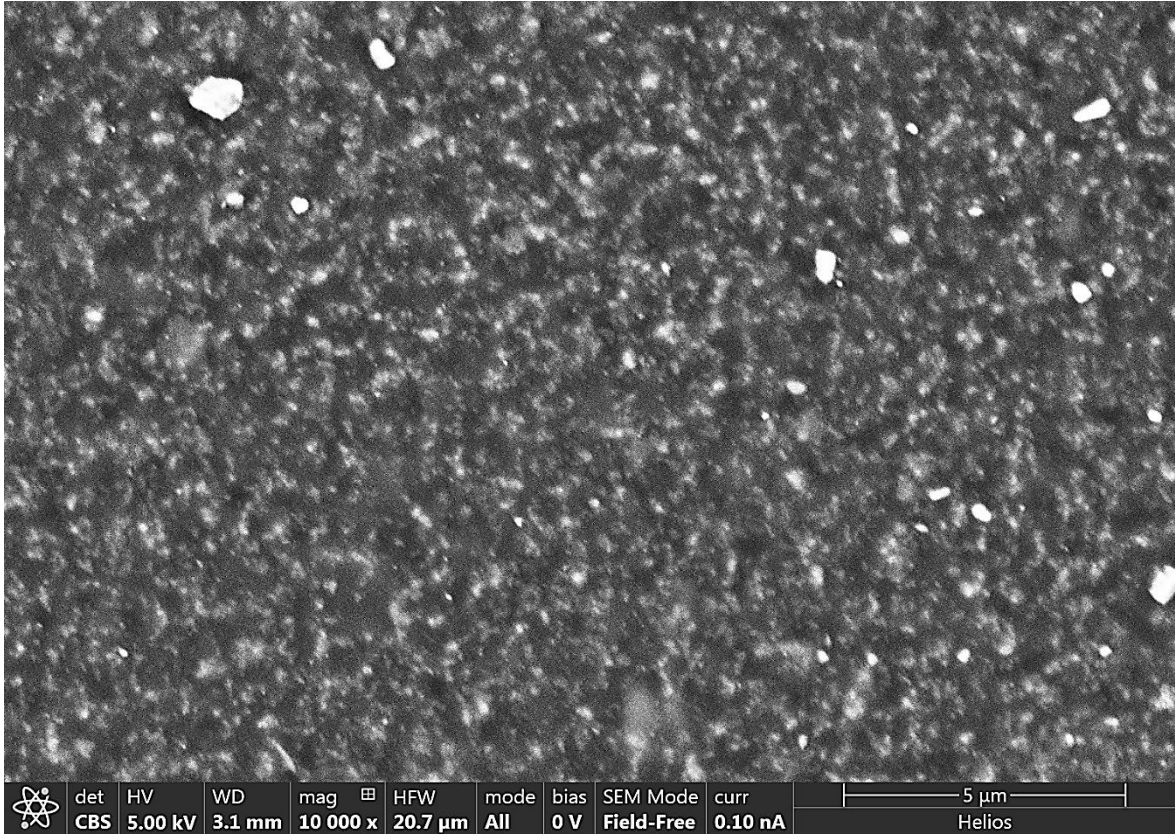
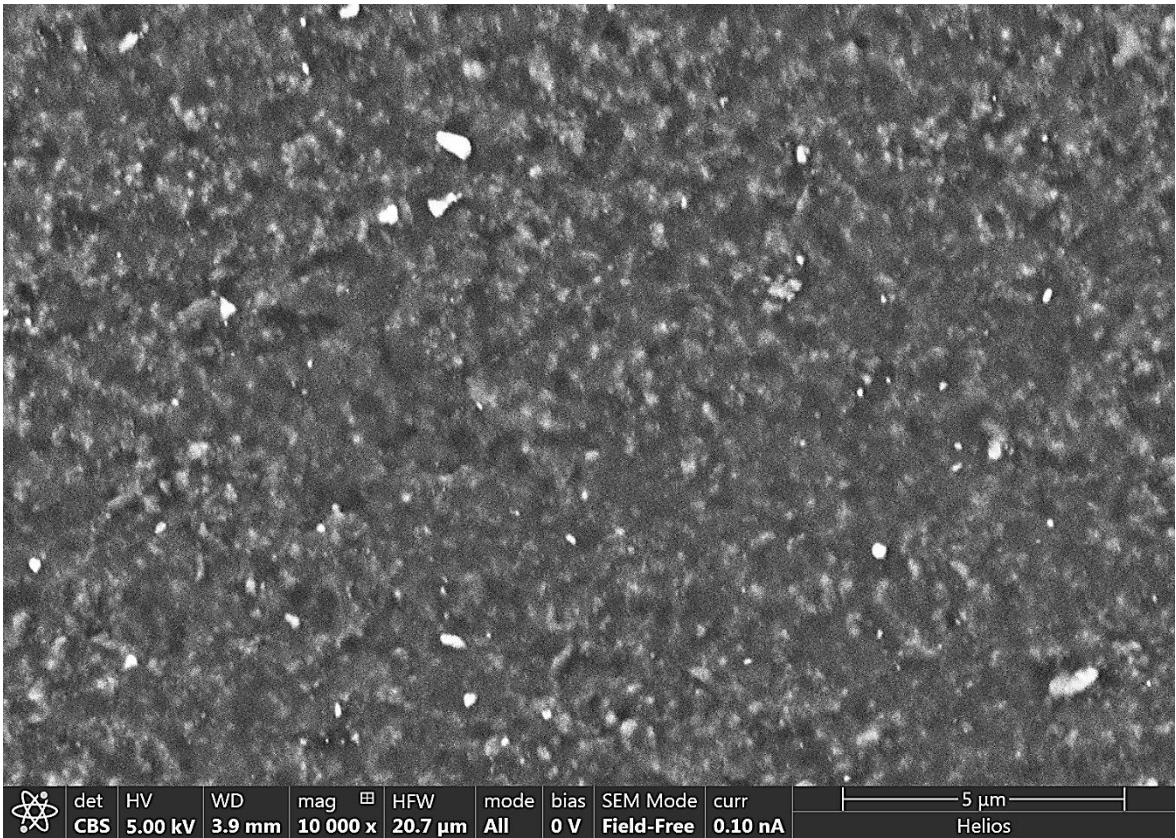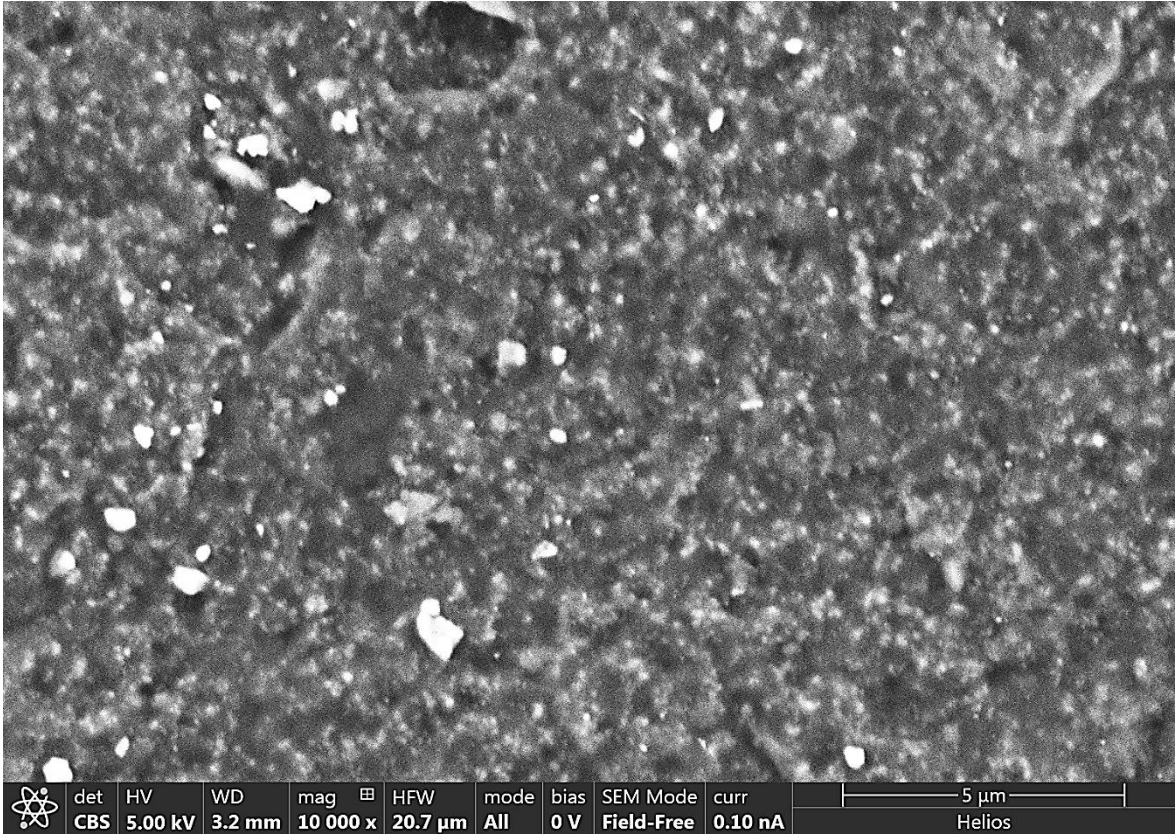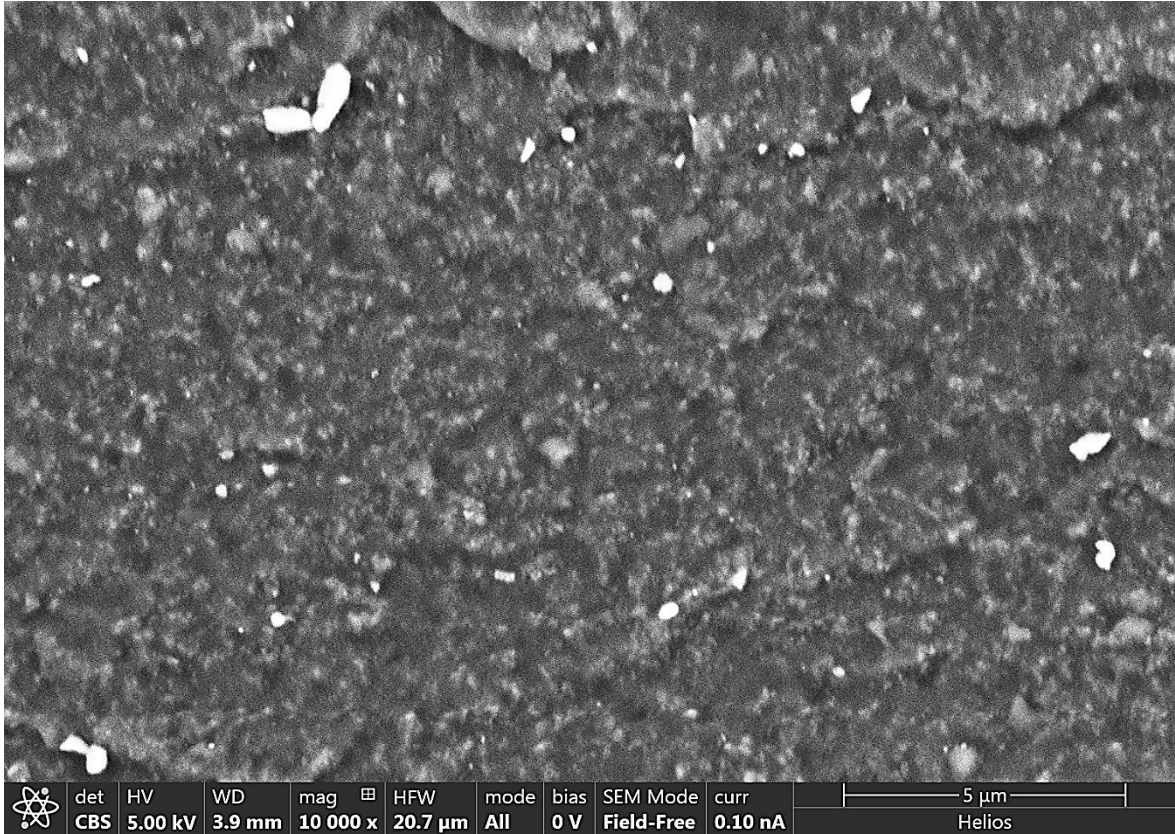xv.   <u>Processed Image, 137 Days Aerobic Aged Sample</u>

xvi.   <u>90 Days Anaerobic Aged Sheet Sample</u>
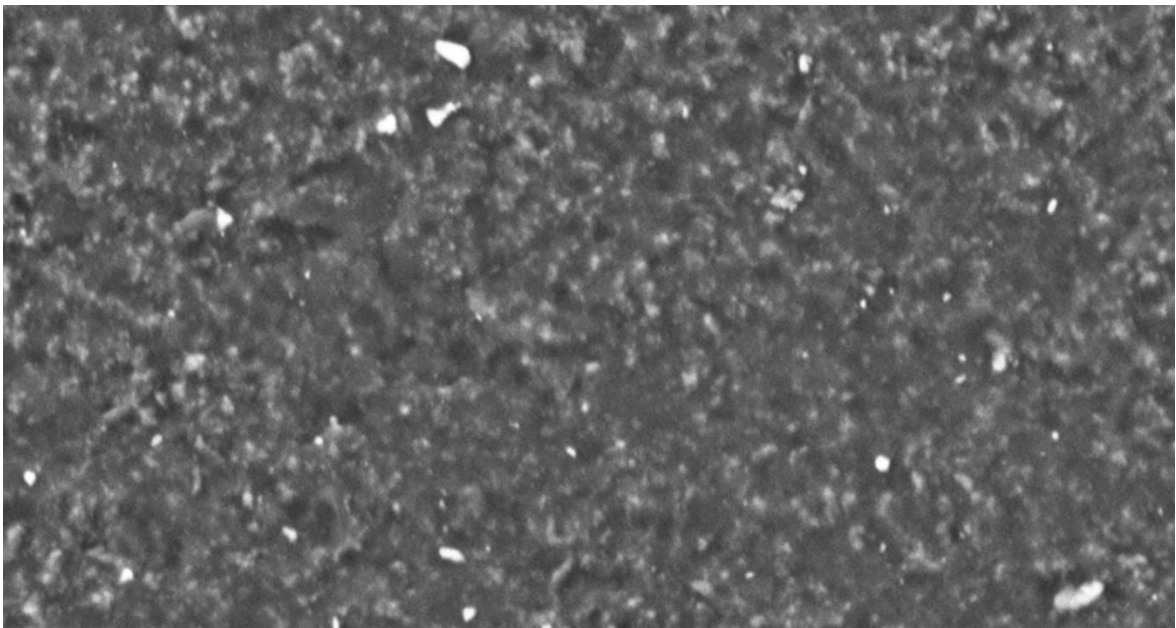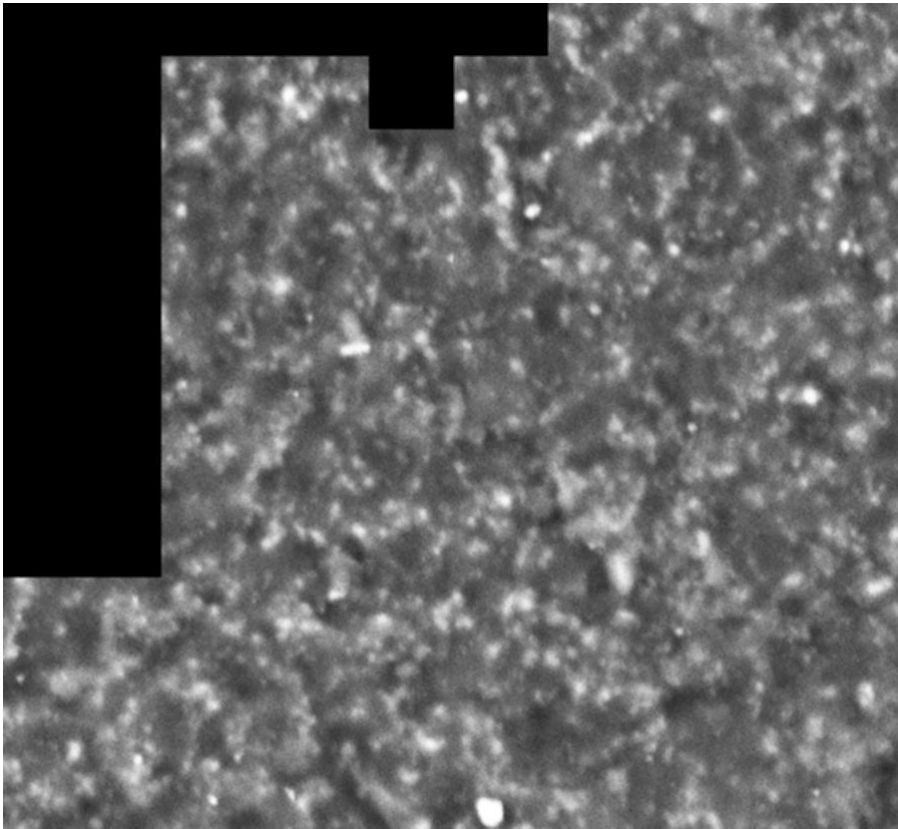
det	HV	WD	mag ⊞	HFW	mode	bias	SEM Mode	curr	5 μm
CBS	5.00 kV	3.9 mm	10 000 x	20.7 μm	All	0 V	Field-Free	0.10 nA	Helios
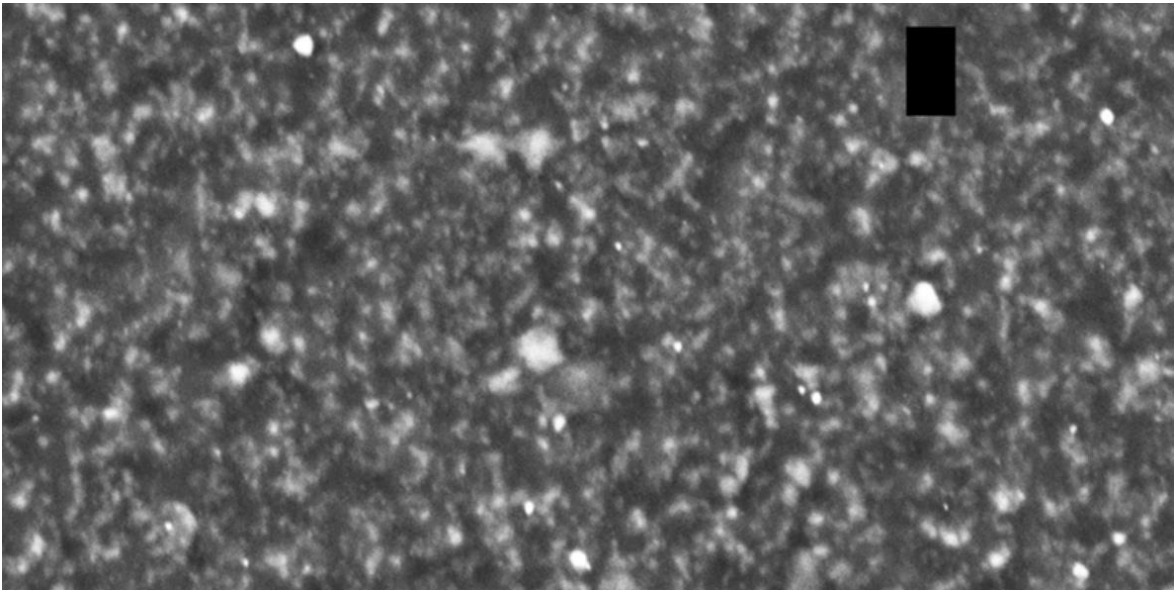
xvii.   <u>Processed Image, 90 Days Anaerobic Aged Sheet Sample</u>

lxxiv
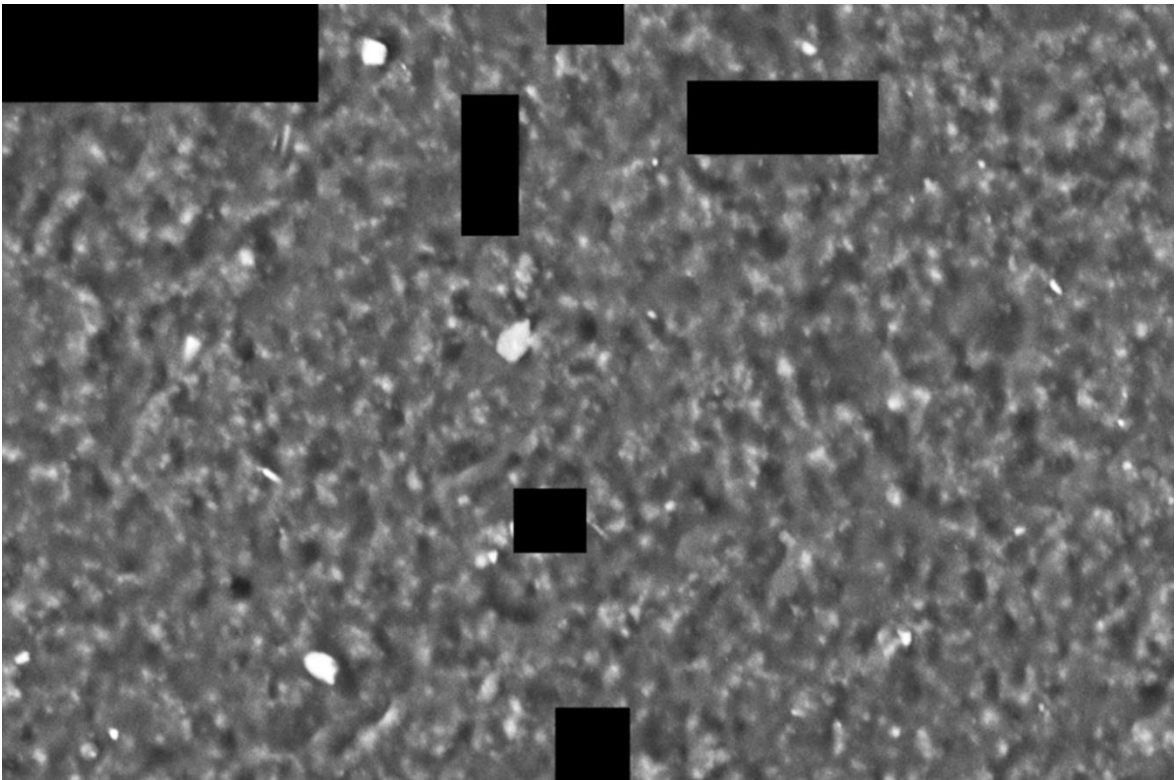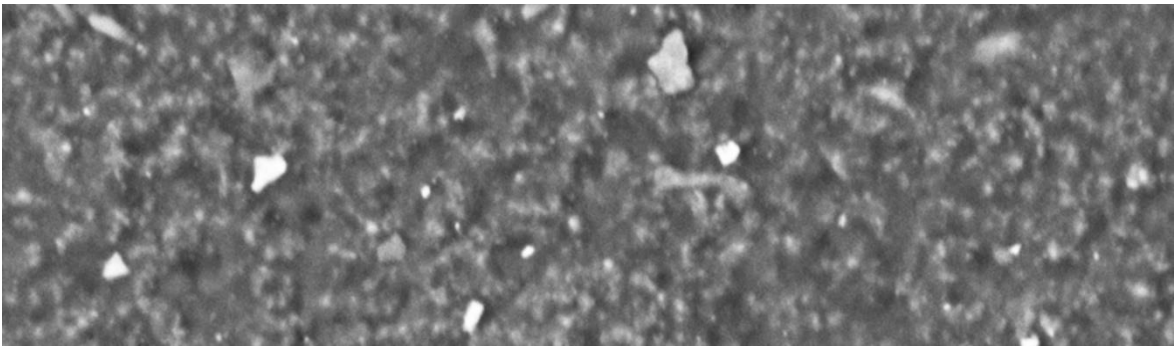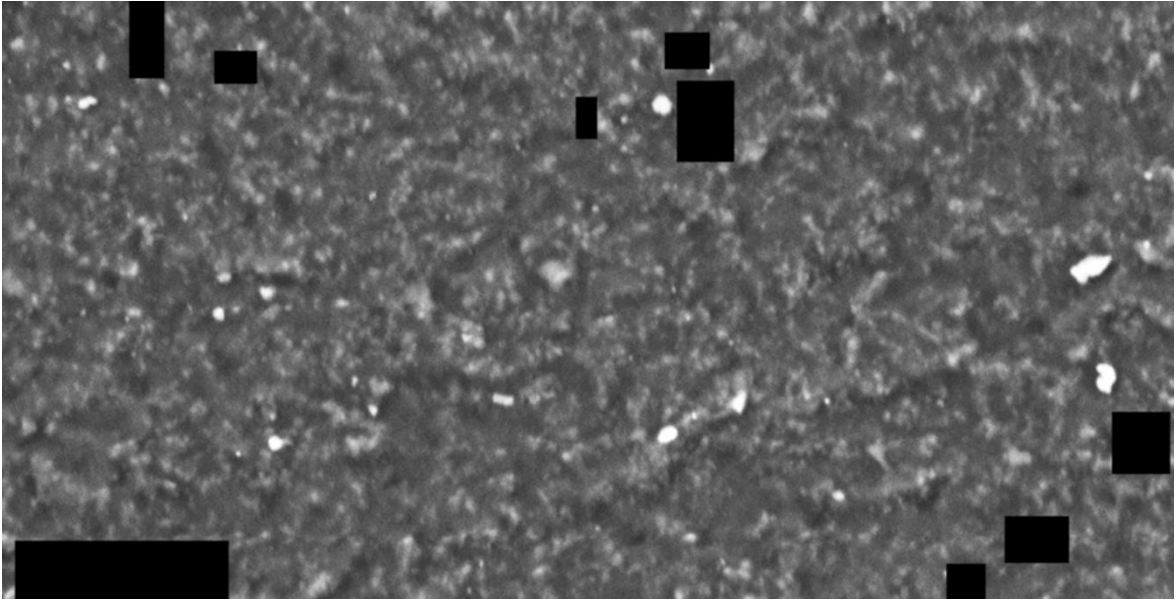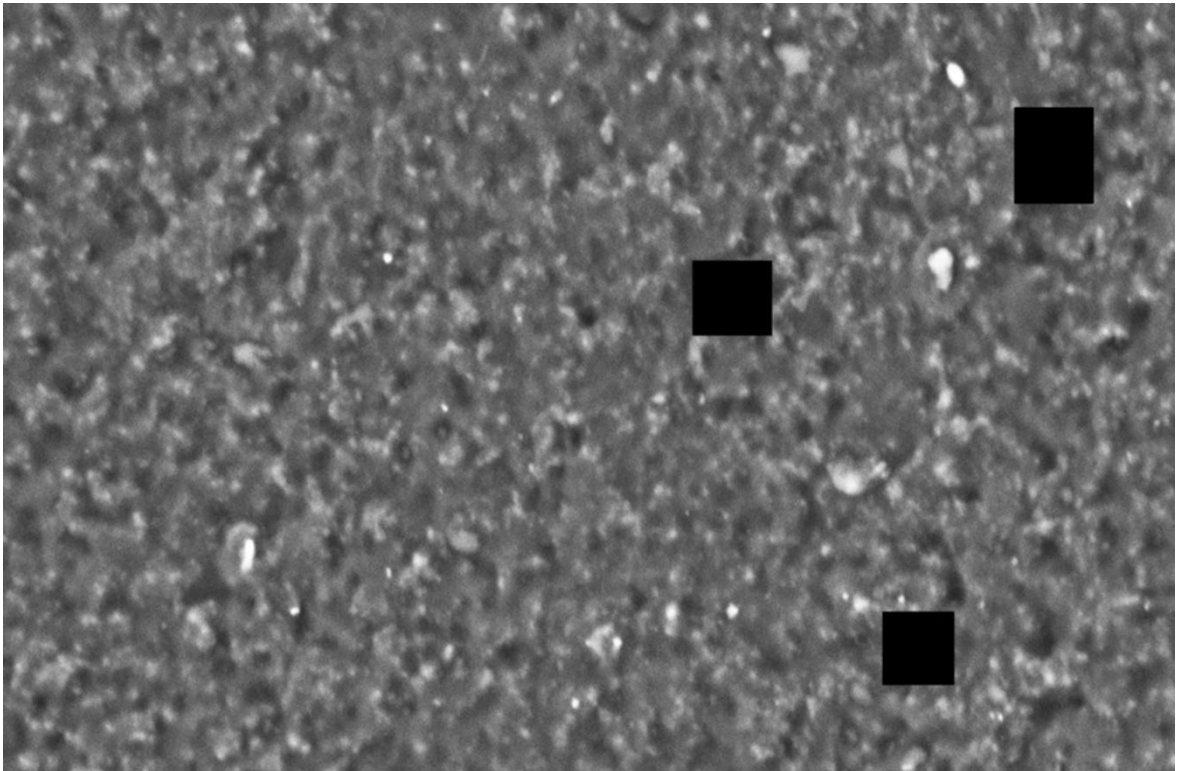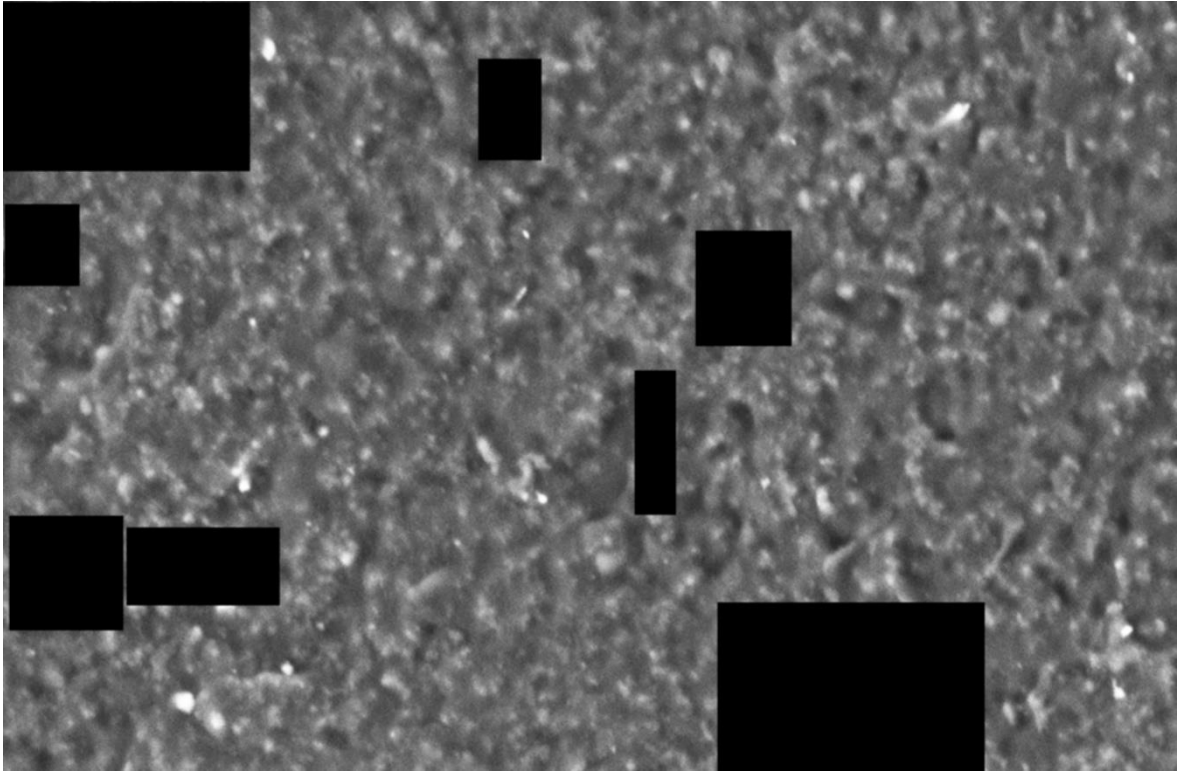
Appendix C.   Additive concentrations measured from GC

i.   Aerobic Aged Samples

Retention Time		13.85	16.15	17.8
Aged Days	Chemical Name	Octadecane	2-Amino-4-cyanomethyl-6-morpholino-1,3,5-triazine	Acetic acid n-octadecyl ester
0		21913181	601831	1054521
0		20048449	544209	827530
4		25053343	490545	829538
7		25844853	446071	693222
16		22672951	87484	283529
24		24200933	0	192627
36		28604807	0	115092
45		30612277	0	30373
56		33673850	0	24133
56		27633882	0	27679
72		27573713	0	0
92		30151149	0	0
108		25580140	0	0
138		37378369	0	0

Retention Time	17.75 18.6 19.45 20.25 21 21.75 22.5 23.2	19	19.35
Aged Days	Chemical Name	paraffin	6PPD	Hexanedioic acid, bis(2-ethylhexyl) ester
0	598912	26264712	914942
0	448673	22920026	738219
4	492885	21260573	908535
7	405947	15587287	829536
16	296470	4850185	613298
24	271553	1270377	496085
36	249001	724410	495330
45	155051	356038	277685
56	91998	333868	283394
56	113857	339043	283445
72	49627	203855	173346
92	45486	167999	99506
108	23195	113264	92487
138	69166	125732	177383

Retention Time		19.5	21.7	22.05
Aged Days	Chemical Name	Eicosyl acetate	DPPD	1,3-Benzenedicarboxylic acid, bis(2-ethylhexyl) ester
0		508048	5500952	1554581
0		398703	4636157	1205626
4		460725	7351214	1336170
7		427790	6538282	1478755
16		270059	4375071	1149901
24		246686	2308050	1123247
36		243461	1742209	1124433
45		157940	368861	698845
56		173807	312557	1006575
56		159377	257704	834653
72		125552	124843	520734
92		56162	96378	1018596
108		59515	68965	1089872
138		141446	71199	1006950

ii.   Anaerobic Aged Samples

Retention Time		13.85	16.15	17.8
Aged Days	Chemical Name	Octadecane	2-Amino-4-cyanomethyl-6-morpholino-1,3,5-triazine	Acetic acid n-octadecyl ester
0		21913181	601831	1054521
0		20048449	544209	827530
6		19833398	702202	799656
12		24266351	794115	825152
19		23220972	682714	766594
28		22433007	747710	768603
38		19751104	728107	701953
49		21126950	812684	845341
60		17515765	718909	762894
74		19127905	639643	636222
88		25008118	856913	741514

Retention Time		17.75 18.6 19.45 20.25 21 21.75 22.5 23.2	19	19.35
Aged Days	Chemical Name	paraffin	6DDP	Hexanedioic acid, bis(2-ethylhexyl) ester
0		598912	26264712	914942
0		448673	22920026	738219
6		452097	16912312	834931
12		493622	10490123	847176
19		462497	4932109	816328
28		490764	4481476	798687
38		473587	2340660	816366
49		545912	798532	951019
60		535139	422938	833296
74		489272	287524	724510
88		605810	368559	881109

Retention Time		19.5	21.7	22.05
Aged Days	Chemical Name	Eicosyl acetate	DPPD	1,3-Benzenedicarboxylic acid, bis(2-ethylhexyl) ester
0		508048	5500952	1554581
0		398703	4636157	1205626
6		380075	6345025	2323787
12		411259	5460361	1585793
19		370096	4073706	1906269
28		365975	4153886	1978379
38		342130	3360621	1777097
49		427029	1817805	1397095
60		394941	519251	1583026
74		324468	316477	1613194
88		392307	553934	1909732